A Thesis presented to the Cranfield Institute of Technology for the DEGREE OF DOCTOR OF PHILOSOPHY

Author: Hurmuze Naziri, B.Sc., D.A.E., A.I.M.

Supervisor: Roger Pearce, B.A., B.Sc., F.I.M.

Department of Materials.

Title: Superplasticity in Zn-based alloys.

17th February, 1972. 1968/70.

PAGE NUMBERING AS ORIGINAL

Abstract

This thesis is concerned with two basic zinc-based superplastic alloys, the virtually single-phase Zn - 0.4 wt % Al alloy and the two-phase Zn - Al eutectoid alloy. The first investigation is concerned with superplasticity in the Zn - 0.4 % wt Al alloy, while the second investigation is devoted to the effect of copper additions on the behaviour of the Zn - Al eutectoid superplastic alloy and the possible mechanisms operating during deformation.

A zinc - 0.4 Al alloy was developed, which showed a remarkable degree of superplasticity at room temperature, and elongations of greater than 500% could be obtained at the relatively fast crosshead velocity of 0.1 inch/min.

The strain-rate sensitivity (m) was found to increase with strain up to 300% on elongation (.35 → .5) parallel to the rolling direction and it was also found to be anisotropic in the plane of the sheet. The strain ratio r was also strain dependent and varied in the plane of the sheet. At 90° to the rolling direction, the strain ratio increased from .35 to .75 after an elongation of 350%, that is, tending to unity (isotropy). Texture determination after straining showed a marked change and agreed qualitatively with the change in strain ratio.

Grain growth occurred at room temperature, but was observed to be inhibited on superplastic deformation.

Surface observations after deformation revealed that grainboundary sliding was taking place; fracture behaviour, though characteristically ductile in nature, varied with strain-rate. This alloy obeyed the Hall-Petch relationship above a certain critical grain size, below which it was inapplicable, due to the occurrence of superplasticity.

Thin-foil transmission electron microscopy showed the importance of a dislocation recovery mechanism in the interpretation of this deformation behaviour, and calculations based on the current theories of volume and grainboundary diffusion, grainboundary sliding and dislocation climb/recovery, showed that a grainboundary sliding/dislocation climb recovery model could reasonably predict the observed strain rate sensitivity and strain-rate. Biaxial tests confirmed the anisotropic properties observed in uniaxial tests and also in punch-stretching the effect of friction on cup height was contrary to that observed with workhardening metals.

In the second investigation, measurements of the flow stress (σ_f) and strain-rate sensitivity (m) over a wide range of strain-rates ($\dot{\varepsilon}$) and temperatures between -75 to 300°C have been made on a range of superplastic alloys, based on the Zn - Al eutectoid, but with additions of up to 1% copper. These additions do not significantly affect σ_f or m above about 150°C. The peak in the m - $\dot{\varepsilon}$ curve is not displaced by these copper additions at temperatures above 150°C. Increasing the grain size (L) increases σ_f for temperatures above about 60°C but decreases σ_f below this temperature. With increasing grain-size, the peak in m-value moves towards lower $\dot{\varepsilon}$. The dependence of σ_f vs. L^a showed that the exponent a was strain-rate dependent and varied from 0.6 to 1 at 250°C. The exponent b in the relation $\dot{\varepsilon}$ vs. $\frac{1}{L^b}$ was independent of stress and varied from 1.8 at 250°C to 3 at 20°C.

The activation energy was grain-size and stress-dependent, and for the smallest grain size (.55 μm), a value of about 14 k.cal/mole was obtained in the superplastic region, while a value of near 20 k.cal/mole was obtained at the low $\dot{\varepsilon}$ region. Creep-rate measurements at room-temperature showed that the secondary creep-rate decreased with increasing copper content by a factor of about 120 between 0 and 1.0% copper. Increasing the grain size from 0.55 μm to 1.75 μm decreased the creep-rate further by a factor varying from 10-50 times and thus an overall gain in creep resistance of 1200 times can be obtained.

Uniaxial tension, torsion and camplastometer tests were used to cover strain-rates between 10^{-3} to 10^{4} min^{-1} in order experimentally to determine the multistage σ_f - $\dot{\varepsilon}$ curve. Hot-torsion stress-strain curves were typical of those shown in previous published work on hot working, and showed that a steady-state stress was obtained during superplasticity. In uniaxial tension, elongations of greater than 1000% were obtained at the very high initial strain-rate of 1.6×10^{1} min^{-1}. Grain coarsening occurred during deformation and was found to be strain-rate and strain dependent.

Thin-foil transmission electron microscopy showed the extensive activity of dislocations and diffusional processes. Dislocation-free structures and rounded interphase boundaries were observed under superplastic conditions. Also, though many of the grains appeared equiaxed after deformation, a variety of odd-shaped grains were observed, particularly in hot torsion, where there was evidence of accelerated spherodization. Fracture behaviour was dependent on grain size, temperature and strain-rate sensitivity.

Calculated σ_f - $\dot{\varepsilon}$ curves, from current theories, suggested that a dislocation-climb-recovery/grainboundary sliding model, based on grainboundary diffusivity was the operating mechanism during superplasticity.

ACKNOWLEDGEMENTS

The author is extremely grateful to his supervisor, Mr. Roger Pearce, for his unfailing encouragement, assistance and patient guidance throughout the course of this work. He also wishes to thank Dr. R. Johnson of the Electricity Council Research Centre, Capenhurst, and Dr. W. T. Roberts of the University of Birmingham for helpful discussions. The use of the Cambridge Instruments Scanning Electron Microscope, made possible by Dr. D. Beasley of the A.W.R.E., Aldermaston, and was greatly appreciated. Also thanks are due to the British Steel Corporation, Swinden Laboratories and the Research Centre, Port Talbot, for the use of the torsion and camplastometer testing machines.

The assistance of the members of staff of the Department of Materials is also much appreciated. In particular, the help of Mr. C. Matthews with the electron microscopy is gratefully acknowledged.

The author is extremely grateful for the financial support received from the Cranfield Institute of Technology, the Imperial Smelting Corporation, Avonmouth, and the Institute of Sheet Metal Engineering during the period August 1968 to December 1970.

Thanks are expressed to Mr. C. J. Swanson and Drs. C. Cross and N. Pipkin of the Imperial Smelting Corporation for the initiation and support of the investigation into the Zn - Al eutectoid superplastic alloys and for their many discussions.

All the material for this research was provided by the Imperial Smelting Corporation.

LIST OF ILLUSTRATIONS

List of Symbols

σ_f	Flow Stress (True)
σ	True Stress
σ_o	Back Stress or Initial Flow Stress
σ^*	Frictional Stress
K	Constant
K_1	Constant (= 0.22)
k	Boltzmanns Constant
k'	Hall-Petch Slope
α	Constant (= 10)
β''	Constant (= 150)
$\dot{\varepsilon}$	True Strain-Rate
$\dot{\varepsilon}_{DV}$ or $\dot{\varepsilon}_{N-H}$	Strain-Rate due to Volume Diffusion or Nabarro-Herring Creep-Rate
$\dot{\varepsilon}_{GB}$	Strain-Rate due to Grain-boundary Diffusion or Coble-Jones Creep-Rate.
$\dot{\gamma}_T$	Total Shear Strain-Rate
$\dot{\gamma}_G$	Average Grain Shear Strain-Rate
$\dot{\gamma}_D$	Diffusional Strain-Rate
$\dot{\gamma}_{GBS}$	Grain-boundary Sliding Shear Strain-Rate
γ_3	Strain-Rate in Grain 3
δ	Average Sliding Rate
$\dot{\delta}_{1,2}$	Grain Displacement Strain-Rate
v_1, v_2	Constant Crosshead Velocity
V	Velocity due to two Grains Sliding
V'	Velocity of Climb

d_o	Initial Diameter
l_o	Initial Length
l_i	Current Length
Δl	Extension or Change in Length
ω_o	Original Width
ω_i	Current Width
A	Cross-sectional Area
A'	Average Cross-section Area of a Grain
$\delta_{1,2}$	Displacement due to Movement of Grain 1 over Grain 2
ε	True Strain
ε_1, ε_2 & ε_3	True Strains in the x, y and z Directions
P	Load
P_A, P_B	Steady State Loads at Velocities ν_1 and ν_2 Respectively
ρ	Dislocation Density
μ	Shear Modulus
b	Burgers Vector
ν	Poisson's Ratio
M	Number of Active Dislocation Sources per Unit Volume.
m	Strain-Rate Sensitivity
w	Grain-boundary Width
L	Grain Size
γ	Strain Ratio
η	Coefficient of Viscosity
H	Distance a Dislocation must Climb
D_v	Volume Diffusion
D_{gb}	Grain-boundary Diffusion
D_p	Pipe Diffusion

Q_v	Activation Energy for Volume Diffusion
Q_{gb}	Activation Energy for Grain-boundary Diffusion
T	Temperature in Degrees Absolute (^oK)
T_m	Homologous Temperature
TEM	Transmission Electron Microscope
SEM	Scanning Electron Microscopy

Other symbols are defined as they appear in the text.

TABLE OF CONTENTS

CHAPTER I

1. Introduction

The development of the Zn - 0.4 % wt Al superplastic alloy was motivated by an earlier investigation by the author on the extended plasticity observed in commercial-purity zinc (1). This work followed from the fortuitous observation that, on rolling a zinc slab to 90% reduction, fine and stable grains of the order of ~ 2 μm in size were produced. On straining at room temperature and at slow strain-rates (~ 10^{-3} min^{-1}) elongations up to 200% were obtained. Micro-structural examination exhibited the presence of impurity particles at the grainboundaries and these were thought to stabilize the fine grains at room temperature. Surface observations of grainboundary sliding and internal observations showing the absence of dislocation and dislocations were characteristic of superplasticity. It was therefore decided to try and produce a virtually single-phase zinc alloy which would be truly superplastic, and perhaps produce higher elongations at higher strain-rate. Also, it was obvious that the interpretation of any structural observations would be easier, and less confusing than in two-phase superplastic alloys. Furthermore, superplasticity exhibited at room temperature reduced the complications encountered in higher temperature tests. Finally, it was hoped that such an investigation would elucidate the mechanisms responsible for superplasticity.

The second investigation was industrially sponsored (Imperial Smelting Corporation, Avonmouth) and was aimed at the development of the well-known Zn - Al eutectoid superplastic alloy, taking into consideration all the practical aspects for its application commercially.

The Zn - Al eutectoid is the most popular superplastic alloy at present since it exhibits a high degree of superplasticity ($m > 0.5$ and > 1000% elongation) at the relatively low temperature of 250°C, low stresses and at reasonably high strain-rates. Unfortunately, the strength and creep resistance, between 20 - 100°C, of this alloy is inadequate for many engineering applications.

In an attempt to improve this, copper additions have been made to this alloy; the selection of copper was a natural one, as it is used as a strengthening addition in most commercial zinc-based alloys. Also it was essential that the improvement of the strength and creep resistance would not affect the superplasticity at 250°C.

It was also decided to correlate the forming behaviour of the various alloys to the uniaxial measured superplastic parameters.

Together with the emphasis being towards commercial requirements, the various mechanistic aspects of superplasticity were also investigated.

Chapter (2) on 'Isothermal Superplasticity' summarises the datas and mechanisms observed in most of the superplastic alloys and is relevant to the two basic superplastic alloys investigated in this thesis. A general chapter (3) on the ductility in the fine-grained zinc-based alloys is included followed by chapters on the investigations of the two basic alloys.

The creep and forming investigations of the Zn - Al eutectoid alloys were carried out at the Imperial Smelting Corporation, Avonmouth, and the results have been included with their permission.

CHAPTER 2

2. Isothermal Superplasticity*

2.1 Introduction

Viscous behaviour, or the ability of certain metal alloys to flow in such a manner so as to produce neck-free elongations of greater than thousand percent, has been with us for nearly forty years. However, it is only in the last 6 years, which marks the graduation of this phenomenon from a laboratory curiosity to serious metallurgical research and the resulting development of superplastic alloys for commercial exploitation (2-6).

Several review papers have been written on this subject (7-10) and very recently, a review article covering all the superplastic alloys investigated to date, has been published by Johnson (11). Therefore, it is not intended to write a comprehensive review in this thesis, but the relevant observations, properties and mechanisms have been summarised and listed in the following sections.

---

* The term 'superplasticity' has been applied to metal alloys which are capable of exhibiting high elongations (200 - 2000%). High elongations are observed in materials having a stable, fine-grain structure (~ 0.5 - 2 μm) and strained under isothermal conditions of temperature, in the region of fifty percent of the melting point of the metal. Large amounts of elongation can also be obtained in certain allotropic metals and alloys by thermal cycling through the transformation temperature while under stress, but this is termed phase-transformation superplasticity.

This thesis is only concerned with fine-grained alloys strained under isothermal conditions, and as such the term 'superplasticity' is used to refer to this particular type of superplasticity only.

2.2 Discovery and Early Investigations

The necessary requirements for superplasticity, that is, an extremely fine, stabilized grain-size of the order of a few microns at a temperature about equal to or greater than fifty percent of the melting point, and deformation in a critical strain-rate range were discovered as early as 1934 by Pearson (12) in the Pb-Sn eutectic. However, it was not before the Russian investigators, Bochvar and Sviderskain's (13) discovery of the superplastic Zn - Al eutectoid, followed by the investigation of several Russian workers into a range of superplastic alloy systems (14-19), (Mg-Al, Mg-Cu, Al-Cu, Al-Si and M-Cu), and the review of all this work by Underwood (7) in 1962, that this phenomenon was investigated in detail.

The credit of rationalizing the superplastic behaviour in terms of elongation, flow stress, strain-rate, temperature and grain size, goes to the collective work of Backofen, Turner and Avery (20) (Zn-Al eutectoid), Avery and Backofen (8) (Pb-Sn eutectic) and Holt and Backofen (21) (Al-Cu eutectic).

2.3 Flow stress, Strain-Rate and Strain-Rate Sensitivity Relationships

Backofen et al (20), realised that the 'neck-free' elongation obtained in uniaxial tension at very low stresses was directly related to the strain-rate. These workers introduced the parameter m, termed the strain-rate sensitivity of the flow stress, from the relationship $\sigma_f = K \dot{\varepsilon}^{m}$ (1) as a measure of the degree of superplasticity,

where σ_f = true flow stress, K = constant and $\dot{\varepsilon}$ = true strain-rate. This empirical equation has since been found to be obeyed by all superplastic metal alloys (10,11,22). Typical m-values range from 0.4 to 0.8, where m = 1 for Newtonian viscous flow.

The basis for necking resistance, with subsequent unlimited elongation, shows a strong dependence on the flow stress and the strain-rate. When the m-value is high, the more rapidly straining material in an incipient neck is strengthened, so that deformation tends to spread out into the less rapidly straining, and therefore weaker, material adjoining the neck. Analytically this can be shown using equation (1) as follows:

$\sigma_f = K \dot{\varepsilon}^{m} = \frac{P}{A}$ where P is the load transmitted through the cross section area A. At any point along a rod in tension,

$\dot{\varepsilon} = \frac{\nu}{l} = \frac{1}{l} \cdot \frac{dl}{dt} = \frac{1}{A} \cdot \frac{dA}{dt}$ (2), where ν is the crosshead velocity, l the gauge length and t the time.

Combining equation (1) and (2):

$$-\frac{dA}{dt} = \left(\frac{P}{K}\right)^{\frac{1}{m}} \left[\frac{1}{A^{1-m/m}}\right] , \qquad (3)$$

therefore, as long as m is < 1, the smaller the cross-section, the more rapidly it is reduced. When m is unity, flow is Newtonian viscous and $\frac{dA}{dt}$ is independent of A, so that any cross-sectional irregularity (or incipient neck) is preserved during straining.

Thus the nearer the m-value is to unity, the less is the likelihood of necking in a tensile specimen, and consequently high elongations will be achieved. This is observed in most superplastic metal alloys. Woodford (22) has shown that a direct correlation exists between the m-value and the percentage elongation for a range of alloys with m-values ranging from 0.002 to 0.8. However, it has been shown by Morrison, (23) that tensile specimen geometry can effect the total elongation. The author observed that a critical notch depth existed below which it had no appreciable effect on the maximum elongation. In the case of a cylindrical tensile specimen, the elongation was dependent on the diameter to gauge-length ratio. An empirical equation was developed relating elongation, specimen geometry, and m-value. For the Pb - Sn eutectic it was found to be:

Total elongation $\simeq b'm^2 \left(^{d_o}/_{l_o}\right) 100$ where b' is a constant equal to 280, d_o and l_o are the initial diameter and gauge length of the specimen.

A rather special feature of superplastic metals is that the m-value varies with strain-rate, and a characteristic dome-shaped, three region, m - $\dot{\varepsilon}$ curve is obtained (Figure 1) and the peak m-value region is the superplastic region. In most superplastic metals, this curve covers four to six orders of magnitude of strain-rate, typically from 10^{-6} to $10 \cdot 1\ min^{-1}$. (8,20,21,23-32,85). The low and high strain-rate regions are considered non-superplastic regions.

The flow stress versus strain-rate relationship curve is S-shaped, and also can be divided into regions (Figure 2). The slope of the tangent at any point to the curve, corresponding to a particular strain-rate, will give the m-value plotted in Figure 1.

Generally, the average slope of each of the three regions is taken as the operating m-value. Typical m-values obtained in the three regions are, $m \lesssim 0.2$ for the low - $\dot{\varepsilon}$ and high - $\dot{\varepsilon}$ regions, and $m > 0.5$ for the intermediate - $\dot{\varepsilon}$ (superplastic) region.

The σ_f - $\dot{\varepsilon}$ and m - $\dot{\varepsilon}$ curves are grain size and temperature dependent. Increasing the grain size moves the m - $\dot{\varepsilon}$ curve to lower strain-rates, while the peak m-value tends to increase. (Figure 3). This effect is only true for grain size increases from 1 μm → 10 μm (21,24,26,29-31,33). Concurrently the σ_f - $\dot{\varepsilon}$ curve moves to the lower end of the strain rate spectrum with increasing flow stress values. (Figure 4) (8,21,23,24,26-28,31,33,36) At a constant grain size but with increasing temperature, the m - $\dot{\varepsilon}$ curve moves to the higher strain-rate end, with an increase in the peak m-value (21,24,26) (Figure 5).

Similarly, the σ_f - $\dot{\varepsilon}$ curve will move to lower flow-stress values, with the superplastic or high m-value region moving towards the higher strain-rate end (Figure 6) (21,24,26,27,31, 35,85).

It has been suggested that the existence of the low - $\dot{\varepsilon}$ region in the S-shaped σ_f - $\dot{\varepsilon}$ curve is only an apparent effect arising out of the presence of a back stress or initial flow or yield stress (σ_o) (26,30,36,37). This approach was adopted on the assumption that the σ_f - $\dot{\varepsilon}$ relationship actually shows a Bingham-type behaviour, i.e.

$$\dot{\varepsilon} = \frac{\sigma_f - \sigma_o}{\eta},$$

$\dot{\varepsilon}$ is the diffusional strain-rate, σ_f the applied and σ_o the initial flow stress, and η the coefficient of viscosity. Therefore the true flow-stress characteristic of the material is represented by:

$$\sigma_f - \sigma_o = \bar{K} \dot{\varepsilon}^{\bar{m}},$$

where $\bar{K}$ is the material constant and $\bar{m}$ the true index of strain-rate sensitivity. Comparing this with the empirical equation (1):

$$\sigma_f = K \dot{\varepsilon}^{m},$$

then

$$\bar{m} = \frac{\sigma_f}{\sigma_f - \sigma_o} \quad m,$$ and its

value is always unity so long as diffusional deformation is significant. $m \to 1$ only when $\frac{\sigma_o}{\sigma_f} \to 0$. Therefore the relationship between stress and strain-rate takes the form shown in Figure 7 which only covers two regions. It has been suggested that this initial yield stress, σ_o, may result from a relatively rate-insensitive grain-boundary sliding resistance (21,24,26,36,37) only present when deformation commences.

2.4 Flow Stress and Strain-Rate Dependence on the Grain-Size:

The relationship between grain-size and flow stress can be expressed in the form -

$\sigma_f \alpha L^a$, where L is the grain size and a an exponent. The values of a determined for a range of superplastic alloys have been found to vary from 0.5 - 3.5. (8,21,24,33,38-40). This exponent is strain-rate and temperature dependent and should be related to the parameter m, though this relationship has not been investigated systematically. Typical a-values, determined at strain-rates where the m-value is high, have been correlated with superplastic behaviour. a = 1 is stated as an indication that grain boundary sliding is predominantly operating, (21). a = 2 is indicative of volume diffusion or Nabarro-Herring creep (41,42) and a = 3 of grain-boundary diffusion creep or Coble-Jones creep (43,44) respectively.

The relationship between grain-size and strain-rate can be expressed in the form:

$$\varepsilon \alpha \frac{1}{L^b}$$

where b has been found to vary from 2 to 5 (8,25,28,33,40,45). This exponent has been found to be independent of stress, but there is no data showing the influence of temperature and m-value on b. Nuttall (40), has shown that in the Zn-Al eutectoid, in the temperature range 150 - 250°C, the exponent b remains constant (b = 2). The value b = 2 indicates the operation of Nabarro-Herring creep and b = 3 Coble-Jones creep respectively.

However, as has been stated by Backofen and Zehr, (28) unique values of a and b will not necessarily be obtained as a combination of mechanisms might be operative during superplasticity.

2.5 Activation Energy

Though it has been stated that superplasticity is observed at a temperature of about fifty percent of the melting point or 0.5 Tm (Tm = homologous temperature), this is merely a 'rule of the thumb' approach, as superplasticity can be observed below and above this value. Ideally, the higher the temperature the higher the degree of superplasticity, provided the structure is

stable and excessive grain-growth or a structural change (i.e. phase transformation) does not take place.

It is recognized that the mechanism or mechanisms responsible for superplasticity are dependent on the thermal contribution. The thermal contribution in the form of activation energy (Q) has been determined for a range of alloys, though activation energy values quoted by many workers are rather conflicting and in some cases different even for the same alloy. In the Zn - Al eutectoid Chaudhari (46) obtained a value of 35 k cal/mole at temperatures above 200°C and a value of 21 k cal/mole for temperatures below 175°C, both values being obtained at the same low (creep) strain-rate. In contrast, in the same alloy, Packer and Sherby (47) and Nuttall (40) obtained a value of 19-25 k cal/mole between 260-200°C, while Ball and Hutchinson (45) obtained a value of 15 k cal/mole. It should be noted that the self diffusion value for zinc is 20 k cal/mole (48,49), while it is 34 k cal/mole (50) for aluminium. The grain-boundary diffusion value for zinc is ~ 14 k cal/mole (48,49). In (47), (40) and (45) the strain-rate region in which the activation energy was determined was also considered to be the superplastic region. However, Alden (27) has shown that variation in grain-size alters the activation energy and the demarcation between the three regions of the $\sigma_f - \dot{\varepsilon}$ curve is not sharp. Alden observed that in a fine-grained Pb - 6Cd alloy, the percent recovery was about eighty and the Q-value was 9.6 k cal/mole, a value close to the grain-boundary diffusion value for lead. However, in the case of the coarse grained material, the percent recovery was only forty and the Q-value was in the region of 19 k cal/mole.

Q-values near the self-diffusion value have been observed in the Al - Cu eutectic (21), Mg-Zn-½ Zr (26), cp zinc (1), Cd-5 Pb (27), Nc-Fe-Cr (38). Values near the grain-boundary diffusion value have been obtained in the Pb-5 Cd (27), Sn - 38 Pb (51), Zn-0.2 Al (52) alloys. Though, the situation might appear complex, a pattern might exist, and this will be discussed fully in Chapter 5.

2.6 Microstructural Observations after Deformation

The microstructures observed are different in the three $\dot{\varepsilon}$ regions.

In the superplastic $\dot{\varepsilon}$ - region, surface observations show grain-boundary sliding and/or the relative movement of grains (grain rotation) in all superplastic metals. (8,21,23,24,26-31,33,35,40 45,46,51,53-57). Meticulous measurements of surface markers (scratch marks) in order to determine the strain contribution by grain-boundary sliding, has shown that this contributes nearly sixty percent of the total strain (29,31). These measurements were made in the range of five to twenty percent elongation, as at higher elongations (> 50%) the surface becomes too rumpled for any meaningful measurements to be made. It is inferred that the grain-boundary sliding contribution is the same even at elongations > 1000%.

Also in this $\dot{\varepsilon}$ - region, the initial equiaxed grains remain equiaxed after deformation, or grains which are elongated at the commencement become equiaxed after deformation, (19,21,23-26, 28,29,31,32,35,36,38-40,45-47,51,53,54,56-65,67-71). Furthermore grain coarsening has been observed in most of the superplastic alloys - Sn - 5 Bi (33), Pb eutectic and alloys (8,28,51), Al - Cu eutectic (21), Al - 17 Cu (72), Zn - Al eutectoid (31,38,49,60), Pb - 5 Cd (27), c.p. zinc (1), Ni - Fe - Cr (38), low alloy steels (23), Ti - 6 Al - 4V (24), the nickel based alloys (IN-100 and U700) (68,69), Tungsten-Rhemium (73), 60 - 40 Brass (71), Al - bronze (71), Cr - 24 Ru (61). However, a few investigators did not observe any coarsening after deformation - Zn - Al eutectoid (47) and the Al - Cu eutectic (70). Other typical observations are the rounding-off of the interphase grain boundaries, while the identical-phase boundaries remain sharp and straight (31,32,47,57,67,70,71,73,74), and the internal structure is virtually free from dislocations, that is, no cells or dislocation entanglements are seen, (23,31,38, 40,45,55,58,76). In the low region, grain boundary sliding is again observed, but as Lee (31) and Holt (54) have stated, the contribution to the total strain is less than thirty percent.

Evidence for diffusional processes operating in the intermediate and low $\dot{\varepsilon}$ - region, has been given by Backofen and his co-workers (26,28,36,77,78). Striation bands are observed on the surface at the tension stressed boundary and on polishing away the surface layer, denuded zones appear at these boundaries, the width of the striation and band being the same. These striations have been observed in the Mg - 6 Zn - 0.5 Zr, the Mg - 0.5 Zr (26,28,77,78) and the Pb - Sn eutectic alloys (28). A point of some difficulty is the absence of internal structural evidence of denuded zones to support the surface observations. However, Lee (31) has found that in the Mg - Al eutectic, striations only occur in the low $\dot{\varepsilon}$ - region, and the internal grain boundaries remain sharp and straight. Also the operation of diffusional processes has been shown by Nuttall (40) in the Zn - Al eutectoid. He observed a precipitate free zones at both the α - α and α - β boundaries, all around the grain, with the grains not exhibiting any directionality, thus suggesting that these observations are not directly associated with the tensile axis and that diffusional processes are not the predominant mode responsible for the superplastic behaviour. However, these observations were taken as supporting the deformation mechanism of grain-boundary sliding.

In the high $\dot{\varepsilon}$ - region negligible grain boundary sliding is observed (29,31). Grains become elongated, while the interphase boundaries remain straight and sharp; reference has been made to the occurrence of fine slip (11,29,31,74). Internal structural observation reveals extensive dislocation entanglement and sub-cell formation (31,38,45,58).

2.7 Methods to Produce a Fine-Grained Structure

As has been stated earlier, the necessary microstructural requirement for superplasticity is a very fine and stable grain-size in the range 0.5 - 5 μm. The smaller the grain size the higher the degree of superplasticity at the higher strain-rates. The minimum grain-size obtained in any alloy appears to be near to 0.5 μm.

It has been shown that, ideally, a eutectoid or eutectic is the easiest composition in which to produce a stable and fine-grained two-phase alloy. The eutectoid or eutectic lamellar structure formed on slow cooling can be broken up by working (rolling or extrusion) to give fine grains. This technique has been employed in several alloys, i.e. Pb - Sn, Cd - Zn, Al - Cu, Cu - Al, Zn - Al, Mg - Al, Bi - Sn and Ag - Cu - eutectic and eutectoid alloys. However, in the case of the Zn - Al eutectoid, fine grains can also be obtained by a decomposition process. (13,20,29,35,45-47,55,76). Though initially the process was thought to occur by a spinodal decomposition (20,40,55) process, very recently it has been shown by Jones and Thomas (79), to be of a non-continuous nature. In the eutectic or eutectoid alloys, the final structure produced consists of an equal-volume mixture of two dissimilar phases. The advantage of this type of structure is the resistance to grain growth and stability at the deformation temperature.

Fine grains can also be obtained in compositions away from the eutectoid and eutectic (29,35,40,54,56). However, a smaller volume fraction of the second phase is present and the grain growth rate or stability of the alloy is reduced. Typical examples are the Pb - Sn (28) and Zn - Al (40,54) system. A 'microduplex' structure composed of ferrite and austenite can be produced in stainless steels centered around 26% Cr and 6.5 Ni with carbon less than 0.3% (58,59). Similarly a two-phase Nickel alloy with 39 Cr - 8 Fe - 2 Ti - 1 Al % wt is produced containing bcc α - Cr phase (.8 μm) which stabilizes the fcc γ - matrix phase (3 μm) (38).

Virtually, single phase material has been produced by the dispersion of particles in the matrix (1,25,27,33,34). Alden (33,34) obtained fine-grained tin by the addition of 1 - 5 % Bi. It was stated that the fine particles of the second phase segregated to the grain boundaries and stabilized the grains. Similar observations have been made in commercial purity zinc (1), in which the impurity particles were seen to segregate to the grain-boundaries.

Powder-metallurgy techniques have been employed in high strength, nickel and titanium based super-alloys (68,69). These super-alloys are difficult to work and working produces inhomogeneties. However, by consolidating and extruding powder particles a homogeneous fine-grained structure is produced. Powder is made by atomization; thus in effect minute ingots consisting of fine grains are produced. The powder metallurgy technique has much to be recommended and it might be possible to obtain even finer grains than those obtained by the present method of rolling or extrusion of ingots.

Fine-grained Al - 17 % wt Cu foils have been produced by splat cooling (72) and Pb - Sn alloys have been produced by electro-plating alternate layers (85) and also by pack rolling (8).

Though it has been accepted that a fine-grained, stable structure is the necessary structural requirement, it has been shown that in a certain number of alloys with a fine grained structure and high m-value, very high elongation values are not obtained. Typical examples are the Cu - Al eutectic (57), 60/40 brass (71) Al - bronze (67,71). Particularly in the 60/40 brass and Al - brass interphase cavitation has been shown to be an important problem (67,71). In the Cu - Al eutectic, the Cu - Al_2 phase exhibits negligible ductility at 520° compared to the α-phase. Therefore the mobility of the interphase boundaries will depend upon the plastic property of the harder phase.

Therefore it would appear that another microstructural requirement for superplasticity is the appropriate plasticity and compatability of the two phases.

2.8 Mechanisms

It was realised by Avery and Backofen (8) that the initial proposal that Nabarro-Herring diffusional creep was the principal mode of deformation in the superplastic region, was not adequate to explain the multi-stage σ_f - $\dot{\varepsilon}$ behaviour. Very appropriately these authors put forward the concept of an additional process and expressed in analytically by

$$\dot{\varepsilon} = \frac{A'\sigma_f}{L^2} + B' \text{ Sin } \beta\sigma_f \qquad (4)$$

where A', B' and β' are constants at a given temperature.

The first term was associated with Nabarro-Herring diffusional creep, which predominates at the low-intermediate $\dot{\varepsilon}$ - region and the second term is attributed to the climb regulated movement of dislocations and predominates at the high - $\dot{\varepsilon}$ - region. In this way they accounted for the falling of the m-values at the high $\dot{\varepsilon}$ - end seen in the Pb-Sn eutectic. However, Packer and Sherby (47) showed that this equation was not in agreement with the experimental results in (8). Secondly, the m-value predicted by the Nabarro-Herring term was unity, whereas the observed m-value was 0.5. The third inconsistency associated with this mathematical model was that the expression did not predict the observed grain-size dependency. Packer and Sherby modified this expression to give a better fit of the results and put forward the expression:

$$\dot{\varepsilon} = \frac{A''\sigma_f^{\,2}}{L^3} + B''\sigma_f^{\,2} \text{ Sin h } \beta''\sigma_f^{\,2.5} \qquad (5)$$

The first term in the expression was taken to represent the mechanism of continuous recrystallization or grain boundary migration, and their microstructural observations in the Zn-Al eutectoid, that:- 1) the rounding of the interphase boundaries 2) the grains remaining equiaxed and 3) no significant change in grain size, were taken as conclusive evidence for continuous recrystallization and/or migration being the predominant mechanism of superplasticity. However, these authors did not seem to apply the expression to their results in the Zn-Al eutectoid and no reference was made as to how the first term is associated with the process of continuous recrystallization or grain-boundary migration.

Holt and Backofen (21) in their investigation of the Al-Cu eutectic, proposed that grain boundary sliding was the rate-controlling mechanism. This conclusion was based on the displacement of surface scratch markers during straining and the linear dependence of stress on grain size ($\sigma_f \alpha L$). The proposed expression was

$$\sigma_f = A''' (\dot{\varepsilon}) + B''' L \dot{\varepsilon}^{0.8} \quad (6)$$

The first term was stated to represent the Bingham yield-stress and the second term grain-boundary sliding.

It was further suggested that to preserve the compatability between grains an additional process in the form of grain-boundary diffusion could be occurring. However, for grain-boundary diffusion to occur the flow stress must be related to the grain-size as $\sigma_f \alpha L^3$, whereas the observed relation was $\sigma_f \alpha L$. At the high $\dot{\varepsilon}$ - region a dislocation strain hardening process was considered to be operative. At the low $\dot{\varepsilon}$ - end strain hardening was produced by the resistance to grain-boundary sliding, which was in turn governed by obstructions at grain-boundaries, forcing deformation in the regions bordering on the boundaries.

The first direct application of a dislocation creep/recovery model was made by Hayden et al (38,58) based on their observations in the Fe-Ni-Cr alloy. The authors observed the superplastic and high $\dot{\varepsilon}$ - region only; the superplastic $\dot{\varepsilon}$ - region showed an m-value of 0.5 over four orders of strain-rate. A dislocation creep mechanism for superplasticity involving the climb-controlled motion of edge dislocation based on Weertman's (80) creep model was then proposed, i.e.,

$$\dot{\varepsilon} = C^1 \frac{\sigma_f^2}{L^2} \exp^{-Q_v/kT} \quad (7)$$

where C^1 is a constant, Q_v the activation energy for volume diffusion, k the Boltzmann constant and T the temperature.

This model predicts deformation by dislocation emission at the grain-boundaries, their moving by glide and climb, and subsequently being annihilated by dislocations of opposite sign or more likely, in boundaries of favourable orientation. Volume diffusion was considered important rather than grain boundary diffusion. At the high $\dot{\varepsilon}$ - region the model predicted dislocation entanglement and cell formation.

Ball and Hutchinson (45) went a step further, and used the concept of dislocation pile-up/climb at grain-boundaries; this could be the mechanism for grain-boundary sliding. The kinetics of flow were explained as the relative motion of groups of grains which were resisted by unfavourably positioned grains. Dislocations were generated in such grains, and these pile-up at opposite boundaries until the back stress produced prevented further sliding. The stress concentration at the head of the pile-up caused accelerated diffusion and dislocation escaped by climb into and along the grain-boundaries. The replacement of these dislocations made possible further grain-boundary sliding.

An expression was developed, following Friedel (81)

$$\dot{\varepsilon} = C'' \frac{\sigma_f^2}{L^2} \exp^{-Q_{GB}/kT} \quad (8)$$

where C" is a constant and Q_{GB} is the activation energy for grain-boundary diffusion.

A stress value calculated using this equation was an order of magnitude higher than that measured, but even so this was considered support for the proposed pile-up model.

Very similar models have been proposed by Alden (27,64), Lee (31) and Naziri and Pearce (11), that is, grain-boundary sliding accompanied by a dislocation climb/recovery process.

Alden (64) states that superplasticity occurs when the sub-grain size equals the grain-size, then dislocations which are produced can move across the grains to interact with the opposite grain-boundary. Depending on this interaction, the rate of grain-boundary sliding will be controlled by different mechanisms -

1) Pile-up against grain-boundaries, 2) climb along grain-boundaries without pile-ups, and finally, 3) grain-boundaries as perfect sinks - sliding controlled by diffusion.

The author favoured the second interaction mechanism and this resulted in the development of an expression similar to those of Hayden et al and Ball and Hutchinson. The expression was found to predict the right order of magnitude of strain-rate for a tin alloy.

The importance of incorporating a dislocation mechanism in any theory was suggested by Fike and Rack (76), after the direct observation of superplasticity in a dynamic experiment done by straining a Zn-Al eutectoid thin foil inside an electron microscope. Observations revealed the existence of extensive dislocation activity accompanied by grain-boundary sliding. Dislocations appeared to be generated and annihilated at the grain-boundaries, without any entanglements occurring. However, the relevance of these observations is criticized on the grounds that the foil is too thin to truly represent the bulk behaviour. Lee and Underwood (154) have strained a similar alloy at 250°C to 450% elongation and then immediately water quenched the specimen in order to freeze the actual structure. Transmission electron microscopy revealed well defined sub-boundaries and sub-grains in the Al-rich (α) phase. Based on these observations the authors proposed the operation of 'dynamic recovery' a similar process which has been stated to occur during the hot-working of normal metals (127).

A dislocation model based solely on the motion of screw dislocations within grains has been suggested by Chaudhari (46). This model has not received any support because explanation of grain-boundary sliding and grains remaining equiaxed is not accommodated in the theory.

A diffusional mechanism incorporating grain boundary sliding has been put forward by the school of Backofen (26,28,30, 36,37), from observations made in the Mg ZK 60 and Pb - Sn alloys, and by Gifkins (82) in the Pb - Th alloy. The Backofen et al theory is based on a proposal by Lifshitz (83) who has shown that diffusional creep must occur with grain-boundary sliding. Even if diffusional creep is considered the only source of deformation grain-boundary sliding is still inevitable. The essence of this argument is illustrated schematically in Figure 8.

The mechanism incorporates non-Newtonian grain-boundary sliding and diffusional (Newtonian) creep acting first in parallel and then in series with the non-Newtonian slip creep. Grain-boundary sliding and diffusional creep is responsible for the high m-value at the superplastic $\dot{\varepsilon}$-region, while slip creep is operative at the high $\dot{\varepsilon}$-region. No change in m-value should occur at the low $\dot{\varepsilon}$-region when the Bingham yield stress due to grain-boundary sliding resistance is taken into account. However, as a diffusional creep model cannot by itself explain the σ_f - $\dot{\varepsilon}$ relationship observed for most of the superplastic materials, the assignment of the Bingham stress is unsupported. A further difficulty is that the nature of the initial flow stress cannot be unambiguously identified (66).

It would therefore appear that the models so far proposed cannot account for the many differences observed in the various alloys. However, it can be concluded that models which have received the most support are based on one or other of the following three basic processes: diffusional creep, grain boundary sliding and dislocation creep/dynamic recovery.

Recently, Hayden (84) has analysed the likely contribution of these three processes under various conditions of stress and temperature. On the bases of the analysis, it is stated that the observed strain-rate during superplastic deformation should be the sum of the separate strain-rates of diffusional creep ($\dot{\gamma}$ D), grain-boundary sliding ($\dot{\gamma}$ GBS) and dislocation creep ($\dot{\gamma}$ G). In general at low stresses diffusional creep should be rate-controlling. At temperatures between 0.4 - 0.65 Tm, grain-boundary diffusion is the dominant mechanism while at higher temperatures > 0.7 Tm, volume diffusion paths will become effective. At the intermediate stress level, grain boundary sliding is the major deformation mode; however, this sliding is governed by the dislocation creep rate within the grains. At 0.4 - 0.65 Tm, the dislocation creep rate is controlled by dislocation pipe diffusion, while at the higher temperature > .7 Tm volume diffusion will become effective.

At higher stress levels the superplastic effect will diminish due to the work-hardening processes of dislocation cell formation, entanglement and pile-ups.

A combined relationship to cater for the various conditions was presented:

$$\dot{\gamma}_T = \frac{\beta'' D_{gb} b^4 \sigma_f}{L^3 kT} + \frac{K_1}{L} \cdot \frac{24\pi(1-\nu) D_p b^3 \sigma_f^2}{L^2 \mu kT}$$

$$\text{(Temp } 0.4 - 0.65 \text{ Tm)} \qquad + \qquad \frac{24\pi(1-\nu) D_p b^3 \sigma_f^2}{L^2 \mu kT} \qquad (9)$$

or

$$\dot{\gamma}_T = \dot{\gamma}_D + \dot{\gamma}_{GBS} + \dot{\gamma}_G$$

The above equation illustrates that the sum of the three strain-rates ($\dot{\gamma}_D + \dot{\gamma}_{GBS} + \gamma_G$) contributes toward the actual strain-rate under the various conditions. The above equation can be further modified if it is considered that maximum grain-boundary sliding is taking place. Ke's (86,87) prediction of the absence of any grain constraint and his treatment of grain-boundaries as viscous material coupled with Friedel's (81) relationship for the velocity of two grains sliding passed each other, the grain boundary sliding strain-rate was calculated to be $\frac{D_{gb} \sigma_f b^2}{L k T}$ Thus equation (9) is altered for maximum grain-boundary sliding to occur ($\dot{\gamma}_{GBS} \rightarrow \max^m$).

$$\dot{\gamma}_T = \frac{\beta'' D_{gb} b^4 \sigma_f}{L^3 k T} + \frac{D_{gb} \sigma_f b^2}{L k T} + \frac{24\pi(1-\nu) D_p b^3 \sigma_f^2}{L^2 \mu k T} \qquad (10)$$

However, at higher temperatures (> 0.7 Tm), volume diffusion becomes effective and the contribution from dislocation creep-rate ($\dot{\gamma}_G$) becomes:

$$\frac{6\pi(1-\nu) D_v b^2 \sigma_f^2}{L \mu \ln(\frac{L}{b}) k T}$$

Therefore for higher temperatures, (9) and (10) becomes:-

$$\dot{\gamma}_T = \frac{\alpha D_v b^3 \sigma_f}{L^2 k T} + \frac{K_1}{L} \cdot \frac{6 \pi (1-\nu) D_v b^2 \sigma_f^2}{L \mu k T} + \frac{6 \pi (1-\nu) D_v b^2 \sigma_f^2}{L \mu \ln(\frac{L}{b}) k T} \quad (11)$$

and

$(\dot{\gamma}_{GBS} \rightarrow \max)$

$$\dot{\gamma}_T = \frac{\alpha D_v b^3 \sigma_f}{L^2 k T} + \frac{D_{gb} \sigma_f b^2}{L k T} + \frac{6 \pi (1-\nu) D_v b^2 \sigma_f^2}{L \mu \ln(\frac{L}{b}) k T} \quad (12)$$

Equation (11) was utilized by Hayden to predict the multistage $\sigma_f - \dot{\epsilon}$ in the Ni - Fe - Cr alloy and excellent correlation was obtained with the experimental values. Strain-rates, for a stress value of 1000 p.s.i., were calculated for a range of superplastic alloys, Pb - Sn, Sn - Bi, Al - Cu and Ti - Al - V (84). The calculated values were found to be of the same order as the experimentally obtained values.

In conclusion it can be said that the analytical solution of Hayden does take into account the various differences in experimental observations and appears to be the right approach towards a final solution.

CHAPTER 3

3.0 Ductility in Fine Grained Zn-based Alloys

High ductility or superplasticity has been obtained in fine-grained zinc-based alloys having either a virtually single-phase or a two-phase structure. Most of the previous work has been concerned with the ductility effect in the single-phase alloys, though recently the two-phase alloys of the zinc-aluminium system has received a great deal of attention due to their very high degree of superplastic behaviour.

The following sections on the single and two-phase alloys summarises the background of these two basic types of alloys.

3.1 'Single-Phase' Fine-Grained Alloys

Rosenhain et al (1920) (88), while studying the constitution and mechanical properties of certain zinc alloys, observed the remarkable pitch-like behaviour at room temperature of certain alloys. He observed that additions of 1% copper and cold rolling produced sheets which behaved differently from the ordinary crystalline materials. He explained this observation by stating that the alloy became amorphous on rolling, and due to the low melting-point of the alloy, the amorphous material existed in a state of comparatively low viscosity, and could therefore flow readily under conditions of slow strain-rates. He further noted that when the amorphous material recrystallised, the alloy reverted back to the crystalline state.

Chadwick (1933) (89), investigated the room temperature rolling and creep behaviour of electrolytic zinc and zinc alloys with dilute additions of Cd, Hg, Fe and Mg. He observed that the alloys softened on rolling and the hardness decreased with increasing rolling reduction (up to 80%). However, soon after rolling, all the alloys were found to exhibit self annealing and grain growth at room temperature, with the exception of the Fe and Mg alloys. These alloys showed a high creep rate, and the creep rates for the .25% Cd and .025% Fe alloys were 7 and 5 times greater than for the .01% Mg alloy respectively. No elongation values were quoted though later in a discussion (90), the author stated that he had obtained elongations in the region of 400%, no reference being made to any specific alloy. Microstructural observations of the rolled products showed that increased reduction in rolling broke up the grains, till finally, fine grains were obtained.

The explanation for the increased creep rate and elongation was that the rolled sheet consisted of groups of crystallites in echelon formation embedded in a mass of amorphous material and crystal fragments, the amorphous material being largely contained in the form

of thin films bounded by overlapping basal planes. Elongation or creep at low loads took place by flow in the amorphous phase, the crystallites moving relative to each other along bands containing amorphous phase. It was also suggested that self-annealing with subsequent grain-growth prevented in certain alloys was due to the stabilization of the amorphous phase, from where recrystallization was supposed to be nucleated.

Following these earlier observations, zinc alloys were developed but primarily as die casting alloys (i.e. Cu/Al/Ti/Zn). After the discovery by Irmann and Von Zeerleder (91,92) in 1949, of the powder metallurgy technique of producing sintered aluminium powder and at its remarkable creep resistance at elevated temperatures, it was not surprising that the zinc researchers tried a similar method in order to improve the creep resistance of zinc.

Lenel (1961) reported the creep behaviour of zinc alloys produced by the powder metallurgy method. A Zn/ZnO powder product produced by consolidating and extruding atomized powder, surprisingly, showed very low creep resistance at room temperature. On the other hand a Zn/.95 Zn/.13 Ti alloy similarly produced showed very much improved creep properties. No explanation could be given for this difference in behaviour, though the fast creep rate of the Zn/ZnO alloy was attributed to the generation of dislocations at the grain-boundaries and grain-boundary creep. A point to note was that the Zn/ZnO alloy was fine grained (5 μm).

A similar investigation of dispersion-strengthened Zn/ZnO alloy also produced by powder metallurgy was undertaken by Tromans and Lund (1966). These authors observed that there was a critical grain-size below which the Hall-Petch relationship did not hold, and also that below this grain-size the creep rate increased with decrease in grain-size. The minimum grain-size material produced was in the region of 1-3 μm and an elongation of about 100% could be obtained at the strain-rate of .002 min^{-1}. Transmission electron microscopy of thin foils, showed the grains to be separated by high-angle boundaries (> 20°) and the ZnO particles tended to be located at the grain-boundaries. This marked increase in flow behaviour was attributed to a complex combination of grain-boundary sliding/migration.

Further attempts to improve the creep resistance by dispersion strengthening using a range of insoluble particles (alumina, graphite, tungsten etc) was undertaken by McCarthy (95). Creep tests showed the improved properties at elevated temperatures; however, surprisingly enough the zinc/tungsten composite was shown to be weaker than even pure zinc. Tensile tests at room temperature showed the composite

to have a strain-rate sensitivity of about 0.2 and an elongation of 100% and reduction in area of 93% could be obtained. This extended plasticity in the Zn-Tungsten was explained by a mechanism based on the strain induced excess vacancies (created by duplex slip), stress distribution effects including relative thermal expansion characteristics and the fineness of the observed slip bands.

It thus appeared that conflicting properties could be obtained using a dispersion-strengthening method. However, it was quite clear that certain types of particles could produce a strengthening effect. This problem was resolved by some excellent collective work of Tromans, Riseborough, Williams and Lund (96-98). The authors, using intermetallic compounds of nickel, chromium and titanium obtained a range of alloys of different grain sizes. Transmission electron microscopy of thin foils revealed that the alloys could be divided into two groups. In the first group the grain-boundaries of the alloys were relatively free from intermetallic particles, while in the second group a fine dispersion of intermetallic particles were concentrated at the grain-boundaries. Testing at room temperature showed the alloys having the grain-boundaries free of intermetallic particles to be very strain-rate sensitive, whereas the alloys with the fine particles at the grain-boundaries were relatively much stronger and less strain-rate sensitive. The key to the strengthening and decrease in strain-rate sensitivity effect was the immobilization of the grains at the boundaries by the particles.

It was further shown that it was necessary for the intermetallic particles to be extremely fine to be effective. Coarsening of the particles markedly reduced the strengthening effect. The only method by which a fine dispersion of particles could be obtained was shown to be by consolidating atomized powder and then extruding.

Naziri and Pearce (1) obtained fine and stable grains of the order of 2 μm in c.p. zinc by room temperature rolling to 90% reduction. This alloy exhibited a strain-rate sensitivity of 0.2 and elongations of 200% were obtained at the crosshead velocity of .002 inch/min. The impurities (0.8% Pb, .05%Cd and .02% Fe) were found to stabilize the grains by segregation of precipitated phases to the grain-boundaries and the prevention of recrystallization and grain-growth. Microstructural evidence showed that grain-boundary sliding was occurring, while activation energy measurements coupled with the absence of any dislocations in the grains suggested that a form of dynamic recovery was the operating mechanism.

In summary it can be said the fine and stable grains at room temperature can be produced in virtually single phase zinc both from a cast ingot and rolling and also from powder consolidating and extrusion methods. A range of particles were tried but the maximum strain-rate sensitivity obtained appeared to be in the only about 0.2 at virtually creep strain-rates.

There appears to be two possibilities for improving the strain-rate sensitivity. The first is to use very fine second phase particles which stabilize the grains and prevent grain-growth at room temperature but do not reduce the strain rate sensitivity. The second possibility would be to produce a stable grain size in the region of 0.5 μm, for this would increase the strain-rate sensitivity markedly, and move it to higher strain-rates.

At the time of this investigation Cook et al (99) reported having obtained a strain-rate sensitivity of 0.8, at room temperature, in a Zn-0.2Al alloy. The alloy was extruded to give a grain-size of 3.5 μm and an elongation of about 450% was obtained at the strain-rate of 10^{-3} min^{-1}. No structural aspects of the deformation behaviour was reported.

3.2 'Two-Phase' Fine-Grained Alloys

The other method of achieving very high ductility in zinc-based alloys is to produce a 50/50 two-phase, fine-grained structure, with a high grain-stability temperature and the consequent increase in the strain-rate sensitivity. In the main, two-phase zinc/aluminium alloys have been observed to exhibit superplastic properties, particularly those of near the eutectoid and eutectic composition.

Bochvar and Sviderskain (1945)discovered a method of producing fine grains in the near-eutectoid composition by quenching from above the eutectoid temperature 275°C (Figure 9) followed by decomposition at room temperature. This produced fine (~ 1 μm) equiaxed, aluminium (α) rich and zinc (β) rich phases in equal proportions. Furthermore, these authors showed that the alloy exhibited a high degree of superplasticity (450% elongation) just below the invariant temperature (275°C). However, it was the systematic study of Presnyakov and Chernyakova (15,16) which illustrated the variation in the degree of superplasticity with composition and temperature (Figure 10). It was also shown that if the alloy was cooled slowly through the eutectoid temperature, then a lamellar structure of α and β phases were produced and the material did not exhibit superplastic behaviour. These authors postulated that in the quenched-decomposed condition the alloy was in a metastable condition, and on heating superplasticity occurred while the alloy reverted to an equilibrium state by the

weakening of the interatomic bonds during transformation. Soon afterwards it was also shown by Presnyakov et al that the elongations were directly related to the strain-rate and the maximum elongation was obtained at a critical strain-rate.

The superplastic behaviour of the Zn-Al eutectoid was thoroughly investigated by Backofen et al (20) who established that the strain-rate sensitivity at 250°C was high and increased with strain-rate within the strain-rate range covered. An m-value of 0.6 was obtained at 250°C and elongations of greater than 1000% were obtained at the crosshead speed of 0.5 inch/min.

Following these investigations, similar investigation of the superplastic behaviour of the Zn-Al eutectoid was undertaken by several authors (Packer and Sherby (47), Chaudhari (46), Holt (29), Kossowsky and Bechtold (56), Alden and Schalder (35), Ball and Hutchinson (45), Nuttall and Nicholson (44,56), Johnson, Packer, Anderson and Sherby (62) and Blenkinsop and Gidley (67)). It was established that the quench-decomposition method was not the only way in which to produce fine grains but that the lamellar structure obtained by slow cooling from above the invariant temperature can be broken up by working (extrusion or rolling) at 250°C. It appeared that whatever the route followed to produce the fine grains, the minimum grain-size obtained was in the region of 0.5 μm. Holt (29) has shown that for the 0.5 μm material the peak m-value of 0.45 was obtained at the relatively fast strain-rate of 3 min^{-1} while for the 1.8 μm grain-sized material, the peak in m-value increases to 0.5 and moves to the lower strain-rate of 6 x 10^{-3} min. It was shown that elongations of greater than 1000% could be achieved at the crosshead velocity 10 inch/min. Furthermore, the superplastic strain-rate range ($m \simeq 0.5$) covers about 3 to 4 orders of magnitude (10^{-2} to 10^{1} min^{-1}). A notable feature of the effect of temperature on the stress is the marked decrease from 22,000 lb/in^2 to a value as low as 500 lb/in^2 at 250°C, the strain-rate being .05 min^{-1} (35).

Most of these earlier investigations were concentrated on the eutectoid alloy, but compositions away from the eutectoid have since been studied; the eutectic (95 wt % Zn - 5 wt % Al) (60), 82 wt % Zn - 18 wt % Al (35), 60 wt % Zn - 40 % wt Al (54) and 70 wt % Zn - 30 wt % Al (40). Previous work had suggested that the high level of ductility falls sharply on changing the composition (16).

Alden et al (35 examined the properties of the quenched 82 % wt Zn and 64 % wt Zn alloys at 250°C. For the high zinc content alloy the m-value (.53) was similar to that obtained for a eutectoid alloy at the strain-rate of 0.5 min^{-1}, while for the lower zinc content alloy, the m-value decreased with increasing

strain-rate. Holt (54) in his investigation of the 60 % wt. Zn alloy observed a maximum m-value of 0.2 for the as-quenched alloy. However, on extruding the quenched product a substantial increase in m-value (0.48 to .37) was obtained in the same strain-rate range. Microstructural observation of the quenched alloy showed large aluminium rich grains, which on extruding were observed to have recrystallized, and this was suggested as the reason for the increase in m-value. No mention was made as to the break-up of the grains to finer grains on extrusion which would have also increased the m-value.

No marked decline in superplasticity is observed in the 70 wt % Zn - 30 wt % Al alloy. Nuttall (40) has shown that at high strain-rates m-values of ~ 0.5 are obtained, similar to those obtained in the eutectoid. However, at the lower strain-rate end the m-value was found to decrease.

In the case of the eutectic composition, mechanical working at about 300°C has been observed to break-up the lamellar structure producing a two-phase structure. The grain-size being fine enough to exhibit an m-value of 0.7 (> 1000% elongation) at the temperature of greater than 285°C (~ 0.85 Tm). Similar structural stability is exhibited in the eutectic and eutectoid alloys and the behaviour is not greatly influenced by holding time before deformation.

Ternary addition of 0.5 wt % magnesium have been made in the eutectoid alloy (35); the magnesium has the effect of slowing the eutectoid decomposition reaction. Alden et al (35) observed that the m-value decreased from ~ 0.5 to 0.33 at 250°C and an elongation of only 200% was obtained at the strain-rate of 1 min^{-1}.

Recently a eutectoid-based alloy called 'ZAM', patent specification quotes 'zinc from 70-82 wt %, magnesium .05 - .2 wt %, up to 2.0 wt % copper and balance aluminium, has been developed by Professors Belk and Smith of the Royal Military College of Science, Shrivenham. It was stated that the material exhibited the normal high degree of superplasticity at 250°C, while the room temperature strength of 50 tons/in^2 can be obtained by a simple heat treatment, possibly by producing a precipitation hardening effect (100,101).

To summarize then. There is no difficulty in obtaining very high ductility in the two-phase Zn-Al alloys, particularly those of eutectoid and eutectic compositions and also a high degree of grain-size stability is maintained at the superplastic temperature.

CHAPTER 4

4.000 Investigation of the Zn - 0.4 % wt Al Alloy

4.100 Experimental

4.101 Material

The zinc - 0.4 wt % aluminium was made from pure materials and cast into steel moulds; the dimensions of the ingot were approximately 12 x 5 x .75 inches. The casting was supplied by the Imperial Smelting Corporation, Avonmouth. A spectrographic analysis of the alloy showed the following impurities:

Table 1

Cd	Cu	Pb	Fe	Mg	Sn
.0004	.0003	.002	.002	.001	.001 wt %

The top and bottom one inch of the slab were cut away in order to eliminate the high porosity regions. The remaining surface was scarfed to a depth of 0.050 inches and then the slab was homogenized at 325-350°C for several hours.

The material was then rolled in a Stanat-Mann two-high mill. The rolls were 5½ inches diameter and 6 inches wide. The rolling speed used was 30 feet per minute, maintained constant throughout the rolling operation. The slab was hot rolled at 300°C to 40-60 percent reduction (102). Initially, it was found that severe cracking occurred if the slab temperature fell below 200°C, so this was overcome by reheating after each pass and not giving too high reductions per pass. The slab was then room-temperature rolled to 90 percent reduction (.040" thick). Several passes at low reduction were necessary as again high reductions could cause severe edge-cracking. During the final reductions at room temperature, the sheet was kept cool by dipping it in iced water between passes.

Immediately after the last pass the sheet was cut to the appropriate sizes and stored in a large flask containing dry ice.

4.102 Tensile Tests

The various mechanical property measurements were determined on an 10,000 lbs Instron testing machine. The constant crosshead velocity available covered the range .002 to 20 inch per minute. The load and the amount of crosshead movement were recorded on a chart, the chart speed covering the range .2 to 50 inch per minute.

Two dimensions of tensile specimens were used.

Initially, 2.5 inch gauge length and 0.5 inch wide specimens were used, but later on 1.25 inch gauge length specimens were used, to conserve material. The specimens were machined in a 'Tensilkut' machine; six specimens could be machined simultaneously.

4.103 Stress (σ) - Strain (ε) relationships

To obtain true stress-true strain curves, the load-extension curve was recorded for the relevant crosshead velocity and converted to true stress and true strain using the relationship:

$$\sigma = \frac{P}{A_o} \quad (1 + \frac{\Delta l}{l_o})$$

and

$$\varepsilon = \ln \quad (1 + \frac{\Delta l}{l_o})$$

where P is the load, A_o the original cross-section area, Δl the extension and l_o the gauge length.

4.104 Flow Stress (σ_f), Strain-Rate Sensitivity (m) and Strain-Rate ($\dot{\varepsilon}$) Relationships.

The true flow stress-true strain rate and the strain-rate sensitivity of the flow stress - true strain-rate relationships were obtained by the step-technique adopted by Backofen et al (20). The procedure involved was to record the load-extension curve at an appropriate chart speed and crosshead velocity. When the maximum steady state load was reached the speed was changed to the next increment in crosshead velocity and the same procedure followed as for the first curve. A typical diagram of the load speed change is shown in Figure 11. Extrapolation of the lower curve (v_2), has been carried out to establish a common strain for both speeds. The strain-rate sensitivity can then be calculated from the expression:

$$m = \log \frac{P_A/P_B}{\text{Log}\ v_1/v_2}$$

Specimens were subjected to nine velocity increases covering the range of .01 to 5 inch/min crosshead velocities. Under these conditions m was identified with the lower velocity (v_2). It was found that by choosing the appropriate chart speeds, it was possible to record accurately the steady state loads.

For crosshead velocities greater than 2 inch per minute, error could be introduced due to the delay in operating the machine. Together with the m - $\dot{\varepsilon}$ relationship, the σ_f - $\dot{\varepsilon}$ curves were also obtained from the load-extension curves. It was observed that the test could be completed within 25-30 percent elongation.

4.105 Strain-Ratio (r)

The strain-ratio was determined from the length and width measurements made on a 10 mm square grid, initially scribed on the flat surface of the specimen gauge length. The tensile specimen was removed from the testing machine after various elongations (20 - 400%) and the grids remeasured with a travelling microscope.

The strain-ratio was calculated from the expression:

$$\underline{r} = \frac{\ln\left(W_o/W_i\right)}{\ln\left(W_i l_i/W_o l_o\right)}$$

where o and i refer to the original and current measurements.

4.106 Texture Determination

Specimens, approximately 0.9 in square were cut from strained tensile specimens.

The sheet specimens were then chemically thinned and polished in nitric acid in order to remove any surface effects which might possibly obscure the results.

The texture were evaluated by the standard diffractometer reflection technique on a Phillip's model diffraction machine equipped with a Siemens texture goniometer. The texture data was obtained from a Geiger counter and suitable electronics so that the diffracted intensity was displayed on a strip chart recording. The goniometer was set at the Bragg angle corresponding to the (0001) and ($0\bar{1}01$) reflections.

The recorded intensities of the diffracted beam were utilized to plot the pole figures. The radiation used was Cu K_α, nickel filtered, at a tube setting of 30 KV, 20 mA.

4.107 X-ray Back-Reflection

A few specimens 0.5" square were examined by this method in order to detect grain coarsening effects. The specimens were chemically thinned and polished in nitric acid, prior to examination, to record the near to surface and interior effects. The radiation used was Cu Kα, nickel filtered, at a tube setting of 30 KV, 20 mA. The exposure time being 45 minutes.

4.108 Optical Microscopy

Mechanical polishing is a source of difficulty in the metallography of zinc. Unless extreme care is taken, mechanical polishing for optical microscopy results in deformation that can obscure the true surface structure. Therefore, a method was adopted whereby the specimen was neither mounted or mechanically polished. The specimen was dipped in concentrated nitric acid which resulted in a vigorous reaction and immediately removed and washed in water, followed by washing in alcohol. The surface was remarkably well-polished, though slight pitting and delineation of the surface occurred. The specimen was then etched by dipping in concentrated hydrochloric acid and immediately removed and rinsed in water. An alternative method due to Ramsey (103), slightly modified, was also used. A large drop of water was placed on the surface and then a drop of fuming nitric acid dropped to make contact at the edge of the pool of water. The subsequent reaction was immediately quenched under the tap and the area opposite to the edge of the acid region was found suitably etched for examination under the microscope.

4.109 Preparation of Thin Foils for Transmission Electron Microscopy

A wide variety of methods are available for the preparation of thin foils (104-107), but the necessary requirement in this investigation was a technique which was quick, did not involve any mechanical cutting and thinning, and which at the same time had a high percentage of success. The method found to meet these requirements has previously been tried successfully to make thin foils in steels (108,109); this involved the chemical thinning of the specimen, followed by electropolishing.

A .040 inch and less thick specimen pieces, cut from the gauge length of the tensile specimen was initially thinned in concentrated nitric acid to a thickness of .002 to .006 inch. Further thinning was accomplished by having the nitric acid in a glass beaker, inside which was a smaller polythene beaker, drilled with small holes to allow quick drainage. The specimen was placed

in the polythene beaker and dipped in the acid; thinning was rapid and by repeated removal of the beaker and rinsing in water, the progress of thinning could be measured and controlled. It was found that where a region collapsed or perforation appeared, the adjoining area was very thin (~ .0005 inch). In this second stage a 50-70% nitric acid in water was used so that the thinning rate could be kept under control and vigorous evolution of gas and possibly warming of the specimen was prevented. The thinned specimen was then held in tweezers so that the perforated edge could be immersed in the electropolishing solution.

Electropolishing was done at room temperature in a solution of 67.5% ethanol in orthophosphoric acid (104,107). An ordinary voltage supplier was used as it was observed that a stabilized voltage supplier was not necessary. A voltage in the range 8-10 volts was found to be ideal, and gave excellent polishing for the average 0.5" to 0.25" specimen area. Figure 12 shows the milliamps versus voltage plot for the above conditions. A wide polishing plateau exists, ranges from 6 to 10 volts. Figure 13 shows typical chemically thinned and polished specimens. The polished specimens were washed in ethanol and dried using a blower. Thin regions near the perforated edge were cut out using a rounded-edge scapel. The cut piece was then 'fished' out using the fibres of the torn edge of a filter paper and mounted between two 3.05 mm diameter, 50 mesh grids, and examined in a Siemens Elmiskop I Electron Microscope.

4.110 Specimen Preparation for Examination in the Scanning Electron Microscope

In order to observe surface effects on deformation, it was necessary to polish the flat surface of the gauge length of a tensile specimen before straining. The tensile specimen was chemically polished in concentrated nitric acid and examined after straining in a Cambridge Instruments Stereoscan Mk.I.

Fracture surfaces were also examined in the Stereoscan, where no initial preparation of the specimen was necessary.

4.111 Biaxial Tests

Hydraulic bulging was carried out on gridded blanks, on a hand-operated machine producing 4.5 inch diameter bulges. The grid consisted of 0.1 inch diameter circles in 0.25 inch squares, and was etched on the material using 'Electromark' gridding equipment.

Punch stretching tests using a 2-inch diameter hemispherical punch with the blank securely clamped around its periphery were carried out on a Hille Engineering Press. Various punch speeds and lubrication conditions were used. Polar grids of suitable dimension were rubber-stamped on the blank.

4.200 Results

4.201 Material

In order to adopt a rolling sequence which would produce a sheet exhibiting the greatest strain-rate sensitivity, some variations were tried. It was decided to hot roll ingots to 40, 50 and 60% reduction, followed by cold rolling at room temperature to give a final thickness of .040 inch. Figure 14 shows the $m - \dot{\varepsilon}$ curves for three differently processed sheets. The sheet which received the greater reduction at room temperature is observed to exhibit the higher strain-rate sensitivity. Therefore, the procedure adopted in this investigation to produce sheets was to hot roll the ingot to 40% reduction, followed by 90% reduction of the hot rolled product at room temperature.

Figure 15 shows the microstructure of the ingot prior to hot rolling. Typical large, recrystallized grains are evident. On hot rolling to 40% reduction, smaller heavily deformed and directional grains are obtained (Figure 16). Slip and twinning are evident and at higher magnification substructure formation is also observed (Figure 17). On subsequent room temperature rolling of the hot rolled product, severe fragmentation of the grains is observed with increasing reduction (Figure 18). Up to 50% reduction extensive slip and twinning is evident. At 75% reduction directionality still exists, with grains becoming too fine to resolve anything but the grain-boundaries. At 90% reduction a consistent fine grained structure is obtained, with no indication of the directionality in the grains, though the rolling direction is indicated by the presence of stringers. Examination of the internal structure showed the grains to be equiaxed and containing a high density of entangled dislocations (Figure 19). Also there is evidence of heavy precipitation and dislocation loop formation. The grain size obtained was in the region of 0.6 μm (4.209).

Hardness measurements were made at increasing percentage reduction during rolling at room temperature. The measurements were done immediately after each pass, within a few minutes. As the zinc sheet was strain-rate sensitive, any variation in indenter time would affect the readings; however, the indenter time was found to be constant. Figure 20a shows the effect of percentage reduction in hardness. The hardness increases to a maximum value of 70 VPN at about 12% reduction, and with further increase in reduction falls rapidly, and finally after 90% reduction a value of 30 VPN is obtained.

4.202 Grain-Growth Effects

Though the rolling procedure was very successful in producing a material with a grain-size of about 0.6 μm, it was soon observed that leaving the rolled sheet at room temperature induced grain-growth. It was discovered that if the sheet was strained

immediately after rolling, repeated elongations of 500 - 550% could be obtained at the crosshead velocity of 0.1 in/min. However, if the sheet was strained after leaving at room temperature for 24 hours, the elongation fell to about 100%. Microstructural examination of a specimen strained after leaving at room temperature for 3 hours, revealed the reason, as shown in Figure 21. Grain-growth has taken place and certain grains have grown at a faster rate. The large grains have deformed by slip, while grain movement of the smaller grains is indicated by the observation of delineated grains and grain-boundaries.

Sheets were left at room temperature for increasing lengths of time and the microstructure examined (Figure 22). Grain-growth occurred quite rapidly at room temperature and a final stable grain-size of 3 - 5 μm was obtained after about eight hours. Hardness measurements after ageing at room temperature showed that the hardness increased from 30 VPN immediately after rolling to the final constant value of 43.6 VPN after about 7 hours (Figure 20b).

However, it was still not clear how an elongation of 500% was obtained if rapid grain-growth was occurring. At the crosshead velocity of 0.1 in/min it will take 100 minutes to elongate a 2.5 in. gauge-length tensile specimen by 500% and in this time substantial grain-growth should have taken place.

However, microstructural examination of a specimen strained to 200% elongation and aged at room temperature for 8 hours, exhibited a surprising structure, for there was now no sign of grain-growth having taken place.

4.203 Grain-Growth Inhibition by Straining

In order to observe the effect of straining on grain-growth, specimens were strained to increasing percent elongation to various points on a load-extension diagram (Figure 23), followed by annealing at room temperature.

Microstructural observation shows that the specimen strained to 25% elongation, well past the peak load, does not show any signs of grain-growth even after 28 hours at room temperature (Figure 24d). However, specimens strained to lesser amounts exhibited grain-growth, though the greater the strain the slower is the subsequent rate of grain-growth at room temperature (Figure 24 a-c).

Also, the 0.2% proof stress was determined from specimens strained to increasing elongations up to 25% and left at room temperature for various intervals of time. Figure 25 shows the effect of strain and grain growth displayed by the proof stress. No increase in the proof stress occurs for the specimen strained to 25%, indicating that no grain-growth has taken place. However, in the unstrained material extensive grain-growth has taken place as shown by the rise in proof stress from 8.8 lb/in^2 to 15.1 lb/in^2 in 10 hours. Further increase in time shows that the stress remains constant at 15.1 lb/in, which suggests that the grains have reached their stable room temperature size. Straining a material to peak load or about 3.4% elongation shows that slight grain-growth has occurred, as indicated by the 0.2% proof stress value lying between the unstrained and strained 25% specimens.

Also strain-rate sensitivity measurements were made by the step technique on specimens strained and left at room temperature to various times. Figure 26 shows the effect of time on the m - $\dot{\varepsilon}$ curves. The m - $\dot{\varepsilon}$ curve for the 25% strained material has not altered even after 24 hours. However, for the specimen strained to peak load (3.4%) and left for 24 hours, the m-value decreases and the peak m-value region of the curve moves to lower strain-rates. For the unstrained specimen, left for 24 hours, the decrease in m-value is quite considerable, that is, from 0.4 to 0.2. The peak m-value (0.2) being obtained at the lower strain-rate end.

Furthermore, it was obvious that in the specimen strained to 25% elongation, the gauge length would have the starting fine grains, while the grips ends, which are not strained, should go through the normal process of grain-growth. This effect was observed by taking X-ray back-reflection photographs from the gauge length and the grip ends. These are shown in Figure 27. The strained gauge-length exhibits a continuous ring pattern, while the coarsening in the grip ends is indicated by the breaking of the continuous ring pattern to a series of spots.

Based on the above observations, the following procedure was rigidly adhered to soon after rolling the sheet and subsequent testing. Immediately after rolling the sheet was cut to the appropriate size and stored in dry ice. Specimens were subsequently tested such that a strain level of 10% elongation was reached within 20-25 minutes after removal from the dry ice. This ensured that grain-growth effects would not influence any of the results.

4.204 Stress (σ) - Strain (ε) Relationships

Figure 28 shows the true stress - true strain curves obtained for the crosshead velocities covering the range .02 to 1 in/min, the strain-rates against each curve being the initial strain-rates. The shape of the curves is dependent on the crosshead velocity and

all the curves show the initial peak stress. However, the maximum stress is the peak stress at the highest crosshead velocity, and there is a gradual change over with decrease in crosshead velocity till, at the lowest crosshead velocity, the peak stress is not the maximum stress. The physical significance of the effect of crosshead velocity is indicated in the elongation values shown in Figure 29. The specimen strained at the crosshead speed of 0.1 in/min exhibits the highest elongation, the elongation decreasing with increase and decrease in crosshead velocity on either side of the maximum elongation of 550% obtained at 0.1 in/min.

In order to observe the degree of anisotropy induced during rolling of the sheet, specimens were cut at 45^{o} and 90^{o} to the rolling direction and strained at the various crosshead velocities. Elongation values obtained in the three directions are shown in Figure 30. The 90^{o} specimen exhibiting the least elongation.

Visual observation of the 90^{o} specimen showed that the edges had a crest and trough type configuration all along the gauge length, while the edges of the 0^{o} specimen were virtually straight. Also, compared to the 0^{o} specimen, the surface of the 90^{o} specimen appeared to be rougher with some fine surface lamination running normal to the straining direction.

4.205 Flow Stress (σ_f), Strain-Rate Sensitivity (m) and Strain-Rate ($\dot{\varepsilon}$) Relationships

$\sigma_f - \dot{\varepsilon}$ curves obtained by the step technique are shown in Figure 31 for specimens strained in the rolling direction (0^{o}), 45^{o} and 90^{o} to the rolling direction. The slope of the curves decreases with increase in strain-rate, the slope being the greatest between the straining-rates 10^{-2} to 10^{-1} min^{-1}. Also the effect of anisotropy is quite evident, the stress values and slope at the lower strain-rate end being the highest for the 90^{o} specimen and the least for the 0^{o} specimen.

The corresponding $m - \dot{\varepsilon}$ curves shows a similar effect, that is, the 90^{o} specimen shows the highest m-values and the 0^{o} specimen the least (Figure 32). It should be noted that in determining the above curve the specimens were strained up to about 30% elongation, the major part of the strain being at the higher strain-rates or crosshead velocities.

In order to investigate the effect of strain on the strain-rate sensitivity and flow stress, specimens were strained at 0.1 in/min crosshead velocity up to 450% elongation and $m - \dot{\varepsilon}$ and $\sigma_f - \dot{\varepsilon}$ determined in the three directions. Figures 33 and 34 shows

the m - $\dot{\varepsilon}$ and σ_f - $\dot{\varepsilon}$ curves for specimens strained different amounts. It is quite evident that the m and σ_f values increases with strain in the three directions of the sheet. Also the peak m-value increases and moves to lower strain rates with increase in strain.

Another notable effect of strain is the decrease in the degree of anisotropy of m with increase in strain. The difference in peak m-value after 10% strain between 90° and 45° direction is .04, 45° and 0° is .025, and 90° and 0° is .065. After straining 300% the difference in peak m-value between 90° and 45° direction becomes .01, 45° and 0° is .01, and 90° and 0° is .02.

4.206 Effect of Grain-Size on the 0.2% Proof Stress

An experiment was now carried out to investigate the effect of grain-size on the transition from superplasticity to normal work hardening behaviour. Specimens were heat treated for 5 minutes at various temperatures to give a range of grain sizes:

Table 2

Temp °C	Grain-size (L) μm
20 (24 hrs)	3.0
200	10.0
250	20.0
300	87.0
250	120.0

Load extension curves were determined for each of the specimens having a different grain-size at the constant crosshead velocity of 0.1 in/min. Figure 35 shows the load-extension curves, together with the mechanical properties for each of different grain-size specimens. The curves for the 0.6 and 3 μm grain-sized specimens are of a similar type in the sense that, after reaching an initial peak load, the load decreases with increasing strain. In the case of the larger grain-size specimens, there is no load decrease with increasing strain. The 10 μm grain sized specimen shows a typical work-hardening type curve where a maximum load is followed by necking and fracture.

The curves for the 20, 87 and 120 μm materials exhibit load-drop kinks, and with increase in grain-size the load-drops occur at progressively lower strains. Also during testing sounds were heard when the load-drops occurred. Elongation measurements to fracture showed the marked fall with increase in grain-size, from 525% for a grain-size of 0.6 μm to 9% for a grain-size of 120 μm. The microstructures of the various grain-size

specimens strained to fracture are shown in Figure 36. No obvious effects of deformation are visible in the 0.6 μ and the 3.0 μ samples. Slip is evident in the 10 μ specimens, and extensive twinning and slip is observed in the three larger grained specimens (20, 87 and 120 μm).

The 0.2% proof stress was determined for each of these specimens and plotted against the reciprocal of the square root of the grain-size (Figure 37). Two slopes are obtained having opposite signs. The drawing of a straight line through the two points representing the smaller two grain-sizes is open to criticism, but a third point could not be obtained, as it was not possible to obtain an intermediate grain-size. Grain-size control is exceedingly difficult in zinc (155).

In order to verify the grain-size effect in a single specimen, a 0.6 μm specimen was strained to 25% elongation, unloaded and heat treated at 200°C for 5 minutes. The specimen was then restrained. Figure 38 shows the recording of the load-extension curve and the effect of increasing the grain-size. The form of the curve changes from a superplastic curve to that of the work-hardening type and a very much higher load is recorded with the specimen failing after only 30% elongation.

4.207 Strain-Ratio (r)

The strain-ratio $\underline{r}$ was obtained for specimens strained at the crosshead speed of 0.1 in/min in the rolling direction (0°) 45° and 90° to the rolling direction and strains up to 400% elongation (Figure 39). Initially, difficulty was encountered in obtaining reproducible values at the high strains due to the expansion of the scriber marks, with the introduction of a wide band on which to position the cross wires. However, this difficulty was resolved by positioning the cross wire at the same edge of the band. The first reading was taken at 20% elongation as this was an accepted value in measuring r-values in normal work-hardening materials. The marked degree of anisotropy in $\underline{r}$ is evident for strains up to 400%. With increase in strain $\underline{r}$-value is increased substantially, i.e. .35 → .78 in the 90° direction, and there is the tendency towards unity.

4.208 Texture Determination

In order to assess the changes in preferred orientation during superplastic deformation, pole figures were determined from strained specimens cut at 0°, 45° and 90° to the rolling direction, for strains up to 300% elongation.

Pole figures for the basal and prism planes before and after deformation are shown in Figures 40 a and 40 b.

Room temperature rolling to 90% reduction in thickness produces a concentration of basal planes inclined at about 22° to the rolling plane towards the rolling direction, while the concentration of the prism planes suggests the [10$\bar{1}$0] direction is parallel to the transverse direction. On straining the material parallel in the 0° direction, the initial strong intensity weakens to 6, while the concentration of basal plane inclination is reduced, till at 300% elongation the basal plane becomes parallel to the plane of the sheet, producing an 'ideal' pole figure. In the case of the prism plane pole figures, with increase in strain, the peak intensity points are lost, and no information could be obtained after straining.

On straining in the 45° direction, the behaviour is quite different, that is, after 300% elongation, the basal plane normals become compressed in the N - S direction and a rotation of 30° occurs from the tensile axis, while the basal plane tilt reduces by 7° to 15° and the texture weakens.

At 90° the basal plane normals are compressed along the N - S axis, while the tilt remains the same with the texture weakening. The change in basal plane tilt with increasing strain for all the specimens is summarised in Figure 41.

4.209 Biaxial Tests

The biaxial tests were done in order to confirm the anisotropic behaviour observed in the sheet plane in the various parameters. Initially tests were done using a 2-inch diameter hemispherical punch at varying strain-rates and under different lubrication conditions. Figure 42 shows that with increasing punch speed, the dome height decreases. Also the radial true-strain, measured from surface grids, showed that the maximum strain was obtained well away from the pole, that the radial true-strain varies in the sheet plane, and that the strain at 0° to the rolling direction is greater than that at 90°. Furthermore, fracture always occurred perpendicular to the 90° direction. In order to ascertain the effect of lubrication on the strain distribution and dome height, Figure 43 shows the true radial strain in the rolling direction for two specimens, one strained to fracture with oil/polythene lubrication and the other without lubrication. The difference in the dome height is evident and the specimen with no lubrication was by far the deeper.

In order to assess the biaxial deformation behaviour in the absence of friction, some 4.5 in dia. hydraulic bulges were produced (Figure 44). The surface strain at the pole of the bulge was about 300%. The anisotropic behaviour of the sheet is apparent from this figure. Circular grid patterns become elliptical on deformation with the major axis in the rolling direction.

It was possible to measure the surface strains in any direction of the sheet and at any point by measuring the major and minor axis strains. Also assuming a constant volume condition these perpendicular strains could be converted to thickness strain using the relationship:

$\varepsilon_1 + \varepsilon_2 + \varepsilon_3 = 0$, where

ε_1, ε_2, and ε_3 are the principal true-strains in x, y and z directions.

Figure 45 shows the plot of thickness strain in the rolling and at 90° to the rolling direction. The thickness strain is the greatest in the rolling direction.

4.210 Microstructural Observations

Specimens were strained to increasing amounts up to 400% elongation at the crosshead velocity and of 0.1 in/min and the microstructure examined on the surface and internally by optical microscopy, scanning electron microscopy and thin-foil transmission electron microscopy.

Figures 18 and 19 show the surface and internal structure of the as-rolled sheet examined within ten minutes of rolling. An extremely fine-grained size structure is apparent. The grain size was measured by the linear intercept method, and at least fifty to a hundred measurements were made at random on about ten negative plates and the fixed magnification used was precalibrated (X10000). The average grain-size of the as-rolled sheet was found to be 0.6 μm. As is evident from the transmission electron micrographs the grains are fairly equiaxed and there is hardly any evidence of directionality. There is a high density of tangled dislocations and fine Al-rich precipitates distributed randomly, with segregation at grain-boundaries. At higher magnification the presence of dislocation loops is very marked; these appear as rings with while spots.

On straining the material to 25% elongation there is a marked decrease in the dislocation density (Figure 46a). The presence of dislocation loops and precipitate particles are quite remarkable.

The microstructure after 100% elongation shows the maintenance of the low dislocation density (Figure 46b). Evidence of dislocation activity is illustrated by the dislocation-dislocation, dislocation-loop, dislocation-precipitate and dislocation-grain-boundary interactions. It is clear from the micrographs that the interior regions of the loops exhibits contrast. Also, apart from the regions inside the loops, the dislocation rings themselves also present contrast effects. For certain inclination of the foils, the dislocation rings were visible.

Figure 46b (X45000) shows a range of precipitate sizes and shapes, precipitate particles being also present in the grain-boundaries. There is also evidence that grain coarsening has taken place, and this is clearly observed in the optical micrographs (Figure 47).

Straining up to 400% elongation shows negligible dislocation density, but a few dislocations were observed, as is shown in Figure 46 c. Some gliding dislocations are caught up by, possibly, both dislocation loops and precipitates.

Surface examination after 50% elongation under the scanning electron microscope shows grain-boundary sliding with intergranular cavitation, the initial sliding taking place at the boundaries normal to the tensile axis (Figure 48). After 200% elongation the extensive grain movement is evident. Intergranular cavitation direction is lost and holes appear all around the grains and the grains are seen to be protruding relative to each other. After 400% elongation the surface rumpling effect is even more marked. Figure 49 is the longitudinal section of the specimen strained 400%. It illustrates the depth of intergranular cavitation resulting from grain-boundary sliding.

Fracture behaviour was studied on specimens strained at three strain rates: 4×10^{-2}, 4×10^{-1} and 8×10^{0} min^{-1} strain-rates for m-values of 0.34, 0.17 and 0.05 respectively. The fracture surfaces were examined by means of scanning electron microscopy (Figure 50). The marked difference in the fracture behaviour is indicated clearly in the case of the two extreme strain-rates. However, both the fracture surfaces are ductile in nature. In the case of the very low m-value (.05) specimen a ductile 'honeycombe' type fracture surface is evidence, typical of a coarse grained 'normal' ductile work-hardening metal.

In the highm-value region (.34) another type of ductile fracture is exhibited, where the two halves of the specimen have separated after deforming to a knife-edge composed of such heavily deformed material that the original features in the structure are obscured.

At the intermediate m-value (.17), there is a mixture of these two types of fracture surface with the void concentration very much smaller, and a fair proportion of 'drawing down' in the fracture area.

4.300 Discussion

4.301 Material

The possibility of obtaining a fine-grained structure in a Zn-0.4 Al alloy has been shown by Lutts and Wegria (110). These authors showed in a micrograph the possibility of obtaining fine grains in this alloy by room temperature rolling. However, no reference was made as to the grain-size and whether the grains remained stable at room temperature, the interest lay simply in the annealed recrystallized structure. The grain-size obtained in this investigation (0.6 μm) by hot and cold rolling has not previously been reported.

Cook and Riseborough (99) have obtained a grain-size of about 3.5 μm in a very similar alloy (0.2 % wt aluminium) by extrusion, while grain-sizes in the region of 0.5 - 3 μm have been readily obtained by the powder metallurgy technique (93-98).

Zinc is classified as belonging to the softer group of metals and as previously stated on room temperature rolling the material undergoes softening after a critical percentage reduction (Figure 20a). Gay, Kelly and Hirsch (111,112) were perhaps one of the first workers to investigate using the x-ray micro-beam technique, the effect of rolling at room temperature (.42 Tm) in a high purity zinc. These authors found that up to a limiting deformation of 20-30% reduction, sub-cells are formed within the grains and for deformations greater than 40% reduction, a limiting sub-cell size (18 μm) and a maximum misorientation angle ($9\frac{1}{2}^{o}$) was obtained followed by spontaneous recrystallization. In the present work the softening of the material gives credence to the hypothesis that this softening is associated with spontaneous recrystallization.

However, Deighton and Parkins (113) have observed a similar softening effect with decrease in grain-size during rolling. These authors state that during the early stages of deformation and grain fragmentation, sub-boundaries are formed. With increasing deformation, sub-boundaries coalesce, thus increasing the misorientation of the sub-grains, until these boundaries become high angle boundaries and the grain-size is decreased. This model could be associated with the observation of Lewis et al (114), during the hot torsion of zinc in the temperature range 0.6 - 0.7 Tm. These authors concluded that the observed structural change was similar to that obtained in creep and the structure obtained was a more advanced stage of substructure formation. Deighton et al's suggestion is more in keeping with the experimentally verified polygonization theory of recrystallization i.e. during the recrystallization of deformed material, (158).

In the present investigation the microstructure of the as-rolled sheet would suggest that a minimal grain-size was obtained,

followed by the introduction of dislocations due to further deformation. This grain-size appears to have been made possible by the presence of the dispersion of the fine, Al-rich particles, these particles effecting recrystallization by restricting boundary migration and dislocation recovery processes. Solute additions of aluminium in zinc has been shown to increase the recrystallization temperature and inhibit boundary mobility (157). Also it has been shown by Baralis et al (115) in a similar alloy, that during the initial stages where dislocation density increases, small dispersed particles occur and in the final stage spherical precipitates particles are formed. In the micrographs (Figure 46) the dark spots are identified as precipitates. The identification of the presence of dislocation loops and precipitates become clearer as shown in Figure 46a.

The formation of dislocation loops during rolling has been observed previously in high purity zinc (116). It is supposed that point defects come from the severe rolling which causes interaction of dislocations on several slip systems and the generation of vacancies in the wake of moving jogs. The concentration of point defects must be large enough to nucleate loops and points to the effect that vacancies apparently can condense into loops as well as induce existing dislocations to climb.

4.302 Grain-Growth Effects

It was observed by Chadwick (89) that the physical properties of rolled zinc was subject to considerable variation according to the impurity content, especially during the period of a few weeks after the rolling. Complete recrystallization took place in an 80% rolled, commercial electrolytic zinc, after a month. However, the addition of 0.02% iron or magnesium was found to prevent recrystallization and grain-growth. In this investigation it is observed that the grains are unstable at room temperature and grain-growth takes place. The grain-growth effect is supported by the increase in hardness (Figure 20b). A similar effect is shown by the increase in 0.2% proof stress and decrease in m-values and the peak in m-value moving to lower strain-rates (Figures 25 and 26).

This apparent grain-size effect is not in keeping with the observation made in normal metals during recrystallization followed by grain-growth. This is the elimination of large densities of dislocations reducing the hardness which will continue to fall during grain-growth after recrystallization (159). However, this effect is observed in the grain-size range where superplastic mechanisms begin to operate and where, with an increase in grain-size, the flow stress increases, while the m-value decreases, with the peak in m-value moving towards lower strain-rates (Section 2.3)

It has been established that grain-boundary migration, either during recrystallization or grain-growth is a function of the grain-boundary structure, the driving force for grain-boundary mobility being due to the increase in grain-boundary area, proportional to

the grain-boundary free energy and inversely proportional to the average grain diameter. Furthermore, the increase in dislocation density will further increase the driving force (146). However, it would appear that the presence of aluminium, the solubility of aluminium in zinc at room temperature being about 0.05%, produces a solute impurity drag effect which should inhibit boundary mobility (157). Therefore it would appear that the impurity drag effect preventing grain-growth is overcome by the combination of these factors and the grain-size increases from 0.6 μm to about 3-5 μm, stable size, at room temperature in about 8 - 10 hours.

4.303 Grain-Growth Inhibition by Straining

The remarkable way in which grain-growth is completely inhibited by a tensile strain of 25% seems unique. It is also evident that the operation of the mechanism of superplasticity must in some way be associated with the inhibition of grain-growth. As is shown in Figure 24, the amount of strain governs the final stable grain-size and so there must be a direct link between dislocation activity and the final grain-size, in these experiments. As previously stated, an additional driving force for grain-boundary migration is a high dislocation density. Figure 46a shows that on straining the material 25% there is a marked reduction in dislocation density. Therefore, it appears that during the superplastic deformation, annihilation of dislocation must be taking place, which subsequently reduces the driving force for grain-boundary migration and prevents recrystallization and grain-growth. One way in which dislocation annihilation has been observed to take place in zinc is by the annihilation of dislocations of opposite signs by rearrangement both by glide and climb leading to dislocations of one size aligning themselves into walls to form small-angle sub-grain boundaries or sub-grain (103).

However, it has been observed in zinc crystals, deformed in tension by basal slip, that recovery by polygonization does not take place and as such recrystallization does not occur. Nevertheless, these specimens can recover there original softness completely by an alternative recovery process (158). One basic process of recovery which can readily take place is by the running together and mutual annihilation of two dislocations of opposite sizes. When the two dislocations of opposite size are not on the same slip plane, climb or cross-slip first occur before annihilation. Therefore in the present case since the as-rolled material has a high dislocation density, on straining this material, the introduction of a considerable surplus of dislocations of one sign, which could well occur, could easily lead to mutual alignment of dislocations of opposite signs and annihilation.

A further possibility is the role which the grain-boundaries can play both as donors and acceptors of dislocations, and which has been observed in zinc (116). Surface observation shows that grain-

boundary sliding is taking place (Figure 48), and observations of 'pure' grain-boundary sliding in zinc bicrystals (119-123) have shown that during grain-boundary sliding dislocations are emitted by the sliding boundary and pass freely through the matrix grain adjacent to the boundary. It was also proposed that, associated with the basic mechanism of sliding, was the climb and glide of dislocations along the boundaries. In the present case, the abundance of vacancies should greatly facilitate the climb and annihilation of dislocations both at the grain-boundaries and in the matrix.

Therefore, it would appear from the present results that total inhibition of recrystallization and grain-growth at room temperature after 25% strain is achieved by possibly a dislocation recovery process. Partial inhibition is realised by decreasing amount of strains, which again must depend on the degree of dislocation annihilation and the subsequent effect on the final grain-size.

4.304 Flow Stress (σ_f), Strain-rate Sensitivity (m) and Strain-rate ($\dot{\varepsilon}$) Relationships.

The step-method of Backofen et al (20) to determine the $\sigma_f - \dot{\varepsilon}$ and $m - \dot{\varepsilon}$ relationships has come under criticism (124-126). It has been stated that during the test, the structure is constantly changing and discrepancies in the $\sigma - \dot{\varepsilon}$ and $m - \dot{\varepsilon}$ relationships will inherently be introduced. However, though discrepancies could have been introduced in the present investigation, the test was employed in a comparative sense under reasonably standard conditions of testing. The values obtained in this investigation can also be compared with a considerable amount of the published data, as almost all the $m - \dot{\varepsilon}$ and $\sigma_f - \dot{\varepsilon}$ relationships have been determined by this technique. Favourable correlation is also obtained on comparing the flow-stress values obtained in single tensile tests with the stress values obtained from the step-method (Figures 28 and 31). The strain-rate sensitivity obtained at 10% strain shows a peak value at about 2×10^{-2} min^{-1} strain-rate (Figure 32). Cook and Riseborough (99) obtained a peak m-value of 0.8 and at the strain-rate of 10^{-3} min^{-1}. This is not surprising since the grain-size of these workers was 3.5 μm as compared to 0.6 μm in this work. Therefore, the peak in m-value should increase and shift to the lower strain-rate end.

The $\underline{m}$ and σ_f values are strain dependent and they also vary in the plane of the sheet (Figures 33,34) and the substantial increase in $\underline{m}$ after a strain of 300% predicts that the structure is constantly changing. Variation in the m-value with strain has been observed previously in steels (23), but in most of the steels investigated, the m-value was observed to decrease with strains up to 300% elongation. However, this variation in m-value was only observed for a particular strain-rate, and the decrease was attributed to the

coarsening of the grains with increasing strain. However, this decrease should, in fact, be an increase with increasing grain size if only the peak value is considered (2.30). This discrepancy is resolved for the Zn/0.4 Al alloy if the effect of grain-size on the entire m - $\dot{\varepsilon}$ curve is considered (Figure 33), and the m-value increase and shift to the lower strain-rate end is consistent with the observation that the grain-size increases with strain.

For the specimen strained in the direction of rolling, at the strain rate of 8×10^{-2} min^{-1} the m-value at 10% strain is .3, which decreases to .22 on straining to 300%. At the other end of the strain rate range, 4×10^{-3} min^{-1}, the m-value has increased from .355 to .5. The highest elongation obtained in this work was at the constant crosshead velocity of 0.1 in/min or an initial strain-rate of 8×10^{-2} min^{-1} (Figure 29). However, with increase in elongatwon, the gauge length is constantly increasing, consequently the strain-rate will be constantly decreasing, till after 550% elongation the strain-rate will have decreased to 4×10^{-2} min^{-1} The reason for the highest elongation at this crosshead velocity becomes clear on referring to the strain-rate path the specimen follows in order to reach the 550% mark. Referring to the 10% m - $\dot{\varepsilon}$ curve and not considering grain-size effects, it is evident that with decrease in strain-rate, commencing from 8×10^{-2} min^{-1}, the m-value is constantly increasing, climbing up to the peak. On the other hand, specimens strained at either end of the peak will have markedly lower m-values, and with decrease in strain-rate the average m-value will be lower than the average m-value obtained at 0.1 in/min. An additional factor which must now be brought into consideration is that the m - $\dot{\varepsilon}$ curve is constantly moving to the lower strain-rates due to the increasing grain-size. Therefore the overall average m-value obtained by the combination of the strain-rate and grain coarsening effects will dictate the elongations obtained. The elongation values obtained for the various crosshead velocities are consistent with the dome-shaped m - $\dot{\varepsilon}$ curve.

The elongation values obtained at 45^{o} and 90^{o} to the rolling direction are shown in Figure 30. It is clear that these values are not consistent with the m - $\dot{\varepsilon}$ values (Figure 32). The m-values increase from 0^{o} to 90^{o} and is the greatest at 90^{o}; therefore higher elongations should have been observed in the 90^{o} direction, followed by the 45^{o} direction. Similar m-value anisotropy effects have been observed by Taplin et al (71) in hot-rolled aluminium-bronze sheets. These authors obtained the opposite effect of higher elongation at 90^{o} and lower elongation at 0^{o}, though no m-values were quoted. In the present case this discrepancy in m-value and elongation could be a result of the surface or internal cracking on a small scale, during hot rolling and room temperature rolling, and the failure of the

specimens cut at 90° was by fracture occurring normal to the tensile axis without the necking to a sharp point observed in the case of the 0° specimen. Premature failures from minute surface laminations also occurred.

4.305 Stress (σ) - Strain (ε) Relationships

The stress-strain curve indicates the response of a material to the structural variations during straining. In highly strain-rate sensitivity materials, the $\sigma - \varepsilon$ behaviour will be governed by the strain-rate. It is accepted that during superplasticity there must be a balance between the softening and the work-hardening mechanism, and under ideal conditions of constant strain-rate, a steady-state condition should be achieved; thus in fact the stress should have a constant value during straining. However, this ideal $\sigma - \varepsilon$ behaviour will be affected by the continuous change in structure and strain-rate if a tensile testing machine operating at a constant crosshead speed is used, and this behaviour is observed in the present investigation, (Figure 28) for, as previously stated, the strain-rate is constantly decreasing while the grain-size is increasing as the test proceeds.

At the highest crosshead velocity of 1.0 in/min the curve reaches a peak value which markedly decreases with strain, a typical observation in superplastic metals, partcularly materials which have a high m-value at relatively high strain-rates (55). At the other end of the strain-rate spectrum the curve for a crosshead velocity of .02 in/min, exhibits virtually no peak, and the stress increases with increasing strain. The difference in this behaviour can be traced to the strain-rate path followed in the $m - \dot{\varepsilon}$ curve, and also to the effect of the increase in grain size on the $m - \dot{\varepsilon}$ curve during straining. At the low strain-rate, the strain-rate follows a decreasing m-value path while at the higher strain-rate an increasing m-value path is followed. Thus the suggestion of the rate of strain-rate hardening and strain-rate softening for the lower and higher strain-rate appears reasonable (4). The curve obtained at the crosshead speed of 0.1 in/min is shown to balance the effects at the higher and lower strain-rates and negligible strain-rate hardening is observed. It should also be noted that the strain-rate path at this velocity gives the highest m-value. Therefore it is suggested that under constant conditions with no strain-rate or grain size changes, an ideal steady state stress-strain should be obtained at the critical strain-rate where the balance between the softening and hardening mechanisms is achieved. This suggestion is supported by the steady-state stress behaviour obtained under constant strain-rate condition during the hot torsion of metals (127). Hardwick et al (128) have stated that the shape of the $\sigma - \varepsilon$ curve is an indication of the deformation mechanism operating, the peak in the curve is associated with the

operation of a restoration process, and its height is an indication of the ease with which restoration occurs. In the case of a high-stacking fault metal like zinc, since restoration by dislocation climb is rapid, only a small peak, if any, should be observed. However, in the present case, a similar analysis of the curves is complicated.

4.306 Effect of Grain-Size on the 0.2% Proof Stress

The degree to which the flow stress of a polycrystal is sensitive to grain-size in terms of the dislocation structure which develops in the vicinity of grain-boundaries was put forward by Hall (117) and Petch (118) and is expressed in terms of the relationship:

$$\sigma = \alpha^* + kL^{-1/2}$$

σ = yield stress, σ^* = frictional stress

k' = Hall-Petch slope

L = Grain-size

The application of this expression to relate the 0.2% proof stress dependence in the grain-size range 0.6 μm to 120 μm, revealed an interesting relationship (Figure 37). For the grain-size range 10 - 120 μm the decrease in stress with increase in grain-size is in accordance with the above expression, but an opposite effect is obtained for the two smaller grain-sizes, where an increase in stress with increase in grain-size is observed. It is evident then, that a critical grain-size must exist at which the Hall-Petch (H-P) relationship is no longer valid.

A similar effect has been observed by Tromans and Lund (94) in the Zn - ZnO power composite covering the grain-size range of 1 μm to 83 μm. Furthermore, the critical grain-size change-over point was strain-rate dependent for with an increase in the strain-rate, the critical grain-size was decreased. The authors stated that the breakdown of the H-P relationship was due to the commencement of grain-boundary sliding.

Two principal analytical models have been evolved that provide semi-quantitative explanations for the experimentally established H-P relationship. One is the original mechanism proposed by Hall and Petch involving a pile-up of dislocations against the grain-boundary. In the second approach (129), stress concentration at grain-boundary was not taken into account explicitly instead use is made of the relationship which expresses the stress in terms of dislocation density.

$$\sigma = \sigma^* \rho^{1/2} \mu b L$$

where ρ is the dislocation density, b the burgers vector and μ the shear modulus.

Experimental verification of the second approach has been made by the use of electron microscopy (130,131). Thus, whichever of these models is applied to the present alloy, the breakdown of the H-P relationship suggests that a process comes into operation which reduces the dislocation density or removes the dislocation pile-ups at grain-boundaries.

In the case of the two smaller grain sizes which do not obey the work hardening model, surface grain-boundary sliding has been observed. Transmission thin foils also show a negligible dislocation density, and suggest the possibility of dislocation generation and absorption by the grain-boundaries, in accordance with the statement made above, and supporting this behaviour are the typical load-extension (L - E) curves and deformed microstructures obtained for grain sizes covering both the superplastic and work-hardening grain sizes (Figures 35 and 36). In superplasticity the load increases to a maximum value and then drops continuously with increasing extension. In comparison the typical work-hardening type curve is observed at a grain size of 10 μm, where the load increases reaching a maximum value, which is maintained during the commencement and necking before fracture. It appears fairly obvious that, since in the normal large-grained material, the load is increased and maintained by an increase in dislocation density due to the interactions and pile-ups, whereas in the case of the superplastic-type curve, mechanisms must come into operation which prevent or retard dislocation interaction and pile-ups.

One of the mechanisms proposed for superplasticity has been based on the concept of dislocation pile-up followed by climb, leading to grain-boundary sliding and the consequent reduction of flow stress (45). Other suggestions based on dislocations involve a dislocation annihilation process by glide and climb along the grain-boundaries (27,31). Thus, the 0.2% proof stress - grain size relationship emphasises the role of dislocations during superplasticity.

This relatively abrupt change from superplasticity to work-hardening behaviour, suggests the possibility of 'switching off' superplasticity in this alloy by a grain-size change, as shown in Figure 38, in which, additionally, the strength of the alloy is increased by a factor of two. The utilization of this treatment could have an important practical significance.

4.307 Strain Ratio (r)

The r-value indicates the degree of resistance to through thickness deformation. If r = 1, then the material is isotropic, i.e. it strains equally in the x, y and z directions. If r is less than one, then the material strains in the thickness direction in preference to straining in the plane of the sheet, and if r is greater than 1, the reverse is the case. The observation in this material of the r-value increasing from .3 to .8, tending towards unity indicates a marked change in the texture introduced on rolling, and the tendency of the material to become random in texture., (Figure 39). Atkinson (132) has reported the strain-dependence of r-value in zinc, but he covered a very much smaller range of values and elongations. Lee et al (24) observed a fall in r with increasing temperature and elongation in Zircaloy-4 and suggested that the value is tending to unity (isotropic), while Pearce (133) has shown an increase in r in commercial purity aluminium from .51 at -196°C to .73 at 400°C. In a non-textured, superplastic Zn - Al eutectoid, since the alloy was produced by a quenching-decomposition process, it has been observed that the r-value remained constant, at unity, up to 400% elongation (40) and it was suggested that the introduction of preferred orientation due to lattice rotation during straining could indicate that a dislocation mechanism might be operating.

The variation of the r-value in the plane of the sheet is consistent with that observed in normal zinc (134). However, the r-values determined in unidirectional rolled zinc are usually the greatest at 90° and the lowest at 0°, the r-value usually being measured at 20% elongation. In this work this trend is not observed, at 20% elongation the 0 and 90° are virtually the same (.35), while in the 45° direction it is (.51). However, with increase in elongation, the rate of increase in r-value is the greatest for the 90° specimen and after 200% elongation, the 90° attains the higher r-value, while the 0° remains the least.

4.308 Texture Determinations

It is well known that hexagonal metals in sheet form exhibits a marked degree of plastic anisotropy. This follows from the fact that plastic anisotropy is associated with the disposition of shear systems relative to the stress axis, and hexagonal metals have a small number of slip systems. In zinc, at room temperature, slip takes place mainly on three slip systems, consisting of the three $[11\bar{2}0]$ directions, in the basal plane, although deformation modes other than basal slip must operate in order to accommodate the slip mechanism.

In zinc, during the rolling operation, reduction in thickness and extension in length are accomplished by rotation of the slip directions within individual grains towards the rolling direction. In accordance with this tendency, the predominating texture of zinc deformed by basal slip is one in which the basal plane lies in or near the rolling plane, although modifications are found. In the typical pole figure of as-rolled Zn - 0.4 Al, (Figure 40a), it is seen that the majority of the grains are oriented with the basal plane about 20° from the plane of the strip in the direction of rolling. On subsequent tensile straining of a strip cut in the rolling direction, the least difficulty is encountered, since the basal normals both along and on either side of the N-S axis suggest the operation of the three slip directions. However, the result of this straining, which is to rotate the basal plane until it becomes parallel to the sheet plane cannot be only due to slip, since work-hardening mechanisms cannot cater for the total strains involved. At 45° to the rolling direction, the behaviour is quite different, since slip is more difficult. However, straining is effective in rotating the basal plane poles together with decreasing the tilt angle (7°). Rotation of the basal plane poles has also been observed in large-grained zinc (135), in which the initial texture of the sheet was similar to that in Figure 40a, and when straining was carried out at 90° to the rolling direction a rotation of the basal poles by 90° took place. It was observed that twinning was necessary to provide accommodation for further slip. In the present case, however, no twinning occurs and therefore accommodation up to 300% elongation must again be provided by another mechanism. At 90°, no basal-pole rotation or tilt occurs. In this direction slip becomes very difficult and crystals with basal plane normals away from the N - S axis govern the slip behaviour. It therefore appears from the present investigation that if a continuous lattice rotation is taking place in order to account for the steady texture changes, a continuous form of recovery mechanism must be operating simultaneously.

The only observation studied so far on a superplastic alloy (Zn - 5% Al) has been by Packer et al (60). These authors strained their sheet only in the rolling direction and obtained a similar pole figure as in Figure 40 a(b). The suggestion of these authors was that a dynamic process of recrystallization or migration must be occurring coupled with crystallographic slip.

4.309 Biaxial Tests

The biaxial tests under the various conditions clearly illustrated the anisotropic behaviour in the sheet and confirmed the behaviour observed under uniaxial tension.

Not unexpectedly, the dome height in punch stretching decreased with increasing speed, in qualitative agreement with the

uniaxial behaviour of superplastic alloys. The observation that under high frictional conditions, i.e. no lubrication between the punch and the sheet, a higher dome produced is quite different from that of work-hardening metals (136). In the case of work-hardening metals, friction over the punch nose isolates a cap of metal that can take no further part in the straining/work-hardening cycle which continues up to fracture.

In the case of non-work-hardening superplastic deformation, when the cap of metal around the pole is prevented (by friction) from deforming, a larger volume of metal, i.e. that between the cap and flank, contributes to the overall deformation and the final dome height is greater. On the other hand under conditions of good lubrication, as the pole cap is not prevented from straining, straining will predominantly take place nearer and around the pole region with very little deformation nearer the flank region, resulting in a lower dome height.

The greater surface strain is shown to occur under hydraulic bulging in the rolling direction (Figure 44), and this is supported by the higher elongation values obtained under uniaxial tension. Also, as is shown in the punch-stretching case, the total strain is less at 90° to rolling, due to the occurrence of failure perpendicular to this direction (Figure 42).

Also the ease of deformation in the rolling direction is supported by the lower flow stresses and texture changes, and the absence of any work-hardening that would 'pass on' the deformation load and force axisymmetrical straining, as in the case in non-superplastic metals exhibiting planar anisotropy.

4.310 Microstructural Observations after Deformation

Optical microscopy indicated the effect of grain-size increase with strain, the grain-size increasing from 0.6 μm to about 1.2 μm after 400% elongation (Figure 47). It has been shown that this increase in grain-size is not only a time-temperature effect but, in fact, is also the result of superplastic deformation. This observation is consistent with the observation made in most of the superplastic alloys (Chapter 2), though a few authors (47, 125) have not found this effect and state that the grain-growth they observed was only due to a time-temperature effect.

The increase in the grain-size, subtracting the time-temperature effect, must be the result of either the change in the strain-rate or strain which takes place during the constant

crosshead velocity tensile test. Lindinger et al (65) have shown in the Ni - Fe - Cr superplastic alloy that the grain size increase is not dependent on the strain but is directly related to strain-rate, i.e. the grain-growth rate increases with increasing strain-rate.

Watt et al (70) in their tests on the Al - Cu eutectic alloy, did not observe any additional grain-growth to that observed due to time at temperature effect and, as these authors strained their material under constant strain-rate conditions, this confirms the strain-rate effect observed by Lindinger et al. Unfortunately, in this investigation, since both the strain-rate and strain were changing during the tensile test, it was not possible to isolate the contribution of these two variables.

Surface observations using the scanning electron microscope clearly shows that extensive grain-boundary sliding, with grain rotation takes place (Figure 48). The extensive rumpling and delineation of the grains relative to each other shows that the surface movement of the grains is continued with increasing elongation. The figure after 50% elongation also shows that the weakest grain-boundary link is normal to the stress axis; however, with increasing strain the sliding tends to become random. The most remarkable observation is the massive cavities which form between the grains and the depth of penetration of these cavities (Figure 49). However, the lack of cavities in the interior of the specimen illustrates the effect of differing constraints upon the grains and shows that surface behaviour cannot be taken as representative of the bulk behaviour.

Rachinger (137) has shown in his study of creep in aluminium that the mechanism of plastic flow at the surface was different from that in the interior, the transition taking place in the surface ten thousandths of an inch. In his experiments the deformation within the grains was computed from measurements of grain dimensions in the longitudinal and transverse directions. It was observed that grain-boundary sliding increased with depth below the surface. Intergranular deformation, therefore, seems to be more predominant on the surface than internally, and in creep at low strains grain-boundary sliding is related to intergranular deformation (138).

The initiation of intergranular cavitation normal to the stress axis suggests the operation of a w-type fracture (138); this is due to the stress concentration being primarily developed at the triple points. However, it can be in part attributed to grain-boundary sliding, but is intensified by the anisotropic effects related to differing orientation of adjacent grains. The other possibility is that the void nucleation at the grain-boundaries could very well occur by the condensation of vacancies to the grain-boundaries and as such would not depend on the generation of stress concentrations due to deformation. This process is suggested due to the presence of a high concentration of vacancies and the large grain-boundary area available for condensation due to dislocation short-circuiting (138).

With increase in strain, sliding is operative along all the boundaries, resulting in extensive intergranular cavitation. The discrepancy of extensive cavitation on the surface, and no visible cavitation in the interior, indicates that an additional process must be operating in order to relieve the stress concentrations at the grain-boundaries and maintain compatability during continuing grain-boundary sliding. In creep of polycrystals there is ample evidence to show that with the operation of grain-boundary migration the propensity for intergranular fracture decreases, and in bicrystals, sliding is believed to be controlled by strain-hardening and recovery effects occurring within the zone (138).

The contribution to the total strain of grain-boundary sliding has been assessed by several authors (29,31). However, it was found that measurements could only be made up to about 50% elongation, as with increase in strain above this, extensive surface rumpling occurred and no meaningful measurements were possible. Based on these low strain measurements it was concluded that as much as 60% of the total strain could be contributed from grain-boundary sliding up to > 1000% elongation. This suggests that grain-boundary sliding strain is linearly related to the total strain, but in creep of several alloys (β - brass, Al and Al - Mg alloys) (139-141) deviation from linearity are observed, and during the initial stages of creep, grain-boundary sliding contributes more to the total strain than in the later stages. Therefore, it would appear that though surface observations are indicative of the operation of certain processes during superplasticity, the direct association of these observations to bulk behaviour should be viewed with sceptisism.

Transmission electron microscopy of thin foils showed that the high dislocation density of the initial, as-rolled material was markedly reduced by straining the material in tension to 25% elongation. The foils also contain many dislocation loops. In addition, no grain elongation was observed. The most striking observation was the dislocation loops. Dislocation loops have been observed previously in zinc and are found to be situated on the (0001) plane and are sessile in character, (116). Other notable observations from these foils are:

1. the linking of dislocation to the grain-boundaries, and
2. the interaction of the gliding dislocations with the loops and with precipitate particles (Figure 46b and 46c).

Figure 46b (X24000) shows a typical loop-dislocation interactions indicating both a combination and repulsion effect. It has been shown that dislocations can act as short circuits for the diffusion of point defects, with the grain-boundaries acting as better sinks for vacancies at the expense of the loops. A typical reaction exhibiting the possibility of this effect is shown in Figure 46b (X24000)(A). Direct evidence of the grain-boundaries acting as sources has been previously observed and it is suggested that it might be happening in this case, where dislocation lines are observed linked to the grain-boundaries. However, the question is, do these

dislocations arrive from the grains and stay in the boundaries, or are they left behind each time a dislocation is generated from the boundary? Lin et al (142) have suggested that if a dislocation bulges out in a loop from the grain-boundary, then dislocations are emerging and if this idea is accepted, then the dislocation in Figure 46c X25000 could be identified as leaving the grain-boundary. Also, a pattern containing trains of dislocations that appear at first sight to be pile-up groups, pressing against the boundary is identified as dislocations arriving at the boundary (Figure 46b) X45000. It can also be seen that the dislocations are generated at the boundary and move across the grains, rather than appear from the interior of the grain.

From these microstructural observations there is evidence of dislocation activity though the general density is remarkably low, but this is in keeping with the dislocation free-structures observed in alloys during superplasticity (Chapter 2).

The observation of the grains remaining equiaxed but increasing in size during deformation needs an explanation. No model proposed has yet explained this observation adequately.

It has been analytically shown by McLean (143) that during grain-boundary sliding, the grains will retain their equiaxed nature. Also, if extensive grain rotation occurs no grain elongation will take place. For energy reasons it is the most equilibrium configuration, though grain-boundary migration has been stated to accompany grain-boundary sliding. It is fairly well established in creep and hot working (127,138) that in order for the grain-boundaries to remain coherent during grain-boundary sliding, recovery processes in the region of the grain-boundaries must take place. This effect is shown by Halliday et al (121) in zinc bicrystals. One process by which this occurs is by grain-boundary migration. Thus, it would appear that due to the instability of the grain-boundary structure brought about by the extensive strain it has to accommodate, grain-boundary structure adjustment must be occurring continuously, in order to attain the next equilibrium configuration, and must be related to the sliding mechanism. This aspect is further discussed in the section on mechanisms.

A noticeable feature is the relatively straight boundaries, which are unlike the rounded or curved interphase ones found in two-phase superplastic alloys. Therefore, the rounded grain-boundary is not a necessary requisite of superplasticity. However, as Packer et al (60) have suggested, when grains of the same kind slide, local hardening at the boundaries can be relieved by migration which creates new, strain-free material, in which sliding can continue. In the case of dissimilar phases hardening of the interphase cannot be relieved by simple migration without redistribution of the solute phase. In the Al - Zn eutectoid superplastic, it is suggested that the β/β grain-boundaries shear, and is confirmed by the present work.

4.311 Fracture Behaviour

In creep and hot working, the rupture mechanisms have been related to the deformation mechanisms, and these former are now well understood. In the case of superplasticity, little has been done to link together the fracture to the deformation behaviour, simply because no studies of fracture behaviour appear to have been carried out. This is not surprising, since it is accepted that with a material showing ductility of up to 1000% elongation, plus the occurrence of grain-boundary sliding, a typical ductile failure would occur. However, since in superplasticity the ductility is directly related to the strain-rate sensitivity or strain-rate, the fracture mode might well vary with the testing conditions.

The effect of high m-value and high elongation is shown in Figure 50 with the specimen eventually pulling down to a knife-edge. The weakest links under superplastic deformation conditions are the grain-boundaries and the evidence of striations suggest the fracture mode to be due to shear at the grain-boundaries (144). Under work-hardening conditions, the nature of the fracture changes to a ductile, cup-and-cone type. In this case internal cavities become large enough to spread rapidly in the transverse direction. In ductile fracture, the initiation and growth of these cavities usually takes place at and around inclusions, second-phase particles, or impurities. This type of fracture is observed in the present alloy in the specimen strained at the high crosshead speed of 20 in/min in which case the m-value was less than 0.1. One possibility of the 'honeycombe' type configuration can be due to either individual or several grains being ripped away at probably the grain-boundaries and leaving behind holes. As is evident from the micrographs holes range from less than and just over a micron in size, the grain size of the alloy. A very similar type of honeycombe network has been obtained by Tipler et al (144) during the creep of Al - Cu alloy, where carbide particles were seen to be in the centre of each dimple, acting as nuclei.

In the present case, Zn - 0.4 Al, no second-phase particles can be seen at the operating magnification. However, transmission electron microscopy of thin foils shows that the second phase Al-rich particles are extremely small and are below resolving power of the scanning electron microscope. So it cannot be established whether the initiation of the cavity by the particle is in the grain-boundaries or in the grain matrix, though the grain-boundary is the weakest and most likely region, and where the particle would be most effective. On the other hand, the high rate of deformation would tend to increase the rigidity at the grain-boundaries. At the intermediate crosshead velocity of 1 inch/min, the honeycomb effect is observed in combination with the striation effect.

These results indicate a change in deformation mechanism with strain-rate and are in qualitative agreement with other results.

4.312 Mechanisms

The proposal of any mechanism or mechanisms for the superplasticity observed in the Zn - 0.4 Al alloy must take into account the following observations.

1. The inhibition of recrystallization and grain-growth by dislocation annihilation on straining the material to greater than 25% elongation.

2. The change in texture and strain ratio r, tending towards isotropy.

3. The transition of the 0.2% proof stress versus grain-size effect from a work-hardening behaviour to superplasticity.

4. Surface observation that grain-boundary sliding takes place.

5. The generation and annihilation of dislocation in order to maintain a dislocation-free structure during deformation.

6. Grain coarsening during deformation.

It is firmly established that during superplasticity, grain-boundary sliding takes place, and plays a major role mechanistically. It has been observed that the contribution of grain-boundary sliding increases with decrease in grain-size (138). It has been found during the creep of large-grain material (typically 100 μm) that steady-state creep rates are obtained under a given set of experimental conditions for grain-sizes differing by more than an order of magnitude; but at smaller grain-sizes the creep rate increases rapidly, due to the increasing amount of grain-boundary sliding. As has been shown in this investigation, a marked change in deformation mechanism occurs at a critical grain-size, and that the resistance at the grain-boundaries collapses and rapid grain-boundary sliding occurs. However, it is apparent that, on purely geometric basis, sliding at the grain interface cannot take place in the absence of any other process, since stress concentration will arise both at the triple points and irregularities or ledges leading to slide hardening (119 - 123). It has been stated that for grain-boundary sliding to occur, there must be accommodation strains in the grain (146); also that sliding cannot exceed 50% of the total strain (143). Therefore, the real question is surely what is the mechanism of grain-boundary sliding?

Lifshitz (83) has correctly pointed out that movement at the grain-boundaries must occur as a natural consequence of diffusional creep, but it is important to recognise that this merely accommodates the grain elongation arising from vacancy diffusion, and it makes no direct contribution to the total strain. Also, models which treat sliding as a Newtonian viscous phenomena appear incapable of accounting for the data obtained under conditions of superplasticity.

Electron microscopy studies of the grain-boundaries has recently led to some important conclusions about the grain-boundary structure and grain-boundary sliding during deformation (Lin and McLean (142), Hale, Ishida, Lin and McLean (147), Ishida and Henderson-Brown (148), Baro, Glieter and Horbogen (149,150) Loberg and Norden (151)). It has been shown that there are only few isolated dislocations in or immediately adjacent to, the grain-boundaries of an annealed unstrained material, but that the dislocation content increases rapidly with increasing strain. Dislocations come into the boundaries from the lattice or are formed in the boundary and thence move into the grains. Glieter et al (150) considered special types of dislocation in the grain-boundary, 'grain-boundary dislocations' which possess non-crystallographic Burgers vectors lying in the plane of the boundary, the dislocation moves in the same way as lattice dislocations. However, Ishida et al (148) and Bell et al (152) state that the dislocations in the grain-boundary retain their crystallographic Burgers vectors. It is suggested that grain-boundary sliding is caused by the movement of these dislocations along the boundary by alternate climb and glide, so that the shear displacement arises from the component of the Burgers vector parallel to the boundary. This statement is based on experimental observations; no splitting of dislocations occurs on reaching the grain-boundary, nor any cases of bowing suggesting possible Frank Read sources in the grain-boundaries. Thus pure glide is not possible but only climb and glide movements. This is a reasonable conclusion in view of the fact that grain-boundary sliding is observed at elevated temperatures. The inference is that the sliding behaviour must be the reflection of the mechanism controlling sliding, and this may or may not be identical with the basic mechanism of sliding.

It has been suggested that because of the linear relationship between grain-boundary sliding and grain deformation under creep conditions in polycrystals and bicrystals, that sliding is uniquely controlled by crystal deformation (146). It is evident that the mechanism controlling sliding must, in particular, exhibit a stress exponent of 2 or strain rate sensitivity of 0.5. Friedel (8), in his deduction of the stress exponent for dislocation climb along grain-boundaries, obtained a value of 2, whilst that for the movement through the intercrystalline barrier to be ≥ 4.5, as observed in creep.

Activation energies obtained in various superplastic metals have been found to be near to the lattice or grain-boundary diffusion values (Chapter 2). The activation energy equal to that for lattice diffusion could be envisaged if vacancies for dislocation climb at the grain-boundaries were predominantly by diffusion through the lattice rather tha along the grain-boundaries. This, however, depends on the test temperature at which grain-boundary diffusion is swamped by lattice diffusion (84).

However, in fine-grain material it would appear that diffusion via the grain-boundaries would be more favourable. In the present investigation no activation energy measurements were made, but an activation energy has been determined by Cook (52), in a very similar alloy (Zn - 0.2% Al) and a value of ~ 10 k cal/mole was obtained a value near to the grain-boundary diffusion value in zinc (14 k cal/mole).

The observation in the present investigation that, during superplasticity, dislocation annihilation occurs, leading to the inhibition of grain-growth suggests that the dislocations are involved in the rearrangement of the grain-boundary structure, lessening the driving force for grain-growth.

It is postulated that dislocations enter the boundaries by slip or climb (148), and once incorporated in the boundaries climb and annihilation can readily occur together with the accommodation of shear displacement and in this way an equilibrium state in the boundary is achieved. A similar suggestion that grain-boundaries act as sinks for dislocations has been proposed by Grabski and Korski (153). They state that for grain-boundaries containing grain-boundary dislocations in a metastable configuration, equilibrium configuration, i.e. change to a 'perfect structure' is achieved by the diffusion and annihilation of certain of the grain-boundary dislocations (grain-boundary recovery).

The observation of grain coarsening during deformation could be explained based on the concept of a metastable grain-boundary dislocation configuration. During a tensile-test under constant crosshead velocities, the strain-rate is constantly decreasing; therefore the structure and the equilibrium grain-boundary structure is to be constantly changing. This statement is supported by the observations of Lindenbergetal (65) and Watt et al (70). Lindinger et al (65) have established in the Ni-Fe-Cr superplastic alloy that the grain-growth rate is directly related to the strain-rate, while Hedworth et al (125) using a constant strain-rate test in the Cu-Al eutectic superplastic alloy observed no grain-growth.

A very similar dependence of strain-rate on the structure is observed during the operation of the dynamic recovery process during the hot working of metals (127). In dynamic recovery sub-grains are formed, the sub-grain size being governed by the strain-rate or temperature. Increasing the temperature has the same effect as decreasing the strain-rate. It has been established that the lower the temperature or higher the strain-rate the smaller the sub-grain-size. However, in these hot working tests the strain rate remains constant and so an equilibrium sub-grain-size is maintained during deformation. There is no reason why a similar relationship cannot exist on superplastic deformation. The structure during superplasticity under decreasing strain-rate will be constantly changing in order to maintain the equilibrium configuration and

consequently grain coarsening is inevitable. Furthermore, it has been inferred that under constant strain-rate conditions, the limiting condition of superplasticity would be reached when the sub-grain size equals the grain size, that is the sub-grain grain size which would have been obtained under similar conditions in a larger grained material.

Deductions from hot working theory involve a dislocation mechanism, and this idea is further supported by the strain-ratio and texture observations. It therefore appears that during the superplastic deformation of this alloy two or more mechanisms may be operating under any given experimental conditions; they may act either sequentially, or non-sequentially. In order to account for the various contributions under different conditions of stresses and temperatures, Hayden (84) has formulated several relationships pertaining to the likely strain-rate contribution by the various operating modes of deformation, diffusion, creep, grain-boundary sliding and dislocation climb/dynamic recovery, which are the mechanisms generally proposed for superplasticity (Chapter 2). Two theories have been formulated for diffusion creep, the first involving volume diffusion (Nabarro - Herring) and other grain-boundary diffusion (Coble - Jones) creep (42-44). The predicted creep rate for the two processes are:

$$\dot{\varepsilon}_{DV} = \frac{\alpha_{DV}\, b^3 \sigma_f}{L^2\, k\, T}$$

and

$$\dot{\varepsilon}_{DB} = \frac{\beta'' D_{gb} b^4 \sigma_f}{L^3\, k\, T}$$

where D_V and D_{gb} are the volume and grain-boundary diffusivity, b the Burgers vector, σ_f the applied stress, L the grain size, k the Boltzmanns constant, T the absolute temperature, α and β are constants usually 10 and 150 respectively.

Therefore the ratio of these two strain-rates should be:

$$\frac{\dot{\varepsilon}_{DB}}{\dot{\varepsilon}_{DV}} = \frac{\beta'' D_{gb}\, b}{\alpha\, D_V\, L}$$

Generally at the lower temperatures (.4 - .65 Tm) this ratio would be greater than unity and hence the grain-boundary path would be dominant and effectively rate controlling. At higher temperatures, the ratio would be less than unity and volume diffusion would be rate controlling.

In the case of grain-boundary sliding occurring, there must be accommodating strains in the neighbouring grain. This is illustrated in Figure 51. For Grain 1 to move a distance δ 1, 2 over Grain 2, there must be a strain in Grain 3. Therefore the rate of displacement ($\dot{\delta}$ 1,2) is proportional to the strain-rate in Grain 3 ($\dot{\gamma}_3$)

$$\dot{\delta}\ 1,2 = K_1\ \dot{\gamma}_3, \quad \text{where } K_1 \text{ is a constant.}$$

If all the boundaries are governed by this relationship, then the average sliding rate $\dot{\delta}$, should be determined by the average grain strain-rate $\dot{\gamma}_G$. If the shear strain-rate from grain-boundary sliding is the displacement rate divided by the average grain size $(\dot{\gamma}_{GBS} = \frac{\dot{\delta}}{L})$, then the equation for grain-boundary sliding strain-rate is:

$$\dot{\gamma}_{GBS} = \frac{K_1}{L}\ \dot{\gamma}^*_G \qquad (13)$$

Thus at any time the overall deformation rate should be the sum of the rates from grain-boundary sliding and grain strain-rate or:

$$\dot{\gamma}_T = \frac{K_1}{L}\ \dot{\gamma}_G = \left(\frac{K_1}{L} + 1\right)\ \dot{\gamma}_G \qquad (14)$$

the average value of K_1 was taken to be 0.22 (139).

It is suggested that since in coarse-grained material there is abundant evidence that the rate of sliding is controlled by the rate of grain deformation (146), there is no reason why a similar trend is not followed in fine grains. Furthermore, in order to take the extreme condition when there is no grain constraint and grain-boundary sliding is a viscous process (K_e - 86,87), the Friedel (8) relationship for the velocity (V) of two grain sliding is:

$$V = D_{gb}\ \frac{\sigma_f\ b^2}{k\ T}$$

Therefore the maximum possible strain-rate from grain-boundary sliding will be:

$$\dot{\gamma}_{GBS\ (Max)} = \frac{V}{L} = \frac{D_{gb}\sigma_f b^2}{L\ k\ T} \qquad (15)$$

* $\dot{\gamma}_G$ represents strain-rate due to grain deformation or dislocation creep (Chapter 2)

So long as equation 13 predicts a strain-rate lower than equation 15 the grain-boundary viscosity plays no part. If, however, equation 13 predicts a faster sliding rate than equation 15 then the rate of sliding should be predicted by equation 15. In this instance

$$\dot{\gamma}_T = \dot{\gamma}_G + \dot{\gamma}_{GBS\ Max}$$

Now for the contribution by grain strain-rate $\dot{\gamma}_G$. Hayden and Brophy (58) developed this contribution of strain-rate based on Weertman's (80) suggestion involving climb controlled motion of edge dislocations or

$$\dot{\gamma}_G = M\ A'\ b\ \frac{V'}{H}$$

where M is the number of active dislocation sources per unit volume, A' is the average cross-section area of a grain, V' is the velocity of climb and H is the distance a dislocation must climb above the plane of a potential dislocation source before the back stress from the dislocation is diminished to the point that a new dislocation may be nucleated.

Following the analysis:

$$M\ A\ b \simeq \frac{b}{L}$$

$$H = \frac{\mu b}{6\pi\ (1 - \nu)\sigma_f}$$

where μ is the shear modulus and ν is the Poisson's ratio.

$$V' = \frac{D_V\ b^2\ \sigma_f}{\ln(L/b)\ k\ T}$$

It is suggested that at intermediate temperatures, the greater flux of vacancies to the dislocation via pipe diffusion rather than via volume diffusion would occur then the velocity of climb becomes:

$$V' = \frac{4\ D_p\ b^3\ \sigma_f}{L\ k\ T}$$

where D_p is the pipe diffusivity.

Therefore at temperature above the transition to pipe diffusivity, the strain-rate due to grain deformation would be:

$$\dot{\gamma}_G = \frac{6\ \bar{\pi}\ (1 - \nu)\ D_V\ b^2\ \sigma_f^2}{L\mu\ \ln\left(\frac{L}{b}\right)\ k\ T} \qquad (16)$$

and below when pipe diffusivity is effective

$$\dot{\gamma}_G = \frac{24\ \bar{\pi}\ (1 - \nu)\ D_p\ b^3\ \sigma^2}{L^2\ \mu\ k\ T} \qquad (17)$$

Thus superplastic deformation is the sum of the separate strain rates of vacancy creep, grain-boundary sliding and dislocation creep. and the various combination have been listed in section 2.8. Figure 52 shows the $\sigma_f - \dot{\epsilon}$ plots determined for both the individual and combined strain-rate contributions superimposed on the experimentally obtained curves. The curve (1) shows the contribution due to only volume diffusion or N-H creep and predicts an m-value of 1 and strain-rates which are about 4 orders of magnitude less. A substantial increase in the strain-rates prediction is obtained when using the grain-boundary diffusion or C-J creep relationship, that is an improvement about 2.4 order of magnitude (2). However, with this improvement the strain-rate is about one order of magnitude lower than experimentally ones, and also is incompatible with the experimental m-value of 0.5. Strain-rates predicted by grain deformation $\dot{\gamma}_G$ (3), the diffusivity path being volume diffusion, though exhibits the appropriate m-value of 0.5, the strain-rate values are four orders of magnitude low. Considerable improvement is achieved if the pipe diffusivity path is considered which brings the curve only one order of magnitude lower with the appropriate m-value (.5) curve (4). However, if the strain-rate contribution due to grain-boundary sliding is added to the grain strain-rate, curves (5) and (6) are obtained. In fact these curves predict the total strain-rate ($\dot{\gamma}_T$) since comparatively the strain-rate contribution due to diffusion creep is negligible. It should be noted that the total strain-rate predicted by the combination of strain-rates of grain strain rate and grain-boundary sliding when volume diffusion is effective, is lower than the strain-rate contribution by grain strain-rate when pipe diffusion is operative. But when the grain-boundary sliding strain-rate with pipe diffusion is added to that due to grain strain-rate, the total strain-rate prediction is about an order of magnitude higher. Therefore, it would appear that the pipe diffusivity path could be effective during grain-boundary sliding coupled with grain deformation. The activation energy observed in the Zn/0.2 Al alloy during superplasticity was 10 k cal/mole, a value near the pipe diffusivity value. A value $^2/_3$ that of volume diffusion suggests either grain-boundary or pipe diffusion, the volume diffusion value for zinc being about 20-22 k cal/mole. The strain-rate prediction on considering grain-boundary sliding to be viscous, curve (7), illustrates that the strain-rates are four orders of magnitude higher with an m-value of 1. Based on these analytical relationships it appears that the rate controlling mechanism responsible for the superplasticity observed in the Zn - 0.4 Al alloy is predominated by a dislocation mechanism. It also suggests that grain-boundary sliding is controlled by a dislocation mechanism, and that deformation within the grains is governing the rate of sliding.

4.400 Conclusions

1. Recrystallization and grain-growth is inhibited by the operation of superplasticity leading to the annihilation of dislocations and the reduction of the driving force.

2. The high degree of superplasticity (m = .5) obtained in the dilute zinc alloy at the relatively low temperature of 0.4 Tm is due to the production of ultra-fine grains of ~ 0.6 μm.

3. Stress-strain curves suggests a steady-state stress during the superplasticity. The maximum flow-stress varies in the plane of the sheet, with the value to rolling being the greatest.

4. The increase in strain-rate sensitivity with strain (.375 → .5) is directly related to the increase in grain size during superplastic deformation. Also the m-value is anisotropic and varies in the plane of the sheet, the 90° direction being the highest.

5. The percentage elongation is dependent on the average m-value for a particular strain-rate path and increases with increase in m-value.

6. The Hall-Petch relationship is obeyed up to a critical grain-size in the range 5-10 μm and below which superplastic mechanisms become effective leading to an opposite effect.

7. The strain ratio $\bar{r}$ and texture changes during straining indicates the tendency towards isotropy and emphasises the importance of a dislocation mechanism.

8. Surface observations show that grain-boundary sliding occurs, and also indicates the difference in the surface and interior behaviour.

9. Grain coarsening occurs during deformation and is dependent on the deformation strain or strain-rate. The grains remain equiaxed after deformation.

10. Transmission electron microscopy shows the negligible presence of dislocations after straining and suggests a mechanism of dislocation annihilation during deformation.

11. The fracture behaviour is directly related to the strain-rate sensitivity parameter, a ductile fracture due to grain-boundary sliding occurring at high m-value (.5), while at the low m-value (.05) a work-hardening type ductile fracture occurs with the precipitate particles acting as possible void initiators.

12. Calculations based on the current models of superplasticity predicts a dislocation model in which the dislocation recovery process operates; also that the grain-boundary sliding which is occurring is controlled by dislocation accommodation within the grains.

CHAPTER 5

5.00 Investigation of the Zn - Al Eutectoid Alloys

5.10 Experimental

5.11 Material

The alloys investigated were supplied by the Imperial Smelting Corporation and were made from high purity (99.99) zinc and commercial purity (99.5) aluminium. The melts were cast into iron moulds. The ingots were then heated above the invariant temperature (275°C) to 375°C for one hour, quenched into water and left at room temperature for one hour before reheating to 250°C and rolling to strips at 35 inch/min. Rolling reductions were approximately 0.025 inch per pass, reheating after every three passes for the first twenty or so reductions, and then every other pass to the final thickness of 0.050 inches. The rolls were preheated to about 100°C and the temperature loss before each reheat was about 15°C. The sheets were then annealed for 5 minutes at 250°C. Table III gives the approximate spectrographic analysis for the various casts of alloys.

Table III

Al	Cd	Cu	Fe	Mg	Pb	Si	V	Zn
20	0.001	0.001	0.03	0.001	0.001	0.01	0.0005	Balance
20	0.001	0.15	0.03	0.001	0.001	0.01	0.0005	Balance
20	0.001	0.50	0.03	0.001	0.001	0.01	0.0005	Balance
20	0.001	1.00	0.03	0.001	0.001	0.01	0.0005	Balance

A 0.15% wt. copper alloy (LZM), produced at the London Zinc Mills by the Hazelett process was also utilized for a number of experiments and for certain other experiments, bar specimens of the straight 80% wt. Zn/20% wt · Al, eutectoid (SP_o) was used. Bars of 1-inch diameter were obtained by extruding cast billets at an extrusion ratio of 10:1 at 250°C. Specimens machined from the bar were homogenized for several hours at 375°C and quenched into iced water, removed from the iced water after eight minutes and allowed to decompose at room temperature for at least a week before testing.

The various grain-sizes were obtained by annealing the sheet in air, followed by room temperature cooling.

5.12 Tensile, Torsion and Camplastometer Tests

Tensile tests were carried out on the Instron tensile testing machine on sheet specimens having a parallel reduced gauge-length of

1.25 inch and 0.50 inch wide. Tests above room temperature were carried out in a Baird and Tatlock air-circulating oven which was modified to fit in the Instron machine and to enclose specimens up to elongations of 1000%. The specimen temperature was measured by clipping or tying a thermocouple to the gauge length and coupling it to a digital voltmeter. The power input to the oven was controlled through a Variac potentiometer and it was found possible to control the temperature within $\pm$ 1.5°C.

In order to assess the temperature variation in the oven along a length, three thermocouples were tied on a 2-inch wide sheet 4 inches apart and the sheet gripped at the two ends. The following were the readings at the top, centre and bottom positions in the oven: 245, 247.5 and 241°C, while at a lower temperature the readings were 161.5, 161.5 and 165°C respectively. Between the top end grip and the load cell, a water cooled jacket was located in order to prevent heating of the load cell. The heating time to 250°C was about 20 to 30 minutes, while to 300°C was about 45 minutes.

For tests below room temperature, a rig was constructed as shown in Figure 53. Ice in water and dry ice (solid CO_2) in acetone were used to obtain the temperatures of 3-5°C and -75°C respectively. Temperature measurement was made by positioning the bulb of a thermometer at the midpoint of the gauge length. The tensile specimen had a gauge length of 1.25 inch and 0.50 inch wide and 7 inch total length, and the length of the specimen ensured that the gauge length was well immersed in the coolant and reduced the rate of loss of temperature through the grips, which were at room temperature. Fracture at the centre of the gauge length was an indication that the temperature was reasonably constant along the gauge length. Tensile tests were also carried out at 20°, 150° and 250°C on a certain number of bar specimens (SP_o) of the Hounsfield No. 14 type, and true stress (σ) and true strain (ε) curves were determined from the standard constant volume relationship.

Torsion tests were done on bar specimens (SP_o) having the dimensions shown in Figure 54. The tests were done on a torsion testing machine at the Swinden Laboratories, BSC, at strain-rates between 3.9×10^{0} and 1.5×10^{2} min^{-1}. A thermocouple was tied to the specimen and the complete specimen including the grip ends was enclosed in the furnace. The specimens were in the furnace for 15 minutes before testing and soon after failure, the specimens were removed and quenched in water. The temperature control at 250°C was within $\pm$ 1.5°C.

The torque (τ) and numbers-of-revolution (γ) data was recorded on an X-Y recorder. From the τ - γ curves the true stress (σ) and true strain (ε) curves were obtained from the following established relationships (163-165):

$$\sigma = \frac{3 + m}{2\pi R^3} \checkmark 3\tau$$

and

$$\varepsilon = \frac{R\,\theta}{L} \Big/ \sqrt{3}\ ,$$

where m is the strain-rate sensitivity, R and L the radius and gauge length of the specimen and the θ the angle of twist in radians (1 rev = 2 $\overline{\Lambda}$ radians).

In order to obtain strain-rates in the range 2.7×10^2 and 4×10^3 min^{-1} cylindrical compression specimens (SP_o) 0.5 inch in diameter and 0.5 inch in length were tested on a Camplastometer at the Port Talbot Research Centre, BSC.

The temperature was controlled between $\pm 2^oC$, and the load-displacement data was recorded on a X-Y recorder. The true stress (σ) and true strain (ε) were determined from the relationships:

$$\sigma = \frac{P}{A_o}\ (\frac{\ell}{A_o})$$

and

$$\varepsilon = \ln\ (\frac{\ell_o}{\ell})$$

where A_o is the cross-sectional area, ℓ_o and ℓ the original and final lengths.

5.13 Preparation of Thin Foils for Transmission Electron Microscopy.

An identical technique stated in section 4.109 was employed but using different chemical thinning and electro-polishing solutions.

For chemical thinning a 50-70% solution of hydrochloric acid in water was used. It was found that during thinning a passive layer tended to build up on the surface. However, if this became excessive it could be removed by a quick dip in concentrated nitric acid.

Electro-polishing was carried out in a solution of 15% perchloric acid in methanol at a temperature of -70^oC, a solution previously used successfully by other workers (40,45,55). Figure 55 shows the plot of voltage against milliamps, where a reasonable polishing plateau, between 15-20 volts, is present. The cooling was achieved by immersing the beaker containing the solution in a larger beaker which contained dry ice in acetone. Specimens were removed immediately after polished areas were observed, (and perforations) and washed in the dry ice/acetone bath followed by washing in ethanol. To obtain the best results the specimens were examined within a few hours of polishing.

Grain size measurements were done by the linear intercept method, negative of the thin foils and at least five plates were measured across 20-30 grains at at least 20 measurements were made from which an average was taken and is quoted as the grain-size.

5.14 Optical Microscopy

Specimens were mounted in the room temperature setting "Plastic Padding" and polished on 600 grade emery paper followed by polishing on the rotating, diamond-impregnated wheels in the usual manner. The etchant used was a mixture of 2 to 5% Nital. It was found exceedingly difficult to obtain scratch-free surfaces for examination at x 1000 magnifications.

5.20 Results

5.21 The Effect of Temperature (T) on the Flow Stress (σ_f)

The σ_f values here quoted were determined from the peak load obtained from single tensile tests for the temperature range -75 to 300°C. In the case of the low-temperature tests (-75°C), the maximum load to fracture was used to calculate the σ_f values. In the case of the two larger-grain material (1.75 and 3.25 μm) yield points were recorded. The effect of two factors, i.e. copper content up to 1 % wt and grain-sizes (0.55, 1.05, 1.75 and 3.25 μm) at three crosshead velocities (0.1, 1 and 20 inch/min) were considered on the σ_f - T relationships. Figures 56 – 59 show the σ_f - T behaviour for alloys with copper additions of 0.15, 0.5 and 1 % wt and covering the various grain-sizes and crosshead velocities. The initial strain-rates are indicated against each of the crosshead velocities. The marked decrease in σ_f with increasing temperature up to 250°C in the four grain-size alloys is quite apparent. The addition of copper has the effect of markedly increasing the σ_f values up to 150°C, the σ_f values increasing with copper content. However, with further increase in temperature up to 300°C, the difference in σ_f becomes negligible. At 20°C and the crosshead velocity of 0.1 inch/min the σ_f values obtained for the 0.55 μm grain-size alloys were 17.5×10^3 lbs/in^2 (0% Cu), 31×10^3 lbs/in^2 (0.15% Cu), 33.5×10^3 lbs/in^2 (0.5% Cu) and 40.5×10^3 lbs/in^2 (1% Cu) while that at 150°C were 1.3×10^3 lbs/in^2 (0% Cu) 2×10^3 lbs/in^2 (0.15% Cu), 2×10^3 lbs/in^2 (0.5% Cu) and 3×10^3 lbs/in^2 (1% Cu). Thus there is no marked effect of copper on σ_f at 150°C and increasing the grain-size to 3.25 μm does not alter this trend greatly. At 250°C most of the alloys exhibit the minimum σ_f value, the exception being for grain-size greater than 0.55 μm and particularly at the highest crosshead velocity (Figure 57c, 58b, 58c, 59c) in which case σ_f decreased up to 300°C). The effect of increasing the crosshead velocity is to further increase the σ_f values, with the effect of copper on the σ_f being maintained. However, at the higher-temperature end, σ_f increases by a greater factor with increase in velocity compared to room temperature, this effect being more pronounced the smaller the grain-size (Figures 60-62). As an example, in the 0 % wt copper alloy, the σ_f at 20°C is increased from 17.5×10^3 lbs/in^2 at 0.1 inch/min to 49.5×10^3 lbs/in^2 at 20 inch/min, while at 250°C σ_f increases from 1.3×10^3 lbs/in^2 at 0.1 inch/min to 12 lbs/in^2 at 20 inch/min, an increase of three and nine times respective, (Figure 60a).

The effect of increasing grain-size from 0.55 to 3.25 μm has a similar effect of increasing the σ_f for the entire temperature range.

Figures 63 to 65 summarizes the effect of crosshead velocity from 0.1 to 20 inch/min and grain sizes from 0.55 to 3.25 μm on σ_f for all the alloys.

The σ_f - T relationship was now determined for an alloy containing 1 % wt copper but having a non-superplastic structure that is, a lamellar structure, compared to the fine-grained equiaxed superplastic structure. Specimens were heated to 350°C for 20 hours and furnace cooled in order to obtain the lamellar structure. Figure 66 shows the effect on σ_f with increasing temperature. The rate of decrease of σ_f with increasing temperature is not so marked as in the case of the equiaxed structure alloy and no minimum σ_f at 250°C is obtained. However at the low temperature end the σ_f values are lower than the finer grained equiaxed structure alloys.

In order to establish the form of σ_f in the equiaxed structure alloy in the region of 275°, the invariant temperature, two grain-size specimens (1.05, 1.75 μm) were heated through the transformation temperature while the specimens were being strained. The temperature of the specimen was continuously recorded with time on an X-Y voltage/time recorder. Since the load-extension (time) was also being recorded at a relatively slow speed of 0.2 inch/min it was possible to plot true-stress (σ) against increasing temperature. Figure 67 shows the curves obtained for the two grain-size alloys. Apparently the stress decreases to a minimum value in the region 290 - 300°C and then increases markedly with further increase in temperature.

A similar experiment was done on a specimen having a lamellar structure and Figure 68 shows the σ - T plot. A marked difference in behaviour is observed. There is no sudden increase in σ, it merely decreases steadily with decreasing temperature.

5.22 Flow stress (σ), Strain-rate Sensitivity (m) and Strain-rate ($\dot{\varepsilon}$) Relationships.

In order to establish the effect of copper content and grain size on the σ_f - $\dot{\varepsilon}$ and m - $\dot{\varepsilon}$ behaviour for the various alloys the Backofen et al step method (section 4.104) was used for the temperature range 20 - 300°C and strain-rate range of 4×10^{-3} to 4×10^{0} min^{-1}. Figures 69-71 shows the effect of increasing the copper content (0 → .15 → 1%) and grain-sizes (0.55, 1.05, 1.75 and 3.25 μm) on the semilog plot of m - $\dot{\varepsilon}$. It is evident that the m-value varies with strain-rate and temperature. The effect of decreasing the temperature from 250°C to 20°C is to move the peak m-value region to lower strain-rates while at the same time the m-value is reduced, e.g. for the 0% wt copper alloy and the grain-size of 0.55 μm (Figure 69a) the m-value reduces from about 0.6 (peak) at 250°C to 0.24 (peak) at 20°C.

A very similar behaviour is observed for the same grain-size in the 0.15 and 1 % wt copper alloy (Figures 70a and 71a) though the effect of increasing copper is to further decrease the peak m-value

once below the temperature of 150°C, e.g. at 100°C, the maximum m for the 0, 0.15 and 1 % wt copper alloy are about 0.4, 0.32 and 0.3, while at 20°C the m (peaks) are 0.24, 0.18 and 0.16. Also, a noticeable feature of m - $\dot{\varepsilon}$ for this grain-size is that for temperatures greater than 100°C and less than 250°C, the three-region, dome-shaped curve is not observed, while at lower temperatures the dome is observed with the m - $\dot{\varepsilon}$ curves moving to the lower $\dot{\varepsilon}$ end (Figures 69a, 70a and 71a). Furthermore, the marked difference in m-values at the higher $\dot{\varepsilon}$ end due to increasing temperature is markedly reduced at the lower $\dot{\varepsilon}$ end, e.g. for the 0 % wt copper alloy the m-value at 250° and 20° at $\dot{\varepsilon} = 2 \times 10^{0}$ min^{-1} is about 0.6 and 0.1 while at $\dot{\varepsilon} = 1 \times 10^{-2}$ min^{-1} the m-value is 0.275 and 0.2 respectively.

Increasing the grain-size up to 3.25 μm effects the peak m-value position, the peak m-value for the entire temperature range of 20 - 250°C moves to the lower $\dot{\varepsilon}$ end, the larger the grain-size the greater is the shift to the lower $\dot{\varepsilon}$ end (Figure 69-71). No marked change in the peak m-value is observed with increasing grain-size at temperatures greater than 150°C, though for the 0 % wt copper alloy (Figures 69 a-d), a slight decrease in m-value (peak) is observed, while in the 0.15 and 1 % wt copper alloy there is a slight increase. However, at the temperatures of 100° and 150°C there is an increase in the m-value (peak) with increasing grain-size, e.g. for the 0.15 % wt copper alloy, the m-value (peak) at 100° and 150°C for the four grain-sizes of 0.55, 1.05, 1.75, and 3.25 μm are 0.31, 0.36, 0.37, 0.34 and 0.4, 0.475, 0.45, 0.5 respectively.

At the lower temperature of 50 and 20°C, increasing the grain-size markedly decreases the overall m-value with increasing copper content (Figures 70 a-d and 71 a-d).

Thus, the overall effect in all the alloys of increasing the grain-size is to decrease the m-value at the higher $\dot{\varepsilon}$ end, while increasing it at the lower $\dot{\varepsilon}$ end for the temperature greater than 100°C.

The various effects of strain-rate and grain-size on the m-value for the temperature range 20 - 250°C in the 0 % wt copper alloy are summarized in Figure 72 a-d.

The m - $\dot{\varepsilon}$ curves at 300°C were only done for the finest-grain alloys. Figures 69a, 70a and 71a shows a complete reversal of the m - $\dot{\varepsilon}$ behaviour, i.e. m → 0.5 at the lower $\dot{\varepsilon}$ end while m → .2 at the higher $\dot{\varepsilon}$ end.

The m - $\dot{\varepsilon}$ curves were also obtained for a 1 % wt copper alloy having a lamellar structure for the temperature range 100 - 300°C (Figure 73). The highest m-value obtained is at the lower $\dot{\varepsilon}$ end while at the higher $\dot{\varepsilon}$ end it is very much lower, e.g. for the 0.55 μm equiaxed grains size alloy (Figure 69a), at 250°C and $\dot{\varepsilon} = 10^{0}$ min^{-1}, m = 0.55 while for the lamellar structure it is

only 0.17. At the lower $\dot{\varepsilon}$ end (10^{-2} min^{-1}) m = 0.3 for both the equiaxed and lamellar structure. However, increasing the grain-size of the equiaxed structure increases the m-value, even at the lower strain-rate end.

From these results corresponding log-log plots of σ_f vs $\dot{\varepsilon}$ were made and these are shown in Figures 74 - 76. The tangent drawn at a particular strain-rate on the σ_f - $\dot{\varepsilon}$ curve corresponds to a particular m-value on the m - $\dot{\varepsilon}$ curve. It is quite apparent that the m-value is constantly changing with strain-rate in all the alloys, and confirms the m-value variations evident in the m - $\dot{\varepsilon}$ curves. Another feature brought out by these curves is the exhibiting of the three-stage behaviour (Section 2.3). In the 0.55 μm grain-size alloys stages 2 and 3 are observed at 20 and 50°C while stages 1 and 2 are observed for the temperatures 150, 200 and 250°C. The effect of copper additions and grain-size naturally increases the σ_f values for the entire strain-rate and temperature range. A notable feature with increasing grain-size from 0.55 to 3.25 μm is the gradual changeover from stages 1 and 2 to 2 and 3 at 250°C. The various effects of strain-rate, grain-size, copper content and temperature on σ_f conforms to the σ_f - T relationship followed in the previous section.

Also, σ_f - $\dot{\varepsilon}$ curves were obtained for a lamellar structure for the temperature range 100 - 300°C (Figure 77). The notable feature is the much higher σ_f values compared to the σ_f values obtained even for the largest, equiaxed grain-size material. The m - $\dot{\varepsilon}$ and σ_f - T curves for the lamellar structure for temperatures below 100°C could not be obtained by the step-method due to the lack of ductility.

In order to varify the reliability of the σ_f values obtained by the step-method, these values were compared with the σ_f values obtained from the single tensile tests. For the 0.55 and 1.05 μm alloys the σ_f values obtained by the two methods are virtually identical, though at the lower temperatures and the higher strain-rates, the values obtained by the step-method were slightly higher (Figures 74a, 74b, 75a, 75b, 76a and 76b). In the case of the 1.75 μm grain-size alloys, the σ_f values determined by the step-method are considerably higher for the 20 and 50°C temperatures and also at higher strain-rates. For the 3.25 μm grain-size alloys, the σ_f values determined by the step-method at 100°C are higher over the entire strain-rate range.

The macroscopic effect of strain-rate and grain-size on tensile test pieces is shown in Figure 78 and 79. Figure 78 shows the effect of increasing crosshead velocity on the elongation for the 0.55 μm grain-size material at a temperature of 200°C. The specimen strained at the crosshead velocity of 20 inch/min exhibits a virtually neck-free elongation (> 800%) and failure has not occurred up to the maximum elongation possible on the tensile machine employed. On decreasing the crosshead speed to 5 inch/min, necking and the decrease in elongation is evident. Further decrease in crosshead velocity to 2 inch/min shows a further decrease in elongation with marked necking.

Similarly the effect of increasing grain-size on elongation at 200°C and at a fixed crosshead velocity of 20 inch/min is shown in Figure 79. The 0.55 μm grain-size specimen exhibits the highest neck-free elongation (> 800%). Increasing the grain-size to 1.05 μm, the elongation (480%) is markedly decreased coupled with the onset of conventional necking behaviour. On further increase in grain-size to 1.75 and 3.25 μm, the elongations drop to 70% and 60% respectively.

In order to determine the $\sigma_f - \dot{\varepsilon}$ behaviour over as wide a strain-rate range as possible, the $\sigma_f - \dot{\varepsilon}$ values obtained by tensile, hot torsion and camplastometer tests for the specimen (SP_o) were plotted on a log-log scale in a single figure (Figure 80). No camplastometer tests were done at 150°C. A good fit of all the results is obtained at 250°C which exhibits the three $\sigma_f - \dot{\varepsilon}$ regions. It is apparent that the overall strain-rate sensitivity, (m) is the slope of the tangent at any point on the curve is about 0.5 in the $\dot{\varepsilon}$ range 10^{o} min^{-1} to 8×10^{-1} min^{-1} and then reduces markedly at higher strain-rate levels. In order to assess the strain-rate sensitivity of the material in the region of the torsion strain-rates, a log-log plot of torque against number of revolutions was made and Figure 81 shows that, though the straight lines does not pass exactly through the three points obtained, an m-value of about 0.55 is obtained. The peak torque values rather than the steady-state values are converted to stress, as this was the procedure adopted for the tensile results. Figure 82 shows the torque revolution (stress-strain) curves, and exhibits the effect of strain-rate and temperature. The curves at 150° and 250° show a rapid initial rise, followed by a levelling off to a steady value which is independent of the number of revolutions to failure. The strain to peak stress appears to increase with increasing strain-rate.

5.23 Flow Stress (σ_f), Grain-size (L) and Strain-rate ($\dot{\varepsilon}$) Relationships

In order to obtain the σ_f - L relationships covering the temperature range -75° to 250°C, the copper-free alloy only was considered. σ_f values for various constant strain-rates were obtained from the $\sigma_f - \dot{\varepsilon}$ curves for the four grain-sizes from Figures 74 a-d, and plots of σ_f versus L were done for a range of constant strain-rates for the temperature range 20 - 250°C (Figure 83 a-g). The slope of the curves are indicated adjacent to each curve. Between the constant strain-rate of 10^{-2} to 10^{o} min^{-1} and temperature range 250°C - 100°C, the slope increases from about 0.6 to 1. At 50°C and 20°C, the slopes at the constant $\dot{\varepsilon}$ of 10^{-2} min^{-1} was about 0.9 At the higher strain-rates and lower temperatures, a decrease in the slope occurs, while at 50 and 20°C the change in behaviour is indicated by the change in the sign of the slope.

A plot of σ_f - L at -75° from σ_f values obtained from single tensile tests (5.21) shows a complete reversal of the σ_f - L behaviour (Figure 83g).

Plots of $\dot{\varepsilon}$ versus L at constant stresses were also done from the σ_f - $\dot{\varepsilon}$ curves for the temperature range 250 - 20°C (Figures 84 a-f) and the best straight line was drawn through the points obtained. The slopes of the curves at each temperature were nearly constant and the values are indicated against each figure. The slope at 250°C is 1.8, while with decrease in temperature the slope increases till at 20°C it is about 3.

5.24 Activation Energy (Q) Measurements

In order to determine the activation energy, the generally accepted relationship between stress, temperature and strain-rate, at low stresses, obtained as a power relationship and used in creep and hot working (127) was employed.

$$\dot{\varepsilon} \alpha A^1 \sigma^{n^1} \exp\left(\frac{-Q}{RT}\right) \quad \ldots\ldots\ldots (18)$$

where A^1 and n^1 are temperature independent constants and R the gas constant.

In superplasticity the relationship between flow stress and strain-rate is $\sigma_f = K \dot{\varepsilon}^m$ (Section 2.3)

or

$$\dot{\varepsilon} \alpha \sigma_f^{\frac{1}{m}} \quad \ldots\ldots\ldots\ldots\ldots (19)$$

therefore equation (18) can be written as $\dot{\varepsilon} \alpha \sigma^{\frac{1}{m}} \exp\left(\frac{-Q}{RT}\right)$,

where

$$n^1 = \frac{1}{m}$$

Thus the slope of the semilog Arrehenius plot of $\dot{\varepsilon}$ versus $1/T$ will give the activation energy. The plots of $\dot{\varepsilon}$ - $1/T$ were done at several constant stresses, the values being obtained from the σ_f - $\dot{\varepsilon}$ curves in Figure 74-76 for the four grain sizes and different copper content alloys and covering the temperature range 250°C to 150°C. The constant stress values were chosen so that they covered different regions of the multistage σ_f - $\dot{\varepsilon}$ regions. Figures 85-87 shows the plots and the Q-values are indicated against each curve.

In the three 0.55 μm grain-size alloys, the activation energy increases by about 20-30% on decreasing the stress from 4000 lbs/in^2 to 700 lbs/in^2, that is, from about 13-14 k cal/mole to 20-22 k cal/mole. The only noticeable effect is the slight increase in Q-value with increasing copper content, i.e. from 13 to 14 k cal/mole at 4000 lbs/in^2 and 20 to 22 k cal/mole at 700 lbs/in^2.

On increasing the grain-size up to 3.25 μm a similar trend is observed, that is, lower Q-values at the higher stresses. However, on comparing the Q-values obtained at a particular stress level in the four grain-size materials, it is found that the Q-value increases and then decreases for the largest grain-size material, e.g. 0 % wt Cu - 16 → 17.9 → 16.5, 0.15 % wt Cu - 16.2 → 19.1 → 18.5 → 17.6, 1 % wt Cu - 15.9 → 20 → 22.4 → 21.1 k cal/mole.

In certain cases a fourth point is included in the Figures representing the values for 100°C. However, in most of the cases this point did not appear to fall on the straight line drawn through the points for the higher temperatures. A similar plot of $\dot{\varepsilon}$ $-^{1}/_{T}$ was done for the alloy (1 % wt copper) but having a lamellar structure. Figure 88 shows that a Q-value of 23.5 k cal/mole is obtained for a constant value of 13000 lbs/in^2.

It is estimated that an error of about ± 5% can be introduced in these Q-value determinations.

In order to correlate the activation energy with the m-value, the m-values were obtained from the m - $\dot{\varepsilon}$ curves (Figures 69) for the appropriate constant stress values for each point on the $\dot{\varepsilon}$ - $^{1}/_{T}$ curves. However, since the m-value varies with strain-rate, average m-values were determined for each of the curves. Thus a plot of average 'm' against Q was done for the 0% copper alloy covering the four grain-sizes (Figure 89). A marked decrease in m-value is accompanied by a substantial increase in activation energy in the material having the smaller grain-sizes of 0.55 and 1.05 μm. In the case of the 1.75 and 3.25 μm grain-sizes the behaviour is not so clear, though it appears that there is a very slight increase in the m-value with the activation energy.

5.25 Tensile Stress (σ), Strain (ε) and Strain-rate ($\dot{\varepsilon}$) Relationships

In a constant-crosshead-velocity tensile test, the increase in strain is accompanied by a decrease in strain-rate and consequently a change in stress. Thus from a single tensile test two relationships can be obtained, that is, the change in stress with increasing strain and change in stress with decreasing strain-rate.

Stress-strain curves were obtained for the alloy composition (1 % wt copper) and the four grain-sizes (0.55, 1.05, 1.75 and 3.25 μm) for the various crosshead velocities at a temperature of 250°C.

Figures 90 a-d shows the effect of crosshead velocities for the different grain-sizes. The flow-stress-sensitivity is indicated by the increase in stress with increase in crosshead velocity. For the 0.55 μm grain-size, near steady-state stresses are observed at the lower velocities, while at the higher velocities a marked decrease in stress with strain is observed as the velocity is increased. Increasing the grain-size up to 3.25 μm further increases the rate of decrease in stress with increasing grain size.

From the results which were used to obtain the $\sigma - \varepsilon$ curves, $\sigma - \dot{\varepsilon}$ curves were obtained by plotting the constantly-changing stress with decreasing strain-rate. Figure 91 shows the plot for the four grain-size materials. Specimens were strained up to about 150% elongation so that the final strain-rate of the higher velocity test would overlap with the initial strain-rate for the lower velocity tests. It is apparent that the curves do not follow a continuous $\sigma - \dot{\varepsilon}$ path and the form changes with grain-size and crosshead velocity. Basically three types of curve are observed. Though types A and B exhibit decreasing stress with strain-rate, the slope at points on the curves is initially high and decreases with decreasing strain-rate for type A, while the slope increases with decreasing strain-rate for type B. Type C which is observed for the 0.55 and 1.05 μm grain-size material for the lower crosshead velocity is a mirror-image of Type B; the initial slope is negative and high and decreases with decreasing strain-rate.

5.26 Microstructures

5.261 Fracture

In a tensile test, extensive necking takes place leading to a change in the stress state and thus in the deformation behaviour in this region, compared to a region well removed from the neck. Fractured specimens of grain-sizes 1.05, 1.75 and 3.25 μm obtained from tensile tests at 20 inch/min crosshead velocity and at the temperatures of 20, 150 and 250°C were sectioned longitudinally and examined.

Figure 92a shows the structures observed in the three grain-sized material strained at 250°C and the crosshead velocity of 20 inch/min. No difference in structure, either at the fracture edge or well away from it is observed in the 1.05 and 1.75 μm grain-size material, but in the 3.25 μm grain-size material elongated grains are observed at the fracture edge. The unetched surface near the edge also revealed extensive cavitation.

On decreasing the temperature of testing to 150°C, grain-elongation at the fracture edge is observed both in the 1.75 and 3.25 μm grain-size material (Figure 92b). With a further decrease in temperature to 20°C, grain elongation at the fracture edge was observed in all the three grain-size materials (Figure 92c).

The approximate elongation values at fracture are listed against each of the micrographs.

5.262 Effect of Strain and Strain-rate on the Microstructure

In order to examine the effect of strain on the microstructure an LZM, 0.55 μm grain-size and 1-inch wide specimen was electro-chemically grid marked and strained at 250°C at a crosshead velocity

20 inch/min (Figure 93). The grid marking enabled regions to be obtained from a single tensile test specimen which had deformed different amounts due to the necking effect and yet introduced a constant time at temperature factor. Also the initial strain-rate was the same for all the regions, though the final strain-rate would of course decrease with increasing strain.

Strain-rate variation effect on microstructure was obtained by straining specimens in a similar manner but at different initial strain-rates corresponding to crosshead velocities of 0.2 and 2 inch/min. After deformation specimens were immediately removed from the oven and cooled. Figure 94 shows the transmission electron micrograph of the starting sheet. There is evidence of slight directionality and the interphase and like-phase grain-boundaries are straight. The two phases were easily identifiable, since the difference in their transparency to electrons due to composition far outweighed that due to orientation. Diffraction analysis confirmed that the lighter grains were the aluminium rich α-phase, while the darker grains were the zinc-rich β-phase. Similar identifications have been made by other authors (45,47).

Figures 95 a-c shows the microstructures of the grips ends and regions strained to 100 and 300% elongation at the crosshead velocity of 0.2 inch/min. Higher elongations were not attempted at this velocity as extensive grain-growth would occur due to the time at temperature effect and mask the effect of deformation upon the structure. All the microstructures examined showed an absence of dislocations. However, other significant observations were made. The grip ends showed that grain-growth had taken place due to the time at temperature though the grain-boundaries remained relatively straight and sharp, with the grains still exhibiting directionality.

After 100% elongation, this directionality is not strong and a certain degree of rounding of the interphase boundaries is evident (Figure 95b). At higher magnification certain observations were made which strongly indicated that diffusional processes were operating. Figure 95b (X 51,000) shows a rounded β-phase (dark) (A) in the α-phase (light). Also a large β-phase (B) appears to have been just cut off from the main body of a β-phase grain.

After 300% elongation similar observations are made but to a greater extent. Though the general appearance of the structure is equiaxed, at higher magnification certain odd shaped and elongated grains in both the phases are observed (Figure 95c). Figure 95 c (X 30,000) shows the marked roundings of the interphase boundaries. The extraordinary way in which a small rounded β-phase (A) (dark) is "suspended" is the α-phase (light) is also observed while the β-phases appears to be in the process of being pinched off. At this elongation coarsening of the strained structure relative to the grip ends was evident.

TABLE IV

Initial Grain Size = L_i = 0.55 ± .025 μm

Crosshead velocity in/min	% elongation	Grain size (L_s) μm	Time (t) at temperate for the final elongation mm	$L_s - L_o$	$\frac{1}{2}\frac{L_s - L_o}{t}$
20	Grip ends (L_o)	.73	5		
	100	.76		.03	.03
	300	.79		.06	.06
	550	.96		.23	.23
	900	1.17		.44	.44
	~2500	~1.30			
2	Grip ends (L_o)	.78	5		
	100	.88		.1	.01
	300	1.0		.22	.022
	550	1.15		.37	.037
	900	1.28		.50	.05
.2	Grip ends (L_o)	.89	30		
	100	1.04		.15	.0025
	300	1.27		.38	.0063

Similarly, observations are made at the higher crosshead velocities of 2 and 20 inch/min, though the diffusional effect is greatly increased with strain (Figures 96 and 97). Figure 96 shows the effect of elongation on the microstructure at the crosshead velocity of 2 inch/min. There is more evidence of the diffusion of the β-phase into the α-phase, with suspended β-phase in the α-phase as shown in Figures 96 b-d. Position A in the Figures shows the possible points where the β-phase is diffusing through the α-phase and cutting it off. At one point figure 96c (X 12,000) position B it appears that the β-phase, while diffusing into the α-phase, possibly through a grain-boundary, is being pinched off by the α-phase, or it could be that the β-phase is diffusing via a grain-boundary into the main body of the α-phase.

Figures 97 a-d shows the structures observed at the highest velocity of 20 inch/min. Some diffusional points of the β-phase into the α-phase are indicated (A). The diffusion of the β-phase via α-phase grain-boundaries is observed clearly in certain instances, e.g. position B, Figure 97d (X 30,000). Figure 79d (X 19,500) shows an example of what might be several grains of the α-phase being cut off at various places by diffusion of the β-phase from either side. However, on observation at lower magnification the general appearance of the structure is equiaxed (Figure 98).

In general it can be said that, the greater the strain, particularly for the two higher velocities, a greater amount of diffusion appears to be taking place. Also, grain coarsening increases with strain for each of the specimens strained at the three different speeds.

In order to isolate the effect of strain-rate and strain on grain-coarsening, grain-size measurements were made. Table IV lists the average sizes for the various deformed regions of specimens strained at the crosshead velocities of 0.2, 2.0 and 20 inch/min. Figure 99 shows a plot of grain-size versus elongation, after subtracting the grain-growth due to time at temperature, for the two velocities. Though a greater amount of grain-growth with strain occurs at the lower velocity, the grain-growth rate is higher for the specimen strained at 20 inch/min.

Also included under this section are the electron micrographs of the specimen strained at even higher strain-rates ($\dot{\varepsilon} = 10^{1}$ min^{-1}) in torsion at the temperatures of 150° and 250°C. At these high strain-rates and high strains, diffusion appears to be even more marked, as shown in Figures 100 and 101. Even at 150°C there is evidence of enhanced diffusion. A greater amount of spherical β-phase in the α-phase due to enhanced diffusion, should also be noted. Also in certain α-phase grains particularly at 150°C there was evidence of dislocation entanglements (Figure 100). Furthermore, straining at both the temperatures of 150 and 250°C has caused grain coarsening in both the centre and edge regions of the diametrical cross-section of the torsion specimen. Grain-growth due to time at temperature effects has taken place in the grip ends, though a greater amount of coarsening has occurred in the strained regions (Figure 102).

5.263 Effect of Grain-Size

The three larger grain sizes (1.05, 1.75 and 3.25 μm) strained to fracture at the crosshead velocity of 20 inch/min at the optimum superplastic temperature of 250°C were examined from the specimens used in obtaining the σ_f values shown in Figures 56b-d.

Figures 103a shows an example of the very sharp and straight grain-boundaries that were present in the undeformed 1.05 μm grain-size alloys.

Figure 103b shows the structure of the same material after about 800% elongation. The most striking changes are similar to those described in the previous section, that is, rounded interphase boundaries and diffusional effects. Note also the absence of dislocations.

In the alloy having the grain-size of 1.75 μm there is still evidence of rounding of the interphase boundaries, i.e. evidence for diffusion activity, (Figure 103c X 30,000). However, an additional observation is the presence of dislocations (Figure 103c X 60,000). In the largest grain-size (3.25 μm), material no marked rounding of the grain boundaries was observed while extensive dislocation networks and entanglement was present (Figure 103d). Dislocations were mainly seen in the α-phase.

5.264 Lamellar Structure Alloys

The structure of an equiaxed specimen (0.55 μm grain-size) heated to 300°C and then strained - in order to determine the σ_f value in the σ_f - T curve (Figure 104) was now examined. Figure 104, (X 19,500) shows that the time at 300°C (~ 45 minutes) was not sufficient to ensure that the entire structure was lamellar before straining. Although the greater proportion of the thin foil examined exhibited a lamellar structure, certain regions did show untransformed or partially transformed equiaxed grains. On examination of a region of the lamellar structure certain significant features are observed (Figure 104, X 60,000). The α-phase (light) is cut at several positions by the diffusion of the β-phase (dark). Also a great deal of spherical β-phase are suspended in the α-phase and at various points (positions marked A) spherical β-phase particles are connected to the main body of the β-phase, i.e. not quite fully imbedded in the α-phase.

In order to see whether the actual deformation was responsible for the cutting of the α-phase a specimen with a true lamellar structure, obtained by heating to 350°C for 20 hours and then cooling in the furnance, was strained to fracture (≃ 150%) at 250°C at a crosshead velocity of 20 inch/min. The fully transformed structure was still evident after deformation, but a significant feature was the diffusion of the β-phase into the α-phase. (Figure 105, position marked A).

5.27 Creep Tests

Creep tests at a constant load (stress = 5000 lbs/in^2) were done at room temperature and at 70^{o}C on the standard creep testing machine.* Figure 106 and 107 show plots of the percentage plastic strain versus time for the different grain-sizes and copper contents. The secondary creep rate is given against each curve. The effect of increasing the copper content upto 1 % wt. copper in the 0.55 μm grain-size material decreases the room temperature creep rate from 2.4%/hr to 0.02 %/hr, an increase in creep resistance by a factor of about 120. On increasing the grain-size to 1.05 μm, the creep rate for the copper free alloy is 0.18 %/hr, while for the 1 % wt copper alloy is 0.0056 %/hr. an increase in creep resistance by a factor of 310. Thus the overall gain in creep resistance at room temperature on increasing the grain size to 1.05 μm and adding 1 % wt copper is by a factor of 427. On further increasing the grain-size to 1.75 μm, the creep rate in the copper free alloy decreases to 0.046 %/hr while that in the 0.15% and 1.0 wt % copper alloys decreases to 0.0043 %/hr and 0.002 %/hr respectively.

Therefore on using the maximum benefit of grain-size (1.75 μm) and copper content (1% wt), an overall gain in the creep resistance at room temperature, of 1200 times can be obtained.

On increasing the temperature from room temperature to 70^{o}C, the secondary creep rate in the copper-free 0.55 μm grain-size material increases from 2.4%/hr to 57.3 %/hr. Increasing the copper content to 1 % wt in this grain-size material, the creep rate falls to a value of 2 %/hr, a decrease in creep-rate by a factor of 29 times. The maximum creep resistance is obtained in the 1 % wt copper alloy with a grain-size of 1.75 μm which exhibits a secondary creep rate of 0.133 %/hr, a total gain on the 0.55 μm and % wt copper alloy by a factor of about 440.

Figure 108 shows the log-log plot of the creep rate against grain size for the different alloy composition.

5.28 Pressure Forming

A standardized test, free bulging, developed by the Imperial Smelting Corporation, was done to assess the formability of the various sheet by free bulging of flat sheets through a circular die. The sheet, about 6 inches square, was clamped by a split-die 3.25 inch in diameter (Figure 109). The tooling with the sheet clamped was inserted in furnace at 250^{o}C and a pressure of 1 atmosphere was applied from one end to blow up the sheet. The temperature was monitored with a thermometer near the sheet and a probe touching the pole of the bulge indicated the height of the bulge. Sheets were bulged to a height of 1.17 inch, this representing an approximate 50% increase in surface area; this criteria has been used previously (167).

* Emec - G35C

Figure 110 shows the bulge height versus time curve for the three grain-sizes (0.55, 1.05 and 1.75 μm) with no copper content and 0.15 and 1.0 wt % copper contents.

The general trend is that the addition of copper does not have any effect on the forming time in the 0.55 μm grain-size material. However, increasing the grain-size to 1.05 μm, a marked increase in forming time is observed in the two copper alloys, with negligible increase in time in the copper free alloy. Increasing the grain size to 1.75 μm, the forming time is markedly reduced for all the alloys, the time increasing further in the two copper-containing alloys. A surprising observation is the slightly higher forming times exhibited for the three grain-sizes of the 0.15 % wt copper-containing alloy over the 1.0 % wt copper alloy.

5.30 Discussion

5.31 The Effect of Temperature (T) on the Flow Stress (σ_f)

One of the main commercial requirements in a superplastic alloy component is a high σ_f at the operating temperature coupled with a very low σ_f at the superplastic or forming temperature. In the present alloy these two temperature ranges would be between 20 - 70°C and 200 - 260°C. Thus, ideally, the requirement for the σ_f - T behaviour would be the retention or negligible decrease of the room temperature σ_f value up to a temperature of 100°C followed by a marked decrease in σ_f till at 250°C, the value is very low, i.e. a 'knee' in the σ_f - T curve.

The need for this type of behaviour is illustrated in the copper-free, finest grain-size, eutectoid (Figure 56a), where with only a slight increase in temperature above room temperature, a drastic decrease in σ_f occurs. One method of improving σ_f with increasing temperature has been shown by Ball et al (45) and by Nuttall (40) by increasing the grain-size. Ball et al showed the σ_f - T behaviour for the grain-size range of 1.1 to 4.5 μm covering the temperature range -175° to 250°C, at a crosshead velocity of .002 inch/min. It was shown that a crossover temperature (0°C) was obtained above which σ_f increased with increasing grain-size and temperature, while below this, σ_f increased with decreasing grain size and temperature. Nuttall (40) showed a similar effect for the grain size-range of 0.57 to 1.60 μm and covered the temperature range 80° - 260°C and the strain-rate range of 0.0046 to 1.1 min^{-1}, also showing the marked increase in σ_f with increasing strain-rate.

In the present investigation, the increase of σ_f in the temperature range 20 to 150°C is brought about by (1) increasing the grain-size and (2) by the addition of copper up to 1% wt. The addition of copper markedly improves the σ_f, particularly up to 150°C, and at the same time, virtually no effect is noticed at 250°C. The increase in σ_f on adding copper is due to a solute hardening effect, as the copper remains in solution at room temperature (the mechanisms of solute hardening are the raising of the yield stress, the introduction of friction stress and the intensification of strain hardening (166)).

Increasing the grain-size showed that a further marked improvement in σ_f could be obtained between the temperature range 20 - 70°C, that is, the knee of the σ_f - T curve moves to the higher temperature end. However, it was evident that there was a certain grain-size above which the σ_f would in fact be lower at room temperature and at lower temperatures but with further increase in temperature the σ_f value becomes higher (Figure 63a). A further complication in the σ_f - T behaviour with grain-size is the effect of the crosshead velocity. Increasing the crosshead velocity further moves the knee of the σ_f - T to the higher temperature end, and thus, in effect, can show improved σ_f - T behaviour (Figures 60-62).

Though increasing the grain-size can give desirable σ_f values at room temperature it markedly alters the forming properties at 200-250°C, as is shown in Figure 79. The three important criteria here are (1) lower stresses at the (2) highest possible strain-rate coupled with the (3) highest degree of superplasticity (m-value). This is clear from Figure 63c. At 20 inch/min and at 250°C, increasing the grain-size from 0.55 to 3.25 μm increases the σ_f from about 3.5×10^3 lbs/in^2 to about 15×10^3 lbs/in^2. The second factor, which deteriorates with this increase in grain-size, is the decrease of the m-value from about 0.6 for the 0.55 μm grain-size to less than 0.2 for the 3.25 μm grain-size also at the crosshead velocity of 20 inch/min or $\dot{\varepsilon} = 10^1$ min^{-1} (Figures 69 a-d). Thus σ_f is controlled by the cumulative effects of grain-size, copper additions and strain-rate.

All the σ_f - T determinations were continued past the invarient temperature up to 300°C, and the σ_f values obtained at this temperature are joined to the σ_f at 250°C. However, this continuation of the σ_f - T curve to 300°C is not justified as has been shown in Figure 67, where the σ_f changes during the transformation were monitored. The low σ_f value obtained at about 290°C indicates that transformation superplasticity (m = 1) contributes, or takes over, before a major proportion of the lamellar structure is introduced, and superplasticity is destroyed.

On comparing this behaviour with an alloy which initially had the lamellar structure, obviously no sudden drop in σ_f value would be expected, and this is shown in Figure 68. However, on consideration of the value of σ_f at temperatures greater than 300°C, it appears that the value indicated by equiaxed → lamellar could very well be increasing with temperature for equiaxed regions, while in the lamellar regions σ_f is decreasing. These two opposing changes can be resolved by considering that in the equiaxed structure the volume of material not transformed can also undergo substantial coarsening, this also increases the σ_f value. Figure 104 which shows coarsened, untransformed grains on heating to 300°C supports the above statement.

5.32 Flow Stress (σ_f), Strain-Rate Sensitivity (m) and Strain-Rate ($\dot{\varepsilon}$) Relationships

The Backofen et al (20) step-method was sensitive enough to detect the small changes in the m-value with changing strain-rate (Figures 69-71). There have been criticisms of this method (124-126) and Stowell et al (57) have stated that errors as high as ± 15% can be introduced. However, m = 0.6 measured in this work corresponds well with values obtained previously in a similar alloy (20,35).

It is important to maintain the highest possible m-value at the highest possible strain-rate, and it has been shown that the addition of 1% wt copper does not alter this parameter at 250°C; this is in qualitative agreement with the negligible effect observed on the σ_f values. The effect of decreasing the temperature on the m-values with the peak m-value moving to the lower strain-rate end and decreasing are typical observations in superplastic metals (Section 2.3). However, at temperature below 150°C, the effect of copper is shown by the decrease in m-value, particularly at room temperature, i.e. for the 0.55 μm alloy the addition of 1% wt copper reduces the m-value ($\dot{\varepsilon} = 10^{-1}$ min) from .24 to .18, while for the grain-size of 1.75 μm the m-value ($\dot{\varepsilon} = 10^{-2}$ min^{-1}) decreases from .125 to .065. This observation supports the effect of copper additions on increasing σ_f.

The high m-values at room temperature compared to those measured in normal work-hardening materials ($m < 0.05$) should be noted, as the m-value can be taken as a parameter to give a rough indication of the creep resistance of a material.

The effect of increasing the grain-size is similar to that established in superplastic metals (Section 2.3), that is, the peak in m-value moves to the lower strain-rates. However the slight increase in m-value (peak) that accompanies this movement to the lower strain-rate end is not clearly exhibited at 250°C, since the peak region is not covered for the 0.55 and 1.05 μm grain-size material. However, at 200°C, the m-values are within 0.05 and no particular trend is followed, though Holt (29) has shown that at 250°C and covering the grain-size range of 0.5 to 1.8 μm an increase of 0.05 in (peak) m-value occurs.

The existence of the three regions (Figure 2) is verified both by the $m - \dot{\varepsilon}$ and $\sigma_f - \dot{\varepsilon}$ relationship. Though the strain-rate range covered was not sufficient to bring out the three regions at one particular temperature, the change over from stage 2 and 3 at room temperature to 1 and 2 at 250°C is substantial evidence. Also this multi-stage behaviour is confirmed by using higher strain-rates by the torsion and camplastometer tests (Figure 80). There have been suggestions by Nuttall (40), in his investigation of a copper free alloy of grain-size 0.5 μm at 250°C, that the m-value remains constant (0.5) for four orders of strain-rate between 10^{-3} to 10^{0} min^{-1}. However, the present results on the alloy with a very similar grain-size does not support this conclusion (Figures 69a, 70a and 71a). The elongation values (Figure 78) also support the change in m-value between the strain-rate range 1.54×10^{1} min^{-1} to 1.54×10^{0} min^{-1}, but this could be fortuitous due to grain coarsening effects (Figure 98). However, after 900% elongation the final grain-size obtained at 2 and 20 inch/min is about 1.2 μm, it finally becomes a constant factor on the elongation values.

Therefore, it would appear that though the σ_f - $\dot{\varepsilon}$ curve can differentiate the three-stage regions and give average m-values operating in these regions, it is unable to detect small changes in the m-value with strain-rate. This is illustrated in Figure 74a where the average slope of the curve has been determined and at the temperature of 250°C the slope predicts an m-value of 0.5 between the strain-rate 10^{o} to > 10^{1} min^{-1} while the m - $\dot{\varepsilon}$ curve and elongation values do not support this.

Further support for the step-method as a way of obtaining the actual σ_f - $\dot{\varepsilon}$ behaviour, is shown by the good agreement obtained between the σ_f values obtained by this method and those obtained by the single tensile tests, (Figures 74-76). The significant point is that at high m-values, i.e. > 0.2, reasonable correlation exists between the σ_f values by the two methods, while at m-values lower than 0.2, work-hardening effects come into operation and therefore particularly at the higher strain-rate end (m < .1) a marked increase in σ_f value will be obtained by the step-method (Figures 74c-d, 75c-d, 76a-d).

5.33 Flow Stress (σ_f), Grain-Size (L) and Strain-Rate ($\dot{\varepsilon}$) Relationships

The relationships $\sigma_f \alpha L^a$ and $\dot{\varepsilon} \alpha L^{-b}$ can be used to predict the possible mechanism operating. In the relationship $\sigma_f \alpha L^a$, the a-values at 250°C have been shown by Holt (29) in a similar alloy to vary with strain-rate and to increase from about 0.7 at 10^{-4} min^{-1} to 1.2 at 10^{-1} min^{-1}. In the present investigation an a-value of 0.6 is obtained at 10^{-2} min^{-1} and 1.0 at 10^{o} min^{-1}. A similar a-value of 1.0 at 1.2 x 10^{o} min^{-1} has also been observed by Nuttall (40). Furthermore, Nuttall has shown that with a decrease in temperature to 150°C, the a-value decreases to 0.5, but does not appear to be strain-rate dependent. In the present work the σ_f - L^a relationship has been covered to a temperature as low as -75°C and it is apparent that the a-value is strain-rate dependent at all temperatures. At 150°C, the a-value is 0.77 at 10^{-2} and increases to 0.9 at 10^{o} min^{-1}.

The variation of the a-value with strain-rate, particularly at the higher temperatures, is appropriate since it has been shown that the strain-rate sensitivity change is associated with the change in a-value. An a-value of 1 has been associated with the possible mechanism of superplasticity as a = 1 is consistent with the highest average m-value (20,29). However, a decrease to a = 0.6 does not mean that some superplastic mechanism will not be operating, but it would appear that a change in mechanism might take place.

The non-linearity of the σ_f - L curves at the higher strain-rates at 250°C and lower temperatures indicates a change to a work-hardening behaviour, as is exhibited by the reversed σ_f - L relationship at -75°C.

The relationship $\dot{\varepsilon} \alpha \frac{1}{L^b}$ where b = 2 at 250°C and independent of stress has been observed in a similar alloy by Ball et al (45) and by Nuttall (40). In the present case a b-value of 1.8 is obtained at 250°C which increases to about 3 at 20°C, the values exhibiting no marked stress-dependency. This variation in b appears appropriate and is consistent with the decrease in the m-value with temperature. The prediction of b = 2 and b = 3 suggests that volume and grain-boundary diffusion respectively will be operating (Section 2.8). However, though no dependency of stress is clearly exhibited at any particular temperature, it would appear that the change in m-value at the various stress-values should produce a change in the slope.

The operation of grain-boundary diffusion (b = 3) at lower temperatures is consistent with the prediction by Hayden (84) that grain-boundary diffusion should be effective at lower temperature between 0.45 - 0.65 Tm, while at higher temperature volume diffusion (b = 2) will take over. In the present case, 250°C is 0.74 Tm while 50°C is ~ 0.43 Tm: thus the increase in the b-value with decrease in temperature is explicable on this model.

5.34 Activation Energy (Q) Measurements

Uncertainty exists as to the thermal contribution responsible for superplasticity in the Zn-Al eutectoid and activation energy values from 15 to 35 k cal/mole have been recorded in the temperature range 260 - 150°C (40,45-47). However, an omission in previous investigations is the possible effect of strain-rate sensitivity on the activation energy, has not been considered, even though the m-value varies with stress and strain-rate.

In hot working of normal large-grained materials it has been shown that the activation energy is uniquely dependent on the deformation mechanism operating (127) and that a Q-value close to the lattice diffusion value is indicative of the operation of dynamic recovery, while a value higher than the lattice diffusion by about 50 - 80% is indicative of dynamic recrystallization. In creep also it has been established that during the operation of recovery processes by sub-grain formation, activation energies close to lattice diffusion values are found (138). However, in creep the m-value does not vary a great deal and is usually in the region of 0.25 to 0.16 while in hot-working the m-value is usually 0.2. In superplasticity the situation is complicated by the variation in m-value from 0.2 to 0.8.

The present results show that the m-value varies with Q-value and that at the higher stresses where the highest m-values exist, a Q-value of 13-14 k cal/mole is obtained, a value close to the grain-boundary diffusion value for zinc. Furthermore, with decreasing stress and m-value the Q-value increases, till a value near 20 k cal/mole is obtained, a value close to the lattice diffusion value

for zinc. Furthermore, the Q-value is grain-size dependent, and for a particular stress level, the Q-value increases with increasing grain-size or decreasing m-value (Figures 85-87). This dependence of the grain-size and stress equivalent to the effect of m-value on the Q-value has not been previously reported in this alloy. However, Lee et al (24) have observed an increase in Q-value with decreasing stress in the Ti - 2Al - 2.5 Sn alloy attributing this to some structural change. Thus, the range of Q-values obtained by previous workers in this alloy is not surprising since no consideration was given to the possible effects of stress, grain-size and consequently the m-value on their results.

A Q-value of 14 k cal/mole in the superplastic region, as exhibited by the $\sigma_f - \dot{\varepsilon}$ curves, predicts that the mechanism is controlled by the diffusion of zinc via grain-boundaries. The rate of diffusion along grain-boundaries is several orders of magnitude greater than the rate through the lattice, while enhanced diffusion which can occur by 'short circuiting' through high-diffusivity dislocation pipes must not be forgotten, and the Q-values for grain-boundary diffusion and pipe diffusion have been said to be the same by Gibbs et al (168) for different metals.

Since the diffusion of aluminium at 250°C is slower than that of zinc at 250°C, and linking this with the measured Q-values, it is apparent that the diffusional flow of the zinc-rich phase is more significant. The change in Q-value with stress or strain-rate and the increase to the lattice diffusion value at the low stress or strain-rate end of $\sigma_f - \dot{\varepsilon}$ (stage 1), substantiates the change in the deformation process as indicated by the σ_f-$\dot{\varepsilon}$ relationship. These experimentally obtained Q-values are consistent with Hayden's (84) prediction that at low stresses lattice diffusion will be effective while at high stresses the controlling diffusivity mode will be either via the grain-boundaries or dislocation pipes or both.

5.35 Tensile Stress (σ), Strain (ε) and Strain-Rate ($\dot{\varepsilon}$) Behaviour.

The stress-strain behaviour of a superplastic metal in tensile testing is complicated by the fact that the strain-rate is continuously decreasing with increasing strain. This continuous decrease in strain-rate consequently affects the m and σ_f behaviour. In addition to this strain-rate factor, grain-growth occurs continuously with strain and increasing strain-rate. In this alloy grain-growth is induced firstly by the time at temperature effects and secondly due to both increasing strain and strain-rate effect (Table IV, Figures 98,99). Straining a sheet with the initial grain-size of 0.55 μm at 250°C, the grain-size after 100% elongation is found to increase to about 0.88 μm at 2 in/min and to about 0.76 min at 20 in/min.

To interpret a σ - ε curve under these conditions is difficult, since one has to consider the influence of decreasing strain-rate and increasing grain-size and so one can obtain a range of σ - ε curves of varying shapes, depending on the counter effects of these two changing parameters (decreasing the stress).

The complexity of the stress behaviour under a uniaxial tensile test can be clearly illustrated by the σ - $\dot{\varepsilon}$ curves obtained from the σ - ε curves (Figure 90,91).

In a superplastic metal, the σ_f - $\dot{\varepsilon}$ behaviour covers three stages as described in Chapter 1 and so under fixed conditions of temperature and structure this relationship should be adhered to with changing strain-rate. However, as seen in Figure 91 this behaviour is not observed and a visual inspection of the change in slope is not compatible with the general σ_f - $\dot{\varepsilon}$ relationship. Also, at the low crosshead velocity and for the finer two grain sizes of 0.55 and 1.05 μm material, negative slopes are obtained due to increasing stress with decreasing strain-rate. Three "characteristic" σ - $\dot{\varepsilon}$ curves (A, B, C) can be obtained (Figure 91). Curve A shows that though the stress decreases with decreasing strain-rate the change in slope decreases with decreasing strain-rate. The source will be due to the grain-size increase and work-hardening processes of dislocation interaction but since in the large-grained material grain-growth will be minimal, work-hardening due to dislocation interactions should be the main source.

In curve C, the stress increases with decreasing strain-rate, this being inconsistent with the σ_f - $\dot{\varepsilon}$ behaviour of superplastic metals. However, the effect of increasing stress becomes more effective at the lower velocities in the finer grain-size materials. The reason for this behaviour lies in the considerable grain-growth that will take place due to increasing strain and time-at-temperature; the time-at-temperature effect increasing with decreasing crosshead velocities. Table IV shows that at the crosshead velocity of 2 inch/min the grain-size increases from 0.55 μm to 0.88 μm after an elongation of 100%. Therefore, it is apparent that with increase in grain-size the increasing stress effect is superimposed on the expected decreasing stress type curve and at the lower velocities the hardening effect due to larger grains is dominant. Type B curve appears to be merely an intermediate type balancing the two stress effects.

Similar types of σ - $\dot{\varepsilon}$ relationship have been observed by Fields et al (169). Type A was referred to a strain-rate softening effect while type C a strain-rate hardening effect. No interpretation of these effects were discussed based on the change in structural morphology.

Naziri et al (1), based on their work on c.p. zinc, predicted that under constant strain-rate condition, the $\sigma - \varepsilon$ behaviour should exhibit a steady state stress during superplasticity. The hot torsion test on the Zn - Al eutectoid exhibited this behaviour (Figure 82).

The shape of the stress-strain curve, i.e. the variation in the peak stress before a steady state is reached, has been said to be dependent on the material, and the subsequent deformation mechanism operating. Hardwick et al (128) have suggested that the peak in the torque/revolution curve is associated with the operation of a restoration process and the peak height is an indication of the ease with which restoration can occur. For aluminium, for example, which has a high stacking fault energy and where deformation climb is rapid, a small peak, if any is observed (dynamic recovery). On the other hand in copper with a low stacking fault energy, dislocation climb is slow, dynamic recrystallization operates and a marked peak is observed. On the other hand Stuwe (170) has shown that a marked peak can occur under conditions of dynamic recovery; and he concluded that dynamic recrystallization is unlikely under hot working conditions. Another significant factor which could alter the peak stress would be any temperature rise, caused by deformation at these high strain-rates (171), and any conclusion concerning the type of restoration mechanism operating based on the peak behaviour would not be generally accepted. Microstructural examination showed that grain coarsening had taken place, and it could be concluded that this was strain-induced, (Figures 101, 102). However, it is difficult to expalin the existence of the steady-state region if one considers that grain coarsening would increase with strain, which would consequently increase the stress. In hot torsion of normal large-grained material in which restoration occurs by dynamic recovery, a constant subgrain size is obtained for a particular temperature and strain-rate, it has been stated that the subgrains are formed before or at the start of the steady-state region and during subsequent deformation the subgrain size is maintained (127). A similar process could be envisaged in a superplastic metal, where, if the grain-size was too fine, then subgrains will not form and the grain-size will grow to the critical size.

5.36 Microstructural

5.361 Fracture

In polycrystalline materials under creep conditions the weakest links are the grain-boundaries and consequently failure occurs as a result of nucleation, growth and coalescence of grain-boundary voids. However, in superplastic metals, by the operation of rapid recovery processes it has been possible to arrest any growth and coalescence of voids at the grain-boundaries thus leading to exceptionally high ductilities. It appears therefore that fracture is a rather complex process depending on the stress distribution, work-

hardening characteristics, and plastic deformation associated with the crack process and also the stresses in the vicinity of the crack tip.

Under tensile testing and in a ductile material, after necking has commenced, all the deformation in the final stages is concentrated around the necking area. In the necked region, the state of stress is not simple tension but one of hydrostatic tension superimposed on the nominal tensile stress.

In normal ductile material distorted grains are observed at the tip prior to final failure and intragranular dislocation and work-hardening effects are responsible for grain distortion (160). In the present case the prominent parameter governing the deformation process in the necked region will be the strain-rate sensitivity. Work-hardening behaviour can be induced at all grain-sizes at 20°C, where m is less than 0.2 and this leads to elongated grains at the fracture tip and an equiaxed structure in the remainder of the specimen (Figure 92c). Obviously, the 'weakest' links in these materials are the grain-boundaries where cracks will be nucleated The clearest indication of the effect of the strain-rate sensitivity parameter is indicated in the fracture tips of the various grain sizes at 150°C, (Figure 92b). The operative m-values for the three grain-sizes 1.05, 1.75 and 3.25 μm are in the region of > 0.2, ~ 0.1 and < 0.05. The presence and degree of grain deformation in the 1.75 and 3.25 μm grain-size materials, indicates the operation of the work-hardening process and lack of accommodation by superplasticity mechanisms. In the case of the 1.05 μm grain-size, in which m > 0.2, the importance of structural inhomogeneties probably become more significant due to anti-superplastic effect at fracture regions reducing the m-value and fracture untraced due to stress concentration. In general, for m < 0.15, grain deformation by a dislocation mechanism operates, leading to grain-deformation and eventual stress concentrations probably at the grainboundaries, while at m ≥ .3 the superplasticity mechanisms relieves any work-hardening effects leading to grain deformation, and thus no deformed grains are observed at the fracture tip, though stress concentration at a local inhomogenity can lead to a marked decrease in m also to cause deformation by a dislocation mechanism before final fracture.

5.362 Effect of Deformation on Structures

Several previous investigations of the surface by means of a marker displacement technique has shown that grain-boundary sliding occurs readily in this alloy. It has been observed that the interphase boundaries become rounded and the grains are equiaxed, while the internal structure is generally free of dislocations. These observations have also been made in this alloy. Most of the authors observed that grain growth had occurred during deformation, though Packer et al (47) state that no coarsening takes place in the Zn - Al eutectoid. Grain growth has been found to occur

in most of the superplastic alloys and Lindinger et al (65) has shown that in the Fe - Gr.-Ni system the growth rate is linearly related to the strain-rate and increases with increasing strain-rate, though Watts et al (70) has found that in the Al/Cu Al_2 eutectic grain growth was only due to a time-at-temperature effect.

In the present investigation it has been shown unequivocally that over and above the grain-growth that occurs due to the time-at-temperature effect, grain-growth occurs and increases with strain or strain-rate or both.

The observations of the internal structure for dislocations by thin foil transmission electron microscopy is dubious, since, if the hot-worked material is held at the deformation temperature for some time prior to cooling, or if cooling is very slow, then the high temperature structure is not retained and significant structural changes can occur (145,172). Time in the region of 1 second for cooling have been shown to arrest the actual deformation process in the high-stacking-fault energy aluminium, but for a low stacking fault energy alloy the time-lag to 'freeze' the deformation structure can be considerably increased, (172).

The only quenching after stopping deformation has been carried out by Lee et al (154) on the Zn - Al eutectoid alloy and these authors showed that sub-boundaries and subgrains are readily observed in the α-phase at strains of 450% elongation and so in the present work, delays of up to 5 minutes before cooling to room temperature could easily have removed any dislocation structure present.

The observation that the grains remain equiaxed was found not to be strictly true, particularly at high strains and strain-rates (Figures 94-98, 100,101), and these fresh observations need an explanation. The significant microstructural features observed were the formation and isolation of both the α and β phases, particularly the α-phase, the formation of small β-spheroids and the penetration of the α-phase grain-boundaries by the β-phase.

This evidence of the diffusivity of both the α and β-phase is supported by the activation energy measurements, which predict the possibility of grain-boundary diffusion and dislocation pipe diffusion (165). Furthermore, diffusion in metals can always be enhanced by plastic deformation to some degree, due to rapid diffusion short-circuiting along dislocations, grain-boundaries or even cracks produced in the deformation (173). In order to produce significantly large enhancements by any of these mechanisms, the number of excess atomic jumps caused either by the motion of the excess point defects in the lattice or by the fast atomic jumping rate along short circuiting paths must be significant compared to the number of atomic jumps occurring in the lattice during ordinary state equilibrium.

Figure 97d (X 30,000) shows the evidence for the diffusion of the β-phase into the α-phase grain-boundary. It is observed that a neck exists with the β-phase spreading sideways into the α-phase grains. It is accepted that the rate of diffusion along the grain-boundaries may be several orders of magnitude greater than the rate through the lattice. It has been stated by McLean and Reed-Hill (158,173) that a diffusing substance will not usually penetrate much further along the grain-boundary than through the lattice for the reason that, where the diffusing substance has to travel along a boundary, it will diffuse sideways into the still pure grains adjoining the boundary. In this way the boundary may supply a thickness of crystal on each side much greater than its own extremely small width. However, it would appear that if the grain-boundary length is short, as is the case in fine-grained superplastic metals, the diffusing material can cut off the two adjoining grains as would seem to be occurring (Figures 96d (x) 30,000 (A), 96e (A) and 97b (A). On the other hand if the grainboundary length is too long, the phase in the boundary could eventually be 'pinched off' by the slower diffusing phase from either side (Figure 96c (B)). However, observations are also made where the β-phasesare pinched and suspended in the α-phase in the form of spheroids. Figure 95b (X 51,000) shows two 'pinched off' large β-phase particles; whether diffusion has taken place via the β-phase boundary is not clear. A further remarkable observation is the formation of a small β-phase spheroid as shown in Figure 95c (X 30,000). The only feasible explanation for this appears to be the existence of a high diffusivity path due to a dislocation. However, enhanced diffusivity effects are observed with increasing strain-rate and Figures 100 and 101 show the spheroidization of α and β-phases particularly the β-phase, observed in specimens after hot torsion at 150 and 250°C. Even at 150°C, the high strain-rate used appears to have accelerated or enhanced diffusion. Optical micrographs confirms that the strain is responsible for the grain-growth (Figure 102).

The observation of rounding interphase boundaries and 'pinching off' of the Cu Al_2 phase by the aluminium has been observed by Stowell et al (57) in the Al/Cu Al_2 eutectic after superplastic deformation. These authors suggested that grain-boundary grooving of the Cu Al_2 grain-boundaries occurred by the diffusion of aluminium and its eventual division. Furthermore, under a normal tensile stress, the equilibrium vacancy concentration at the Cu Al_2 grain-boundary is increased, and these vacancies will flow (probably via grain-boundary) to the Al/Cu Al_2 interfaces and diffusion currents will be most intense in the vicinity of the grain-boundary cusps. Vacancies in the Cu Al_2 lattice will probably diffuse along internal boundary and in the interface boundaries to give the shape change depicted in Figure 111.

Possibly a very similar diffusional effect due to deformation and concurrent hot-working is the accelerated spheroidization observed in pearlitic steels. One suggestion for this accelerated spheroidization by Robbins et al (174) is that the formation of excess vacancies during plastic deformation (plastic deformation may create lattice vacancies, such as by the motion of jogged screw dislocations).

could then enhance carbon diffusion by the formation of carbon vacancy complexes and also iron diffusion by increasing the number of sites for diffusion. Another suggestion was that the rate-controlling mechanism was the enhanced diffusion of iron in the ferrite due to the introduction of large angle sub-boundaries in the ferrite brought about by dynamic recovery. These boundaries could then provide short circuiting paths for the diffusion and "pinching-off" the lamella . This second mechanism was later shown to be the controlling process by Chojnowski et al (175) in a pearlitic steel and also found to be true in the case of a Cu/Cu Al_2 eutectic lamellar alloy, as shown by Butcher et al (176). In the Cu/Cu Al_2 alloy, spheroidization occurred during hot tensile testing and 'indented' and 'p nched' regions were found in both the phases. A fine polygonal structure was observed across the Cu Al_2 phase and was believed to be high angle boundaries through which diffusion had occurred.

Similar observations were made in the present investigation in a lamellar structure, Zn - Al eutectoid alloy, confirmed the occurrence of spheroidization (Figure 105). Furthermore, it is clear that the β-phase is the most active diffusing material due to higher percentage of 'indented' or 'pinched off' α-phase, and this substantiates the observations made in the equiaxed structure that the β-phase is the more active phase.

5.37 Mechanisms

Any mechanism accounting for the superplastic deformation in the alloy investigated must explain the experimental dependence of strain-rate sensitivity and stress on the strain-rate, grain-size, temperature and microstructural observations.

Previous work has supported three prominent mechanisms operating, diffusional creep, grain-boundary sliding and dynamic recovery. The operation of any of these mechanisms must be examined on the basis of the relationship obtained in the present alloy at the superplastic strain-rate:

$$\dot{\varepsilon} = A \sigma^2 D_{gb}/L^2$$

In vacancy creep mechanisms, in the form of either lattice or volume diffusion and grain-boundary diffusion are invoked, in order to explain the observed experimental data several inadequacies appear. The prediction of a linear relationship between stress and strain-rate ($\varepsilon\alpha\sigma$), a strain-rate sensitivity of unity and the difficulty of reconciling general observed equiaxed grains after large elongations makes all of these improbable as the rate controlling mechanism. However, as the microstructural evidence and activation energy measurements have illustrated, it does play an important role in the deformation.

Figure 112 shows the predicted strain-rate values by both volume and grain-boundary diffusion and the values are one order of magnitude on either side of the experimentally-observed curve (curves 1 and 2). The observation that volume diffusion is effective at the low strain-rate end while grain-boundary diffusion is effective at the superplastic strain-rate end substantiates the activation energy values at these two strain-rates. However, the strain-rate and stress dependence on the grain-size obtained were two and one respectfully, while the ideal values for volume and grain-boundary diffusion to be completely operative are two and three respectively.

The diffusional observations give credence to the operation of grain-boundary sliding as put forward by Lifshitz (83), Backofen et al (26) and Gifkins et al (82).

However, the support for a dislocation recovery mechanism as rate controlling also requires the operation of diffusional processes and that recovery leads inevitably to grain-boundary sliding has been shown by the experimental observations in Zn - 0.4% wt Al, in the last chapter, and this view has been put forward by several authors for this particular alloy (45,56,76,154). Figure 112 (curves 3,4,5 and 6) shows the strain-rate prediction by a dislocation recovery/grain-boundary sliding and dislocation recovery/grain-boundary sliding/diffusional creep as put forward by Hayden (84) and explained in Sections 2.8 and 4.312. It illustrates that in order to obtain the right order of strain-rate sensitivity at the appropriate strain-rate level a combination of deformation processes must be considered. In the present allow it is shown that diffusional processes will inherently operate at the temperature of deformation (0.74 Tm). However, the necessity of a high concentration of point defects for both volume and grain-boundary diffusion and consequently leading to spheroidization via grain-boundaries, sub-boundaries and dislocation short-circuiting paths suggests the operation of a dislocation recovery process. Lee et al (154) have shown the direct evidence of quenched in sub-grains and sub-boundaries to occur in the α-phase in this alloy. The specimen examined had a grain-size of 1.5 μm and was examined after 450% elongation at 250°C obtained at the strain-rate of 2×10^{-1} min^{-1}. Similar observation of sub-structure formation have been observed by Ball et al (45) in both the α and β phase, the specimen grain-size was 2.5 μm and was strained to 80% elongation at 250°C at the strain-rate of $\dot{\varepsilon} = .5 \times 10^{-1}$ min^{-1}. However, in the present case the starting grain-size was only 0.55 μm, the specimen being strained to various elongations at 250°C and 1.5×10 min^{-1} and probably coupled with the conditions of tensile testing the probability of observing any dislocations would be rare.

Under hot working condition in normal metals in which dynamic recovery has been established to occur the sub-grain size is found to be uniquely dependent on the temperature and strain-rate of deformation, and it has been shown that the stress obtained by any combination of temperature and strain-rate is empirically related to sub-grain size formed by the relation (127).

$$\sigma = k L^{-1/2}$$

where k is a constant.

Thus in the case of aluminium for a stress value of 4000 lb/inch as observed for the 0.55 μm grain-size at 1.5×10^{-1} min^{-1} (20 inch/min) a sub-grain size of about 2 μm is predicted.

In the case of the larger grain-size investigated in this work, i.e. 1.05 and 1.75 μm, the predicted sub-grain size would be about 1.5 and 0.7 μm. However, this estimation has not taken into consideration the marked grain-growth that takes place and particularly the increased grain-sizes obtained at higher strains and strain-rates. Thus for the 0.55 μm grain-size specimen strained at 1.5×10^{-1} min^{-1} (20 inch/min), the grain-size after 300% elongation, the grain-size increases to 0.8 μm and after ~ 2000% elongation the grain-size is ~ 1.3 μm. Similarly in the specimen strained at 1.5 min^{-1} (2 inch/min) after 100% elongation the grain-size is ~ 0.8 μm while after 900% elongation it is ~ 1.3 μm. Thus the effect of increasing grain-size is to increase the stress value in the $\sigma = k L^{-1/2}$ relationship and consequently predicts markedly smaller sub-grain sizes. Another factor which might have an effect on the stress value is the dcreasing strain-rate with strain and which will offset the increase in stress due to increasing grain-size. However, the observation in the 1.75 and 3.25 μm grain-size material under identical conditions of temperature and strain-rate dislocation entanglement and substructure formation lends support to a dislocation based mechanism, (Figure 103).

No microstructural observation could be made at the low strain-rate end, stage 1 (Figure 1) when the m-value again decreases. The difficulty is the marked grain-growth effect masking any structure observations. However, the activation energy measurement indicates that volume diffusion comes into effect. The suggestion that in fact this stage is non-existent once σ_o (Bingham Stress) is taken into account (Section 2.3) still needs clarification as to the source (66). Johnson (11) has suggested a glide/viscous drag creep in this strain-rate range. The grain coarsening as could very well be inevitable when sub-grains are not formed and in large grained superplastic alloys in which substructures are formed grain coarsening will probably not be due to deformation.

Nuttall (40) has stated that if a dislocation mechanism is operative and grain elongation occurs, to eliminate directionality and continuously maintain an equiaxed structure grain spheroidization must take place.

The recent geometrical model of McLean (143) based on the glide and climb of grain-boundary dislocations with boundary diffusion with the retention of equiaxed structure may well be that has been

proposed, provided it is assumed that grain-deformation is inevitable and the boundaries thus can act as both donors and absorbers of dislocations. The sequence of events is depicted in Figure 113. The dislocations shown in the AD and CD boundaries glide towards the triple junction ACD, and then move, main by climb, along the AC boundary. At the triple junction ABC the climbing dislocation splits again into its components which move, mainly by glide this time, along the AB and BC boundaries; proceeding in this way they can travel large distances in continuous matter. As the dislocations climb along AC, material is fed to this boundary from the adjoining boundaries such as AD and CD; thus, diffusion creep occurs in the direction indicated by the curved arrows and in consequence grains B and D approach each other. These events occurring repeatedly brings grain B and D into contact, when grain-boundary tension equilibrium will cause the grains to adjust to configuration in Figure 113b. Other boundaries such as AD and EB take over the role of AC, so eventually grain D and E come into contact and there is again a readjustment. The repetition of this sequence can continue the large extension until the specimen is a few grains across.

5.38 Creep Tests

The creep resistance in the present alloy has been brought about by two methods, that is, by solid solution alloying which is well established (138) and by increasing the grain-size, a method unique in that this method of improving creep resistance has little effect in normal large grain normal work-hardening material. In broad terms the copper used as the alloying element is retained in solid solution resulting in higher dislocation densities and usually an increase in the rate of work-hardening. In the present alloy, it has been shown that the effect of copper is felt between the temperature range up to about 100°C. The creep resistance produced at these temperatures must have been brought about due to the resistance of dislocation recovery and deformation primarily though other additional interaction is possible (166).

The second method of creep strengthening obtained by increasing the grain-size has been shown to have little effect in normal materials, although creep rate has been shown to increase with increased grain-boundary sliding.

In the grain-range which exhibits superplasticity the parameter m can be taken to give an indication of the creep rate. Since in creep, $\dot{\varepsilon} \alpha \sigma n$ (138) and in superplasticity $\sigma \alpha \dot{\varepsilon}^{m}$ it follows that $n = \frac{1}{m}$ and that for a particular stress value, the higher the m-value the higher the creep rate. In the present case at 20 and 50°C though the m - $\dot{\varepsilon}$ curves exhibit lower m-values the higher the grain size, at higher temperature it has been that with increasing grain-size the (peak) m value is maintained though it moves to slower strain-rates.

However, the σ_f - $\dot{\varepsilon}$ curves illustrate that σ_f is markedly increased for the entire strain-rate range when increasing the grain-size. Therefore, in the relation $\dot{\varepsilon} \alpha \sigma^{1/m}$ even if the m-value is the same the higher the stress the greater the resistance to creep-rate. The present creep-rate results with increasing grain-size exhibits this effect.

The flow stress during creep is mainly governed by the dislocation density within sub-grains which generally has a constant value during steady-state creep. The size of the sub-grain being inversely proportional to the applied stress and indirectly to the temperature and strain-rate by their effective stress (177). Also the occurrence of grain-boundary sliding in the smaller grain-size could be controlled by crystal deformation alongside boundaries will have an associated effect. McLean (178) has shown that increasing the creep rates at finer grain sizes are the results of faster grain-deformation as well as increased area of sliding.

5.39 Pressure Forming

The free bulging test has been shown by Thomson et al (167) to be a reliable method of assessing the macro-formability of superplastic metal sheets. In the present investigation it was also found to be a sensitive simulative test, but there are important parameters which can introduce anomalies.

A significant factor is the thickness strain distribution around the bulge hemisphere. It has been shown (167) that the m-value has a marked influence on the thickness strain distribution and the higher the m-value the lower is the thickness variation from the flange to the pole. With this tendency for strain distribution, coupled with the fact that straining is generally more advanced at the pole, it follows that the height at failure will rise with m-value.

The m-value that has been considered is the peak m-value, this being considered the relevant criteria since in a bulge test the initial strain-rate is zero, the bulging rate increases with bulge size, the rate being controlled by the pressure.

Though previous work has shown the effect of m on bulging, no work has considered the effect of grain-size where the peak m-value which in fact increases with increasing grain-size, though the peak m-value moves to lower strain-rate. In the present case the thickness strain distribution around the bulge circumference did not vary with grain-size. Therefore, the forming time criteria in the present case is the forming pressure used. Since in the larger grained material the stress necessary to obtain the maximum m-value is very much higher than that required in the smaller grained material, the time to reach the maximum deformation rate will be higher. Further more, since the strain-rate of the operating peak m-value is lower in the large-grained material the deformation rate will be arrested for larger strains.

Thus, in effect, in order to obtain a fixed bulge height at the same time, higher pressure will be needed with increasing grain-size and the time of formability is not indicated by the peak m-value, though the formability is still assessed by the peak m-value. A more reliable parameter to rate the formability time in this case would be K in the empirical equation $\sigma = K\dot{\epsilon}^m$, where the K value is the stress at $\dot{\epsilon} = 1$.

A structural change which occurs during straining a superplastic metal is the influence of strain-rate and strain (Section 5.35) of increasing the grain-size over and above the normal coarsening observed due to the time at temperature effect. Therefore, in a bulge the strained region increases from the flange to the pole. Also at the pole the deformation rate is the greatest. Thus a grain strengthening will be introduced, it being the most at the pole and decreasing towards the flange region, this strengthening effect passing on the strain to the smaller grain size regions. This argument finds support from the observations made in the superplastic Zn - 0.4 % wt Al alloy (Section 4.309) under biaxial stretching. As has been shown in this alloy marked grain coarsening occurs with strain. Also it was found that when the appropriate strain-rate was utilized to obtain the maximum cup depth, fracture took place, well away from the pole.

5.40 Conclusions

1. The addition of 1% wt copper to the Zn/Al eutectoid is desirable since it increases the σ_f markedly up to a temperature of 20 - 100°C, at the same time decreasing the m-value in this temperature range, while at the superplastic deformation temperature of 200 - 250°C it has negligible effect both on the σ_f and the m-value.

2. Though increasing the grain size reduces the σ_f at room temperature, the rate of decrease with increasing temperature is decreased with the σ_f at 250°C being increased though not markedly. The $\sigma_f - \dot{\varepsilon}$ and $m - \dot{\varepsilon}$ curves shift to lower strain-rate end.

3. The peak strain-rate sensitivity was in the region of 0.6 and was obtained for the grain sizes 0.55, 1.05, 1.75 and 3.25 μm in the strain-rate region of 10^1, 2×10^0, 4×10^{-1} and 6×10^{-2} min^{-1} respectively. Uniaxial elongations of greater than 1000% could be obtained in the 0.55 μm grain-size material at the relatively fast initial strain-rate of 1.54×10^1 min^{-1} (20 inch/min).

4. The activation energy (Q) for the temperature range varied with σ_f and also the m-value. A value of about 14 k cal/mole was obtained at the stress level for superplastic deformation, while a value near 21 k cal/mole was obtained at the low stress region.

5. Torsion experiments under constant strain-rate conditions showed that during superplastic deformation a steady-state stress is maintained.

6. The relationship between strain-rate, stress and grain size during superplasticity at 250°C can be described by the relation:

$$\dot{\varepsilon} \alpha \sigma^2 \, D_{gb}/_{L^2}$$

7. Fracture behaviour at the fracture tip is dependent on the m-value. For m-values of about ~ 0.3 no grain elongation was observed while of m-value of < 0.2 elongated grains were readily obtained.

8. Considerable grain-growth occurred during deformation in the 0.55 μm material, and after an elongation of 2000% at the initial strain-rate of 1.54×10^1 min^{-1} (20 inch/min) and temperature of 250°C a grain size of about 1.3 μm was obtained. Grain coarsening after deducting the time at temperature effect, occurred with strain and strain-rate.

9. Generally, the structure was equiaxed after superplastic deformation, but at higher magnification a number of odd shaped grains were observed.

10. Microstructural evidence showed that interdiffusivity took place readily with the consequence of rounding off the inter-phase boundary, spheroizadization of both the phases but particularly the β-phase and the diffusion of the β-phase via the α-phase grain-boundaries.

11. Calculation of the strain-rate contribution by lattice and grain-boundary diffusion and dislocation recovery/grain-boundary sliding mechanisms illustrated the role of grain-boundary diffusion in the superplasticity, though it is necessary to introduce a dynamic recovery model to obtain the right order to m and $\dot{\varepsilon}$ and explain the experimental observations.

12. It is shown that adding 1% wt Cu in the 0.55 μm grain size material the secondary creep rate at room temperature can be reduced by a factor of 120, while increasing the grain size to 3.25 μm in the same alloy, the secondary creep rate is reduced by a factor of 1200.

13. The free fall bulging method indicated that at 250°C the addition of copper had a negligible effect upon the forming time, while increasing the grain-size from 0.55 to 1.75 μm the time increased by a factor of 3.5 to 10 times, the times increasing with copper content in the copper-containing alloys.

14. Alloys have been developed in which a range of ductility (50 - 2500% elongation) can be obtained based on the requirements of σ_f - $\dot{\varepsilon}$, forming time and creep resistance.

5.5 Recommendation for Future Work

1. Since it has been shown that superplastic deformation takes place under steady state conditions a similar approach should be taken as has been taken by the school of hot working and freeze the actual structure obtained in hot torsion under variable conditions. It would then be possible to examine the frozen structures at the various region of the $\sigma - \dot{\varepsilon}$ curve. Furthermore, with the very high strain-rates available it will be possible to obtain the sub-grain size dependent on the strain-rate and it is envisaged that a critical strain-rate exists at which the subgrain size should be equal to the grain-size. Similarly, it could be shown that the sub-grain size is not dependent on the initial grain-size.

2. With the advent of the one million volt electron microscope it would be possible to examine the structure during deformation in the microscope. The possibility of observing the bulk behaviour is very high since it has been shown by Fujita et al (179) that a penetration of 4 to 8 μm can be obtained at 500 KV in aluminium and that the critical foil thickness for the observation of bulk behaviour of dislocations was > 3 μm. Therefore, in the Zn - Al eutectoid alloy there should be no difficulty in obtaining a penetration of at least 3 μm if not more and since the grain-size is only 0.55 - 1.0 μm the capability of seeing through layers of 3 to 4 grains should ensure the operating deformation mechanism. Figure 114 is a micro-graph of a foil made and examined in the N.P.L., IMV electron microscope and shows overlapping grains.

3. A great deal of work can be done to relate the formability of this alloy in relation to the range of variation of the parameters (σ_f, m, L, % elongation) under the various formability processes of vacuum and pressurising forming and closed die forging.

APPENDIX

Calculations for Volume Diffusivity (D_v) and Grain-Boundary Diffusivity (D_{gb})

Zinc/0.4 Al alloy

$$D_v = D_{ov} \exp^{-Q_v/RT} \qquad \text{(Ref. 181)}$$

and

$$D_{gb} = D_{ogb} \exp^{-Q_{gb}/RT} \qquad \text{(Ref. 181)}$$

where
$D_{ov} = 0.4\ cm^2/sec$ (Ref. 48,49)
$D_{ogb} = 0.5\ cm^2/sec$ (")
$Q_v = 21.5$ k cal/mole (")
$Q_{gb} = 14$ k cal/mole (")
$R = 1.98$ cal/deg/ g atom
$T = 297^oK$

$$D_v = 0.4\ e^{\frac{-21500}{1.98 \times 297}}$$

$$\therefore \quad \underline{D_v = 1 \times 10^{-16}\ cm^2/sec}$$

$$D_{gb} = 0.5\ e^{\frac{-14000}{1.98 \times 297}}$$

$$\therefore \quad \underline{D_{gb} = 2 \times 10^{-11}\ cm^2/sec}$$

Zn/Al eutectoid

$D_{ov} = 0.4\ cm^2/sec$

$D_{ogb} = 0.5\ cm^2/sec$

$Q_v = 23$ k cal/mole

$Q_{gb} = 14$ k cal/mole

$R = 1.98$ cal/deg/ g atom

$\therefore \quad D_v = 1.5 \times 10^{-10}\ cm^{-2}/sec$

and $\quad D_{gb} = 1 \times 10^{-6}\ cm^{-2}/sec$

References

1. H. Naziri and R. Pearce, J.I.M., 1969, 97, p.326.

2. D. North, S.M.I., Jan., 1970.

3. L. T. Feng, paper presented at the Automotive Engineering Congress, Detroit, Michigan, Jan., 12-16th, 1970.

4. D. S. Fields, Jr. and T. J. Stewart, paper presented at the Conference on 'Mechanics of Forming Superplastic Alloys' July, 2nd, 1970, at UMIST, England.;

5. W. A. Backofen, Steel 1969, Dec., 15th, p.25.

6. Forging of High Strength Metals - Mech. Eng., March, 1970, p.37.

7. E. E. Underwood, J. Metals, 1962, 14, p.914.

8. D. H. Avery and W. A. Backofen, Trans. A.S.M., 1965, 58, p.557.

9. P. Chaudhari, Science and Technology, 1968, Sept.

10. H. Naziri and R. Pearce, S.M.I., 1969, Jan.

11. R. Johnson, Metals and Materials, 1970, 4, (9), Sept.

12. C. E. Pearson, J.I.M., 1934, 54, p.111.

13. A. A. Bochvar and Z. A. Sviderskain, Izv. Akad. Nauk. SSSR, Otdel. Tekn. Nauk., 1945, 9, p.821.

14. A. A. Bochvar, Izv. Akad. Nauk. SSSR, Otdel, Tekh. Nauk, 1948, 5, p.649.

15. A. A. Presnyakov and G. V. Starikova, Iza. Akad. Nauk. SSSR, Otdel. Tekh. Nauk, 1959, 1, p.75.

16. A. A. Presnyakov and V. V. Chervyakov, The physics of Metals and Metallography, (SSR, English Translation), 1959, 8(1), p.165.

17 A. A. Presnyakov and V. V. Chervyakov, Russian Metallurgy and Mining (SICT), 1960, 35, p.1289.

18 A. A. Presnyakov and G. A. Starikova, Physics of Metals and Metallography (SSSR, English Translation), 1961, 12 p.84.

19 A. A. Presnyakov and G. A. Starikova, Russion Metallurgy and Mining (SICT), 1963, 4, p.65.

19a A. A. Presnyakov, A. Y. Coban and V. V. Cherryakova, Thur. Fiz. Khim. 1961, 35, p.1289.

20. W. A. Backofen, I. R. Turner and D. H. Avery, Trans. A.S.M., 1964, 57, p.980.

21. D. L. Holt and W. A. Backofen, Trans. A.S.M., 1966, 59, p.755.

22. D. A. Woodford, Trans. A.S.M., 1969, 62, p.291.

23. W. B. Morrison, Trans. A.S.M., 1968, 61, p.423.

24. D. Lee and W. A. Backofen, TMS., AIME., 1967, 239, p.1034.

25. T. H. Alden, Trans., A.S.M., 1967, 60, p.274.

26. W. A. Backofen, F. J. Azzarto, G. S. Murty and S. W. Zehr, 'Ductility', A.S.M., 1968.

27 T. H. Alden, Trans. A.S.M., 1968, 61, p.559.

28. S. W. Zehr and W. A. Backofen, Trans. A.S.M., 1968, 61, p.301.

29. D. L. Holt, TMS., AIME., 1968, 242, p.25.

30. A. Karim and W. A. Backofen, Mat. Sci. Eng., 1968/69, 3, p.306.

31. D. Lee, Acta Metallurgica, 1969, 17, p.1057.

32. A. R. Marder, TMS., AIME, 1969, 245, p.1337.

33. T. H. Alden, Acta Metallurgica, 1967, 15, p.469.

34. T. H. Alden, TMS., AIME., 1966, 236, p.1633.

35. T. H. Alden and H. W. Schalder, TMS., AIME., 1968, 242, p.825.

36. W. A. Backofen, G. S. Murty and S. W. Zehr, TMS., AIME., 1968, 242, p.329.

37. A. Karim, Scripta Metallurgica, 1969, 3, p.887.

38. H. W. Hayden, R. G. Gibson, H. F. Merrick and J. H. Brophy, Trans. A.S.M., 1967, 60, p.3.

39. D. H. Avery and J. M. Stuart, paper presented at the 14th Sagamore Army Materials Research Conference, N.Y., August, 1967.

40. K. Nuttall, Ph.D. Thesis, 1969, Manchester University.

41. F. R. N. Nabarro, Report of Conference on the Strength of Solids, Bristol (1947), Phy. Soc. of London.

42. C. Herring, J. of App. Phys., 1950, 21, p.437.

43. R. I. Coble, J. of App. Phys., 1963, 34, (6), p.1679.

44. R. B. Jones, Nature, 1965, 207, p.70.

45. A. Ball and M. M. Hutchinson, Metal Sci. J., 1969, 3, p.41.

46. P. Chaudhari, Acta Metallurgica, 1967, 15, p.1777.

47. C. M. Packer and O. D. Sherby, Trans. A.S.M., 1967, 60, p.23.

48. E. S. Wadja, Acta Metallurgica, 1954, 2, p.184.

49. G. A. Shirn, E. S. Wadja and H. B. Hutchinson, Acta Metallurgica, 1953, 1, p.513.

50. F. Garofalo, 'Fundamentals of Creep and Creep Ruputure in Metals', 1965, N.Y., (Macmillan).

51. H. Chine and T. H. Alden, TMS., AIME., 1967, 239, p.710.

52. R. C. Cook, M.A.Sc., Thesis, 1969, University of British Columbia, Canada.

53. W. B. Morrison, TMS., AIME., 1968, 242, p.2221.

54. D. Holt, TMS., AIME., 1968, 242, p.740.

55. K. Nuttall and R. B. Nicholson, Phil. Mag., 1968, 17, p.1087.

56. R. Kossowsky and J. H. Bechtold, TMS. AIME., 1968, 242, p.716.

57. M. J. Stowell, J. L. Robertson and B. M. Watts, Metal Sci. J., 1969, 3, p.41.

58. H. W. Hayden and J. H. Brophy, Trans. A.S.M., 1968, 61, p.542.

59. R. C. Gibson, H. W. Hayden and J. H. Brophy, Trans. A.S.M., 1968, 61, p.85.

60. C. M. Packer, R. H. Johnson and O. D. Sherby, TMS. AIME., 1968, 242, p.2485.

61. J. R. Stephens and W. D. Klopp, TMS. AIME., 1968, 242, p.1837.

62. R. H. Johnson, C. M. Packer, L. Anderson and O. D. Sherby, Phil. Mag., 1968, 18, p.1309.

63. H. W. Schalder, Trans. TMS. AIME., 1968, 242, p.1281.

64. T. H. Alden, paper presented at the International Conference on Interfaces, Melbourne, August, 1969, p.207.

65. R. J. Lindinger, R. C. Gibson and J. H. Brophy, Trans. A.S.M., 1969, 62, p.222

66. D. Lee, Scripta Metallurgica, 1969, 3, p.893.

67. P. A. Blenkinsop and J. A. F. Gidley, paper presented at the Colloquium on Heat Treatment and Metallurgy in Metal Forming, University of Aston in Birmingham, March, 1969.

68. S. H. Reichman, B. W. Castledine and J. W. Smythe, Int. J. Powder Metallurgy, 1970, 6, (1), p.65.

69. S. H. Reichman, B. W. Castledine and J. W. Smythe, SAE. 700140, 1970.

70. B. M. Watts and M. J. Stowell, Tube Investments, Technical Report, 1970.

71. D. M. R. Taplin, G. L. Dunlop, S. Sagat and R. H. Johnson, Report No. Jan. 1970, Solid Mechanics Division, University of Waterloo, Canada.

72. G. Beghi, R. Matera and G. Patti, J. Mat. Sci., 1970, 5, p.820.

73. M. Garfinkle, W. R. Witze and W. D. Klopp, TMS. AIME., 1969, 245, p.303.

74. D. Lee, Met. Trans., 1970, 1, p.309.

75. H. E. Chine and D. Lee, Acta Metallurgica, 1970, 18, p.315.

76. K. D. Fike and H. J. Rack, Trans. A.S.M., 1969, 62, p.539.

77. A. Karim, D. L. Holt and W. A. Backofen, TMS. AIME., 1969, 245, p.131.

78. A. Karim, D. L. Holt and W. A. Backofen, TMS, AIME., 1969, 245, p.2421.

79. R. D. Jones and K. G. Thomas, Phil. Mag., 1970, 22, (176), p.427.

80. J. Weertman, J. App. Phys., 1955, 242, p.1193.

81. J. Friedal, Dislocations, (Addison-Wesley), Cambridge, Mass. (1964).

82. R. C. Gifkins, J.I.M., 1967, 95, p.373.

83. I. M. Litshitz, Soviet Phys., JETP., 1963, 34, (6), p.1679.

84. H. W. Hayden, International Nickel Co. Ltd., Paul D. Merica Research Laboratory, N.Y., Technical Paper 688-OP, 1970.

85. P. J. Martin and W. A. Backofen, Trans. ASM., 1967, 60, p.352.

86. T.S. Ke, Phys. Rev., 1948, 73, p.267.

87. T. S. Ke, J. App. Phys., 1949, 20, p.274.

88. W. Rosenhain, J. L. Haughton and K. E. Bingham, J.I.M., 1920, 23, p.261.

89. R. Chadwick, J.I.M., 1933, 51, p.93.

90. R. Chadwick, J.I.M., 1934, 54, p.131.

91. R. Irmann, Technische Rundschau (Bern).

92. A. Von Zeerleder, Zeit fur Metallkunde, 1950, 41, p.228.

93. F. V. Lenel, Progress Powder Met., 1961, 17, p.107.

94. D. Tromans and J. A. Lund, Trans. A.S.M., 1966, 59, p.672.

95. W. H. McCarthy, Ph.D. Thesis, 1966, Department of Material Science, Stanford University, U.S.A.

96. N. R. Riseborough and J. A. Lund, Trans. A.S.M., 1968, 61, p.722.

97. J. A. Lund and D. Tromans and S. F. Radtke, Int. J. Powder Met., 1968, 4, p.41.

98. D. Tromans, N. R. Riseborough, A. J. Williams and J. A. Lund, Trans. Japan Inst. Metals., 1968, 9, Supplement, p.603.

99. R. C. Cook and N. R. Riseborough, Scripta Metallurgica, 1968, 2, p.487.

100. New Scientist and Science Journal, 1971, Jan. 29th, p.196.

101. P. Rogers, 'Zam-unalloyed winner' Business Guardian, 1970, Jan. 24th.

102. C. W. Roberts and B. Walters, J.I.M., 1949-50, 76, p.557.

103. J. A. Ramsey, J.I.M., 1951-52, 80, p.167.

104. I. S. Brammar and M. A. P. Dewey, 'Specimen Preparation for Electron Metallography', 1966: Oxford (Blackwell).

105. G. Thomas, 'Transmission Electron Microscopy of Metals' 1962, (Wiley).

106. D. H. Kay, edited by, 'Techniques for Electron Microscopy', 1965: Oxford (Blackwell).

107. W. J. McG. Tegart, 'Electrolytic and Chemical Polishing of Metals and Alloys', 1961, (Pergamon Press).

108. B. J. Ginn and E. D. Brown, Brit. Weld. J., 1965, 12, p.2.

109. L. G. T. Davy, R. C. Cochrane, M. J. Collins and S. G. Glover, JISI, 1966, Nov.

110. A. Lutts and J. Wegria, CNRN, 1967, (11), p.63.

111. P. Gay and A. Kelby, Acta Cryst., 1953, 6, p.172.

112. P. Gay, P. B. Hirsch and A. Kelly, Acta Cryst., 1954, 1, p.41.

113. M. Deighton and R. N. Parkins,

114. G. P. Lewis and W. J. McG. Tegart, J.I.M., 1964, 92, p.249.

115. G. Baralis, P. Gondi, G. Scandola and I. Tangerini, TMS, AIME, 1968, 242, p.1927.

116. A. Berghezan, A. Fourdeux and S. Amelinckx, Acta Metallurgica, 1961, 9, p.464.

117. E. D. Hall, Proc. Phys. Soc. London, 1957, 64, p.747.

118. N. J. Petch, JISI, 1953, 174, p.25.

119. C. A. P. Horton and C. J. Beevers, Acta Metallurgica, 1968, 16, p.733.

120. C. A. P. Horton, N. B. W. Thompson and C. J. Beevers, Metal Sci. J., 1968, 2, p.19.

121. M. D. Halliday, C. A. P. Horton and C. J. Beevers, Metal Sci. J., 1969, 3, p.145.

122. R. L. Bell, N. B. W. Thompson and P. A. Turner, J. Mat. Sci., 1968, 3, p.524.

123. C. A. P. Horton and C. J. Beevers, Metal Sci. J., 1969, 3, p.195.

124. Conference on Superplasticity, Leeds University, March, 1969.

125. J. Hedworth and M. J. Stowell, Tube Investment Report, 1970.

126. Conference on 'Mechanics of Forming Superplastic Alloys' July 2nd, 1970, at UMIST.

127. J. J. Jonas, C. M. Sellars and W. J. McG. Tegart, Metals and Metallurgical Reviews, 1969, 14, No.130.

128. D. Hardwick and W. J. McG. Tegart, J.I.M., 1961-62, 10, p.221

129. J.C.M. Li, TMS. AIME., 1963, 227, p.239.

130. D. G. Bradon and J. Nutting, JISI, 1960, 196, p.160.

131. A. H. Keh and S. Weissman, 'Electron Microscopy and Strength of Crystals' (Wiley), N.Y., 1963, edited by G. Thomas and J. Washburn.

132. M. Atkinson, 'Assessing Normal Anisotropic Sheet Metal' Steel Co. of Wales, Report MR/E/22a/5, 1966.

133. R. Pearce, 'The Effect of Temperature on Plastic Strain-Ratio' in Commercial-Purity Aluminium'. Inst. Sheet Metal Eng., Report BDDRG-DDR/WG11/12A, 1967.

134. H. Naziri and R. Pearce, Int. J. Mech. Sci., 1968, 10, p.681.

135. D. H. Rogers and W. T. Roberts, Int. J. Mech. Sci., 1968, 10, p.221.

136. R. Pearce, Design Eng. Series, Metals, Vol 1, Chpt. 18, p.145, 1970.

137. W. A. Rachinger, J.I.M., 1952-53, 81, p.33.

138. F. Garofalo, 'Fundamentalo of Creep and Creep-Rupture in Metals', 1966, (McMillian).

139. J. A. Martin, M. Herman and N. Brown, TMS, AIME, 1957, 209, p.78.

140. H. Brunner and N. J. Grant, TMS AIME., 1960, 218, p.122.

141. A. W. Mullendore and N. J. Grant, TMS AIME, 1963, 227, p.319.

142. T. L. Lin and D. McLean, Metal Sci. J., 1968, 2, p.108.

143. D. McLean, Metal Sci. J., 1970, 4, p.144.

144. H. R. Tiplev, L. H. Taylor, B. E. Hopkins, Metals Sci. J., 1970, 4, p.167.

145. W. J. McG. Tegart, 'Ductility' p.133, 1968, A.S.M. Metals Park (Ohio).

146. R. N. Stevens, Met. Review., 1966, 11, p.129.

147 K. F. Hale, Y. Ishida, T. L. Lin and D. McLean, 1966, Sixth International Congress for Electron Microscopy, Kyoto, edited by R. Uyeda (Tokyo: Maruzen), p.295.

148 Y. Ishida and M. Henderson-Brown, Acta Metallurgica, 1967, 15, p.857.

149 G. Baro, H. Gleiter and E. Hornbogen, Mat. Sci., Eng., 1968, 3, p.92.

150 H. Gleiter, E. Hornbogen and G. Baro, Acta Metallurgica, 1968, 16, p.1053.

151 B. Loberg and H. Norden, Arkiv for Fysik, 40, p.413. ; (Institute of Metals, International Conference, Amsterdam, 1970).

152 R. L. Bell and T. G. Langdon, J. Mat. Sci., 1969, 3, p.313.

153 M. W. Grabski and R. Korski, Phil. Mag., 1969, p.707.

154 E. V. Lee and E. E. Underwood, Met. Trans., 1970, 1, p.1399.

155 R. T. Derricott and J. C. Wright, (DDR/WGII/10C/66/S.M.I., 1966, p.1.

156 R. E. Reed-Hill, 'Physical Metallurgy Principles', (Van Nostrand), p.399.

157 P. Niessen and W. C. Winegard, J.I.M., 1963-64, 92, p.300.

158 R. E. Smallman, 'Modern Physical Metallurgy', 1963 (Butterworths), p.230.

159 H. Hu and R. S. Cline, TMS, AIME., 1968, 242, p.1013.

160 W. J. McG. Tegart, 'Elements of Mechanical Metallurgy', 1966, (Macmillan Co.) N.Y.

161 G. J. Smithells, 'Metals Reference Book', 1967, (Butterworths).

162 R. Hill, 'A Mathematical Theory of Plasticity', 1950, (Clarendon Press) Oxford.

163 F. A. Hodierne, J.I.M., 1963, 91, p.267.

164 H. Ormerod and W. J. McG. Tegart, J.I.M., 1960-61, 89, p.94.

165 D. S. Field and W. A. Backofen, Proc. Amer. Soc. Test. Mat., 1957, 57, p.1295.

166 D. McLean, Mechanical Properties of Metals, (Wiley), 1962.

167 T. H. Thomsen, D. L. Holt and W. A. Backofen, Metal Eng. (Quart), 1970, May, p.1.

168 G. B. Gibbs and J. E. Harris, paper presented at Conference on Interfaces, Melbourne, 1969.

169 D. S. Fields, Jr. and T. J. Stewart, paper presented at the Conference on 'Mechanics of Forming Superplastic Alloys', July 2nd, at UMIST, Manchester.

170 H. P. Stüwe, Deformation Under Hot Working Conditions, ISI, Publication 108, 1968.

171 M. J. Luton and C. M. Sellars, Acta Metallurgica, 1969, 17, p.1033.

172 H. J. McQueen, J. of Metals, Jan., 1969, p.131.

173 D. McLean, Grain-boundaries in Metals, (Oxford), 1957.

174 J. L. Robbins, O. C. Shepherd and O. D. Sherby, J.I.S.I., Oct., 1964, p.804.

175 E. A. Chojnowski and W. J. McG. Tegart, Metal Sci. J., 1968, 2, p.14.

176 B. R. Butcher, G. C. Weatherly and H. R. Pettit, Metal Sci. J., 1969, 3, p.7.

177 O. D. Sherby, A. Goldberg and J. E. Dorn, Trans. TMS., AIME., 1954, 46, p.681.

178 D. McLean, J.I.M., 1951-52, 81, p.293.

179 H. Fujita, Y. Kawasaki, E. Furubayashi, S. Kajiwara and T. Taoka, Japan J., App. Phys., 1967, 6, p.214.

180. J. H. Brophy, R. M. Rose and J. Wulff, The Structure and Properties of Materials, Vol. II, (Wiley), 1964.

Fig 1

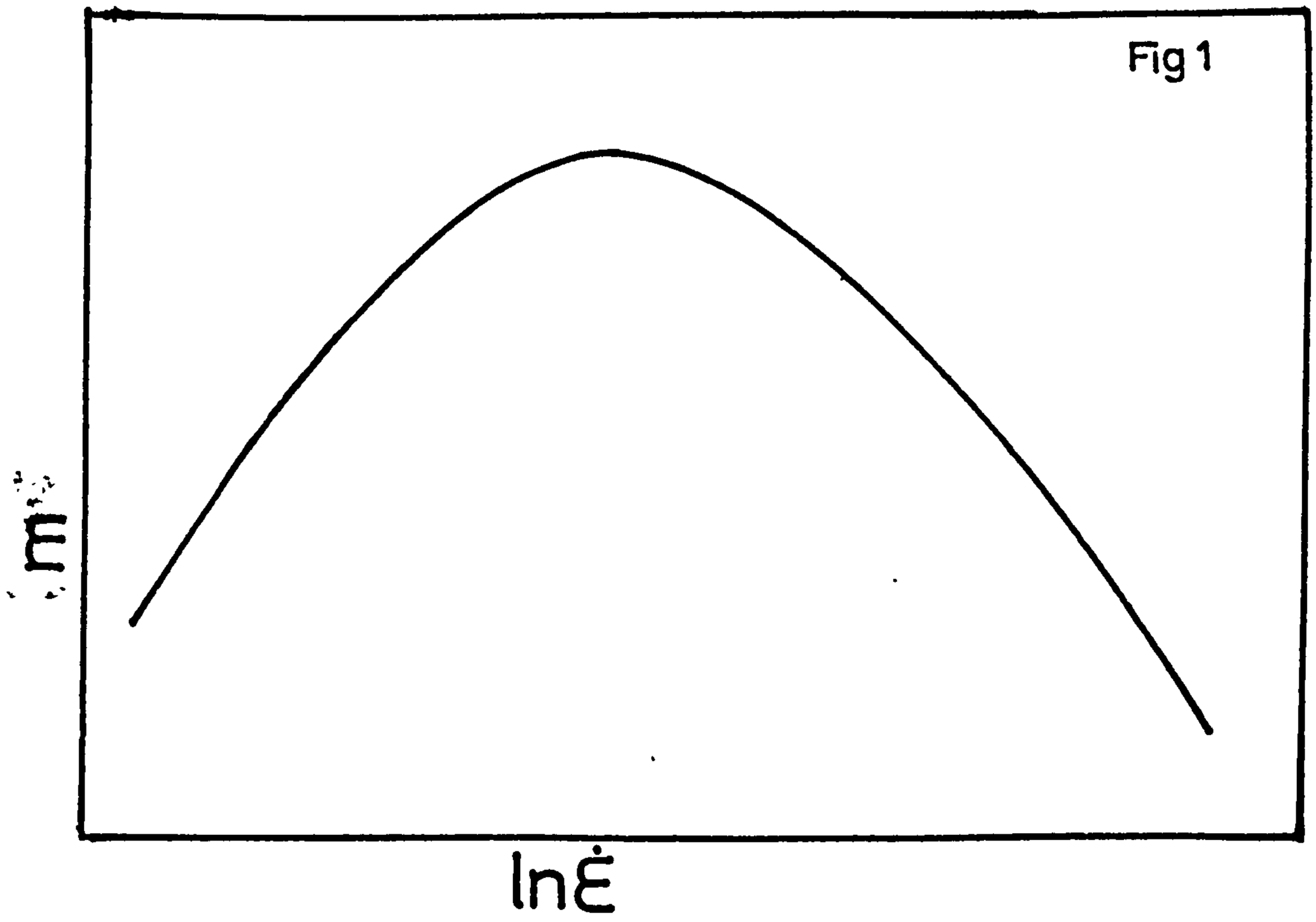

Fig 2

Figures 1&2 - Schematic illustration of the relationship between flow stress (σ_f), strain-rate sensitivity (m) and strain-rate ($\dot{\epsilon}$) for superplastic alloys, contrasting the low-$\dot{\epsilon}$ and high-$\dot{\epsilon}$ behaviour with that in the superplastic region.

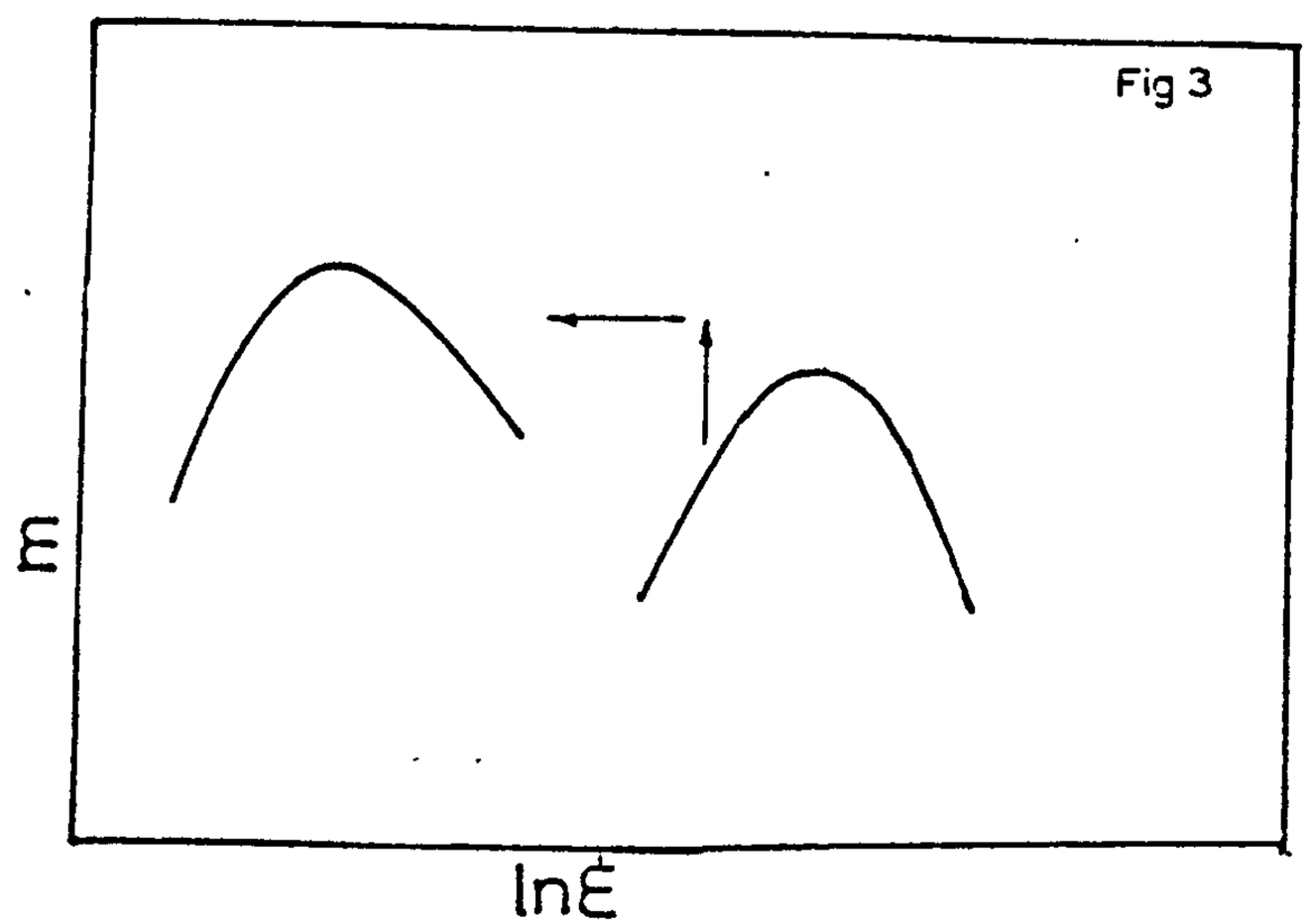

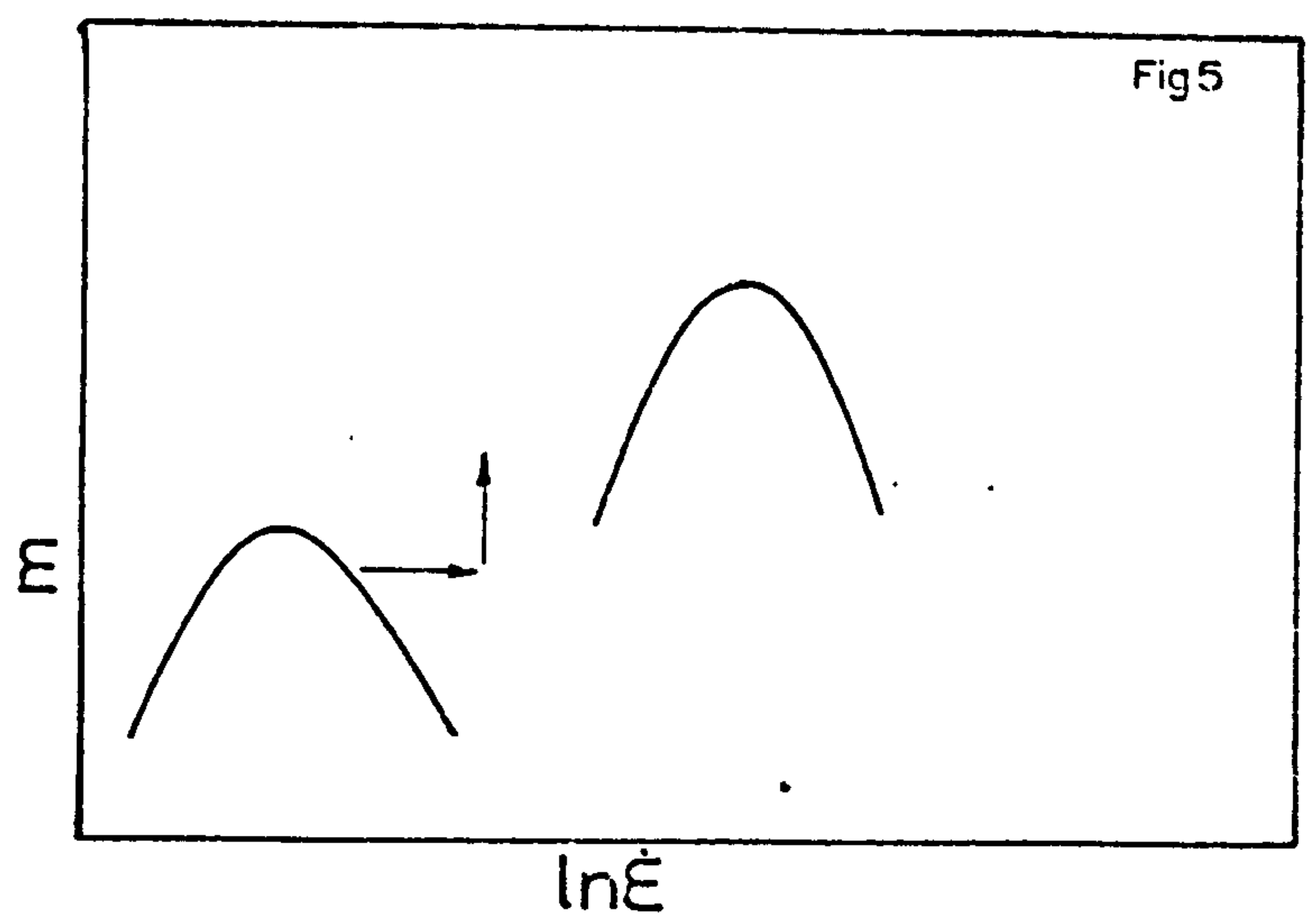

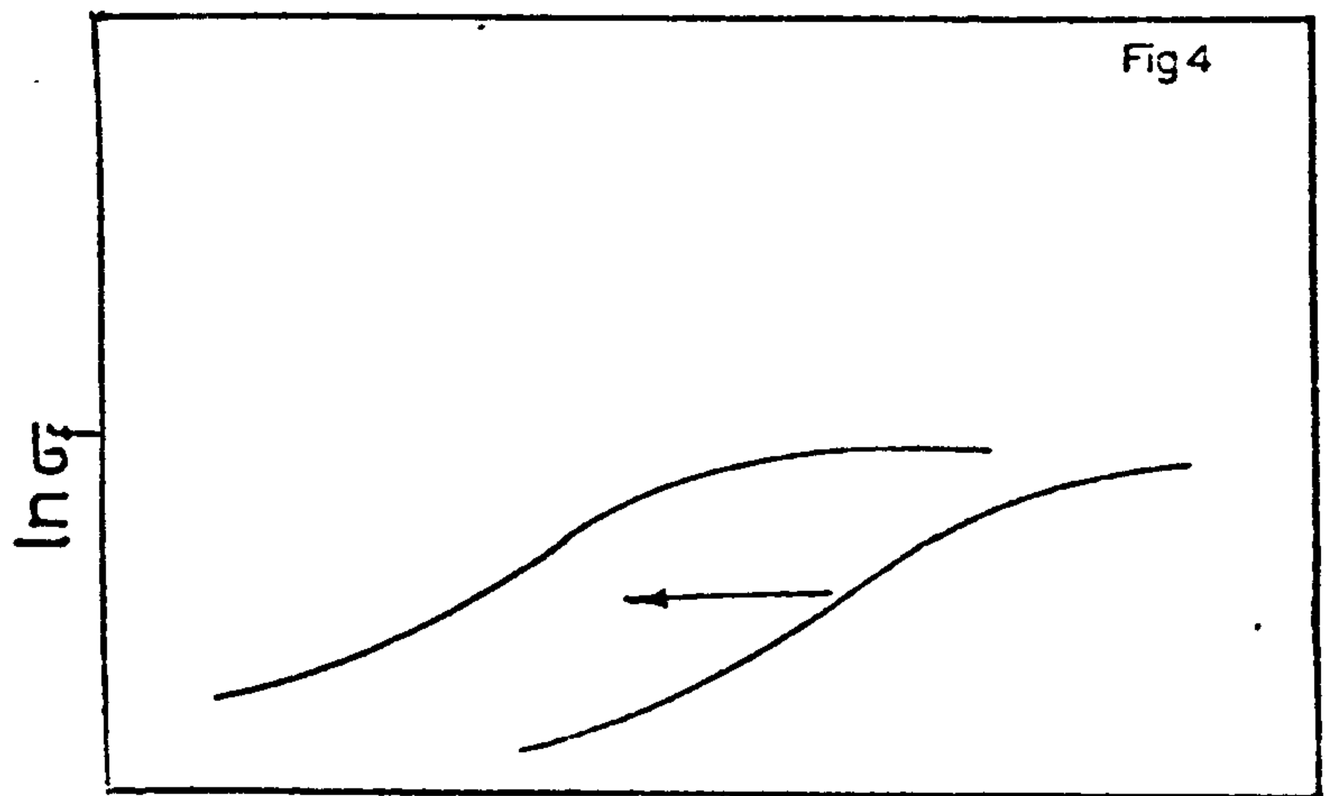

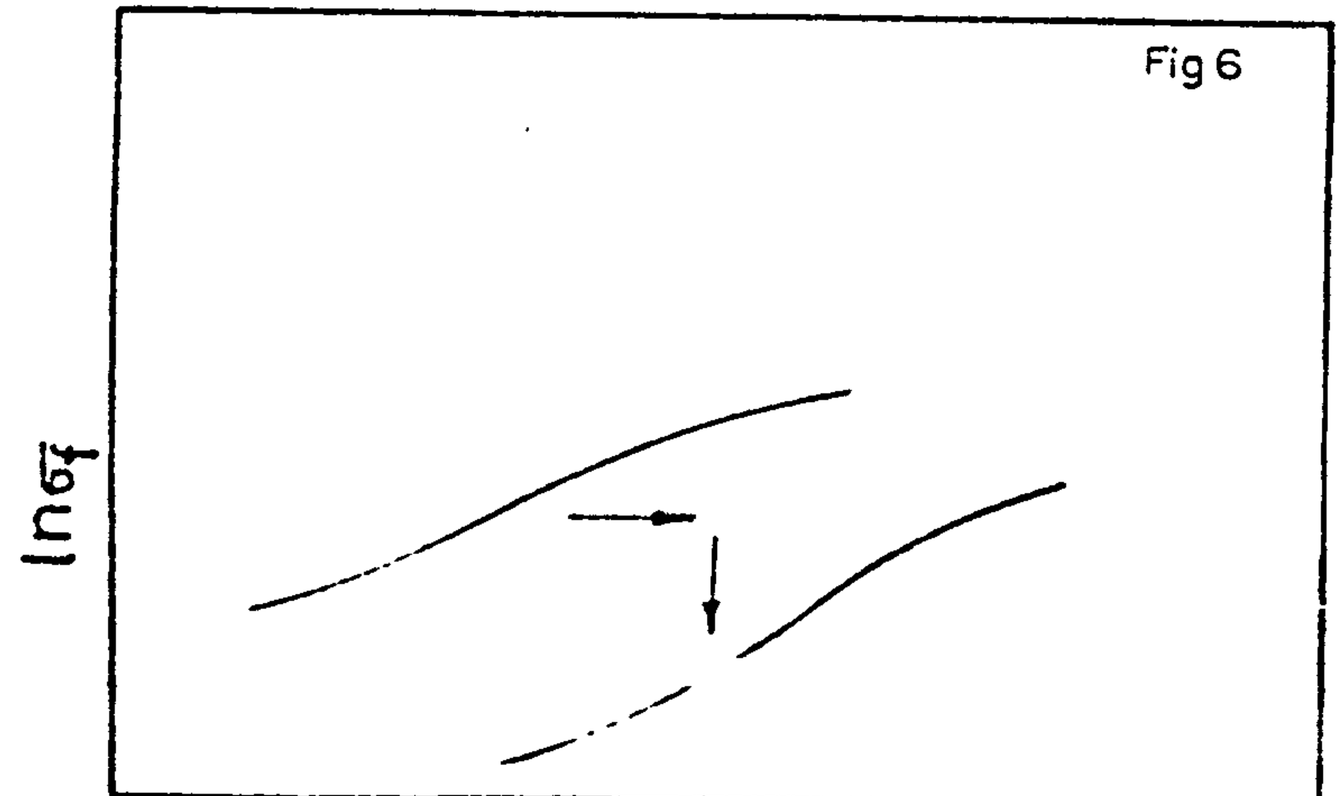

Figures 3&4 - Schematic illustration of the relationship between m vs $\dot{\epsilon}$ and σ_f vs $\dot{\epsilon}$ showing the effect of increasing the grain size at constant temperature.

Figures 5&6 - Schematic illustration of the relationship between m vs $\dot{\epsilon}$ and σ_f vs $\dot{\epsilon}$ showing the effect of increasing temperature.

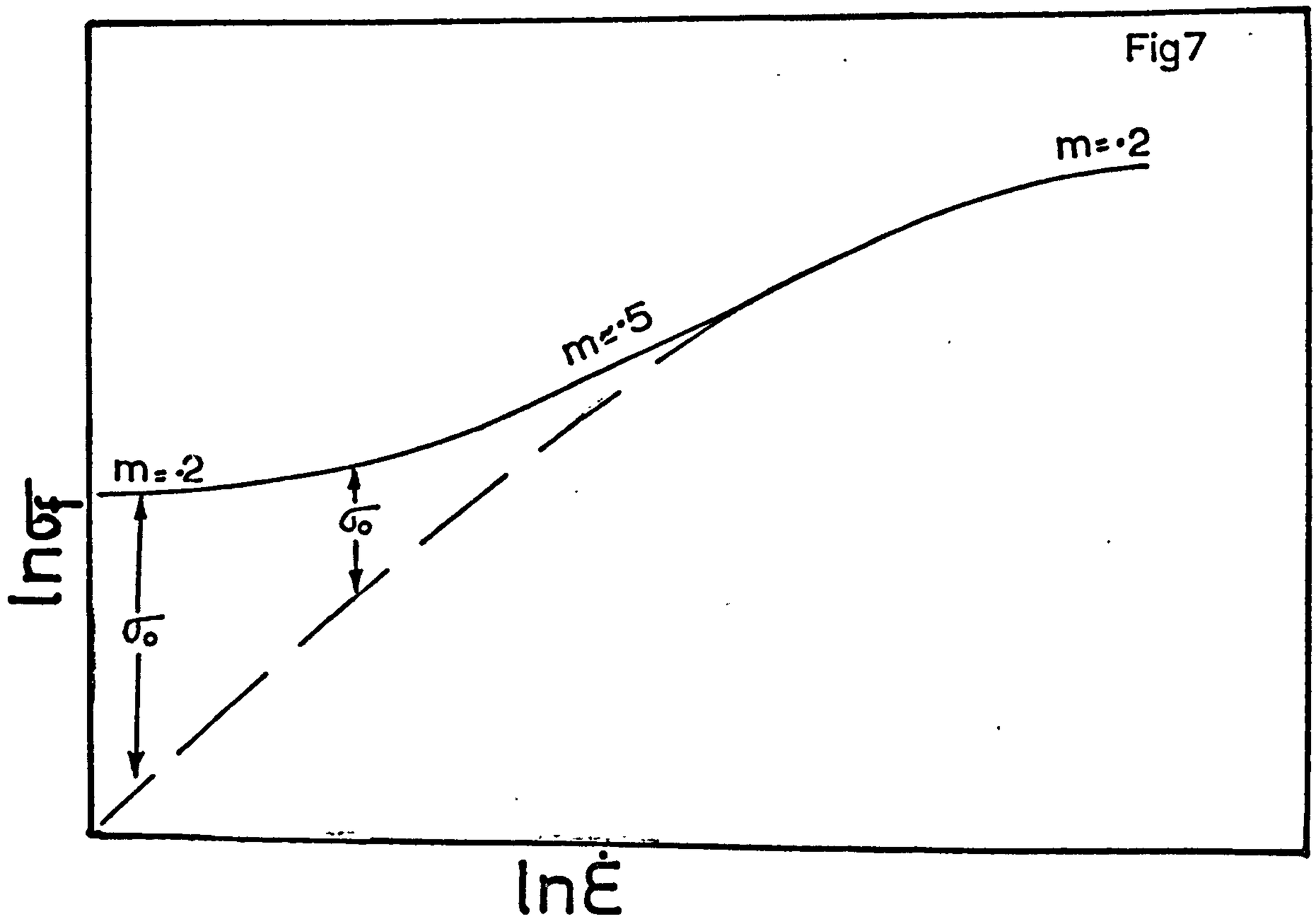

Figure 7 - Typical relationship between flow stress (σ_f) and strain-rate ($\dot{\epsilon}$) for superplastic materials.
The effect of subtracting a constant-backsstress term (σ_o), shown by the broken line.
Slope= strain-rate sensitivity.

Fig8

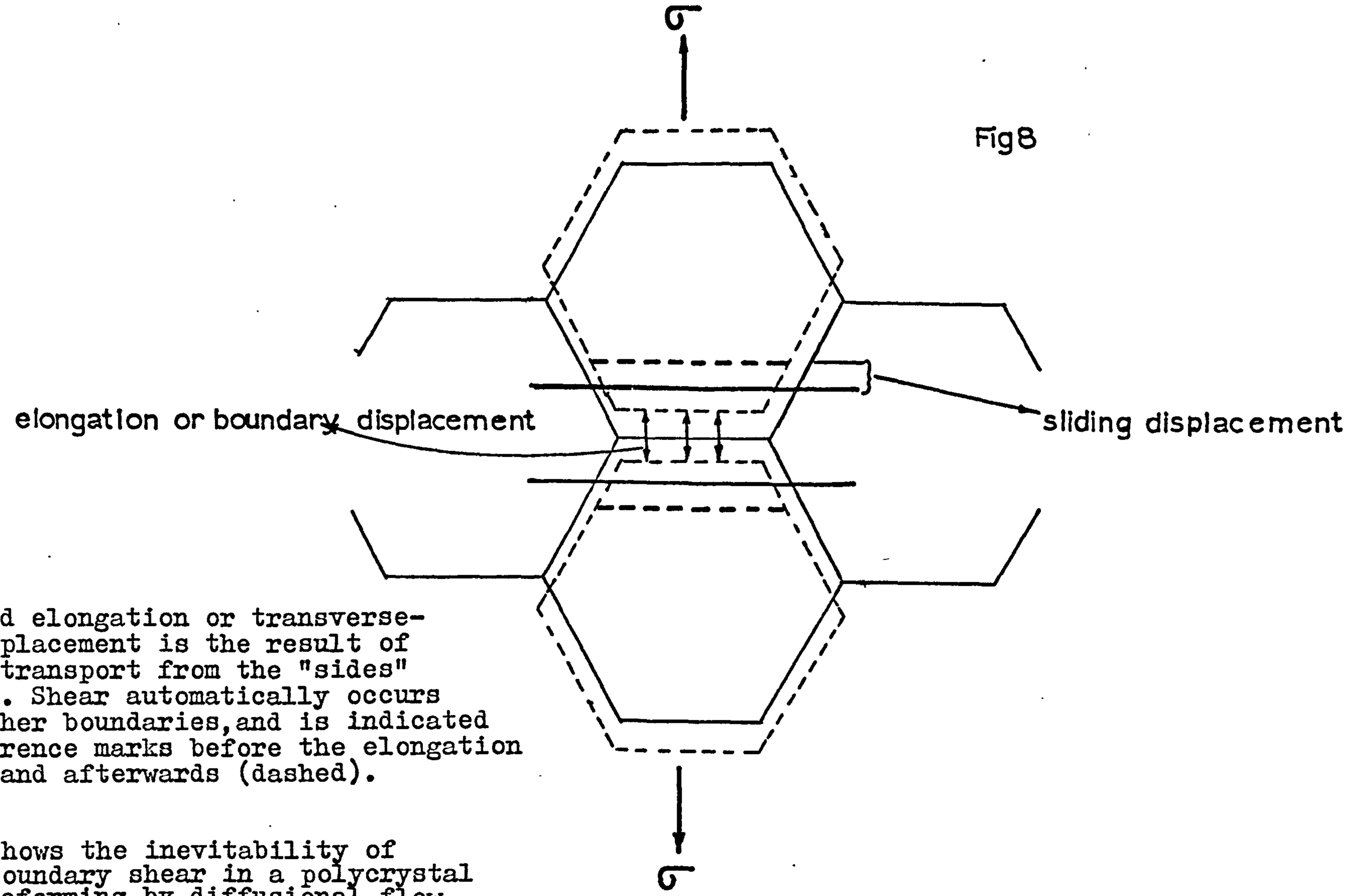

The indicated elongation or transverse-boundary displacement is the result of diffusional transport from the "sides" of the grain. Shear automatically occurs along the other boundaries, and is indicated here by reference marks before the elongation (continous) and afterwards (dashed).

Figure 8- Shows the inevitability of boundary shear in a polycrystal deforming by diffusional flow.

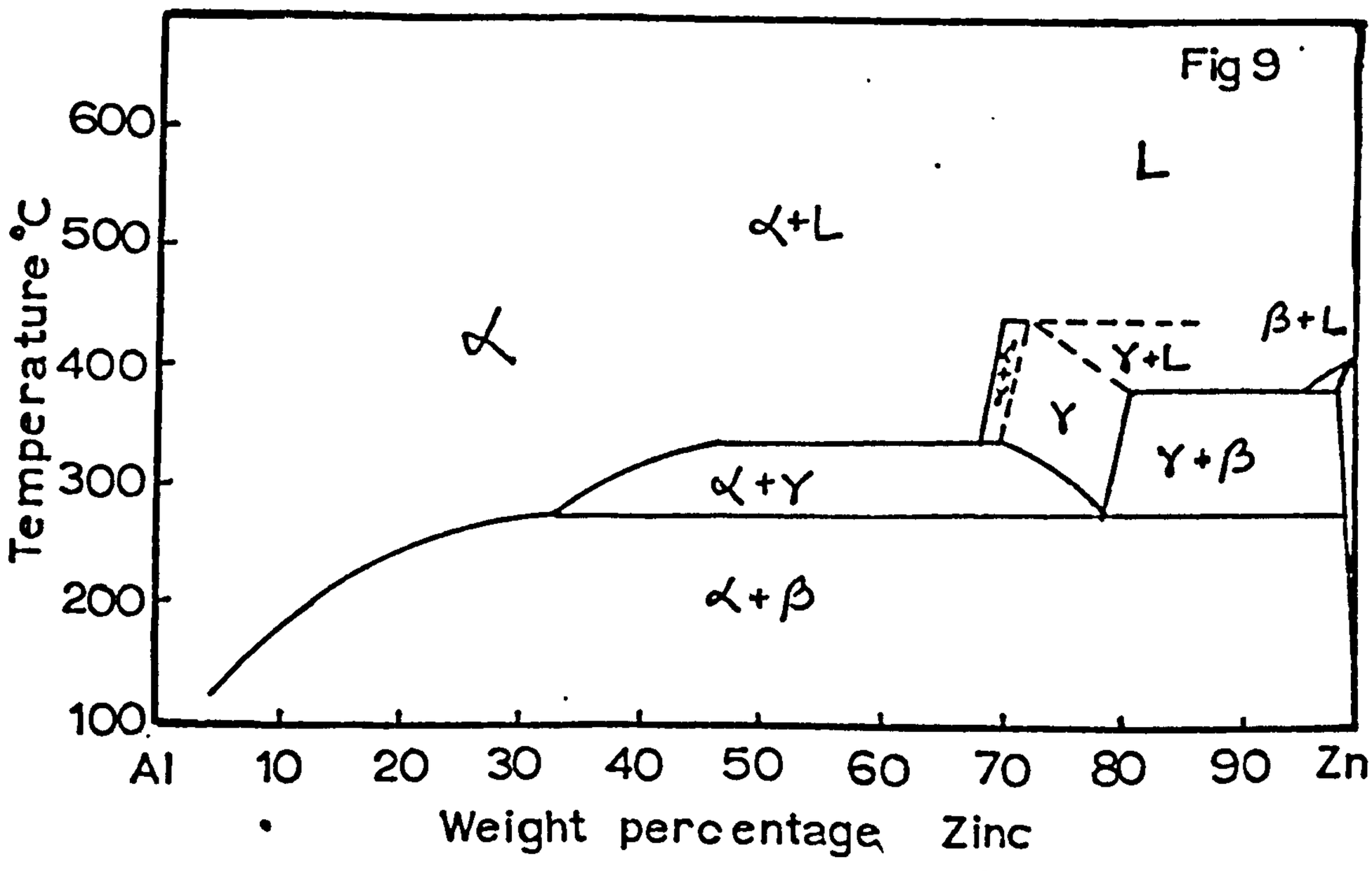

Figure 9 - The zinc-aluminium equilibrium diagram (Reference 19a).

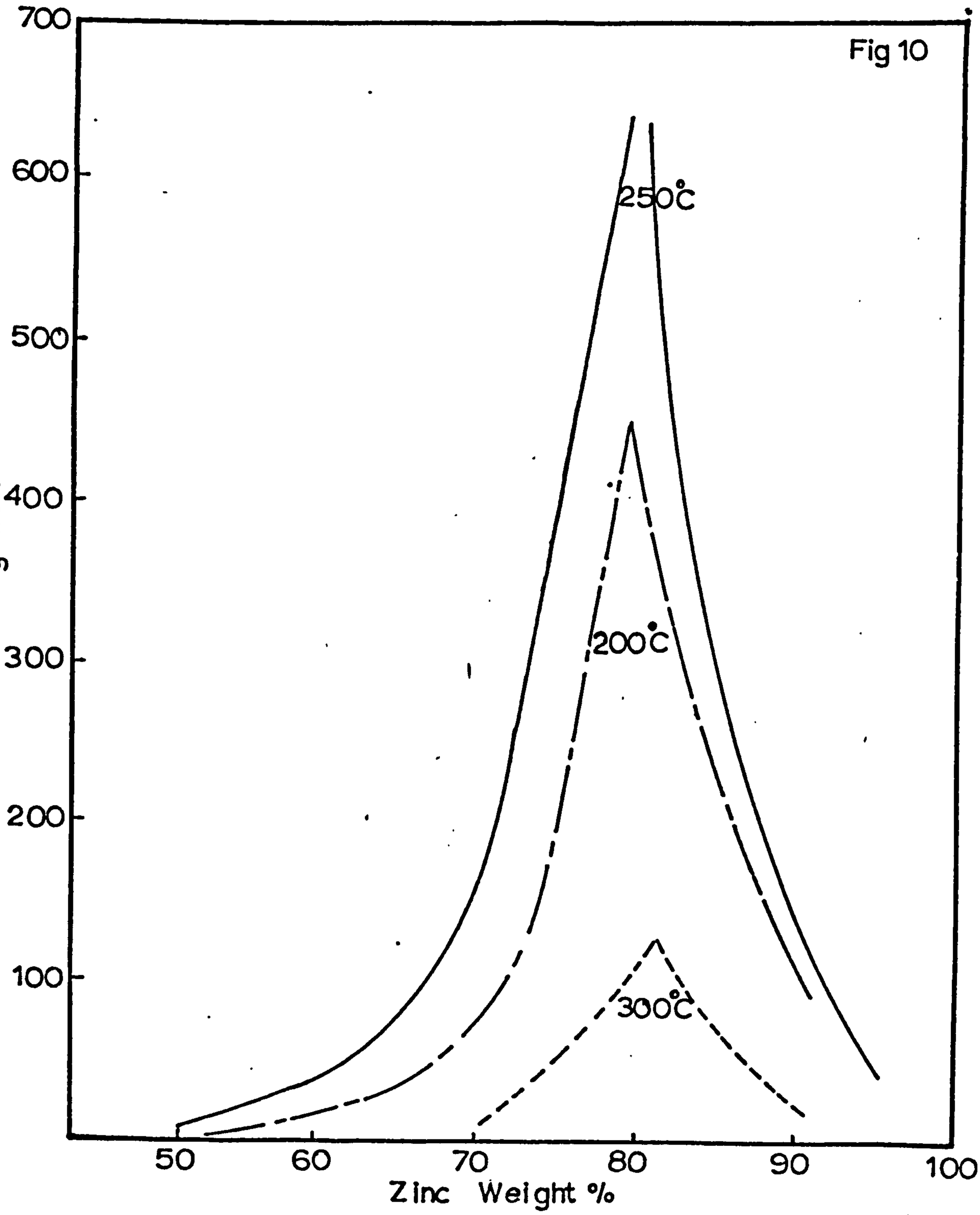

Figure 10 - The effect of composition and temperature on the percentage elongation in the Zn/Al system (Reference 16).

Fig 11

$$m = \frac{\log(P_A/P_B)}{\log(v_1/v_2)}$$

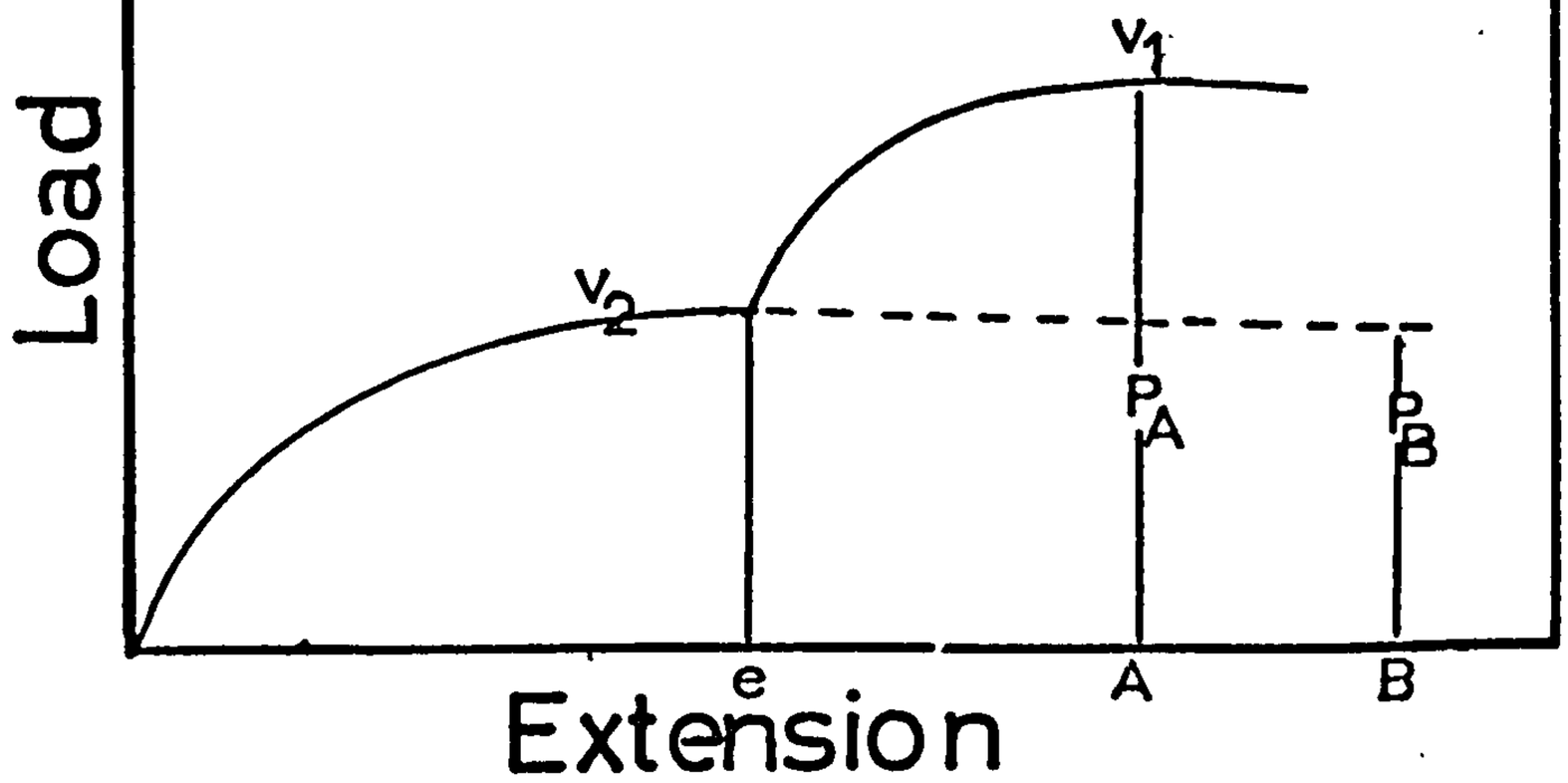

Figure 11 - A schematic load-time diagram representing a velocity change from v_2 to v_1 at extension e. Extensions A and B represent the same strain at the different pulling speeds.

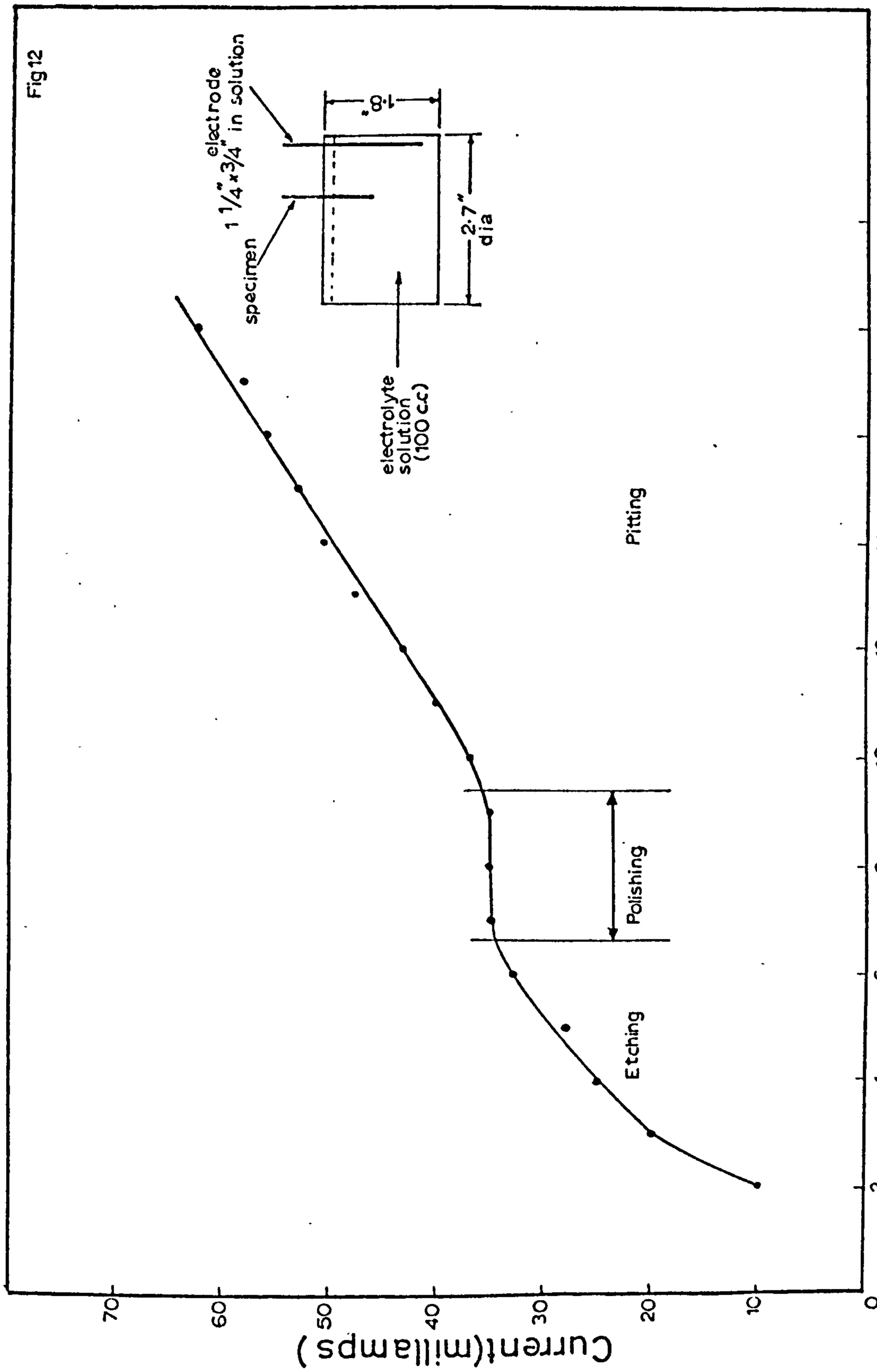

Figure 12- The current/voltage relationship for electropolishing foils of the Zn/0.4Al alloy.

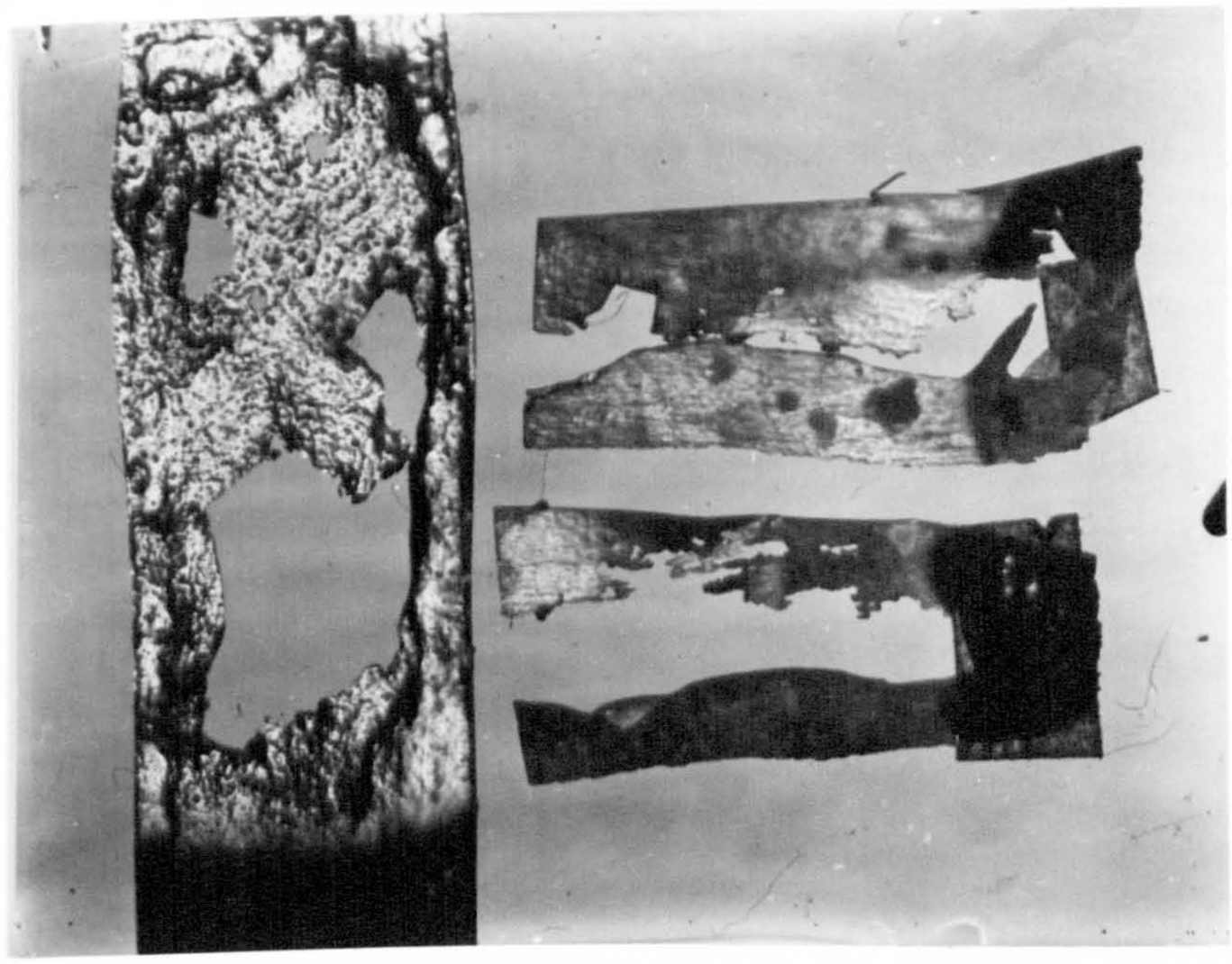

Figure 13-Specimens after chemical thinning and electropolishing. The edges are suitable for transmission electron microscopy. (x5).

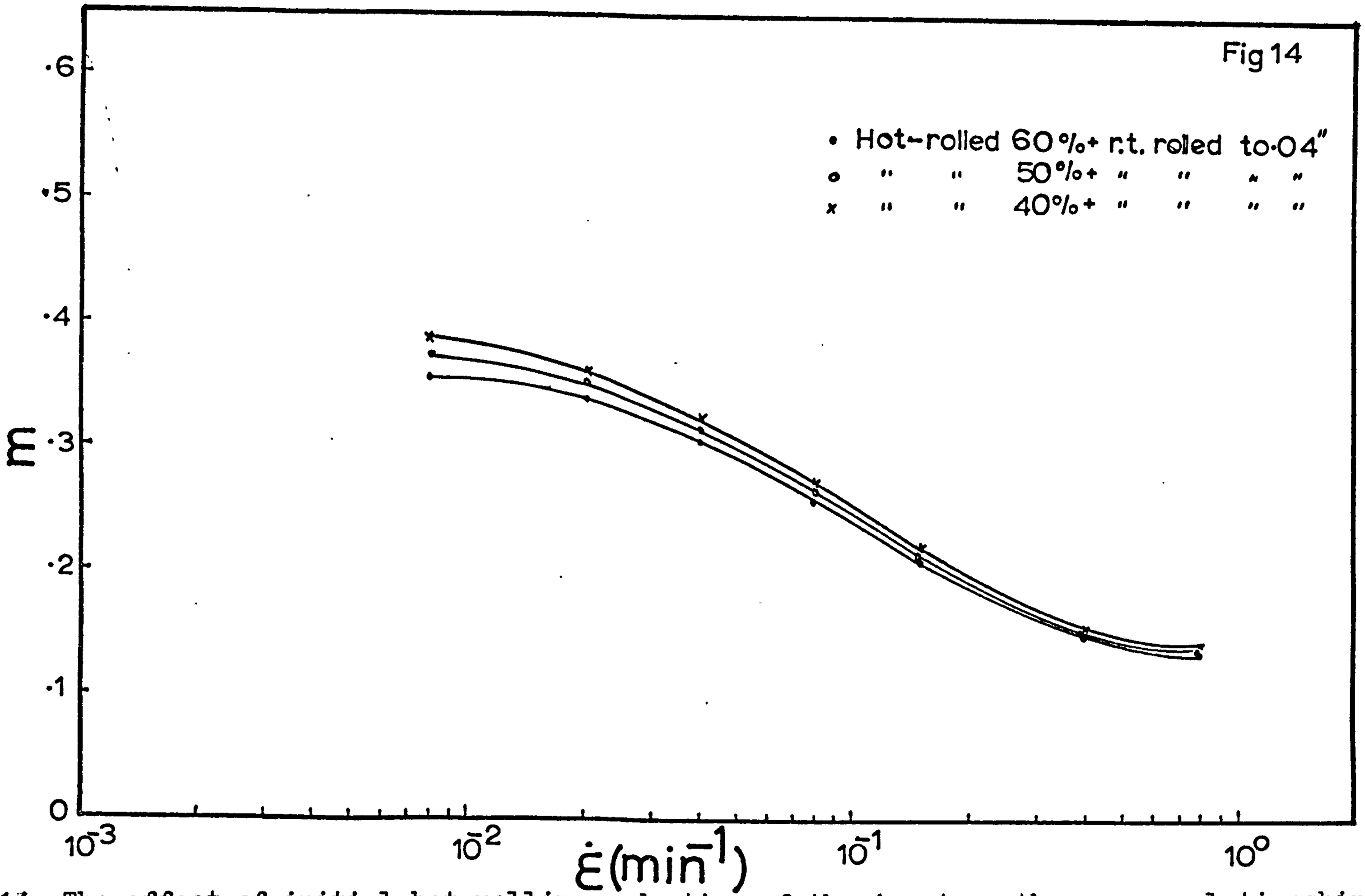

Figure 14- The effect of initial hot rolling reduction of the ingot on the m vs relationship.

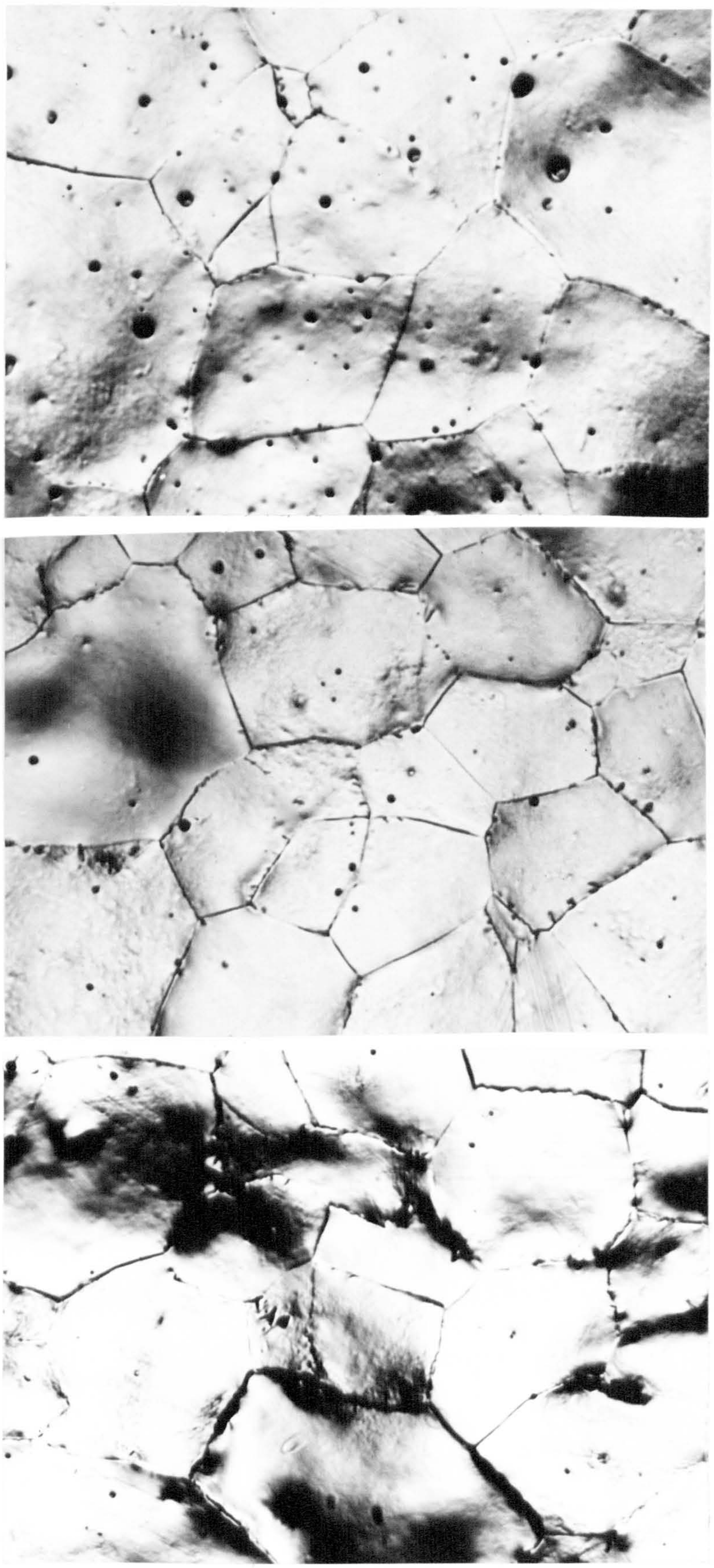

Surface

Longitudinal Section

Transverse Section

Figure 15-Microstructure of the cast ingot , homogenized for several hours at about 350°C.(x150).

Surface

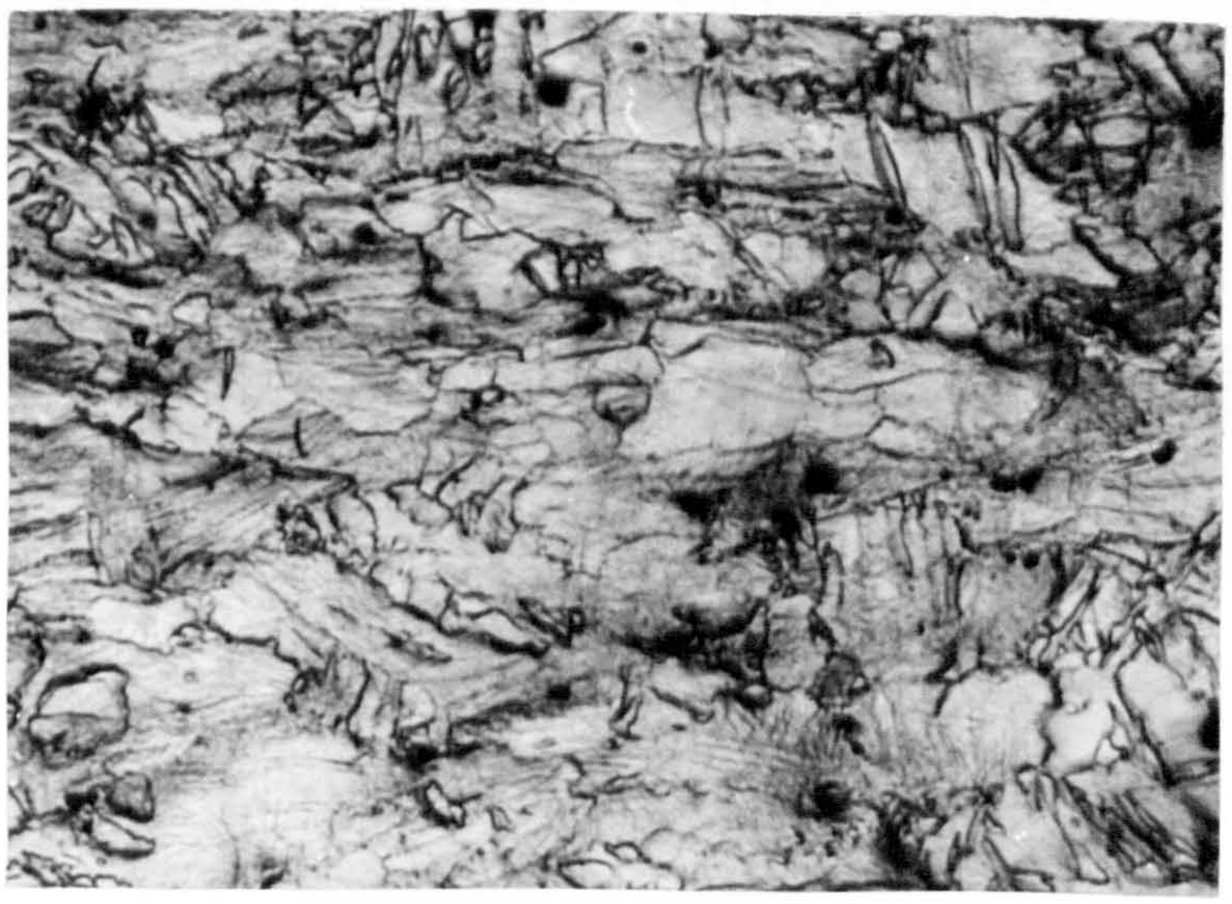

Longitudinal Section

Transverse Section

Figure 16- Microstructure of the 40% reduction, hot rolled slab.(x150).

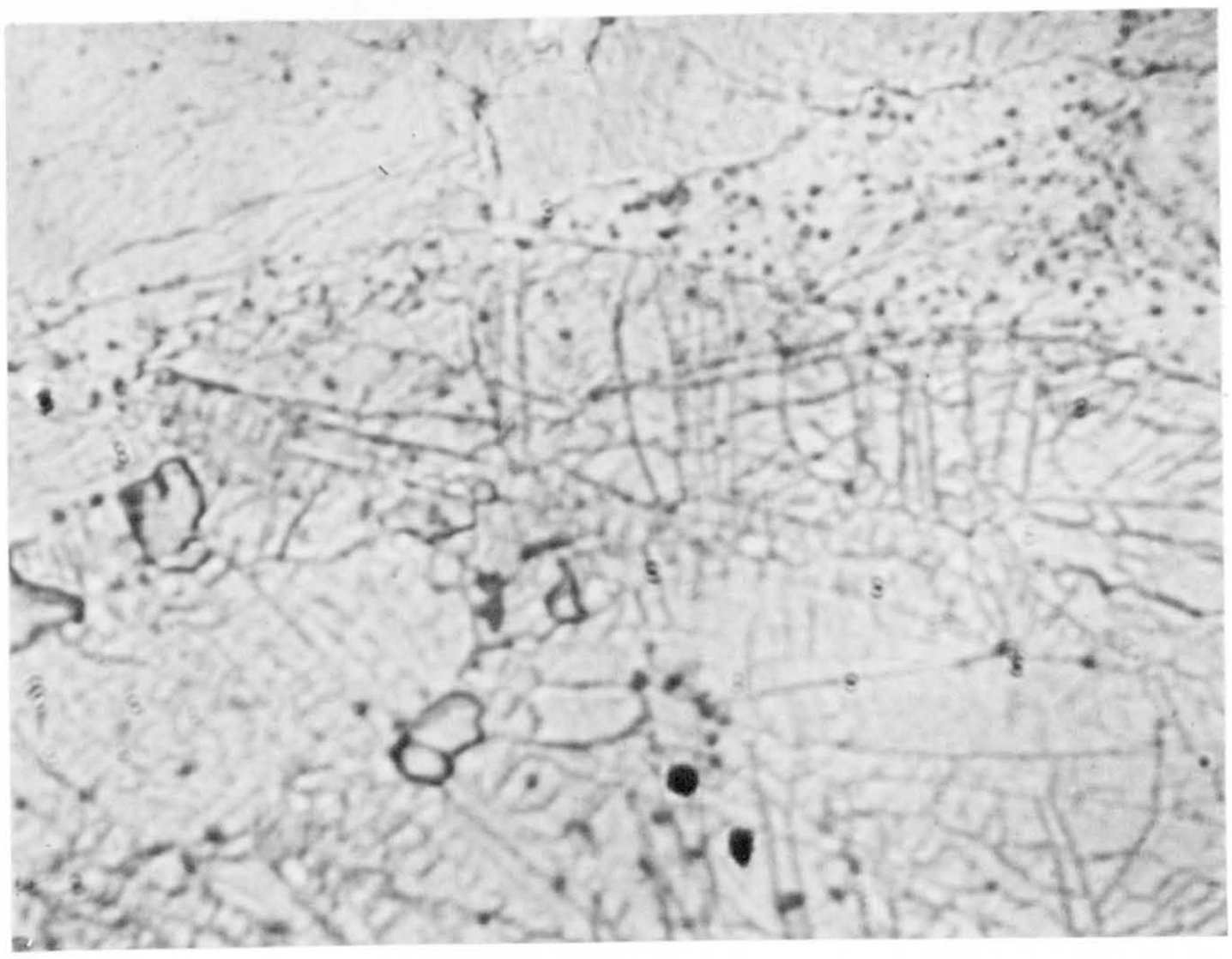

Figure 17-Substructure formation in the 40% reduction, hot rolled slab. (x1500).

Rolling Direction
(Surface)

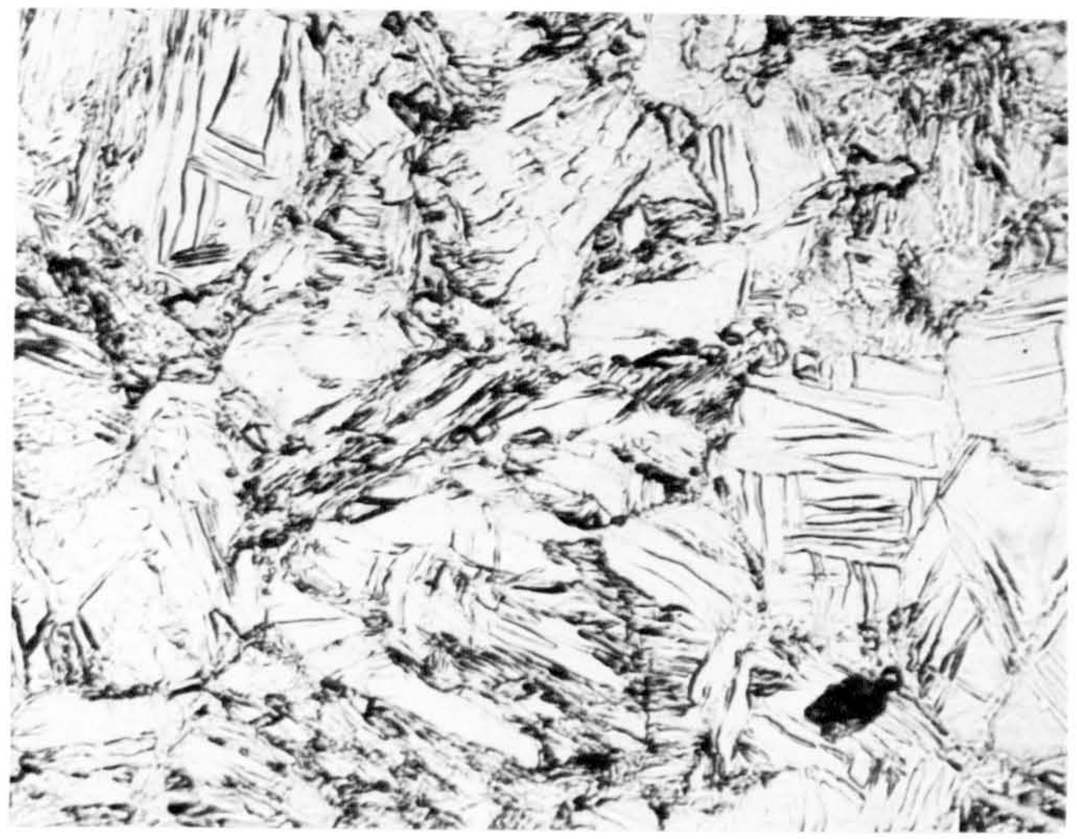

25%

37.5%

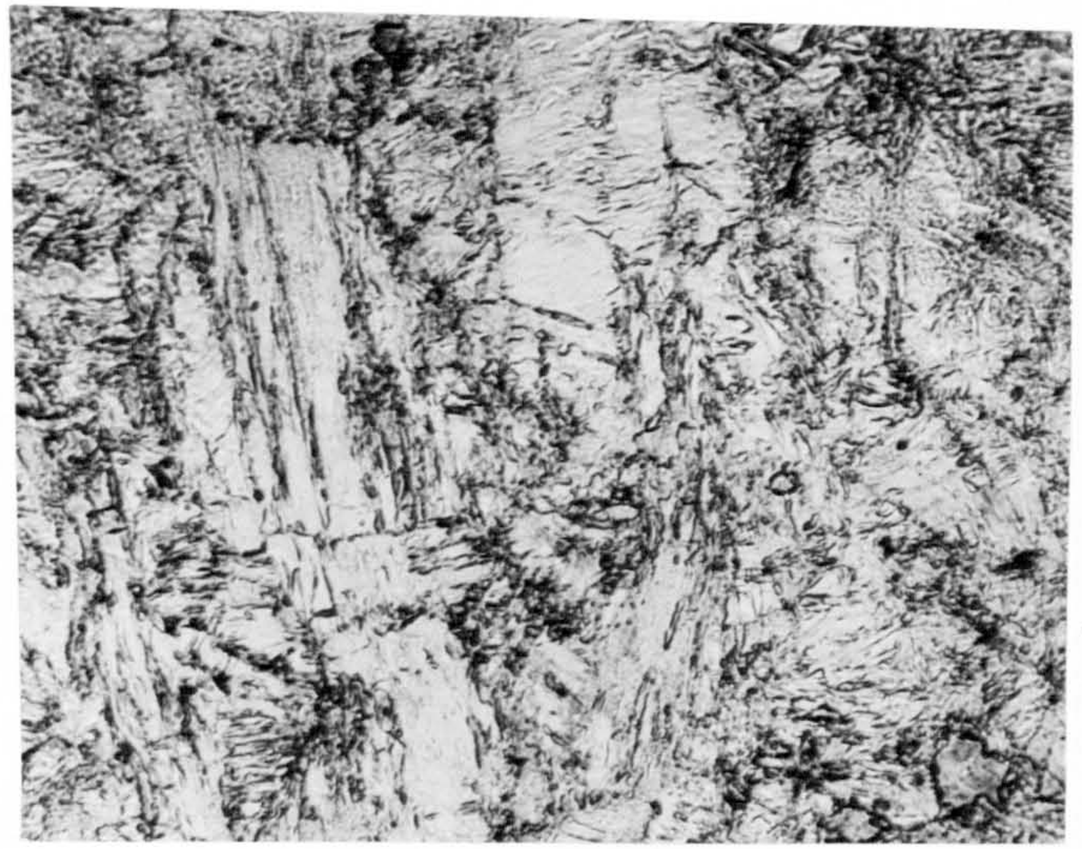

50%

62.5%

75%

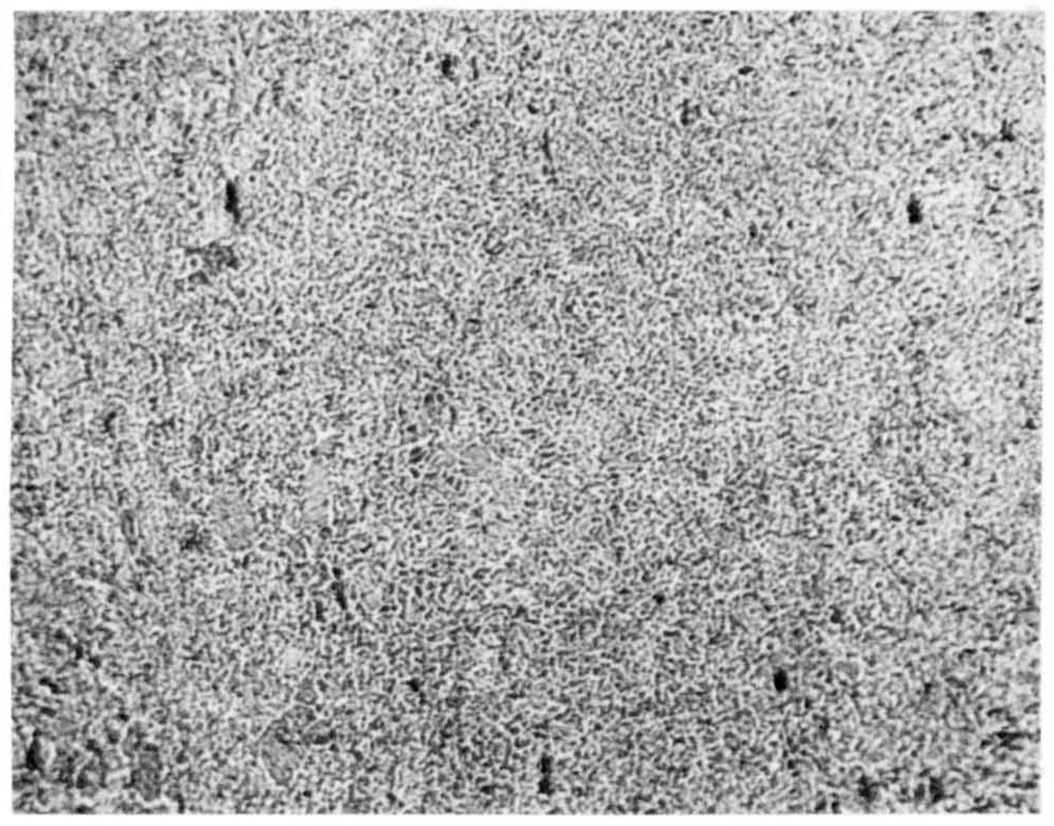

90%

Figure 18- Microstructures after increasing amounts of percentage reduction during room temperature rolling.(x300).

x15000

x25000

Figure 19-Microstructure of the 90% reduction, room temperature rolled sheet examined within fifteen minutes after the final pass.(TEM).

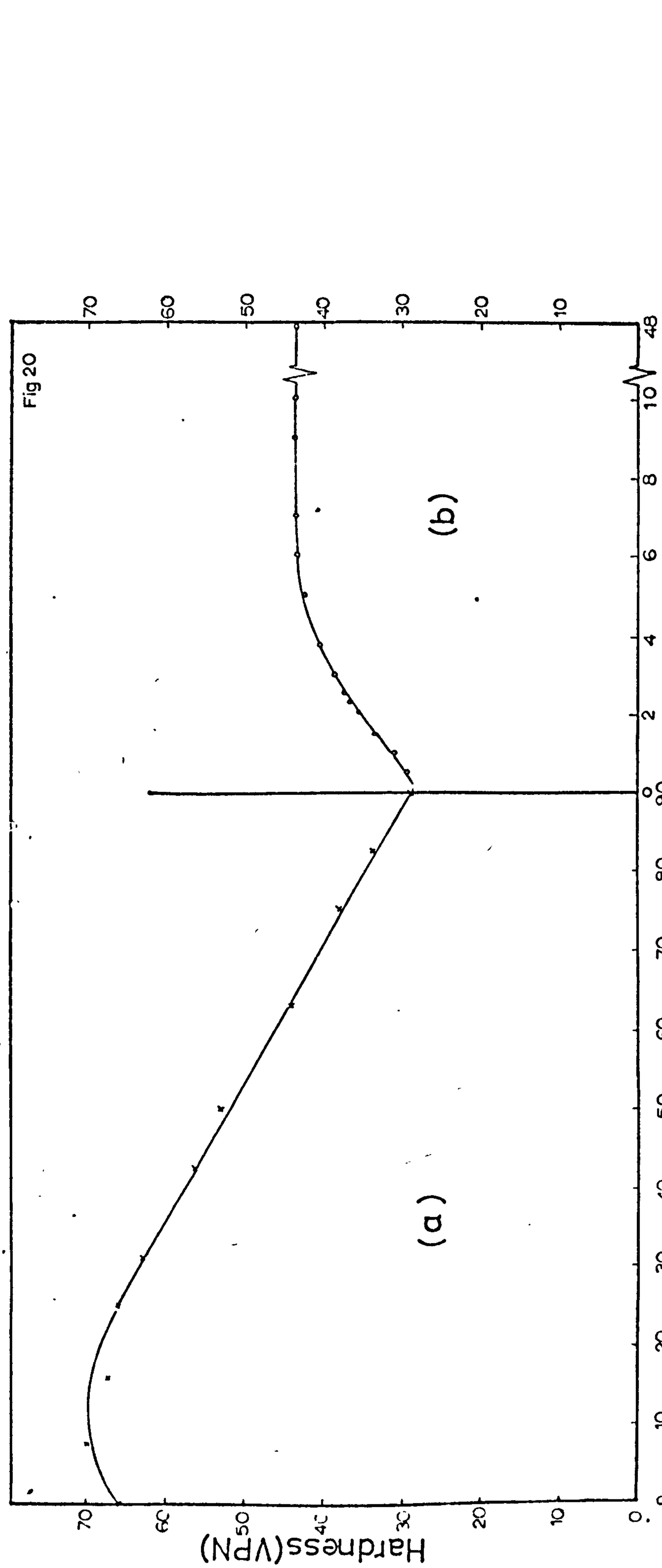

Figure 20a—The effect of percentage reduction at room temperature on the Vickers Hardness No.

Figure 20b—The effect of room temperature ageing of the as rolled sheet on the Vickers Hardness No.

Figure 21-Microstructure of the as rolled sheet strained 200% at 0.1 in/min crosshead velocity after ageing at room temperature for 3 hours. The surface of the gauge length was chemically polished before straining. (x3000).

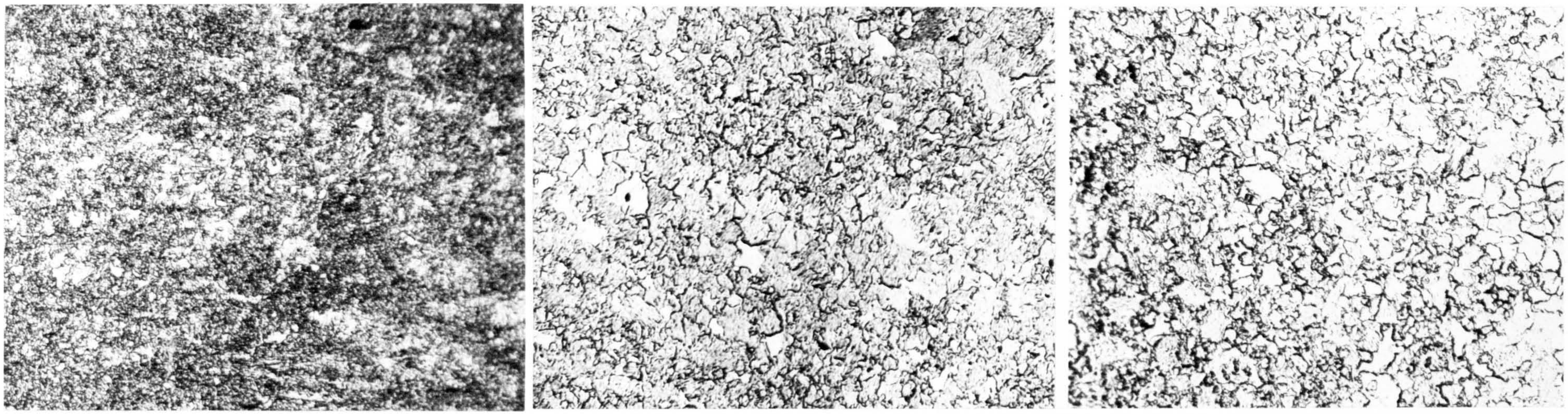

45 minutes | 2½ hours | 4 hours

6 hours | 8 hours | 3 days

Figure 22- Microstructures showing grain growth at room temperature of the as rolled sheet. Surface.(x300).

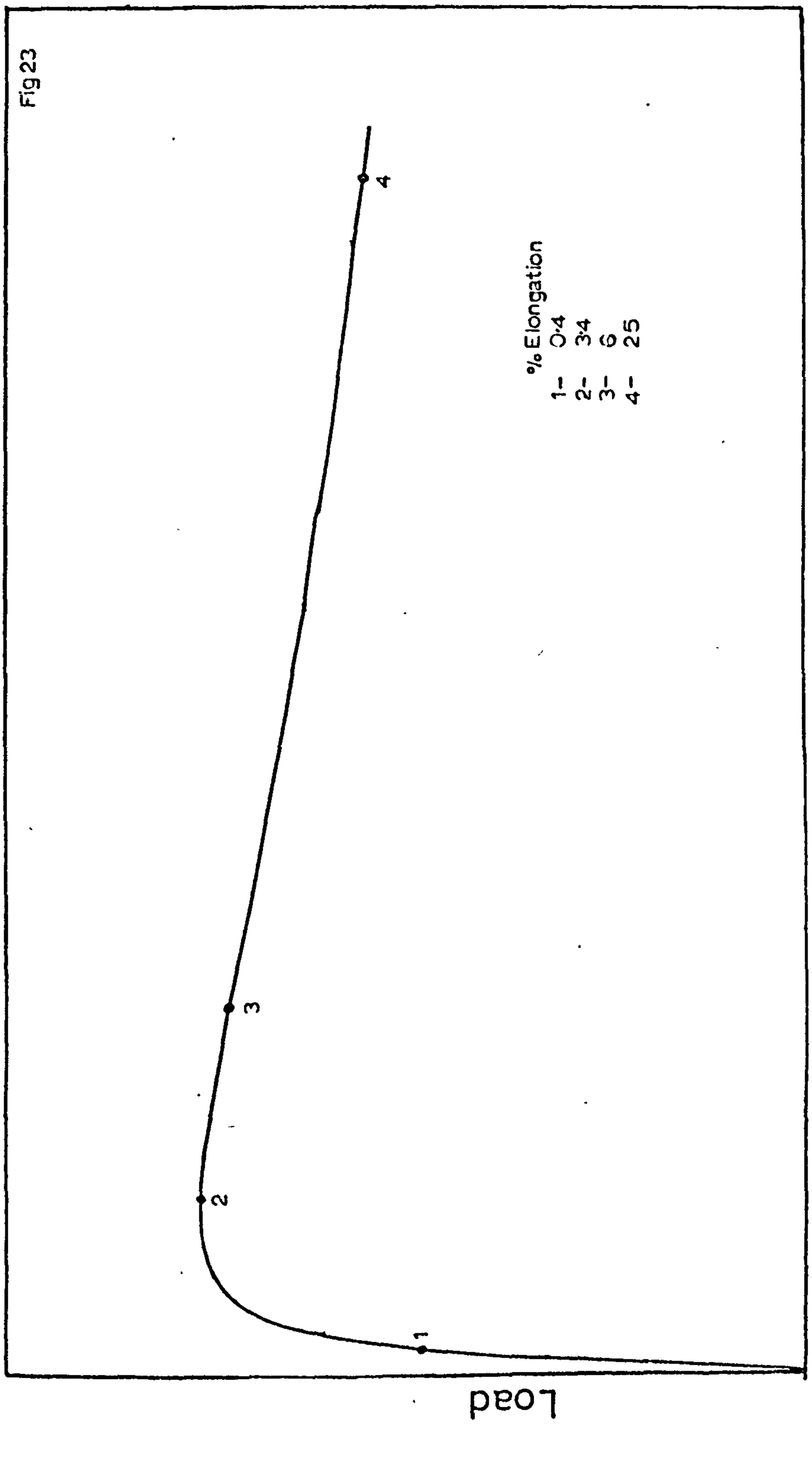

Figure 23- A typical load-extension curve obtained at room temperature on at a crosshead velocity of 0.1 in/min. The curve exhibits points specimens were strained followed by room temperature ageing.

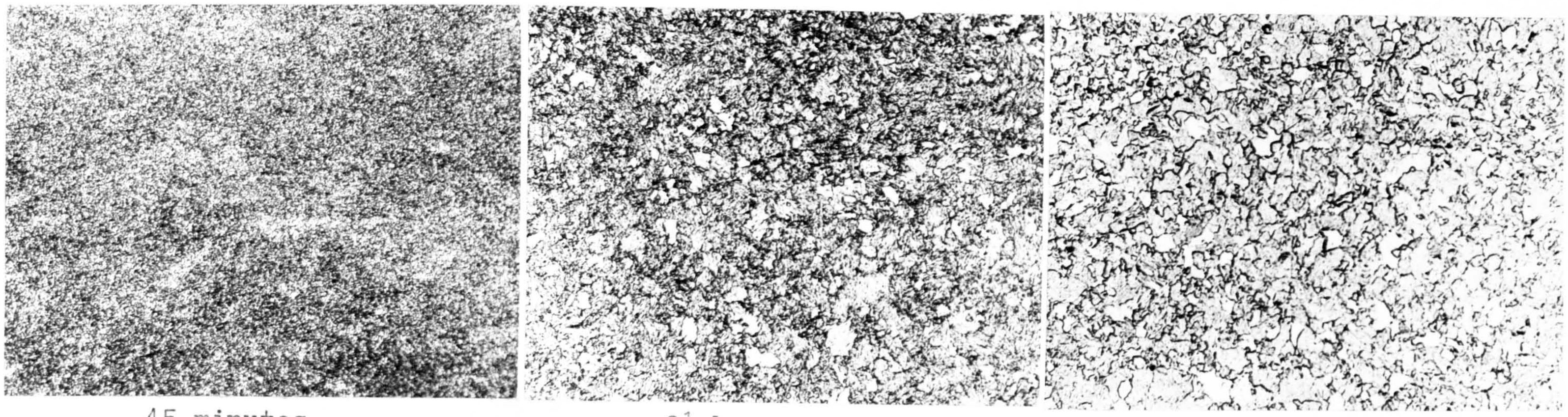

45 minutes | $2\frac{1}{2}$ hours | 28 hours

Figure 24a- Shows the effect of 0.4% elongation on grain growth at room temperature. Surface.(x300)

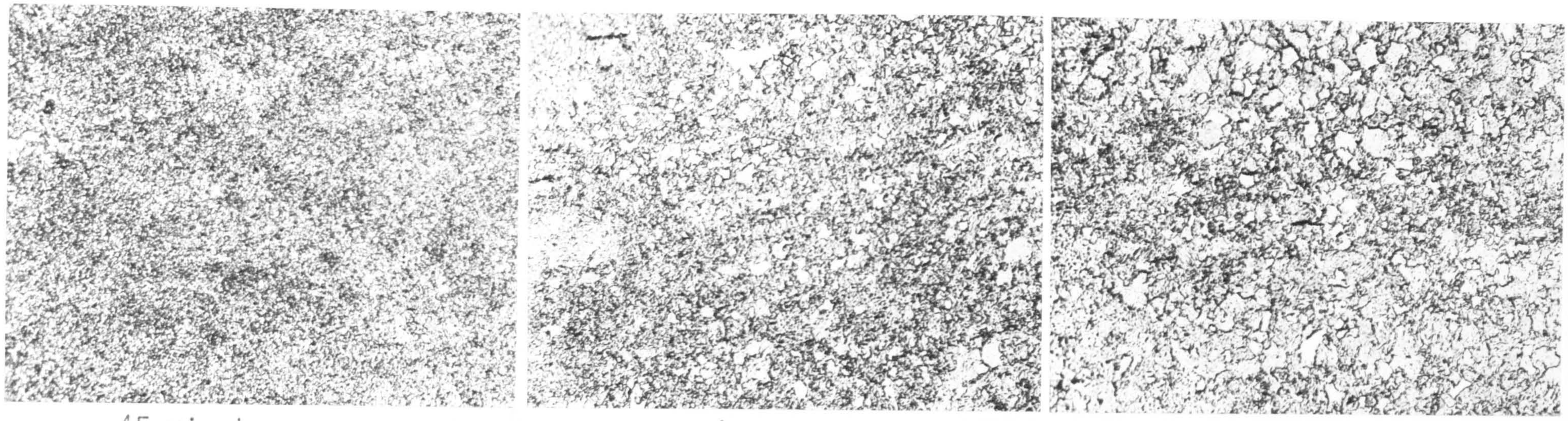

45 minutes

$2\frac{1}{2}$ hours

4 hours

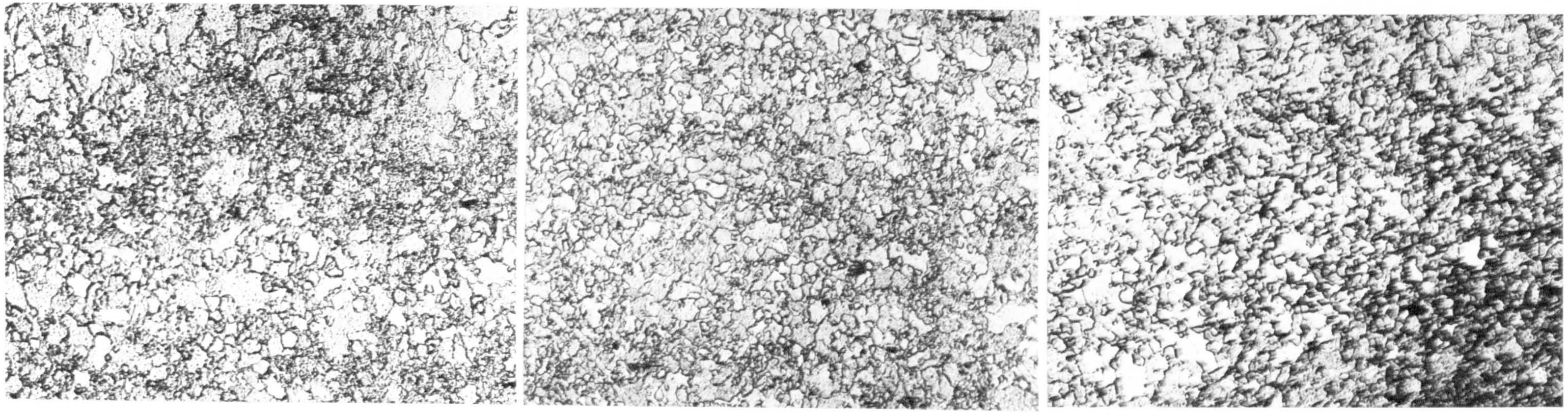

6 hours

8 hours

28 hours

Figure 24b- Shows the effect of 3.4% elongation on grain growth at room temperature. Surface.(x300).

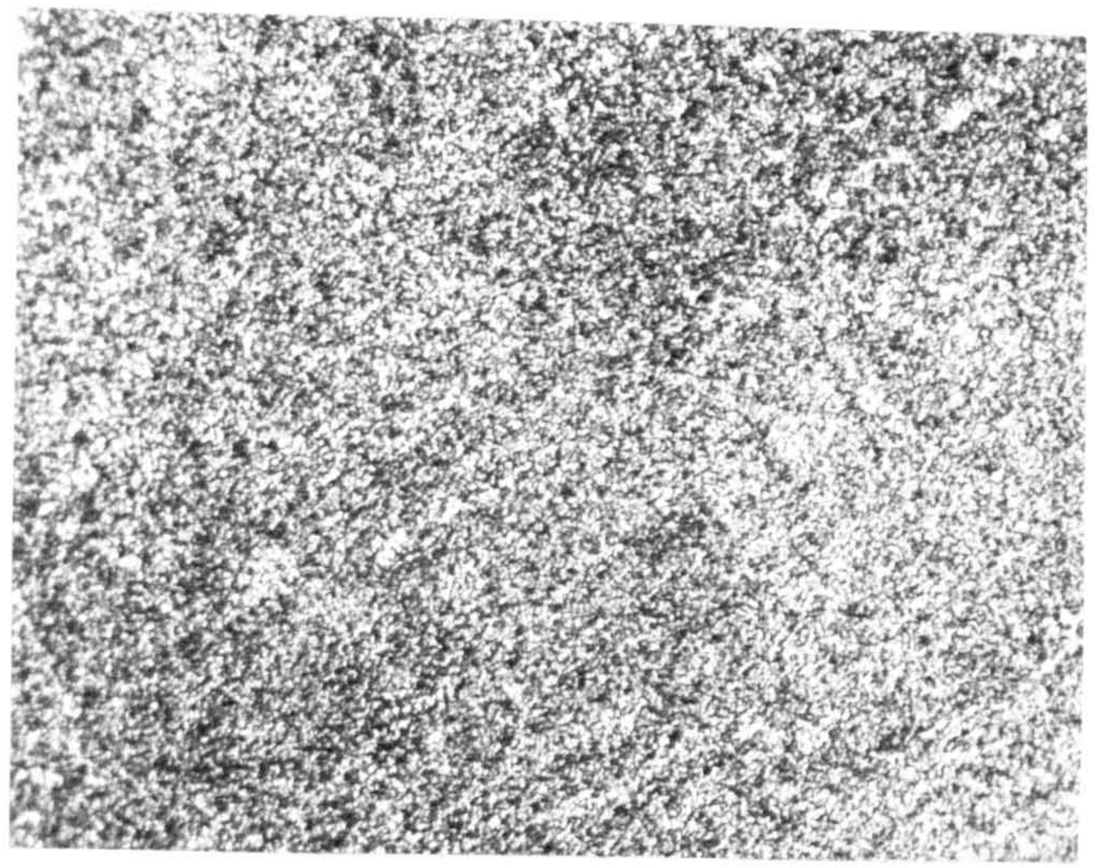

45 minutes

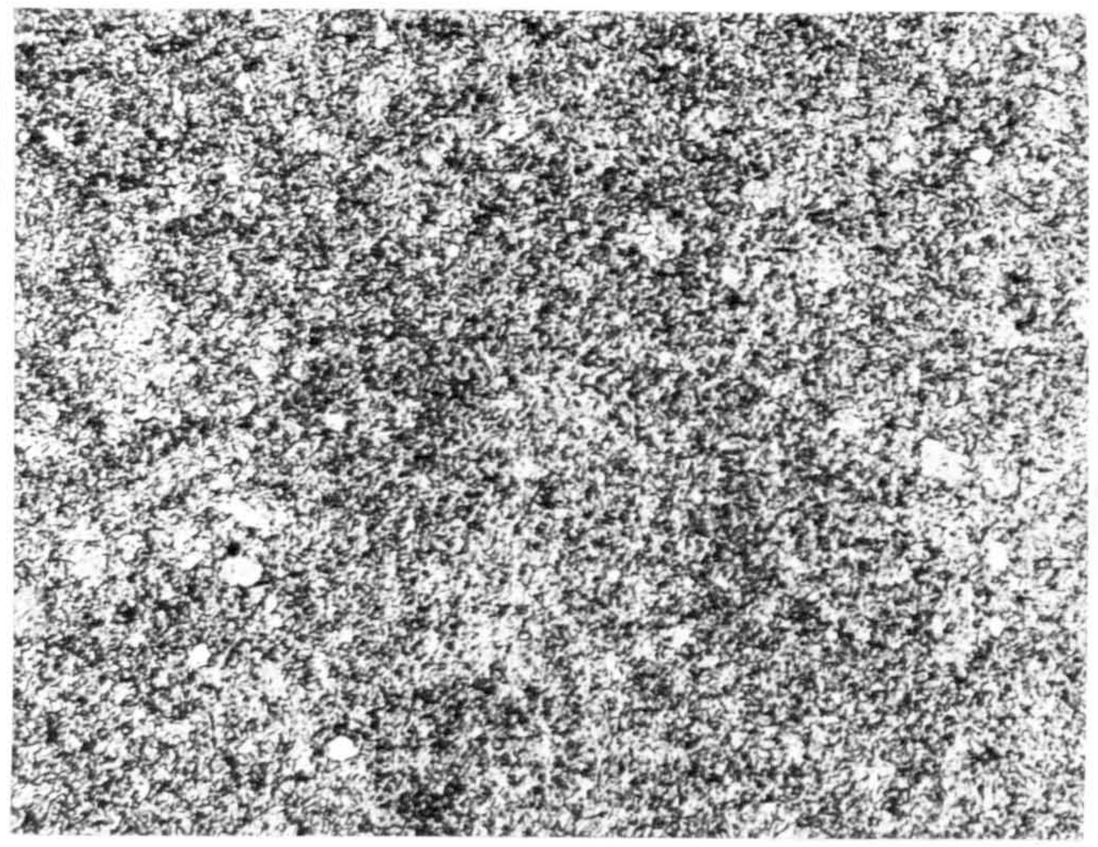

$2\frac{1}{2}$ hours

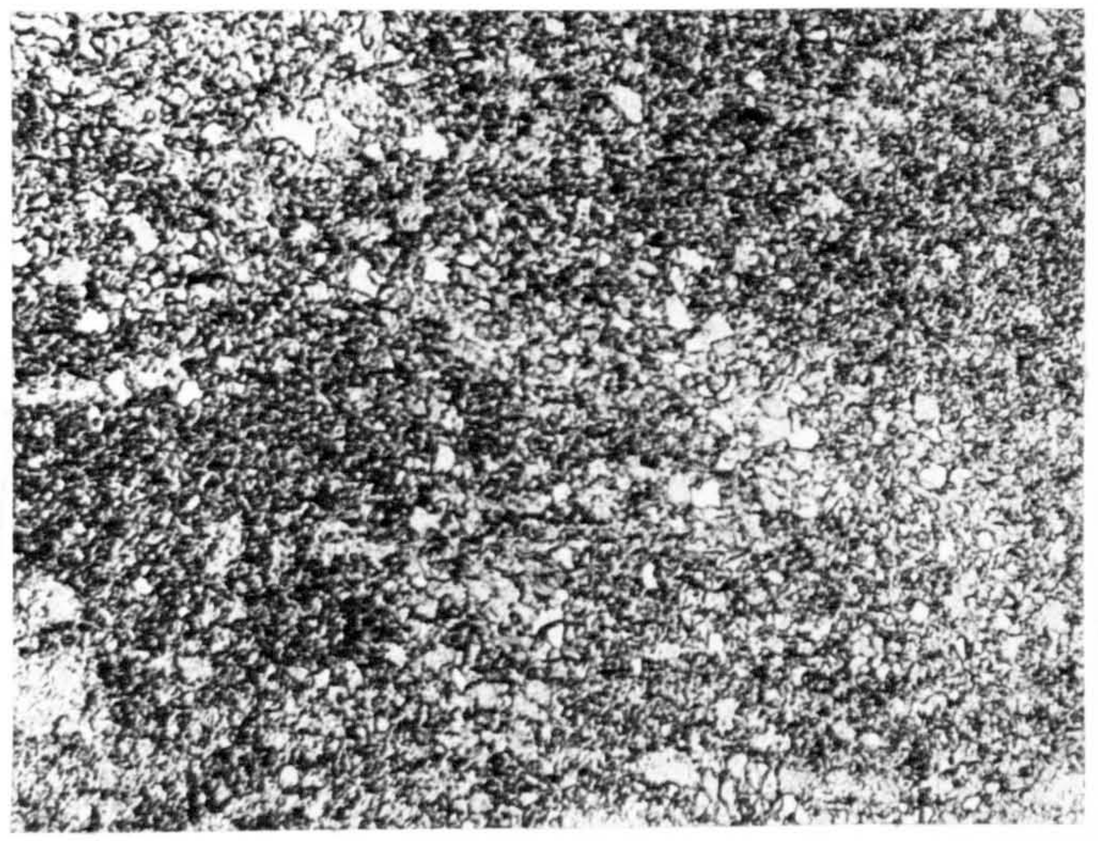

4 hours

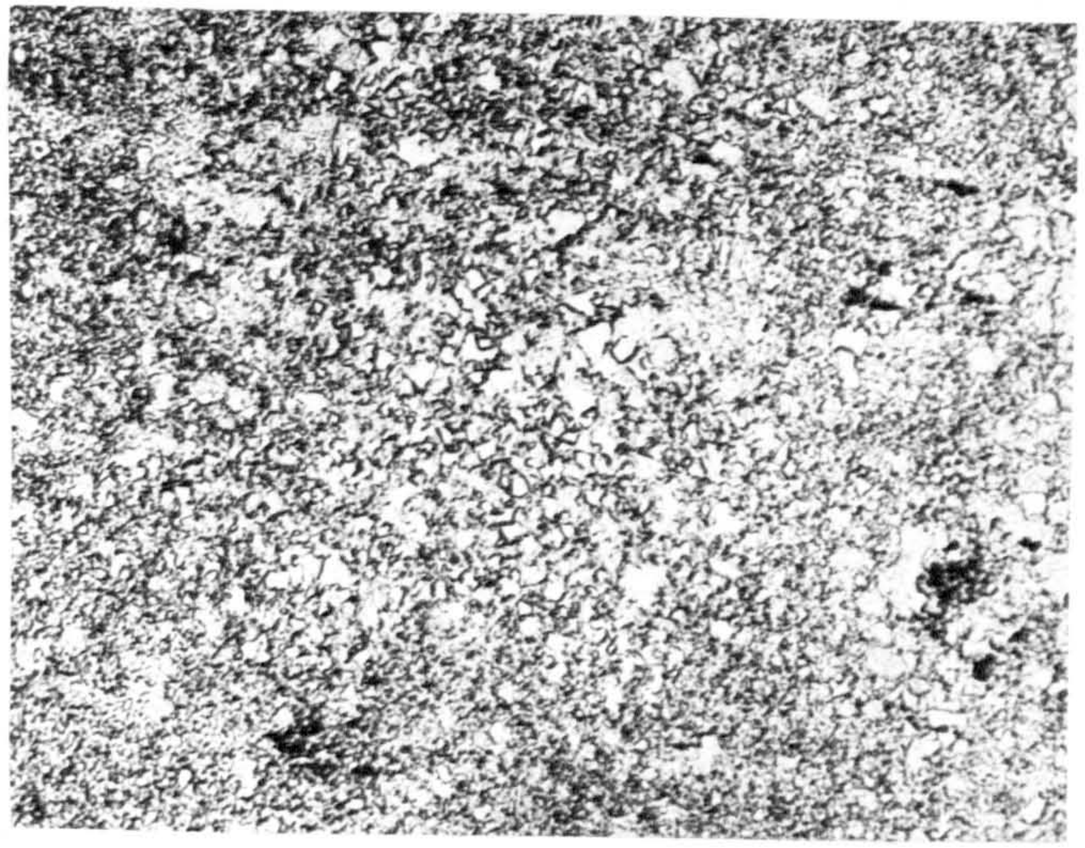

6 hours

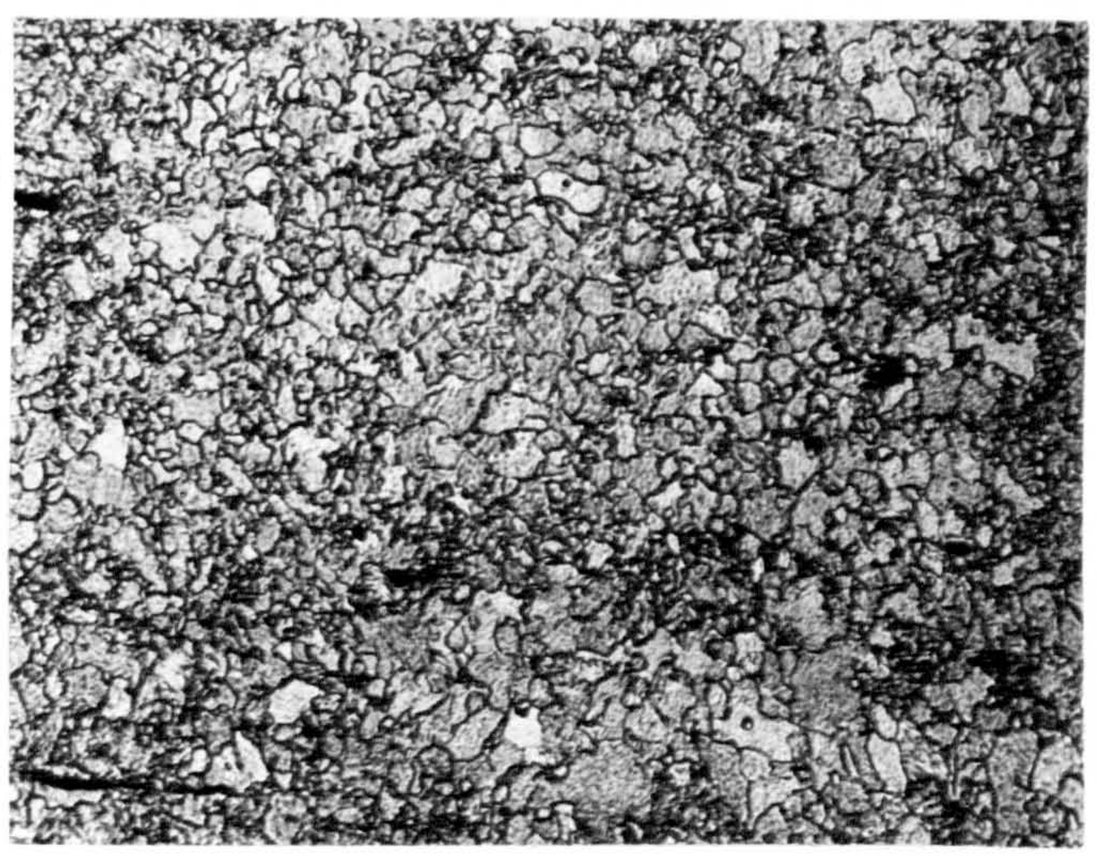

8 hours

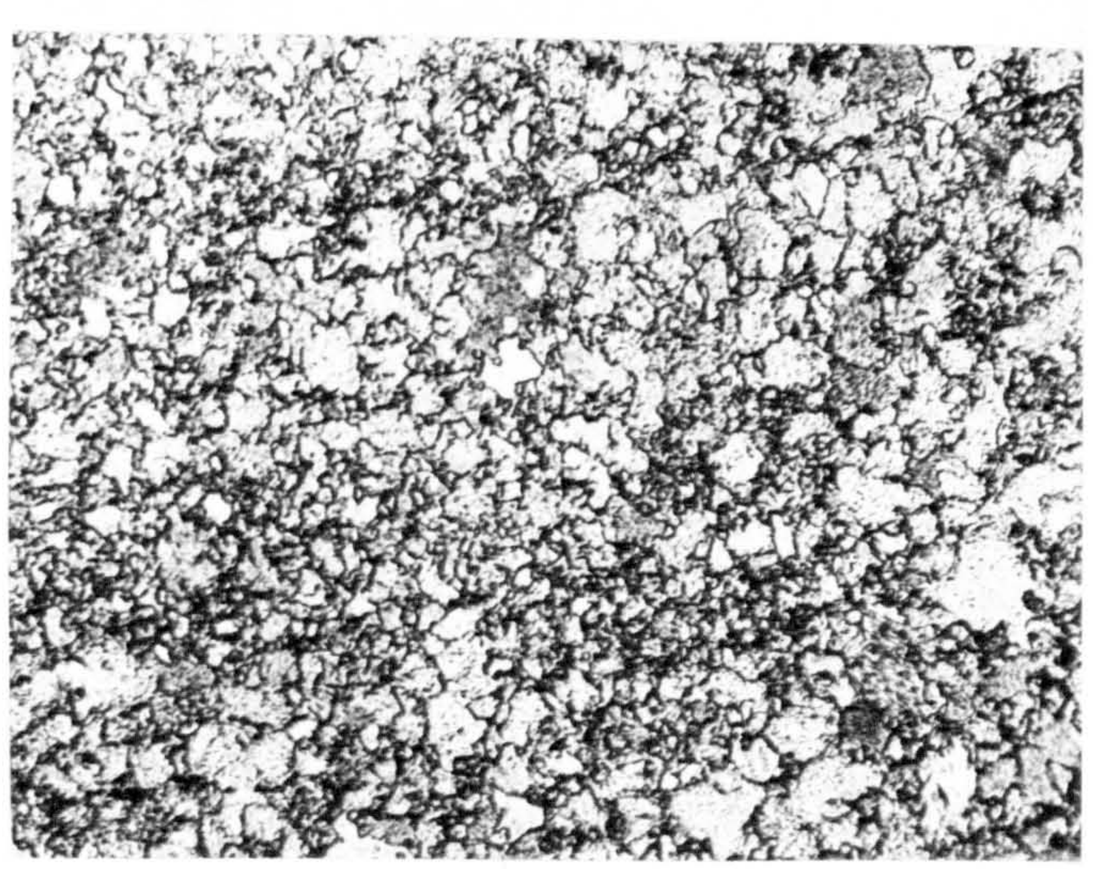

28 hours

Figure 24c- Shows the effect of 6% elongation on grain growth at room temperature. Surface.(x300).

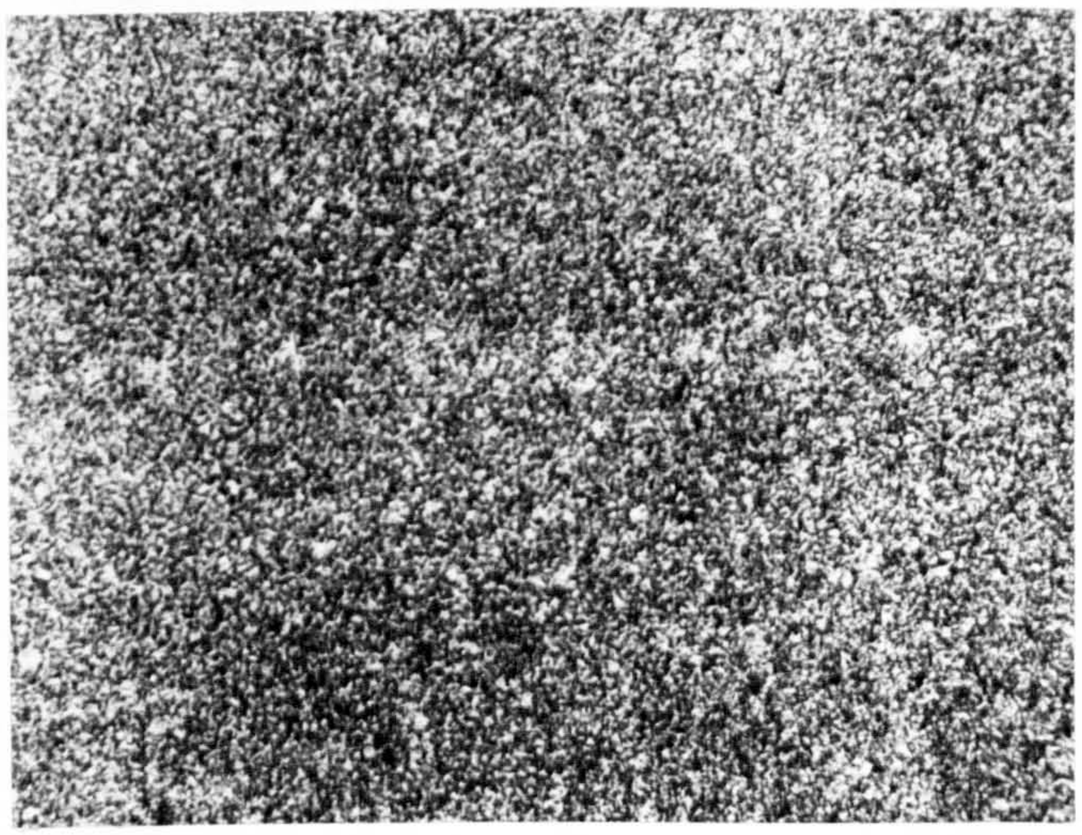

Figure 24d-Shows the effect of 25% elongation on grain growth at room temperature. Surface.(x300).

Figure 25-The effect of % elongation, as indicated in Figure 23, on the 0.2% proof stress determined after increasing room temperature ageing.

Fig 25

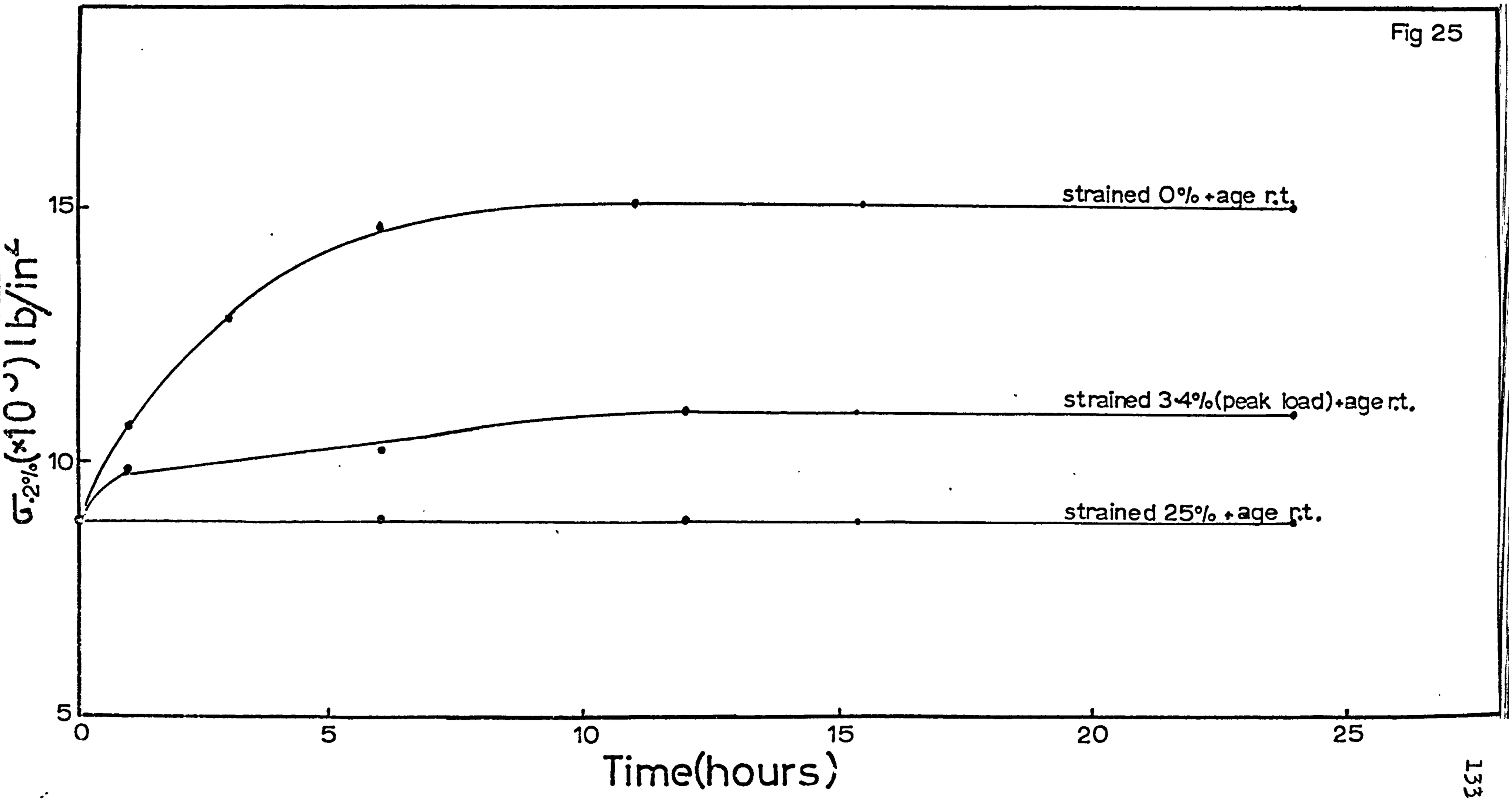
15
10
5
$\sigma_{.2\%}(\times 10^3)$ lb/in^2
strained 0% +age r.t.
strained 3·4%(peak load)+age r.t.
strained 25% +age r.t.
0
5
10
15
20
25
Time(hours)

Figure 26- The effect of % elongation, as indicated in Figure 23, on the m vs relationship determined after increasing room temperature ageing.

Fig 26

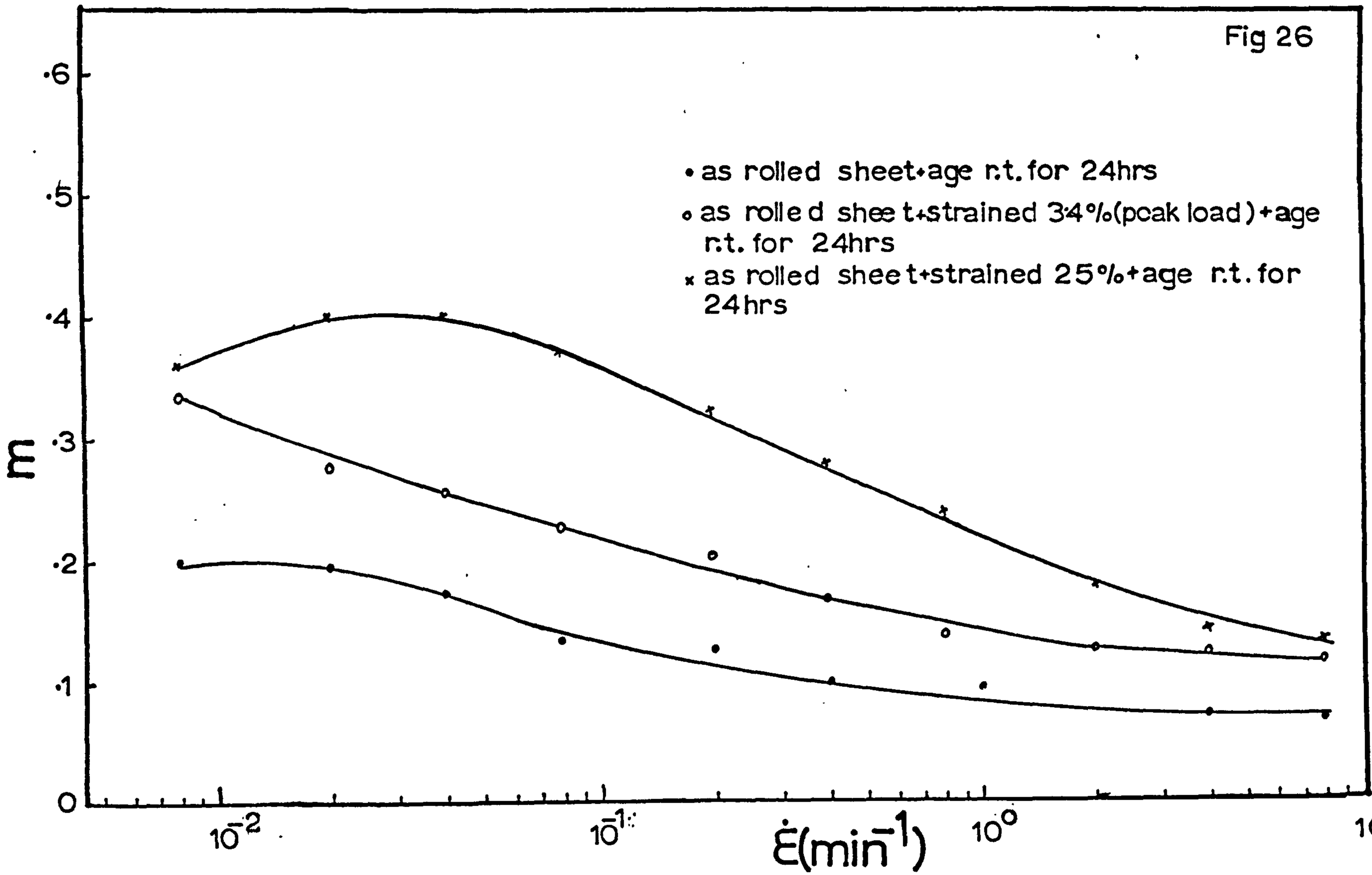
• as rolled sheet+age r.t. for 24hrs
∘ as rolled sheet+strained 3·4%(peak load)+age r.t. for 24hrs
× as rolled sheet+strained 25%+age r.t. for 24hrs
m
·6
·5
·4
·3
·2
·1
0
10^{-2}
10^{-1}
10^{0}
10^{1}
$\dot{\varepsilon}(min^{-1})$

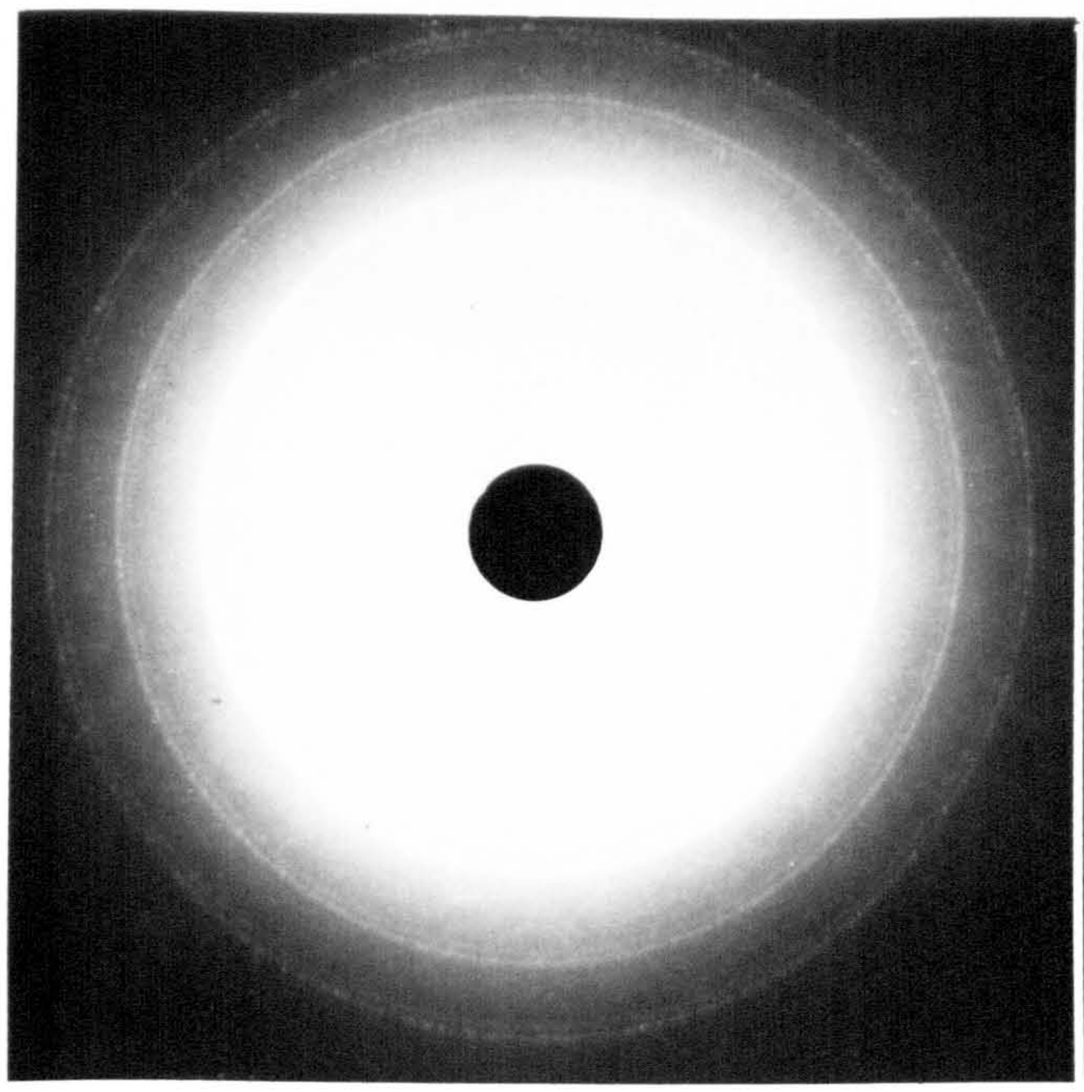

(a)

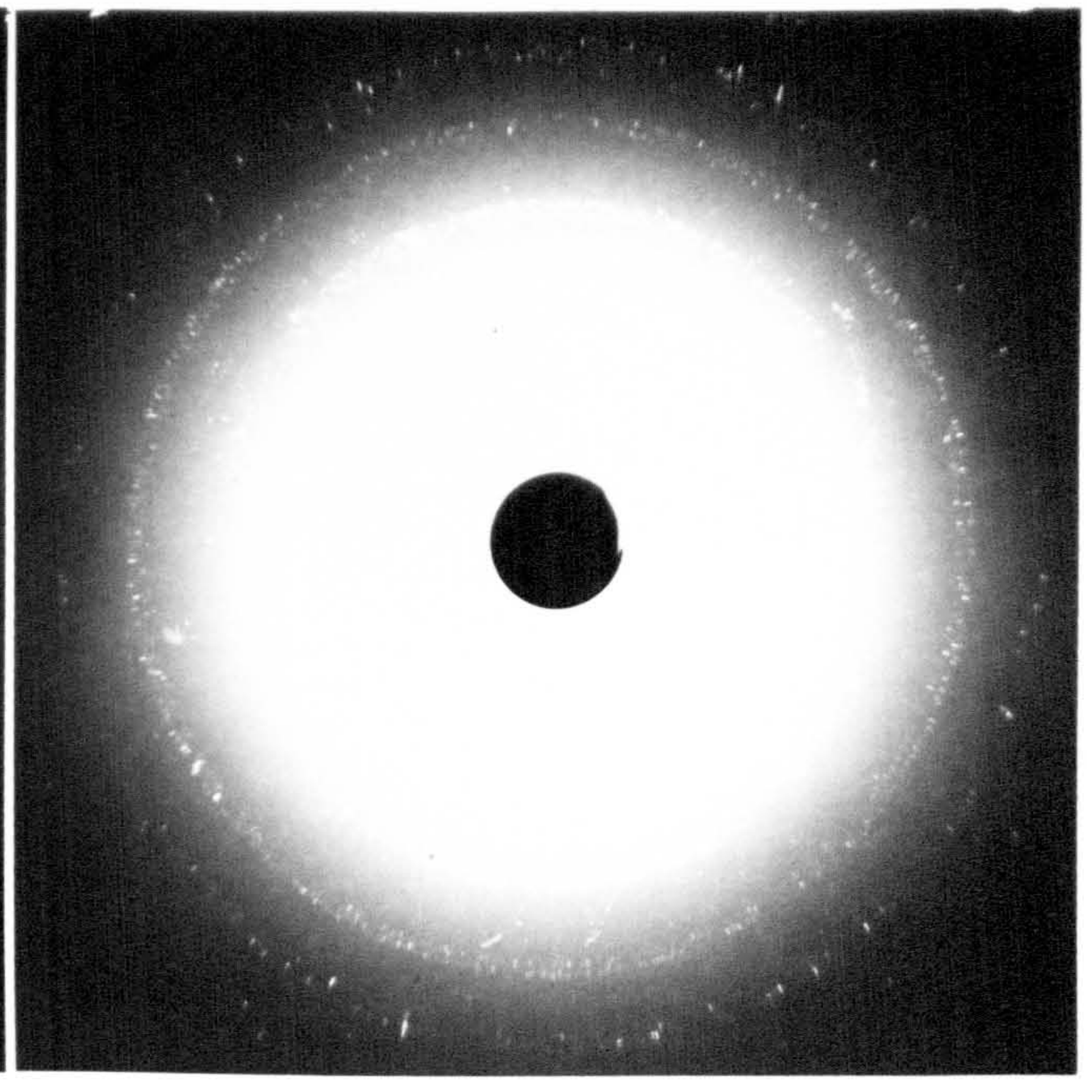

(b)

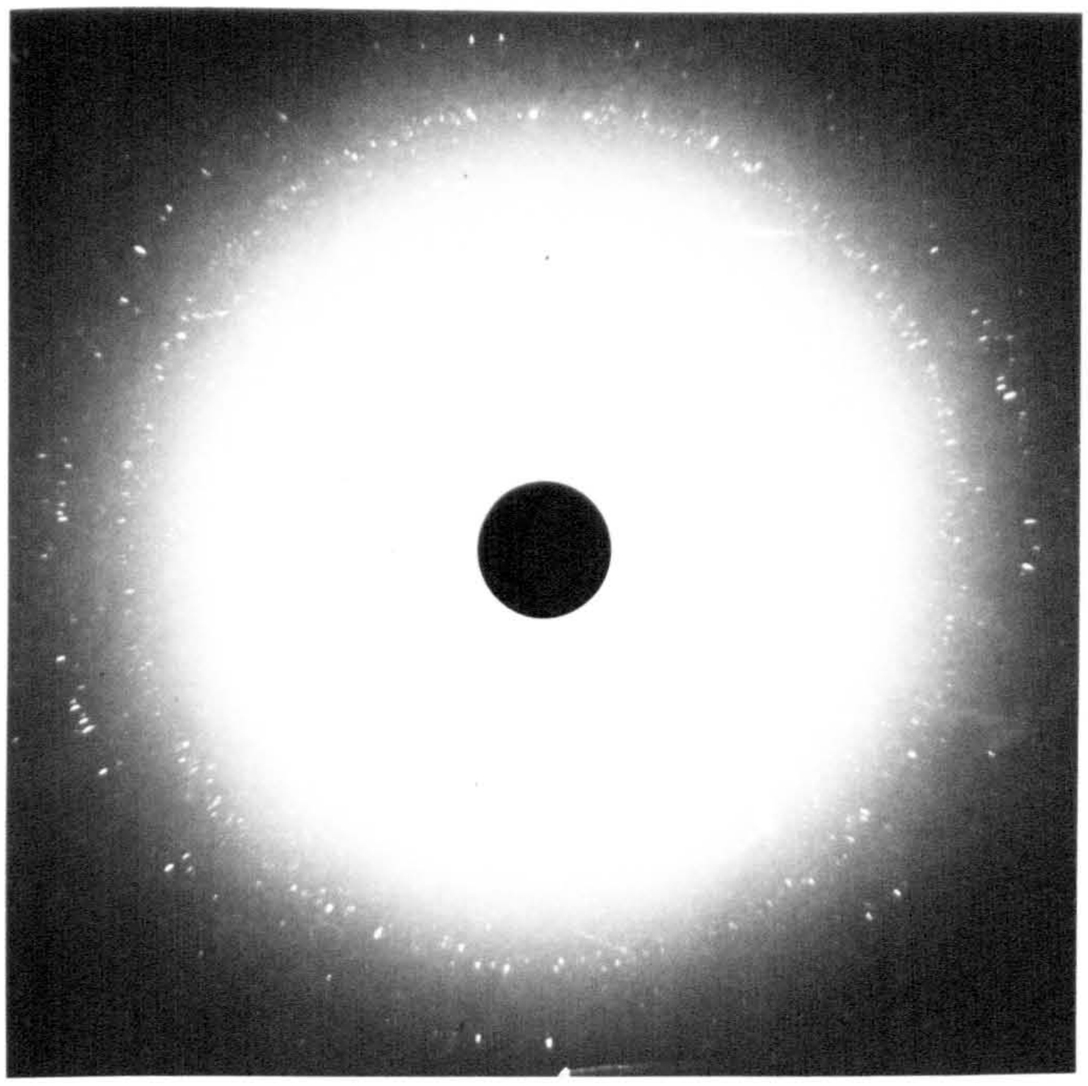

(c)

Figure 27- Shows X-ray Back Reflection Patterns.
(a)-Gauge length strained 300% and aged at room temperature for 1 week.

(b)-Grip end of the same specimen as (a), aged at room temperature for 1 week.

(c)-The as rolled sheet aged at room temperature for 1 week.

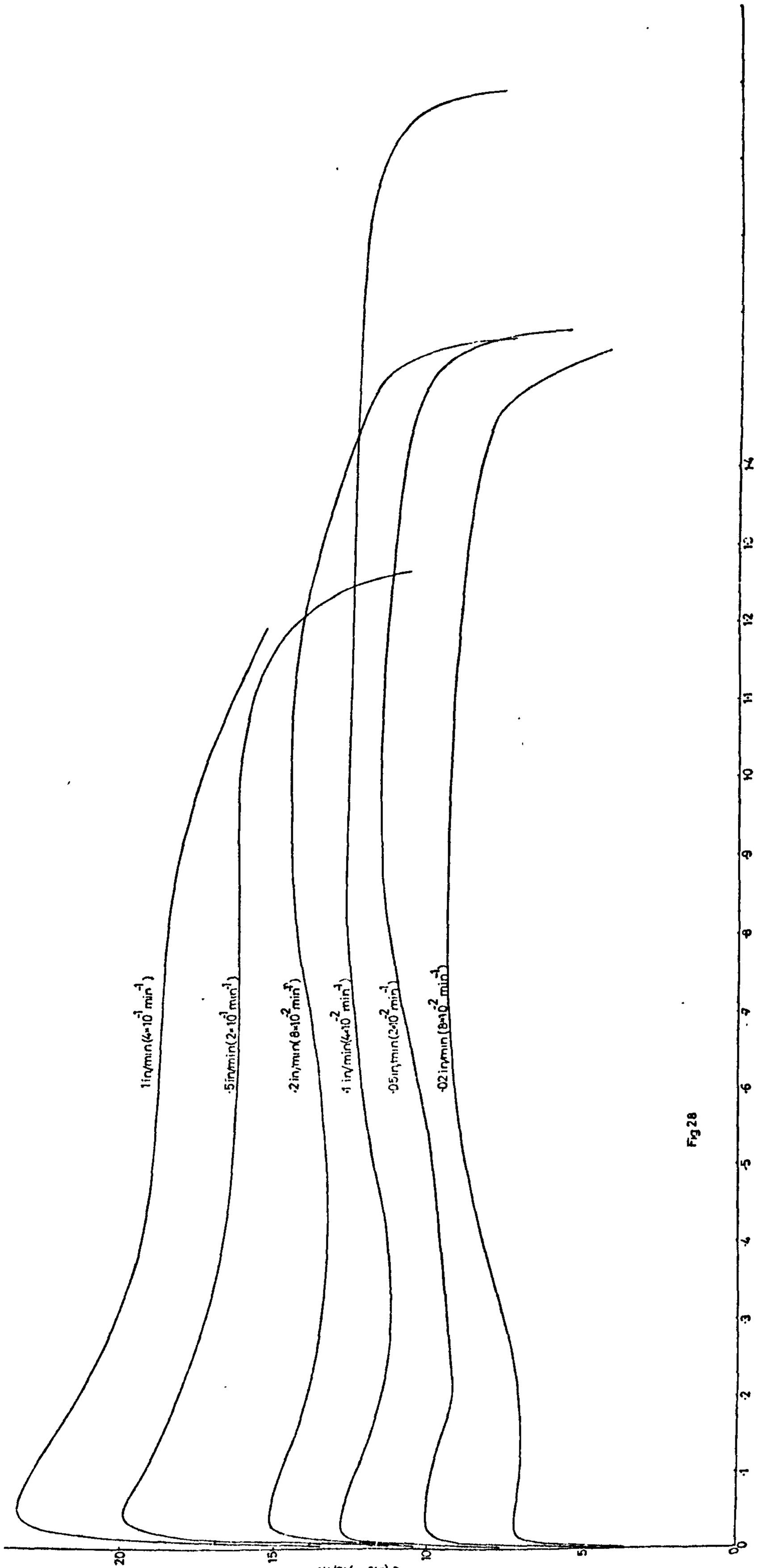

Figure 28- True stress/true strain curves obtained at room temperature for velocity range of .02 to 1 in/min (strained in the rolling direction).

Figure 29–Shows the effect of crosshead velocities on the % elongation obtained on straining at room temperature.

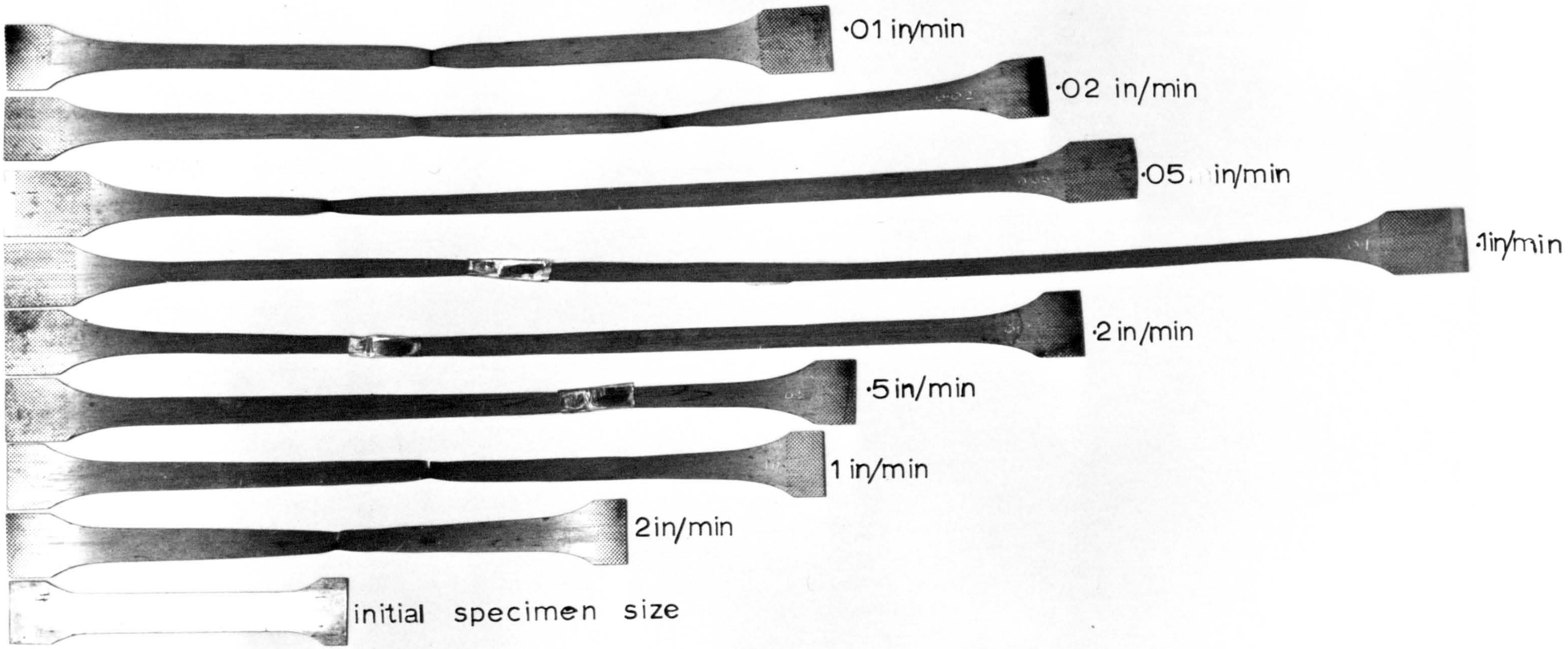
·01 in/min
·02 in/min
·05 in/min
·1in/min
·2 in/min
·5 in/min
1 in/min
2in/min
initial specimen size

Figure 29

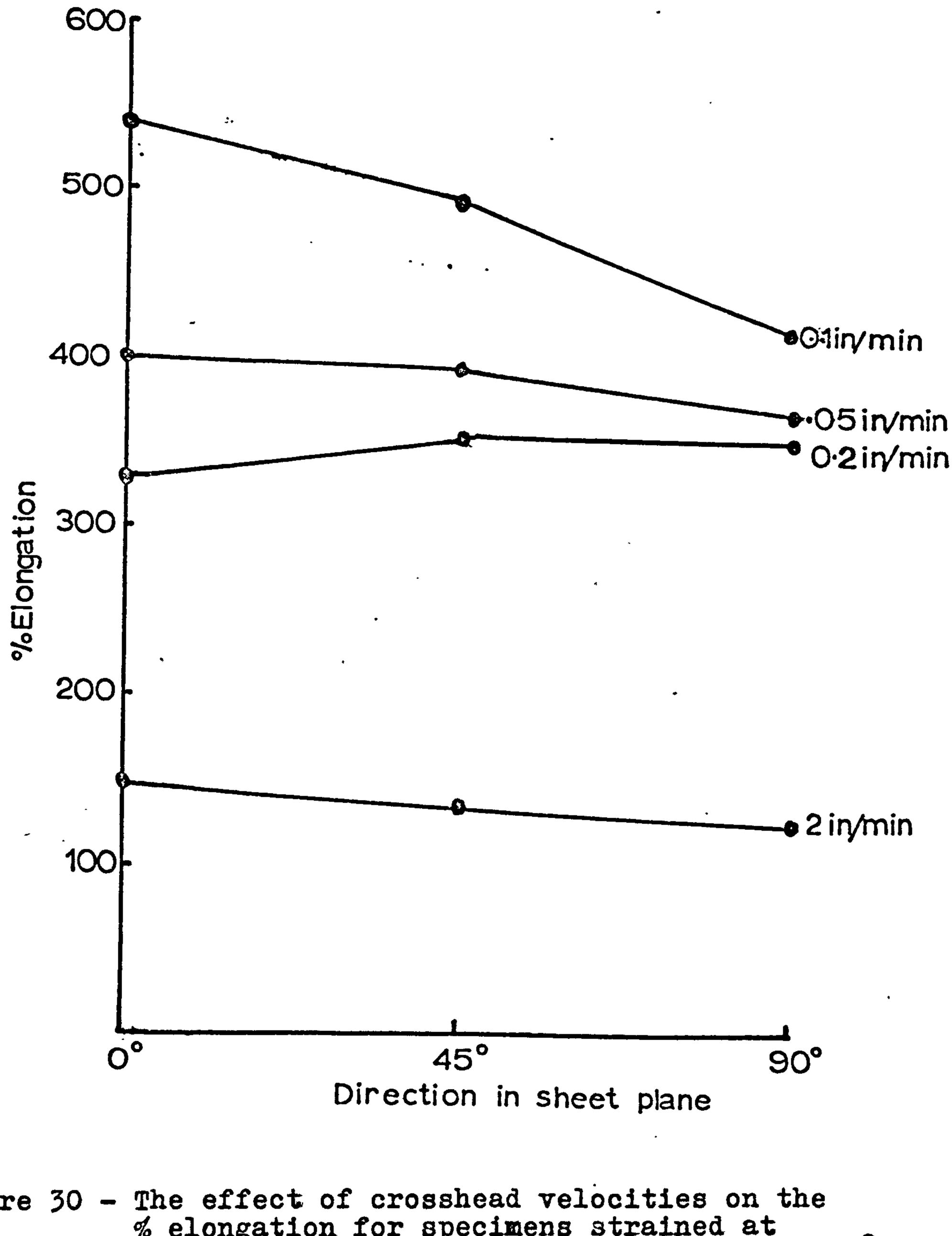

Figure 30 - The effect of crosshead velocities on the % elongation for specimens strained at room temperature in the rolling direction(0^{o}), 45^{o} and 90^{o} to the rolling direction.

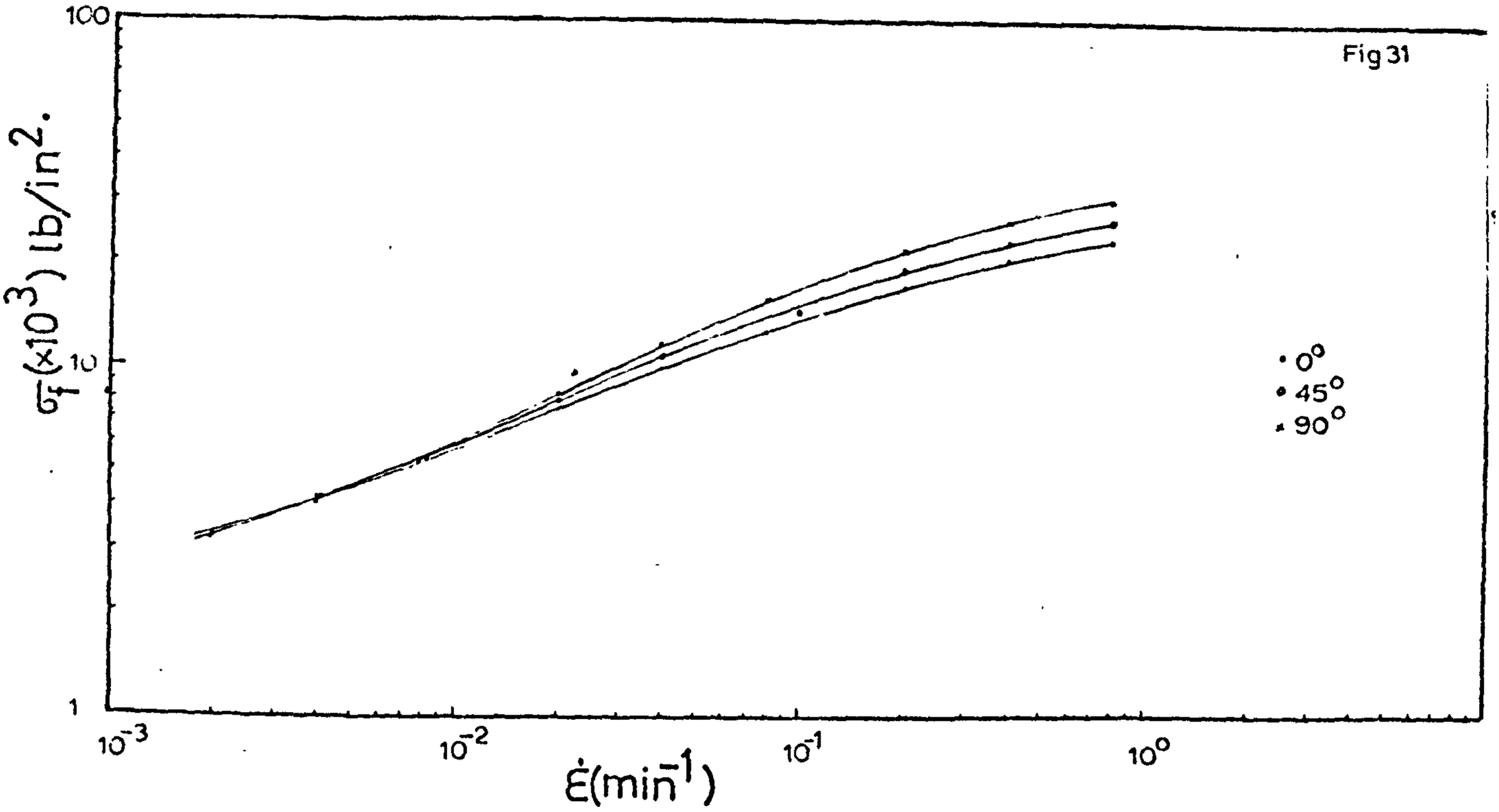

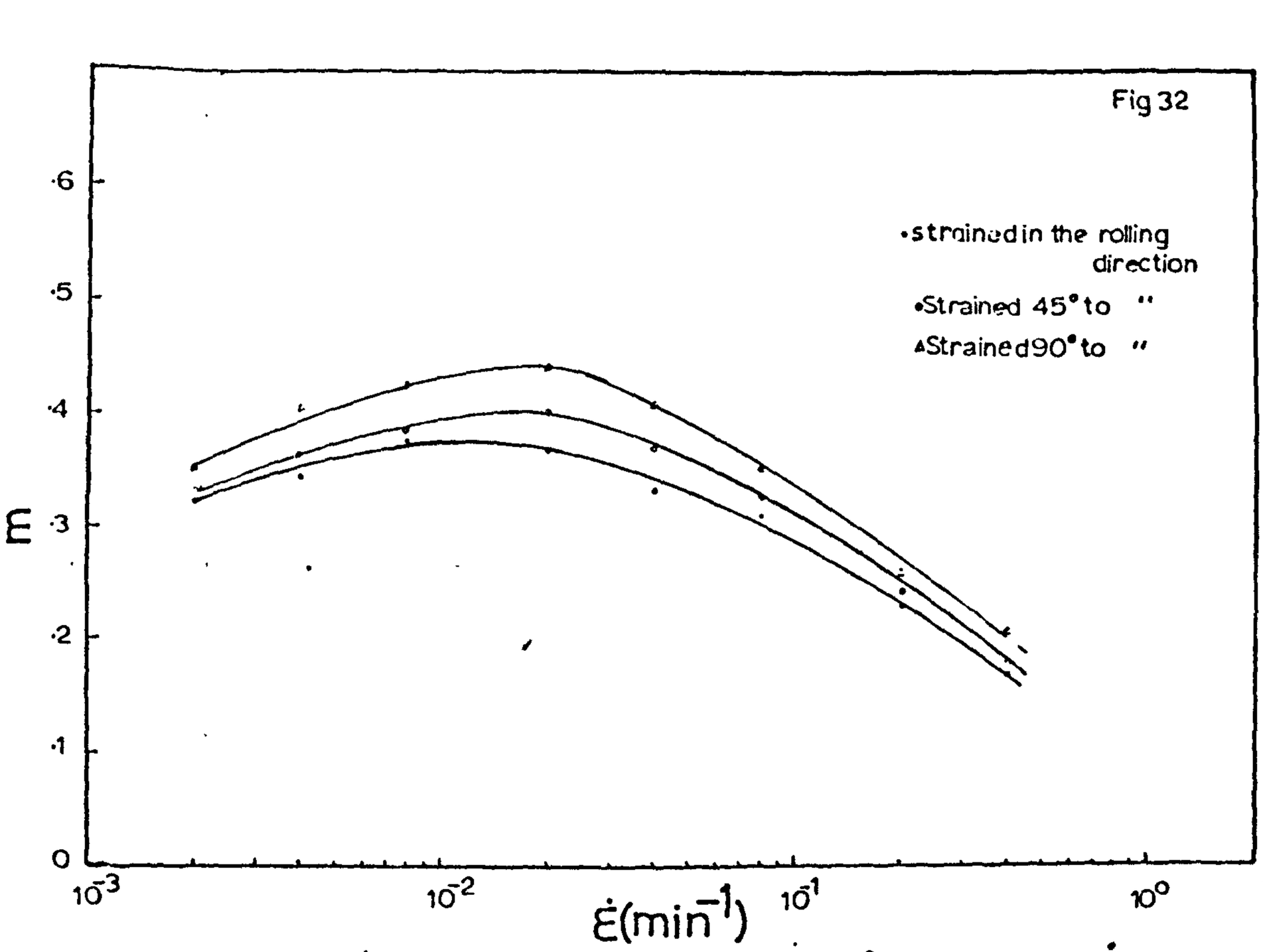

Figures 31 & 32 - Shows the $\bar{\sigma}_f$ vs $\dot{\epsilon}$ and m vs $\dot{\epsilon}$ anisotropy in the sheet plane.

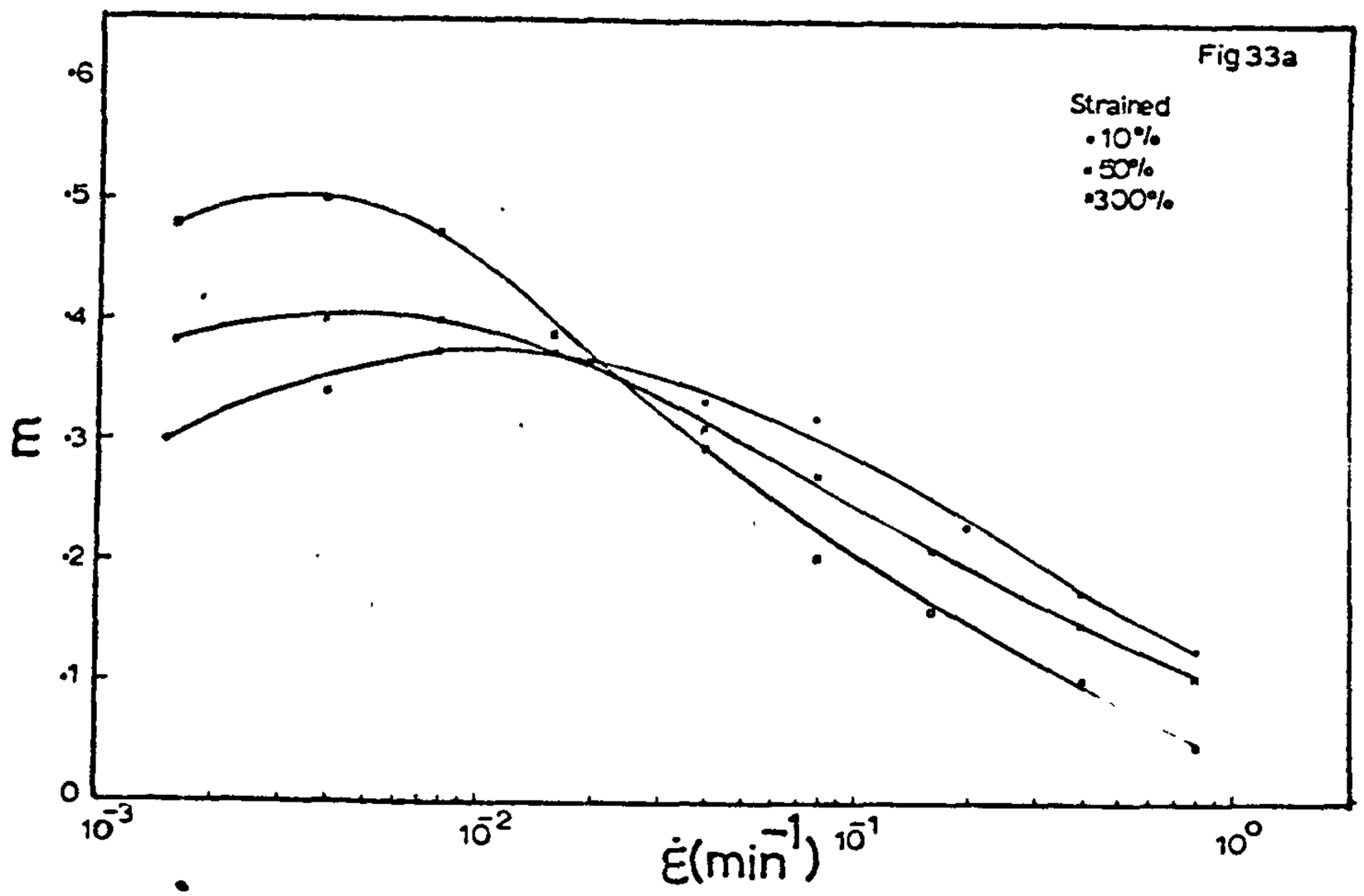

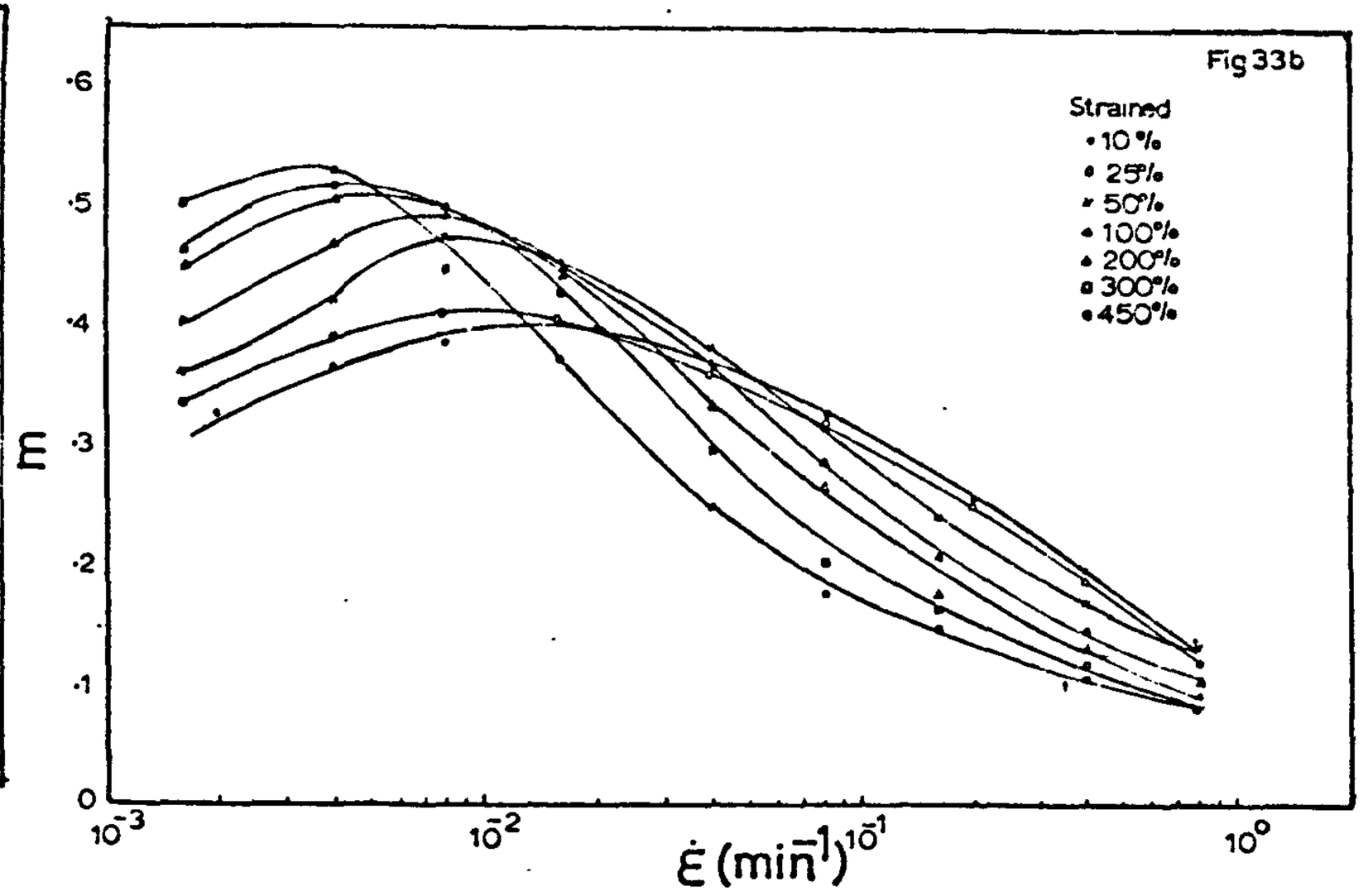

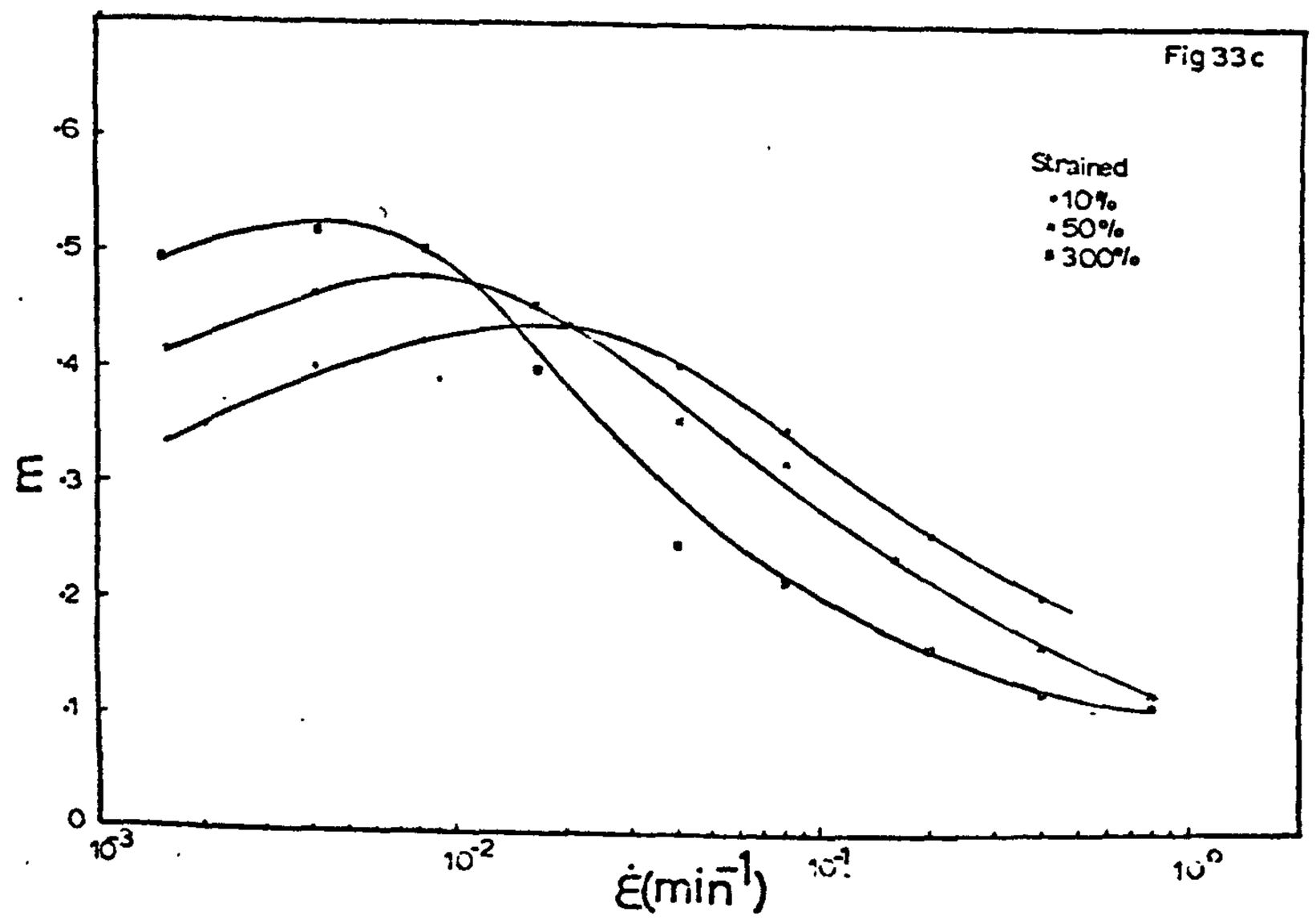

Figure 33a-c - The effect of increasing % elongation on the m vs $\dot{\epsilon}$ relationship determined in the rolling direction(0°), 45 and 90° to the rolling direction.

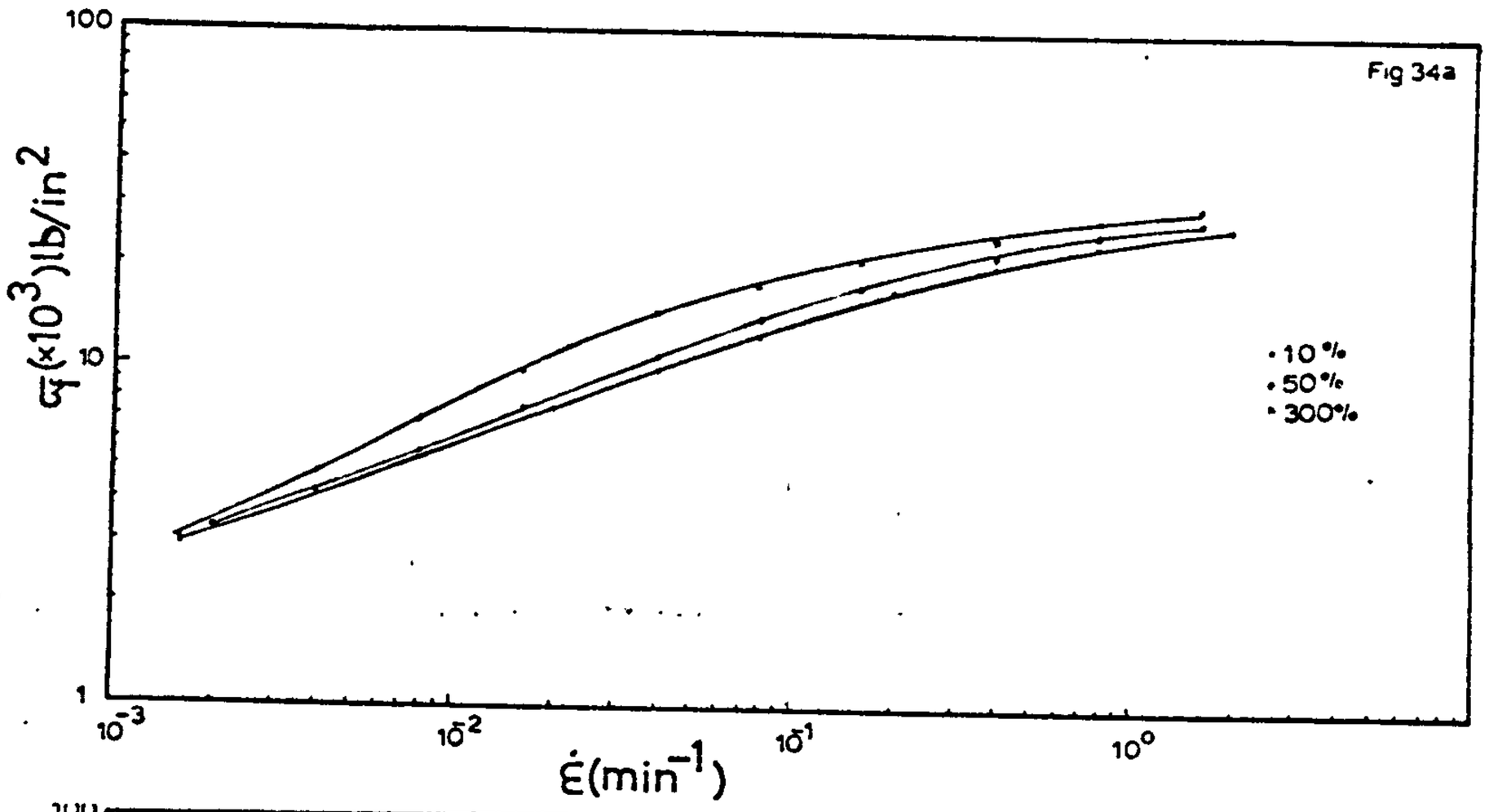

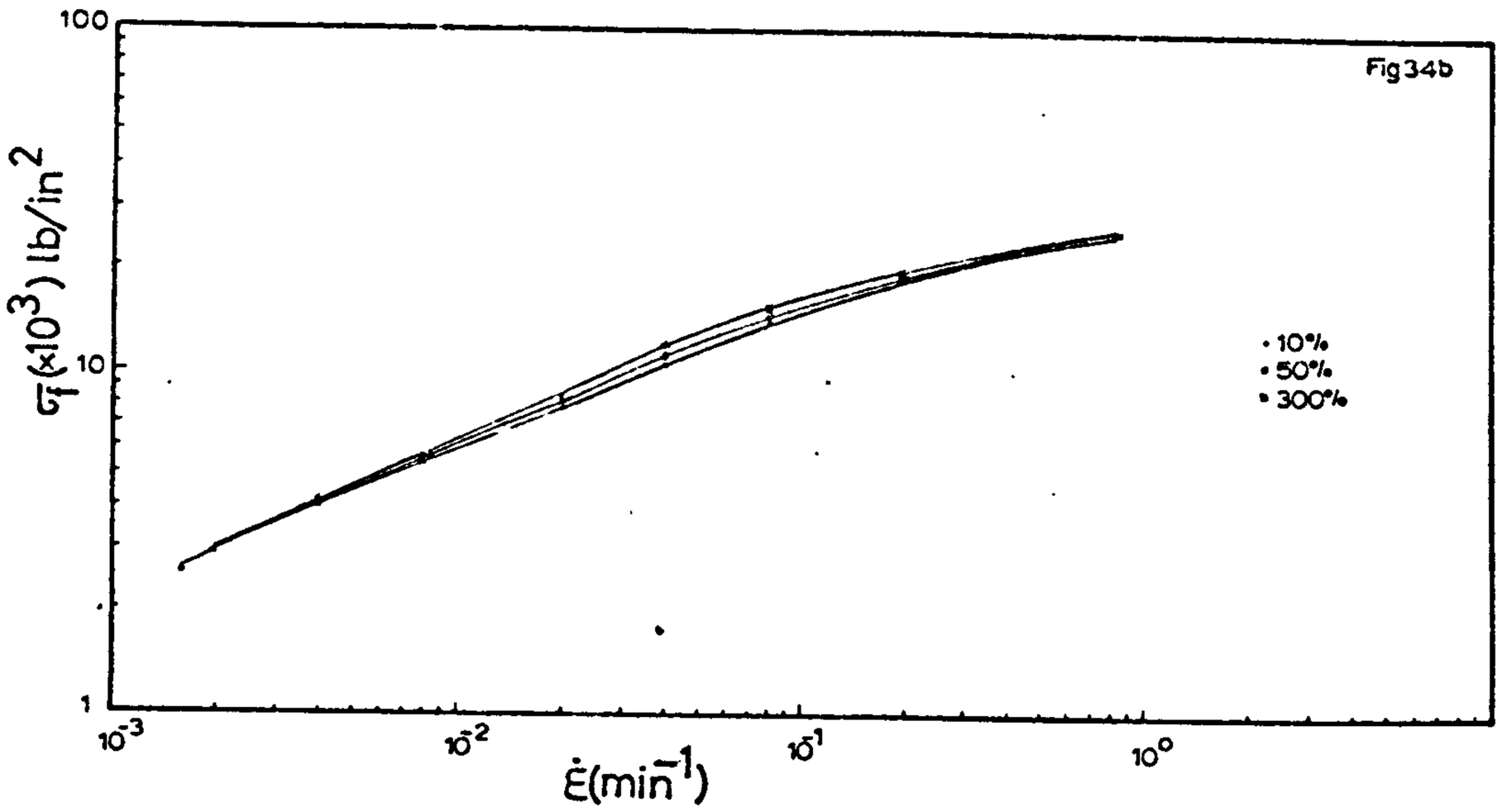

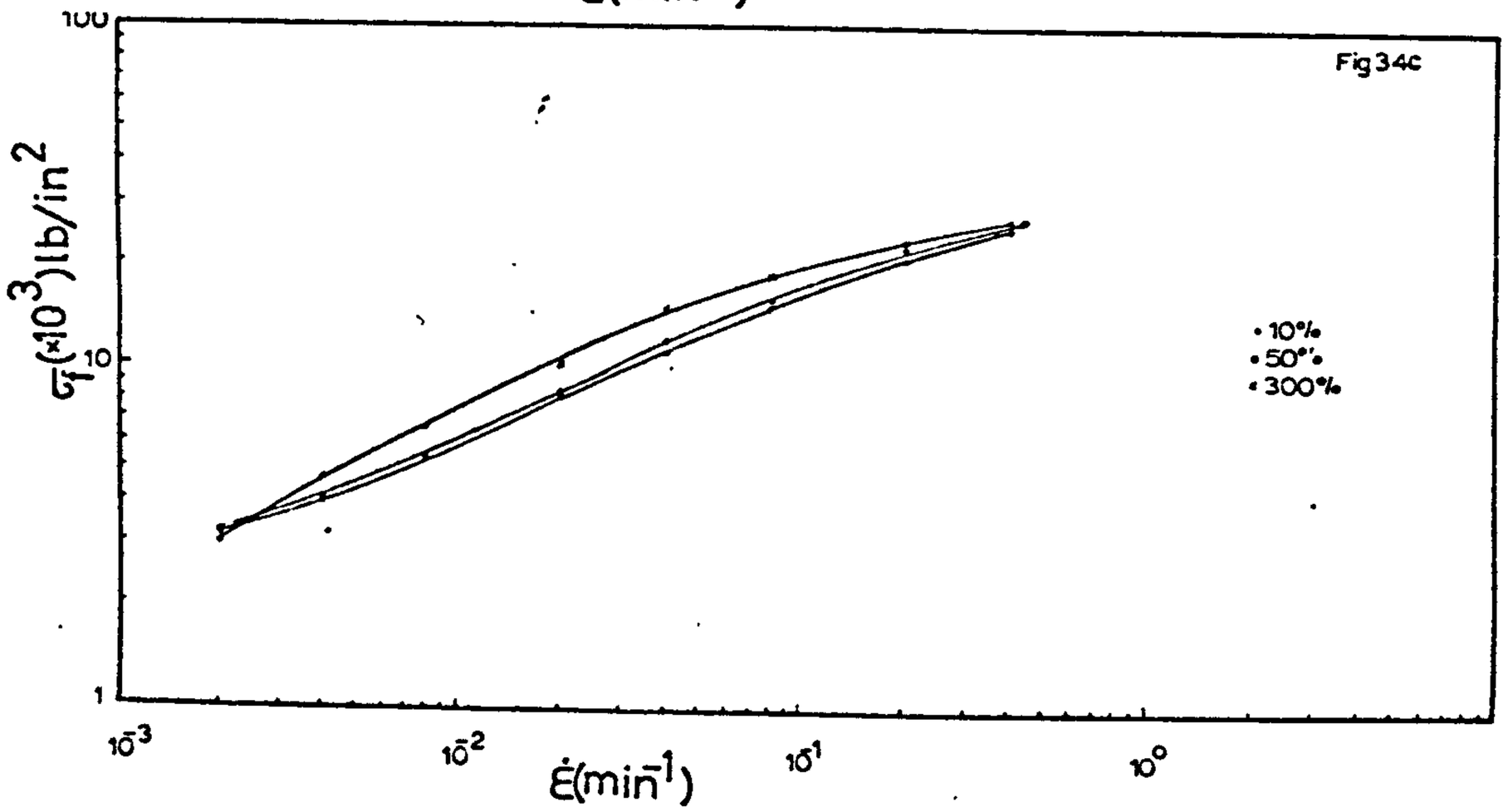

Figure 34a-c- The effect of increasing % elongation on the σ_f vs $\dot{\epsilon}$ relationship determined in the rolling direction(0°), 45 and 90° to the rolling direction.

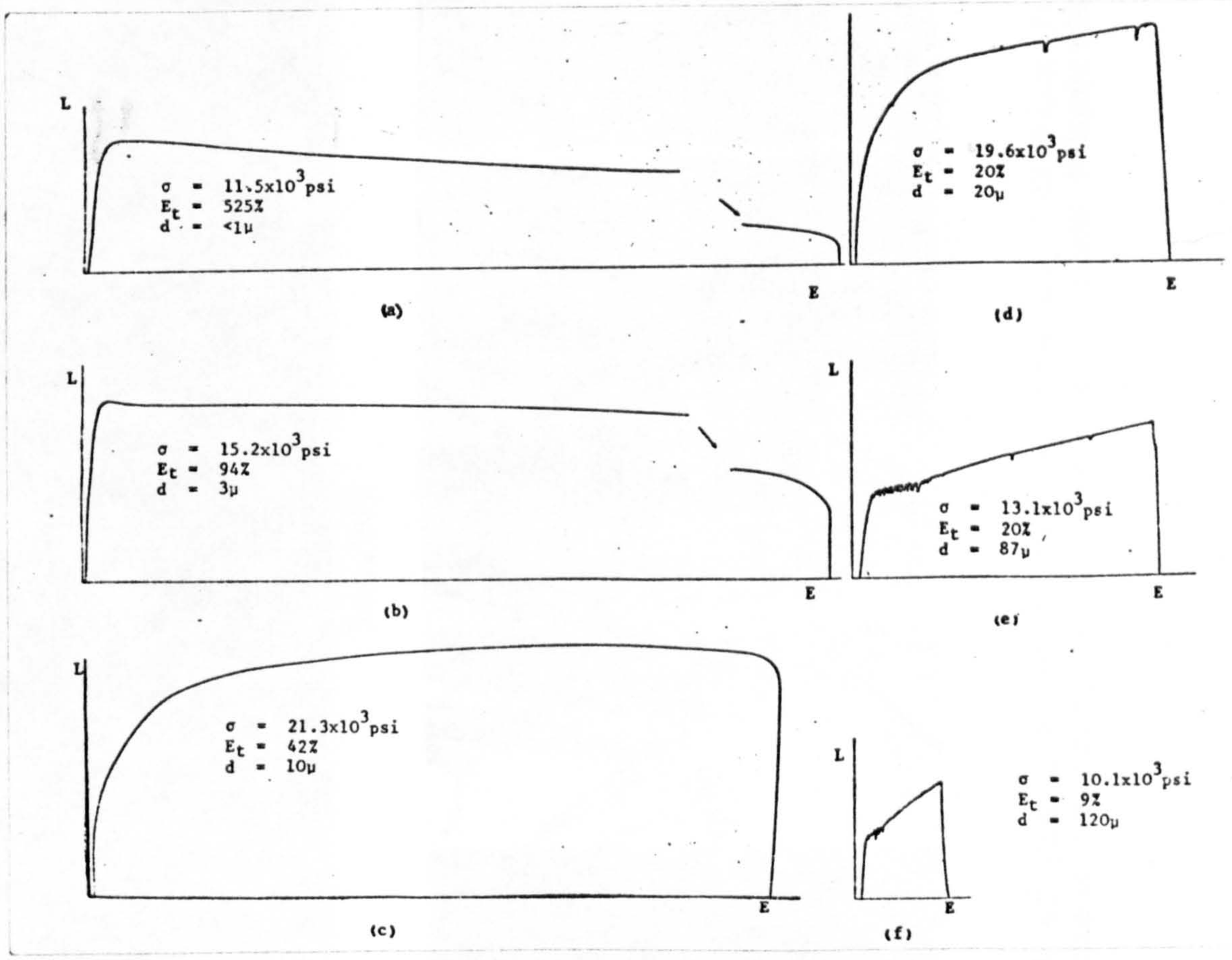

Figure 35 - The effect of grain size on the load-extension curves, % elongation, and maximum engineering stress.

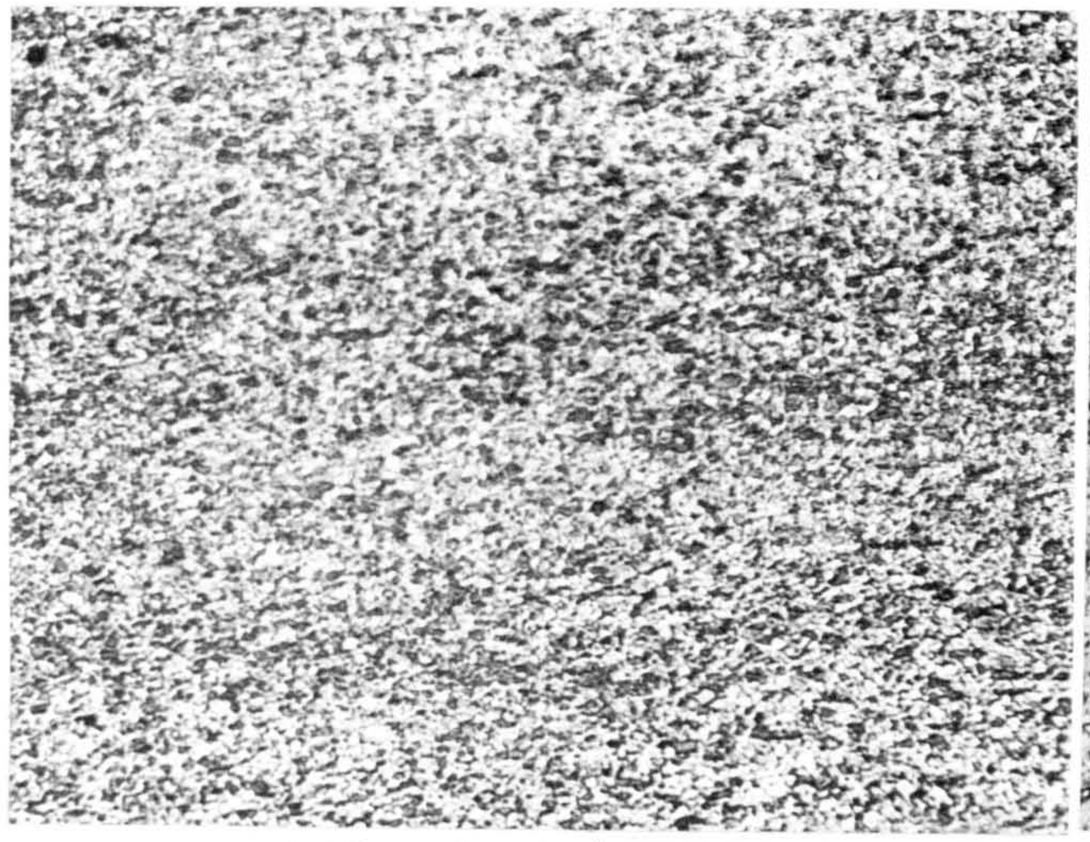

0.6um.525%

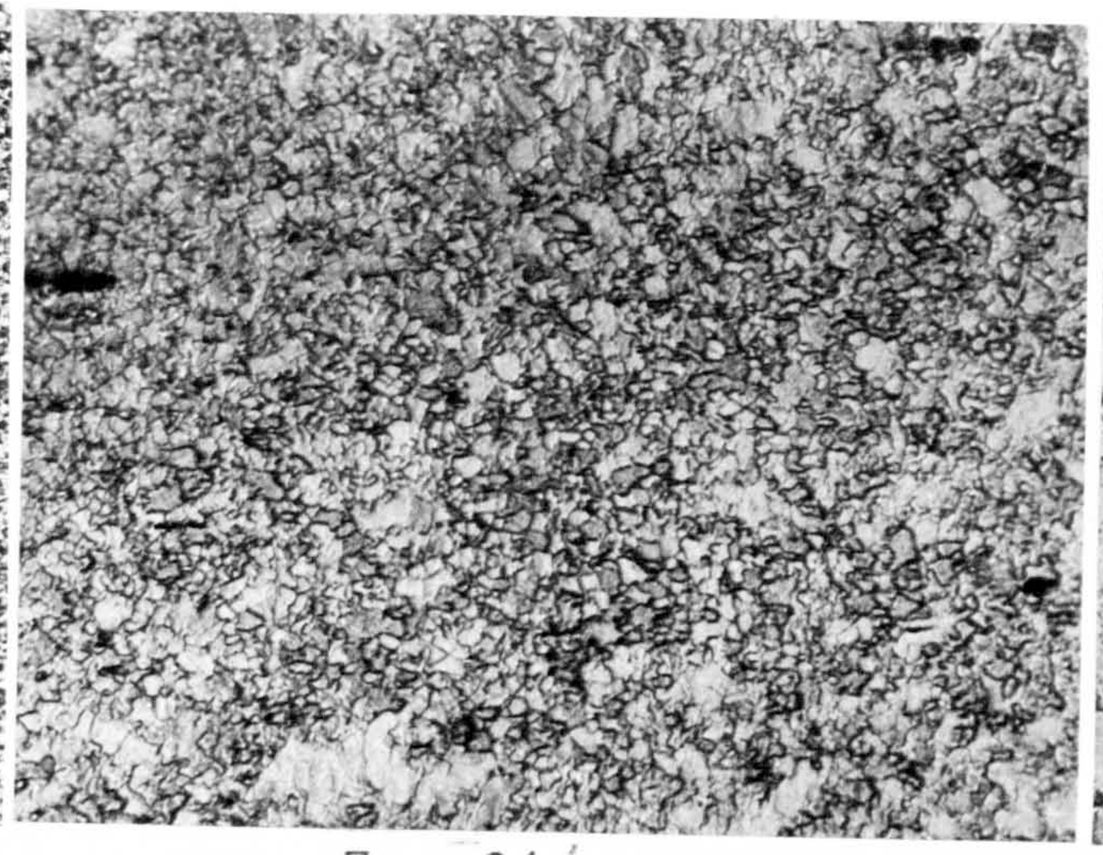

3um, 94%

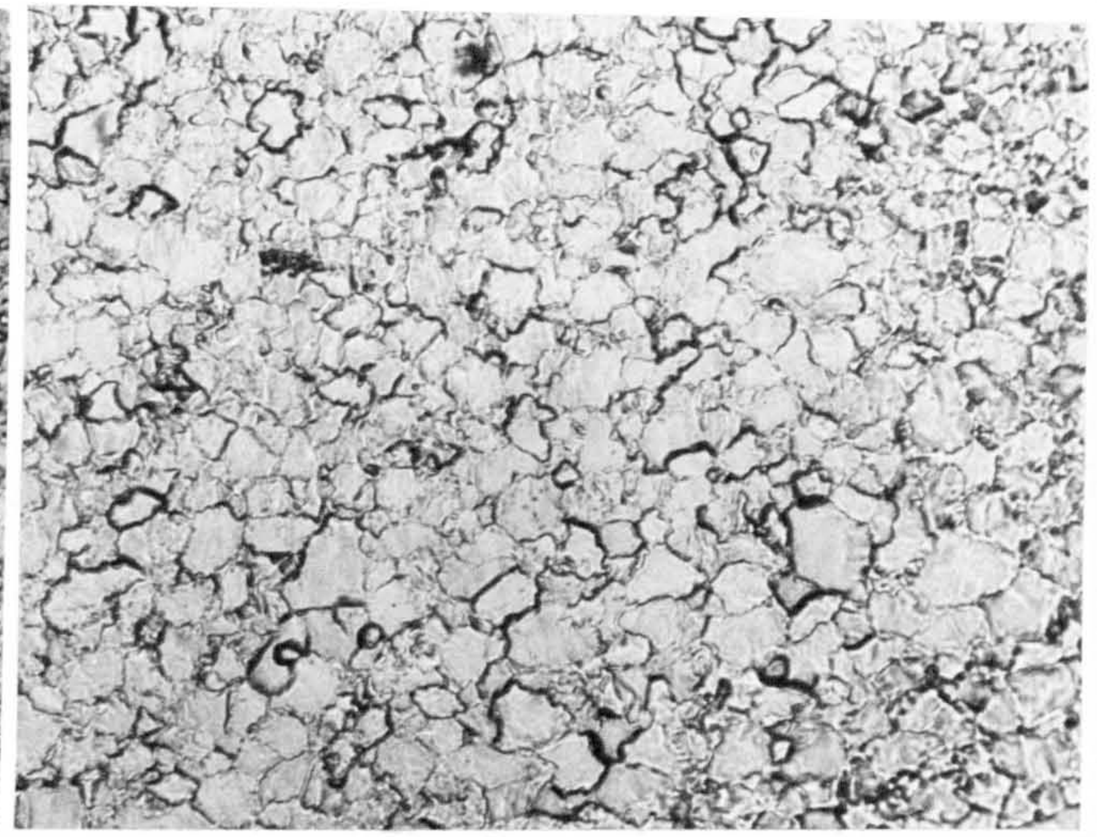

10um, 42%

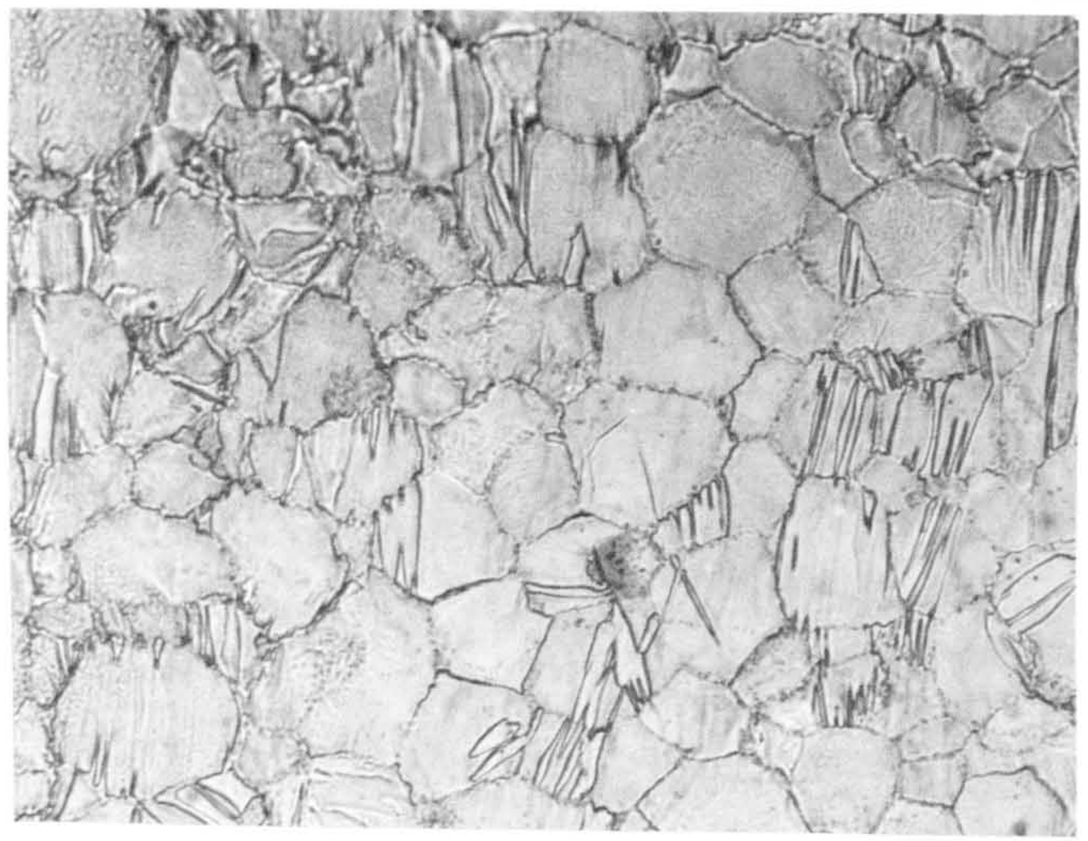

20um, 20%

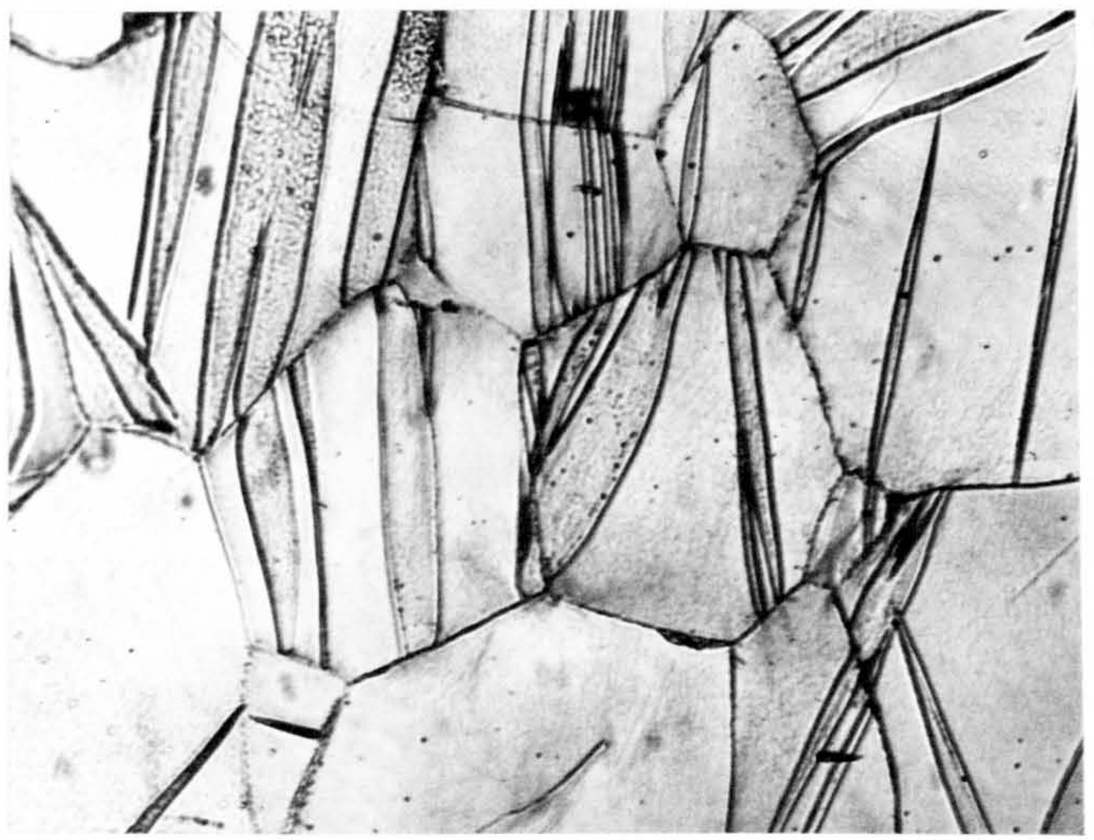

87um, 20%

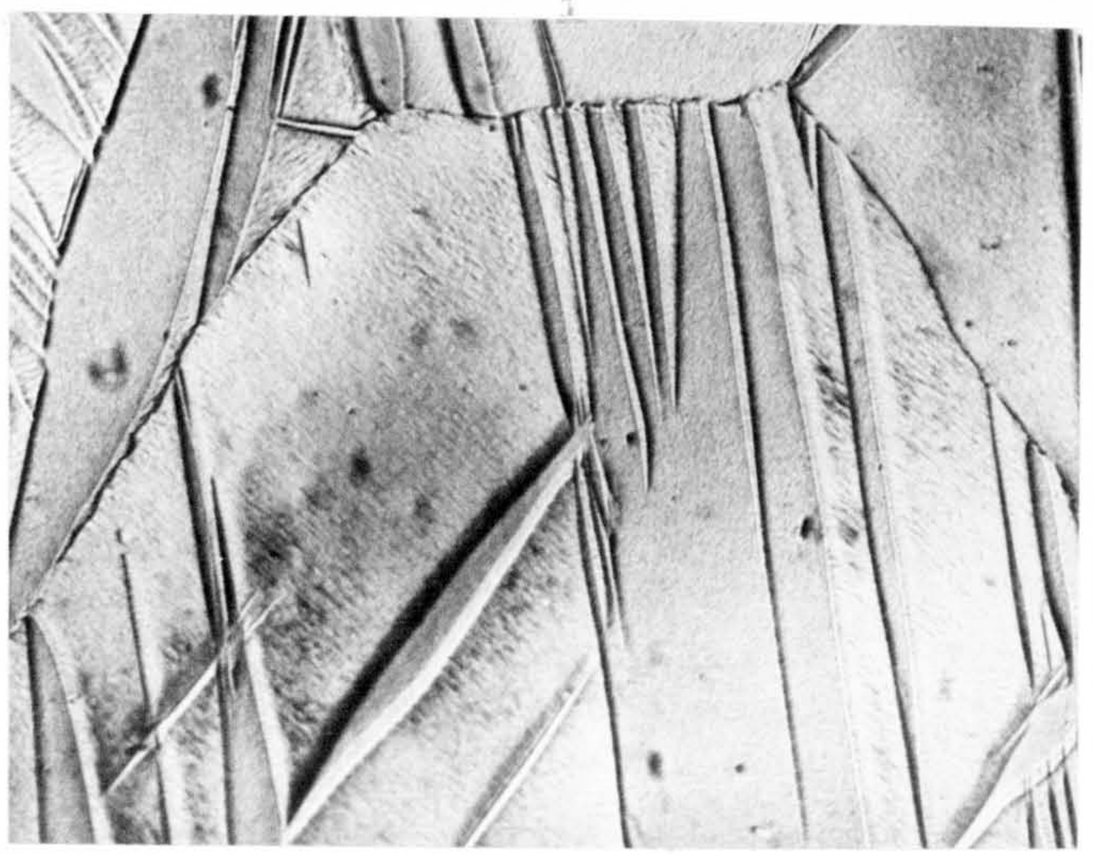

120um, 9%

Figure 36- The effect of grain size on the deformation behavior for specimens strained at a crosshead velocity of 0.1 in/min at room temperature upto fracture.(x300). Surface.

Fig 37

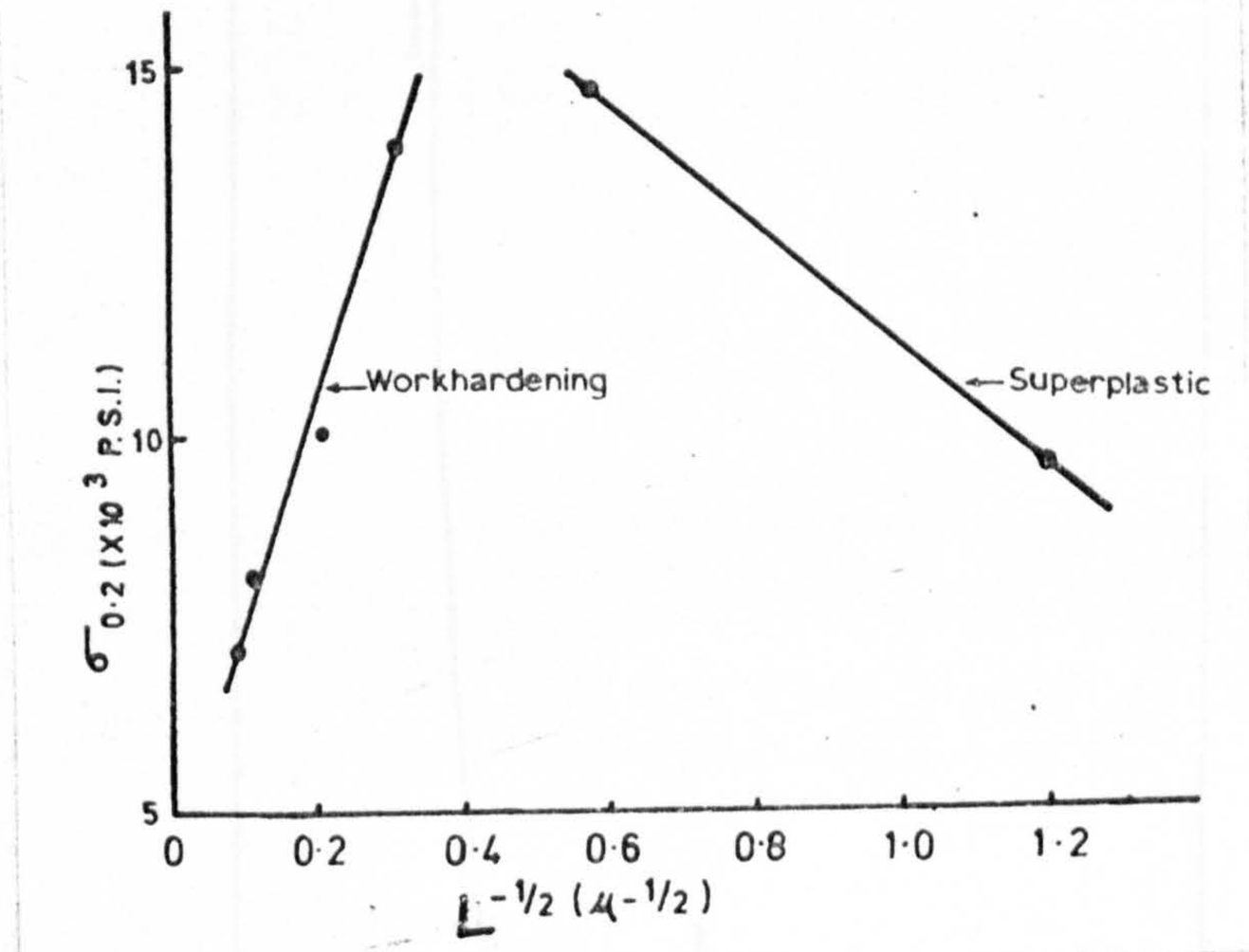

Figure 37 - The Hall-Petch relationship of the 0.2% proof stress ($\sigma_{0.2}$) vs grain size($L^{-\frac{1}{2}}$).

Fig 38

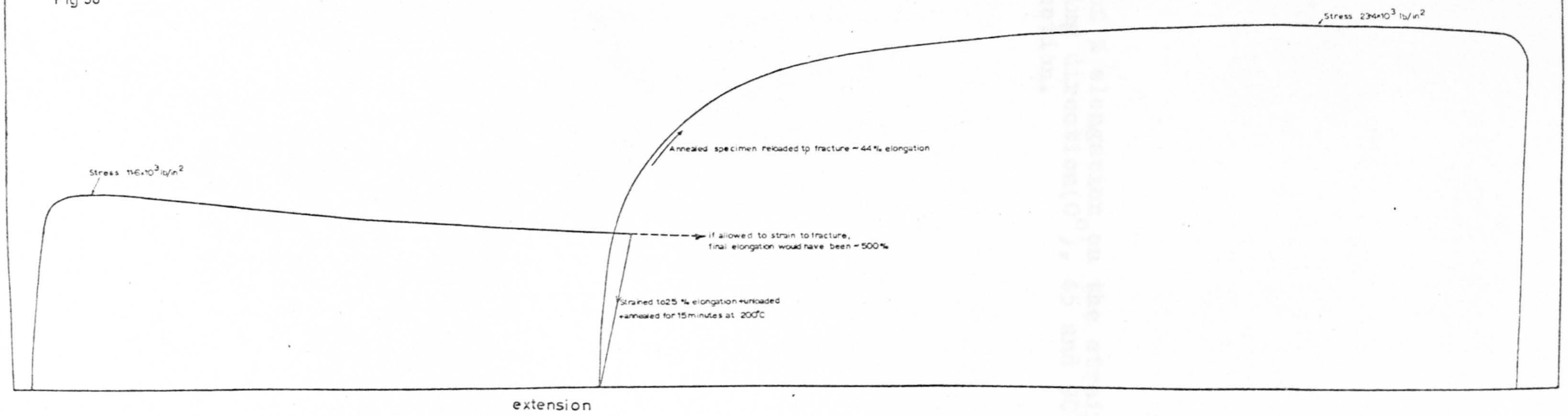

Figure 38- The load/extension curve of a 0.6um grain size material strained to 25% elongation, unloaded, annealed at 200°C for 5 minutes and then restrained to fracture.

Figure 39- The effect of % elongation on the strain-ratio $\bar{r}$ in the rolling direction(0^{o}), 45 and 90^{o} to the rolling direction.

Fig 39

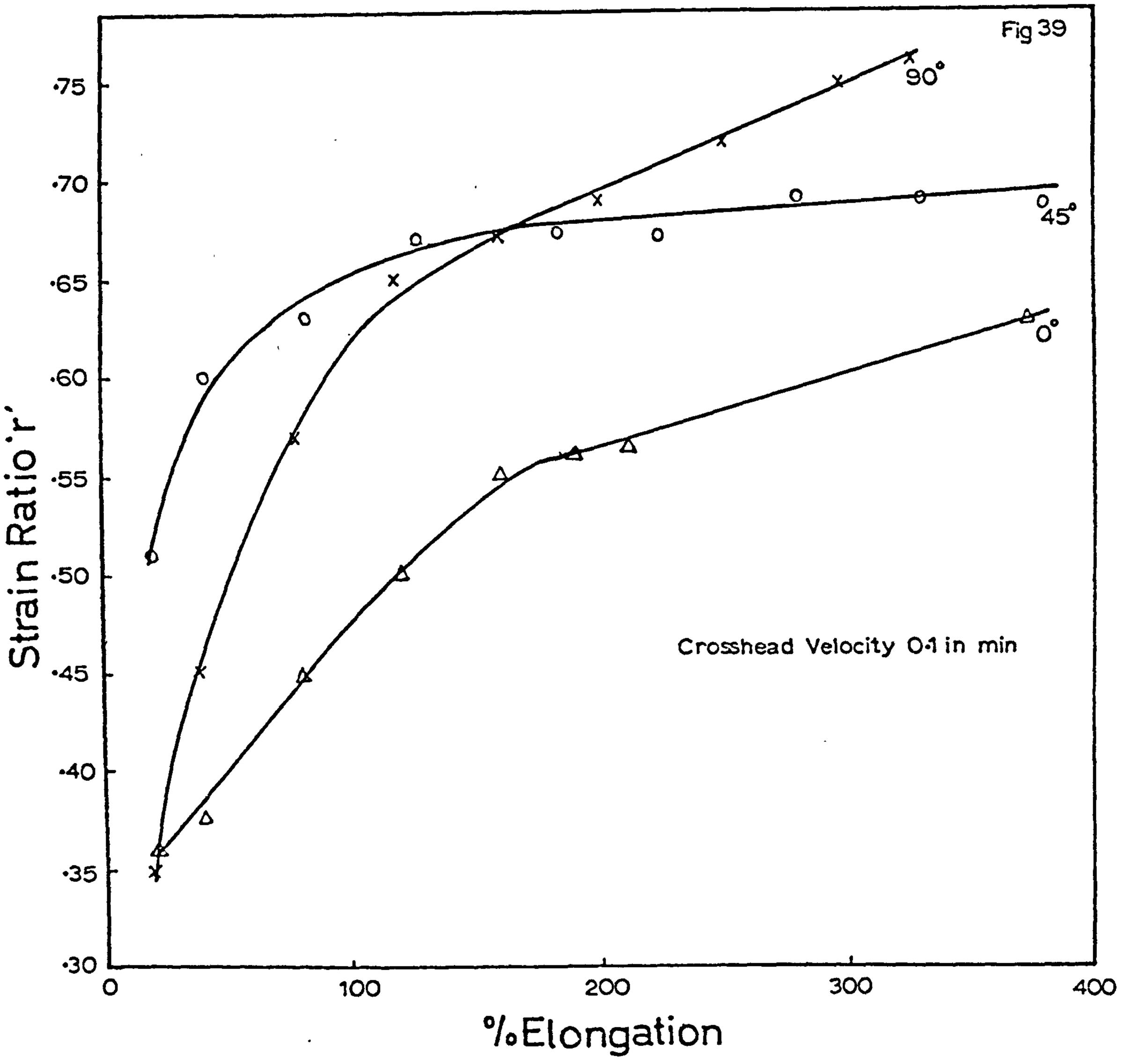
Strain Ratio 'r'
·75
·70
·65
·60
·55
·50
·45
·40
·35
·30
0
100
200
300
400
%Elongation
90°
45°
0°
Crosshead Velocity 0·1 in min

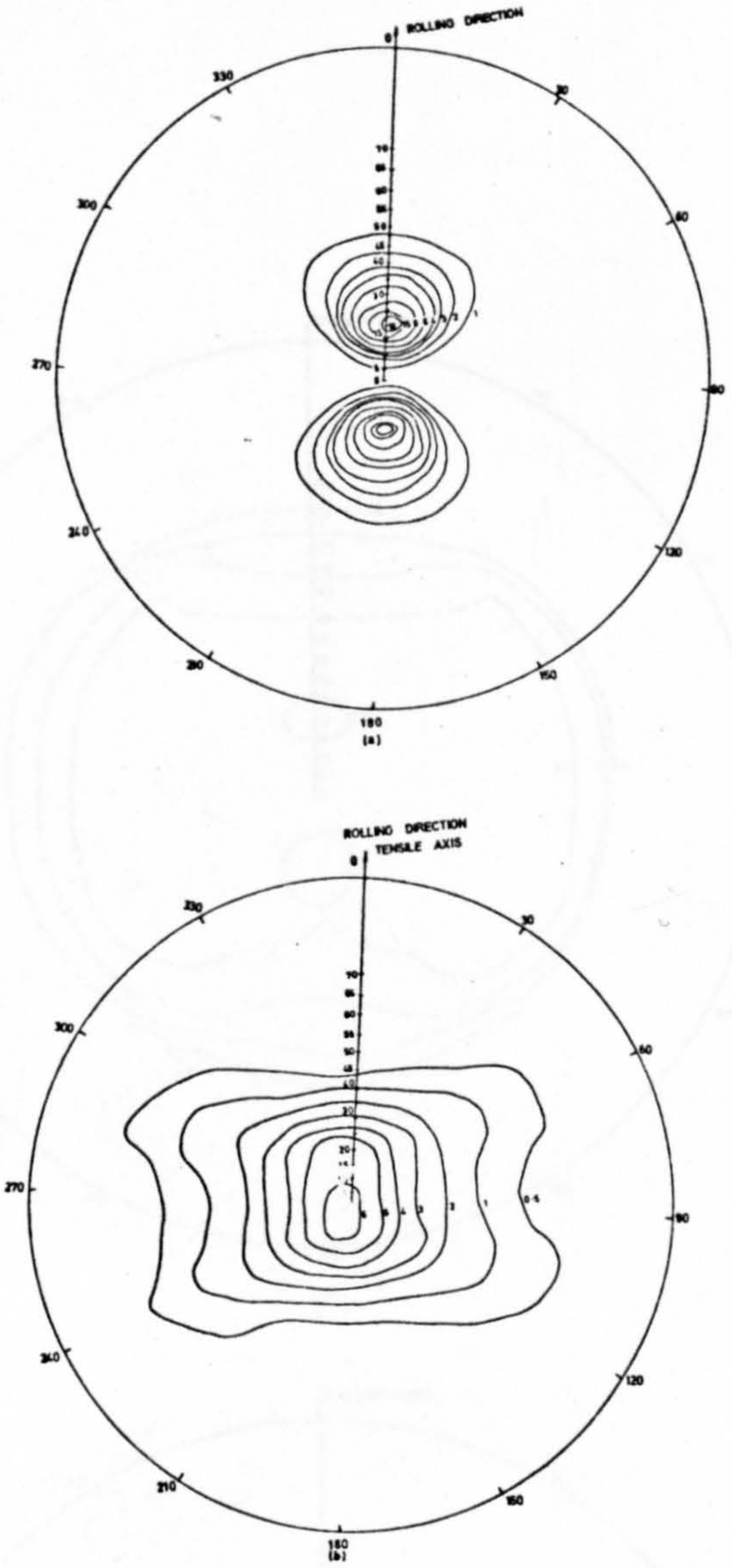

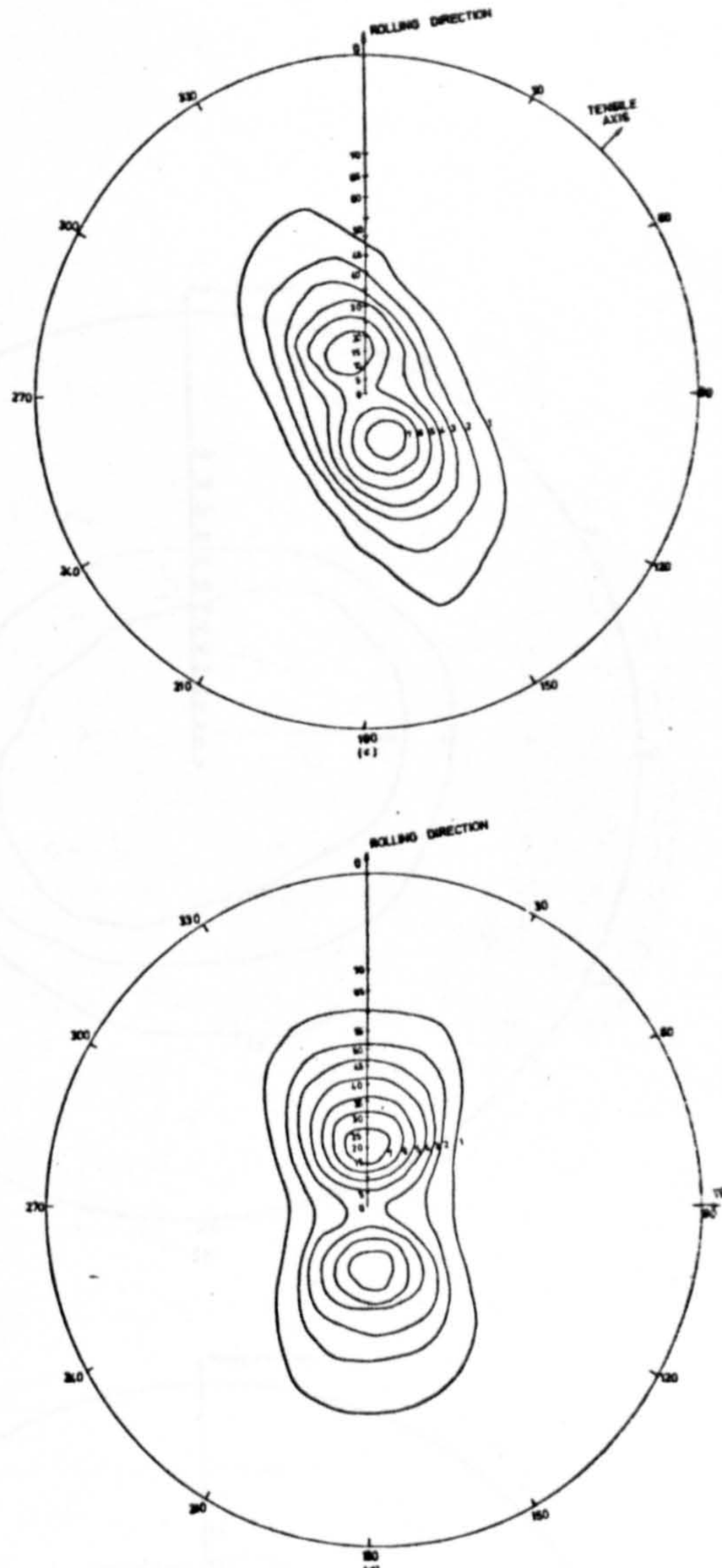

Figure 40a - Basal Plane pole figures for specimens (a) as-rolled sheet, (b), (c) and (d) strained in the rolling direction (0°), (45°) and (90°) to the rolling direction.

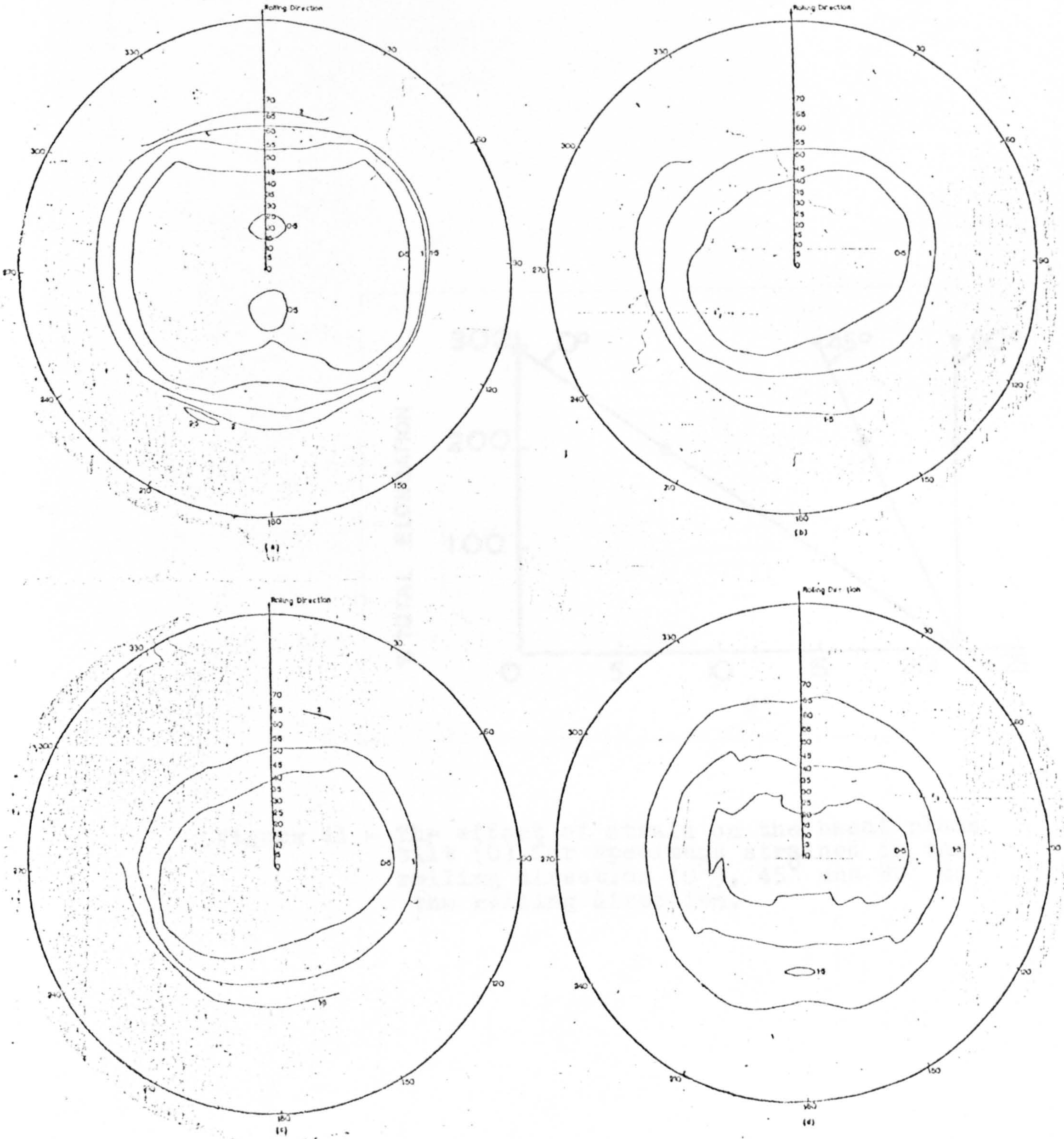

Figure 40b-Prism plane pole figures for specimens(a) .as-rolled sheet,(b),(c) and (d)strained in the rollingdirection (0^{o}), 45 and 90^{o} to the rolling direction.(x300%).

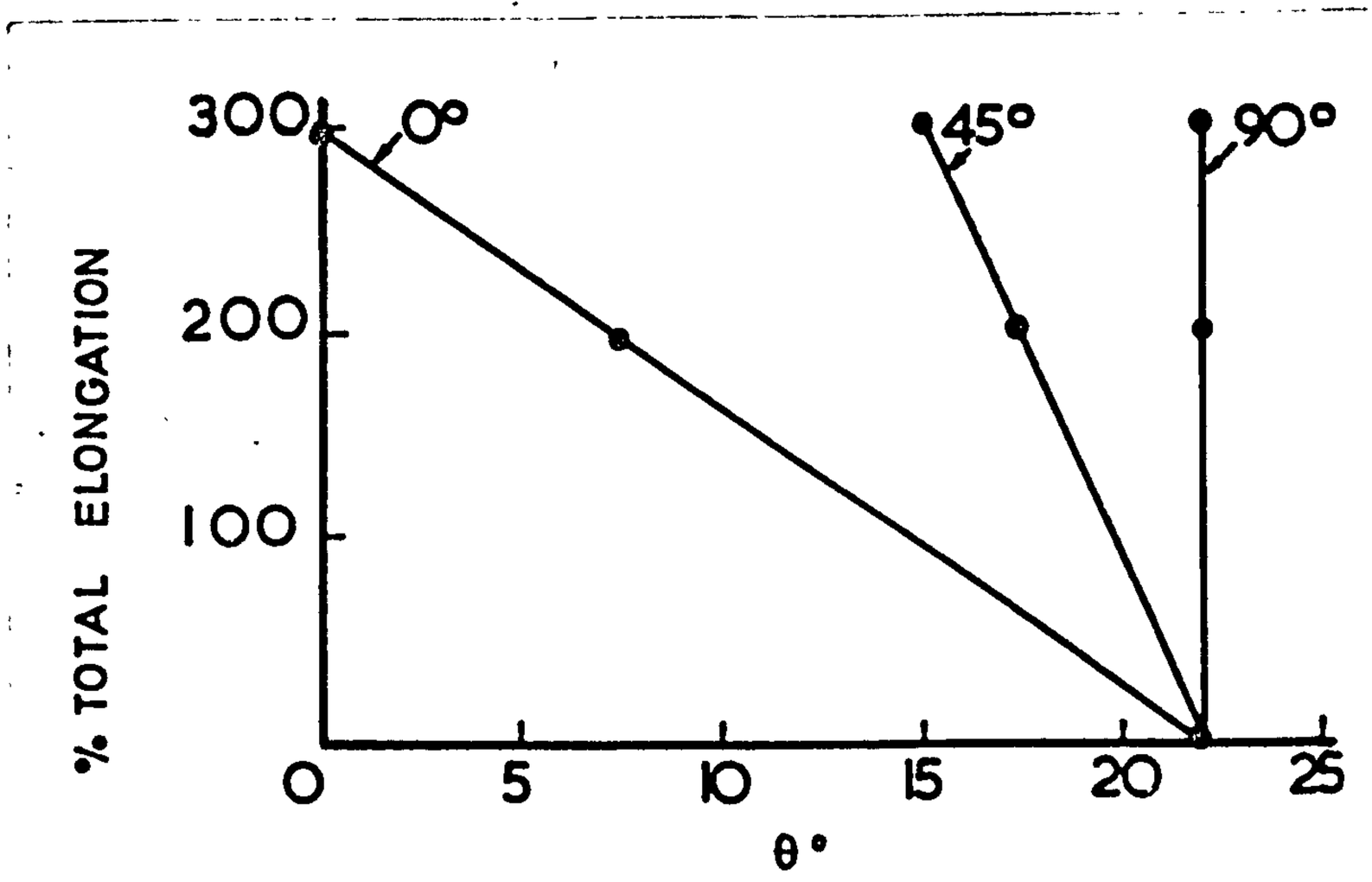

Figure 41 - The effect of strain on the basal plane tilt (θ) for specimens strained in the rolling direction (0°), 45° and 90° to the rolling direction.

Fig 42

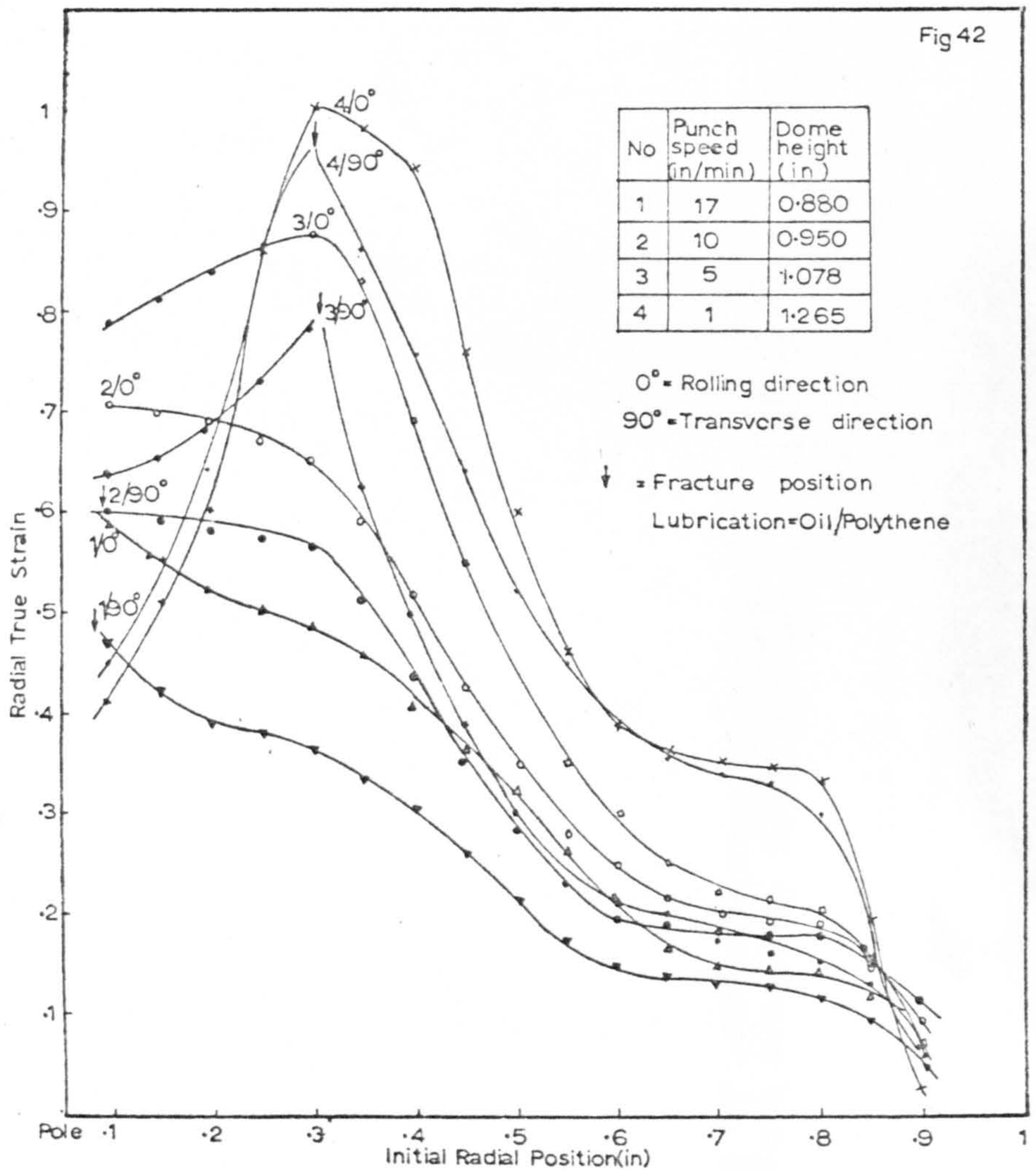

No	Punch speed (in/min)	Dome height (in)
1	17	0·880
2	10	0·950
3	5	1·078
4	1	1·265

0°= Rolling direction

90°=Transverse direction

↓ = Fracture position

Lubrication=Oil/Polythene

Figure 42- The effect of punch speed on the dome height, fracture site and maximum strain.

Fig 43

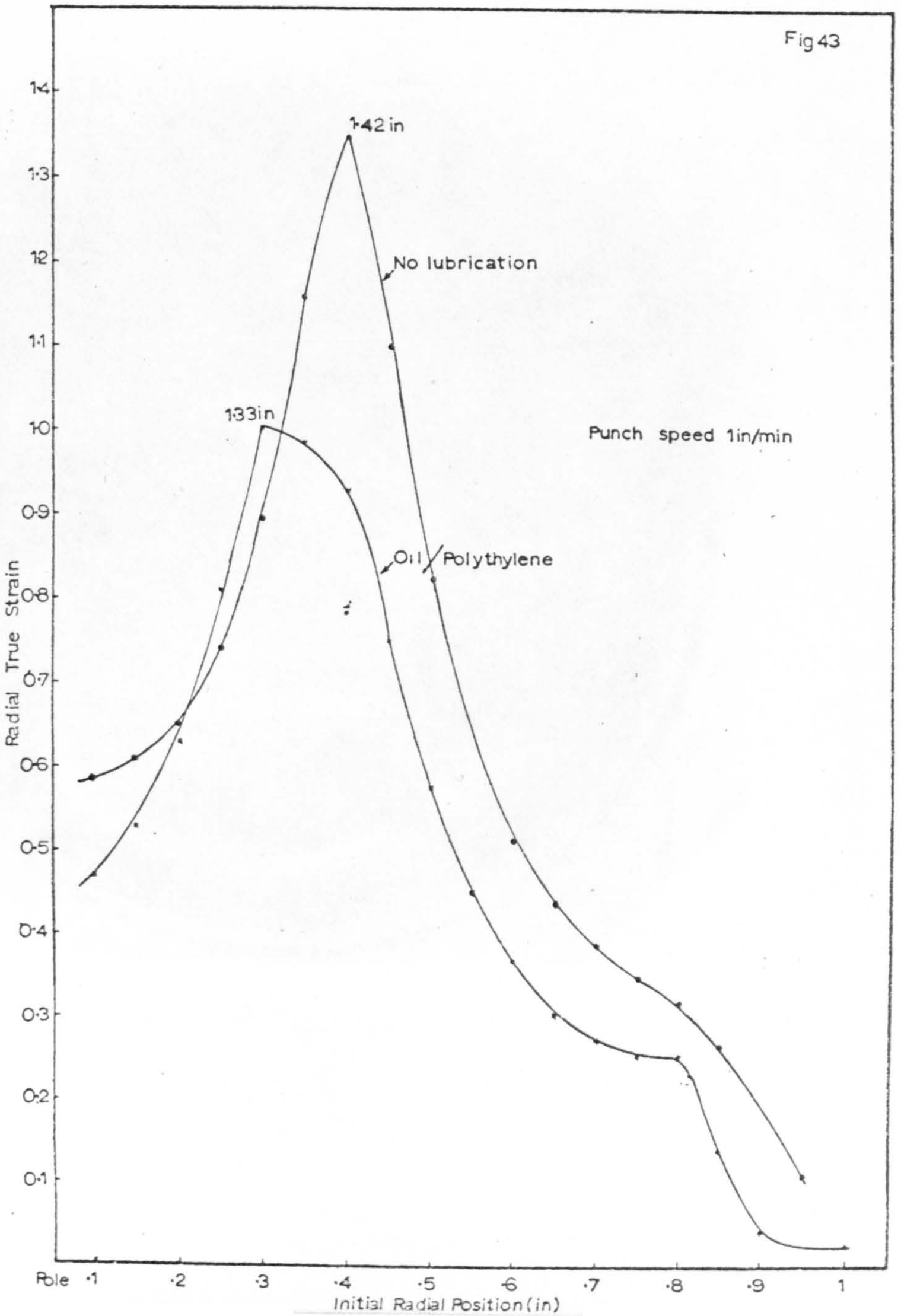

Figure 43- The effect of lubrication on the dome height and strain distribution.

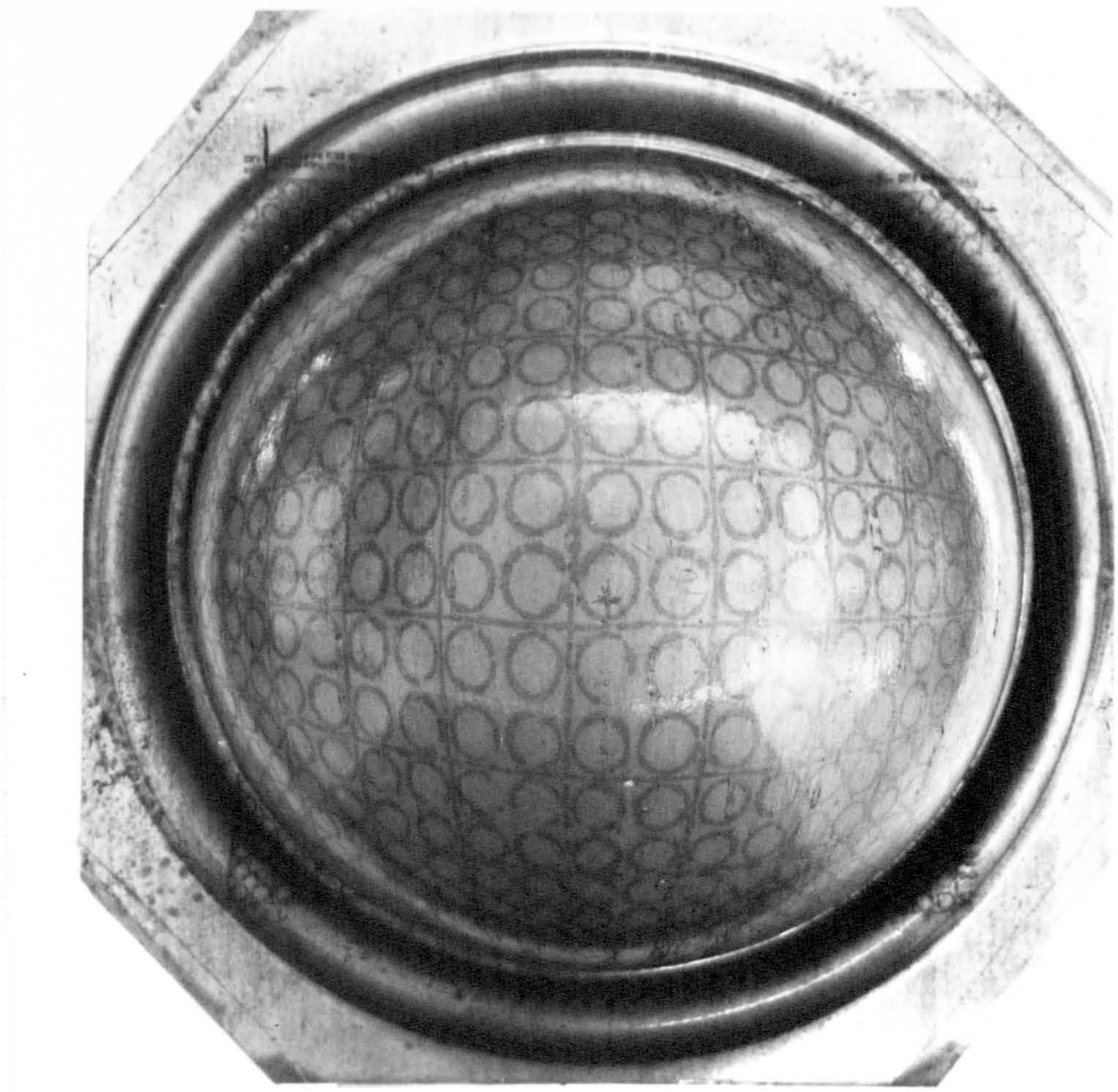

Figure 44- Plan view of the 4.5 inch diameter bulge. Note the " elliptical deformation" at the pole.

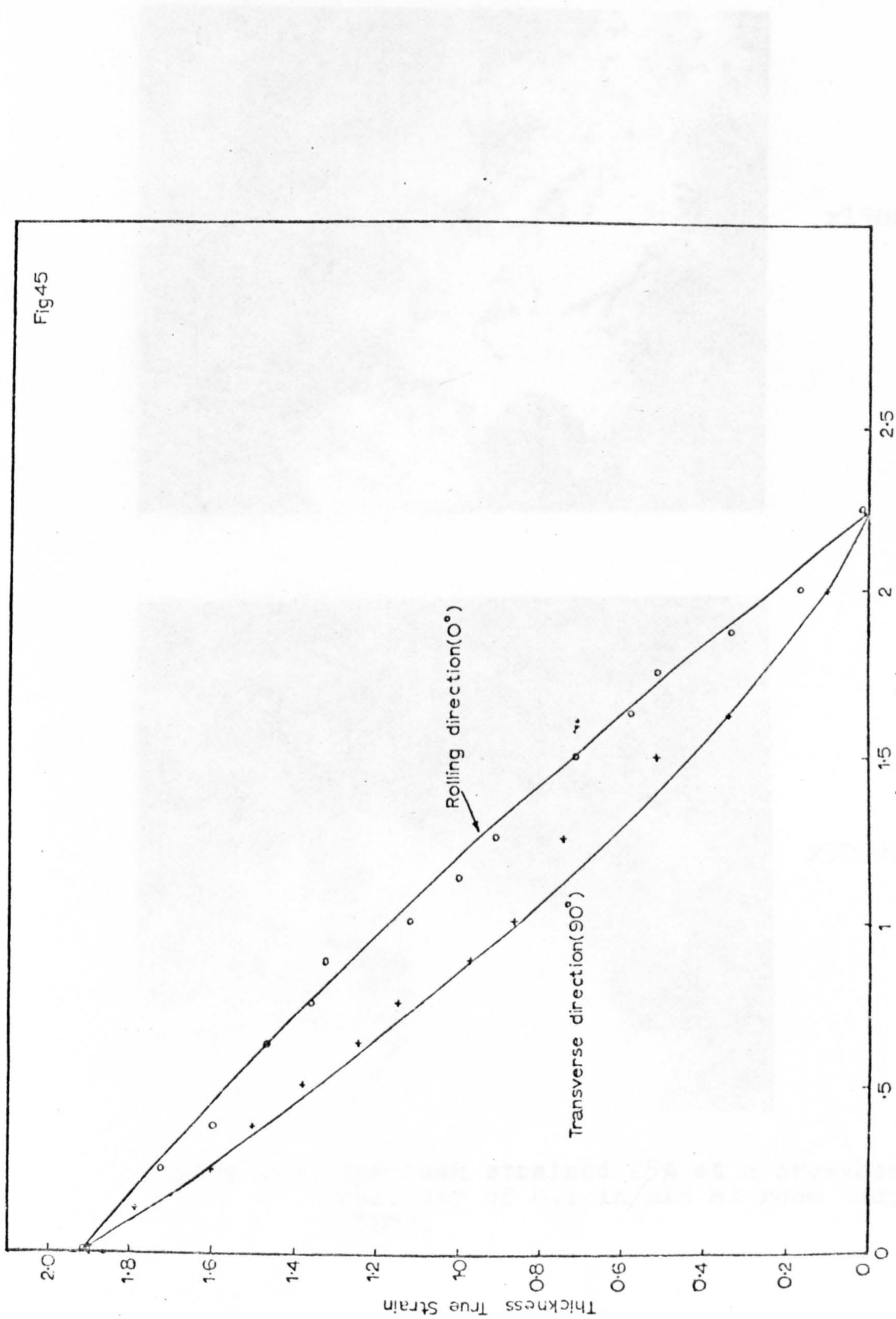

Figure 45- Pole variation in the thickness strain with direction of 4.5 diameter bulge.

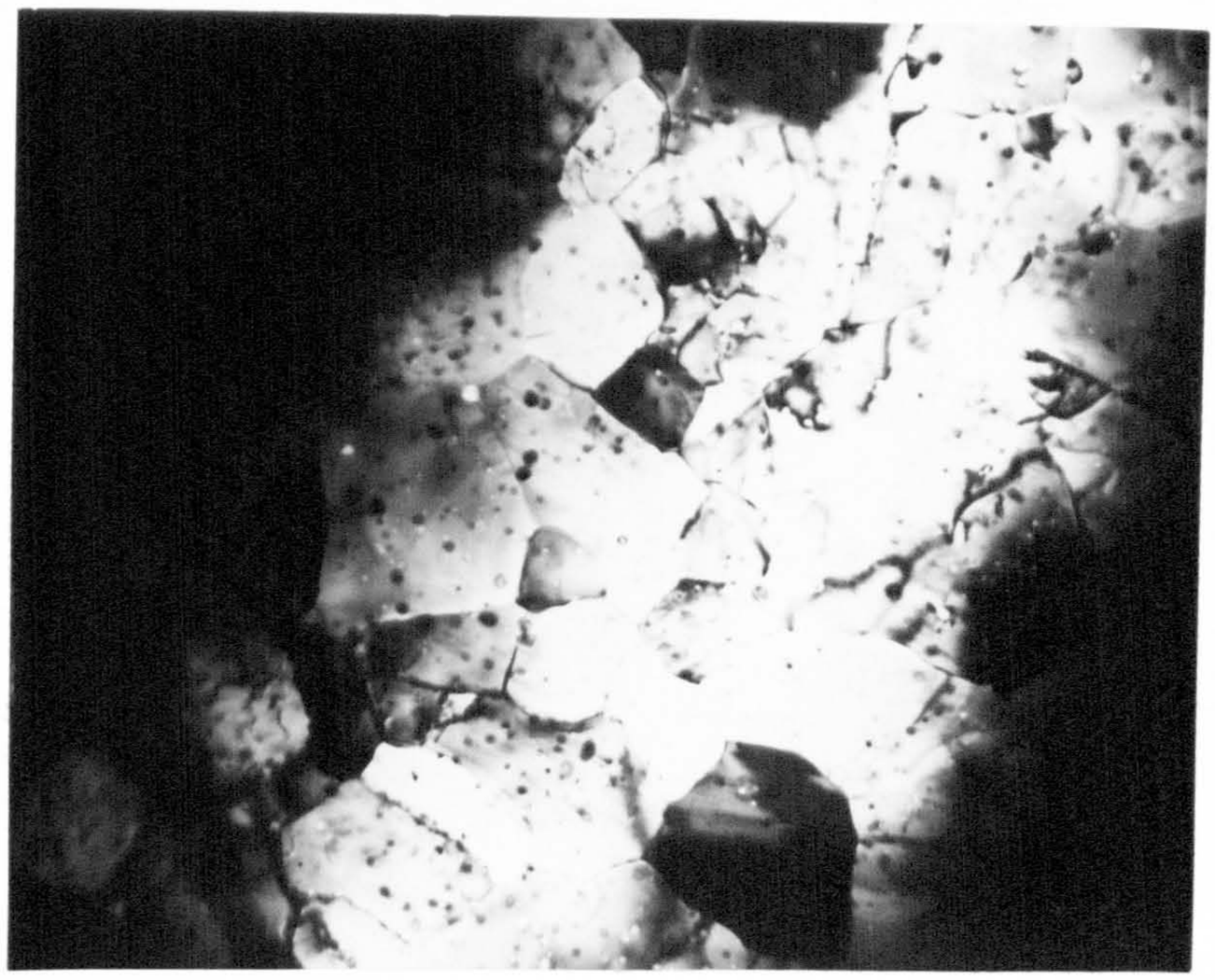

x15000

x30000

Figure 46a- Specimen strained 25% at a crosshead velocity of 0.1 in/min at room temperature. (TEM).

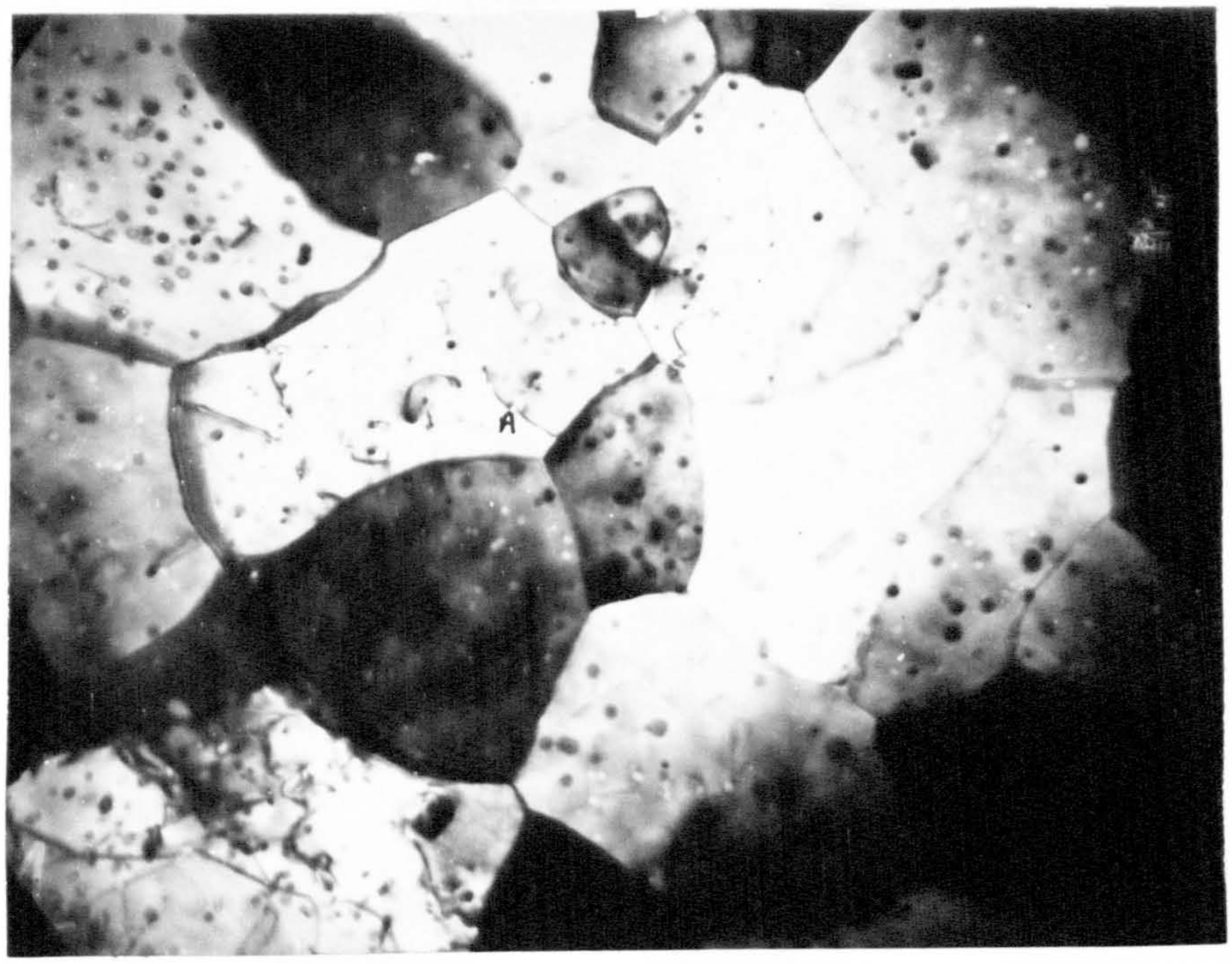

x24000

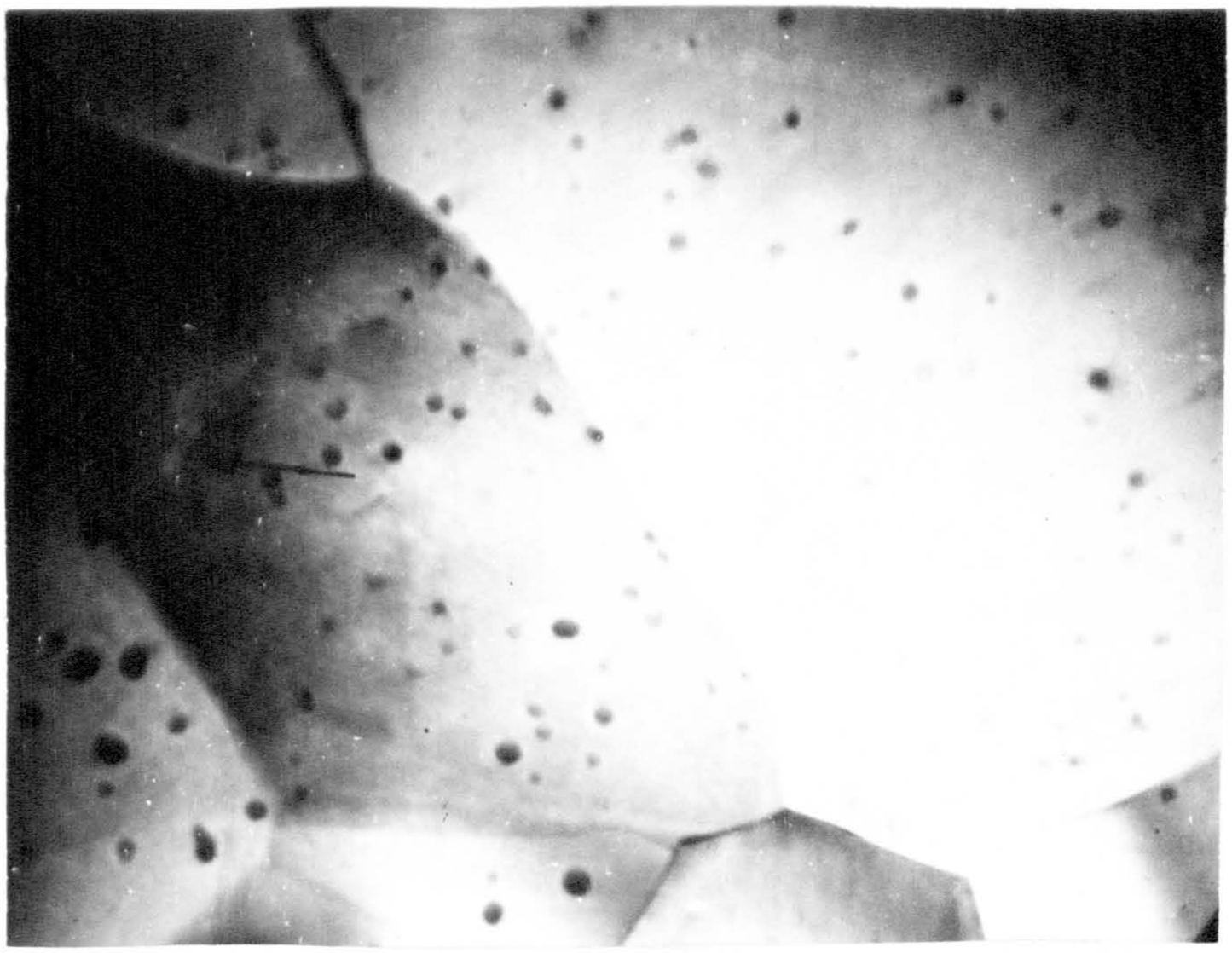

x40000

Figure 46b- Specimens strained 100% at a crosshead velocity of 0.1 in/min at room temperature. (TEM).

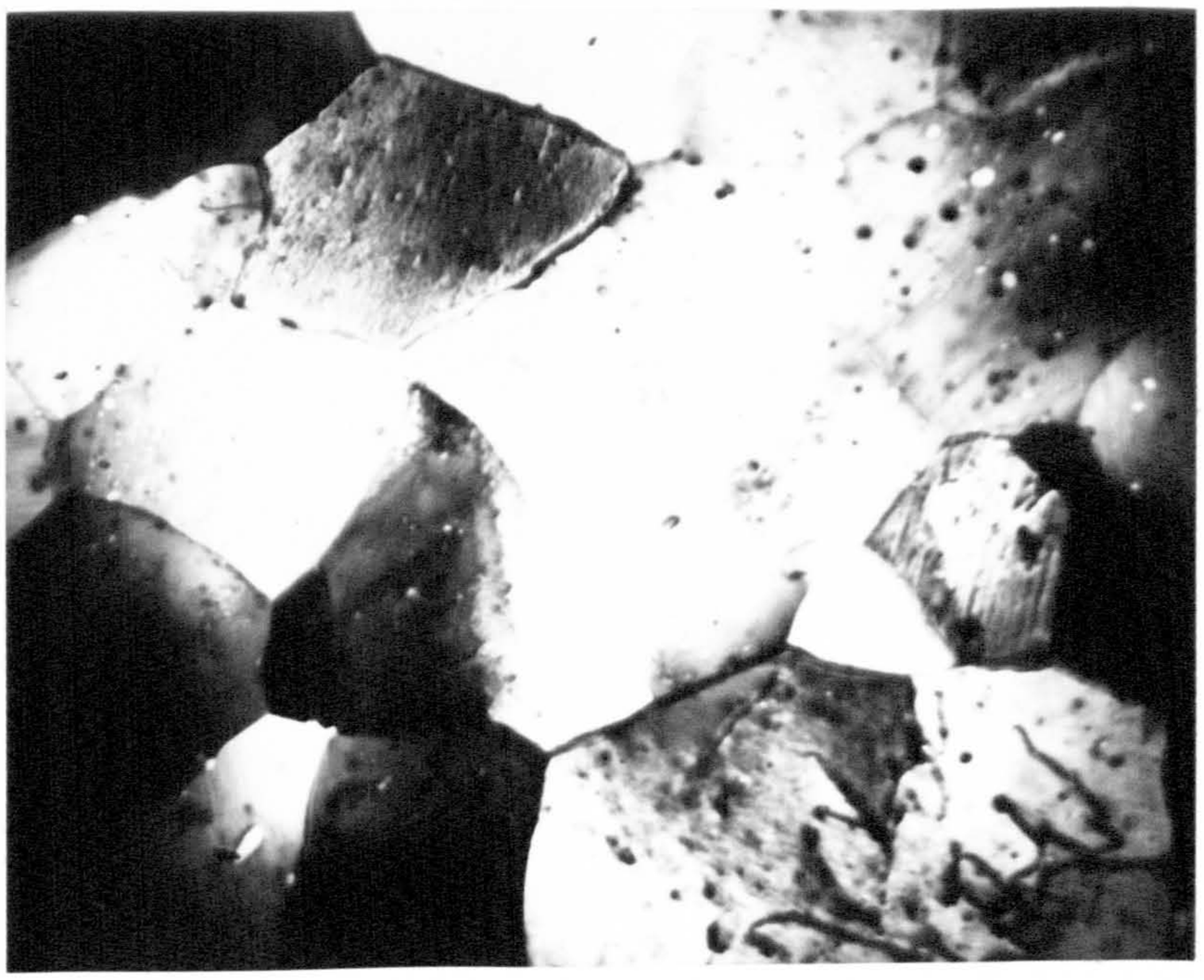

x15000

x25000

Figure 46c- Specimen strained 400% at a crosshead velocity of 0.1 in/min at room temperature. (TEM).

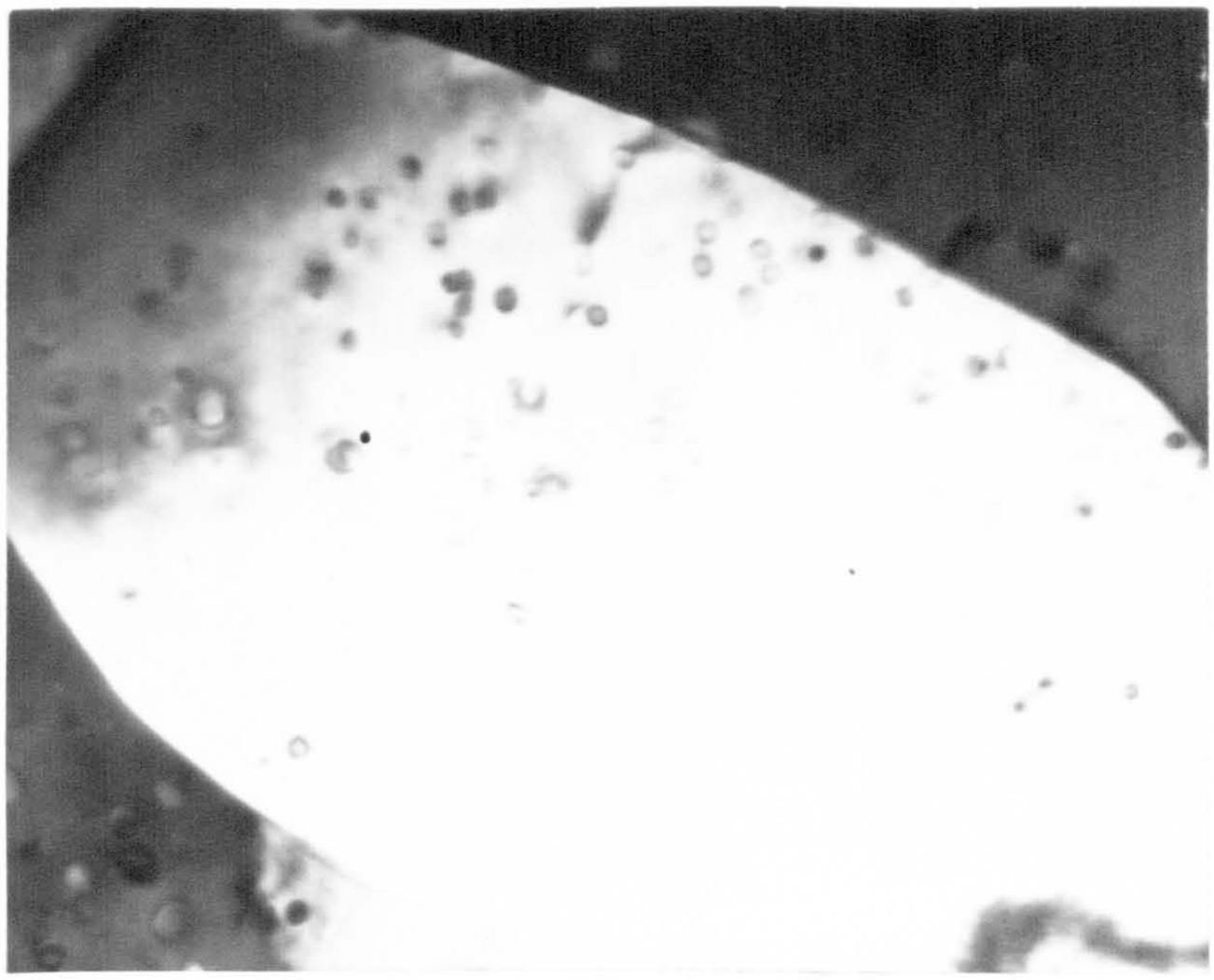

x60000

Figure 46c- Specimen strained at a crosshead velocity of 0.1 in/min at room temperature.(TEM).

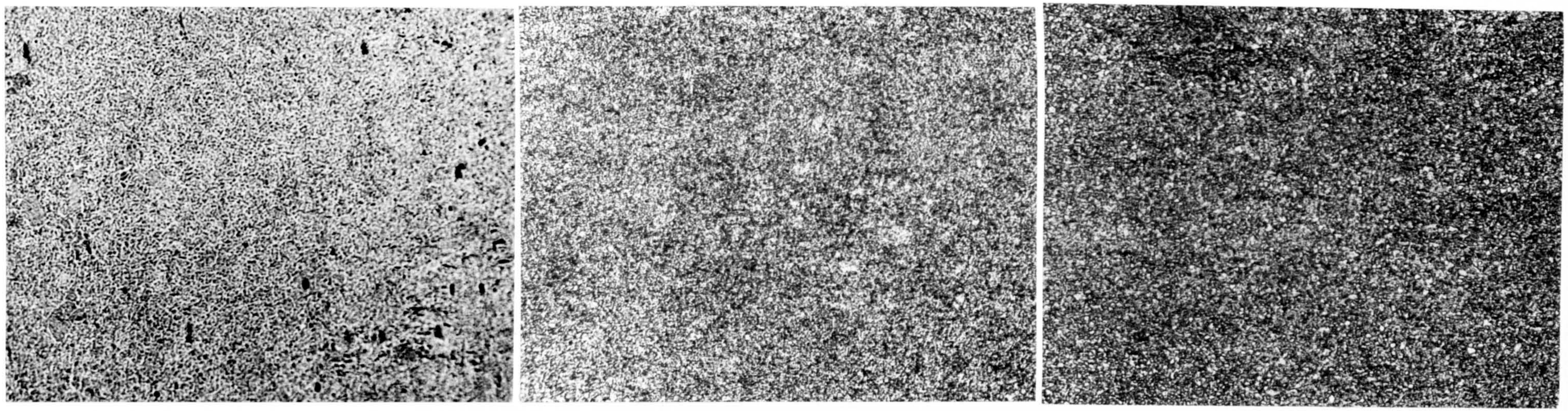

0% 25% 100%

200% 400%

Figure 47-Shows the increase in grain size with increase in strain.A crosshead velocity of 0.1 in/min was used.Surface.(x200).

rigure 48- The effect of strain on the surface behaviour. The gauge length was chemically polished before straining at room temperature at a crosshead velocity of 0.1 in/min.(SEM).

scratch mark perpendicular to the tensile axes.

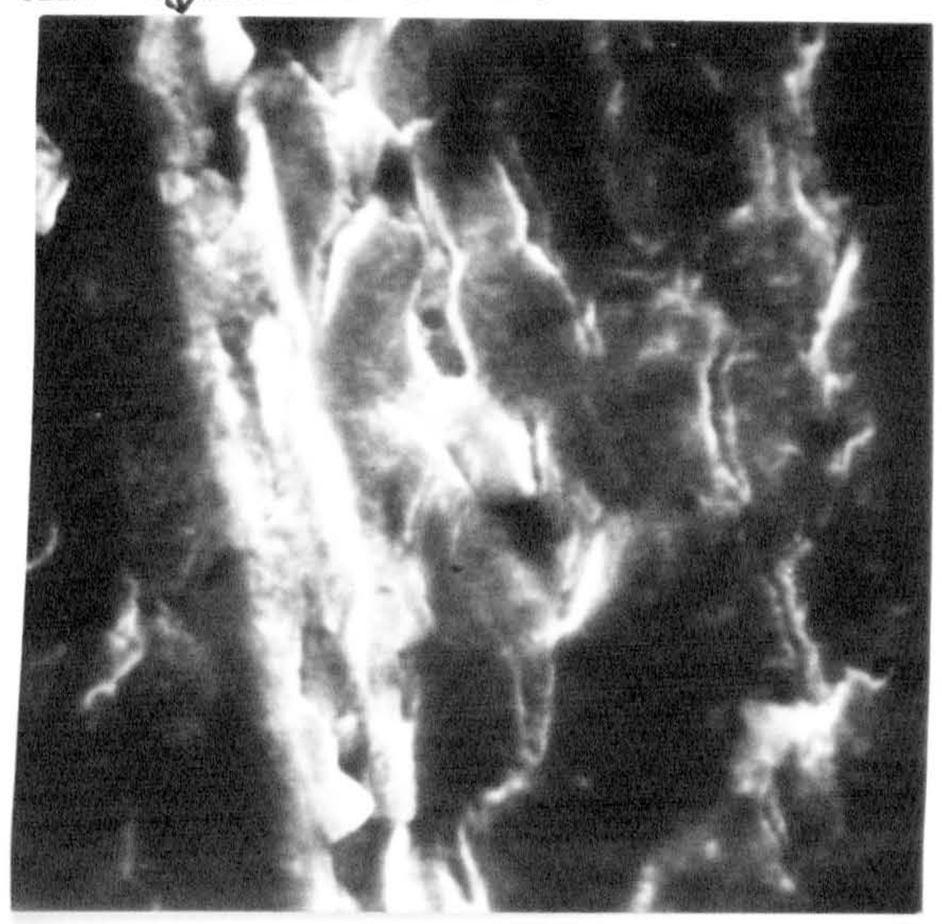

50%

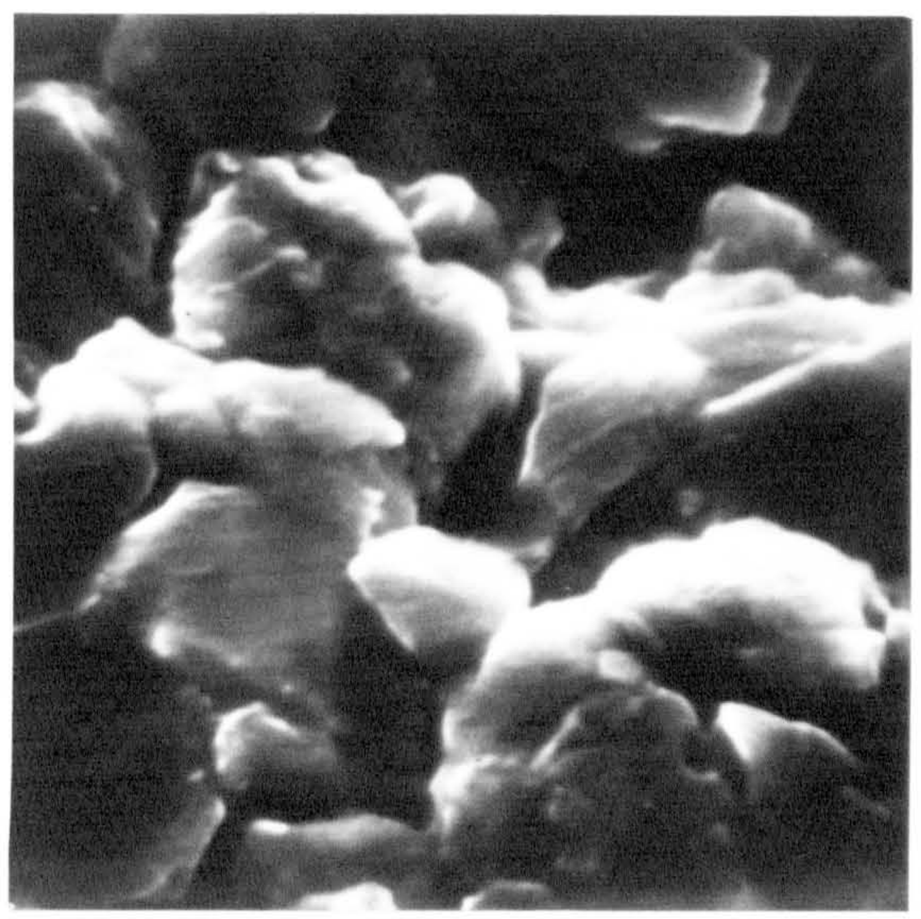

200%

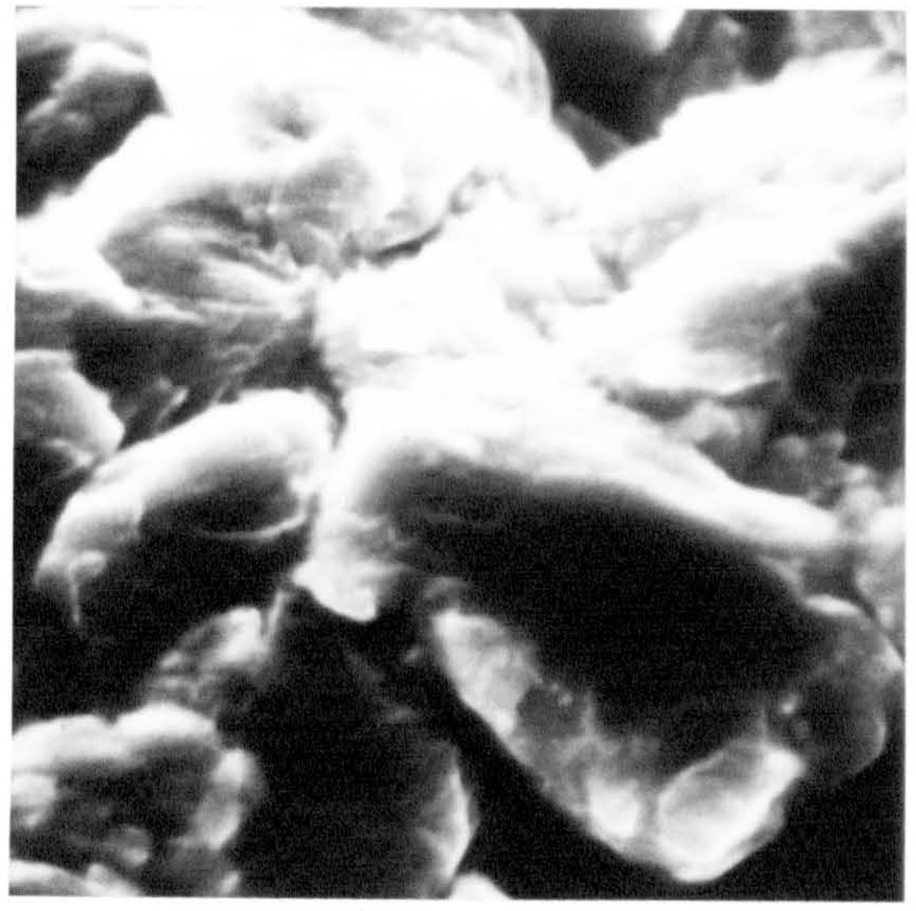

400%

x10000

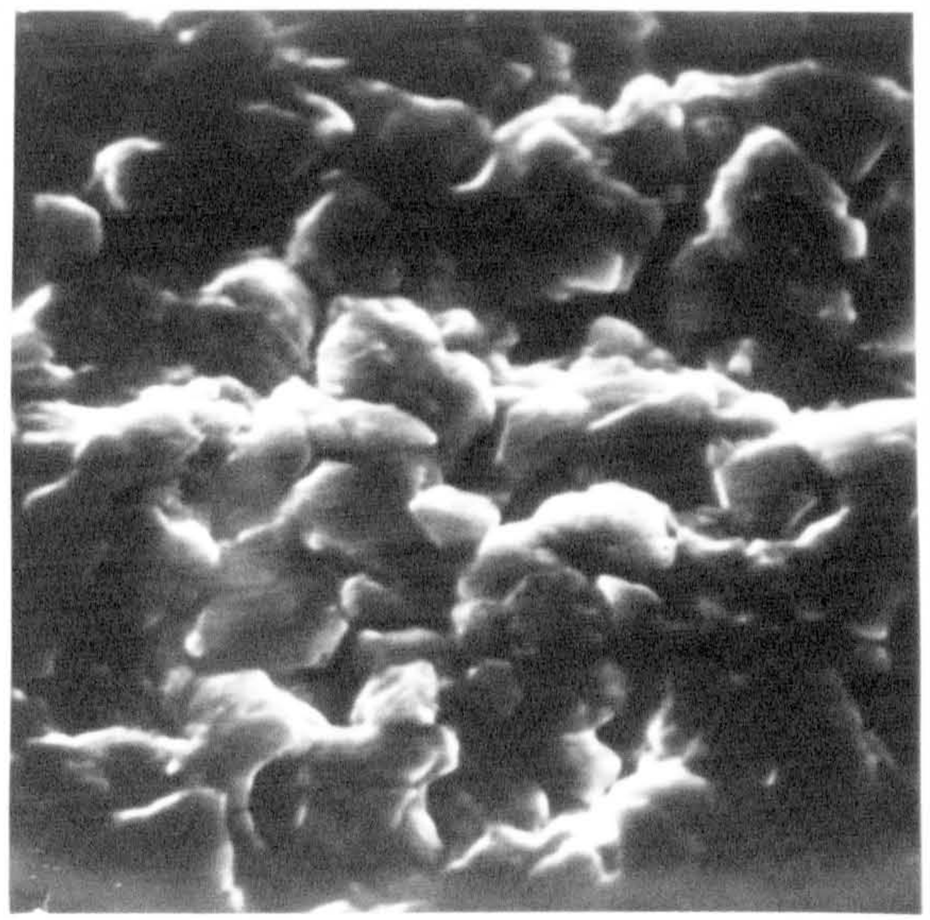

200%

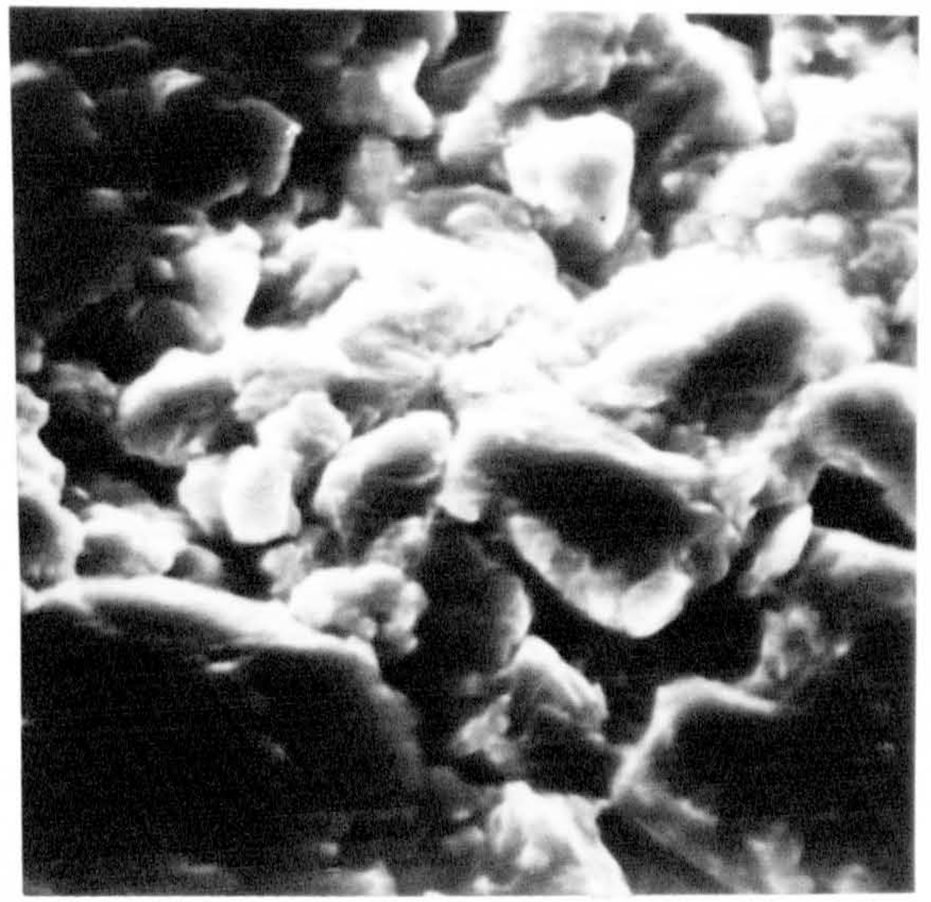

400%

x5000

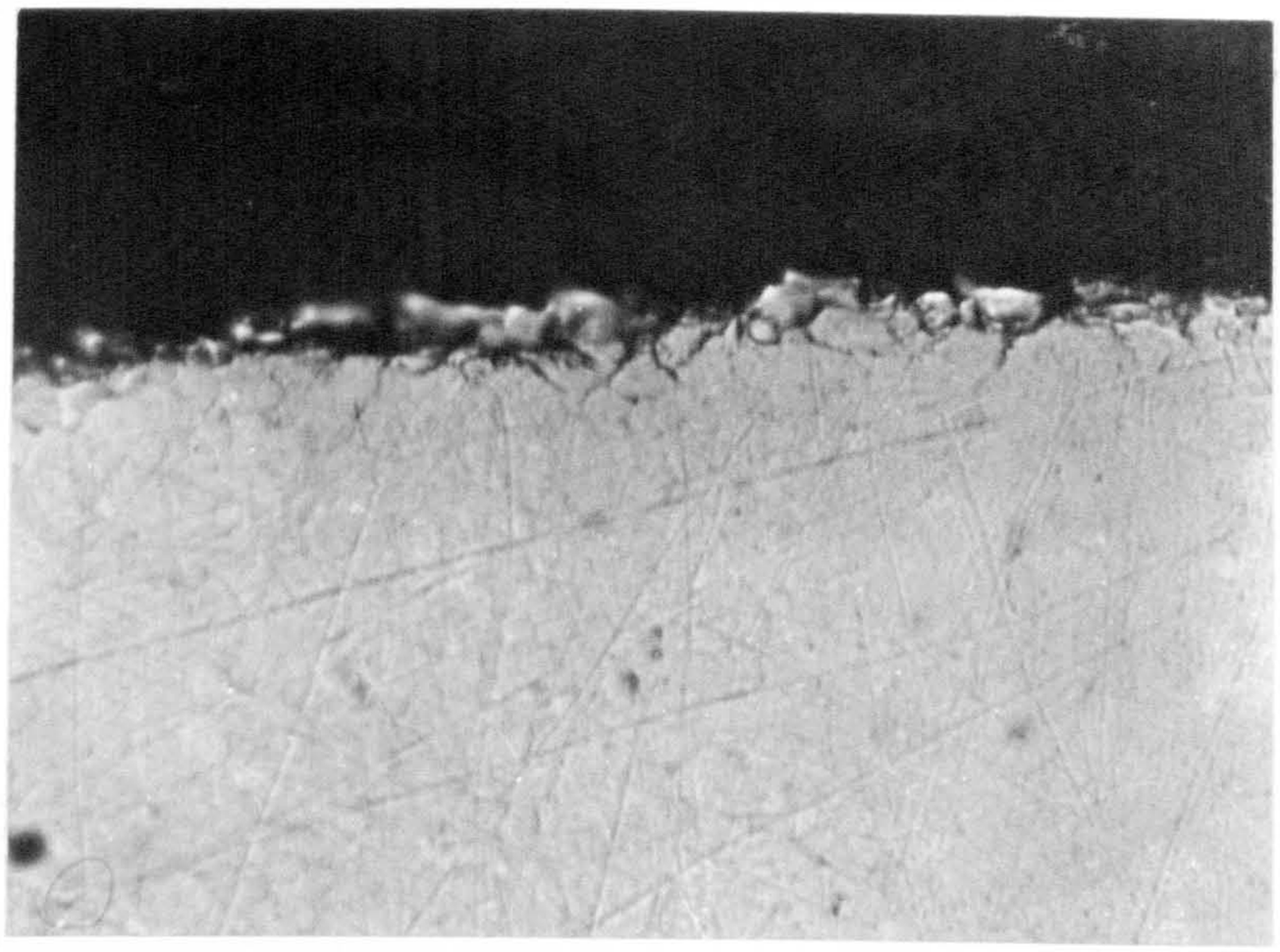

Figure 49- Shows the longitudinal section of the surface of a specimen strained 400% at the crosshead velocity of 0.1 in/min. (x1000).

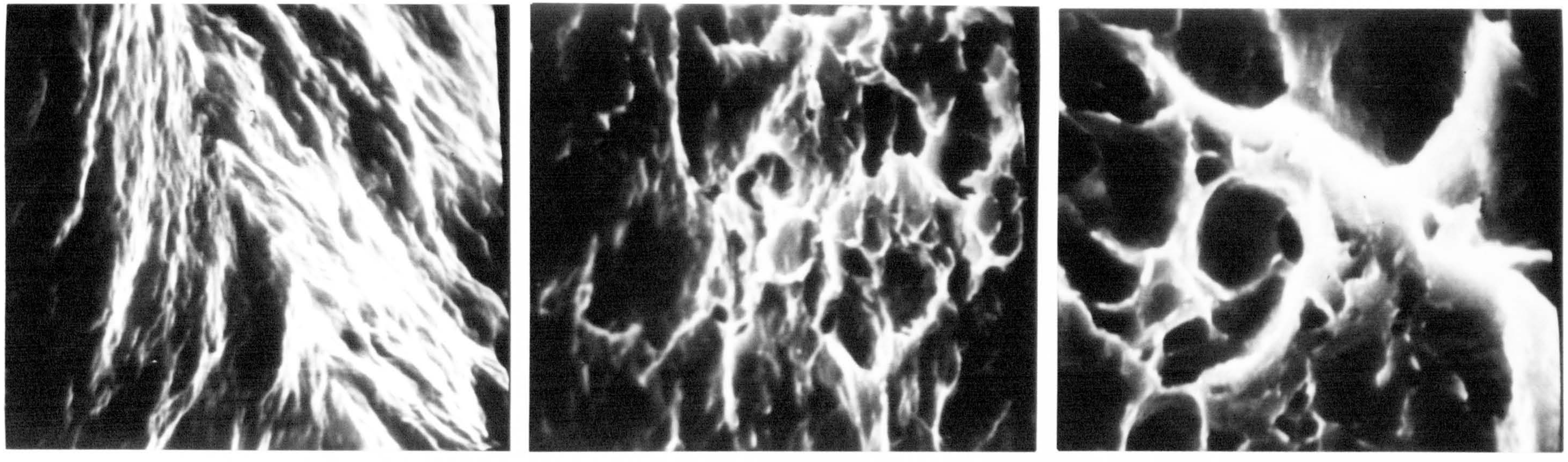

x10000

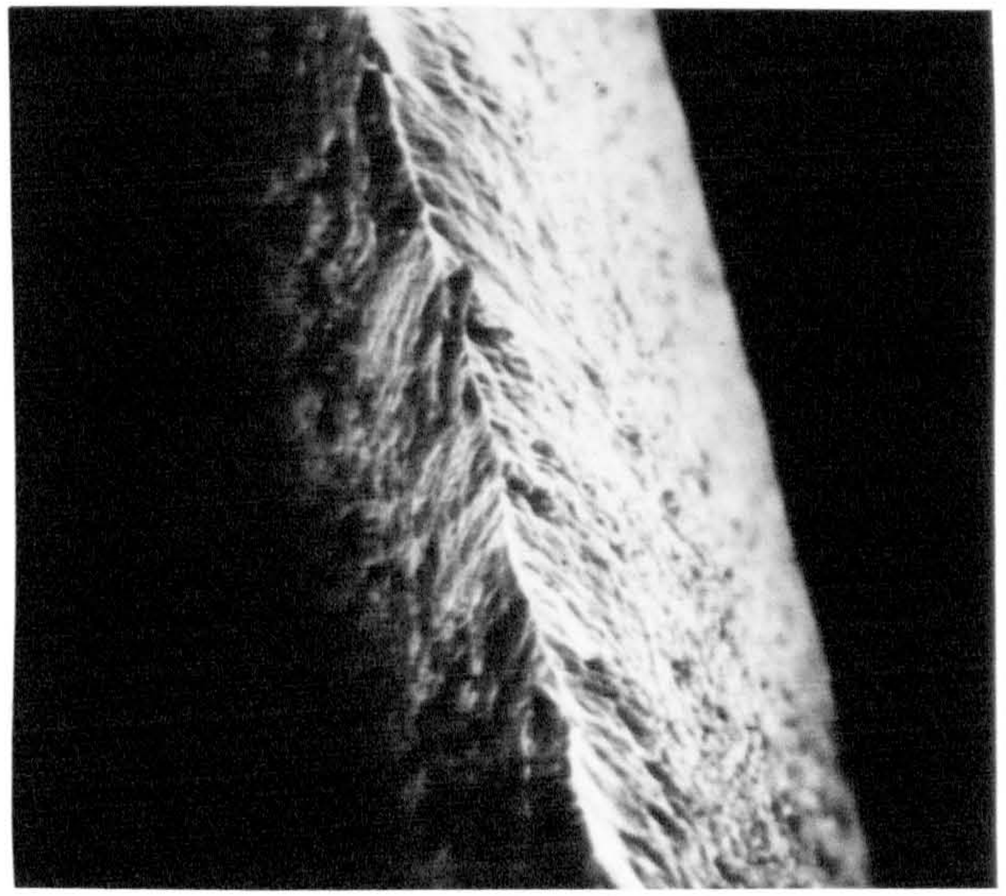

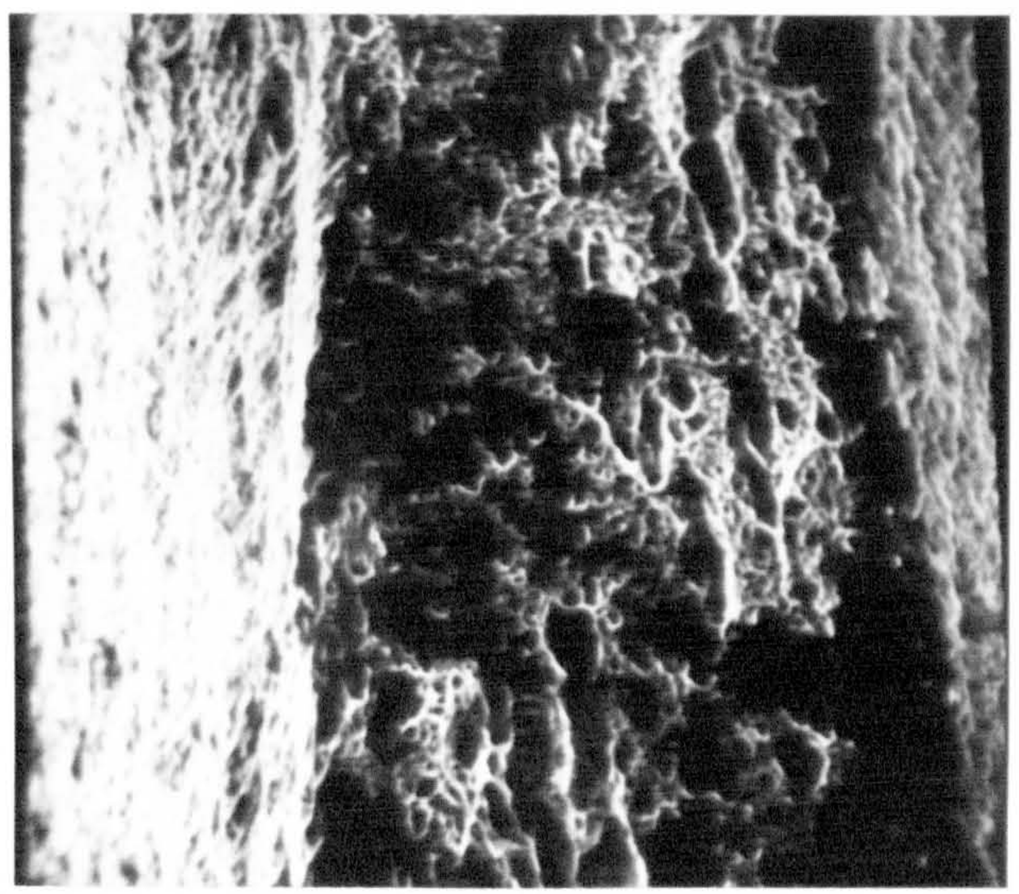

x5000

0.1in/min,400%.m=.34. ($4x10^{-2}min^{-1}$)

1in/min,200%.m=.17. ($4x10^{-1}min^{-1}$)

20 in/min,50%.m=.05. ($8x10^{0}min^{-1}$)

Figure50-The effect of crosshead velocities on fracture behaviour.(SEM).

Fig 51

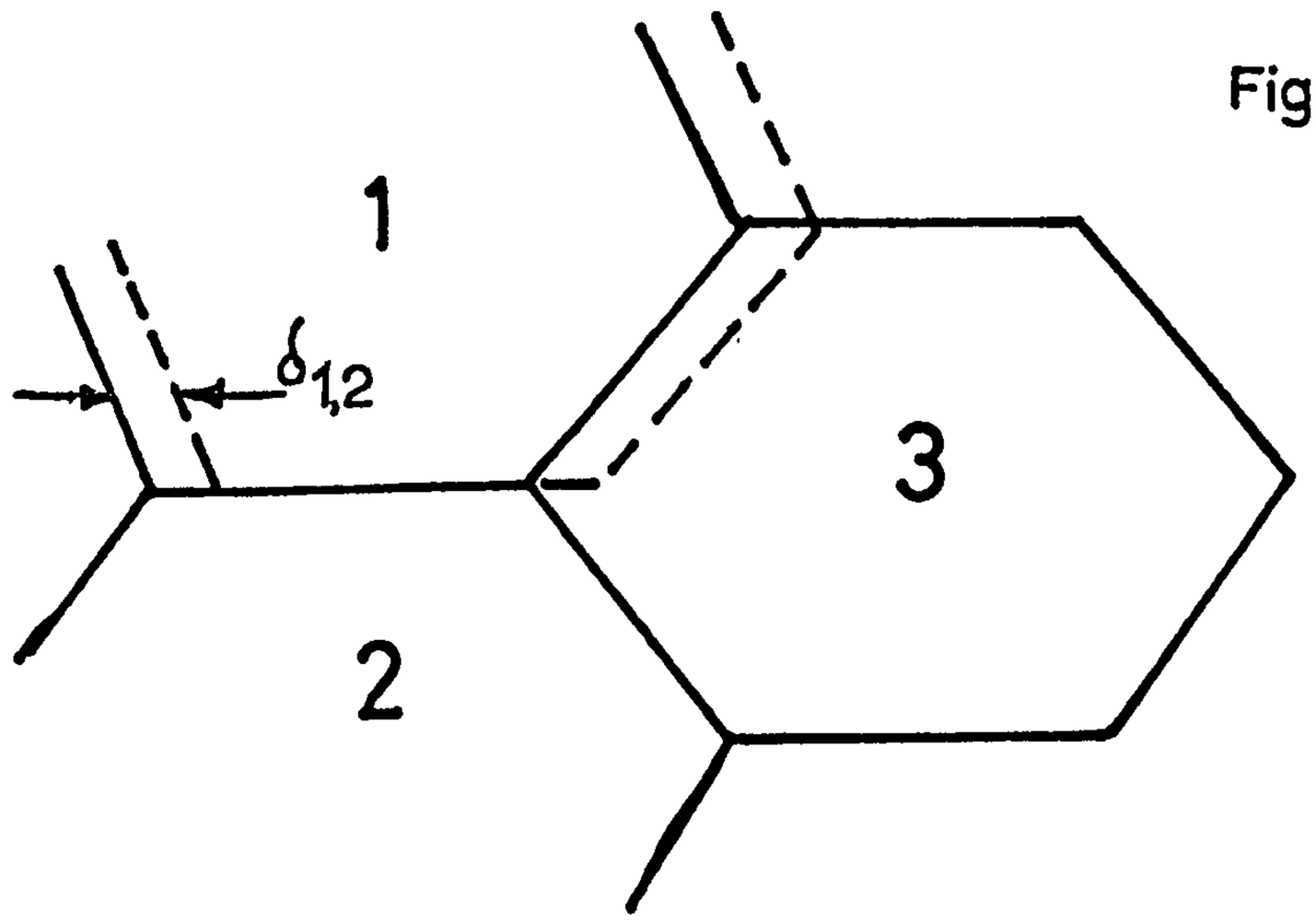

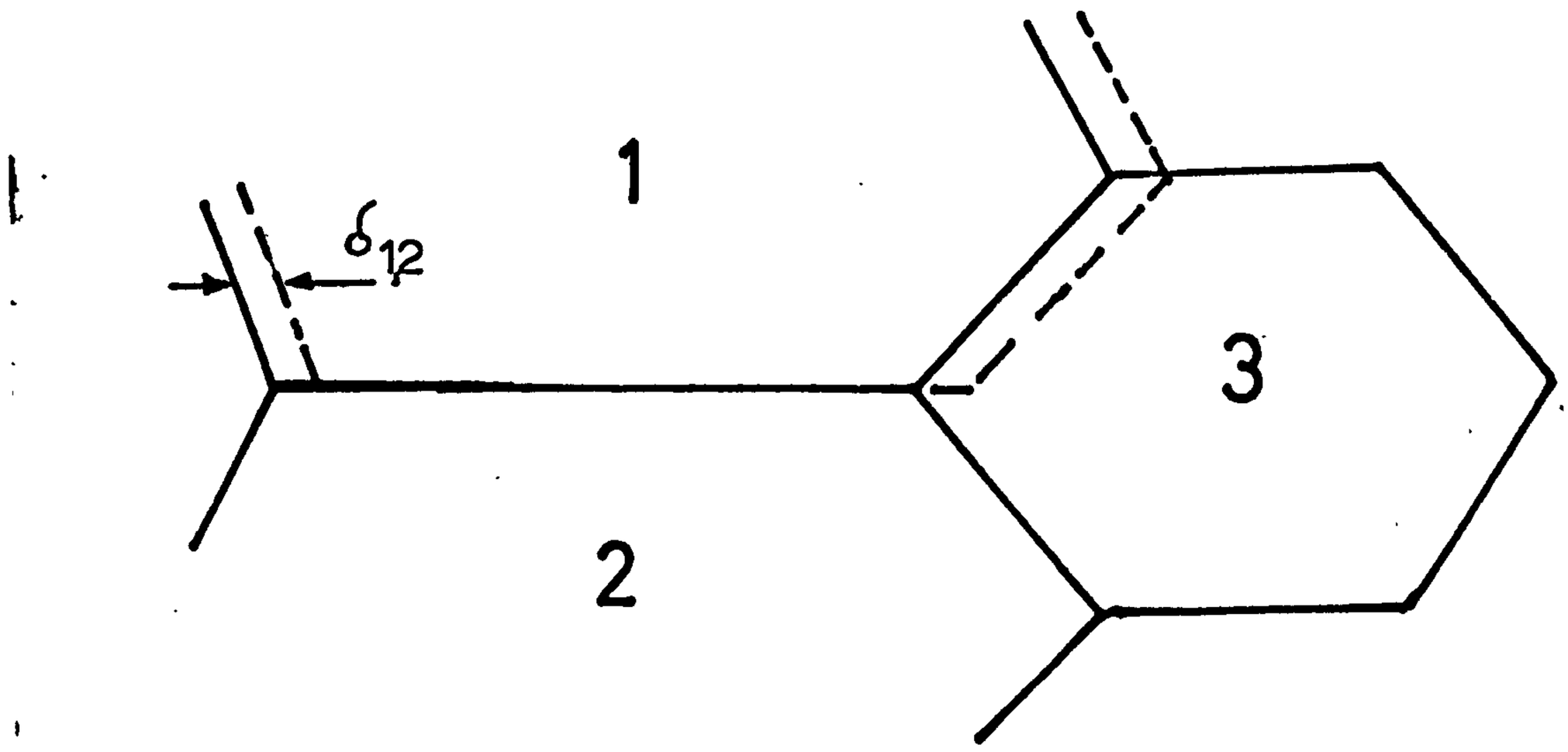

Figure 51 - Schematic illustration for the need of accomodating grain strain to permit grainboundry sliding.

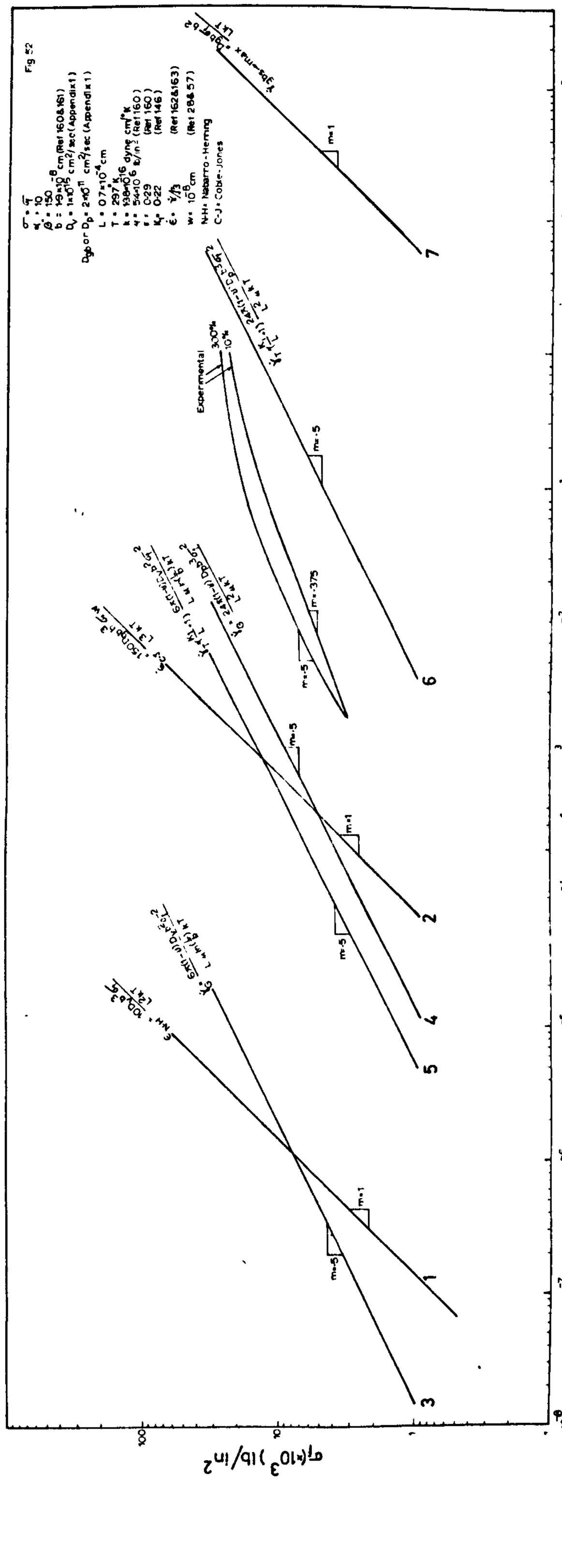

Figure 52- σ_f vs $\dot{\epsilon}$ relationship for the superplastic alloy Zn/0.Al alloy calculated from various strain-rate contributing mechanisms.

Fig 53

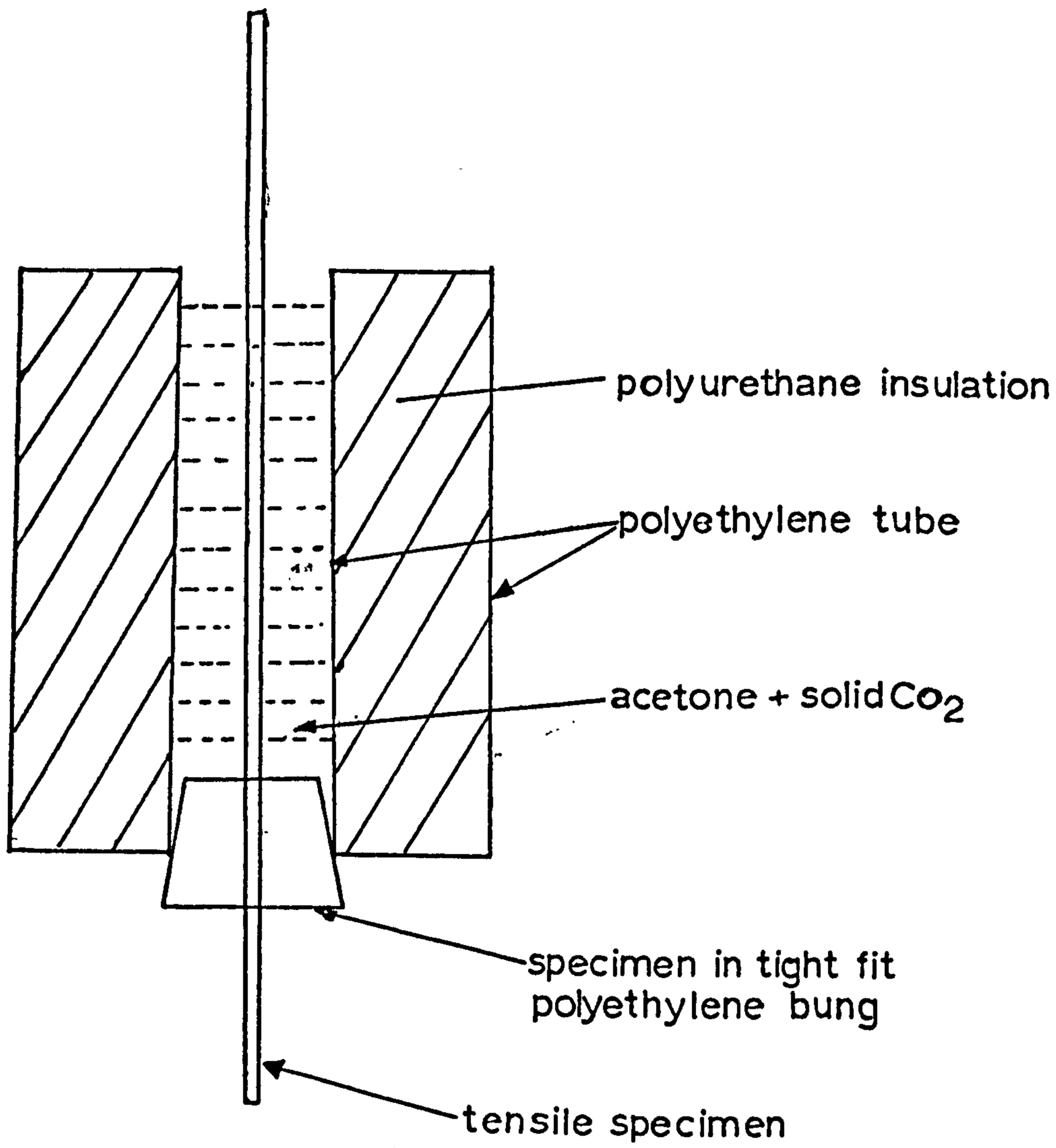

Figure 53 - Schematic diagram of the method employed to strain tensile specimens at -75° C.

Fig 54

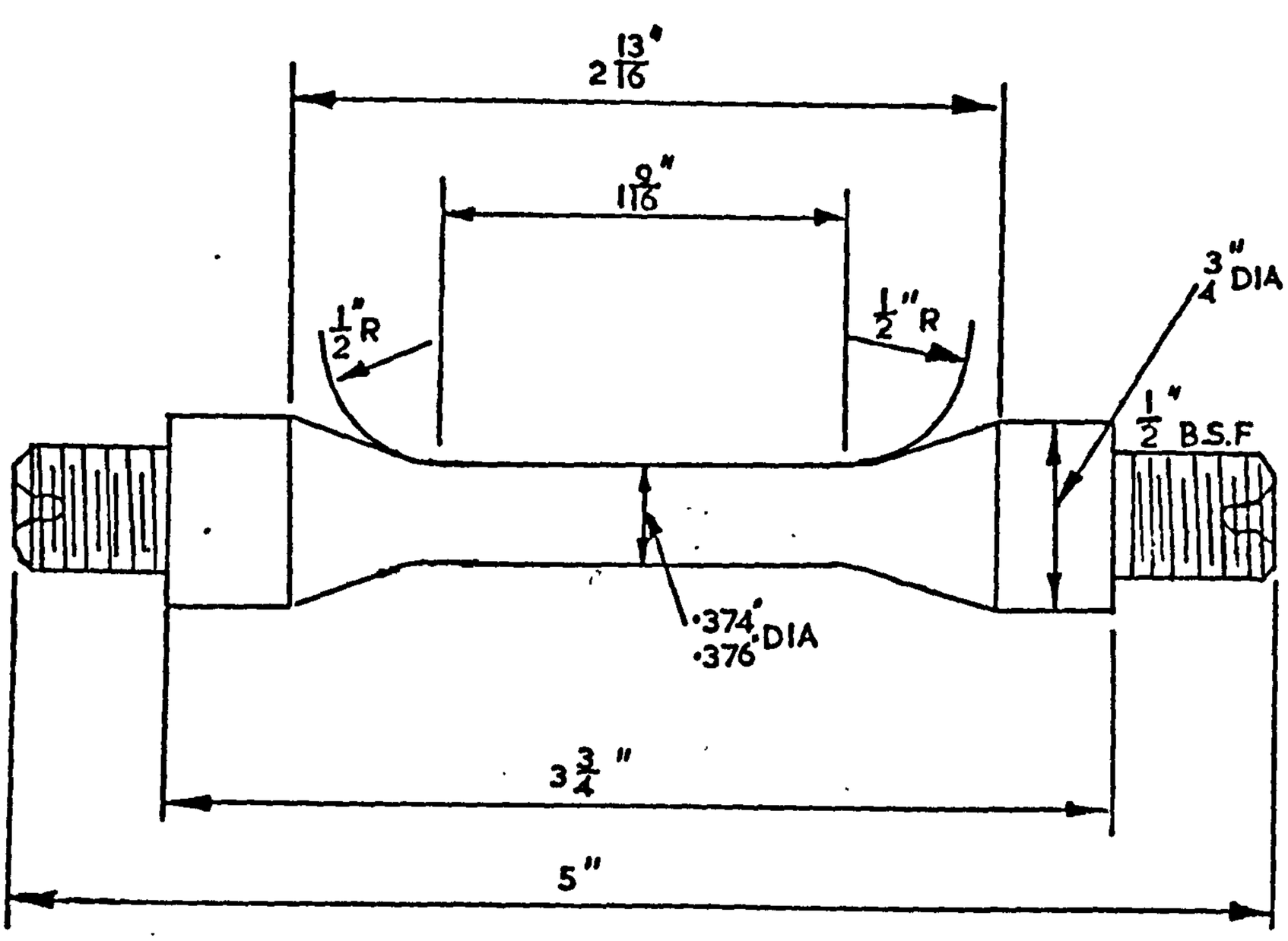

Figure 54 - Dimensions of the torsion specimen.

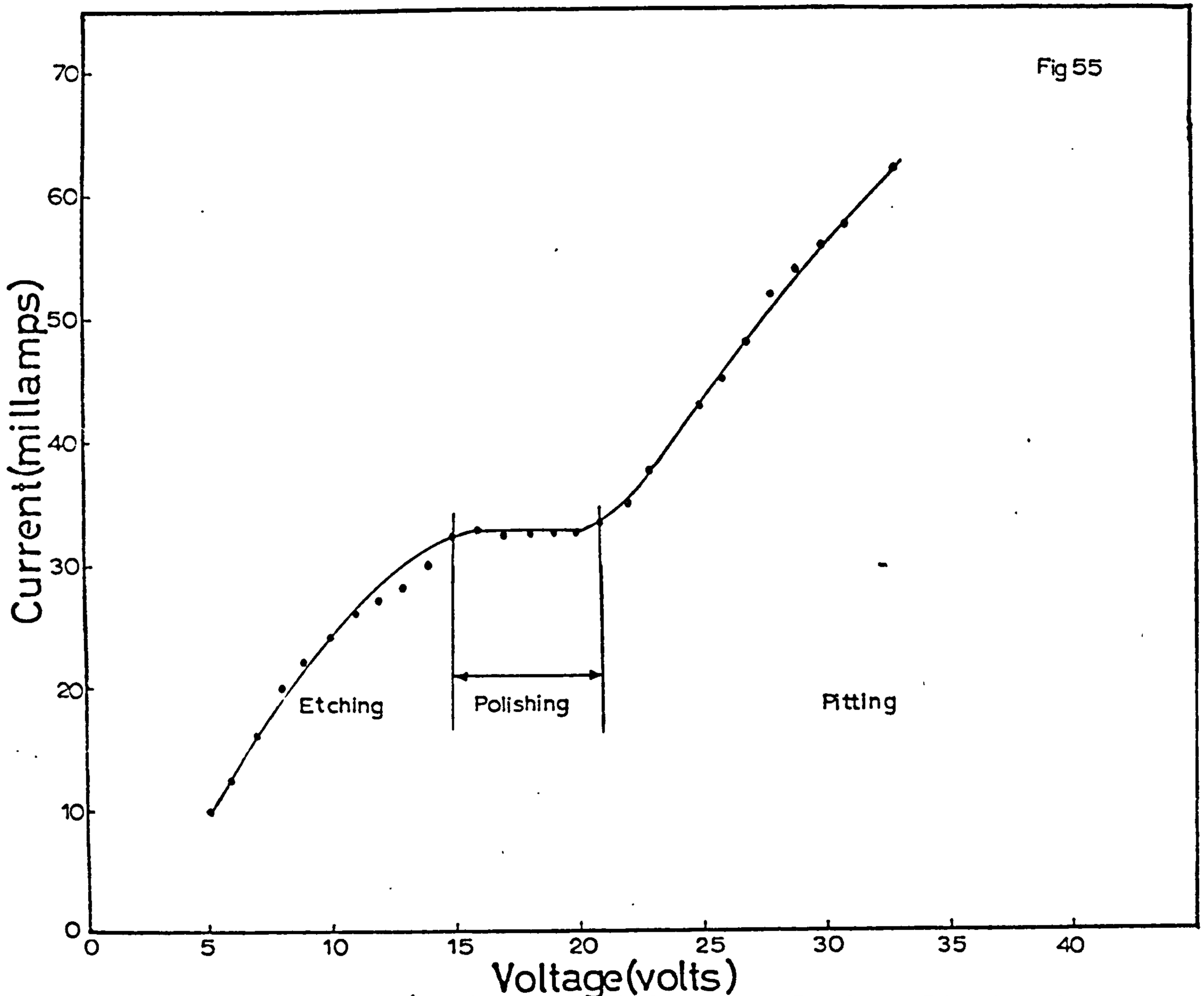

Figure 55-Showing the current/voltage condition for electropolishing to produce thin foils of the Zn/Al eutectoid alloy.

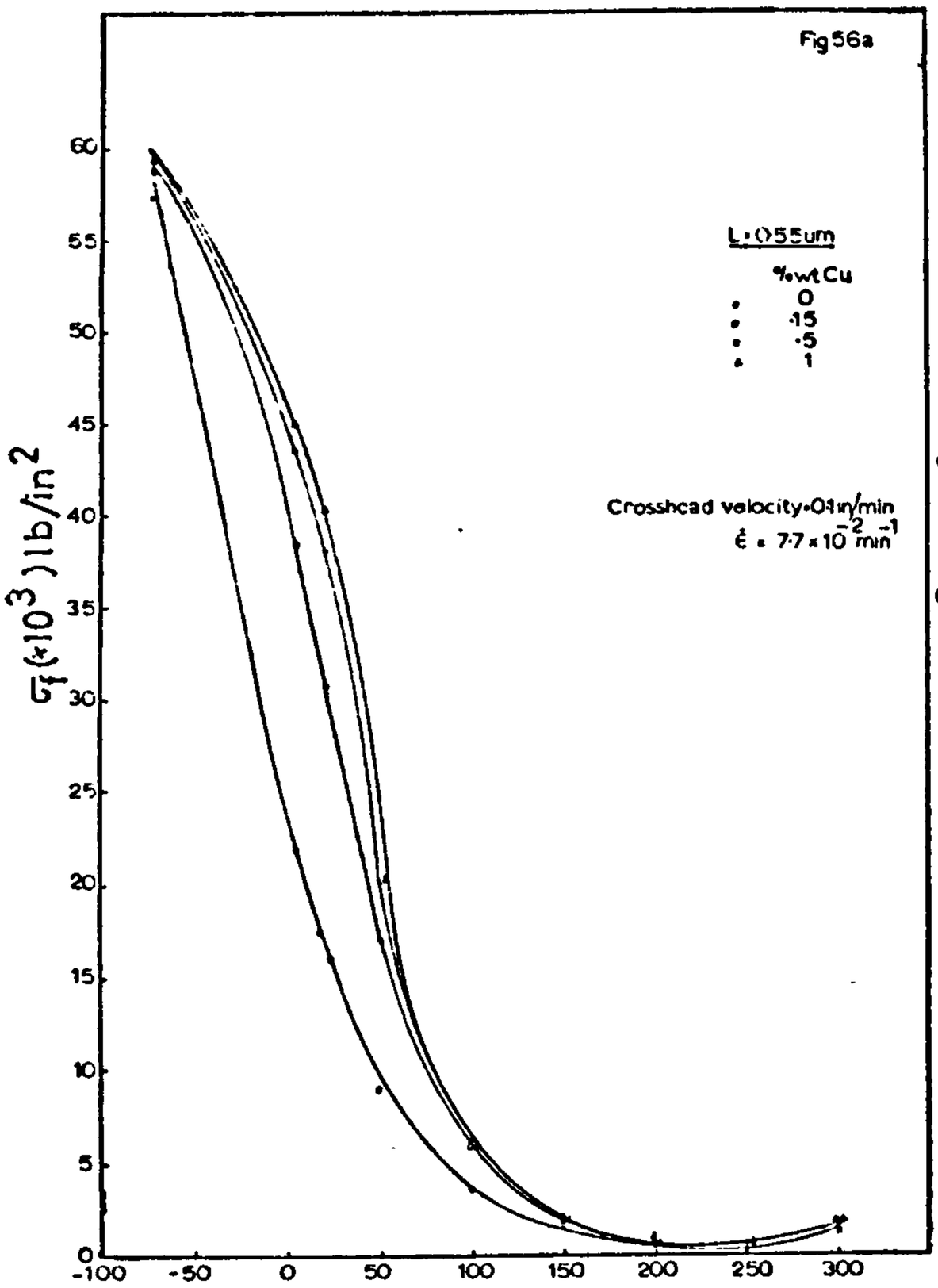

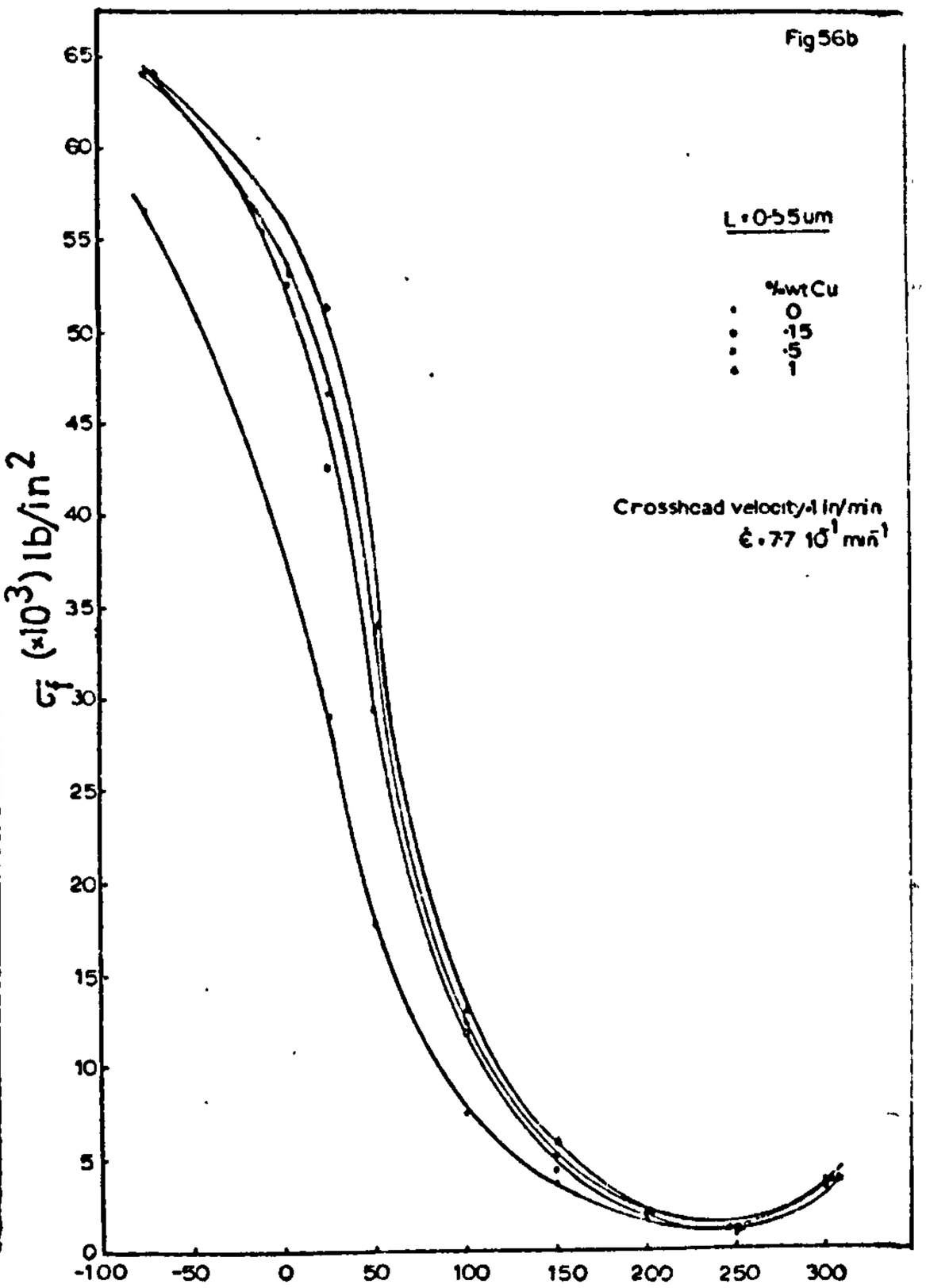

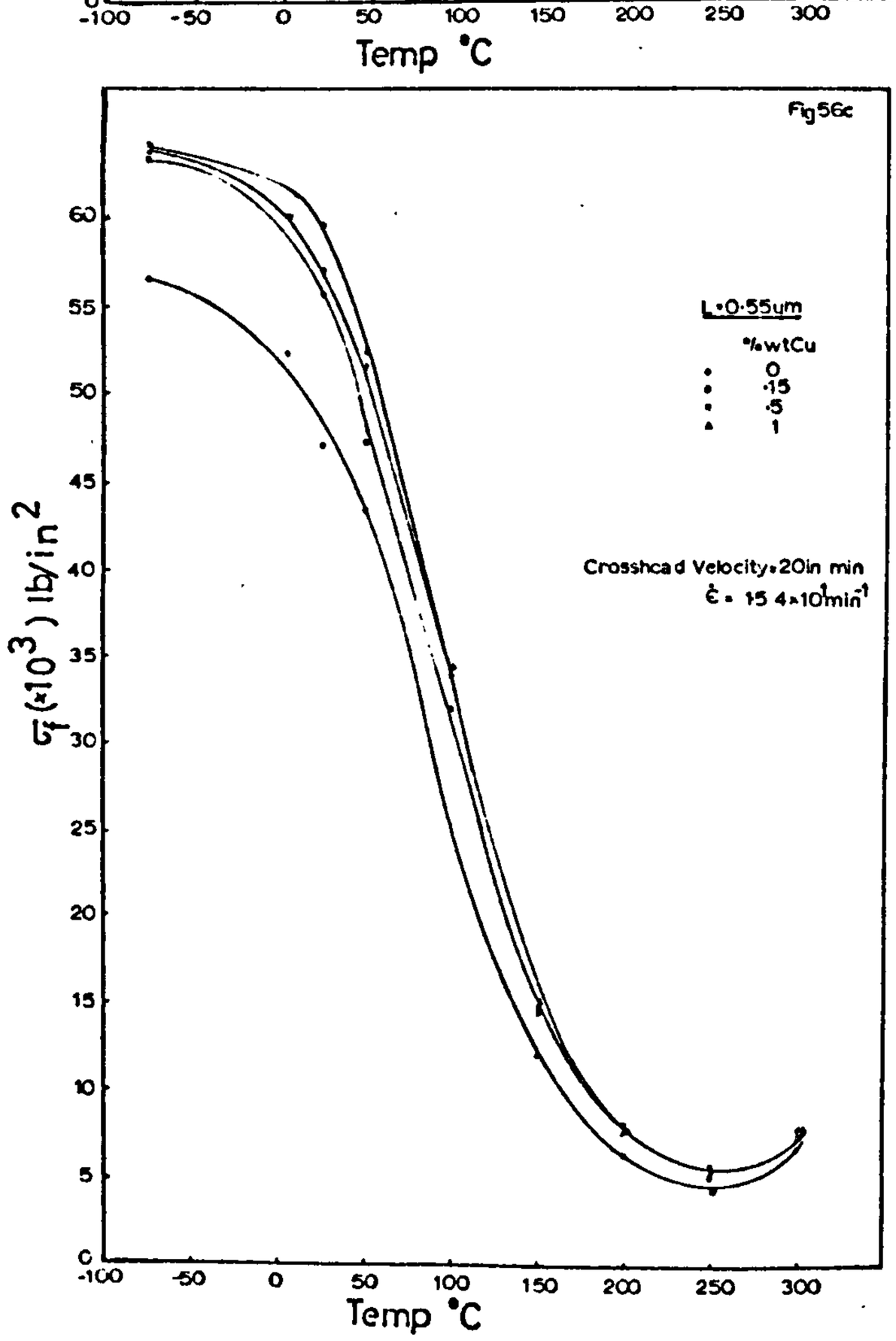

Figure 56a-c - The effect of temperature on the flow stress for the various copper containing alloys (L=0.55um) at three crosshead velocities.

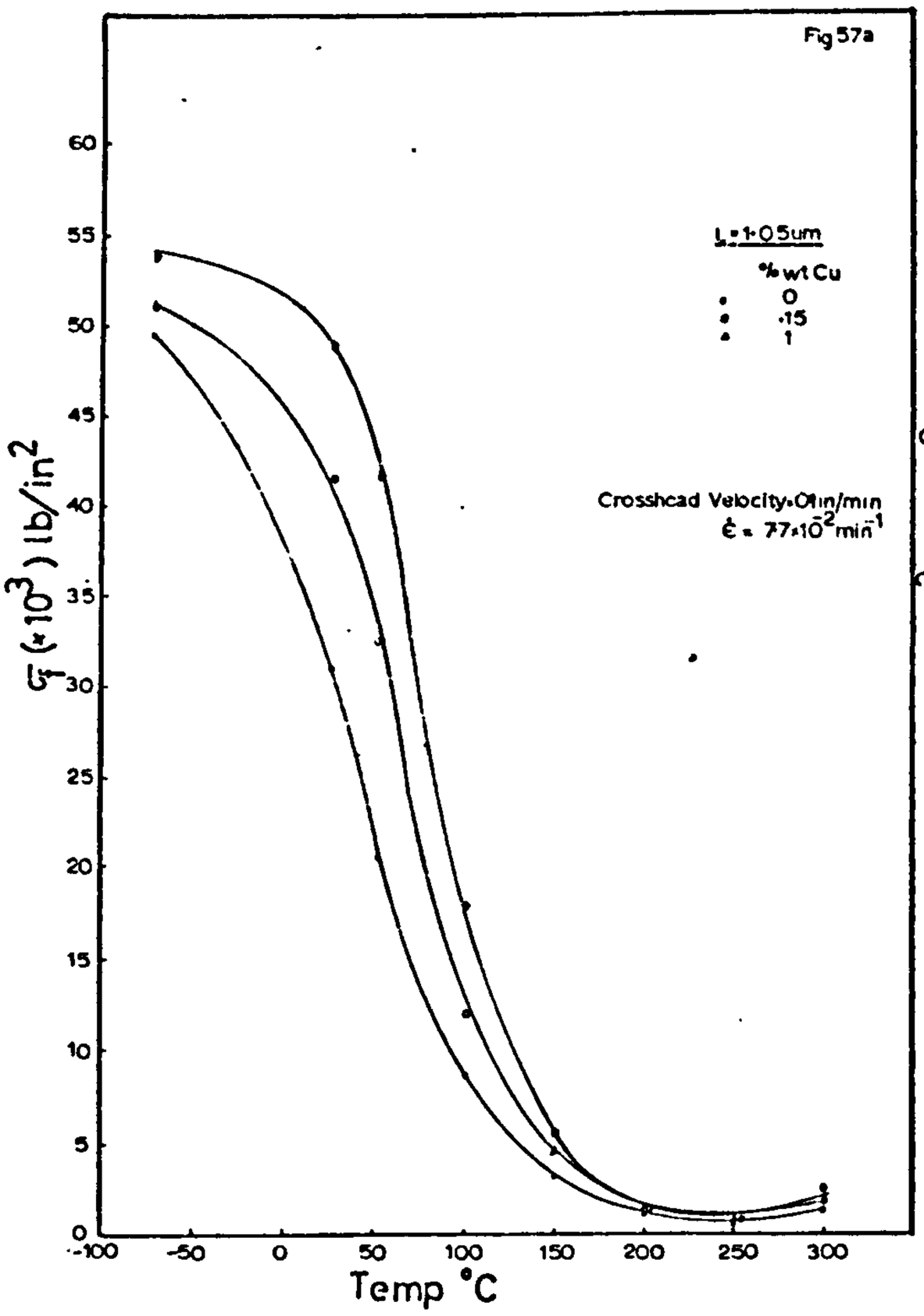

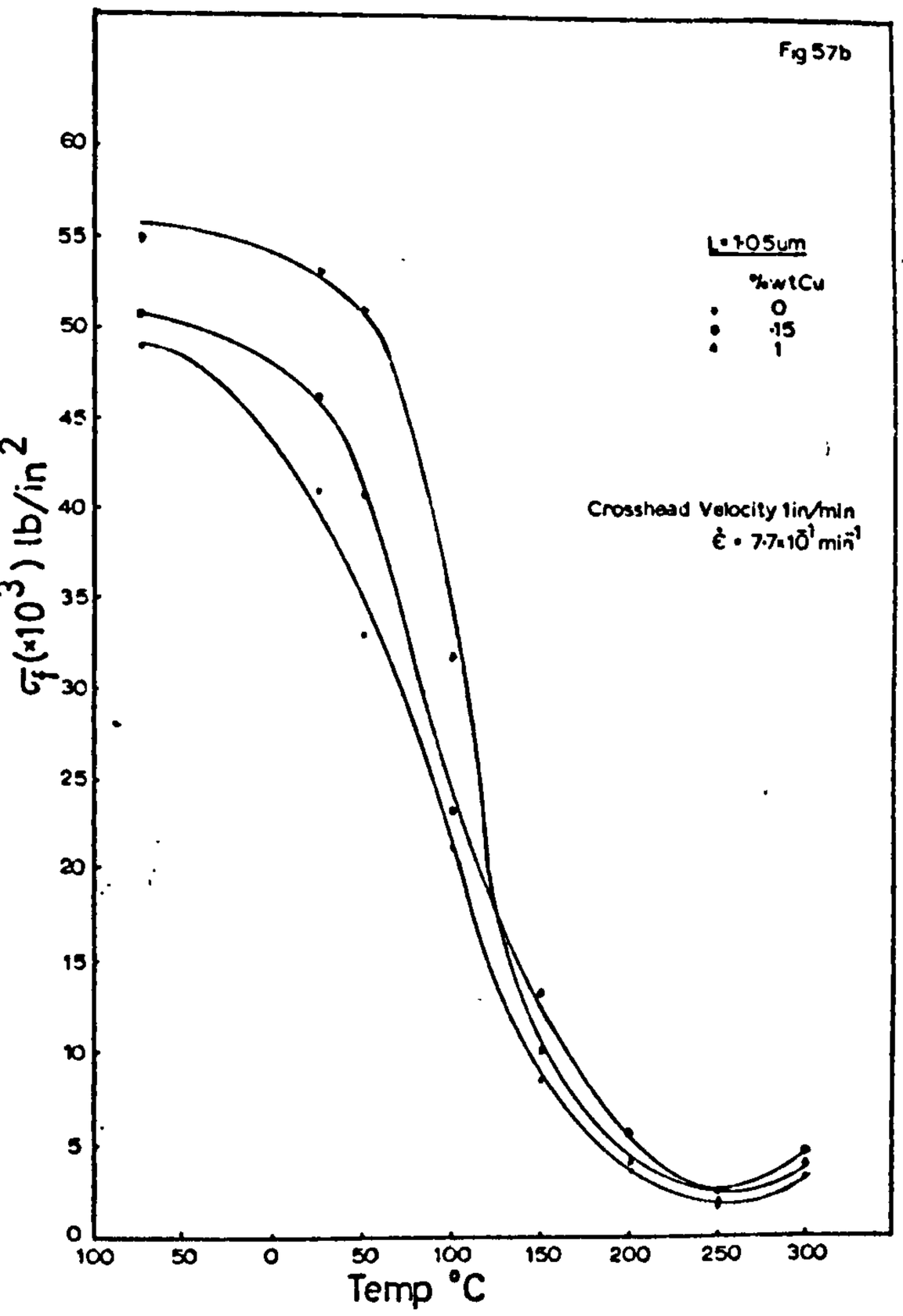

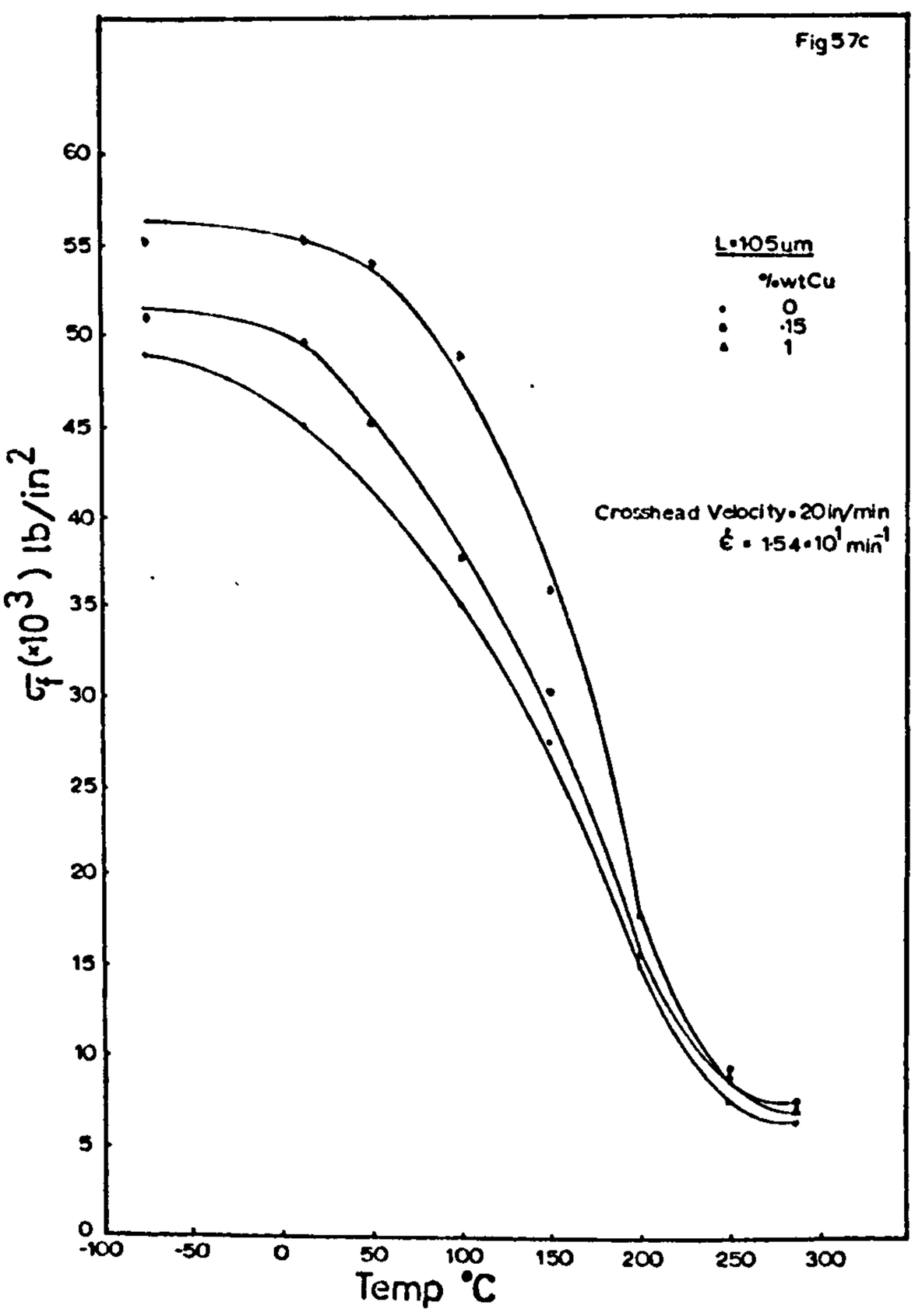

Figure 57a-c - The effect of temperature on the flow stress for the various copper containing alloys (L=1.05um) at three crosshead velocities.

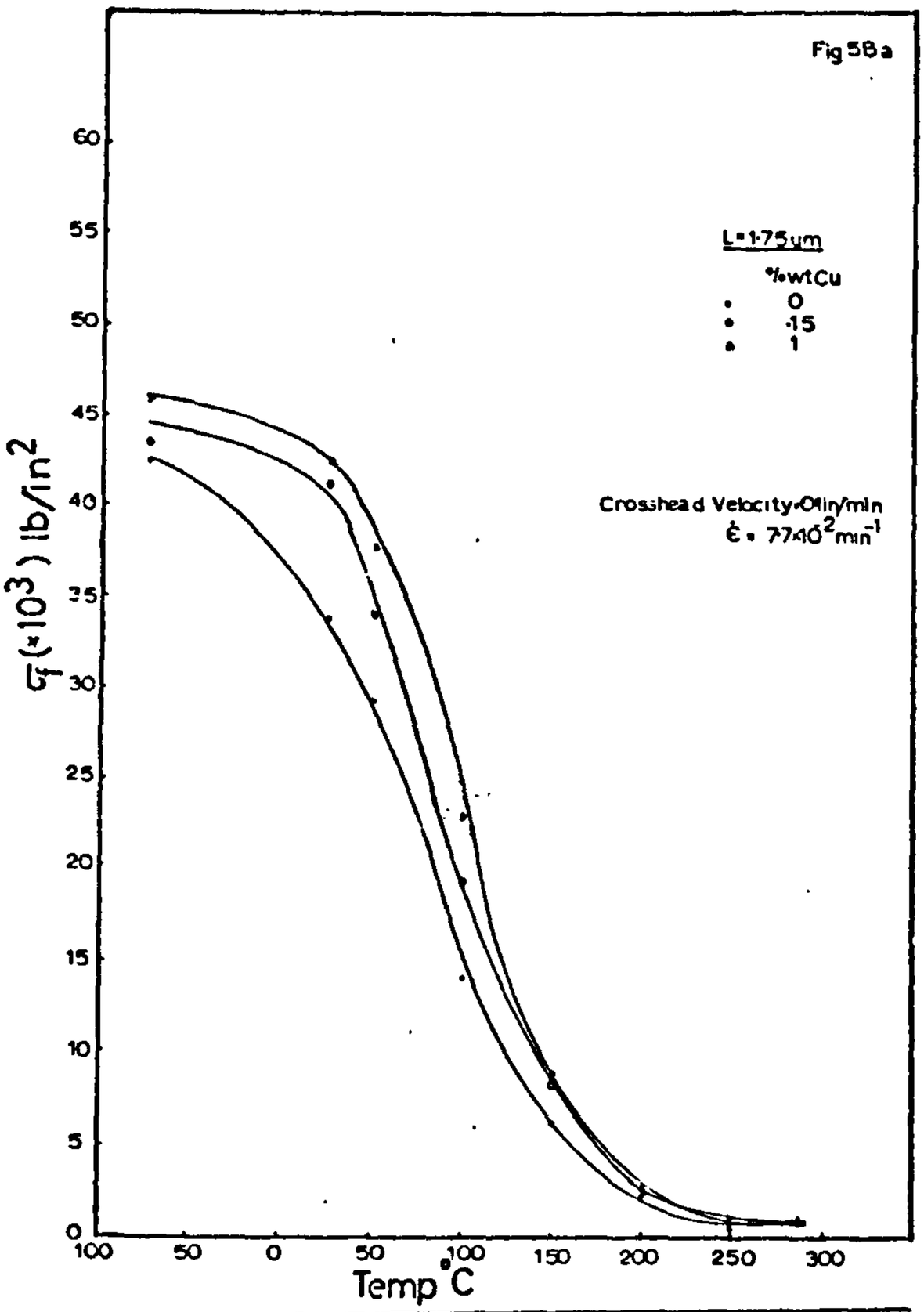

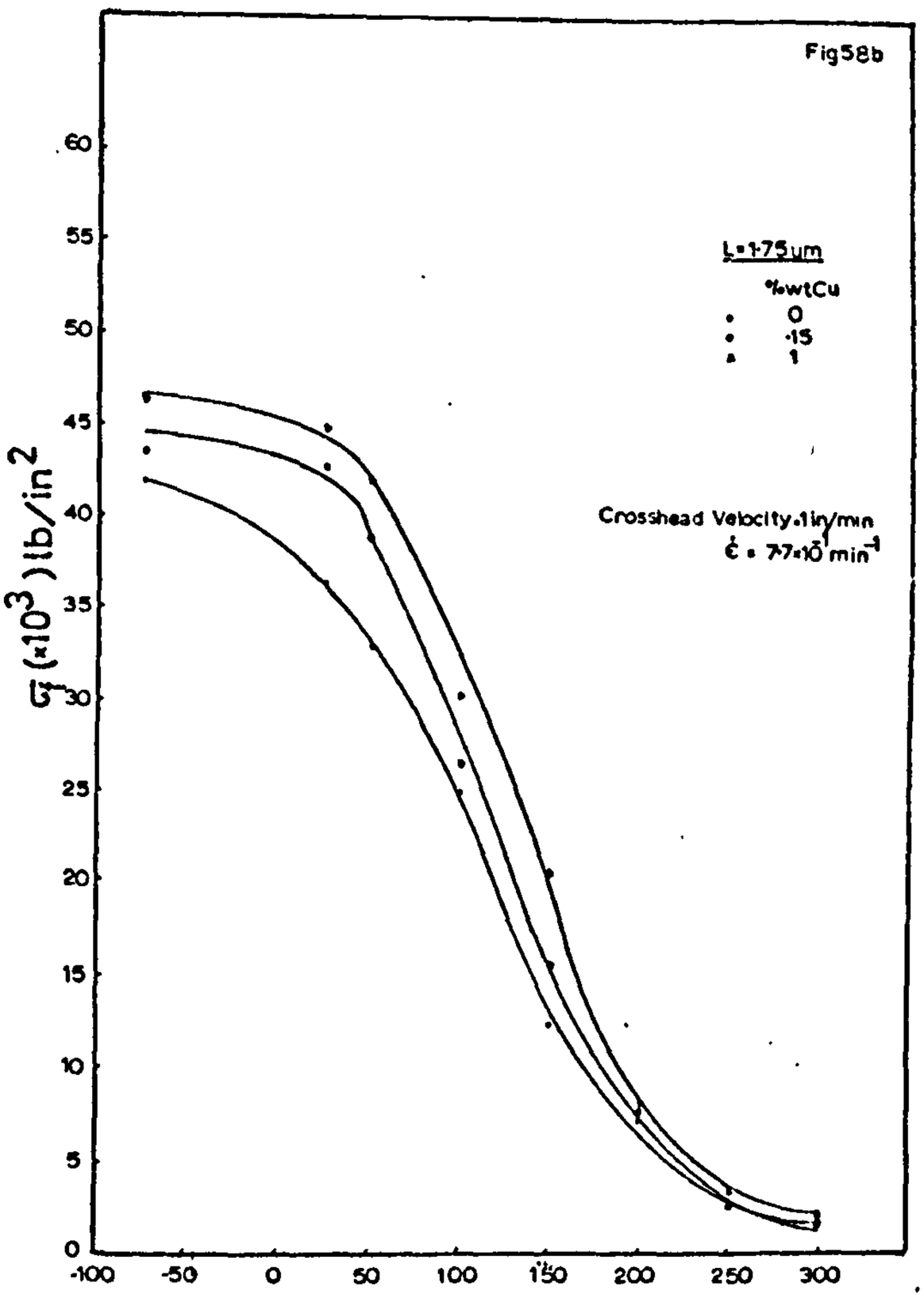

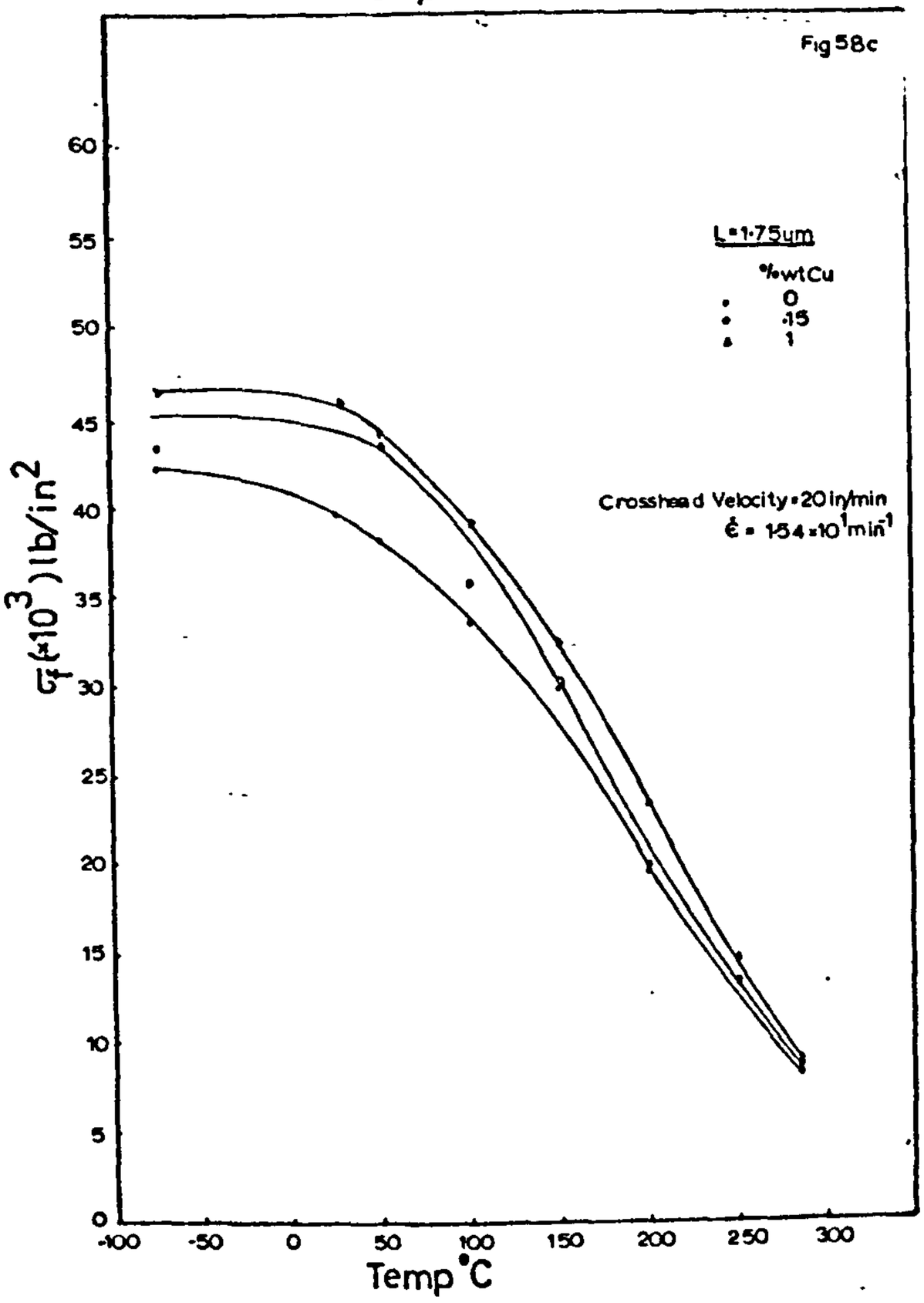

Figure 58a-c - The effect of temperature on the flow stress for the various copper containing alloys(L=1.75um) at three crosshead velocities.

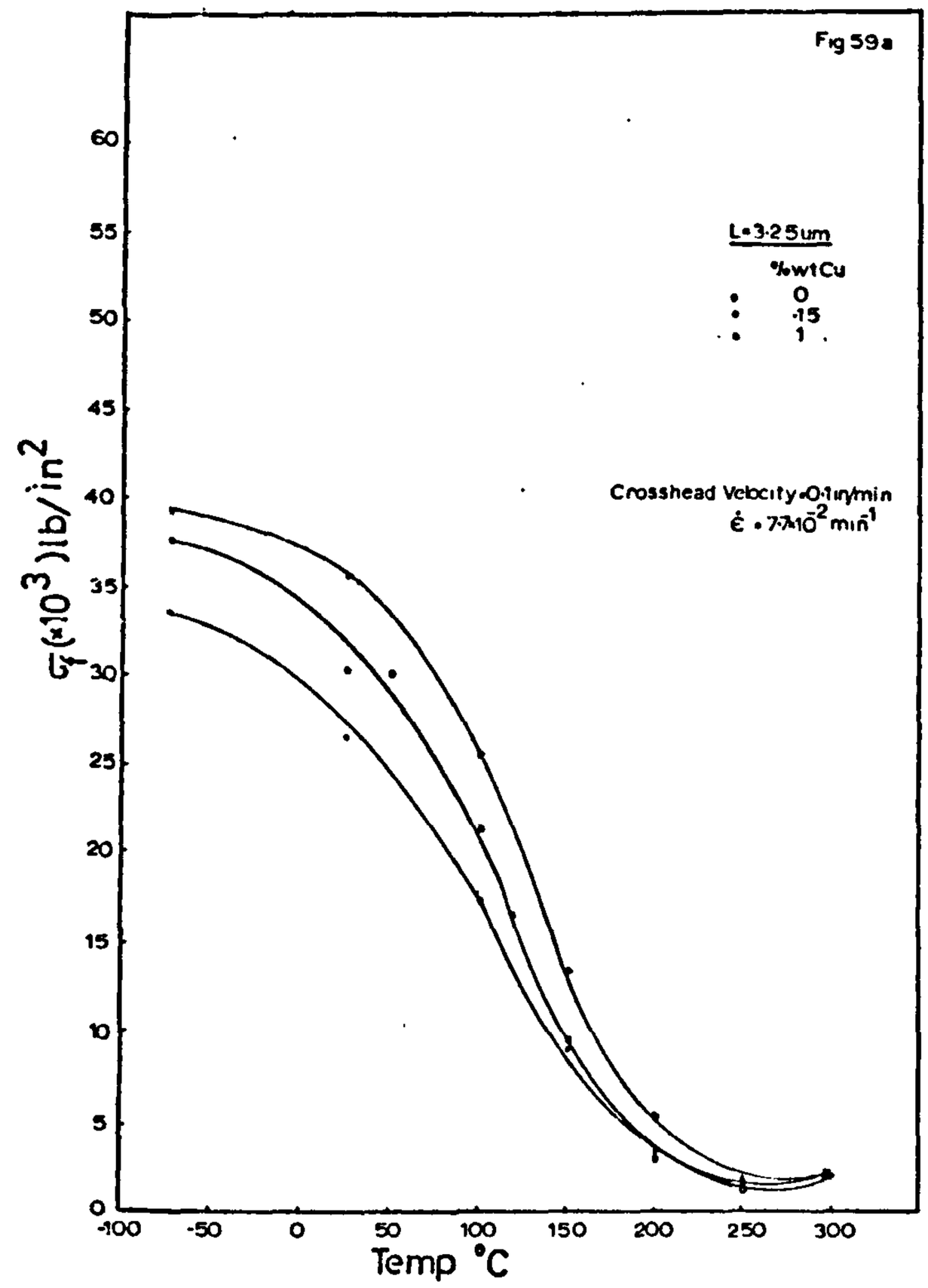

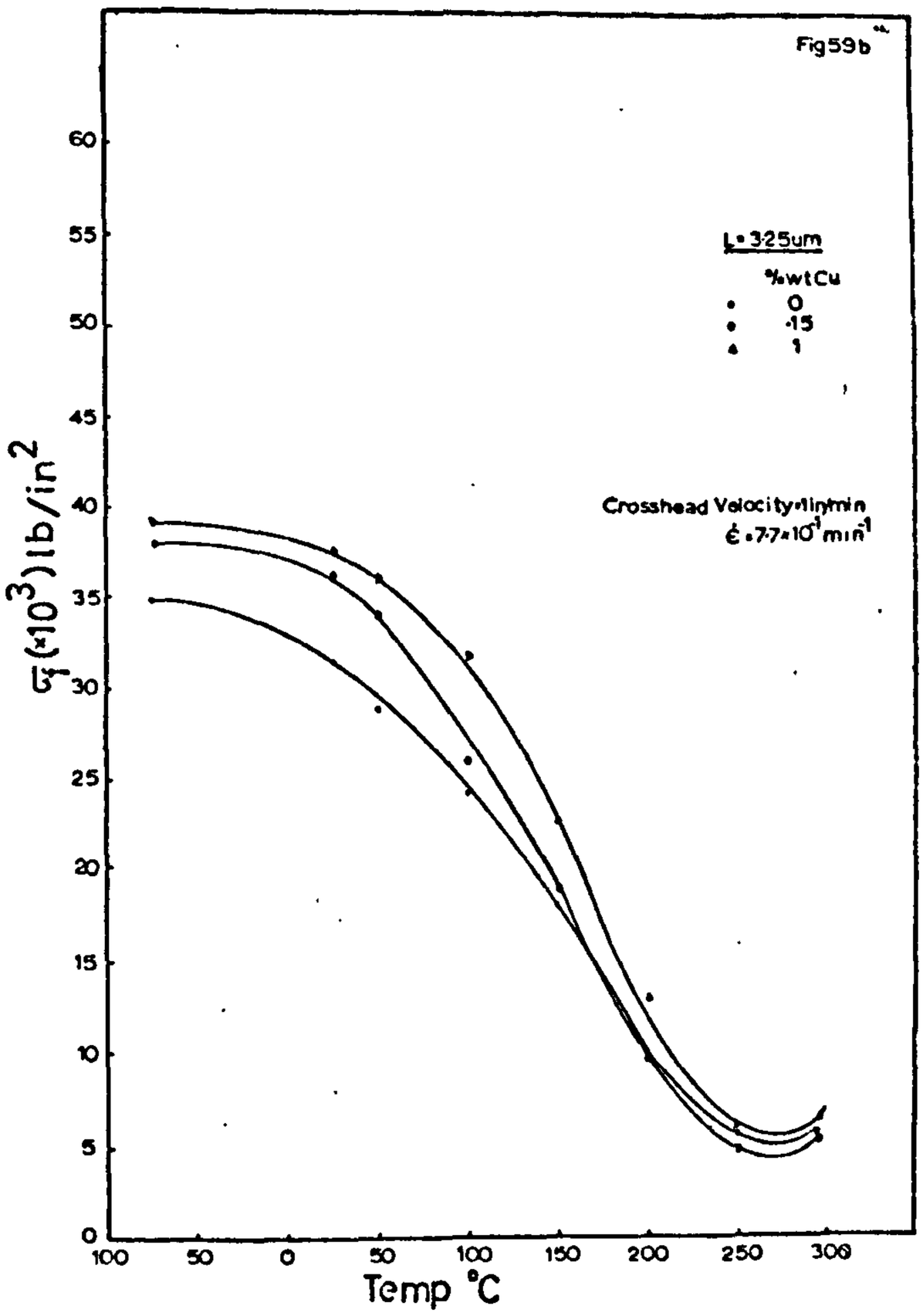

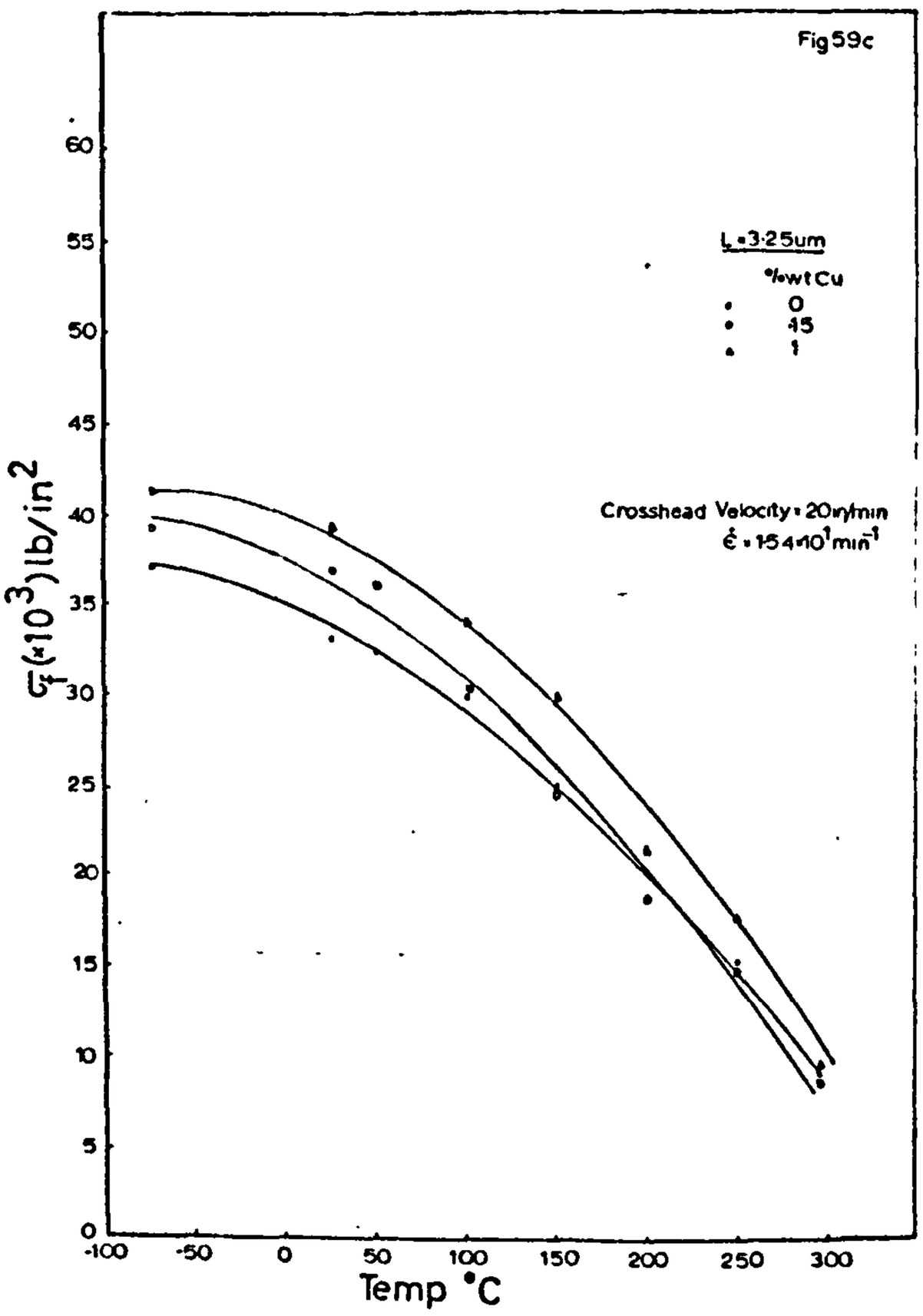

Figure 59a-c - The effect of temperature on the flow stress for the various copper containing alloys(L=3.25um) at three crosshead velocities.

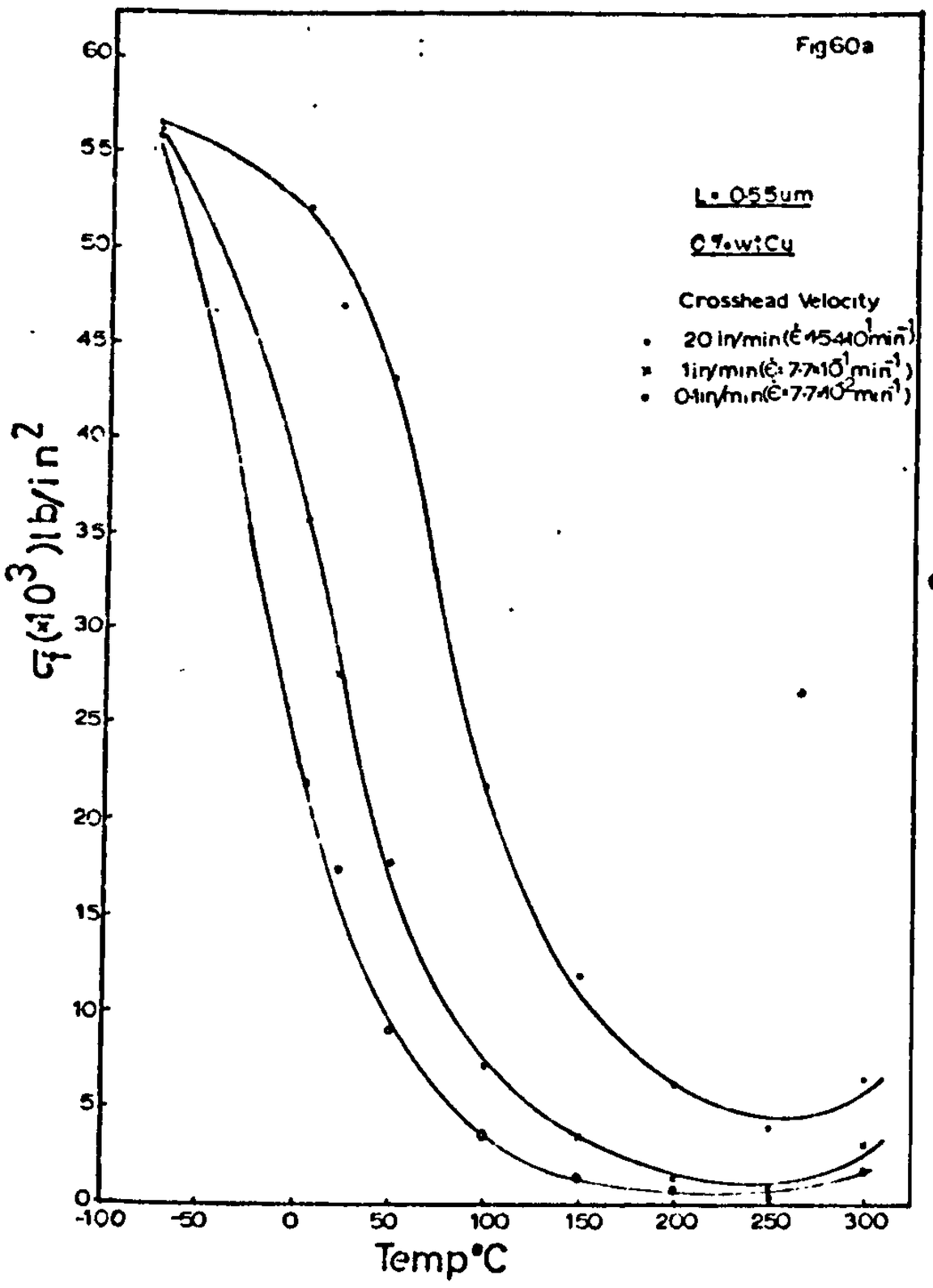

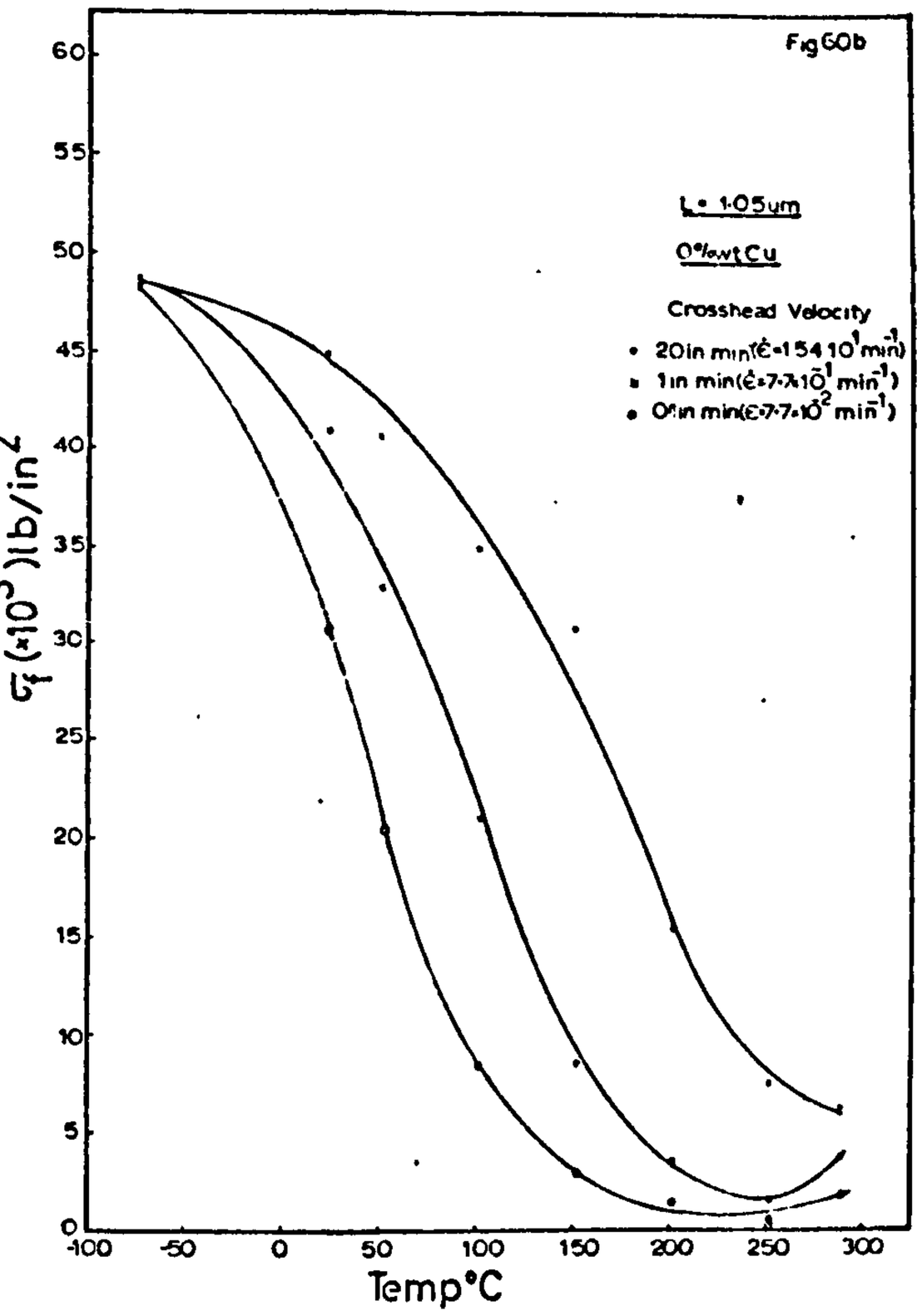

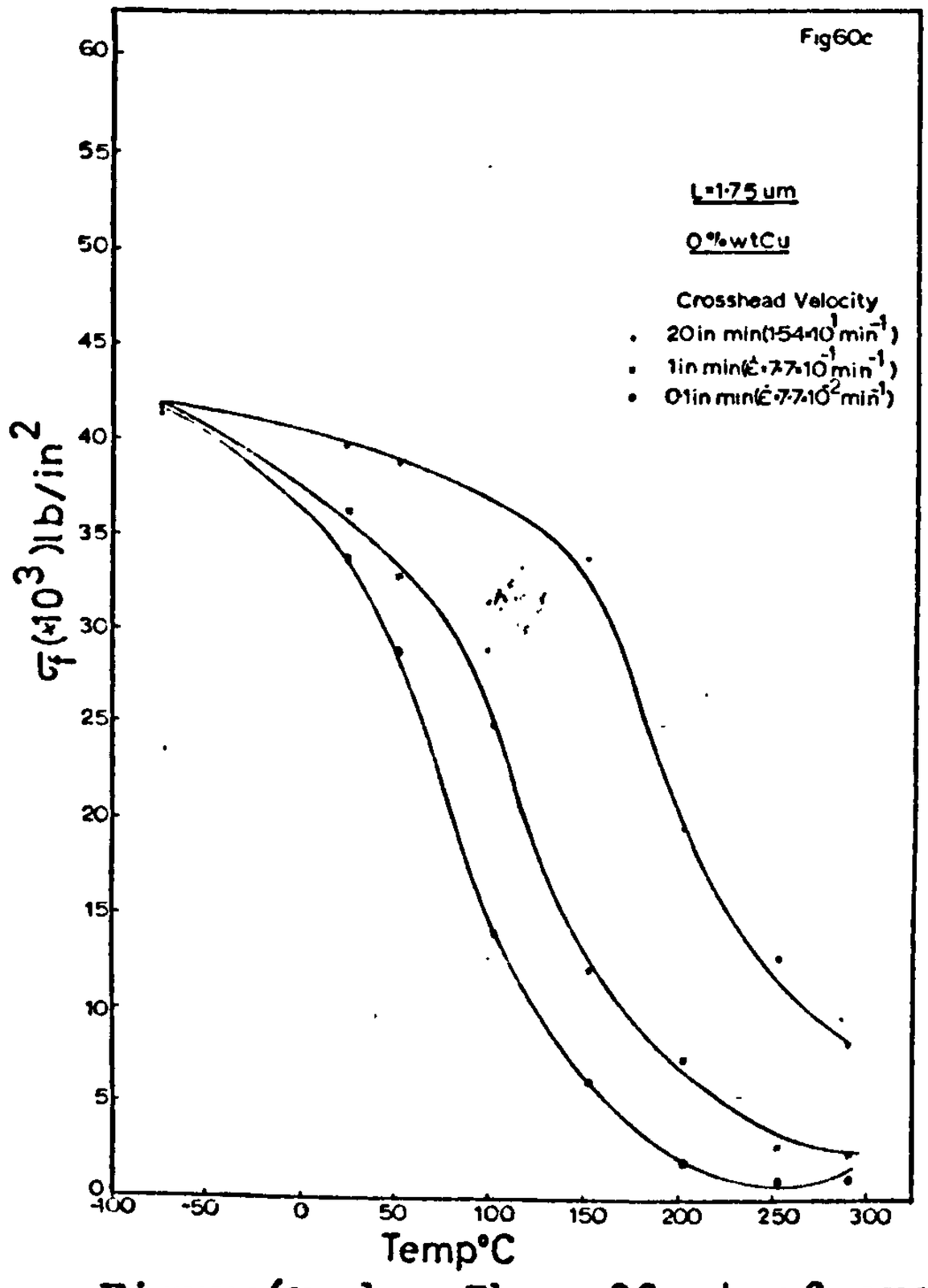

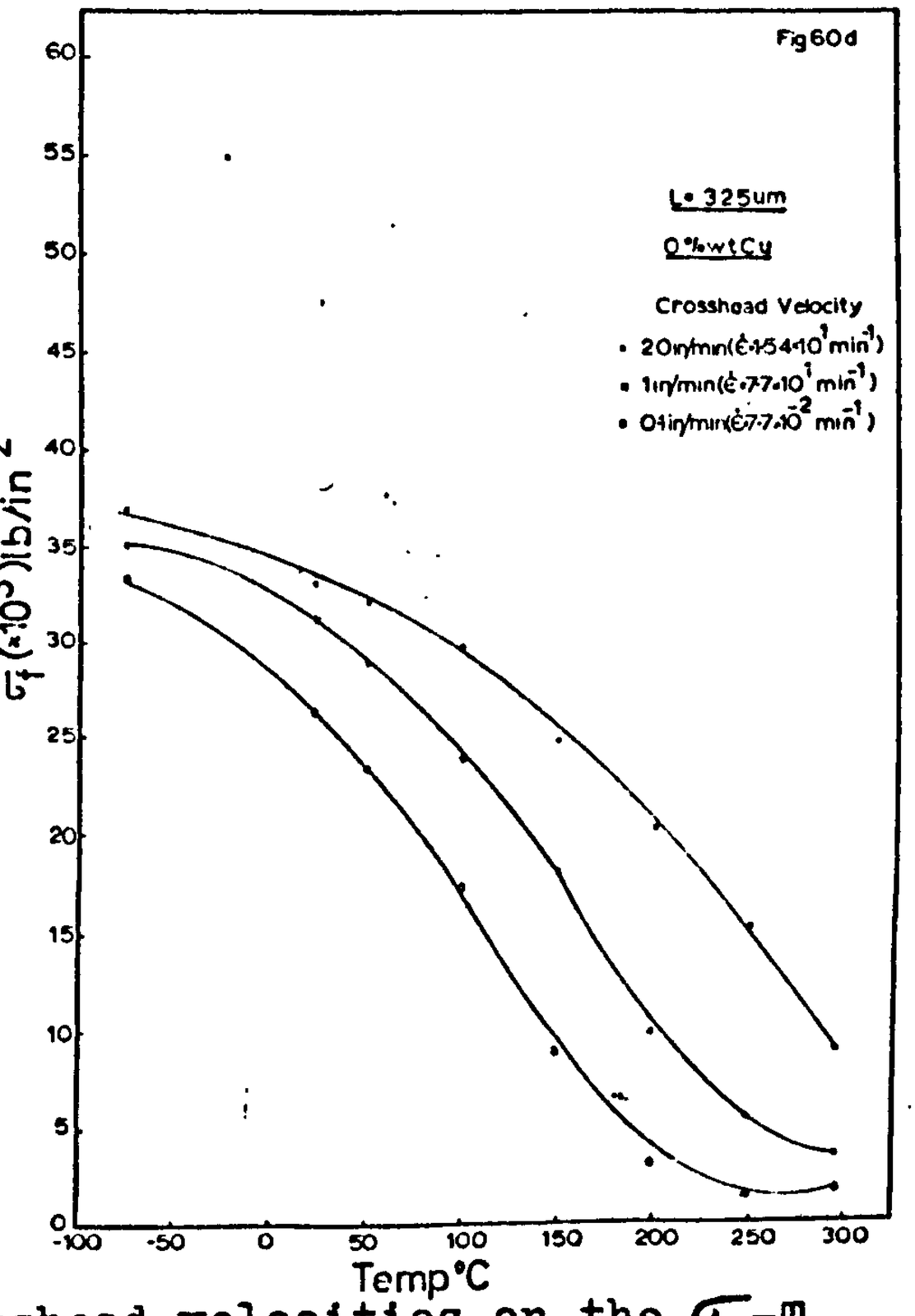

Figure 60a-d - The effect of crosshead velocities on the σ_f-T behaviour for increasing grain sizes (0%wt Cu).

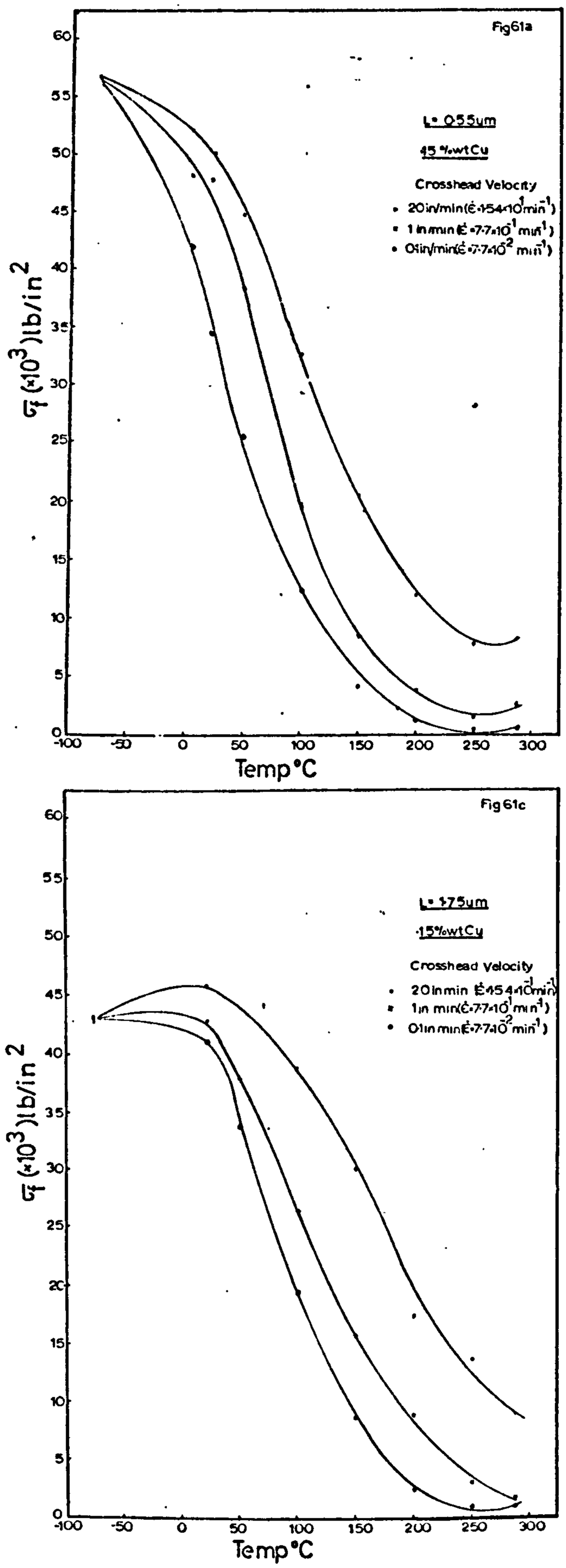

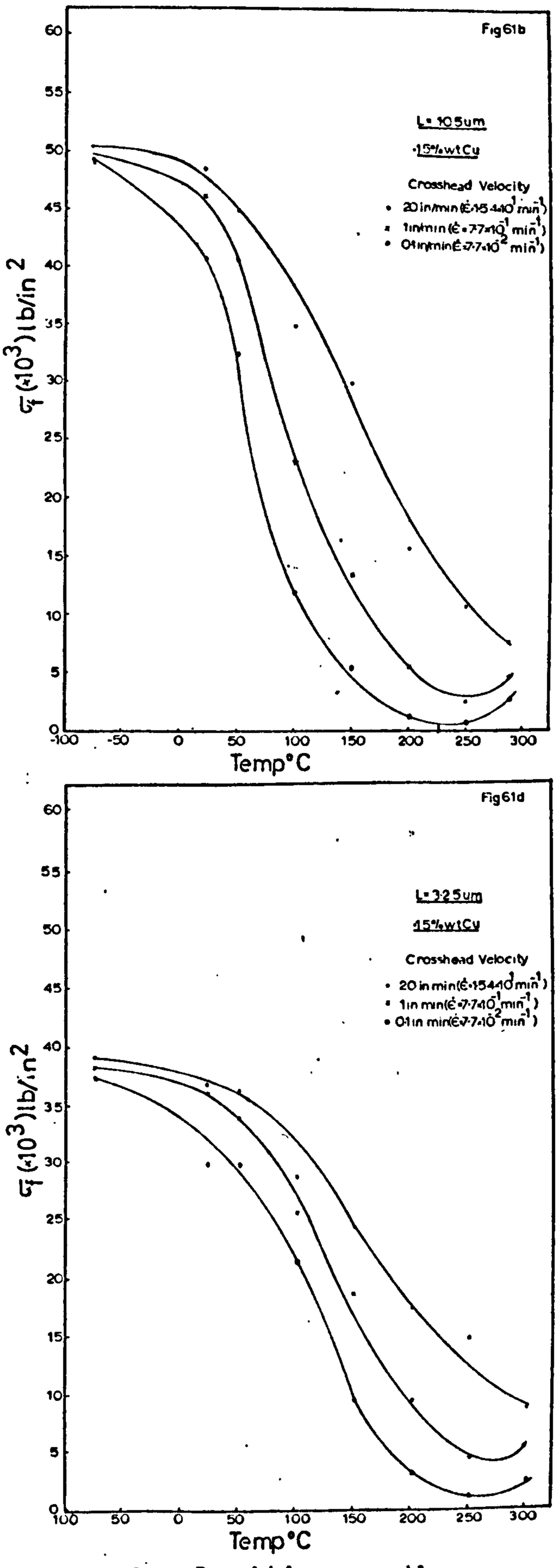

Figure 61a-d - The effect of crosshead velocities on the σ_f-T behaviour for increasing grain sizes (0.15%wt Cu).

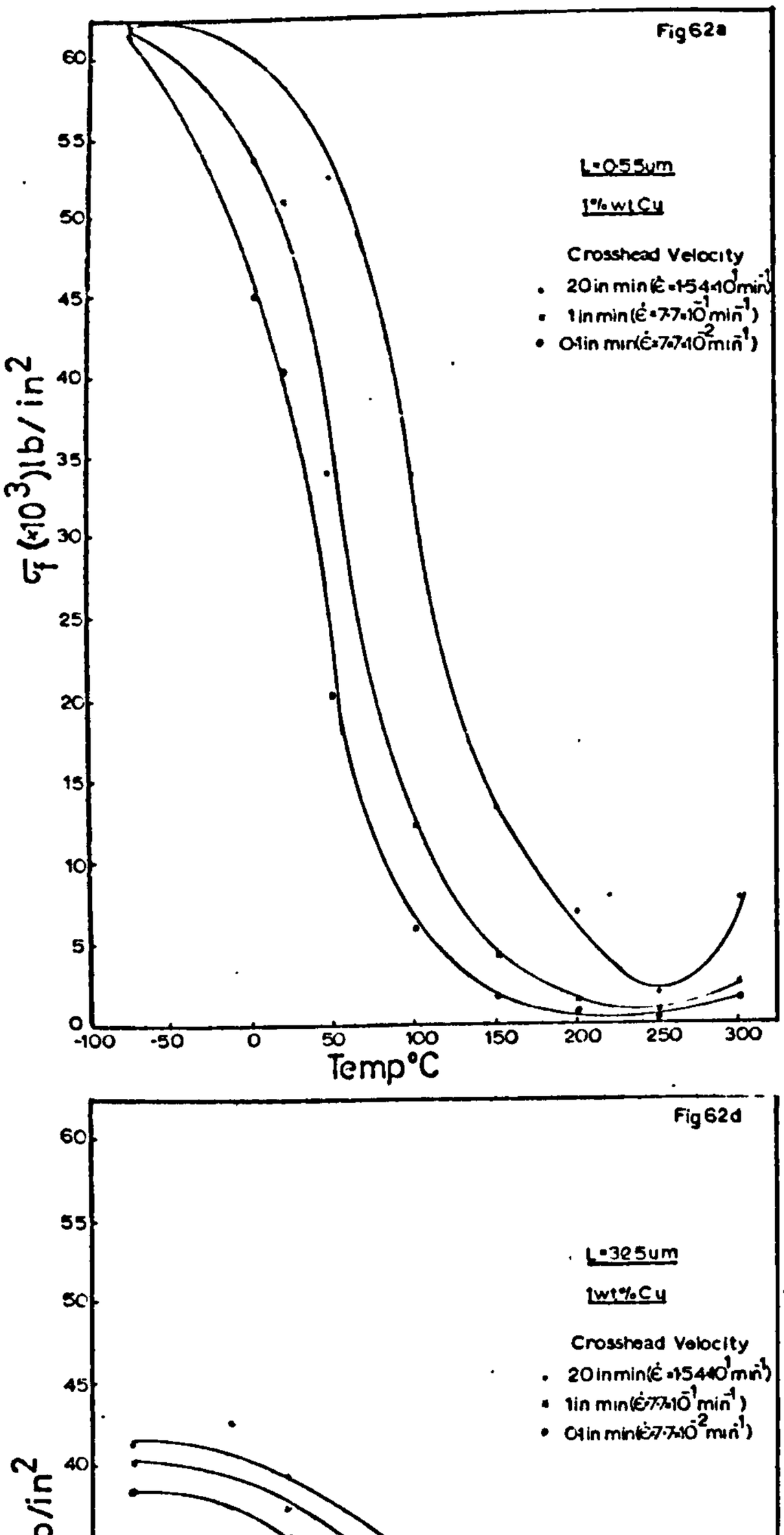

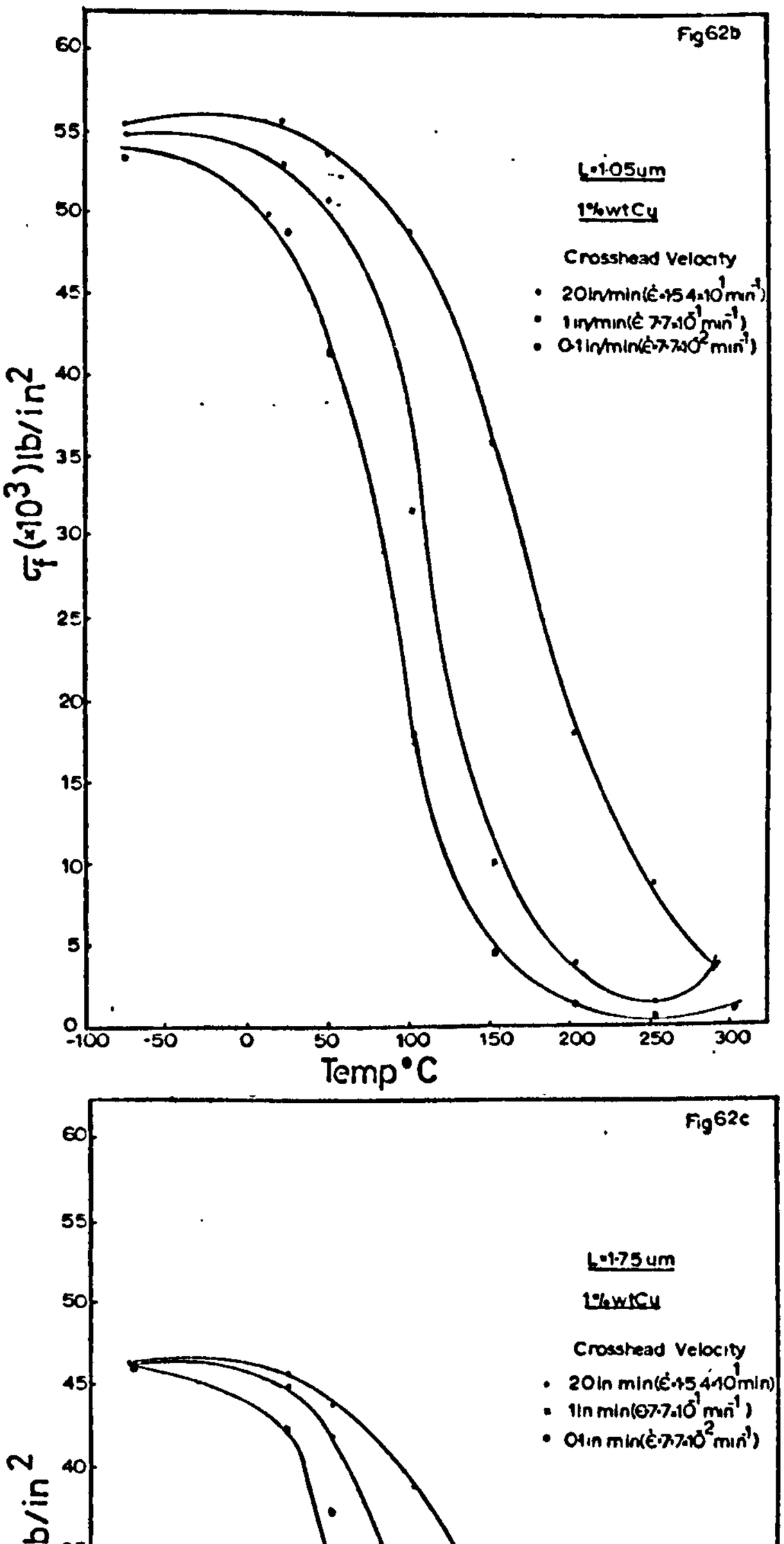

Figure 62a-d - The effect of crosshead velocities on the σ_f-T behaviour for increasing grain sizes (1%wt Cu).

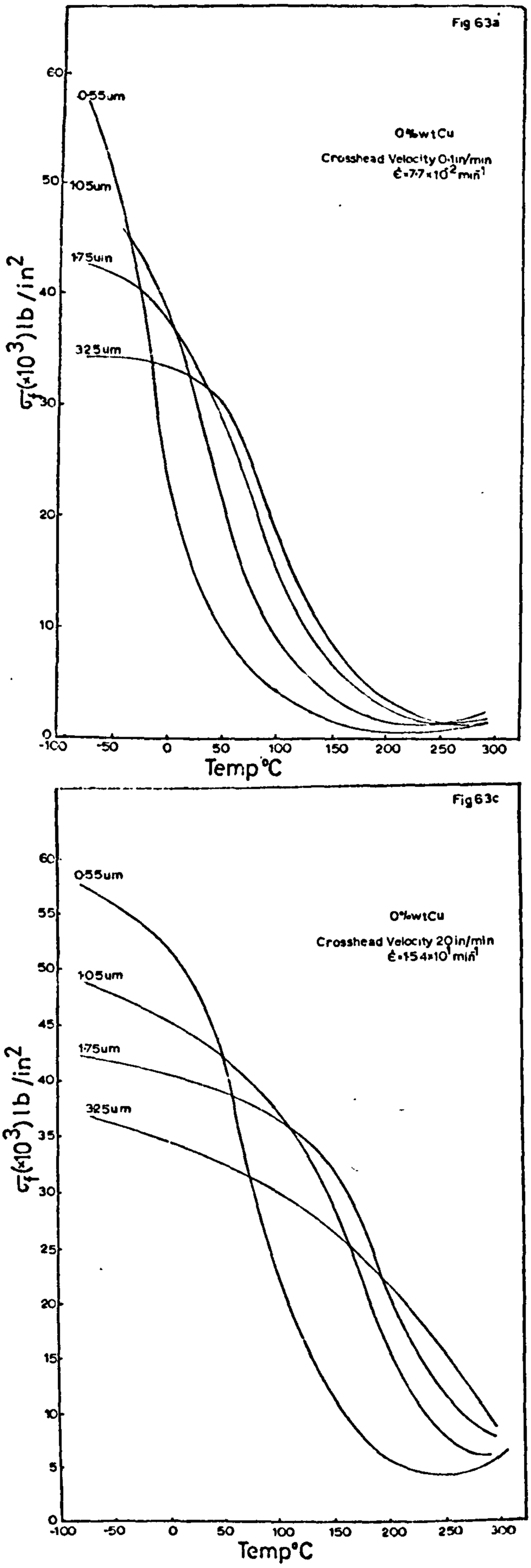

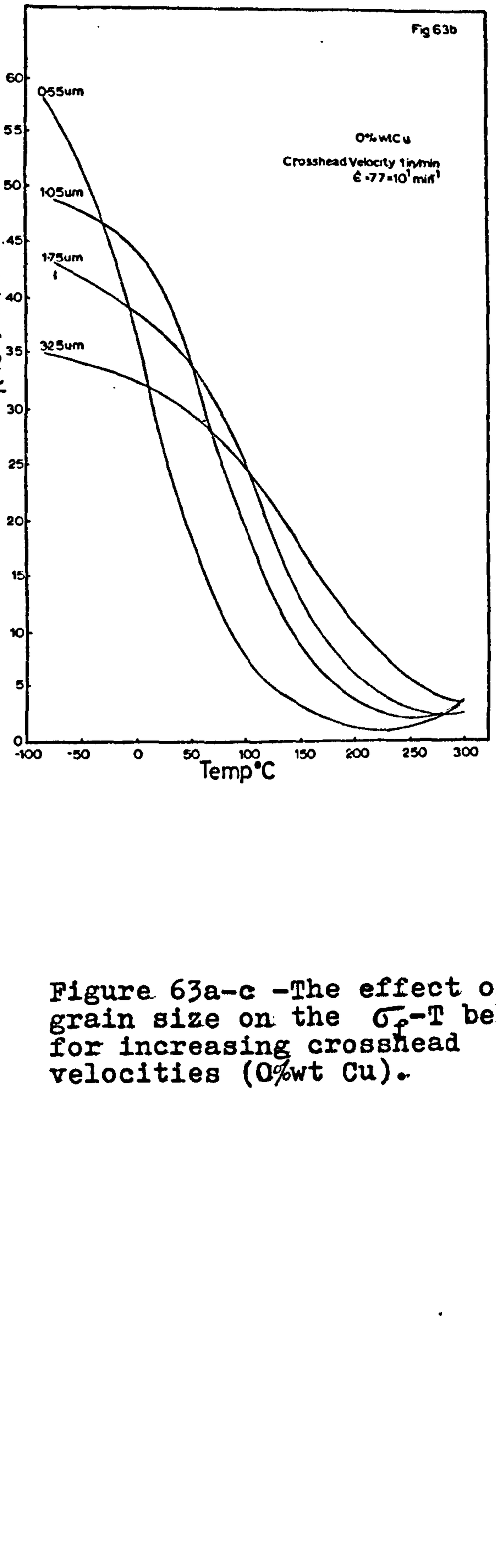

Figure 63a-c -The effect of grain size on the σ_f-T behaviour for increasing crosshead velocities (0%wt Cu).

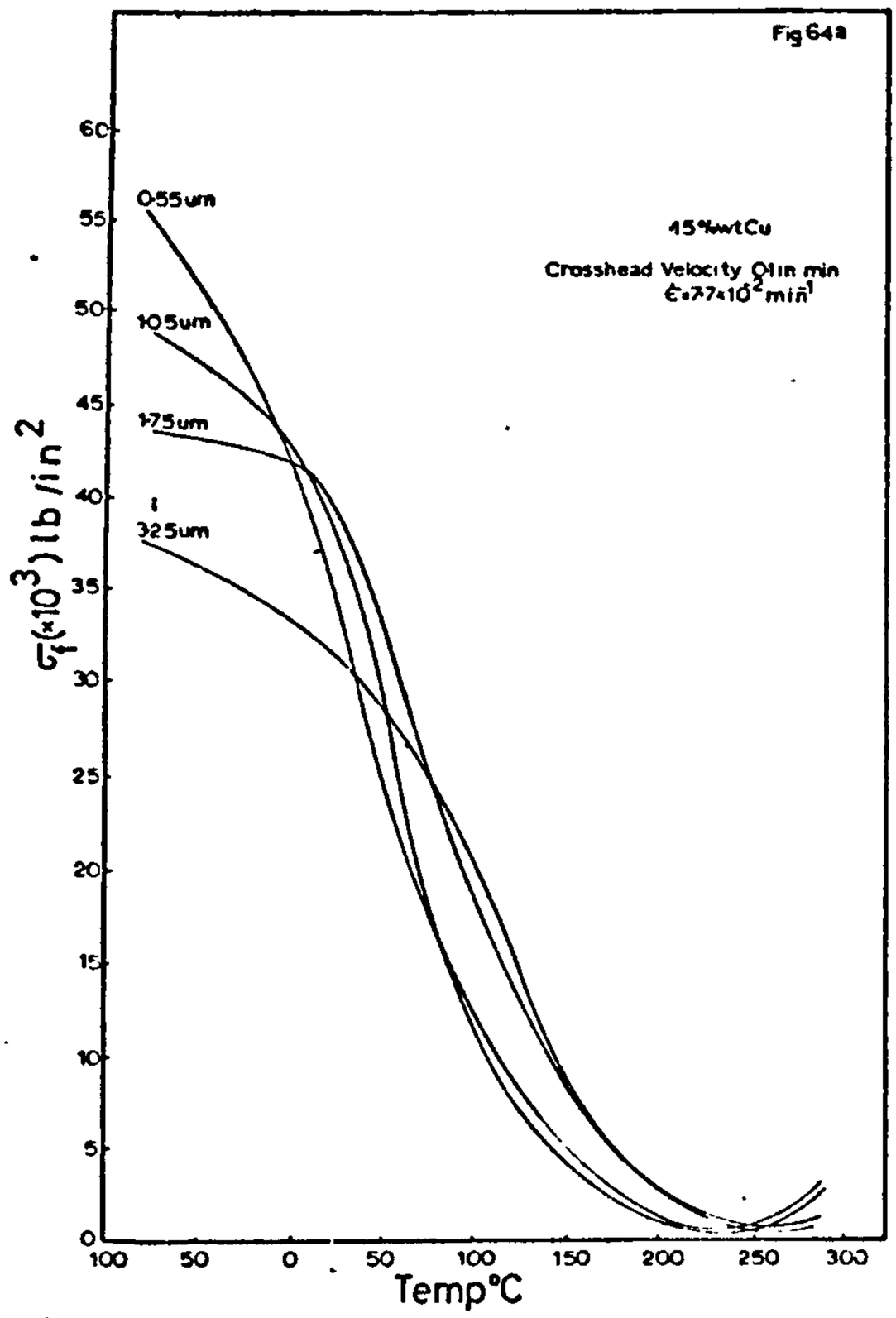

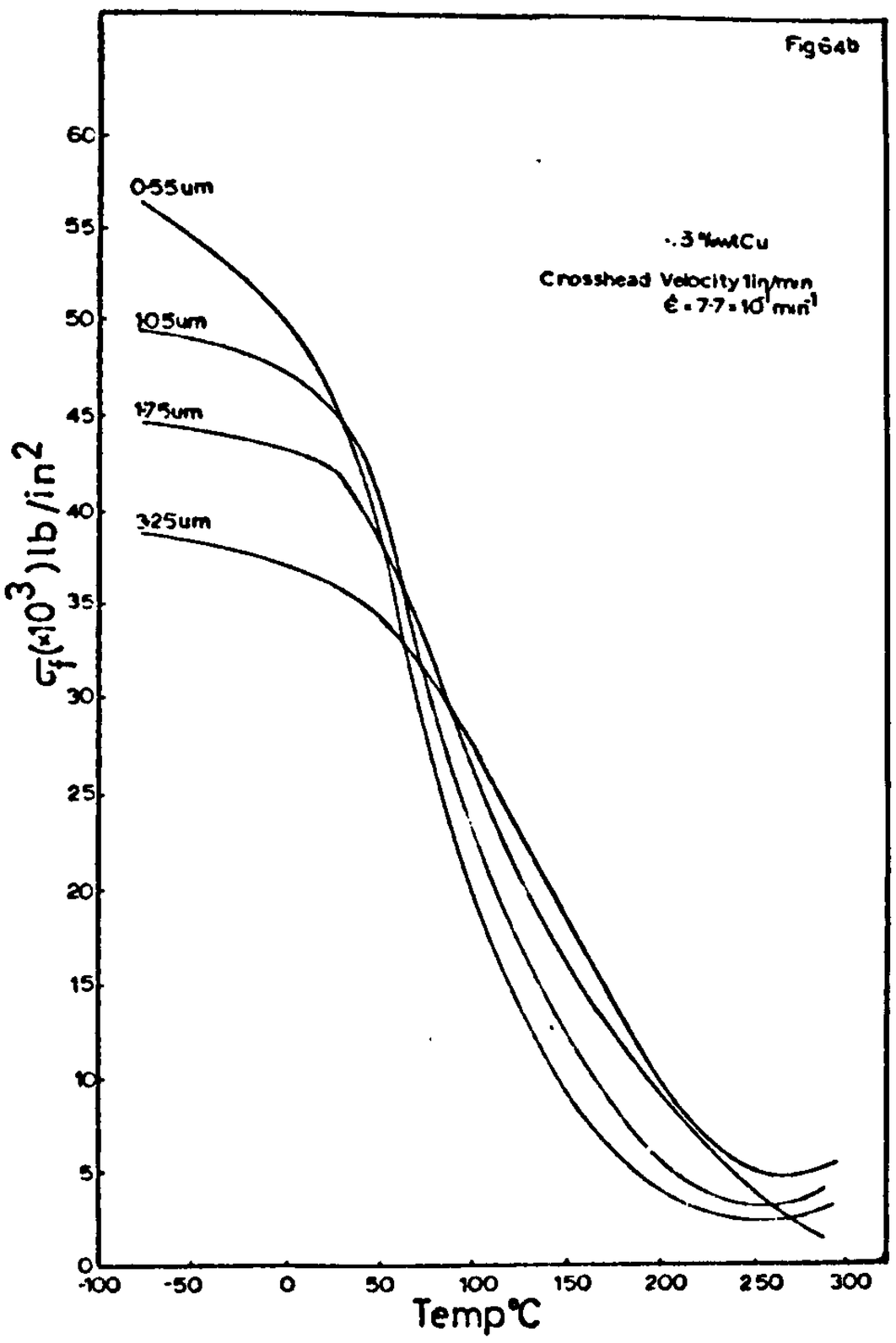

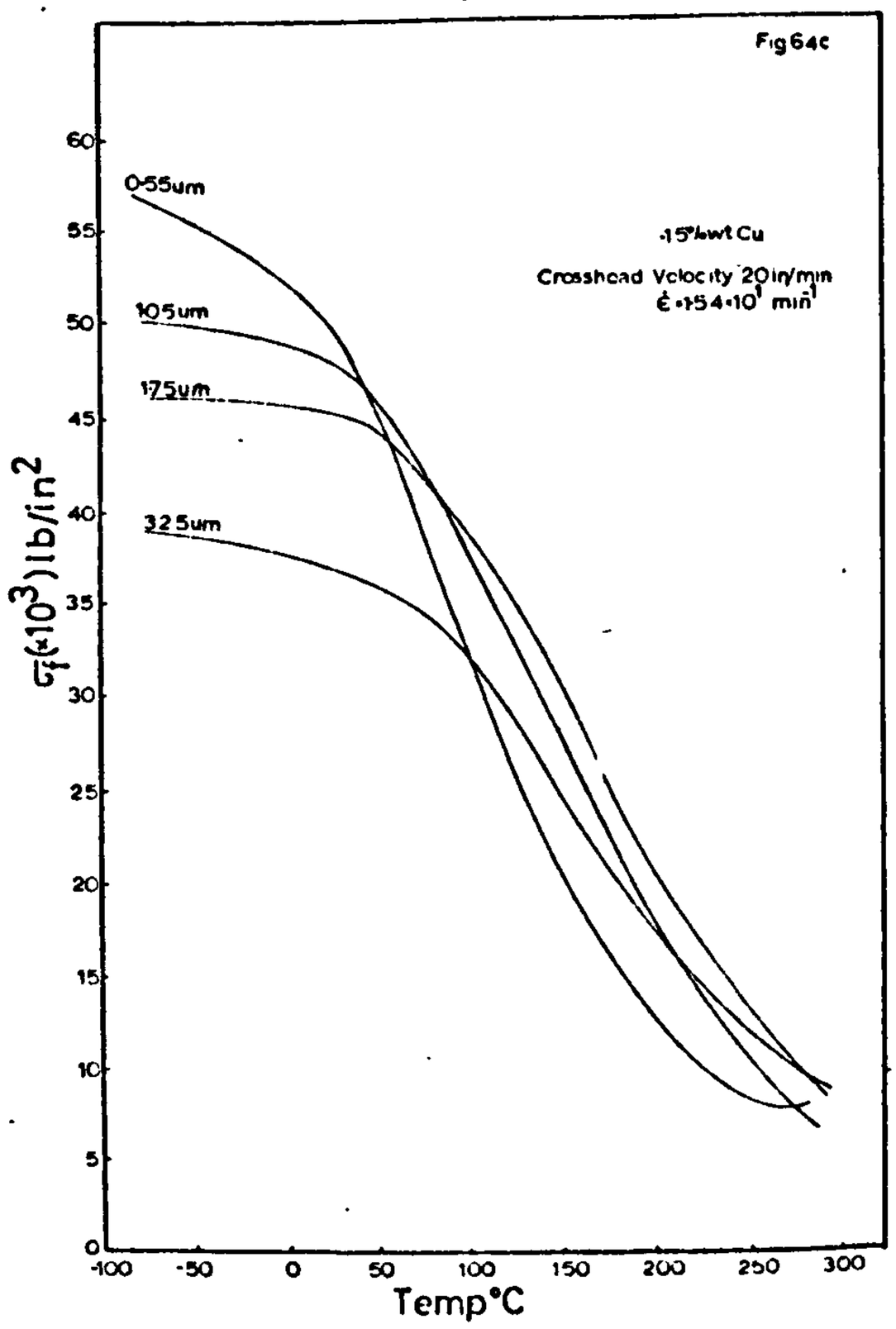

Figure64a-c - The effect of grain size on the σ_f-T behaviour for increasing crosshead velocities(0.15%wt.Cu).

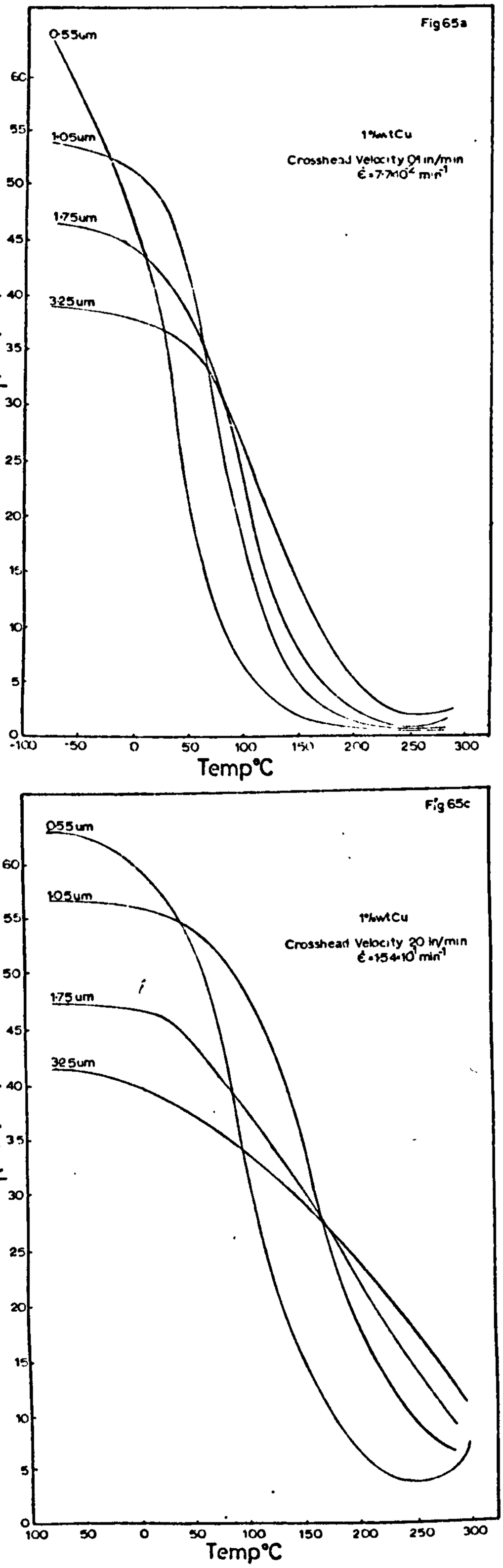

Figure 65a-c - The effect of grain size on the σ_f-T behaviour for increasing velocities (1%wt Cu).

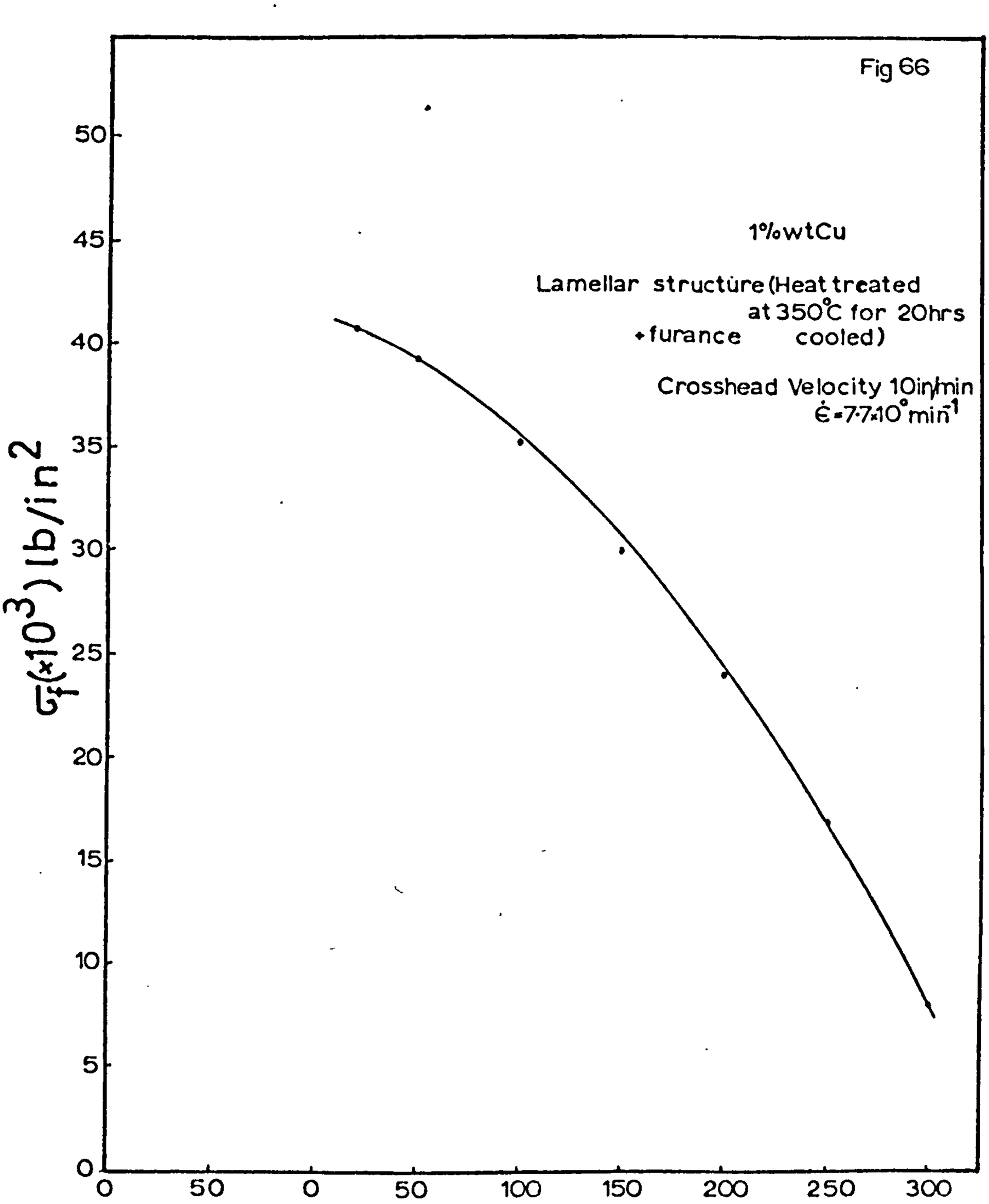

Figure 66 - The σ_f-T behaviour of a lamellar structure alloy.

Fig 67

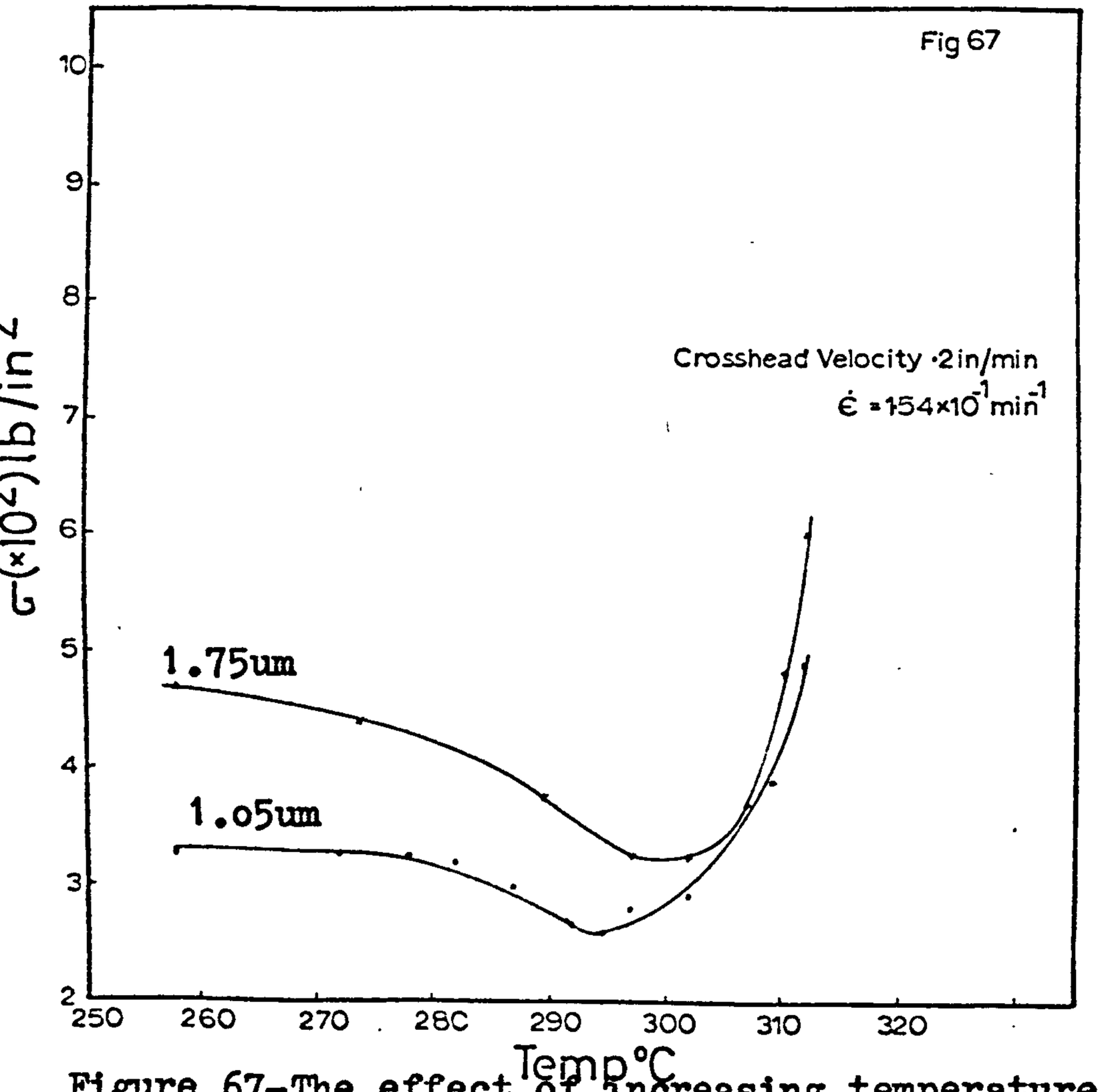

Figure 67-The effect of increasing temperature on the stress during a single tensile test of an equiaxed structure alloy.

Fig 68

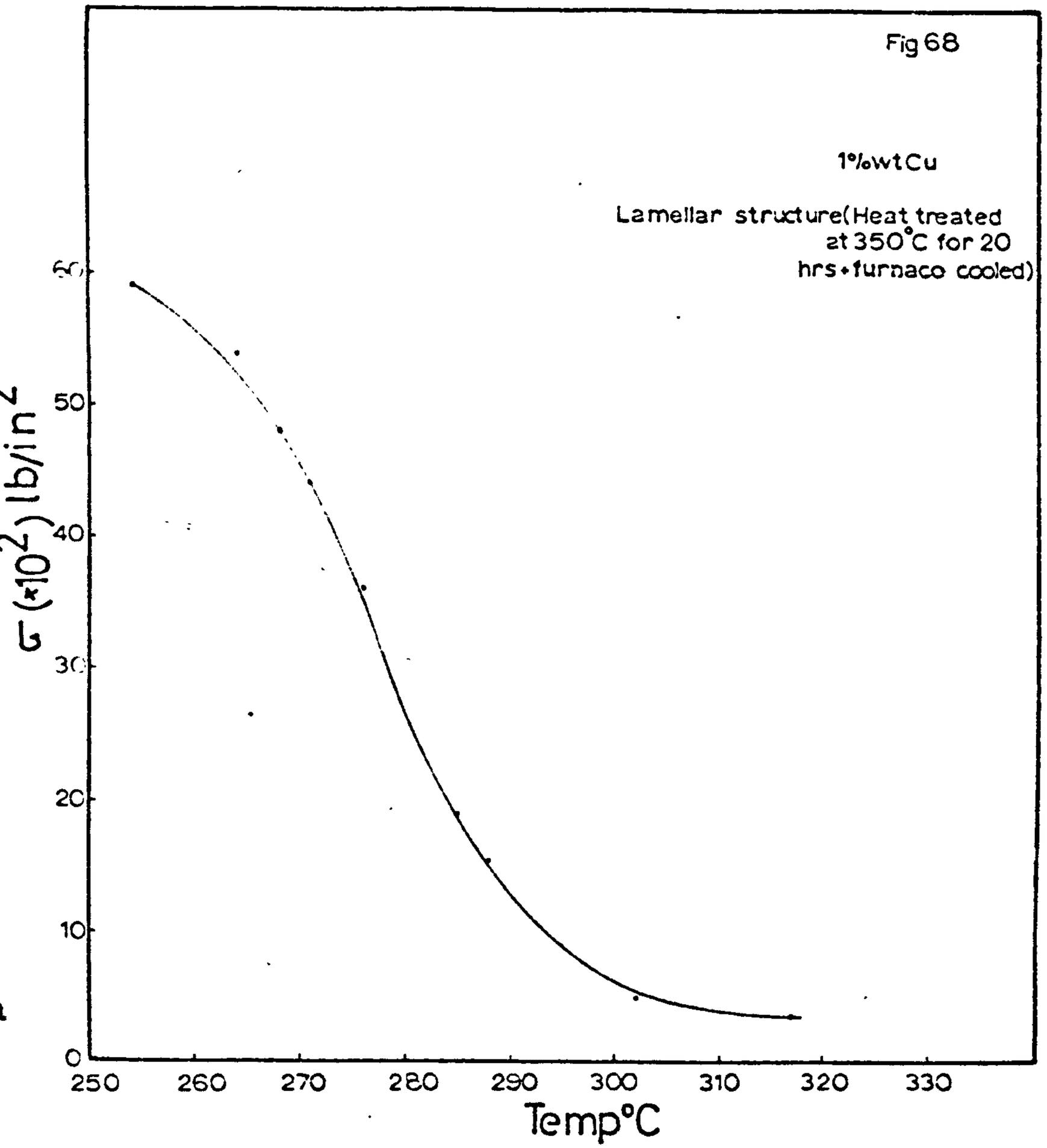

Figure 68-The effect of increasing temperature on stress during a single tensile test of an lamellar structure.

Figure 69- The effect of temperature on the m vs $\dot{\epsilon}$ relationship with increasing grain size (0%wt Cu).

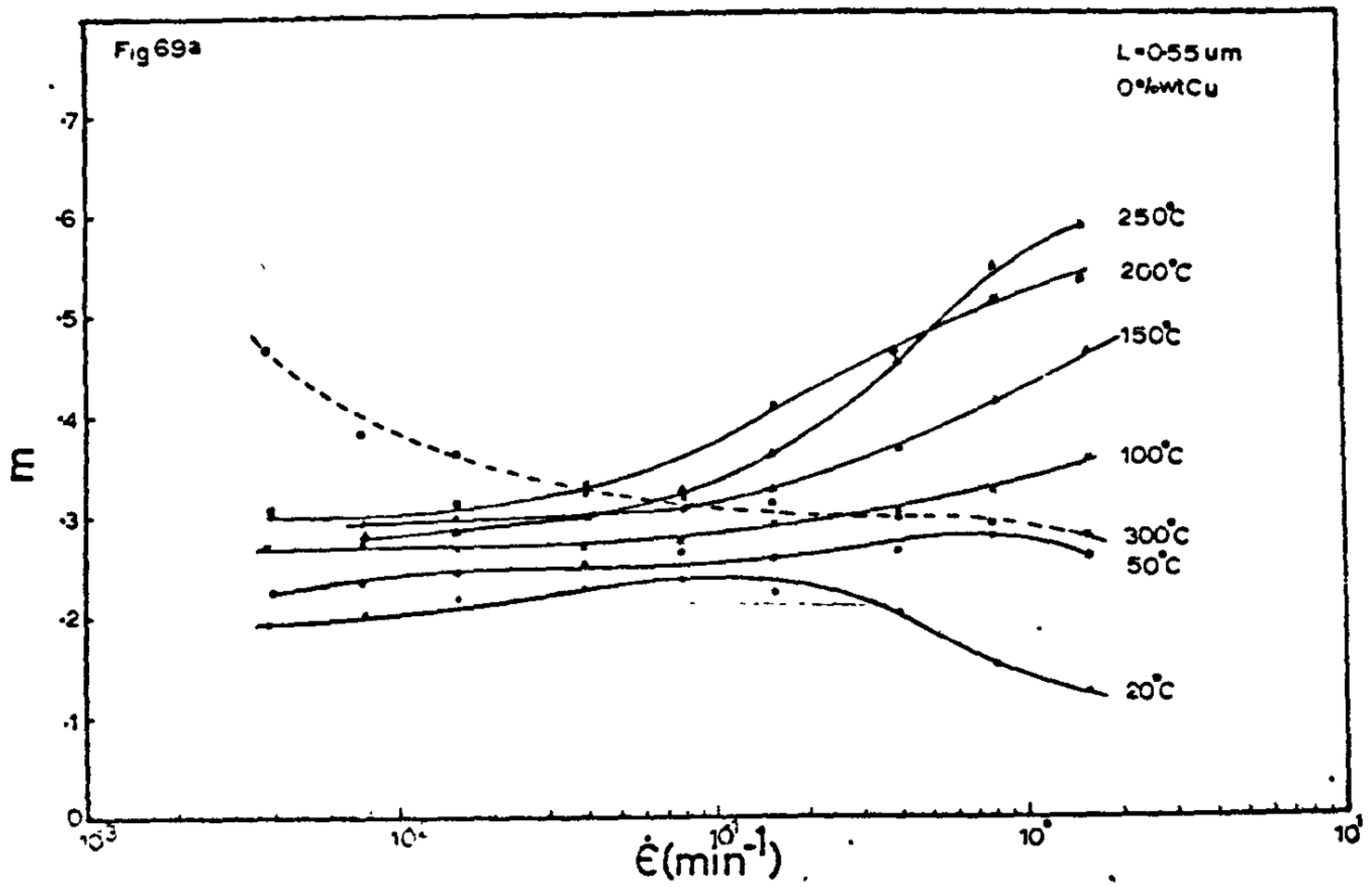
Fig 69a
L=0·55 um
0%wtCu
250°C
200°C
150°C
100°C
300°C
50°C
20°C
m
Ė(min⁻¹)

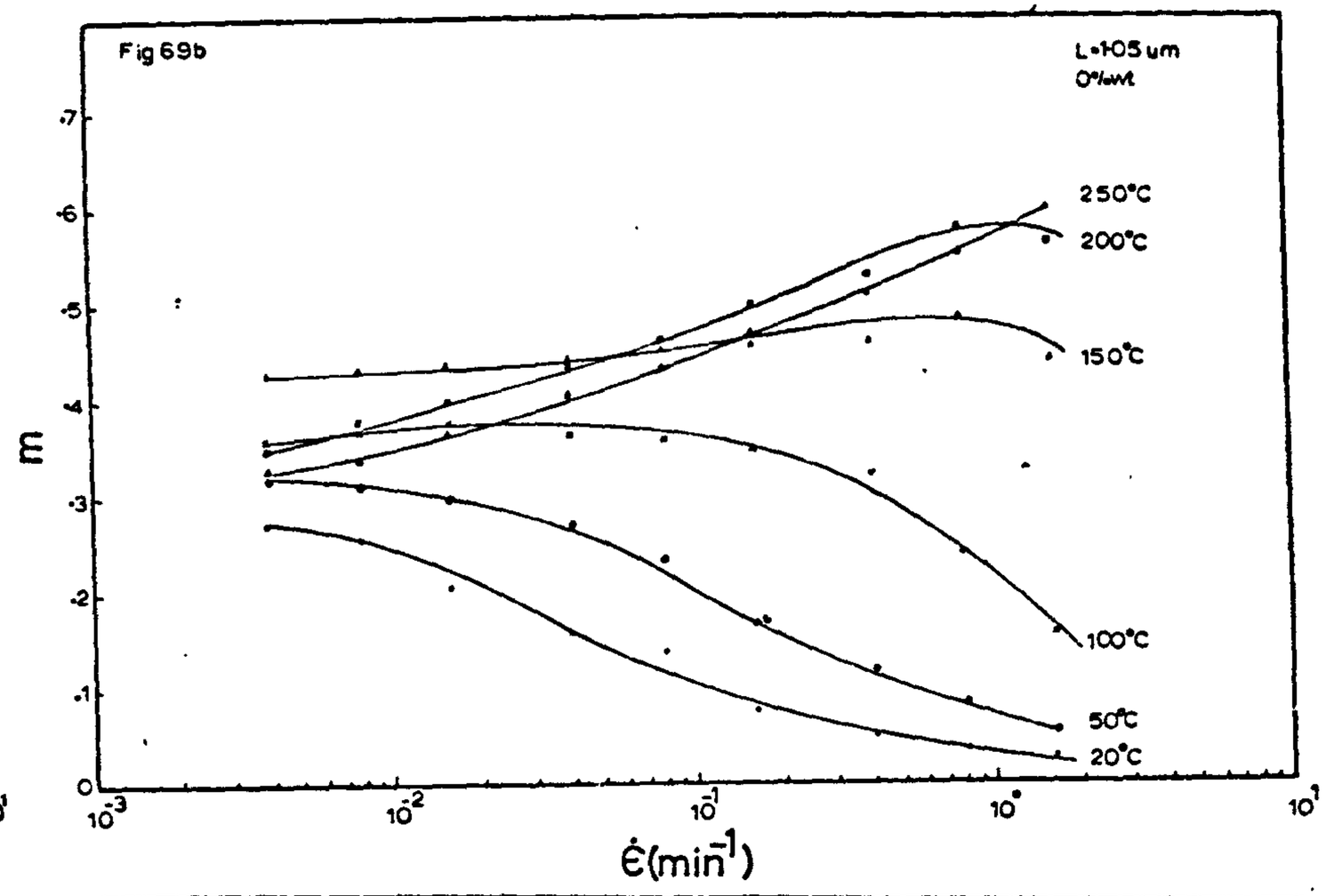
Fig 69b
L=1·05 um
0%wt
250°C
200°C
150°C
100°C
50°C
20°C
m
Ė(min⁻¹)

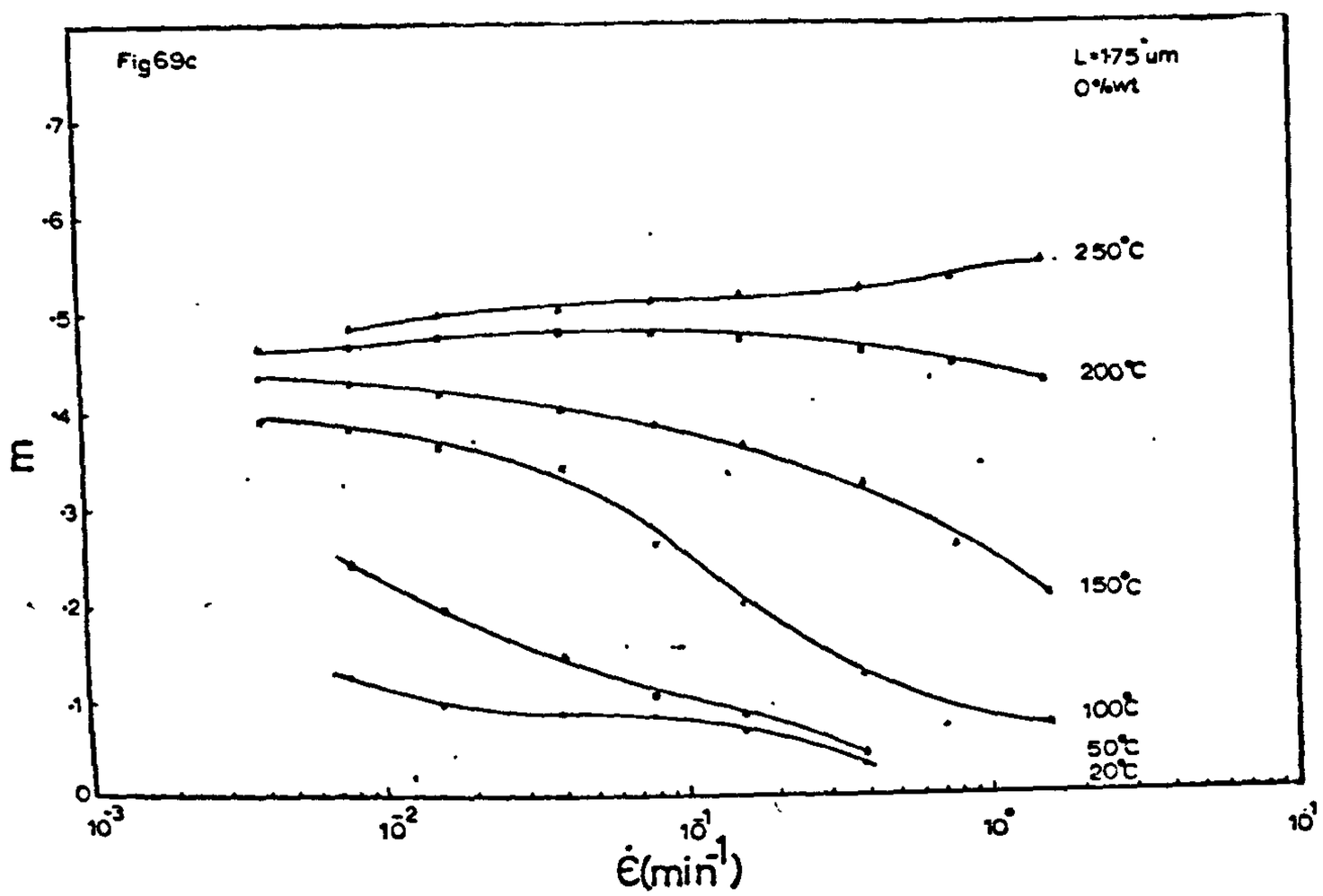
Fig 69c
L=1·75 um
0%wt
250°C
200°C
150°C
100°C
50°C
20°C
m
Ė(min⁻¹)

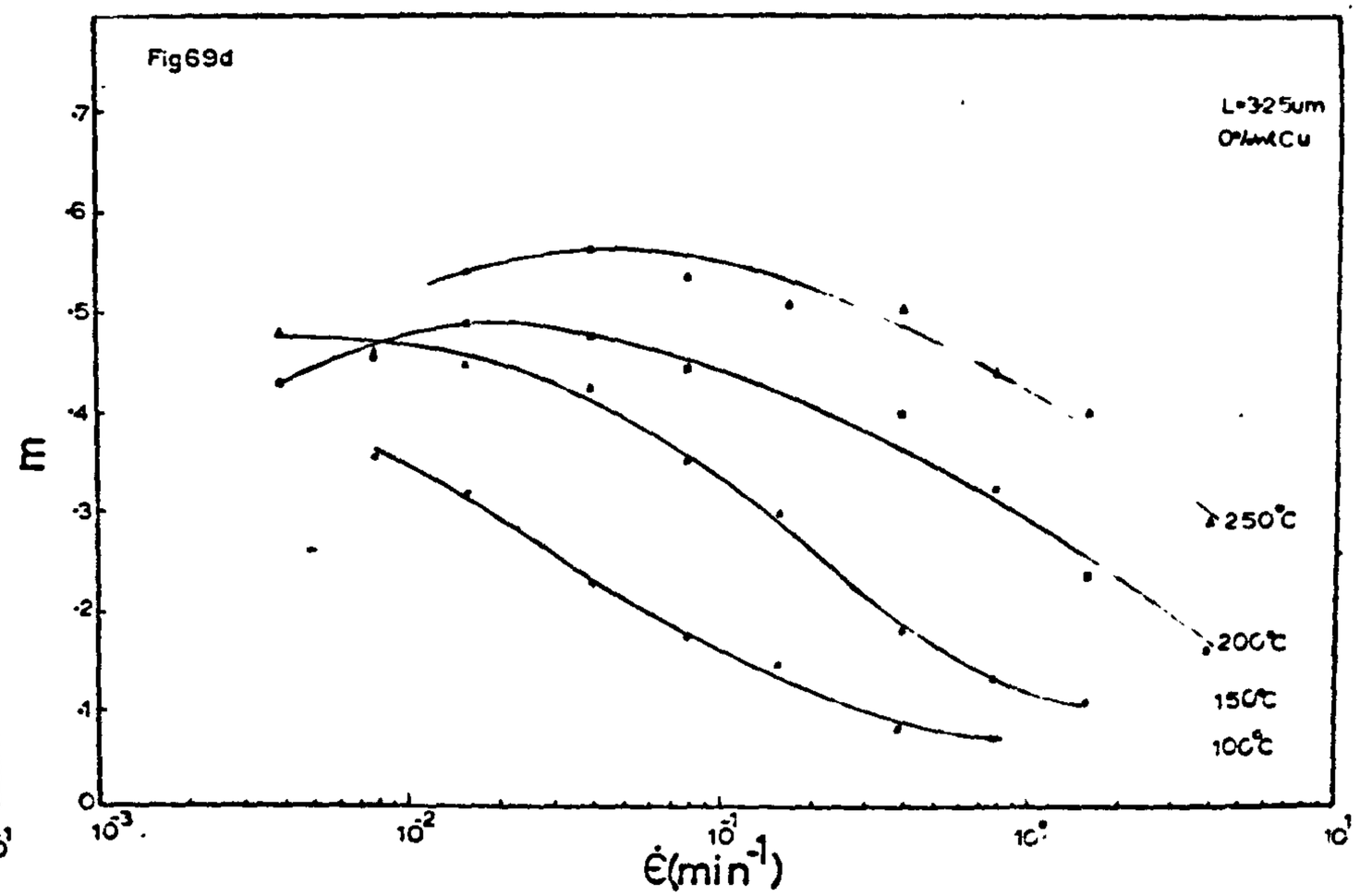
Fig 69d
L=3·25um
0%wtCu
250°C
200°C
150°C
100°C
m
Ė(min⁻¹)

Figure 70-The effect of temperature on the m vs $\dot{\epsilon}$ relationship with increasing grain size (0.15%wt Cu).

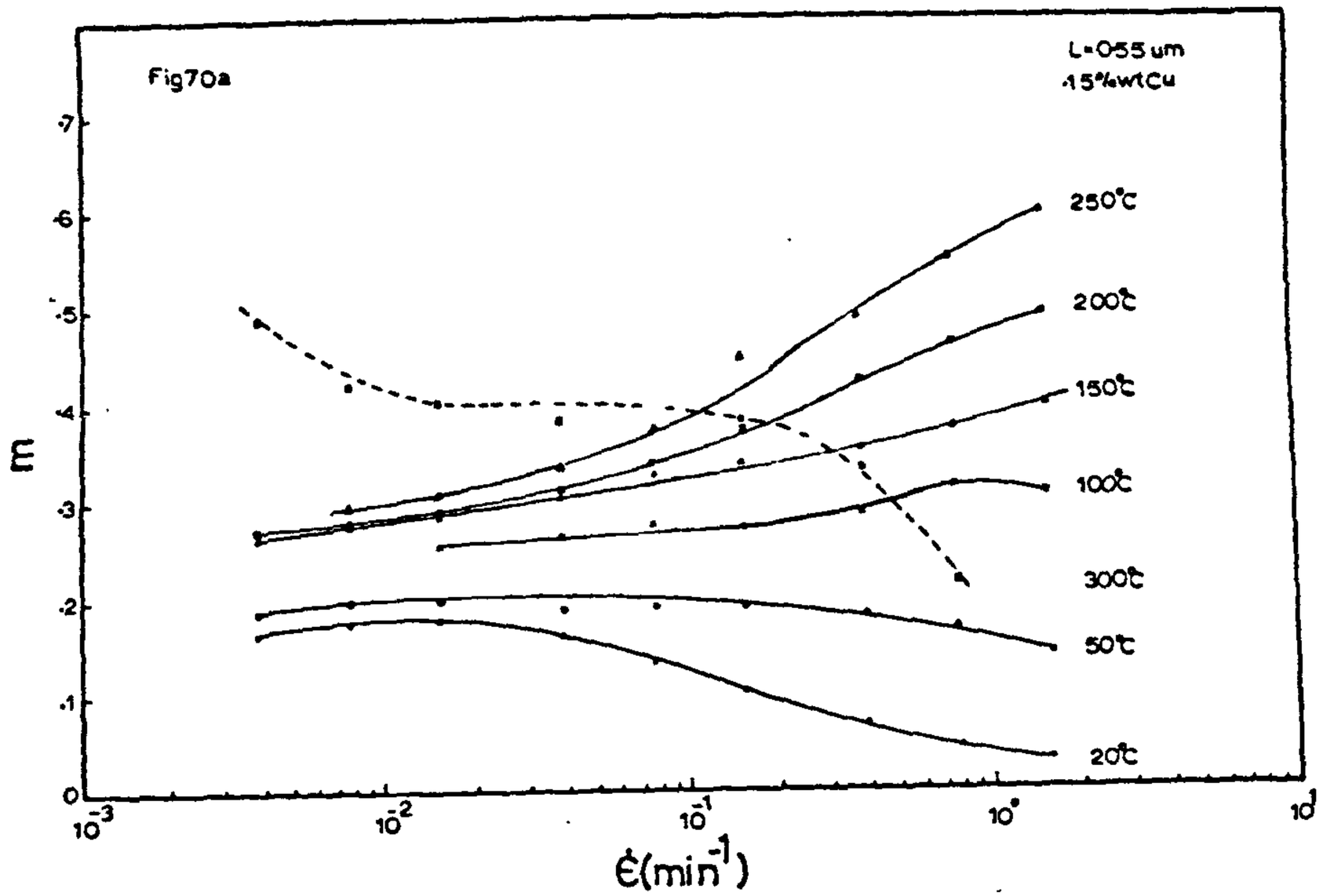
Fig70a
L=055um
15%wtCu
250°c
200°c
150°c
100°c
300°c
50°c
20°c
m
$\dot{\epsilon}(min^{-1})$

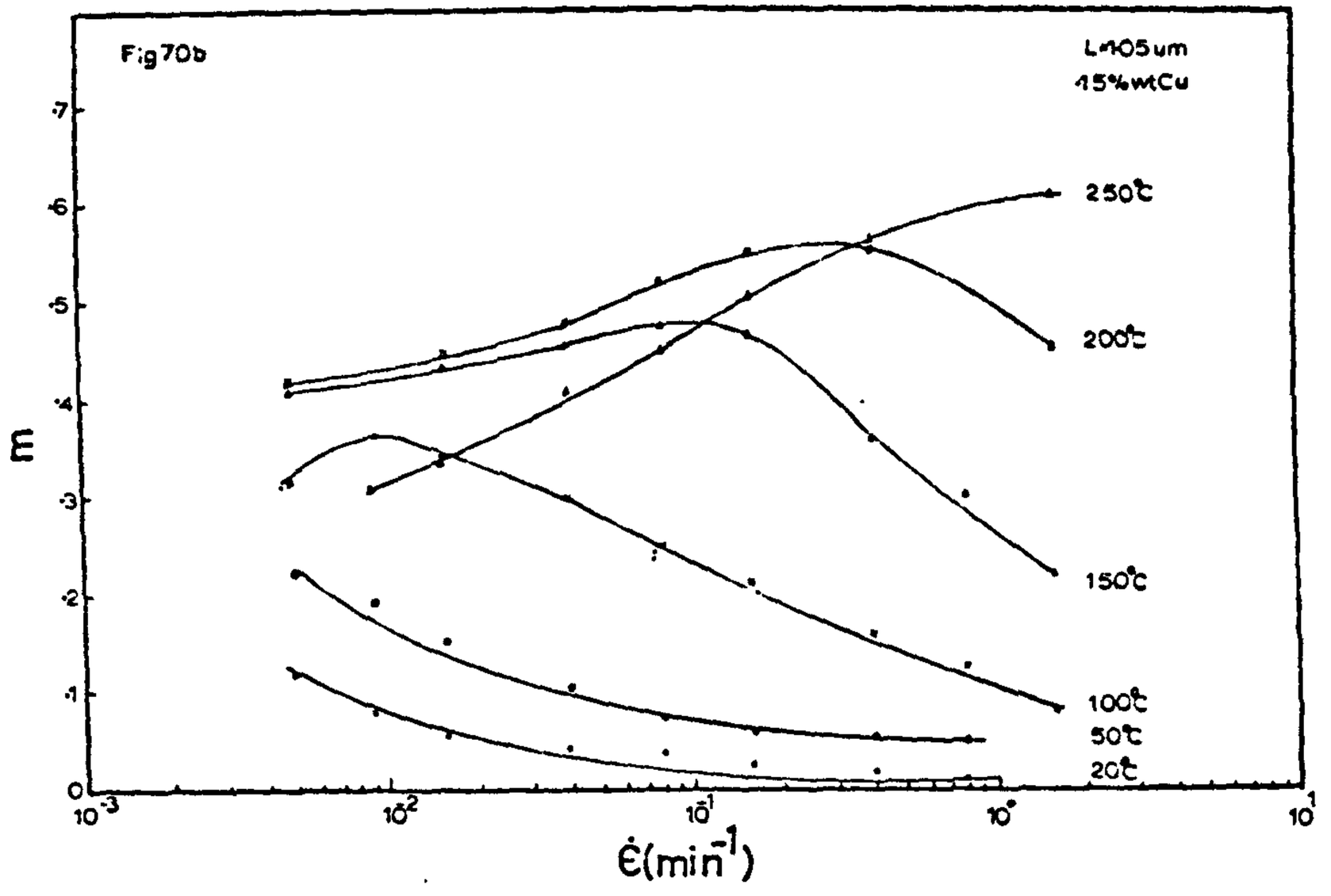
Fig70b
L=105um
15%wtCu
250°c
200°c
150°c
100°c
50°c
20°c
m
$\dot{\epsilon}(min^{-1})$

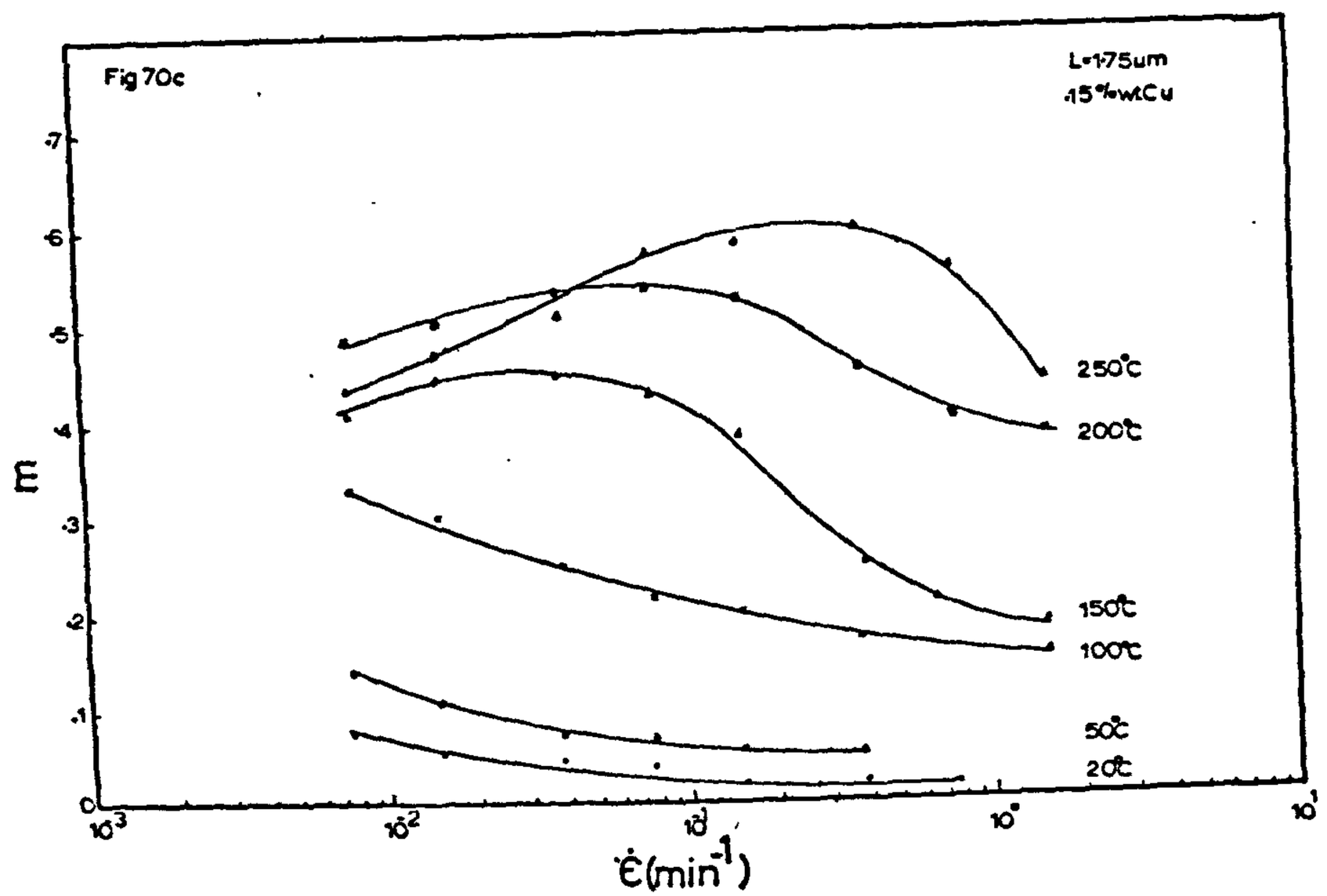
Fig70c
L=175um
15%wtCu
250°c
200°c
150°c
100°c
50°c
20°c
m
$\dot{\epsilon}(min^{-1})$

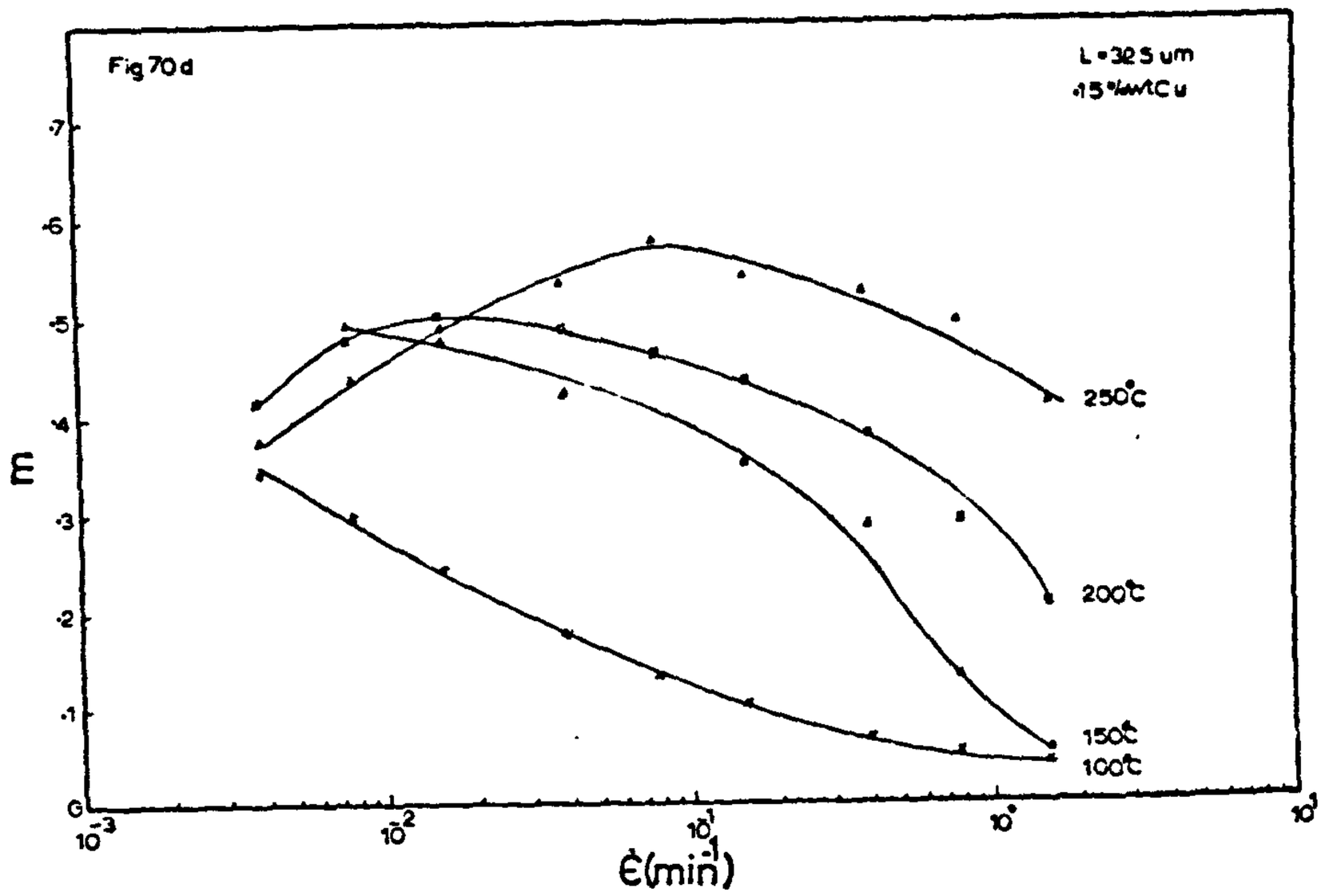
Fig70d
L=325um
15%wtCu
250°c
200°c
150°c
100°c
m
$\dot{\epsilon}(min^{-1})$

rigure 71-The effect of temperature on the m vs $\dot{\epsilon}$ relationship with increasing grain size (1%wt Cu).

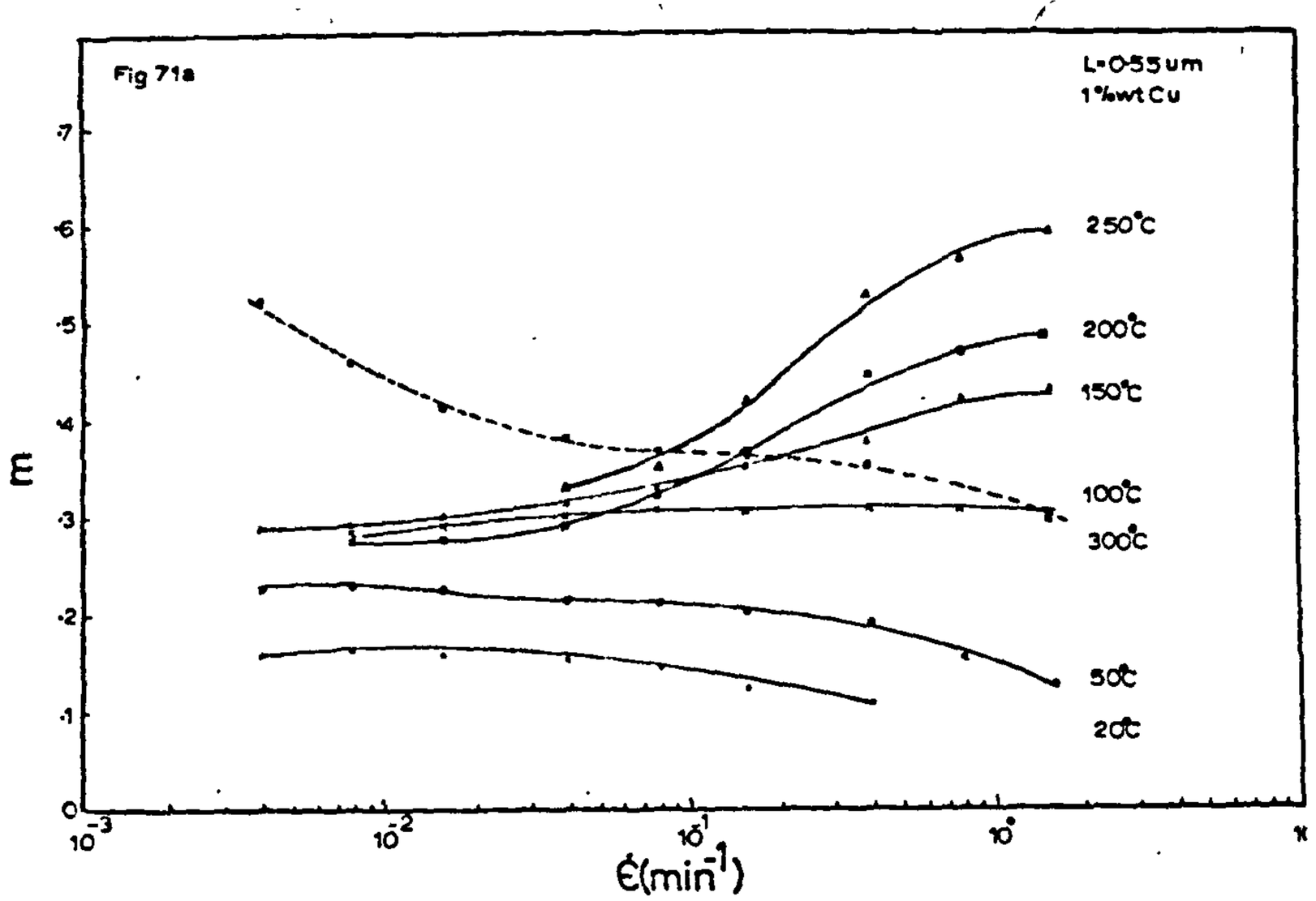
Fig 71a
L=0·55um
1%wtCu
250°c
200°c
150°c
100°c
300°c
50°c
20°c
m
Ė(min⁻¹)

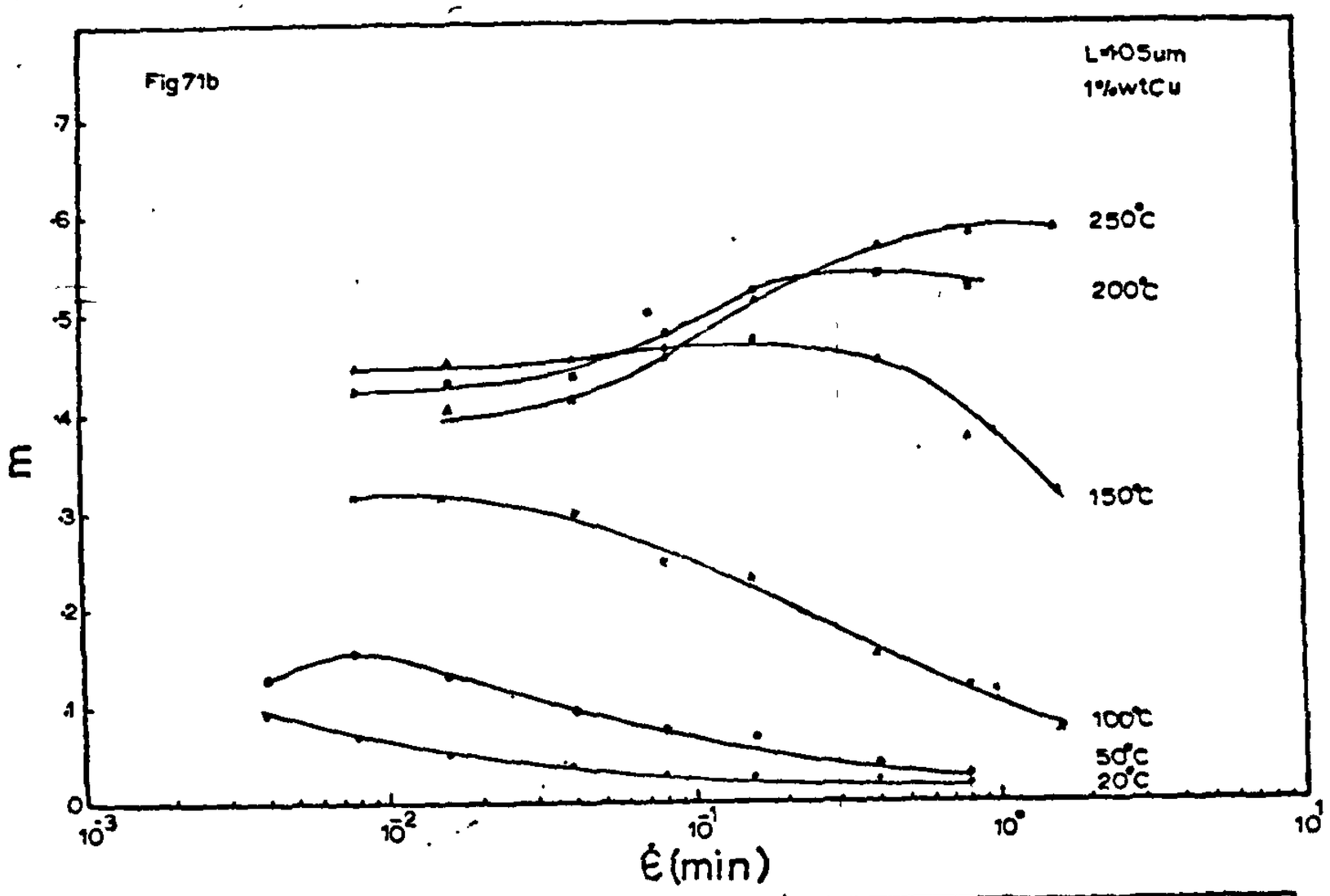
Fig 71b
L=1·05um
1%wtCu
250°c
200°c
150°c
100°c
50°c
20°c
m
Ė(min)

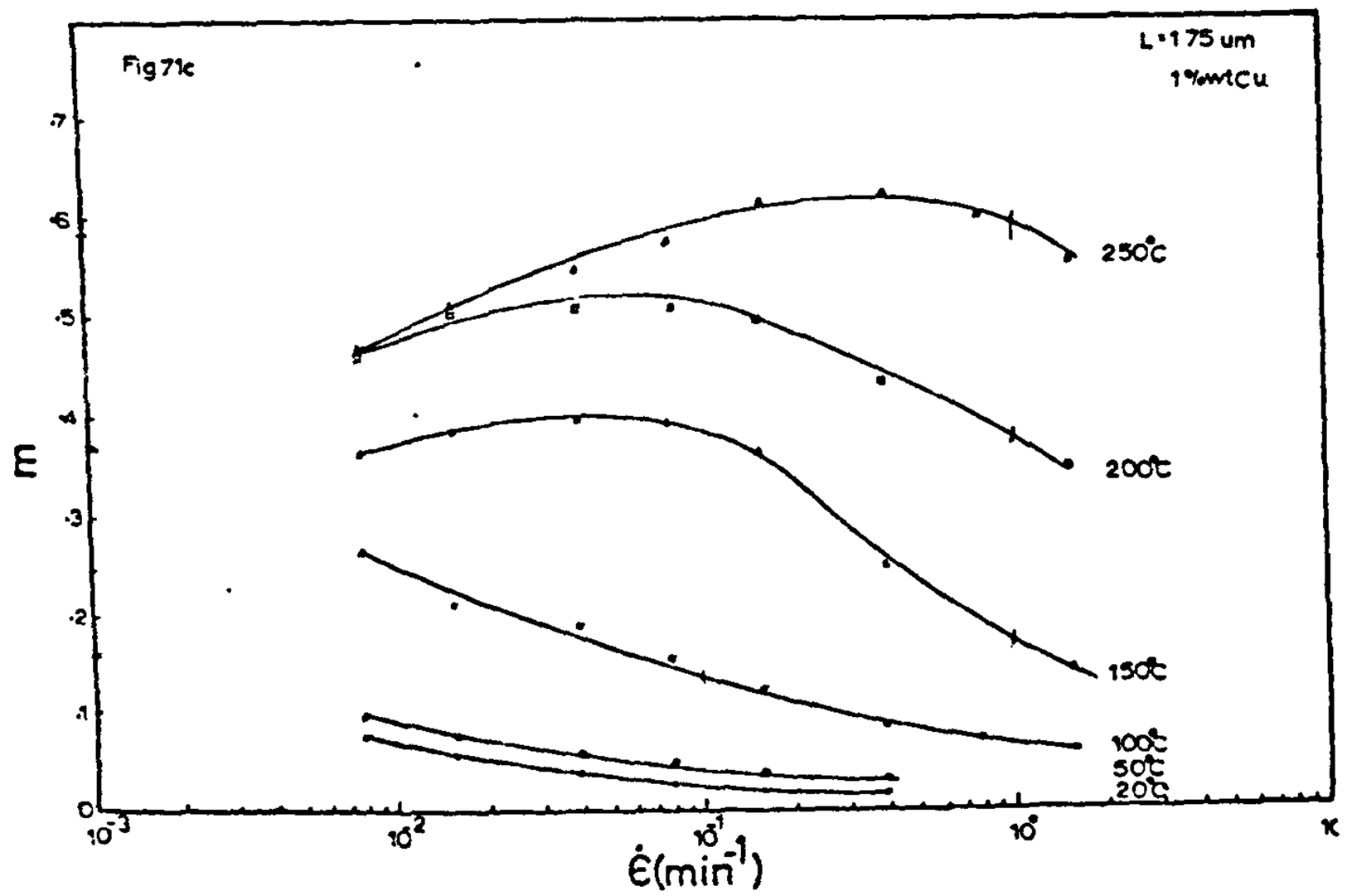
Fig 71c
L=1·75 um
1%wtCu
250°c
200°c
150°c
100°c
50°c
20°c
m
Ė(min⁻¹)

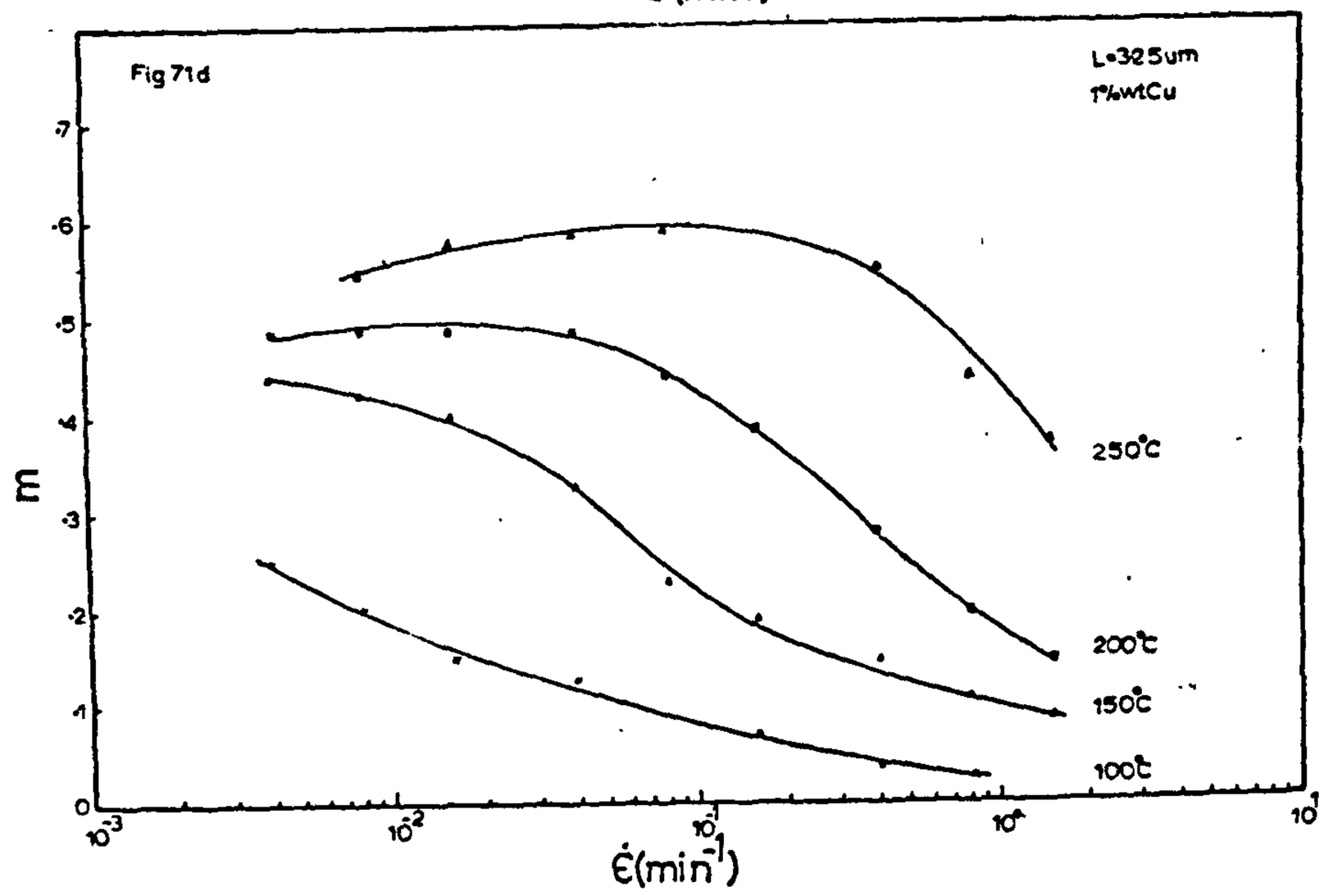
Fig 71d
L=3·25um
1%wtCu
250°c
200°c
150°c
100°c
m
Ė(min⁻¹)

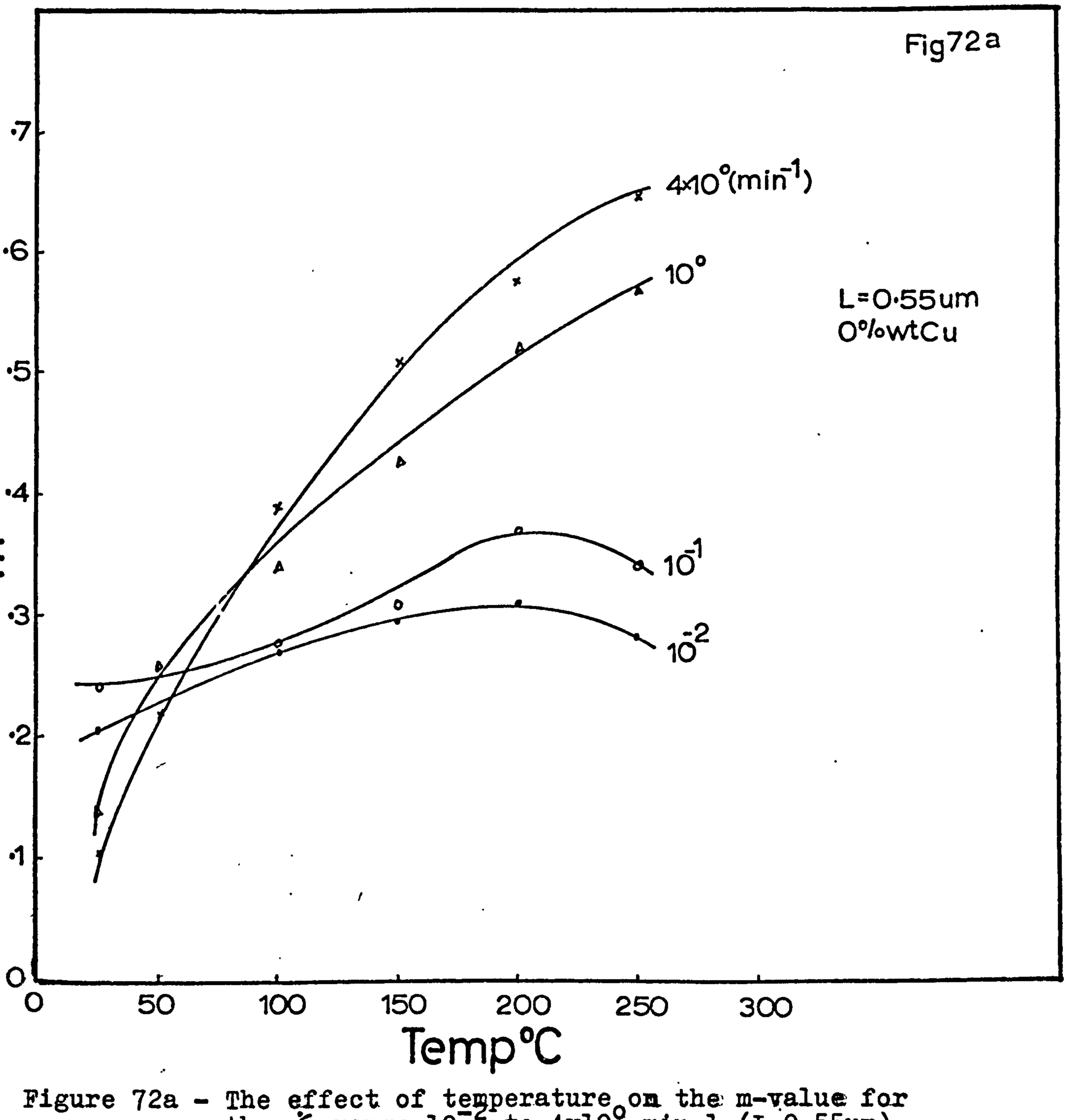

Figure 72a - The effect of temperature on the m-value for the $\dot{\epsilon}$-range 10^{-2} to $4x10^{0}$ min-1 (L=0.55um).

Fig 72b

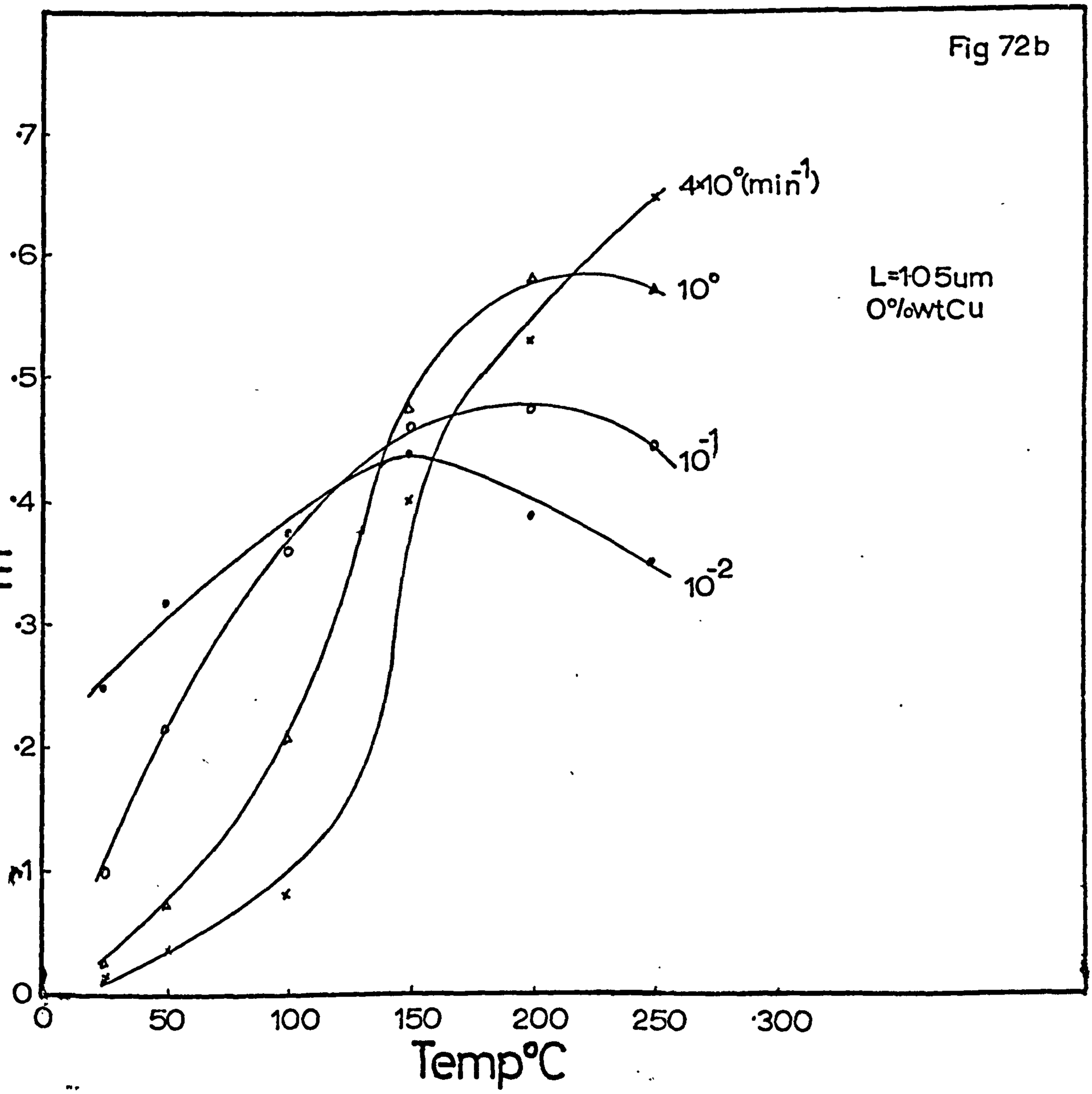

Figure 72b - The effect of temperature on the m-value for the $\dot{\epsilon}$-range 10^{-2} to $4x10^{o}$ min^{-1} (L=1.05um).

Fig 72c

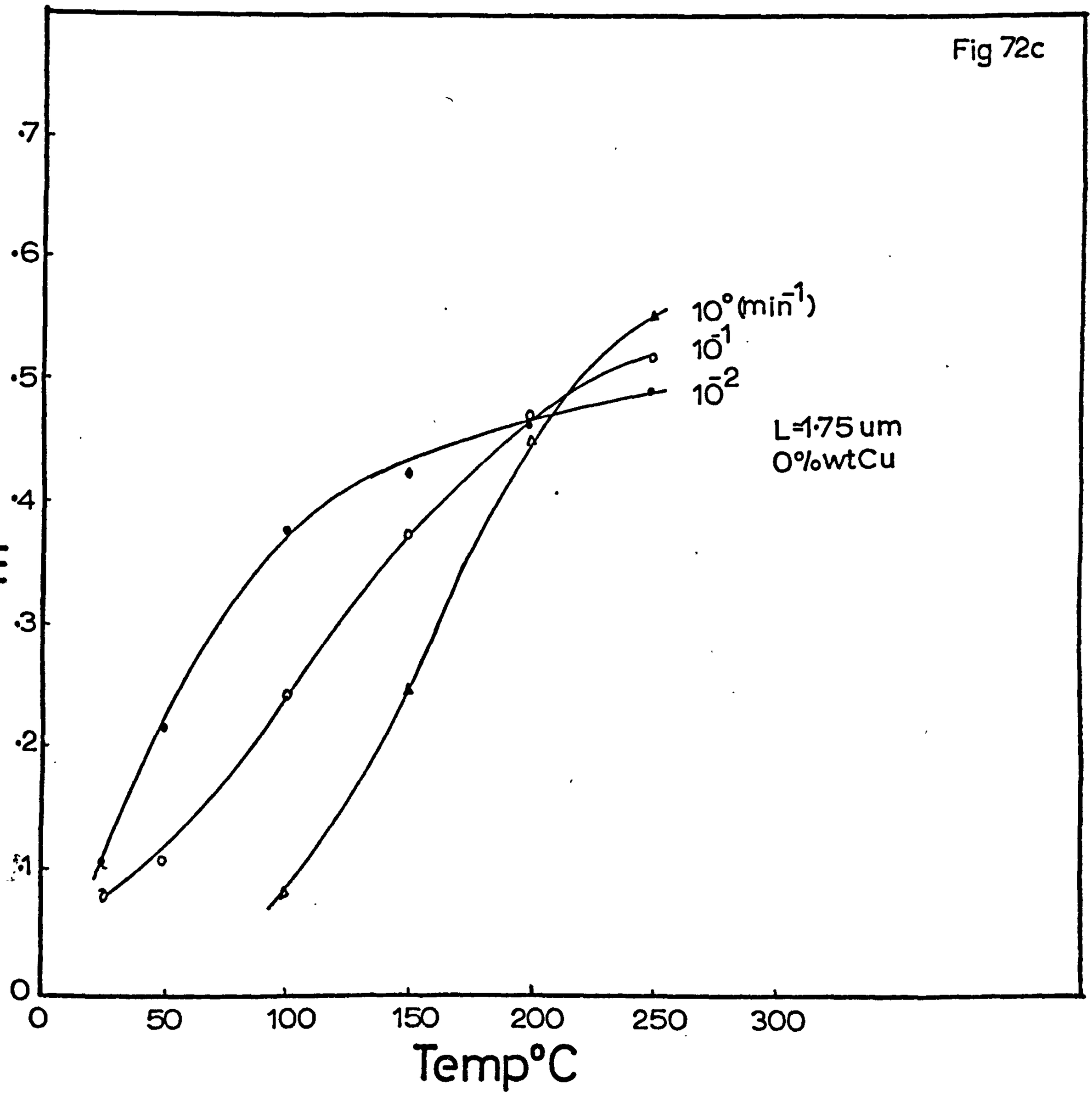

Figure 72c - The effect of temperature on the m-value for the $\dot{\epsilon}$-range 10^{-2} to 10^{0} min^{-1} (L=1.75um).

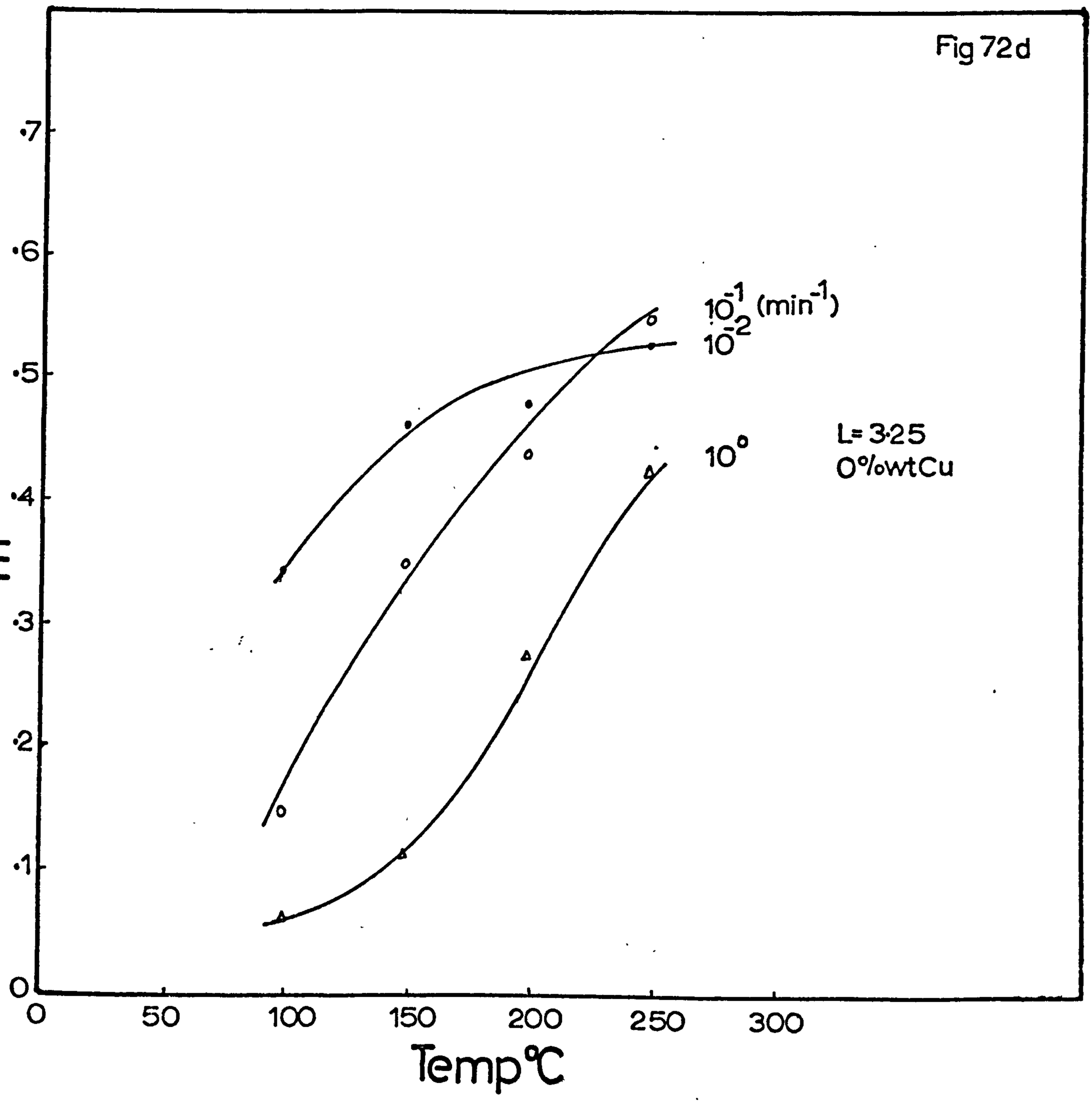

Figure 72d - The effect of temperature on the m-value for the $\dot{\epsilon}$-range 10^{-2} to 10^{0} min^{-1} (L=3.25um).

Figure 73-The effect of temperature on the m vs $\dot{\epsilon}$ relationship for a lamellar structure.

Fig 73

Lamellar structure
1%wtCu

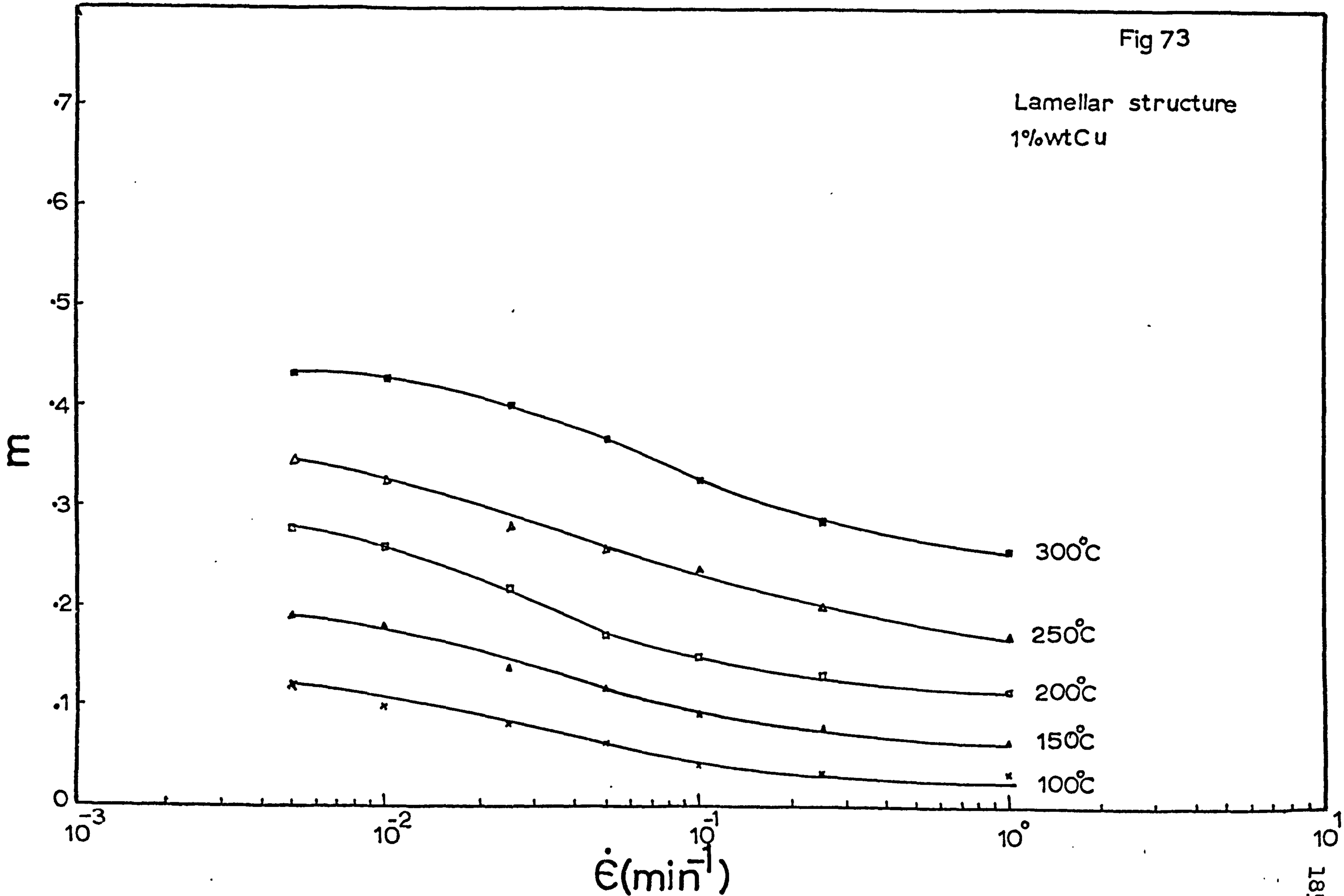

Figure 74-The effect of temperature on the σ_f vs $\dot{\epsilon}$ relationship with increasing grain size (0%wt Cu).

Fig 74a

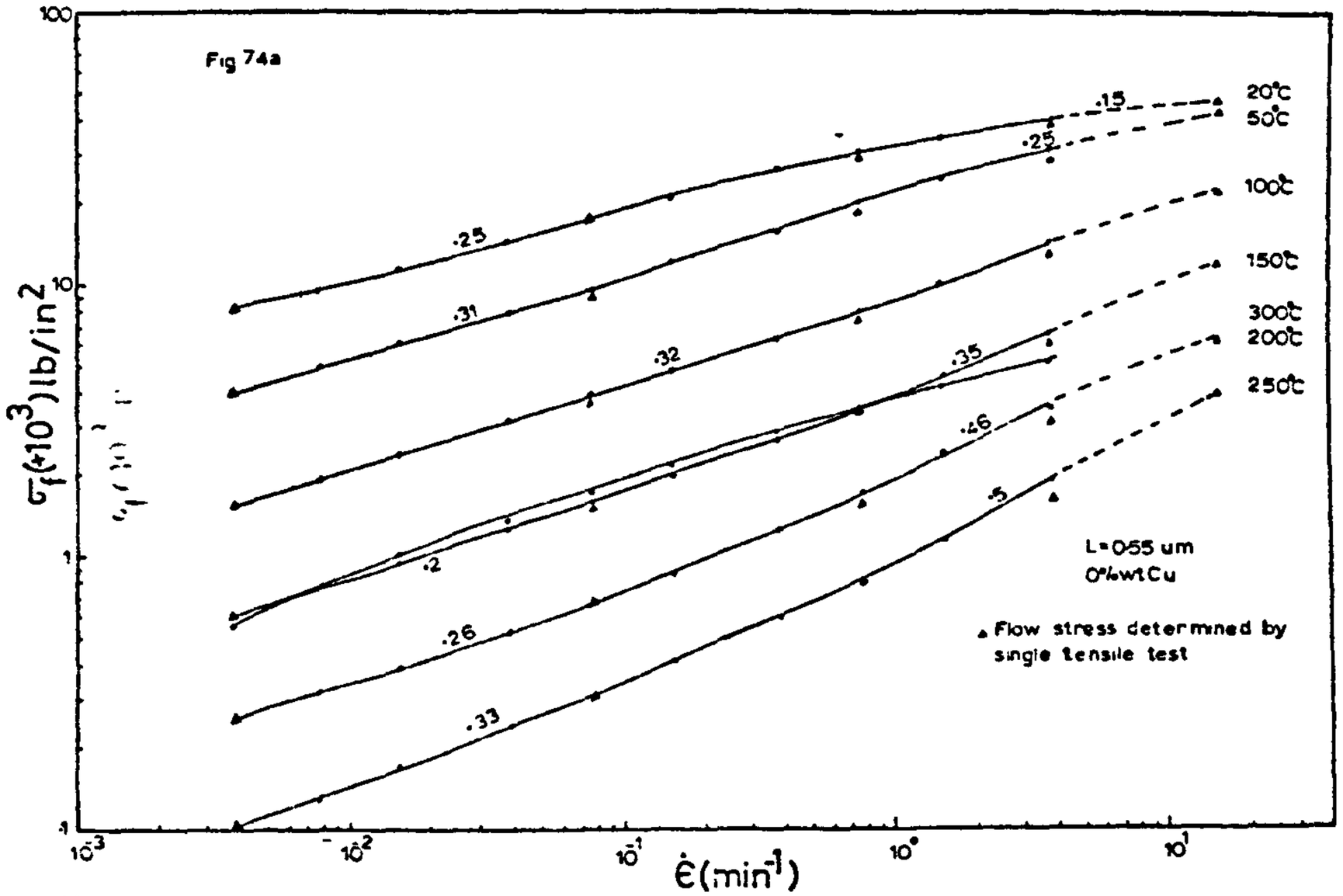

Fig 74b

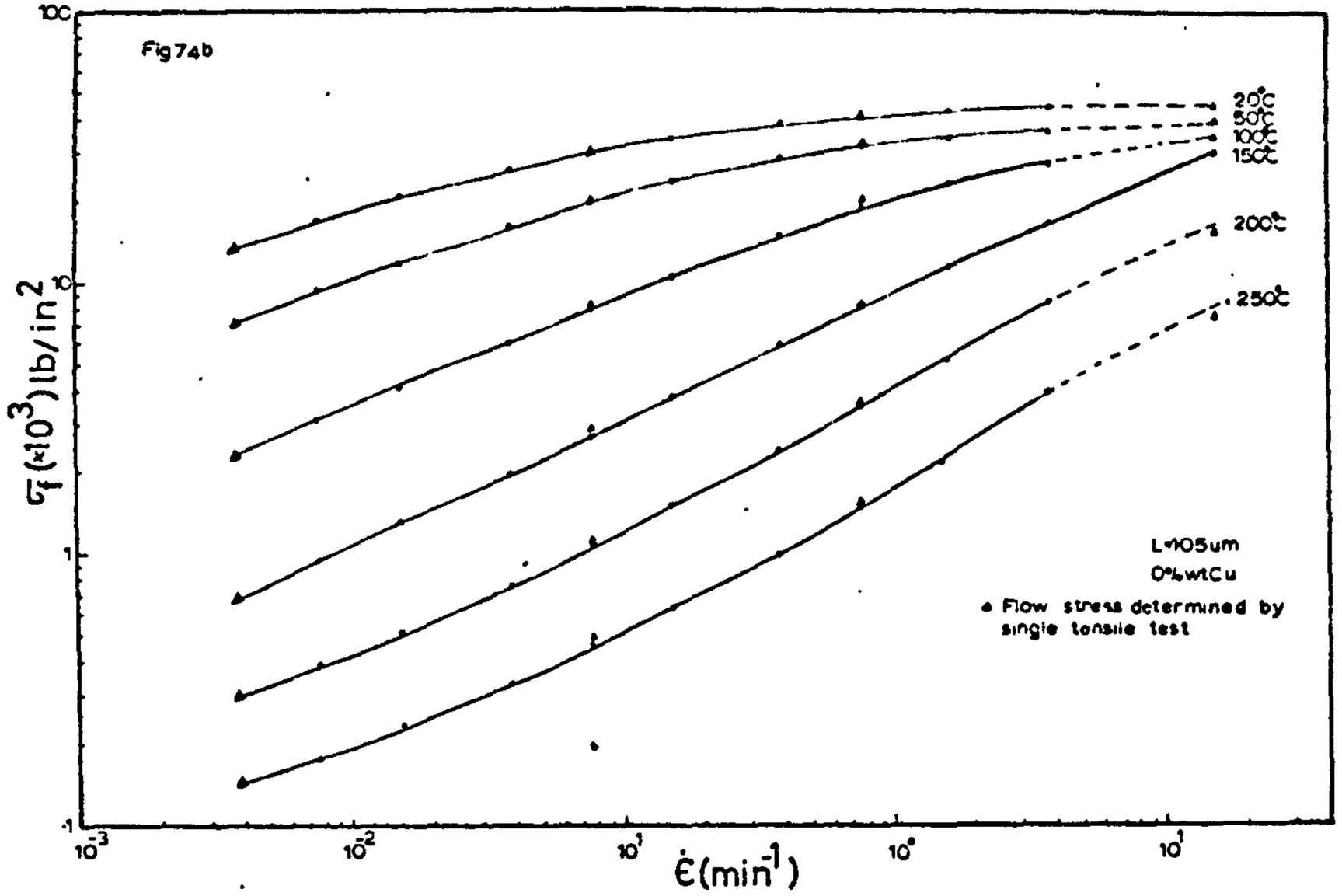

Fig 74c

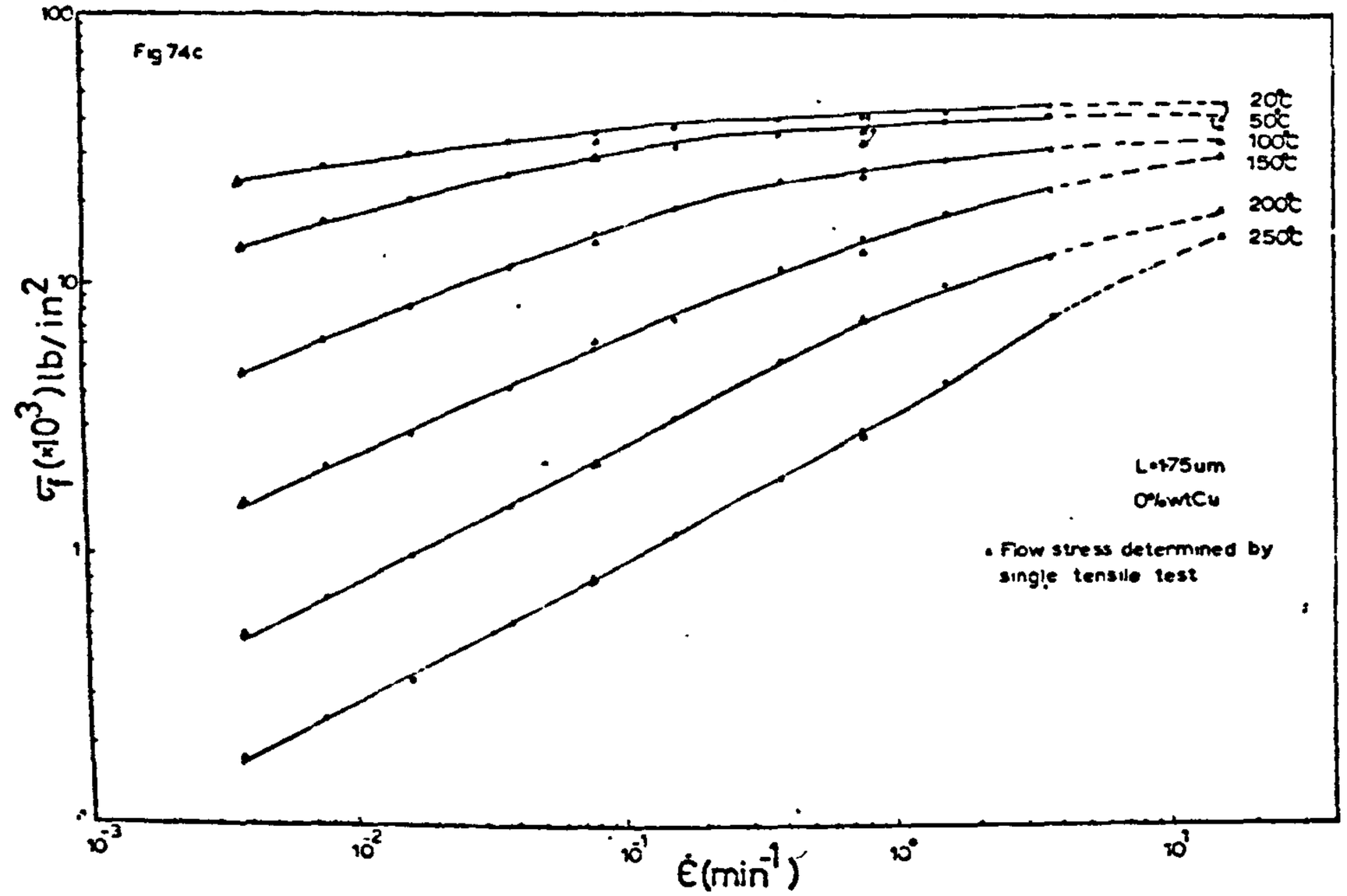

Fig 74d

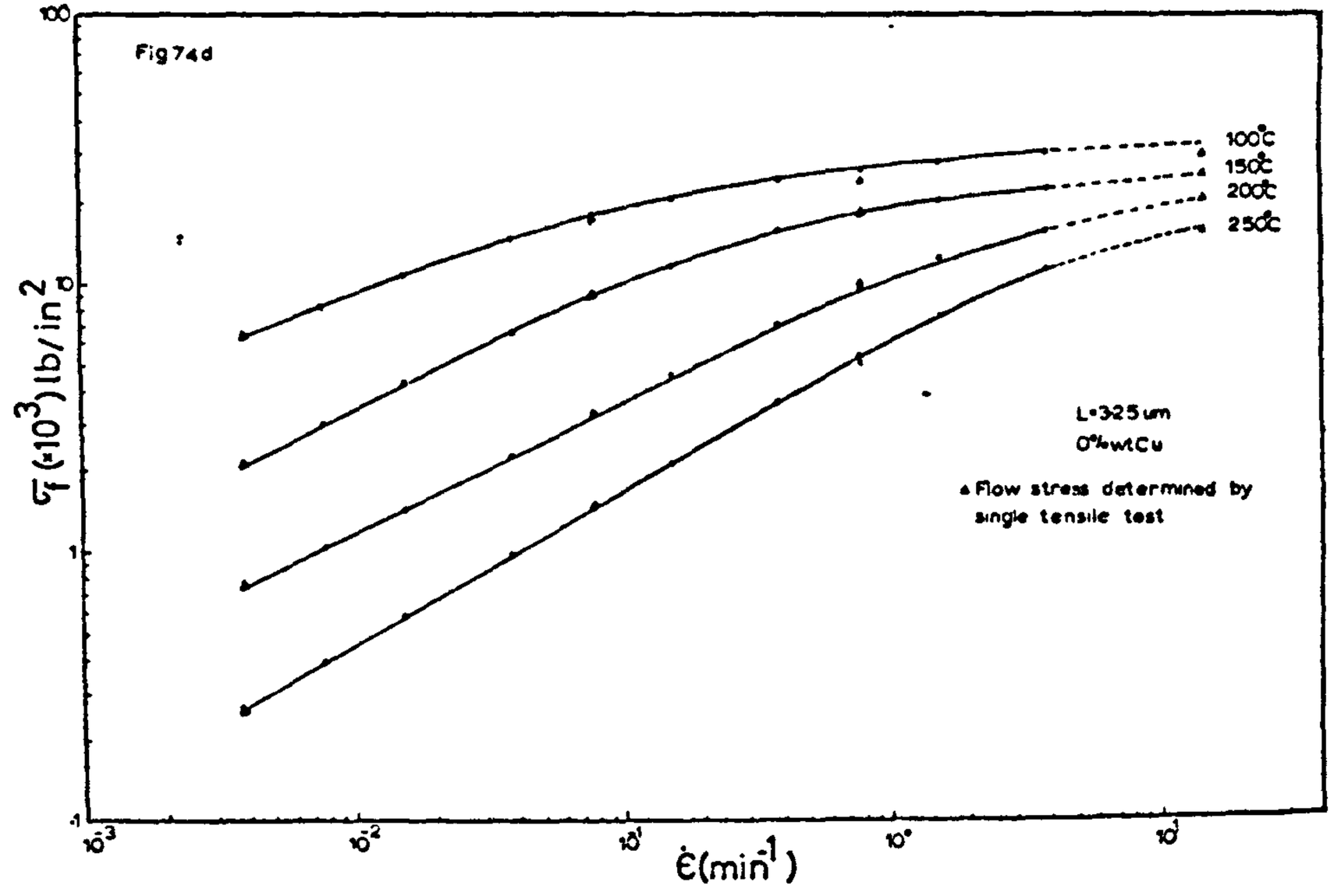

Figure 75-The effect of temperature on the σ_f vs $\dot{\epsilon}$ relationship with increasing grain size (0.15% wt Cu).

Fig 75a

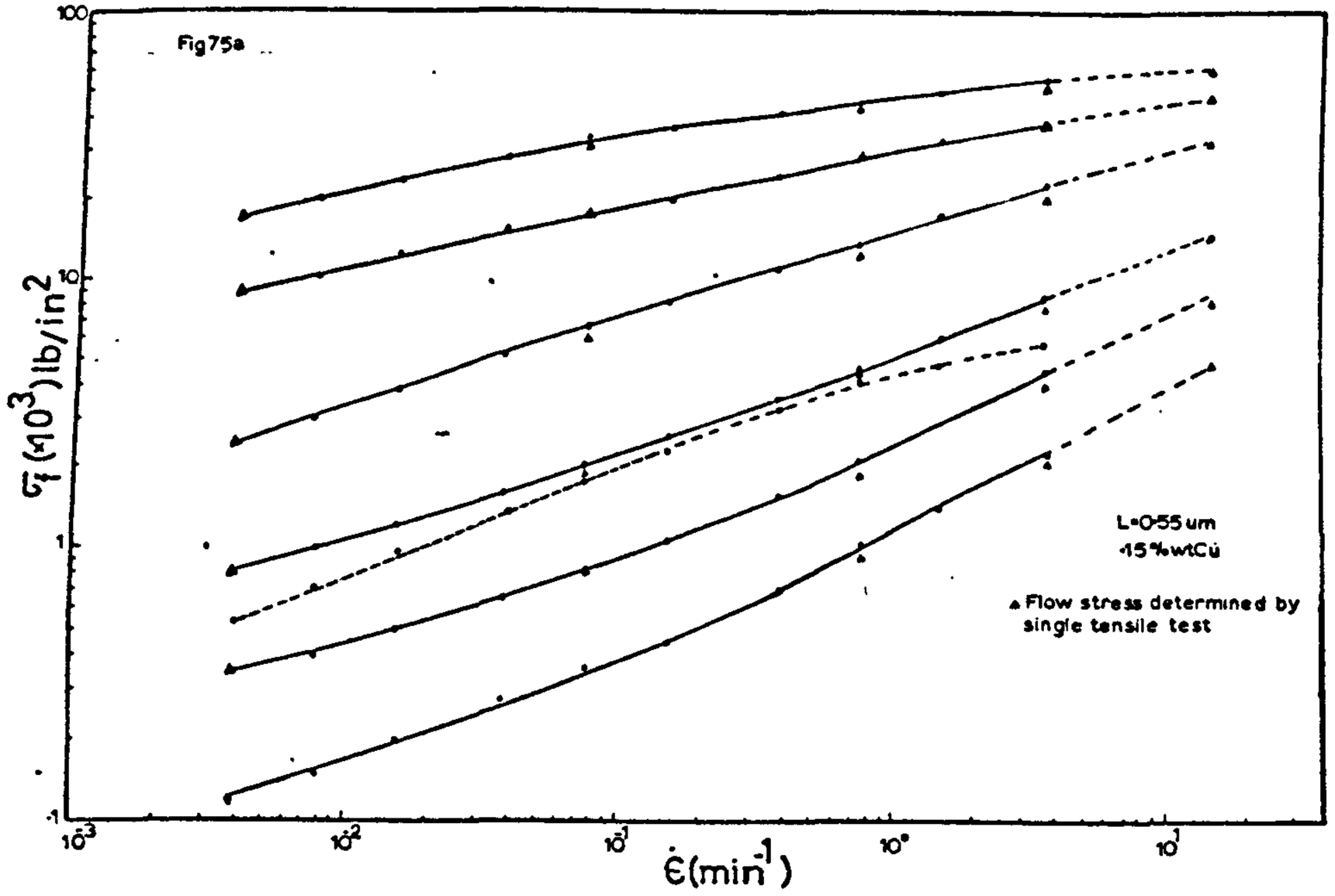

Fig 75b

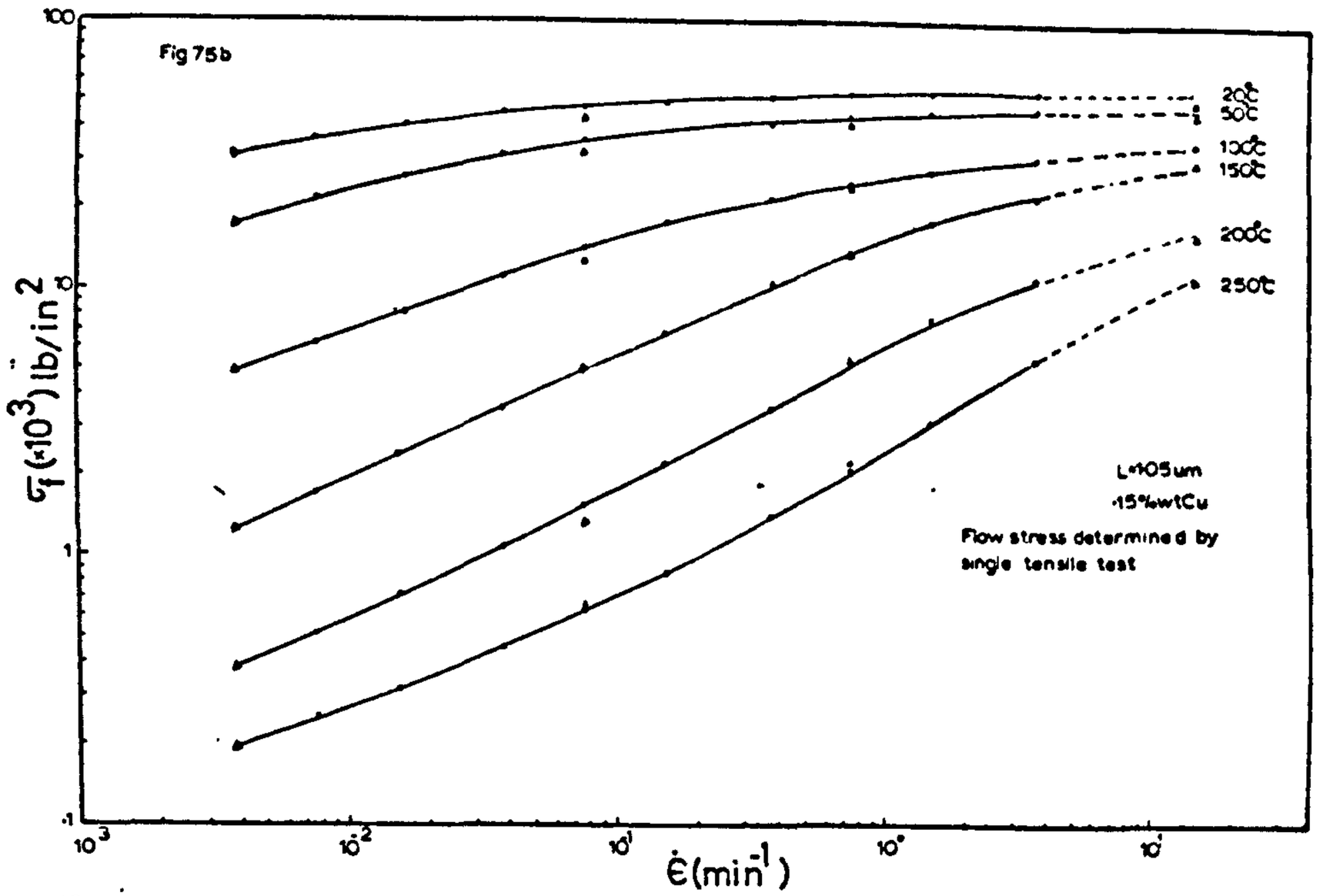

Fig 75c

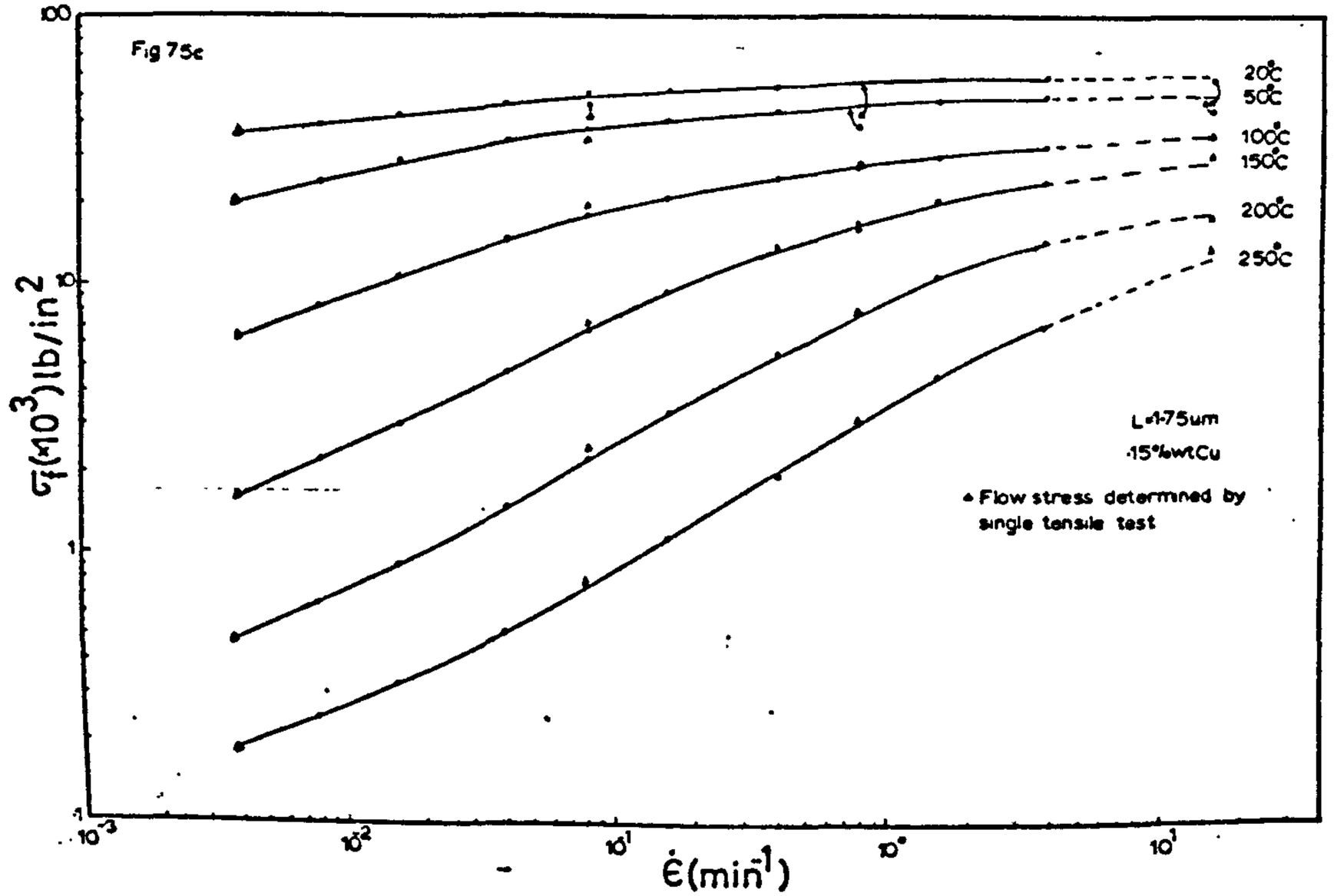

Fig 75d

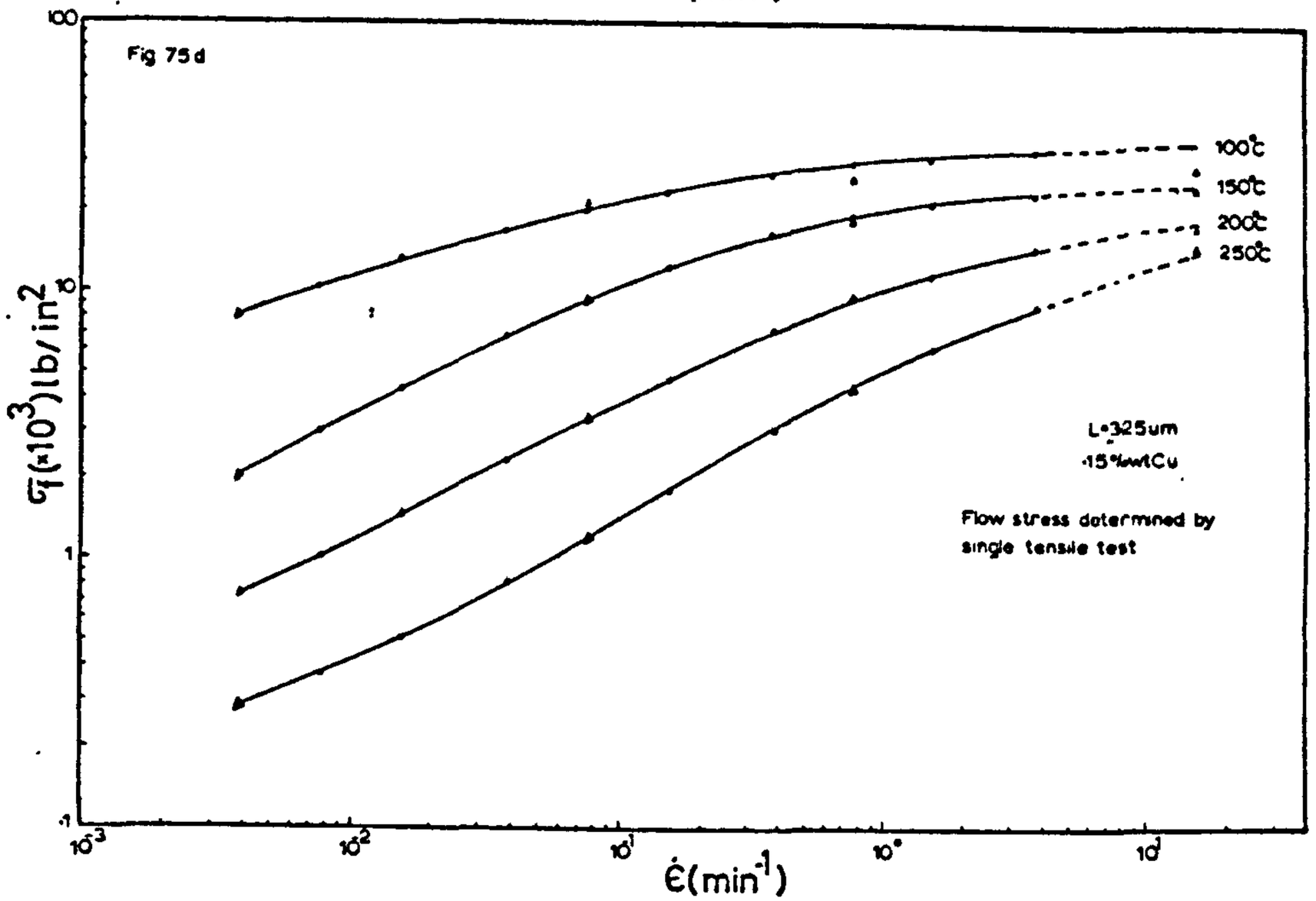

Figure 76- The effect of temperature on the σ_f vs $\dot{\epsilon}$ relationship with increasing grain size (1% wt Cu).

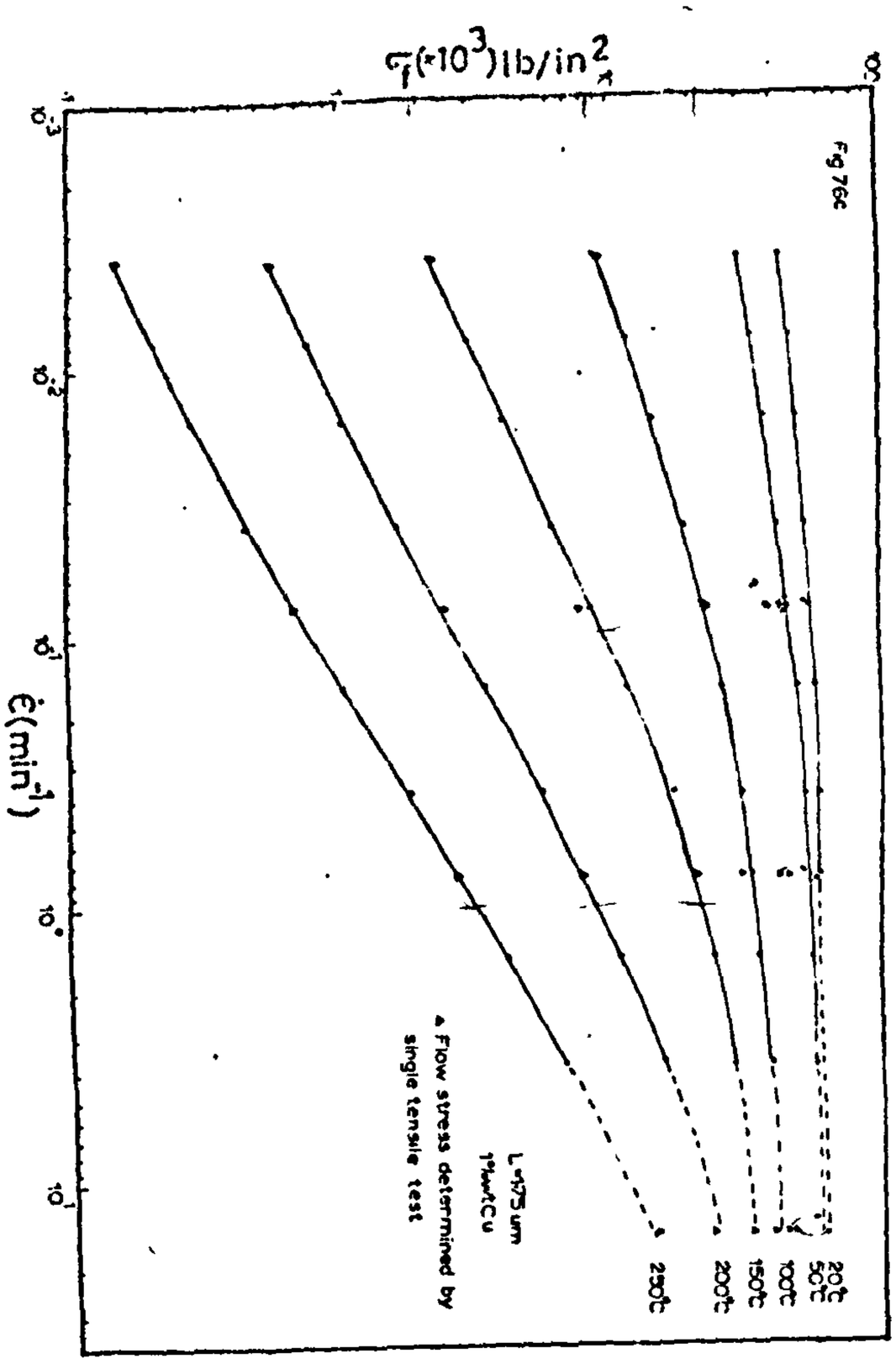
$\sigma_f(\times 10^3)$ lb/in^2
$\dot{\epsilon}$(min^{-1})
20°c
50°c
100°c
150°c
200°c
250°c
L=675 um
1%wtCu
▲ Flow stress determined by single tensile test

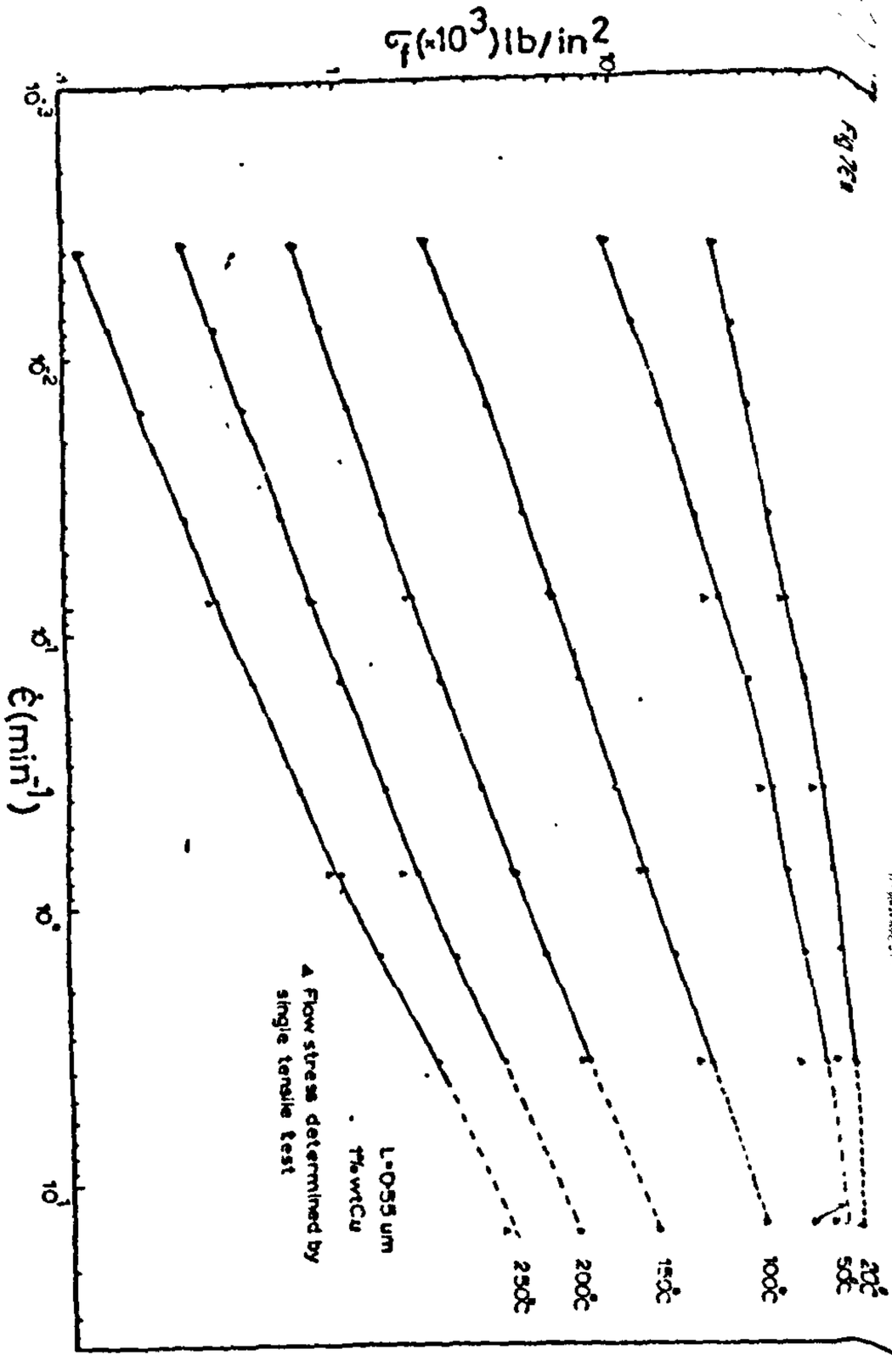
$\sigma_f(\times 10^3)$ lb/in^2
$\dot{\epsilon}$(min^{-1})
20°c
50°c
100°c
150°c
200°c
250°c
L=0.55 um
1%wtCu
▲ Flow stress determined by single tensile test

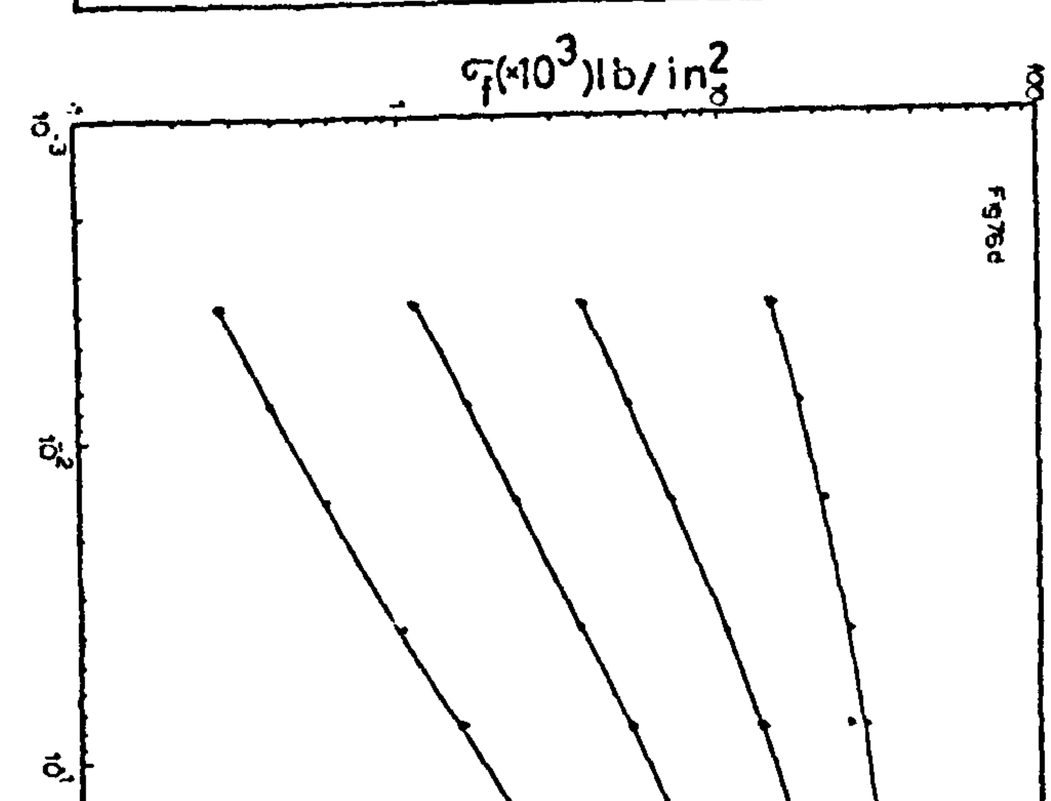
$\sigma_f(\times 10^3)$ lb/in^2
$\dot{\epsilon}$(min^{-1})
100°c
150°c
200°c
250°c
L=325 um
1%wtCu
▲ Flow stress determined by single tensile test

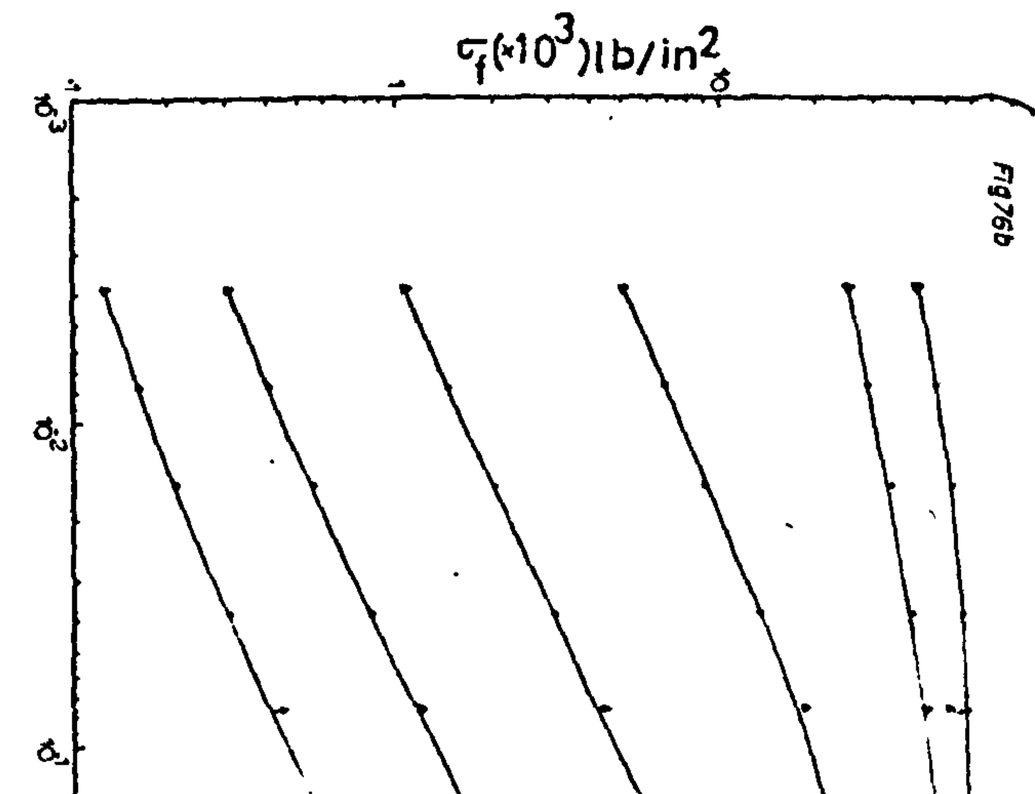
$\sigma_f(\times 10^3)$ lb/in^2
$\dot{\epsilon}$(min^{-1})
20°c
50°c
100°c
150°c
200°c
250°c
L=105 um
1%wtCu
▲ Flow stress determined by single tensile test

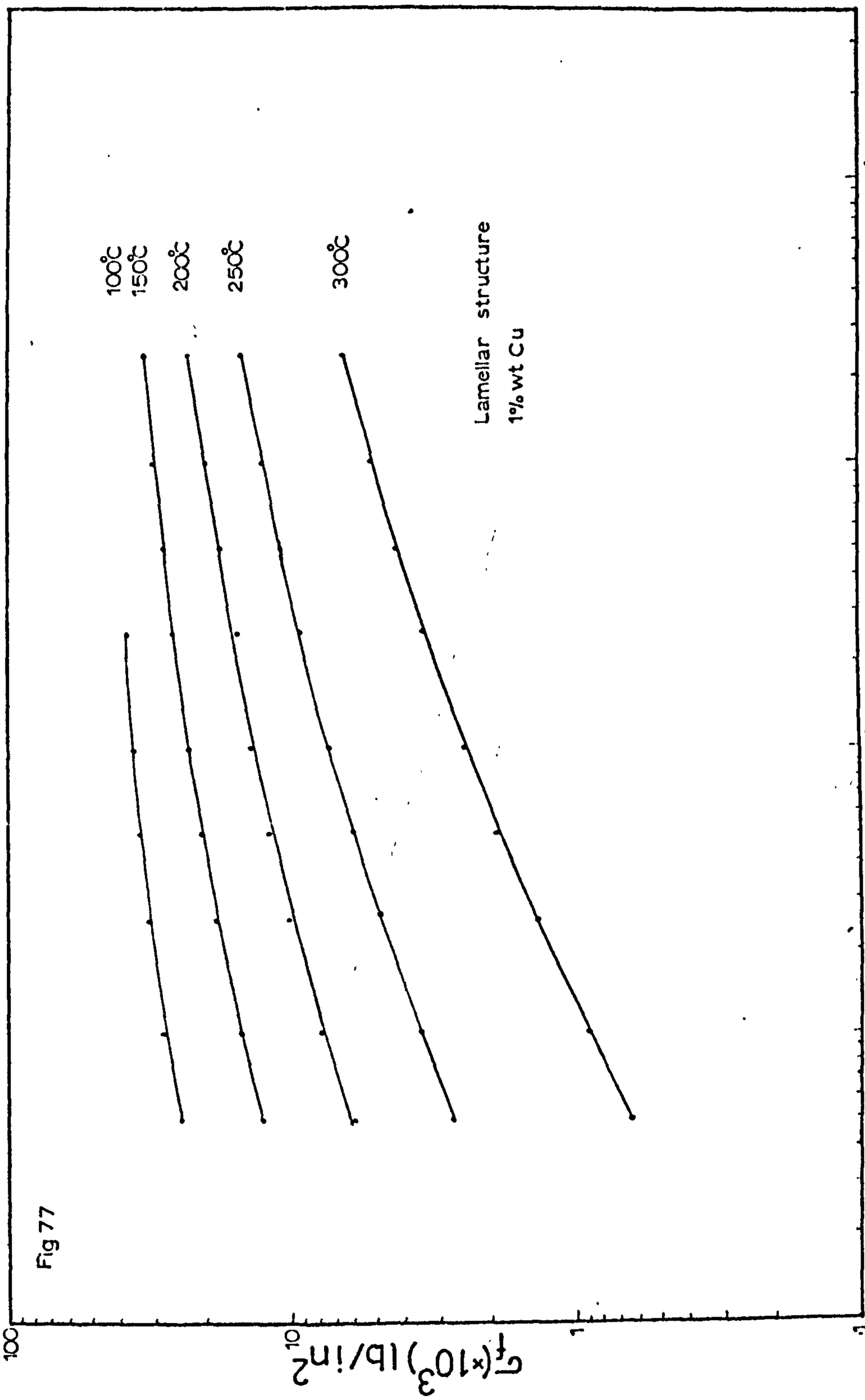

Figure 77- The effect of temperature on the σ_f vs $\dot{\epsilon}$ relationship for the lamellar structure.

Figure 78- Shows the effect of increasing crosshead velocity on the % elongation for a 0.55um grain size material strained at the temperature of 200°C.

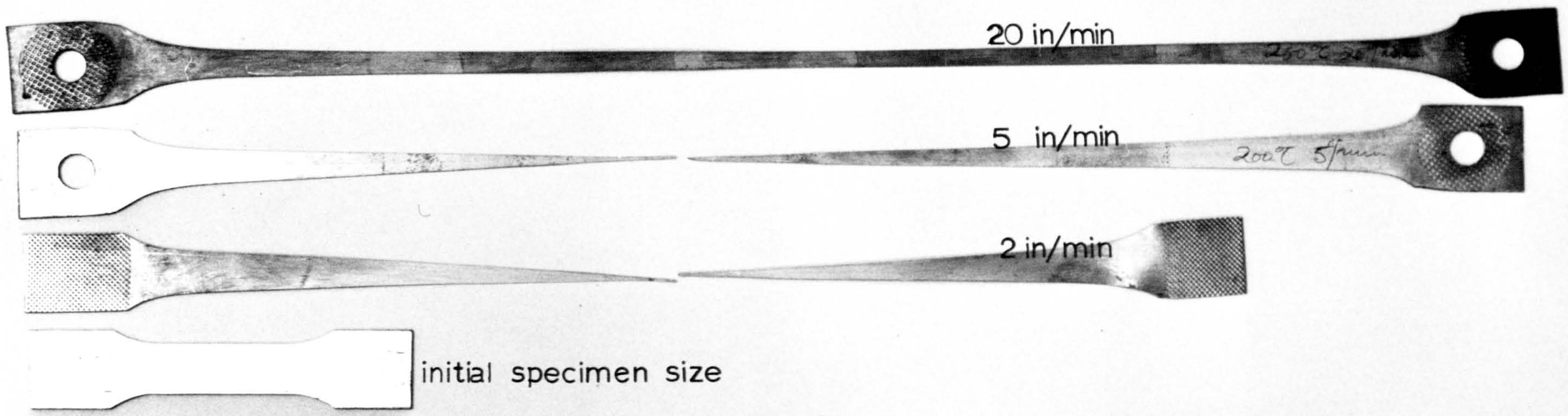

Figure 78

Figure 79-Shows the effect of grain size on the % elongation for a fixed crosshead velocity of 20 in/min and the temperature of 200°C.

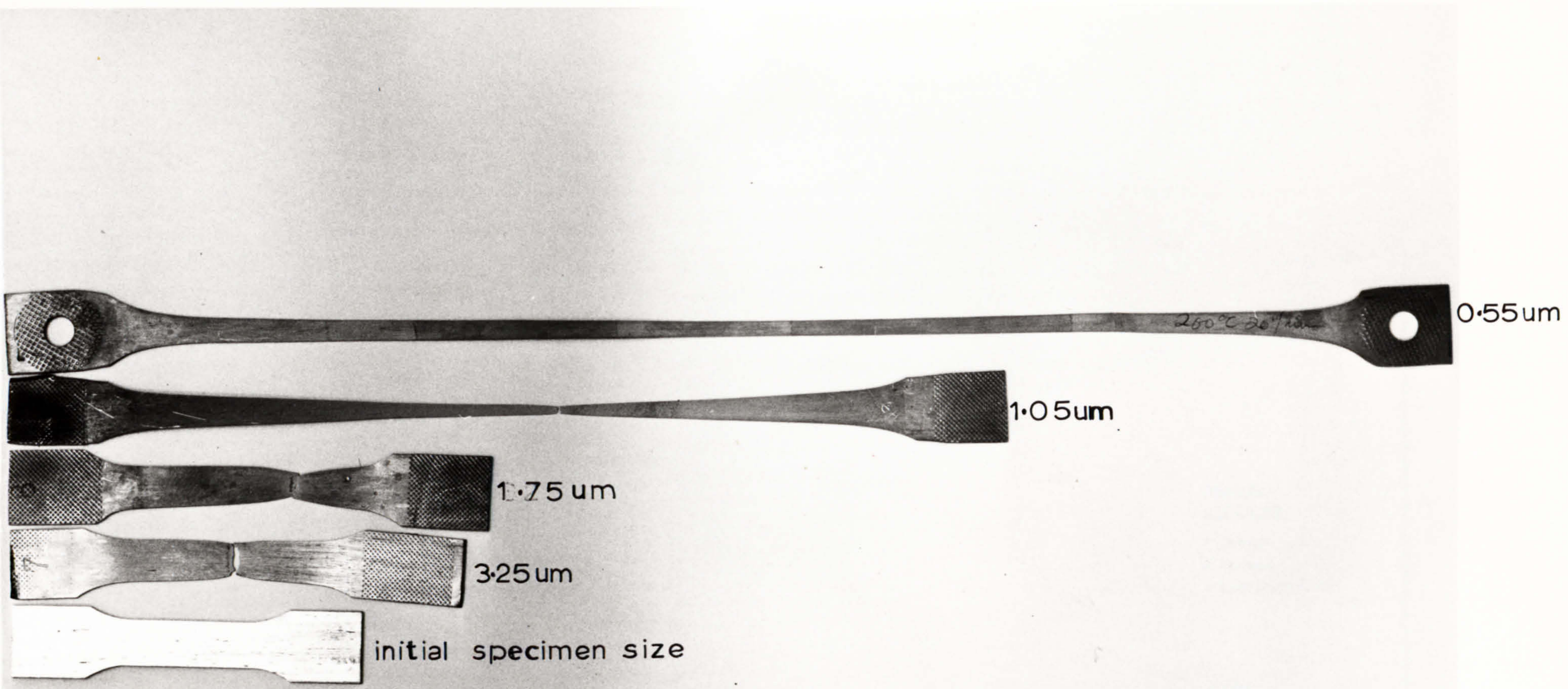

Figure 79

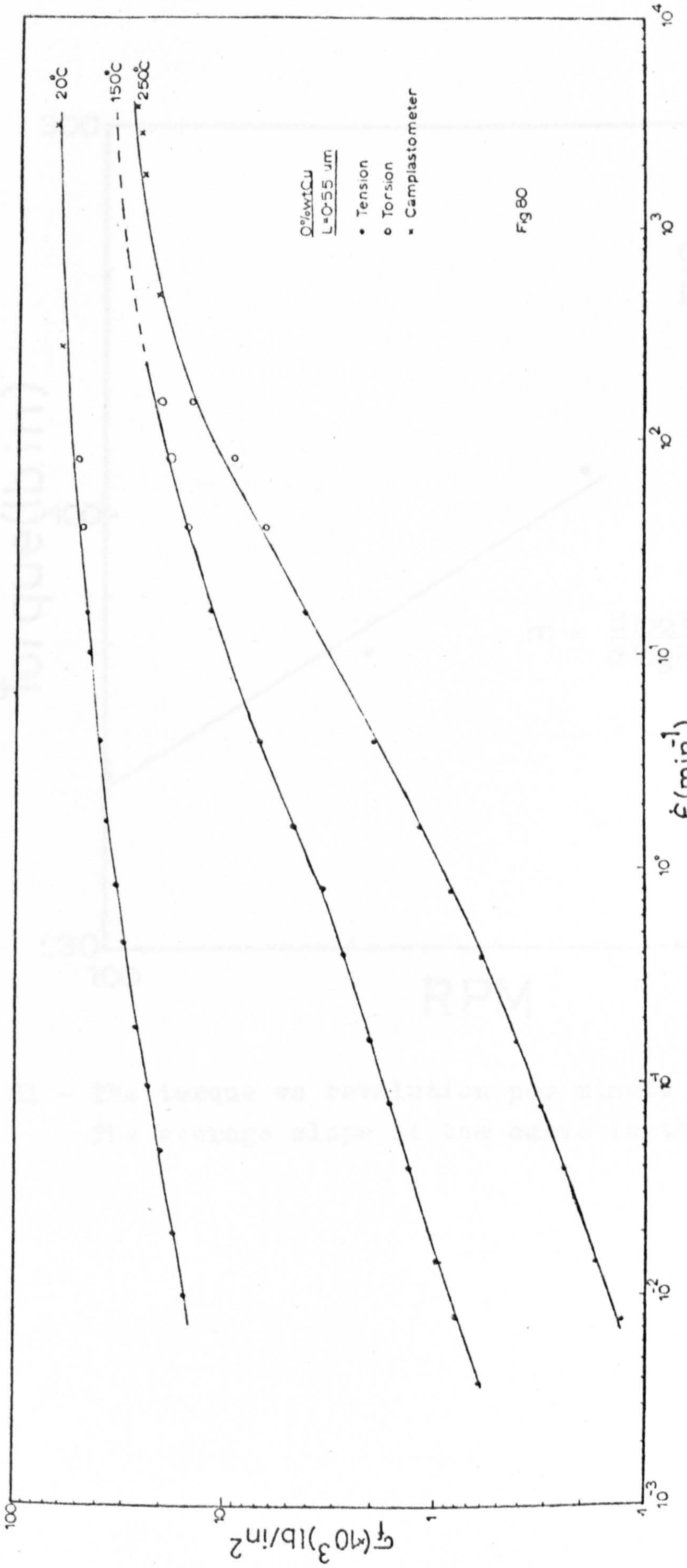

Figure 80-σ_f vs $\dot{\epsilon}$ relationship determined using the tensile, torsion and camplastometer results to cover seven order of magnitude of strain-rate.

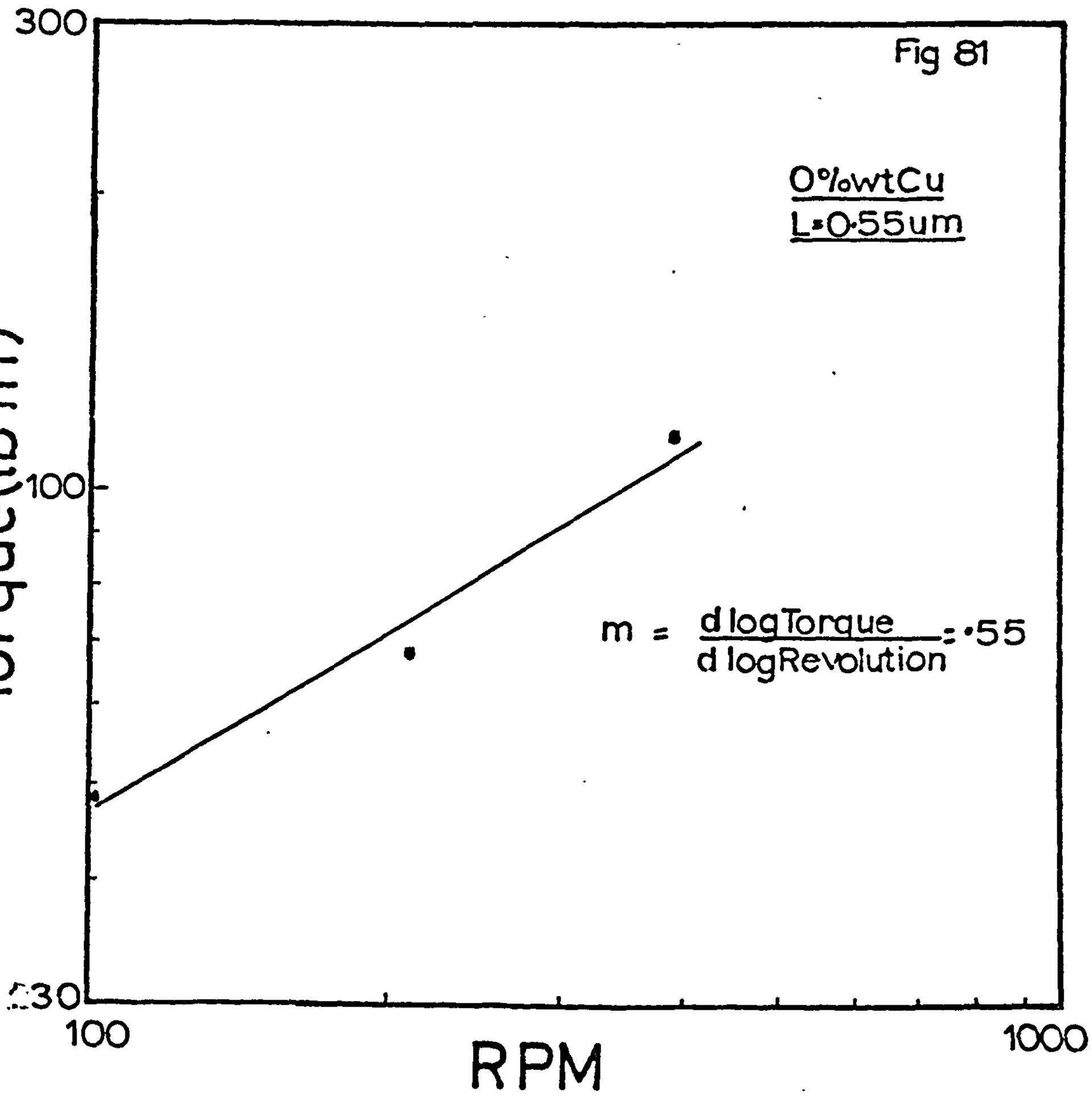

Figure 81 - The torque vs revolution per minute relationship. The average slope of the curve is the m-value.

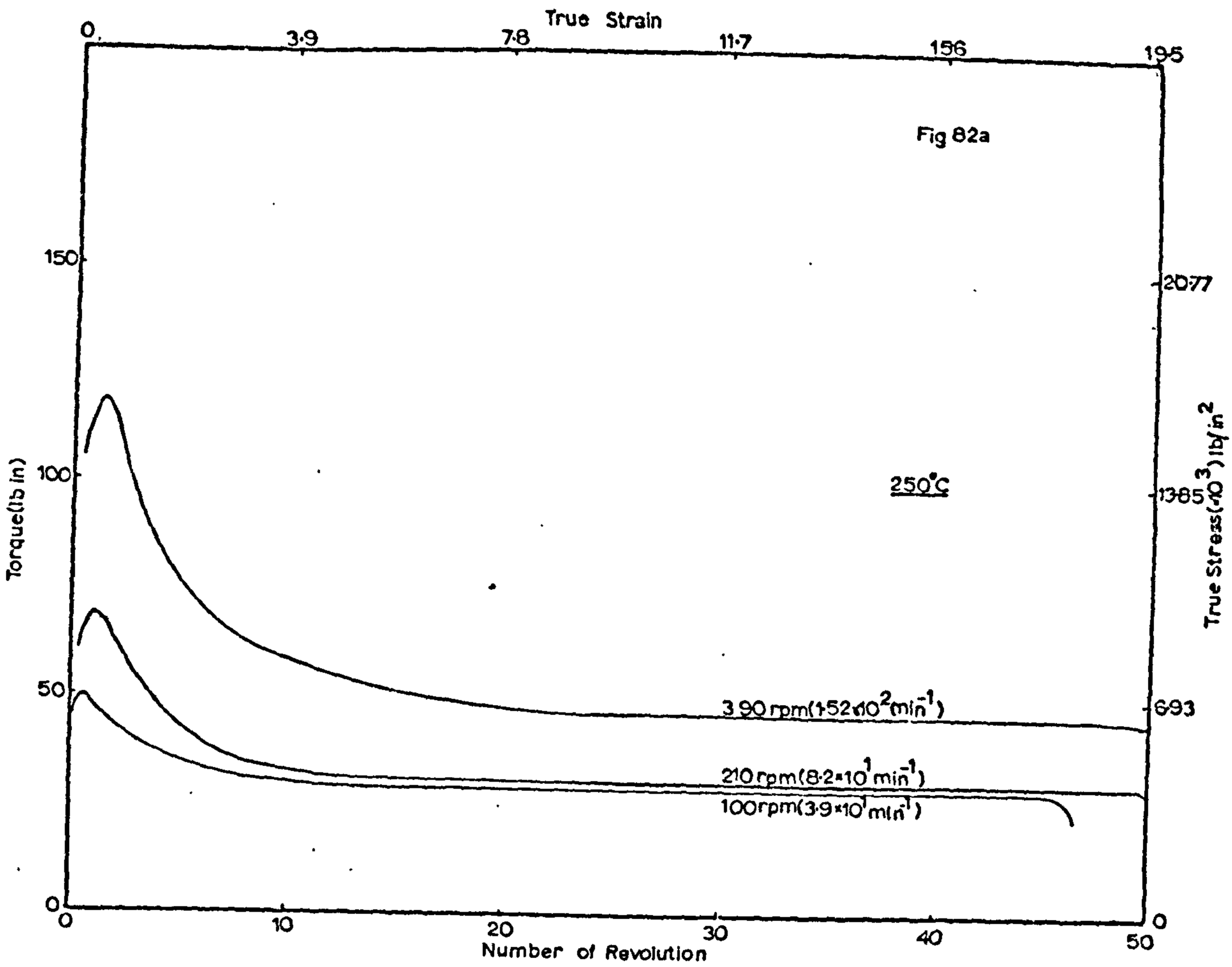

Fig 82a

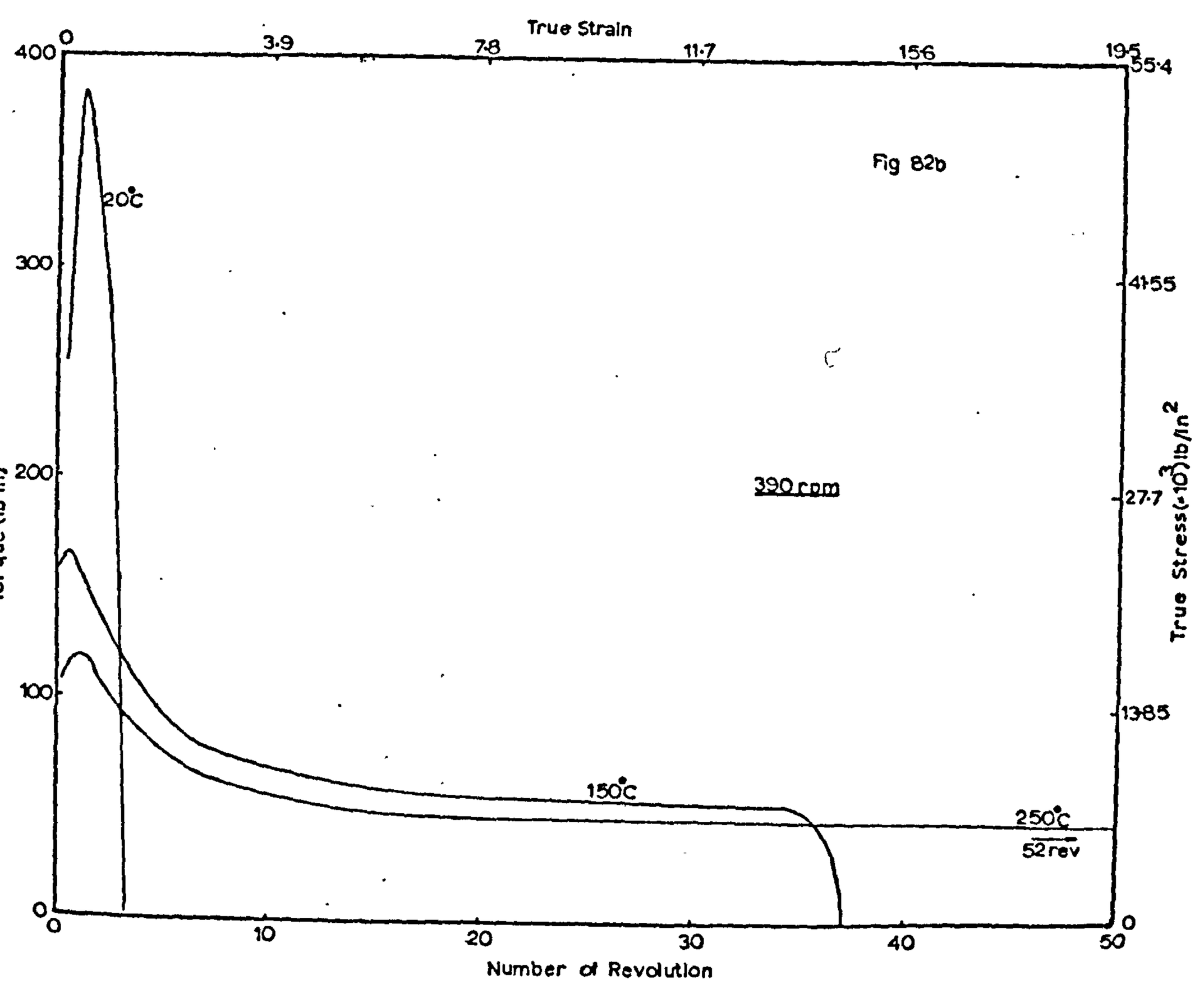

Fig 82b

Figure 82a - Torque/revolution curves at 250°C for different constant strain-rates.

Figure 82b - Torque/revolution curves at 390 rpm and at 20,150 & 250°C.

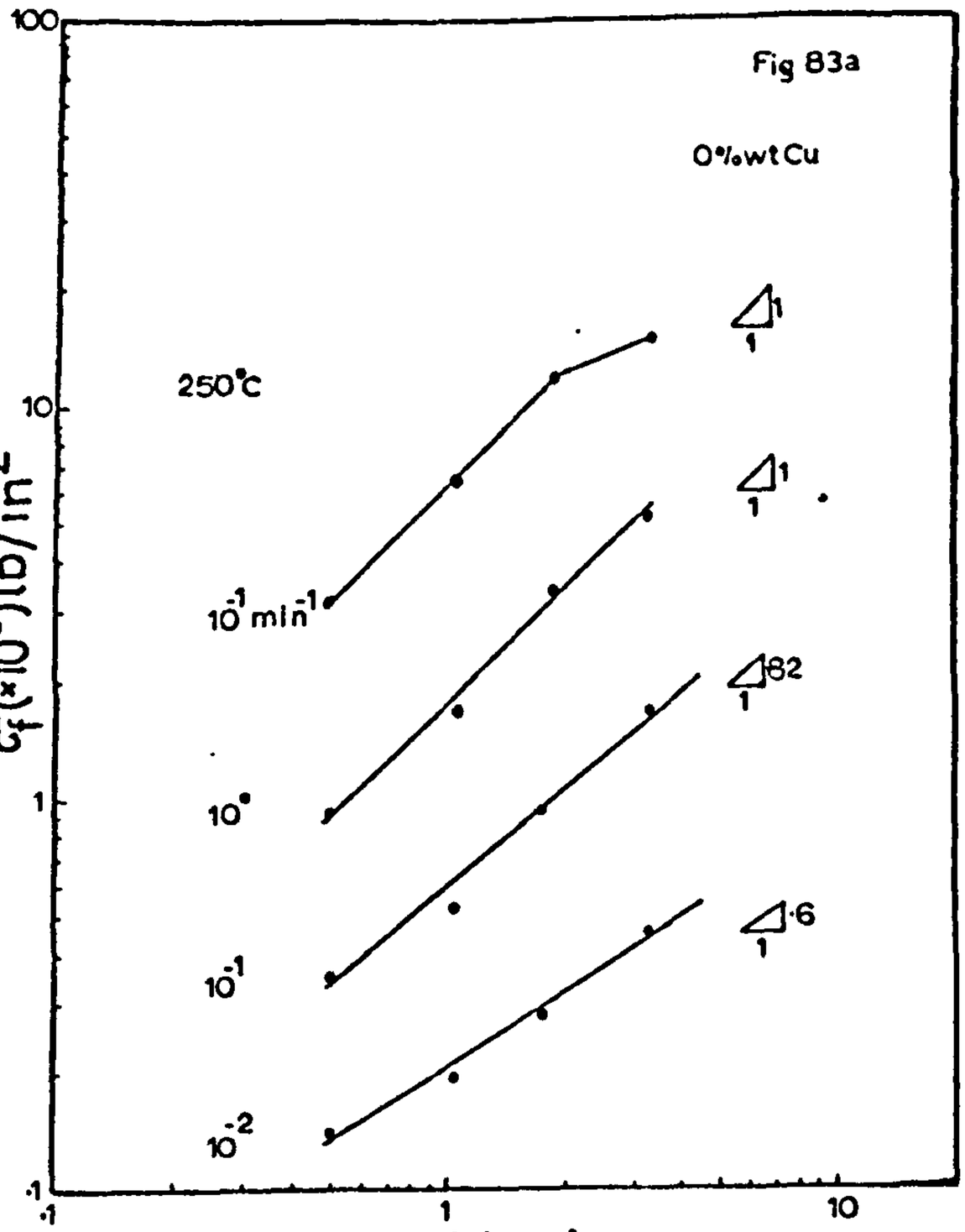

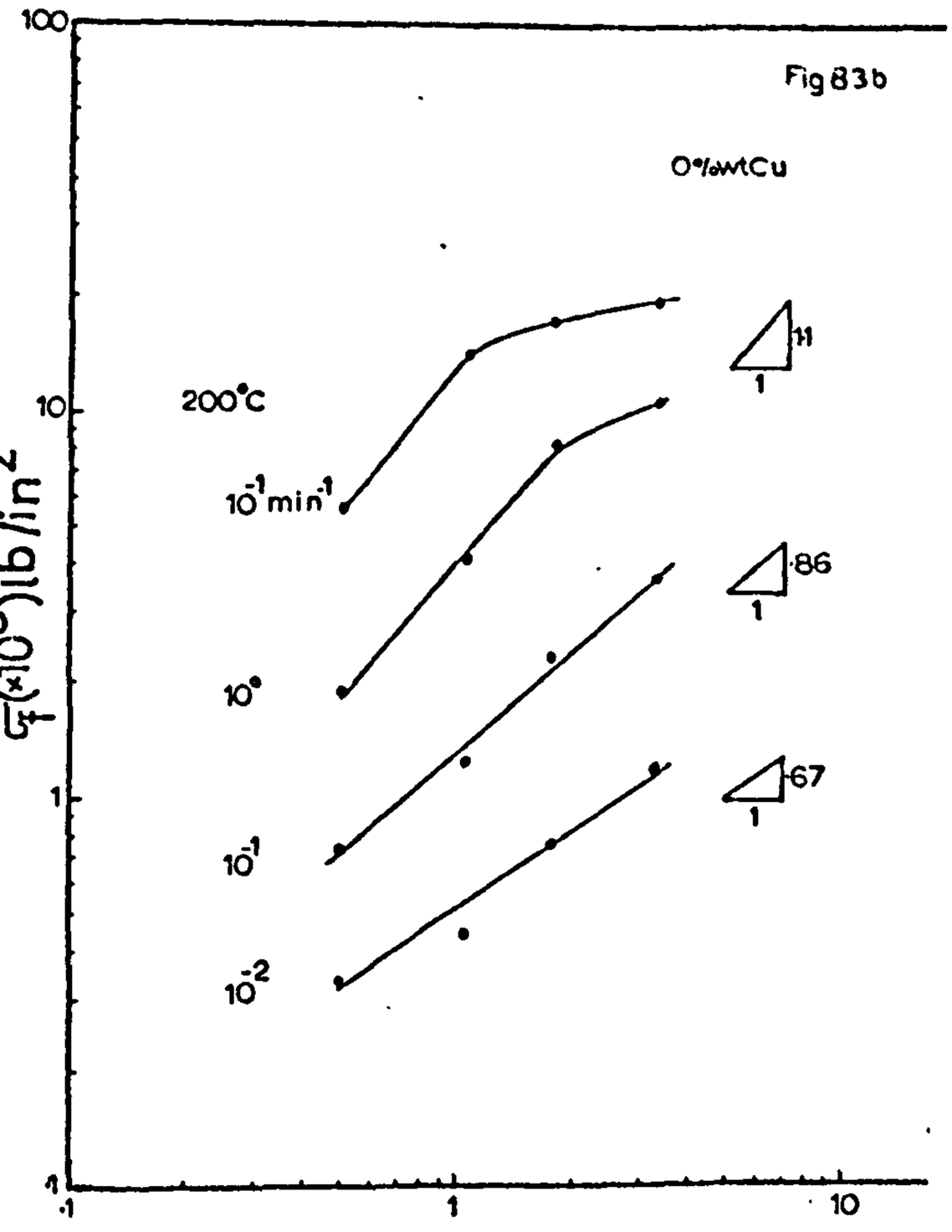

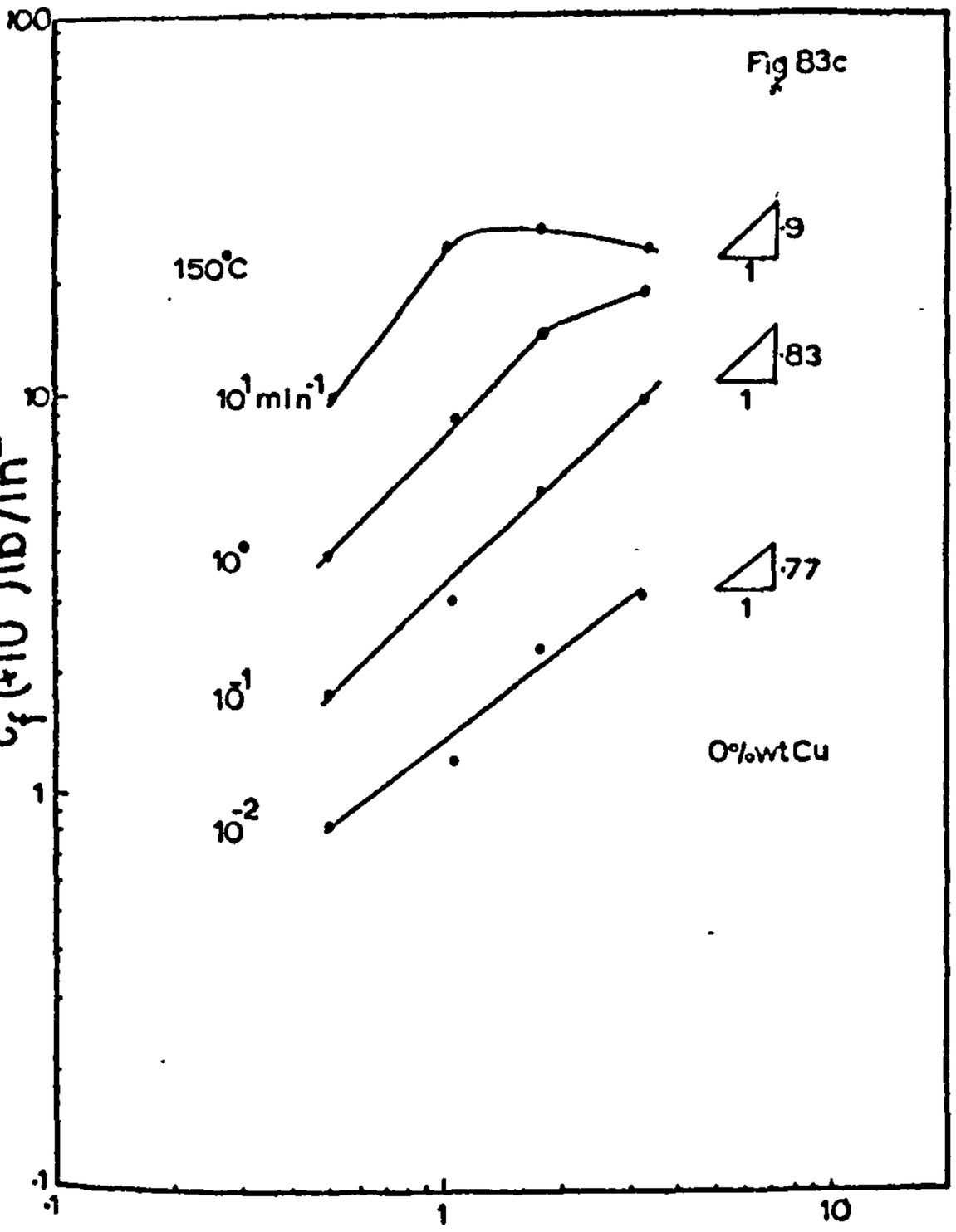

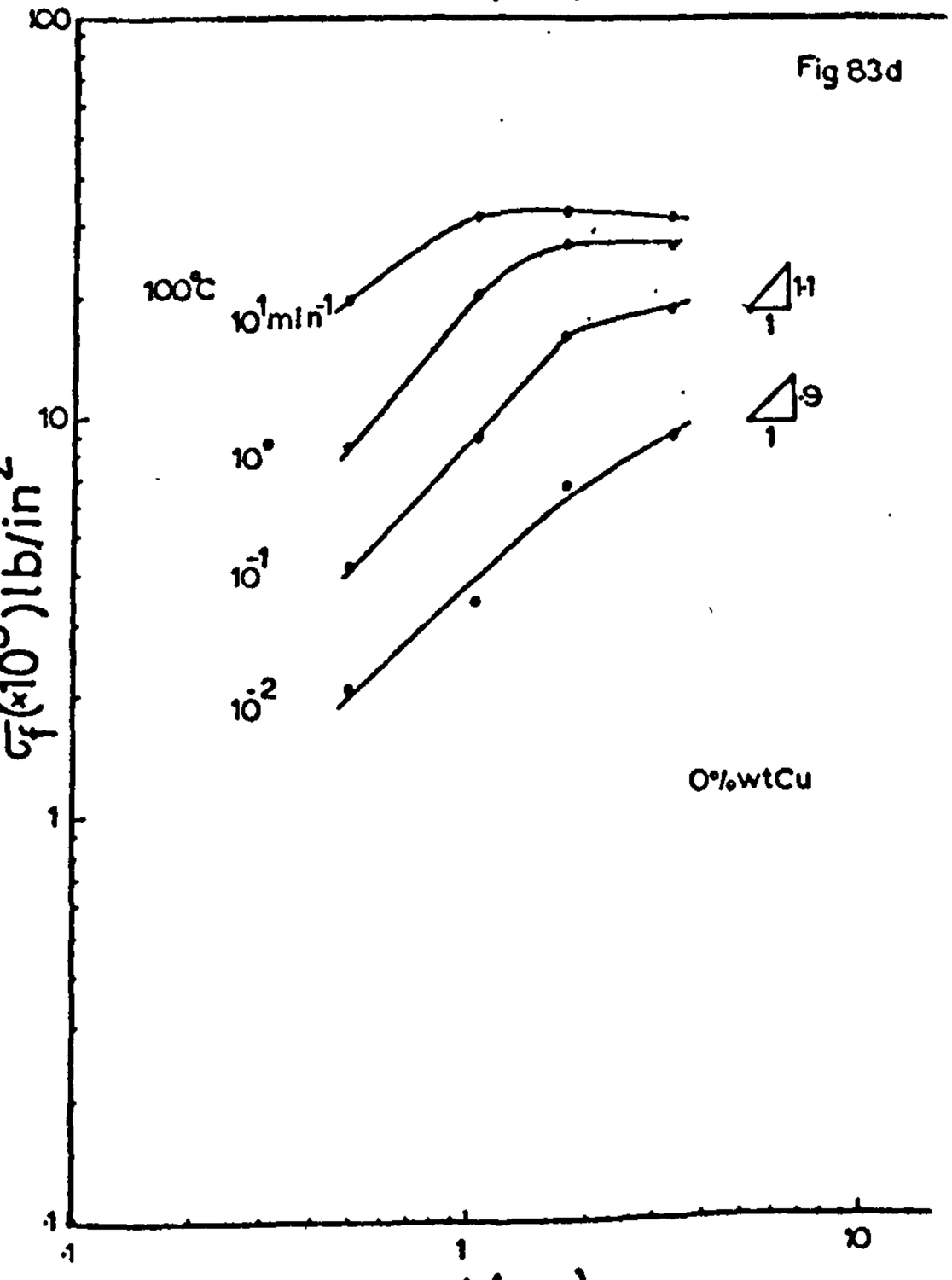

Figure 83a-d - Log/log plots of σ_f-L at different strain-rates for the temperatures 250,200,150 & 100°C. The slopes of each curves are indicated.

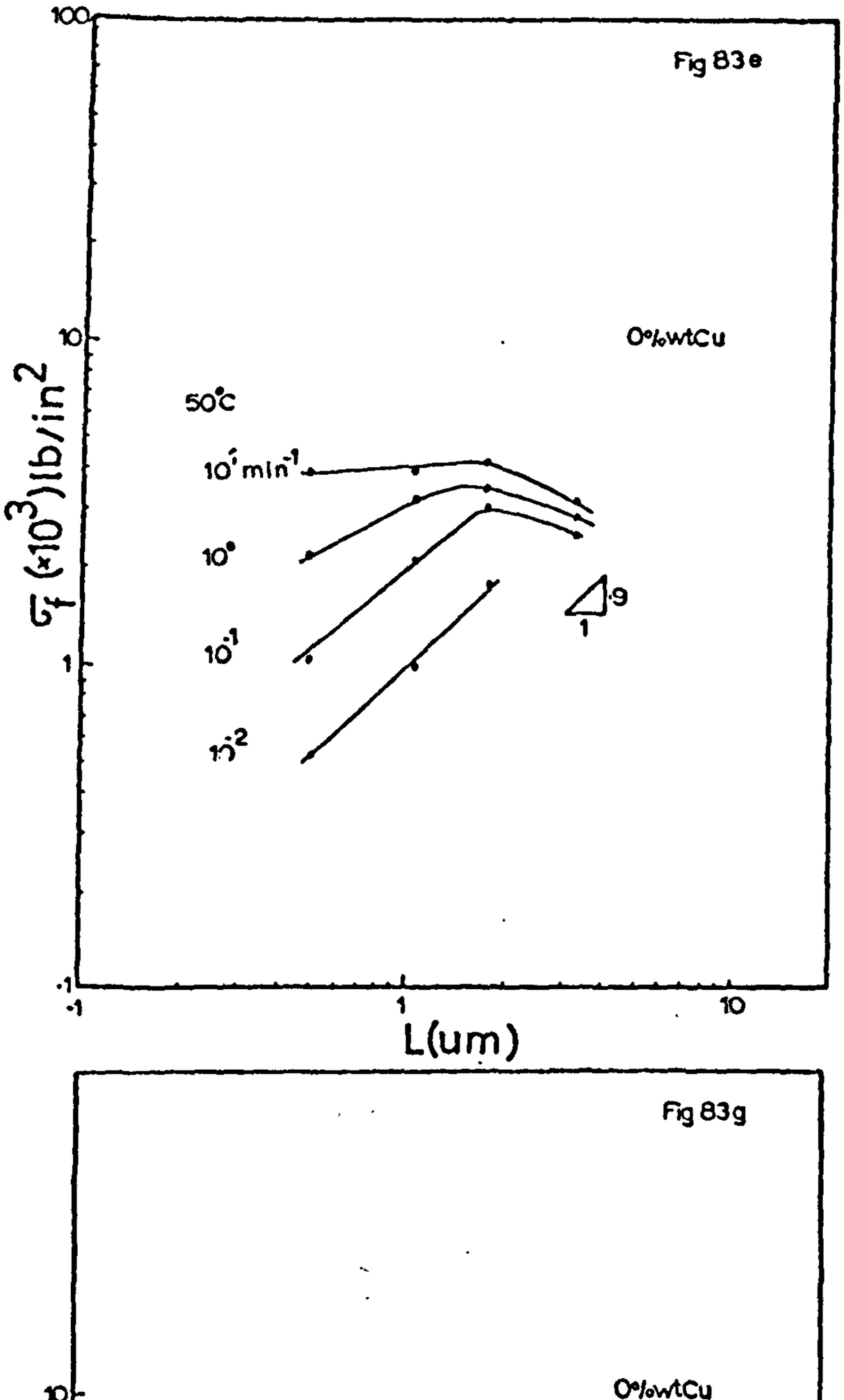

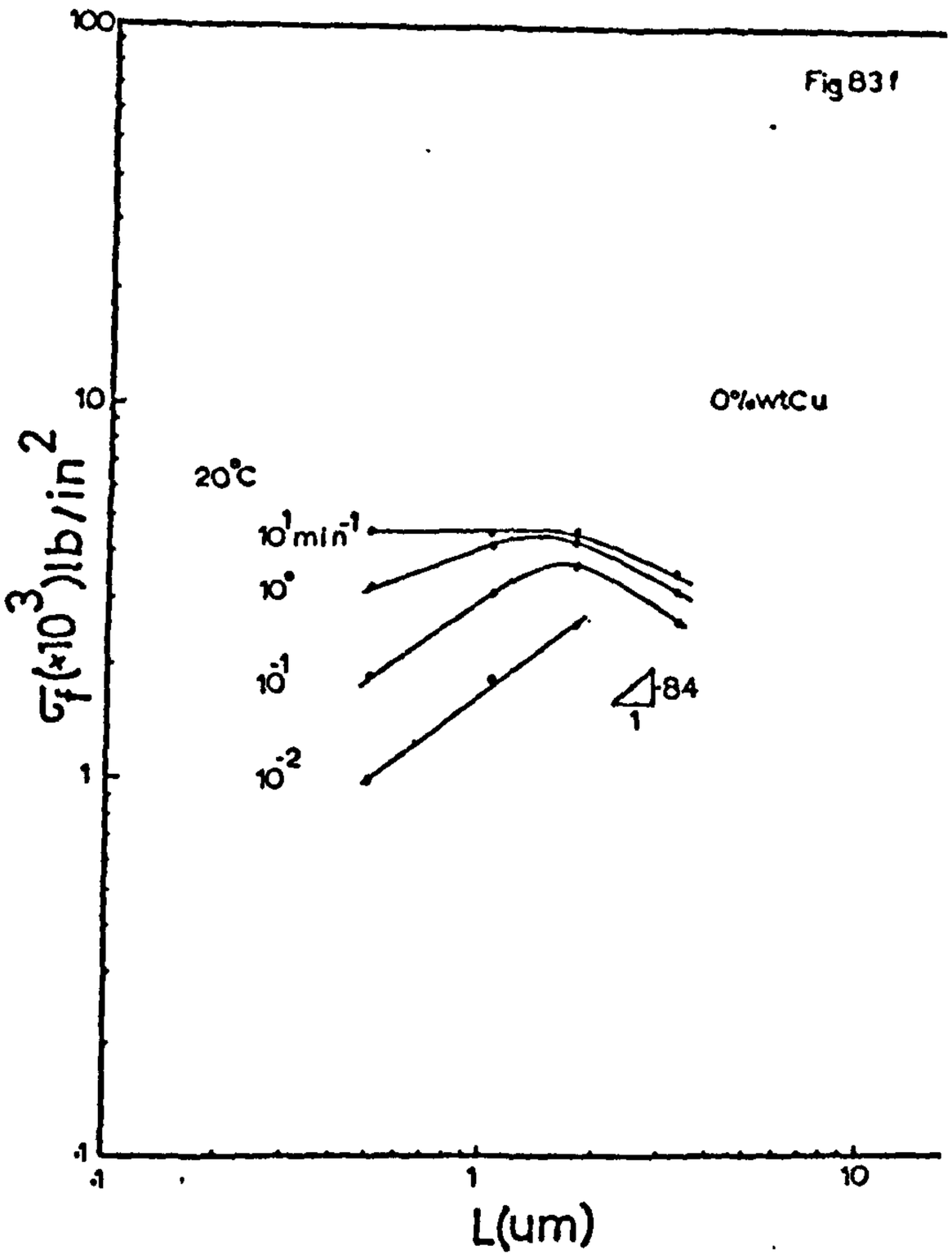

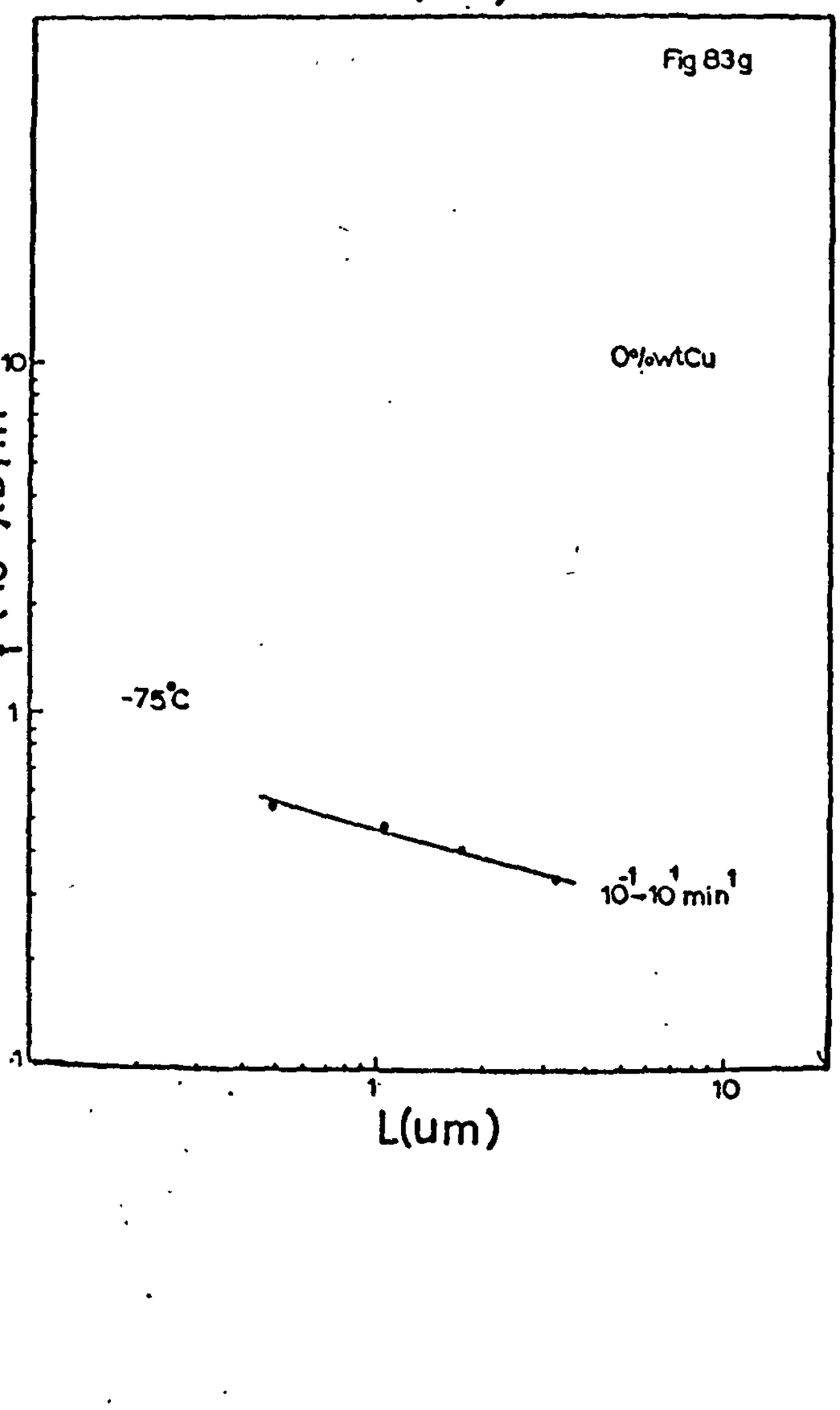

Figure 83e-g - Log/log plots of σ_f vs L at different strain-rates for the temperature -s 50,20& -75°C.
The slopes of each curve are indicated.

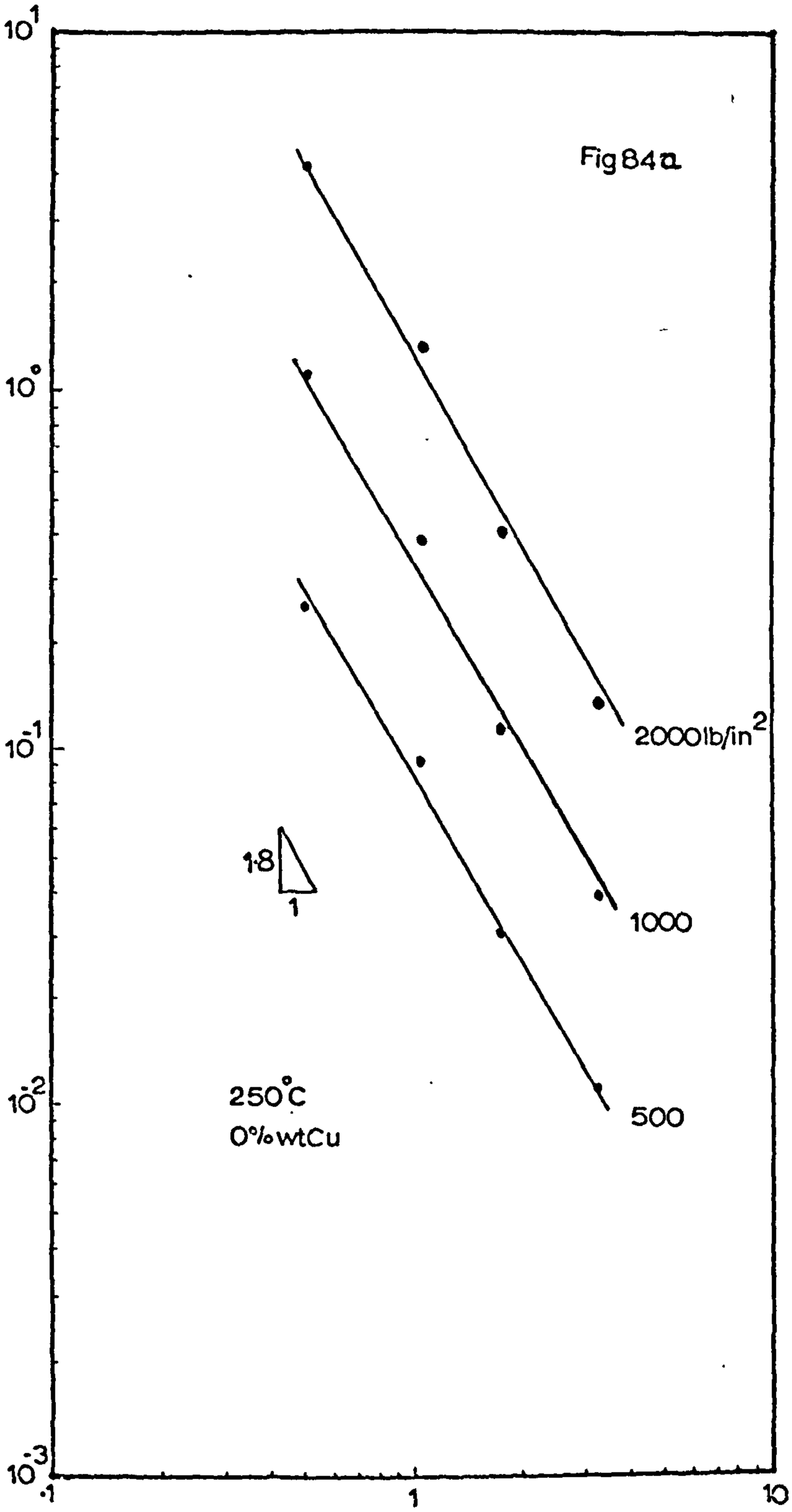

Figure 84a - Plots of $\dot{\epsilon}$ vs L at various constant stresses for the temperature 250°C. The slope of the curves are indicated.

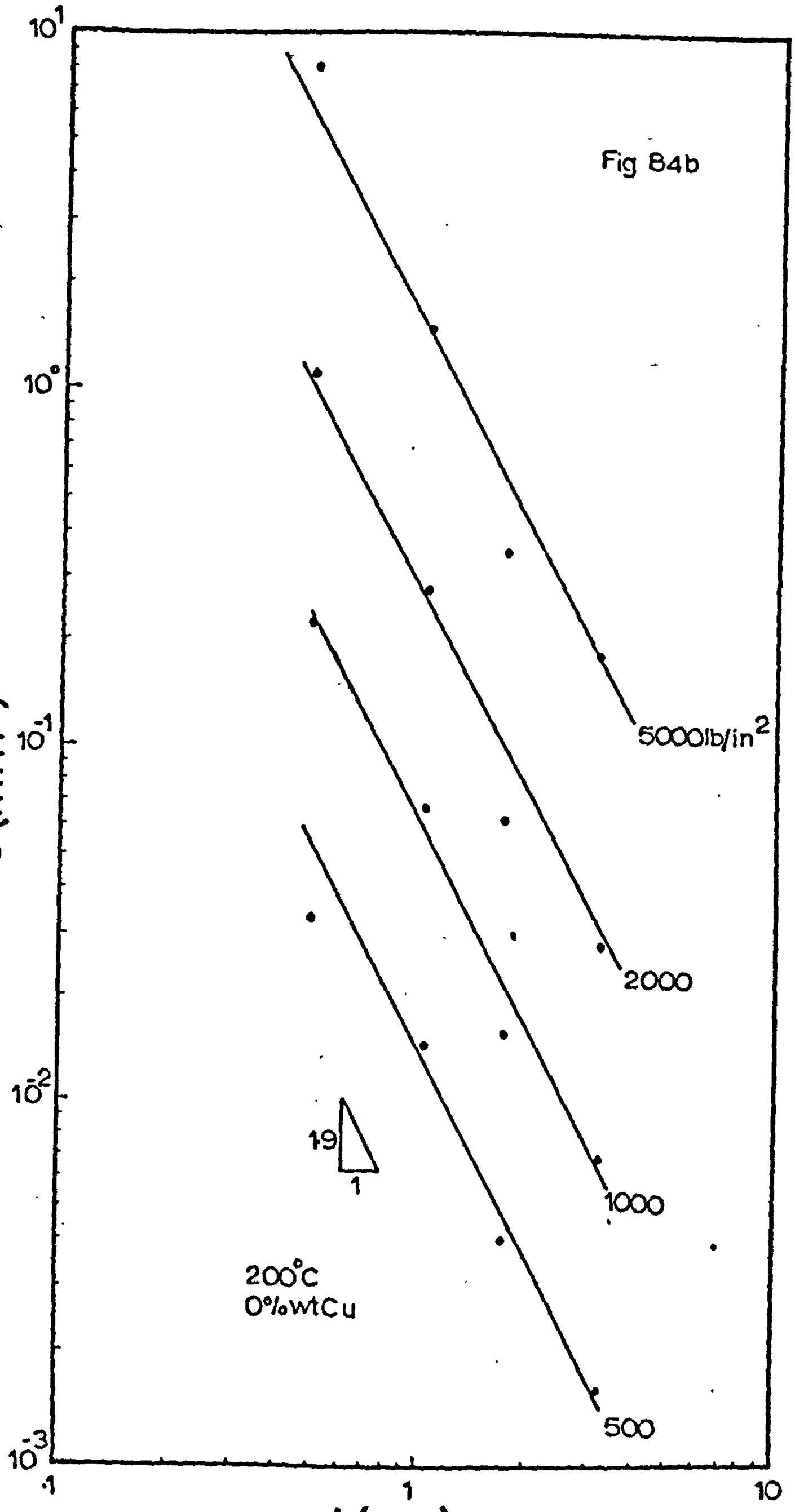

Figure 84b - Plots of $\dot{\epsilon}$ vs L at various constant stresses for the temperature 200oC. The slope of the curves are indicated.

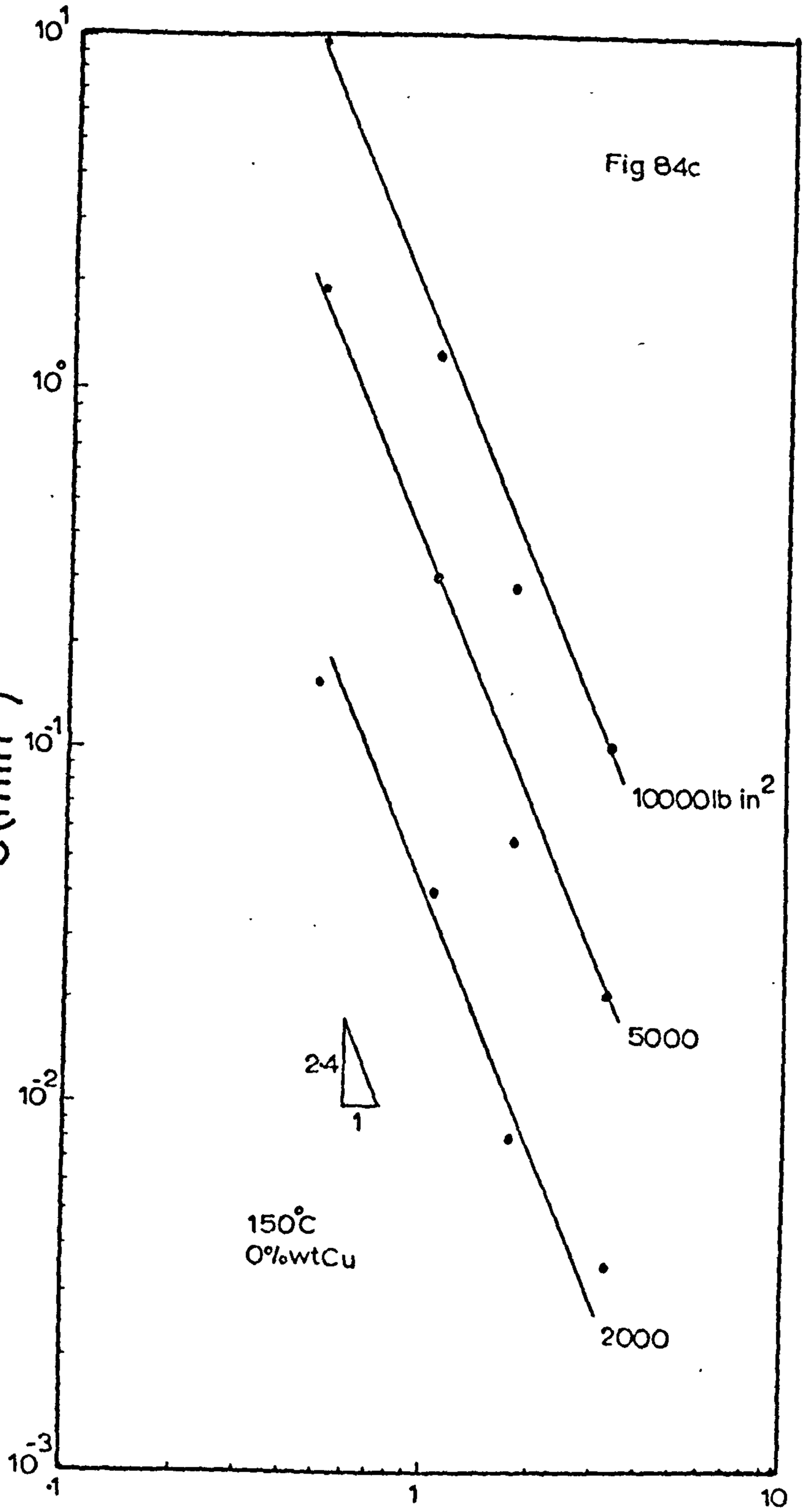

Figure 84c - Plots of $\dot{\epsilon}$ vs L at various constant stresses for the temperature 150°C. The slope of the curves are indicated.

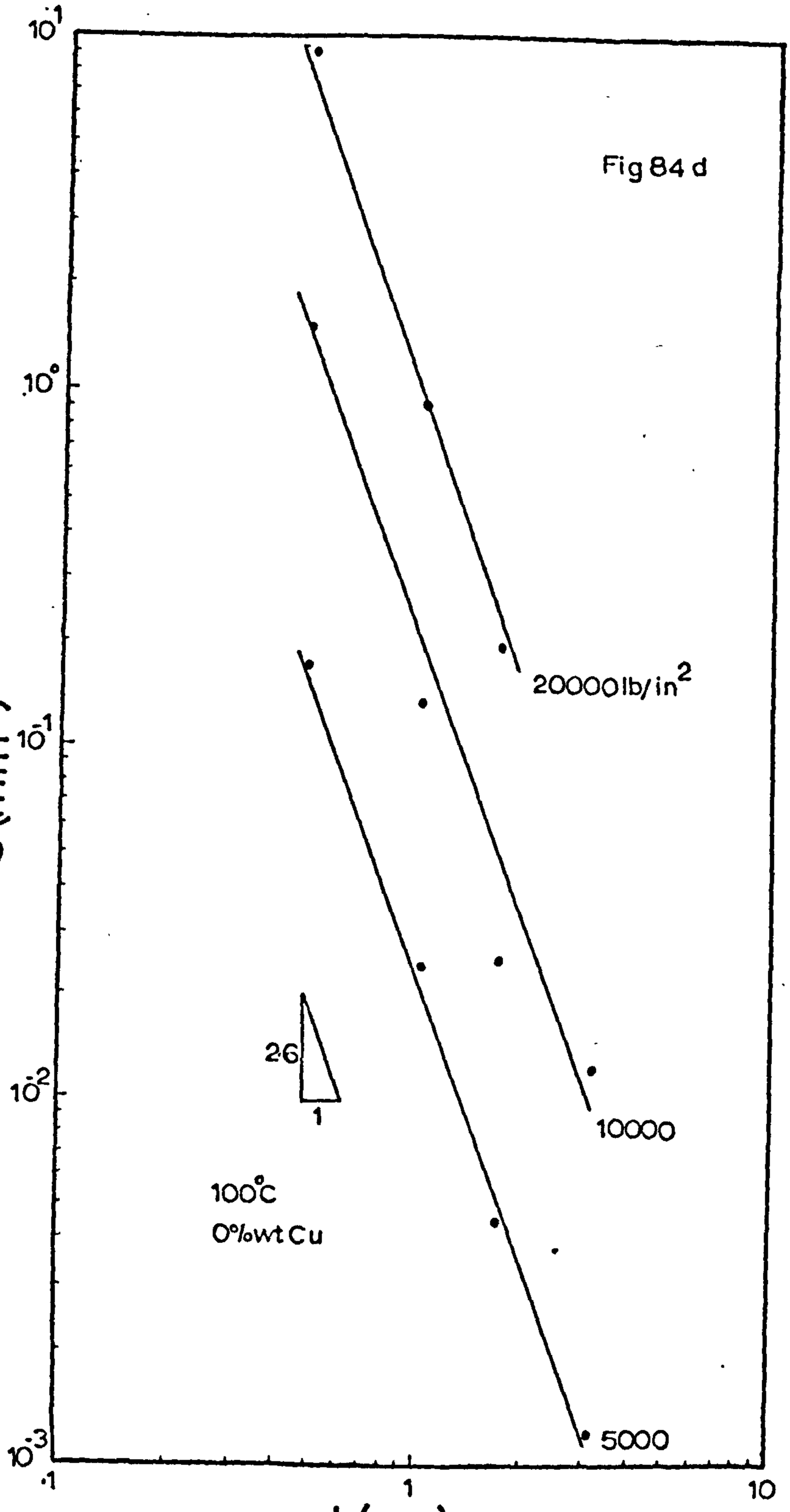

Figure 84d - Plots of $\dot{\epsilon}$ vs L at various constant stresses for the temperature 100°C. The slope of the curves are indicated.

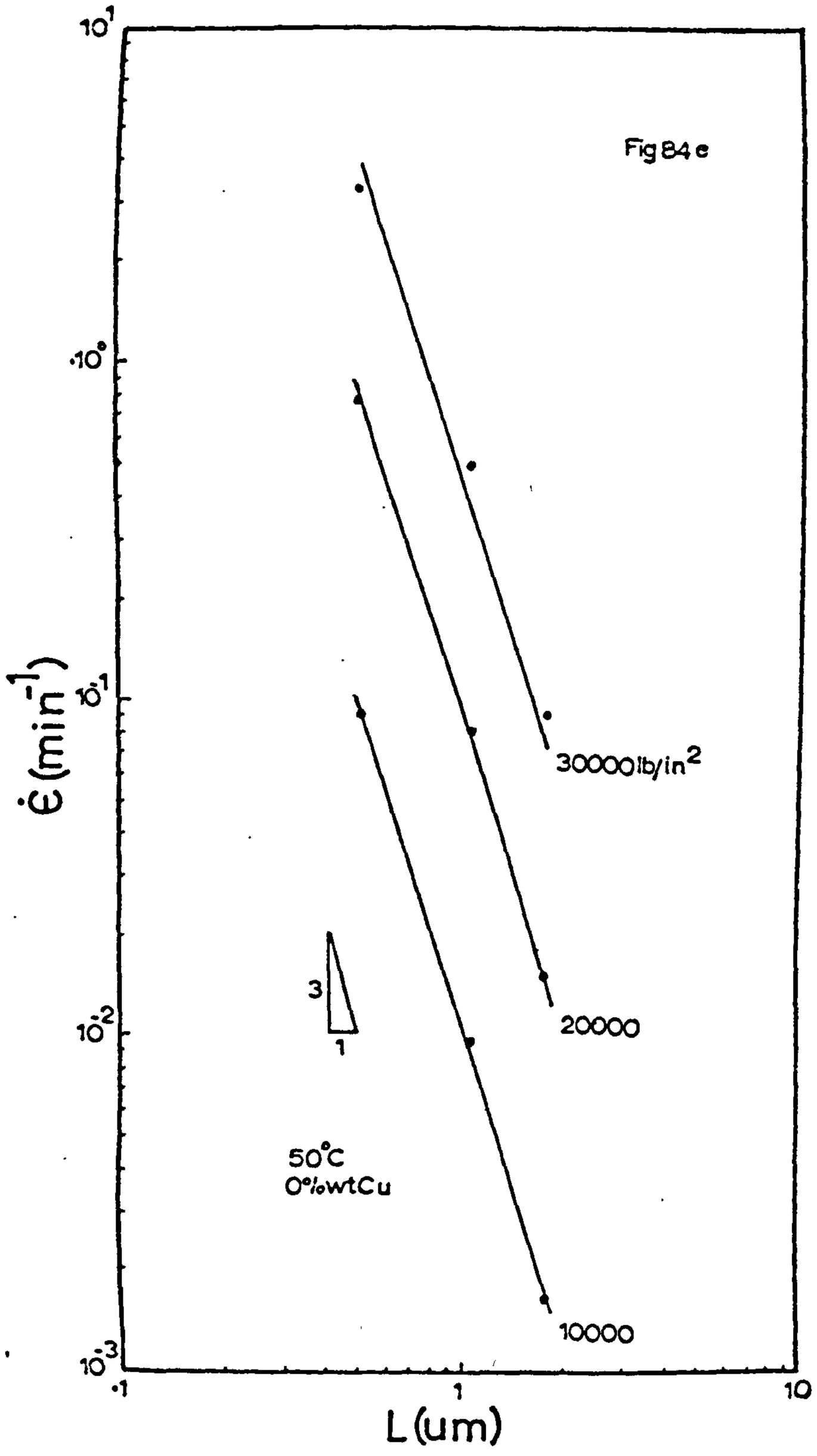

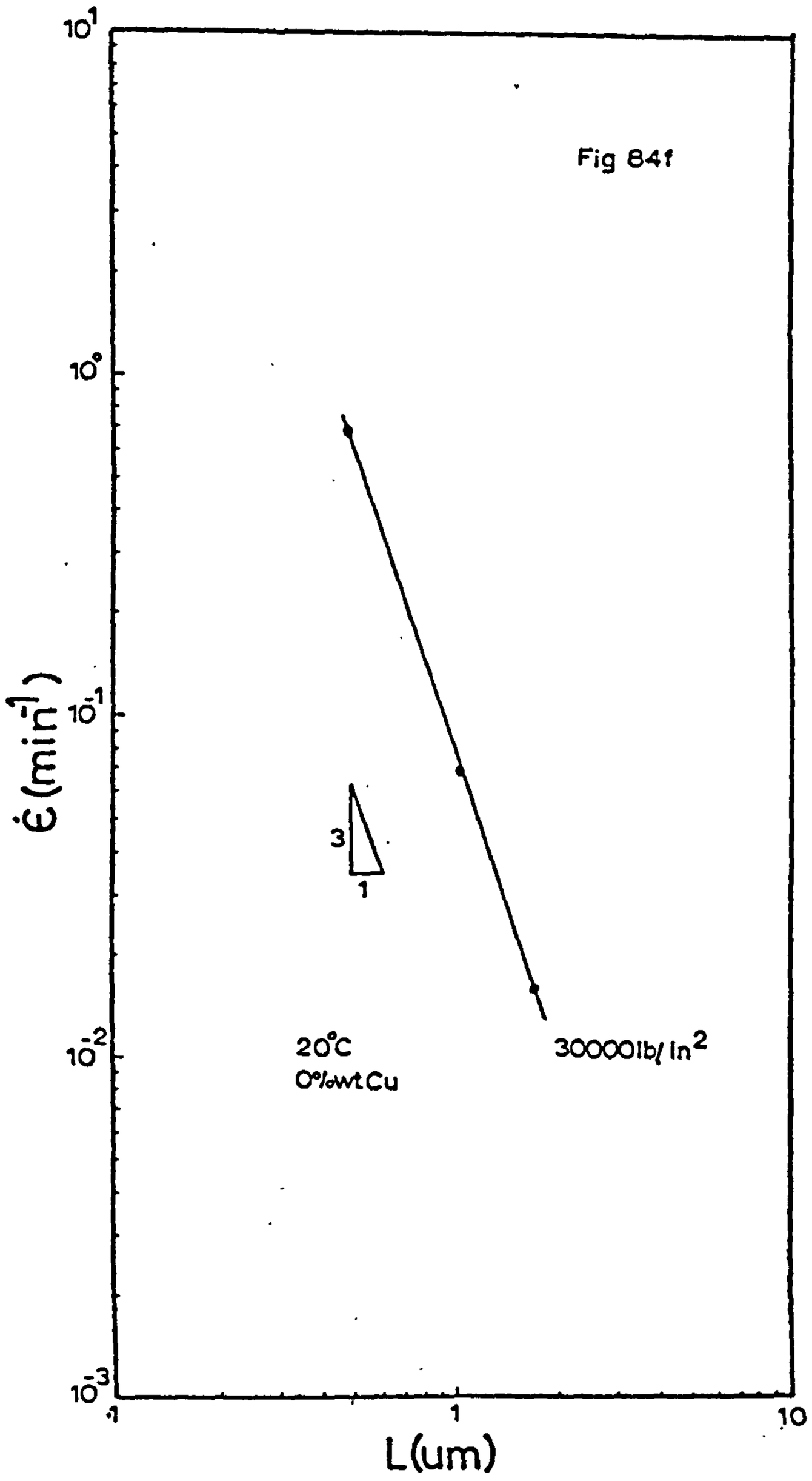

Figure 84e-f- Plots of vs L at various constant stresses for the temperature range 50 and 20°C. The slope of the curves are indicated.

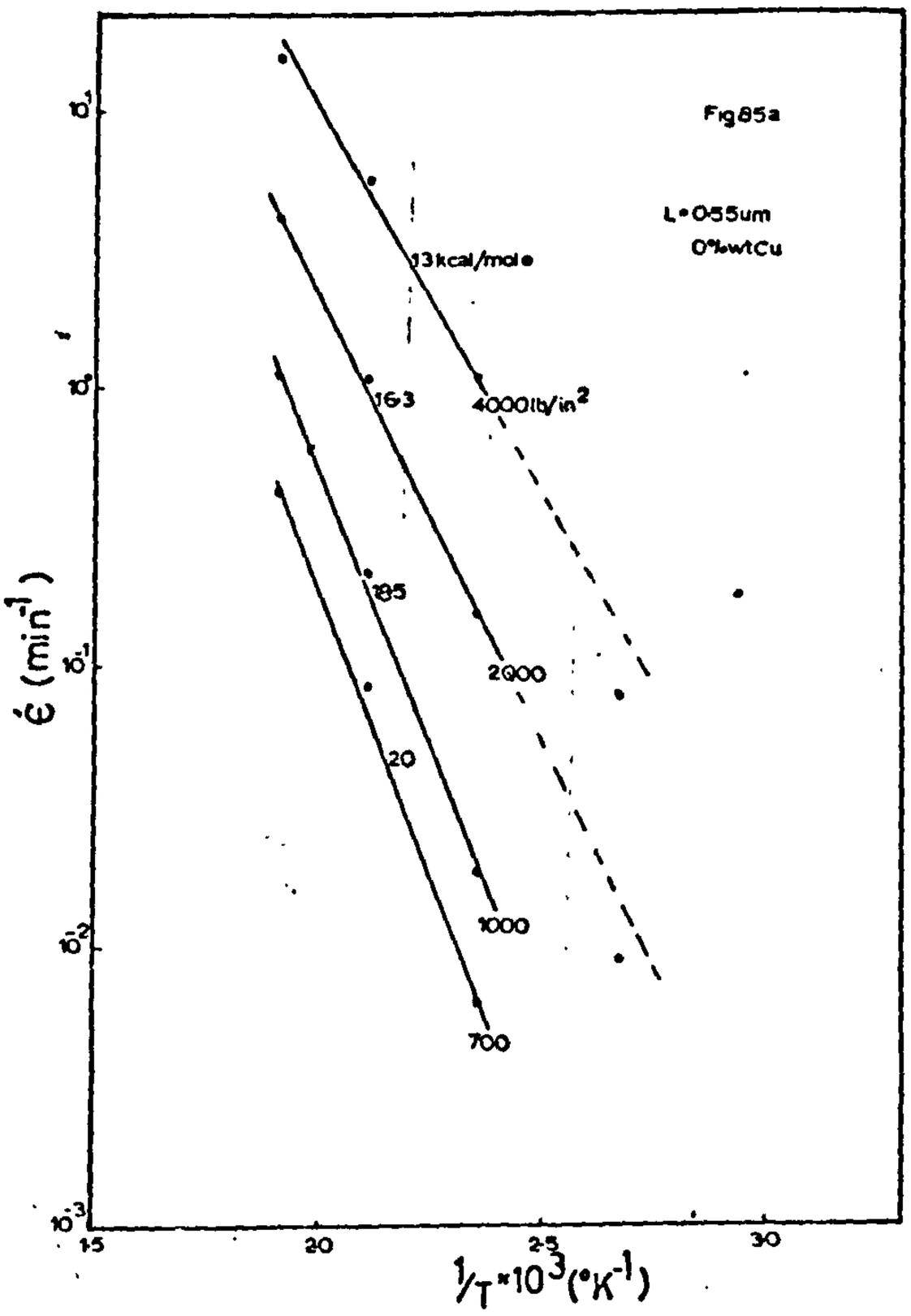

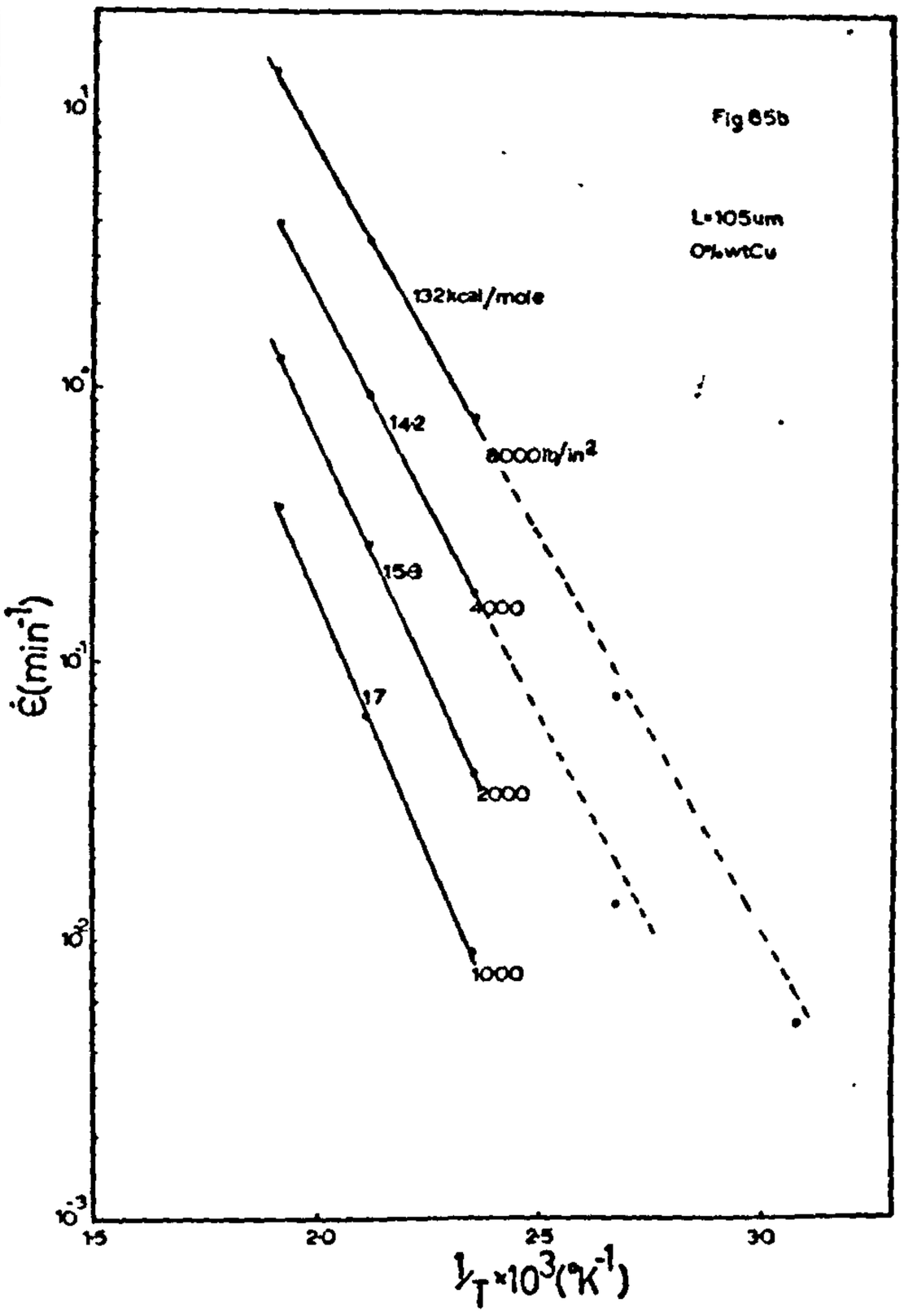

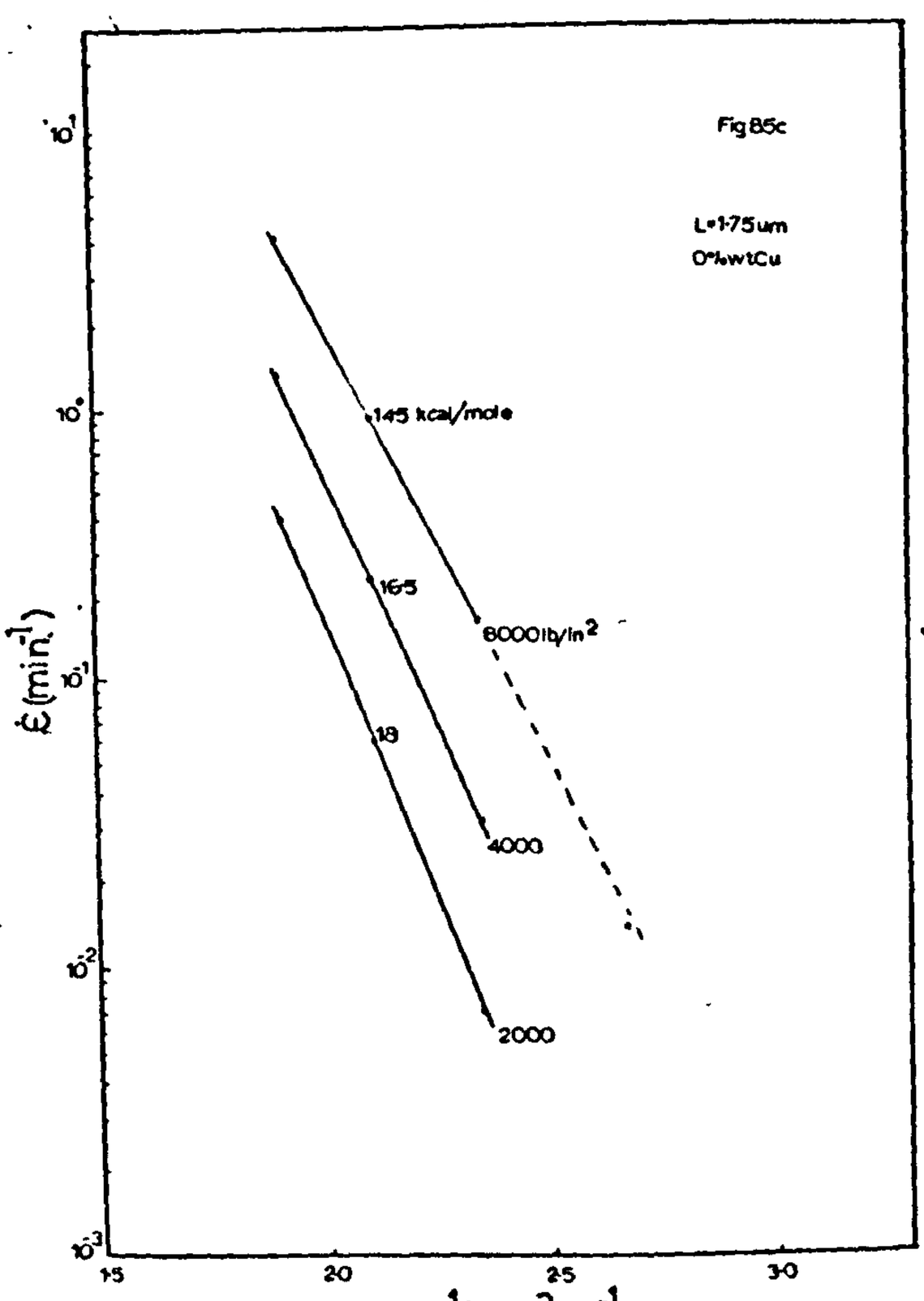

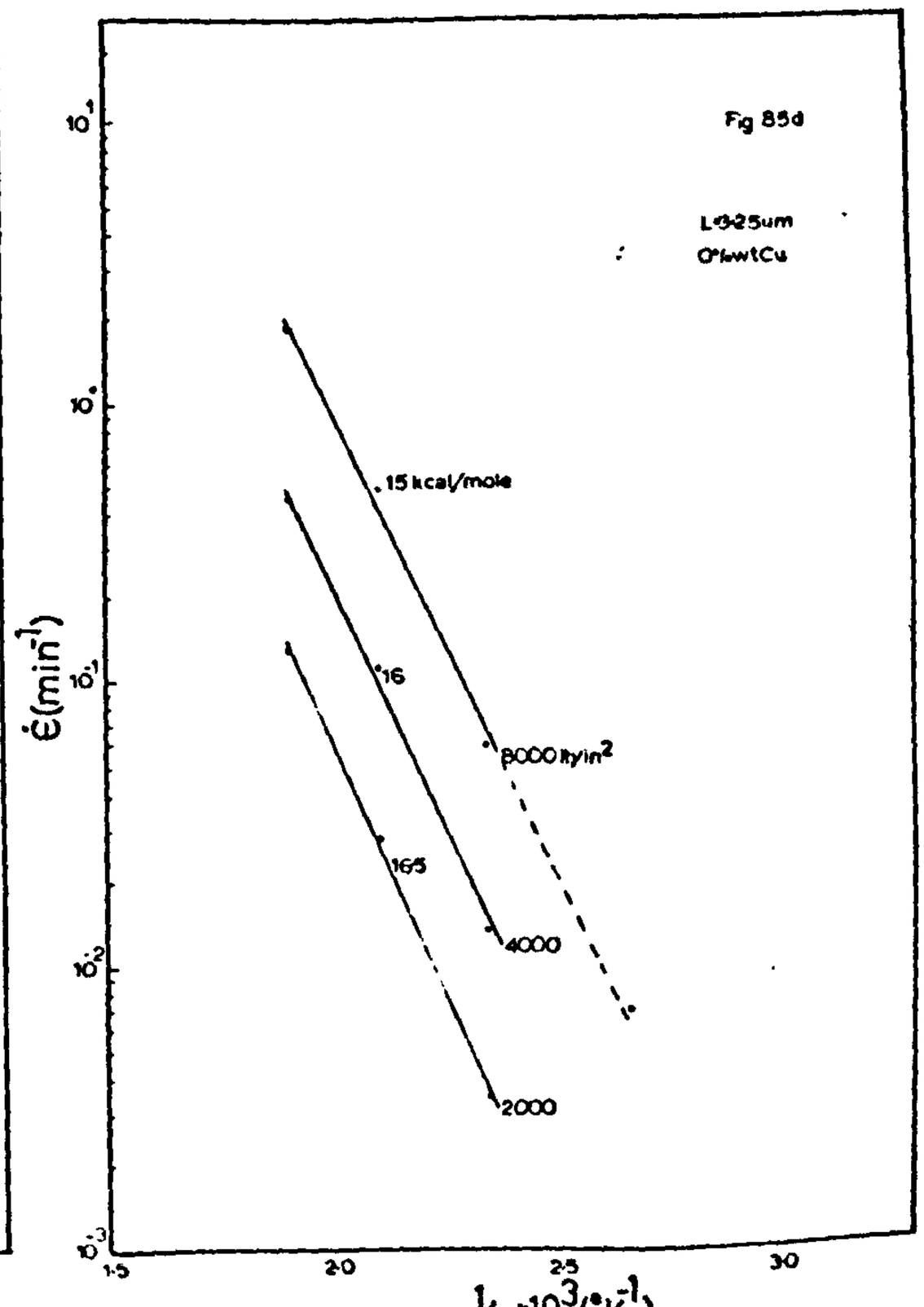

Figure 85a-d - The activation energy determined from the slope of the $\dot{\epsilon}$ vs 1/T curves at constant stresses for the temperature range 150 to250°C. L=0.55,1.05,1.75 & 3.25um.

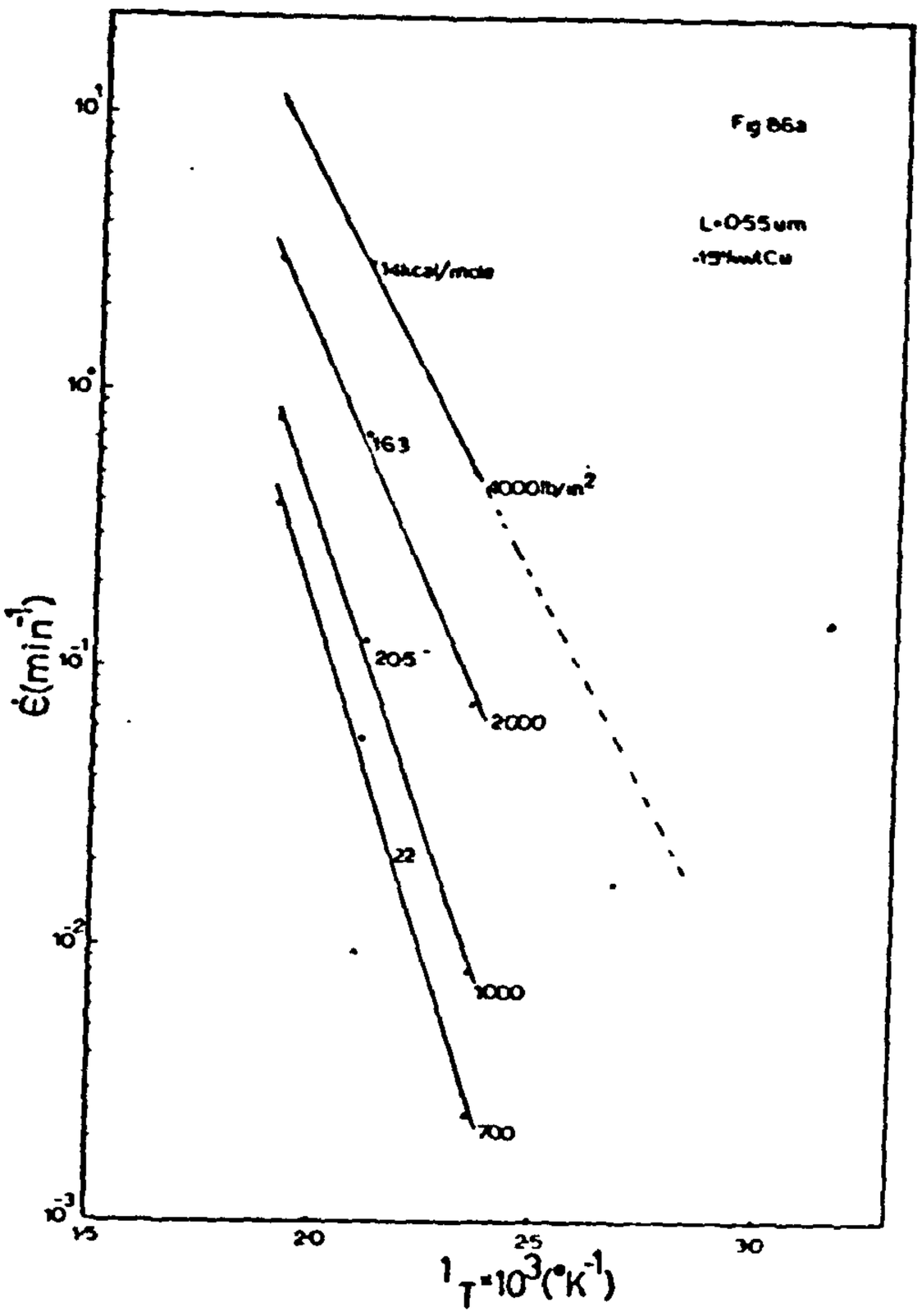

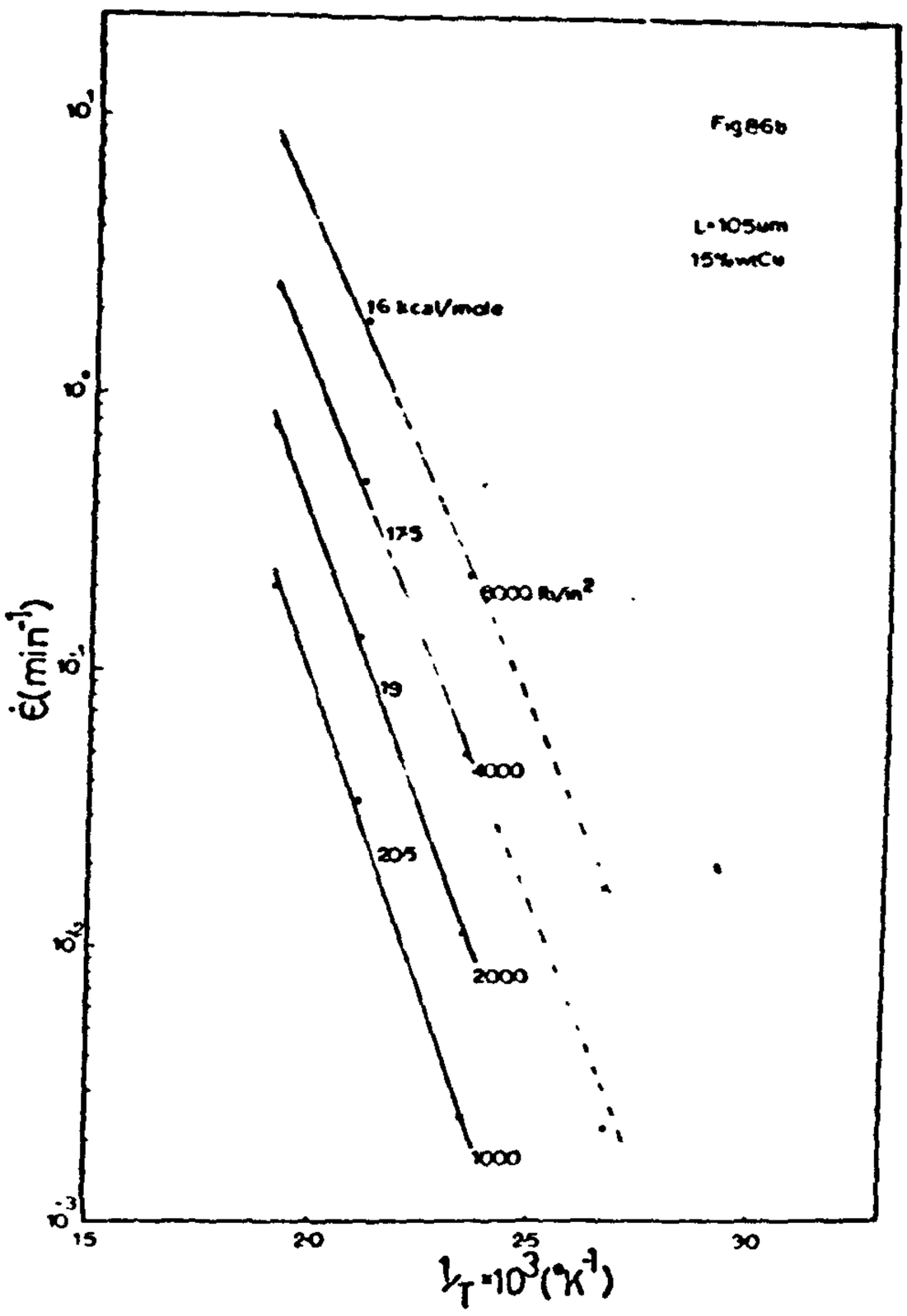

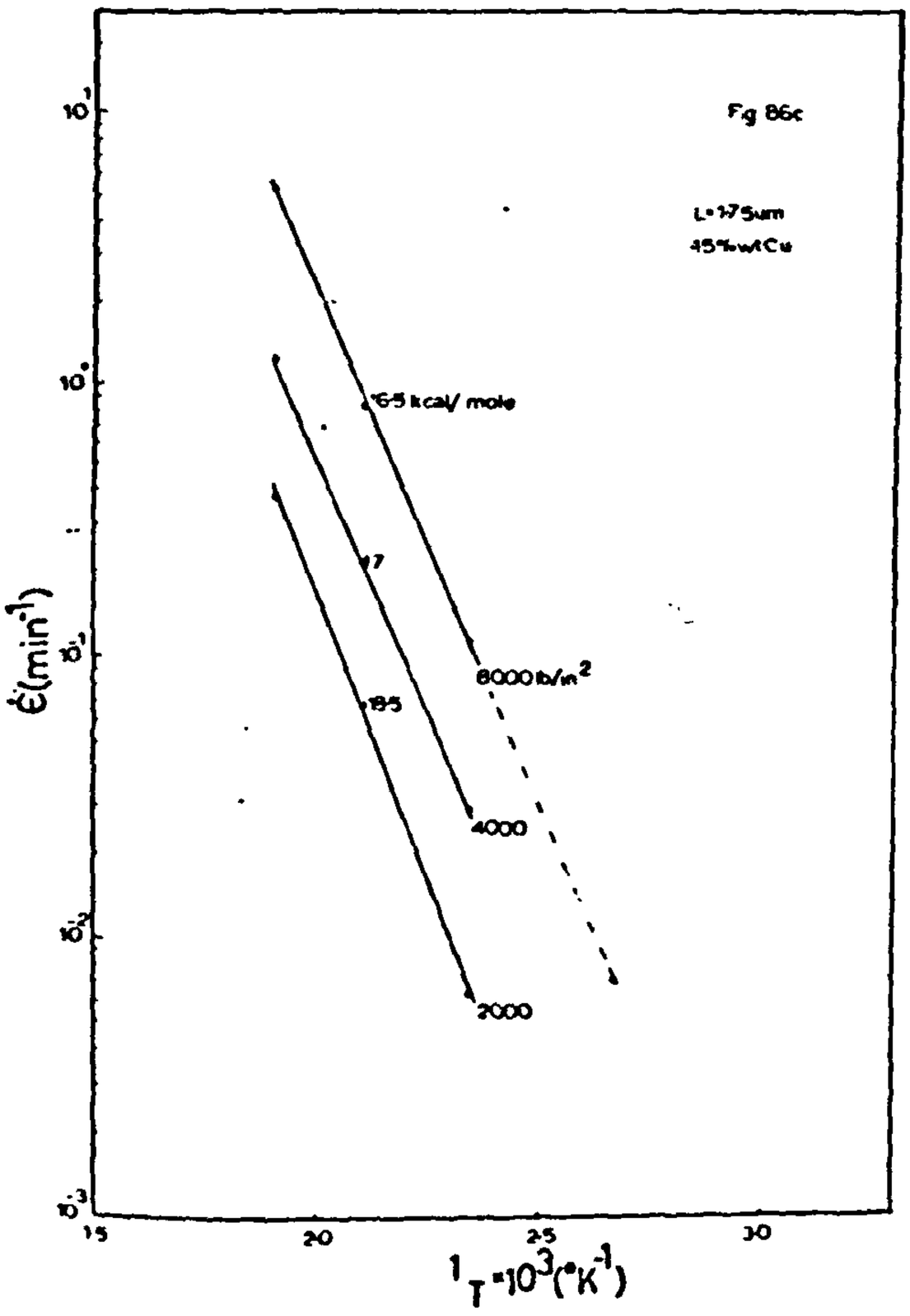

Figure 86a-c - The activation energy determined from the slope of $\dot{\epsilon}$ vs 1/T at constant stresses for the temperature range 150 to 250°C. L=0.55, 1.05 and 1.75 um.

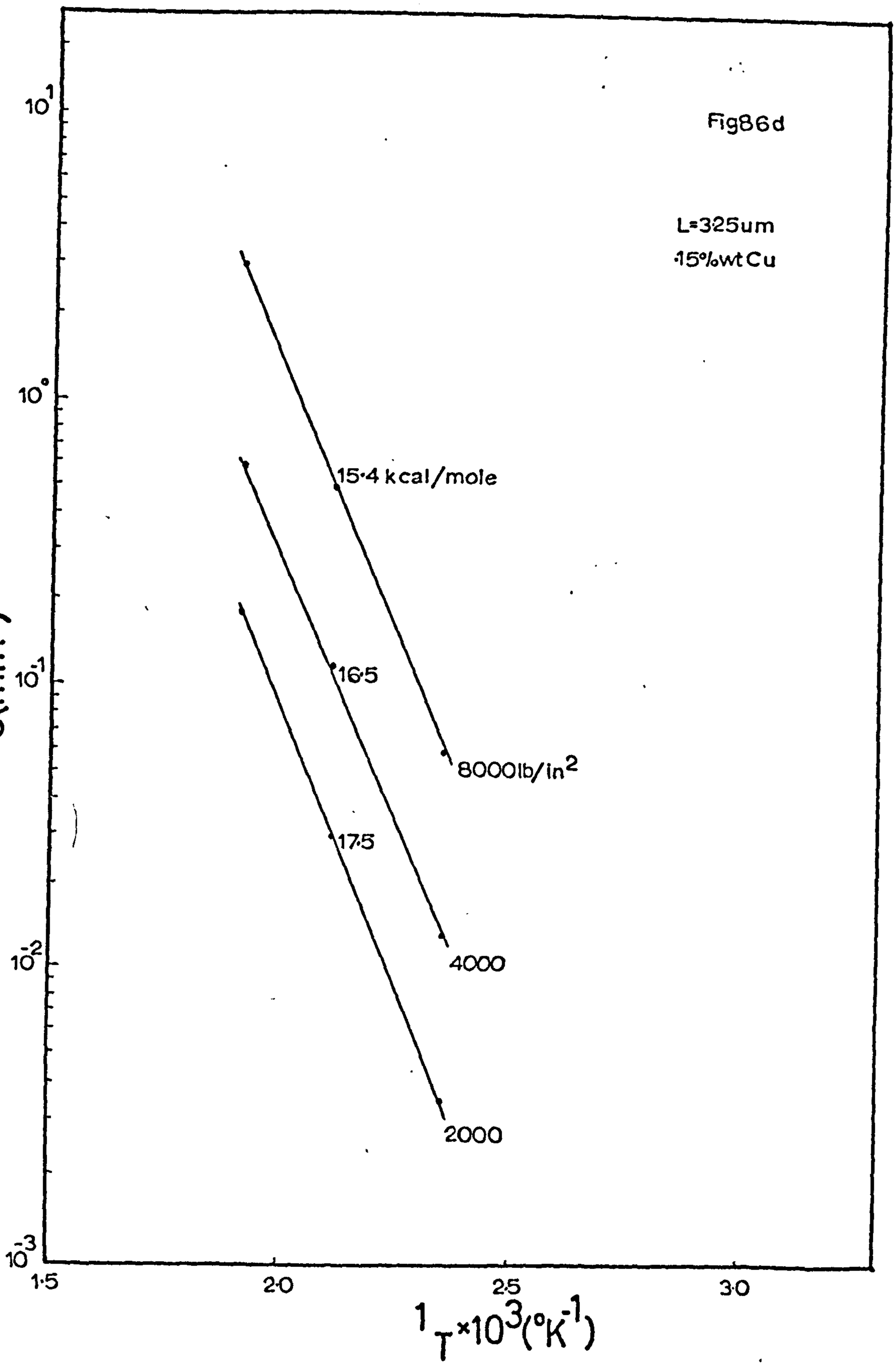

Figure 86d - The activation energy determined from the slope of $\dot{\epsilon}$ vs 1/T curves at constant stresses for the temperature range 150 to 250°C.

L=3.25um.

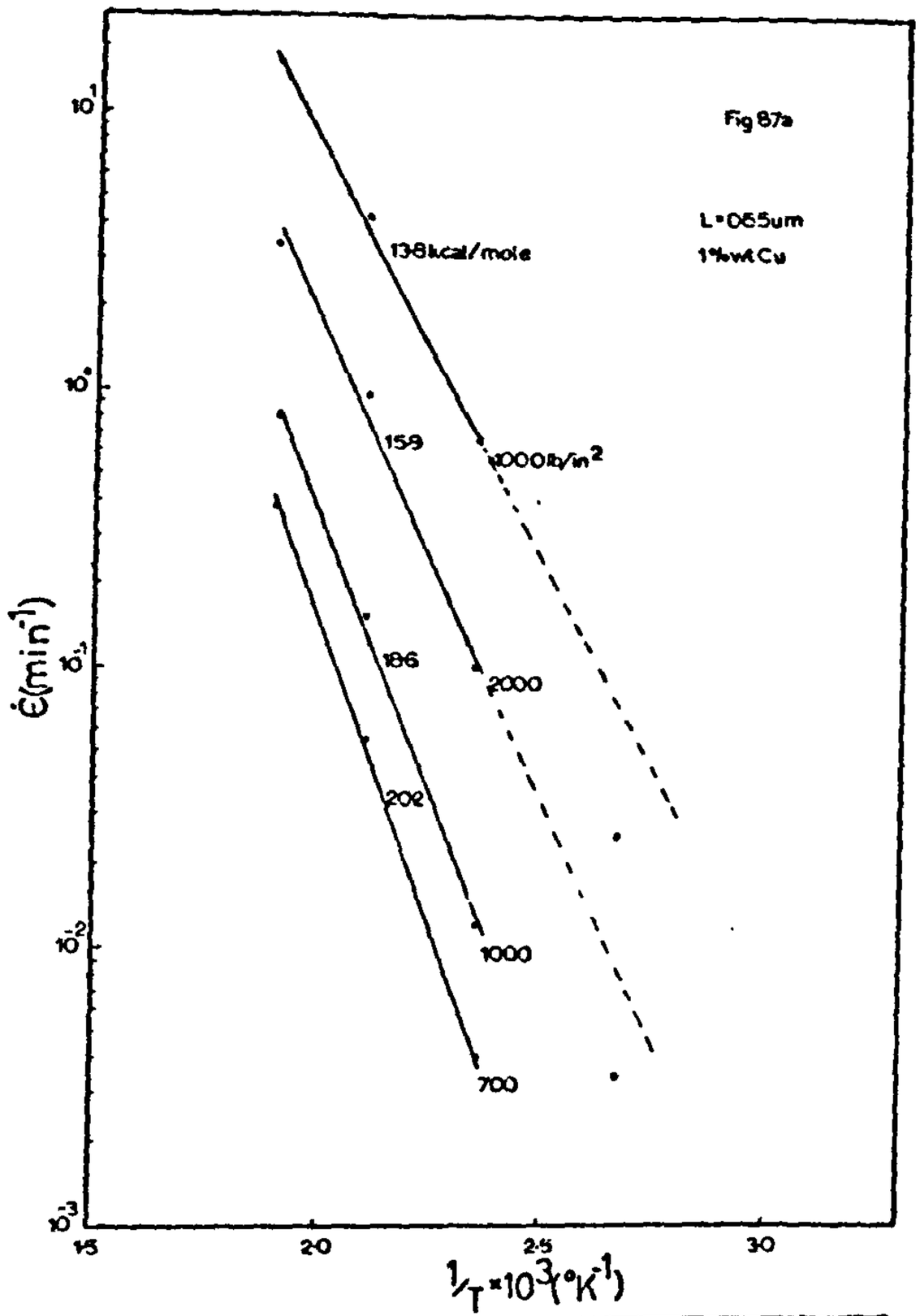

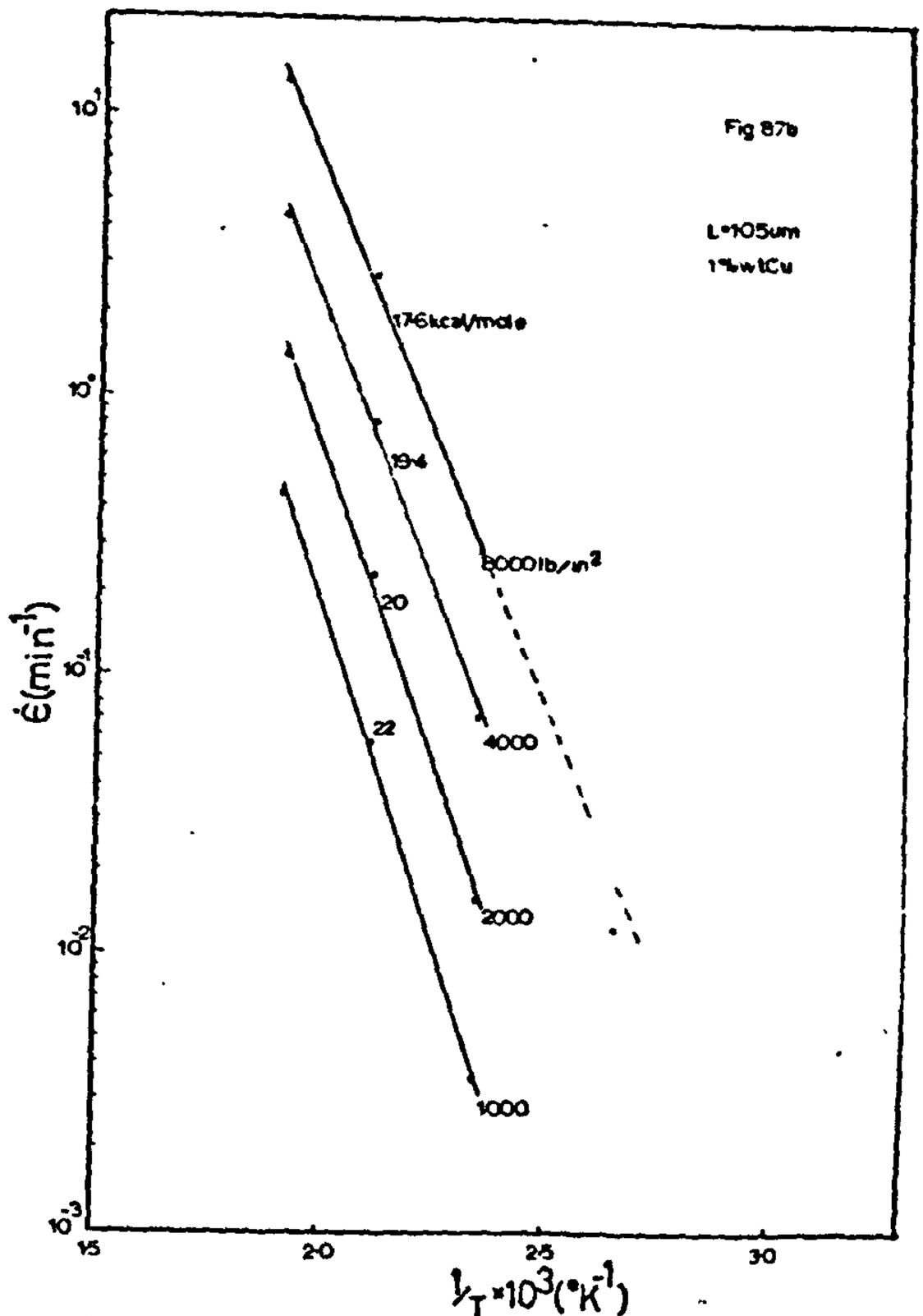

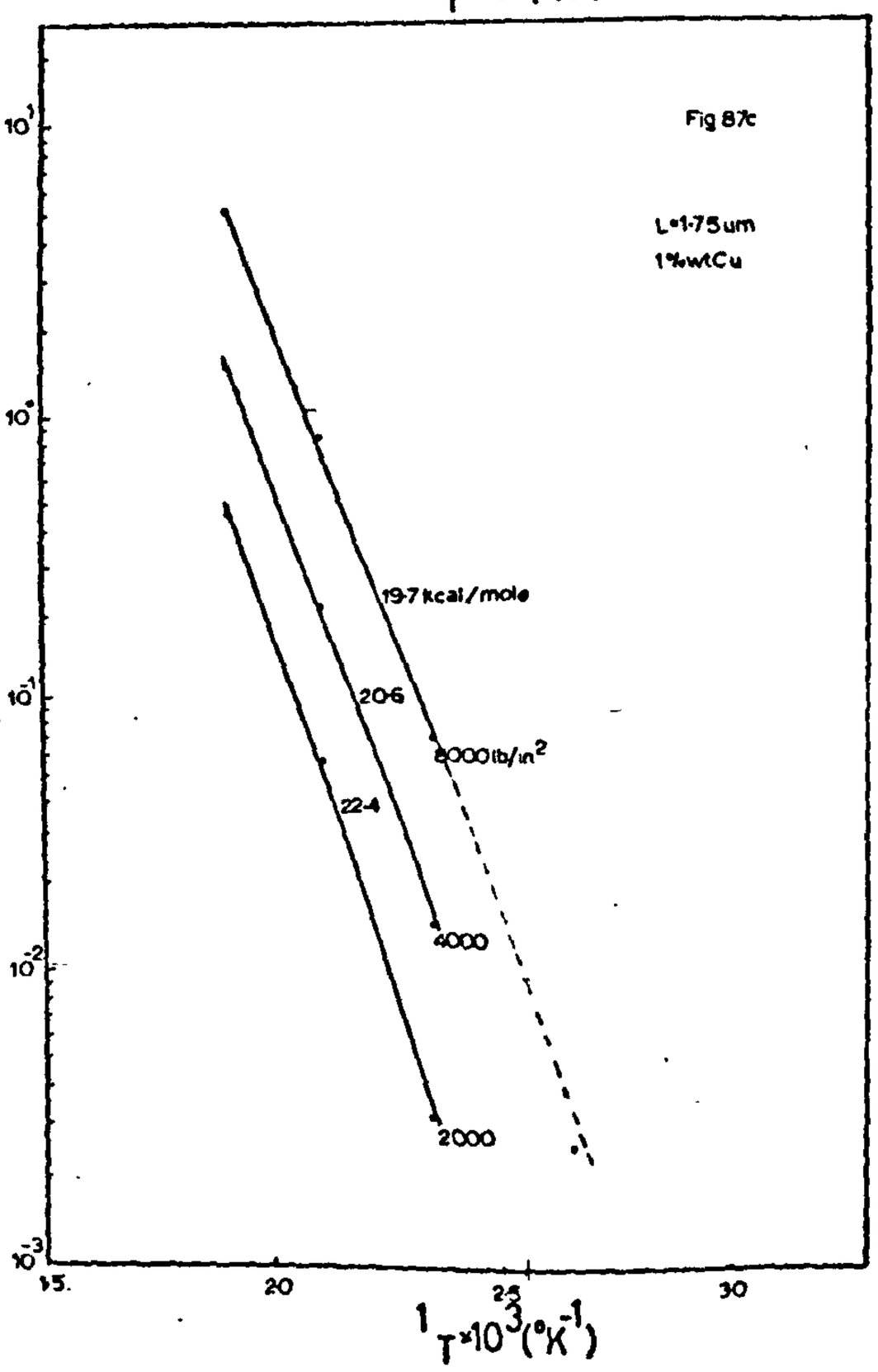

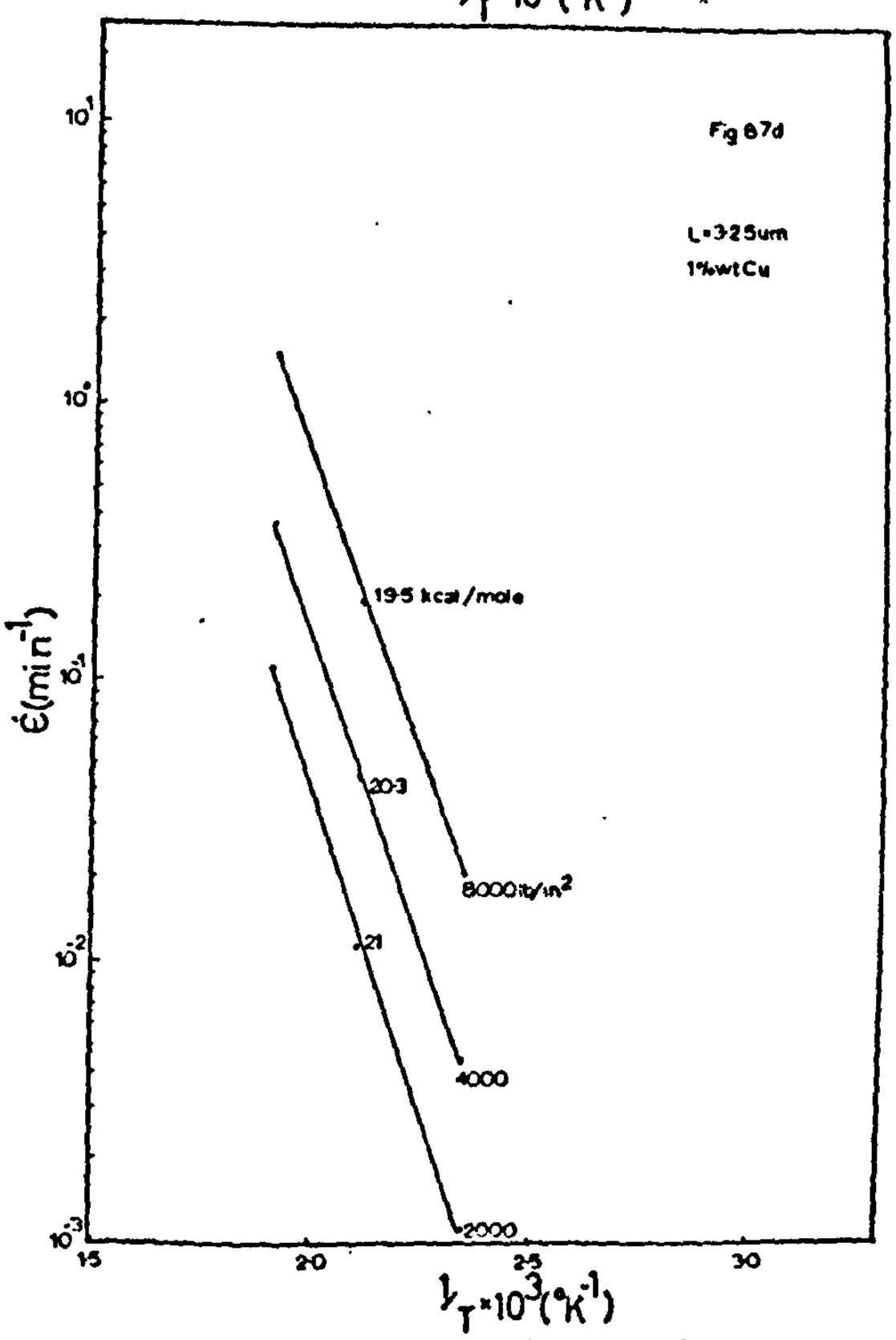

Figure 87a-d - The activation energy determined from the slope of the $\dot{\epsilon}$ vsl/T curves at constant stresses for the temperature range 150 to 250°C. L=0.55,1.05,1.75 and 3.25um.

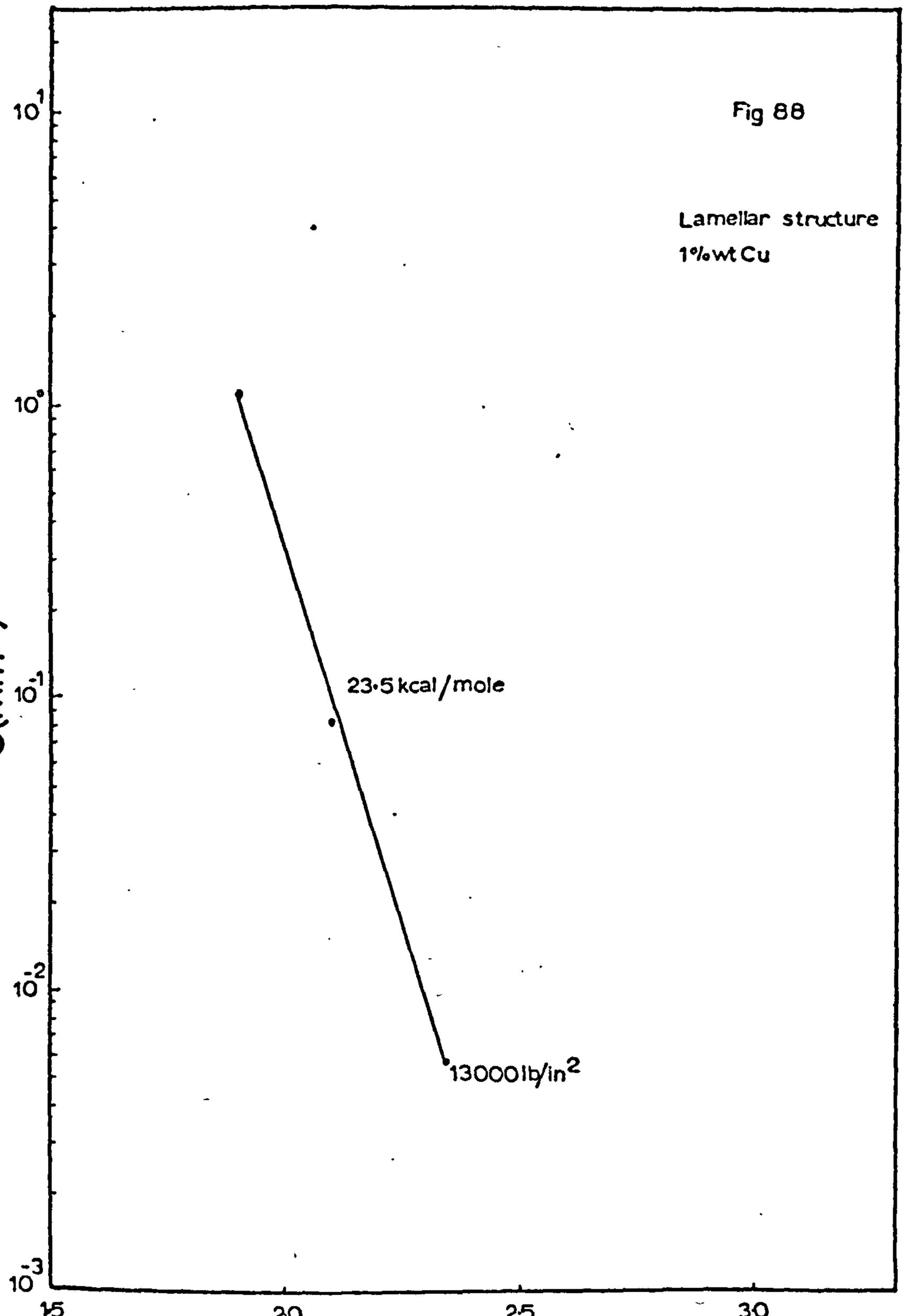

Figure 88 - The activation energy determined from the slope of the $\dot{\epsilon}$ vs 1/T curves for a lamellar structure alloy.

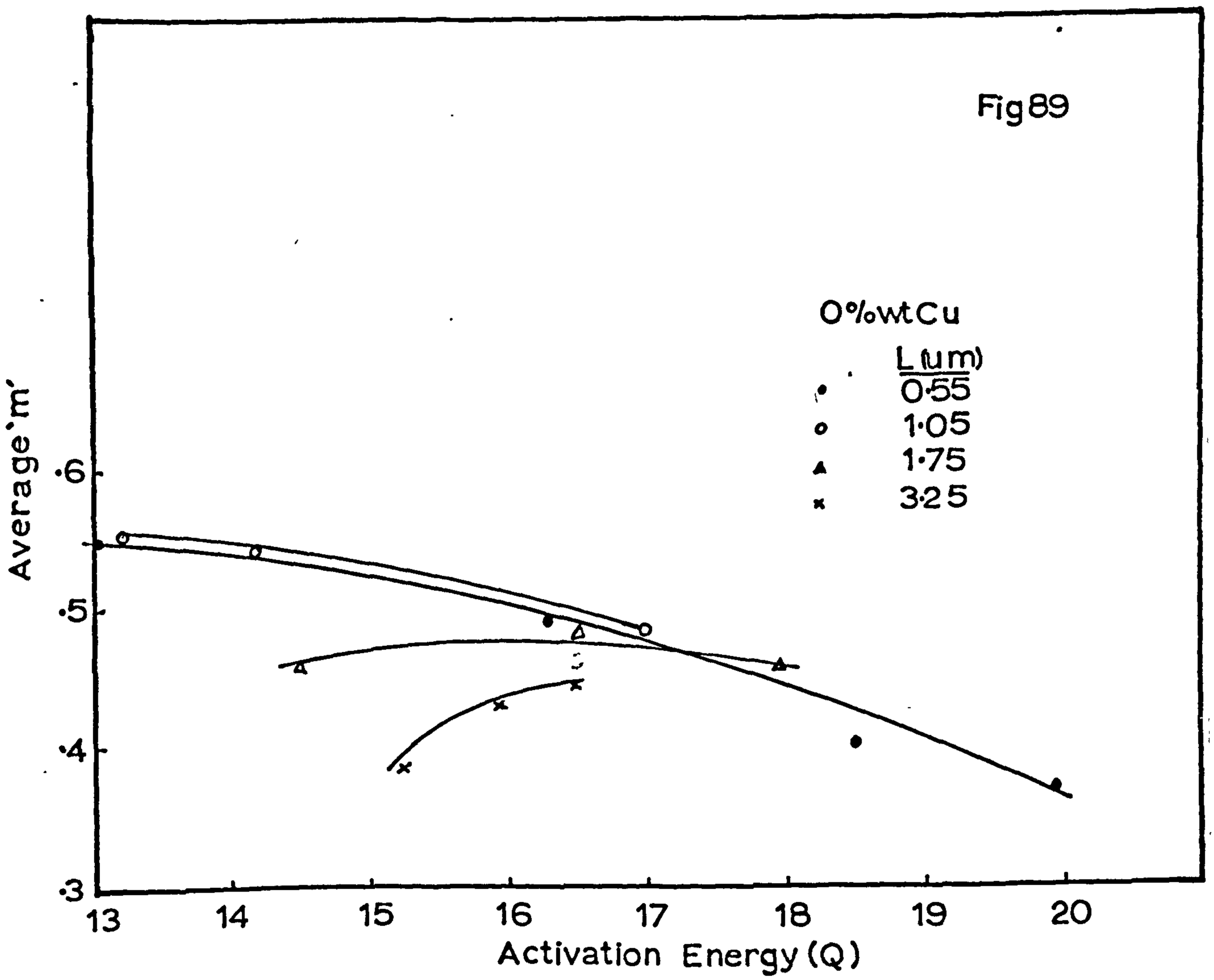

Figure 89 - The average 'm' versus activation energy relationship for the different grain size materials.

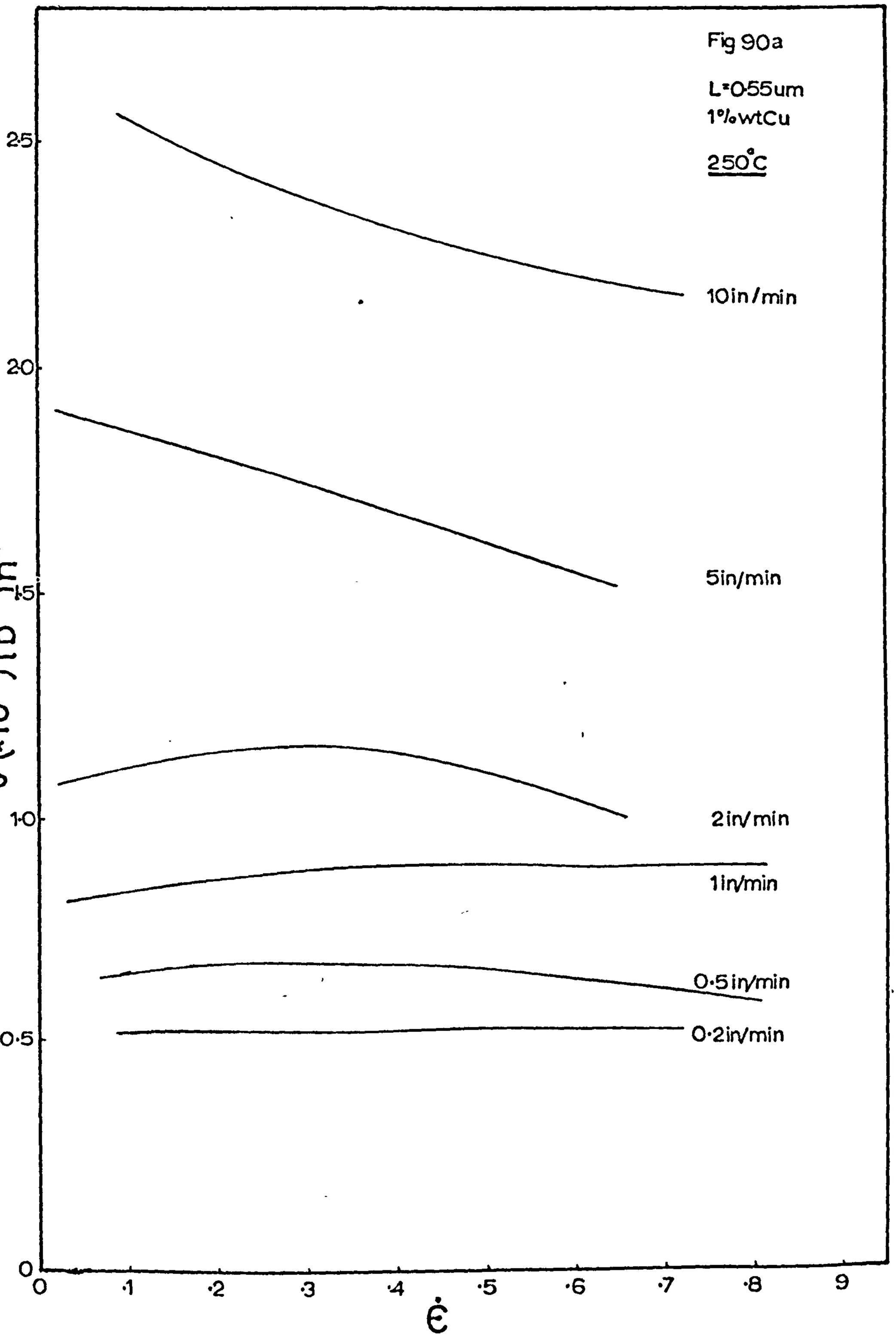

Figure 90a - Stress/strain curves determined for the 0.55um grain size alloy at 250°C.

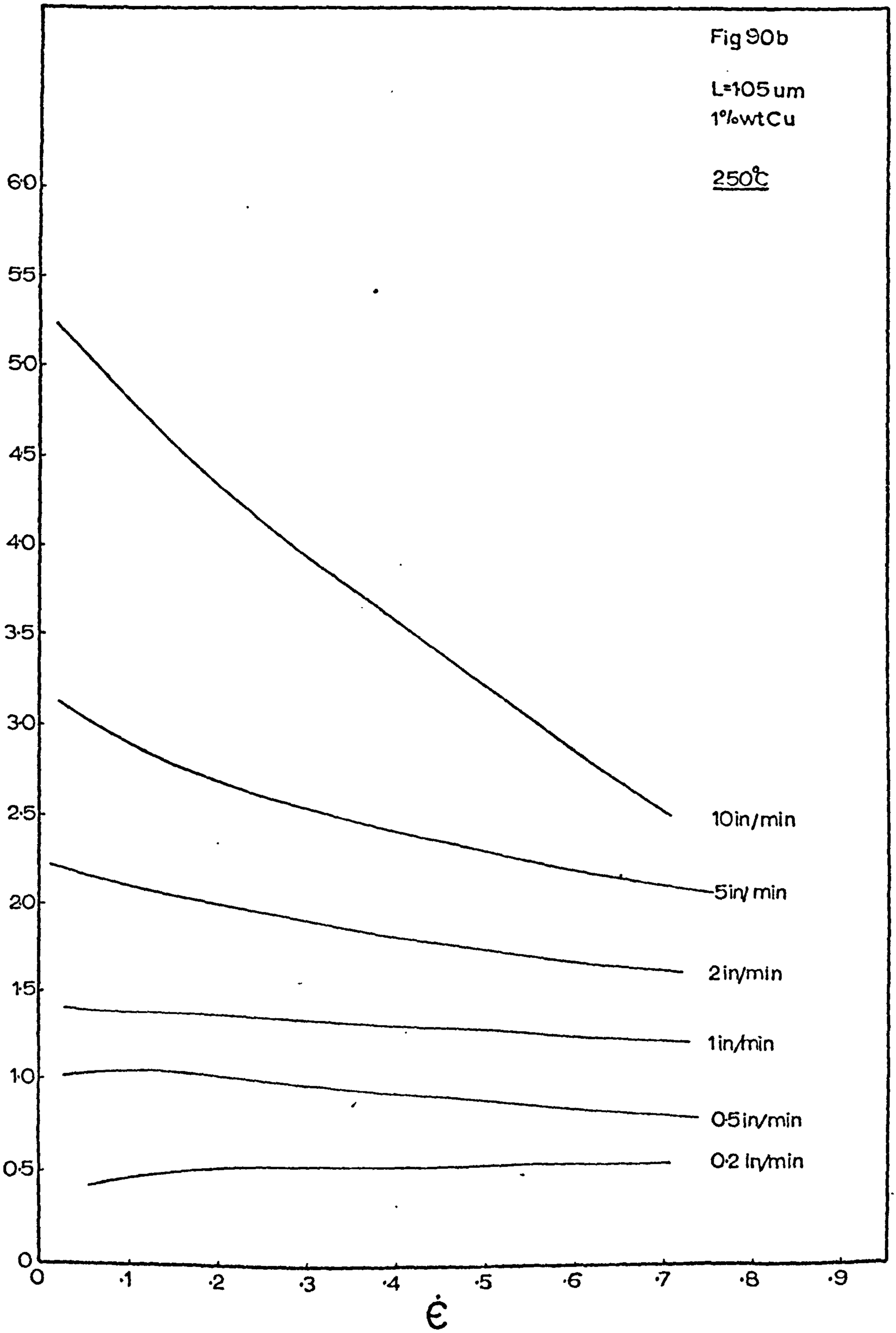

Figure 90b - Stress/strain curves determined for the 1.05um grain size alloy at 250°C.

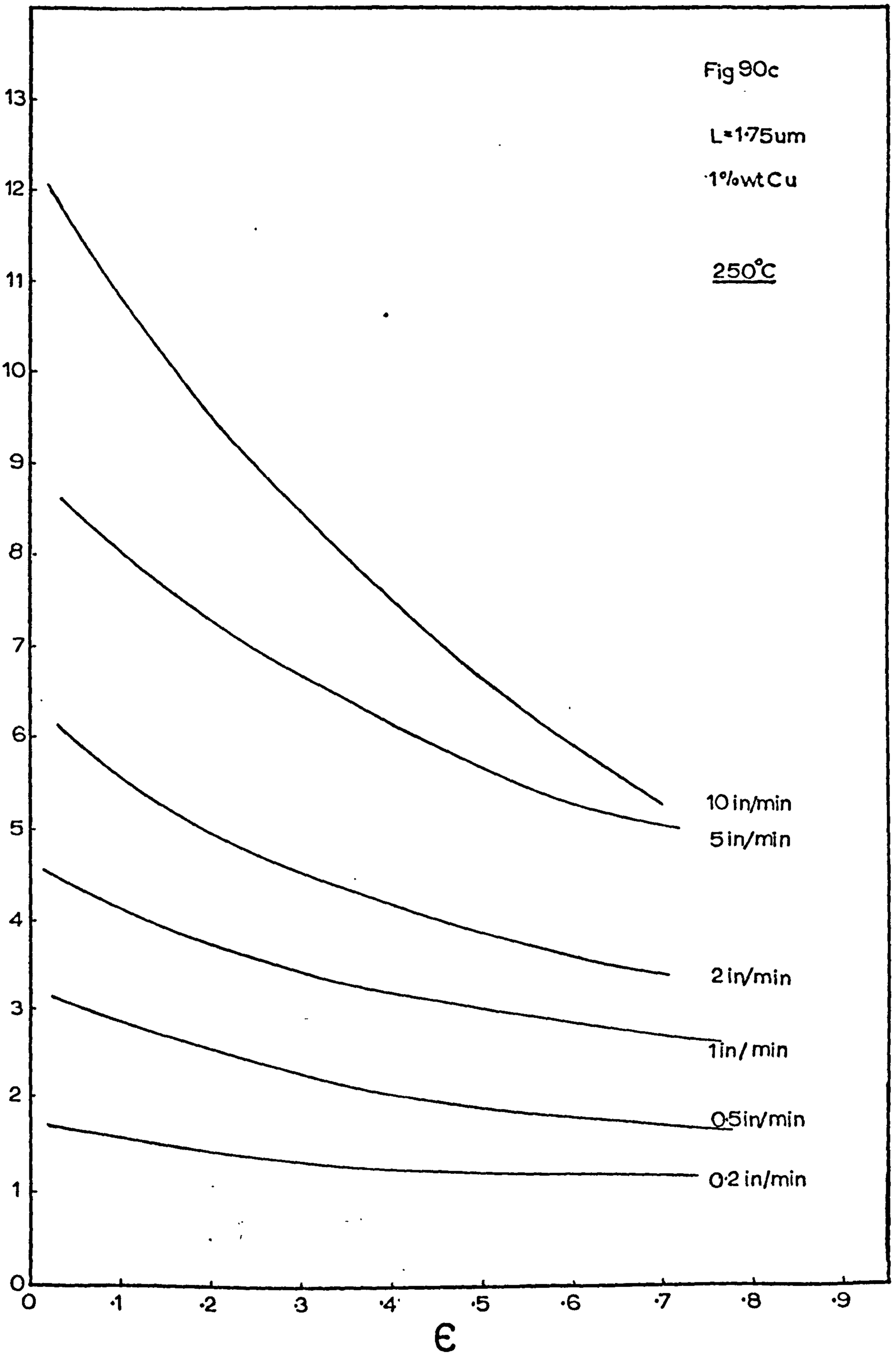

Figure 90c - Stress/strain curves determined for the 1.75um grain size alloy at 250°C.

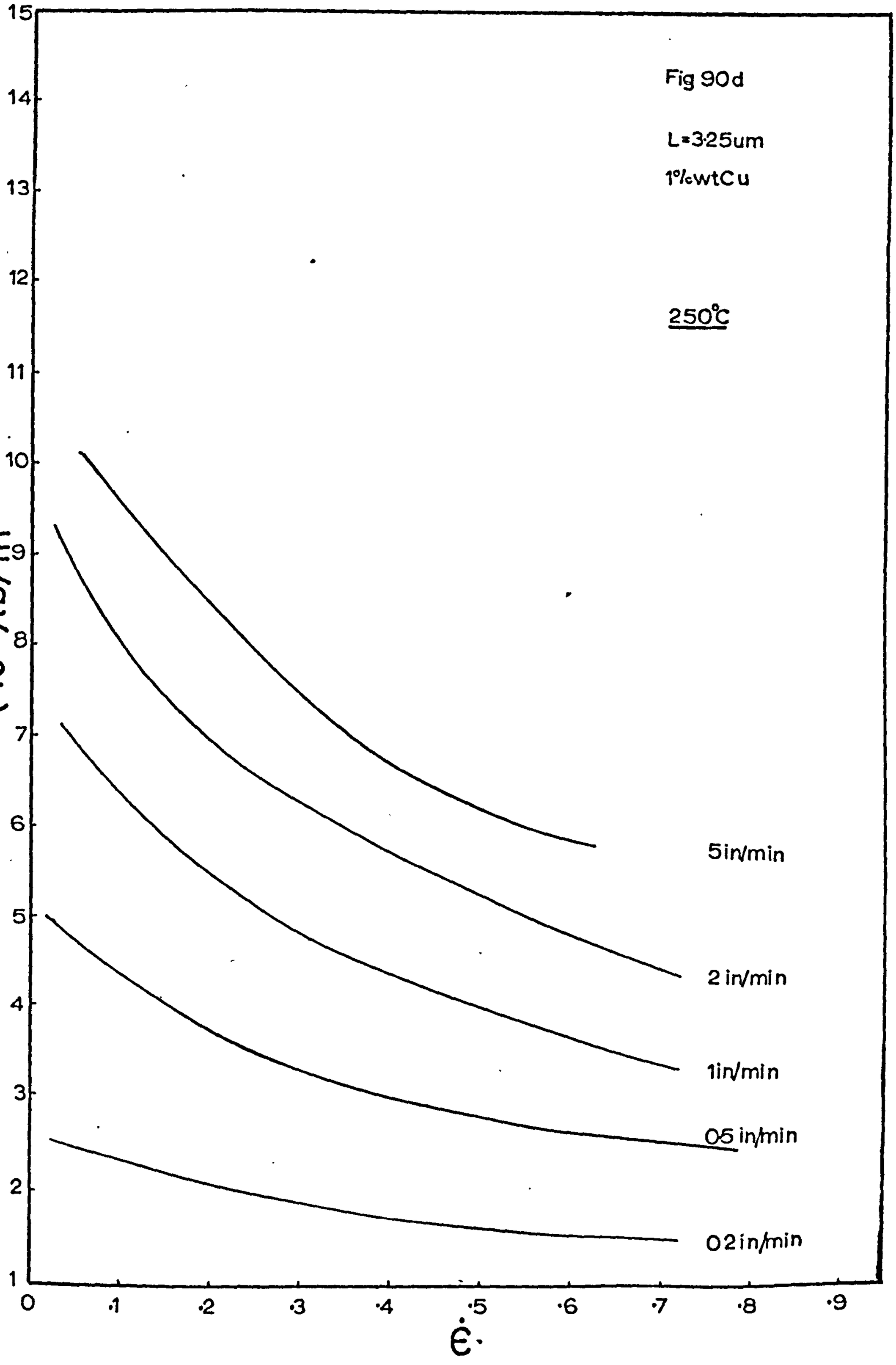

Figure 90d - Stress/strain curves determined for the 3.25um grain size alloy at 250°C.

Figure 91- Stress/strain-rate curves determined from the stress/strain curves(Figure 90).

Fig 91

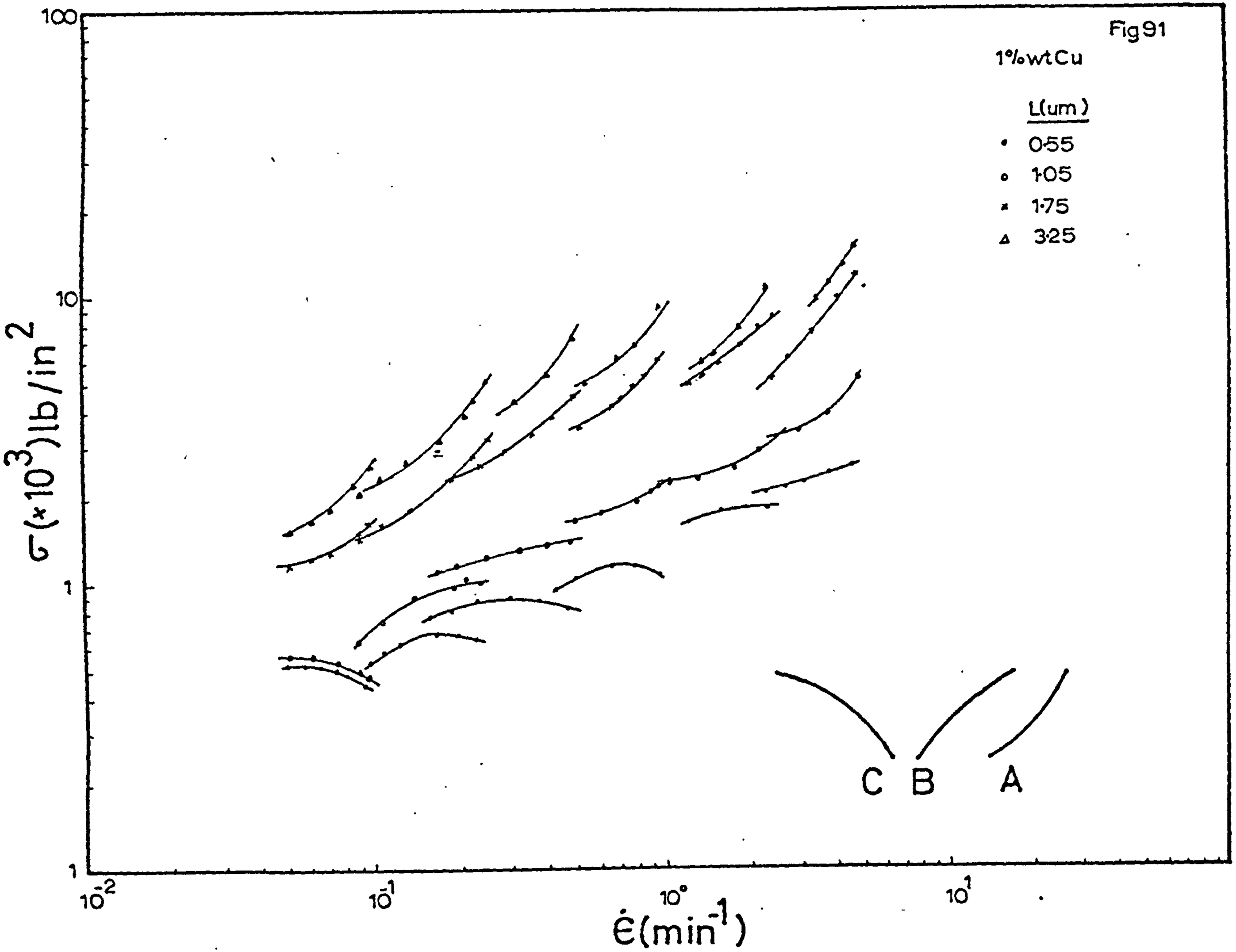
1%wtCu
L(um)
• 0·55
o 1·05
x 1·75
Δ 3·25
100
10
1
1
σ(*10^3)lb/in^2
10^-2
10^-1
10^0
10^1
Ė(min^-1)
C B A

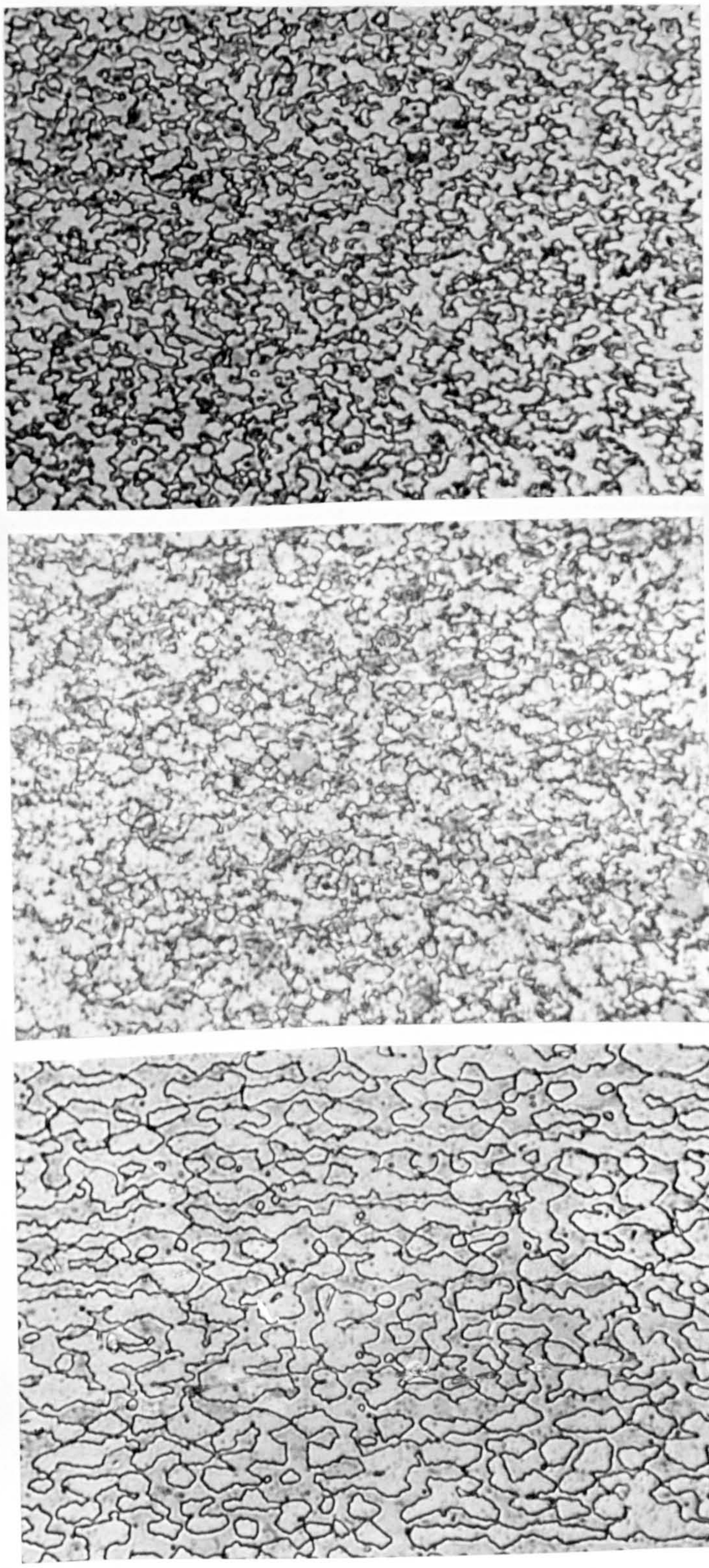

800%
1.05um

400%
1.75um

100%
3.25um

Figure 92a- Specimens strained to fracture at 250°C and at a crosshead velocity of 20 in/min. (xlooo). Longitudinal Section.

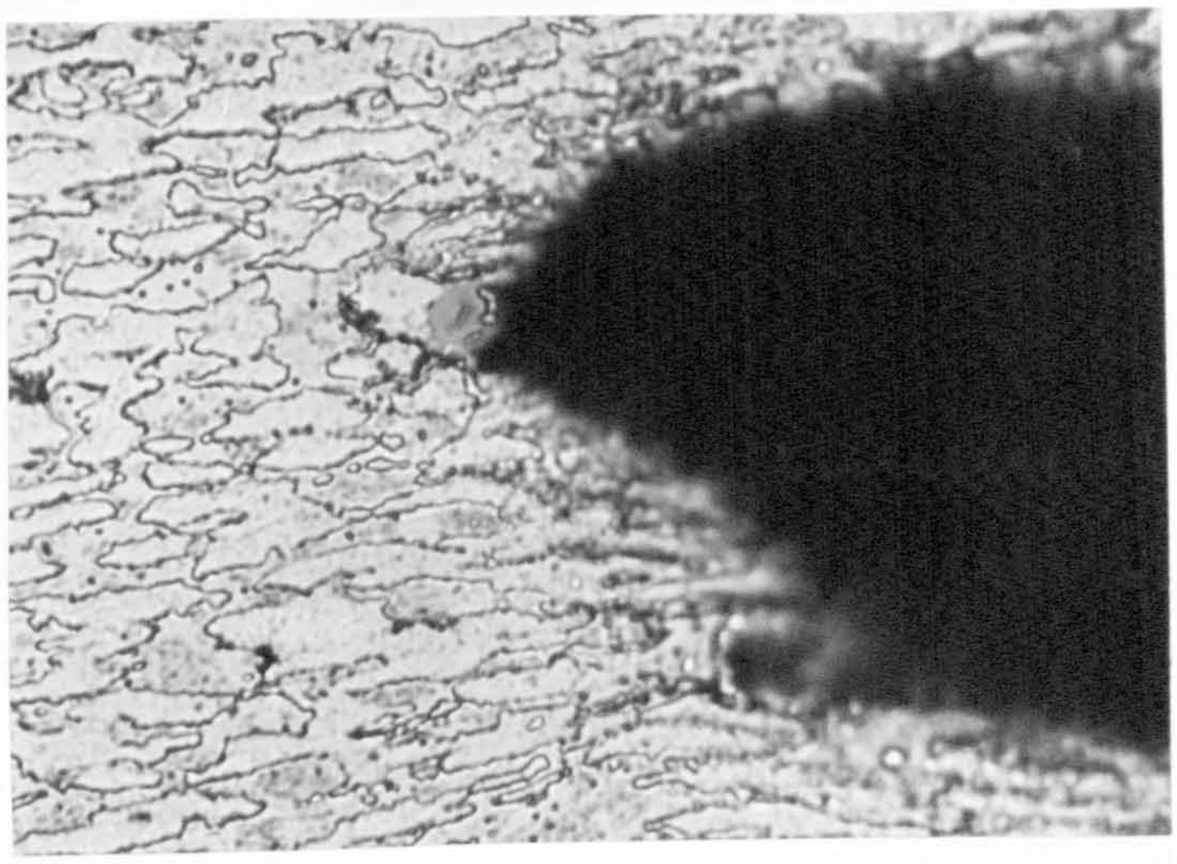

100%
3.25um

Figure92a- Shows the fracture edge of the 3.25um grain size specimen.(x1000). Longitudinal Section.

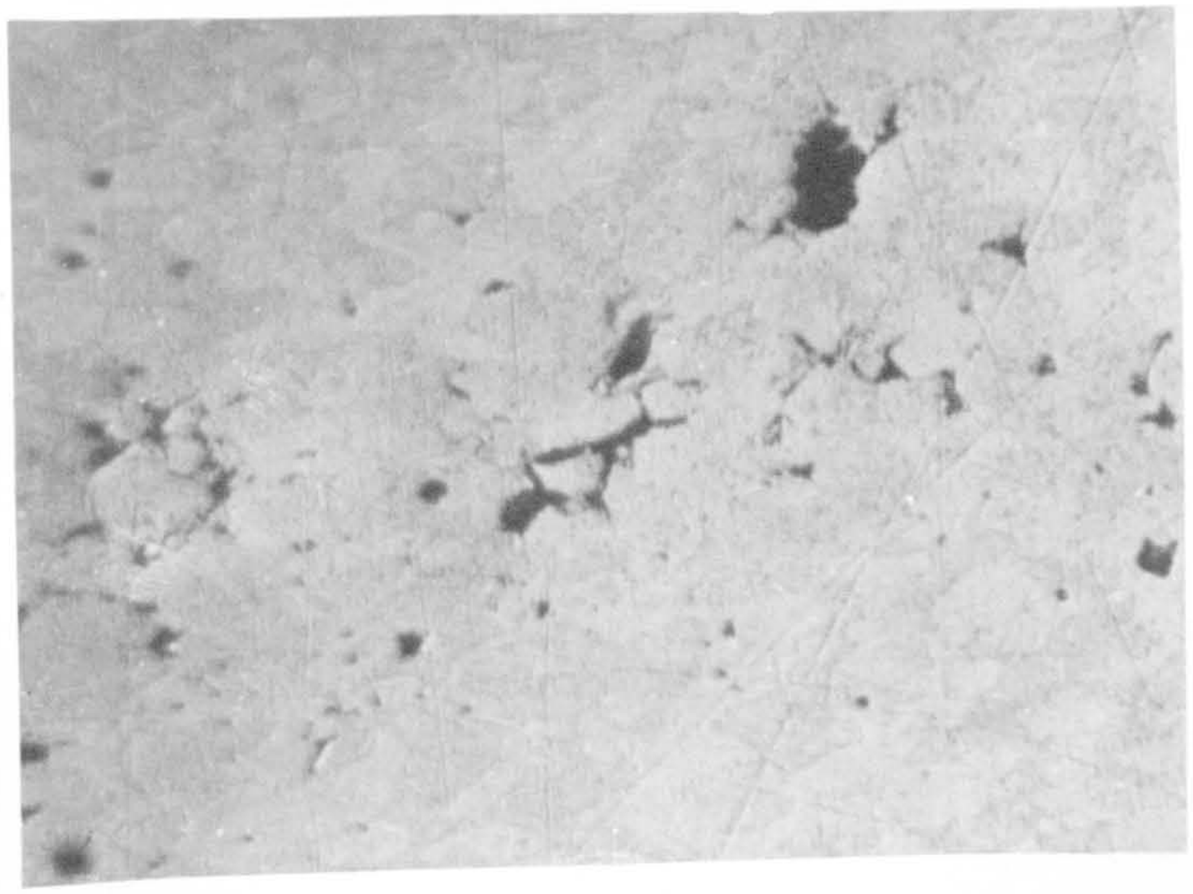

Figure 92a-Showing the cavities formed in the 3.25um grain size specimen which has been strained at 250°C and at the crosshead velocity of 20 in /min.(x1000). Longitudinal Section.

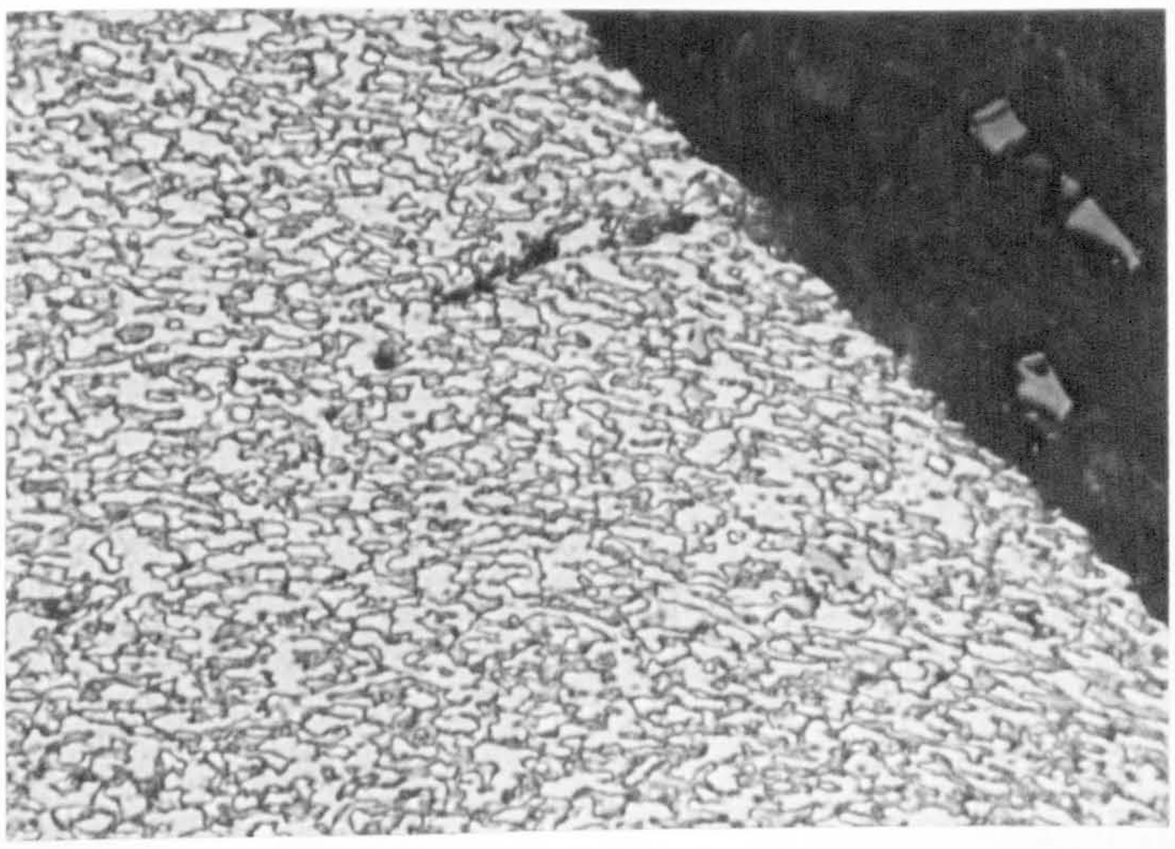

10%
1.05um

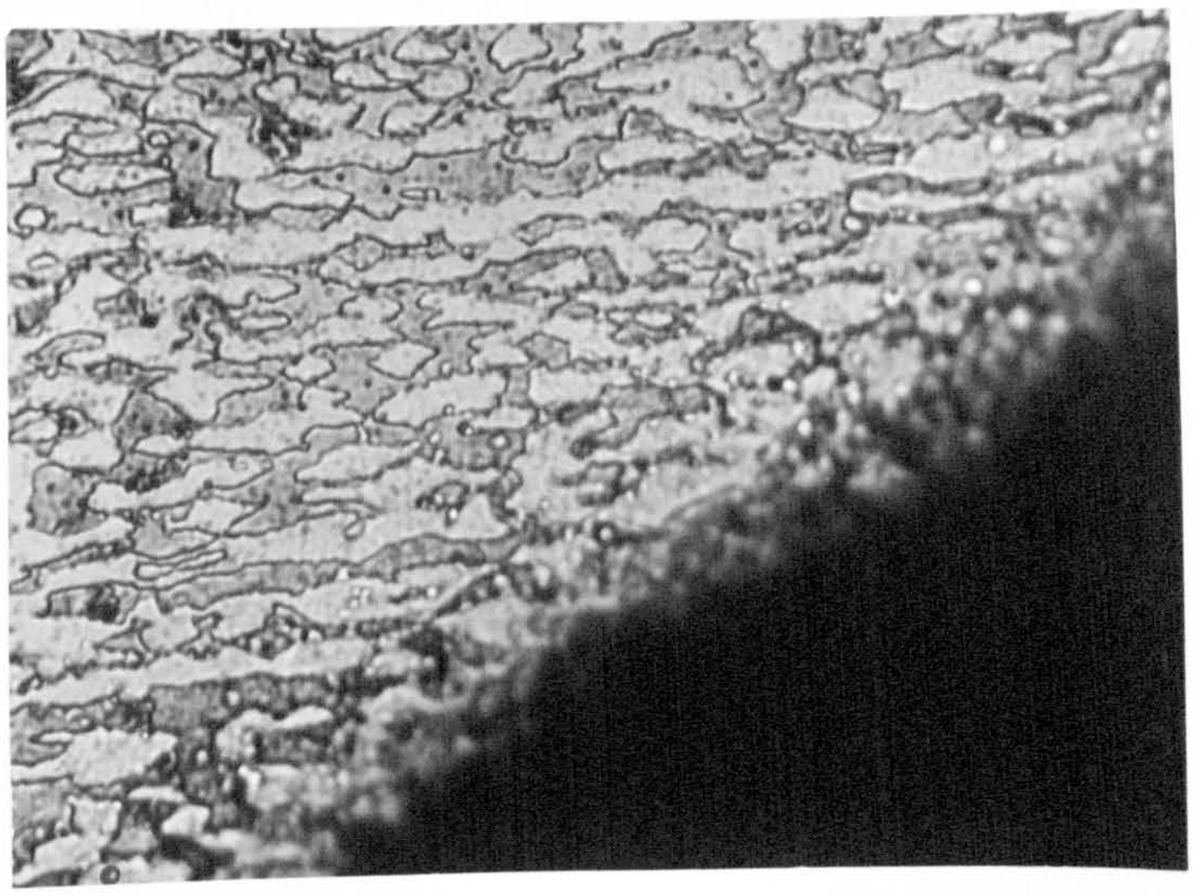

10%
3.25um

Figure 92c- Specimens strained to fracture at 20°C and at the crosshead velocity of 20 in/min. (x1000). LongitudinalSection.

Figure 93-The grid marked specimen showing regions strained different amount.

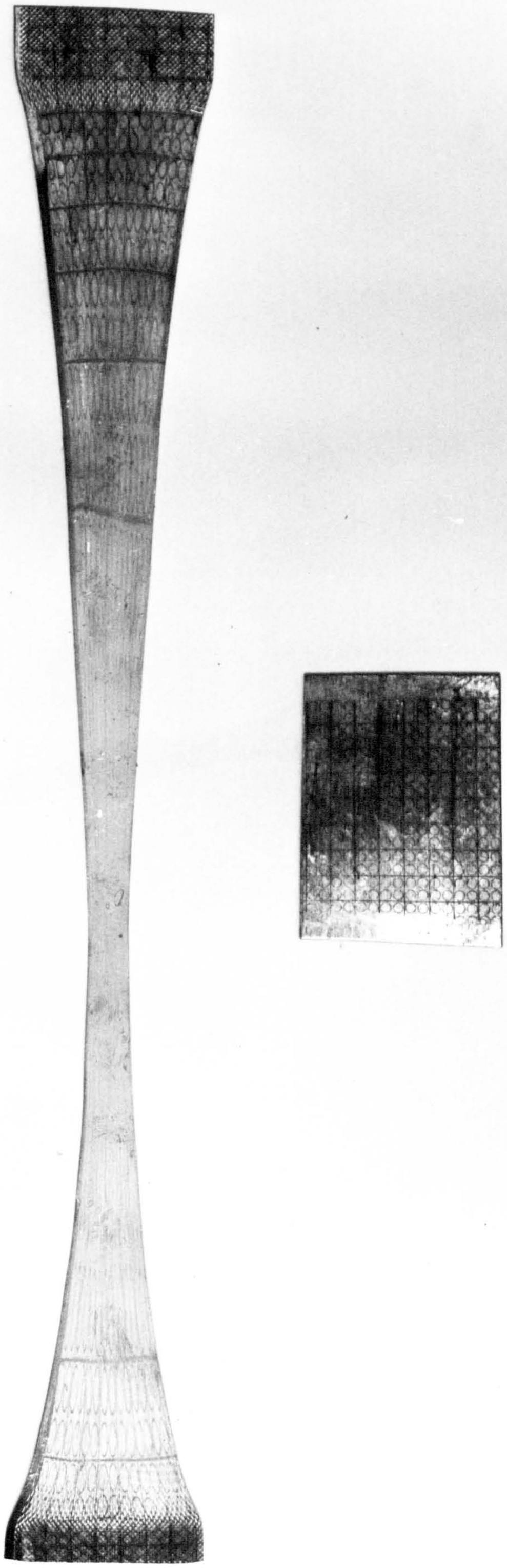

Figure 93

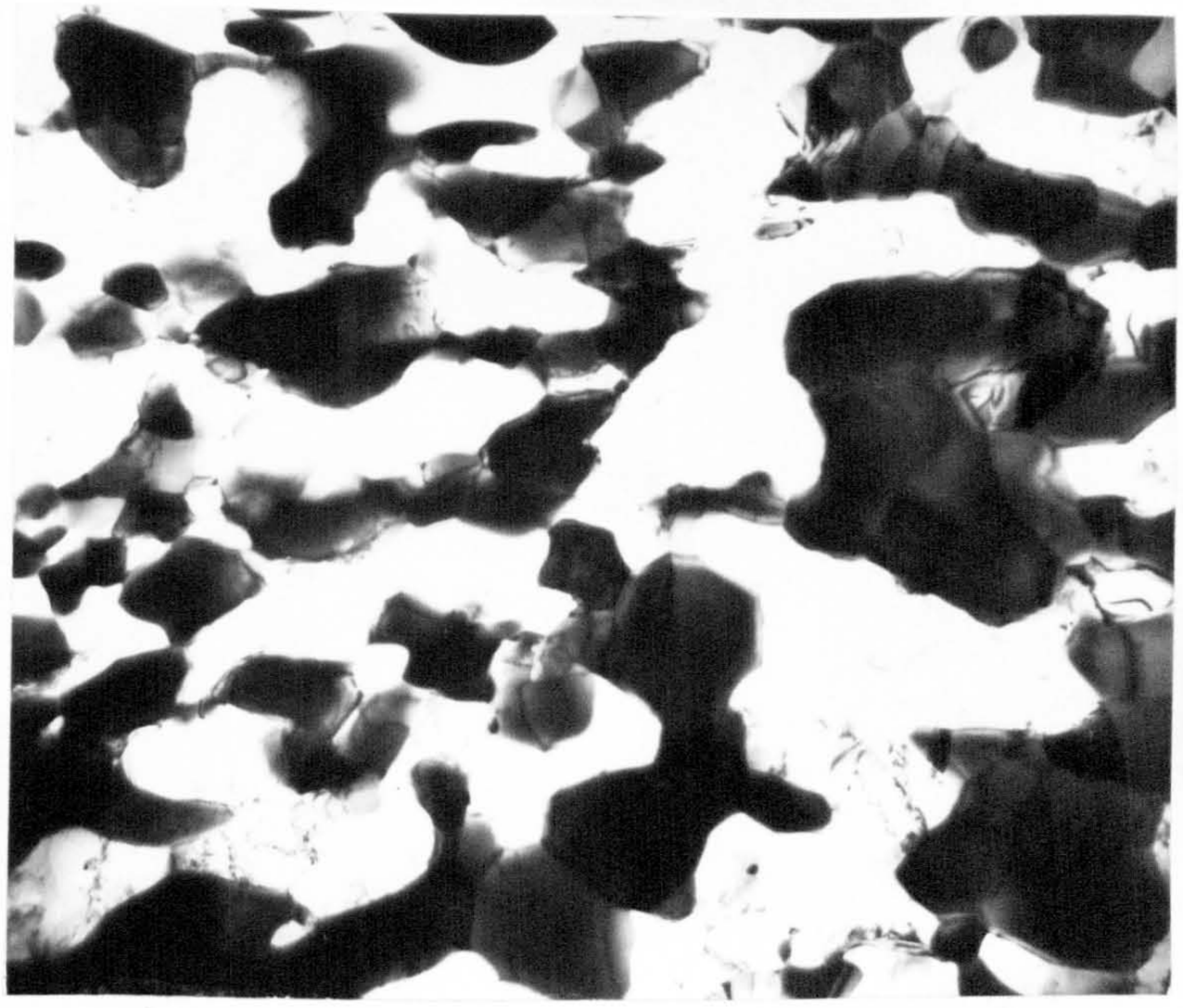

x12000

x20000

Figure 94-As received sheet.(TEM).

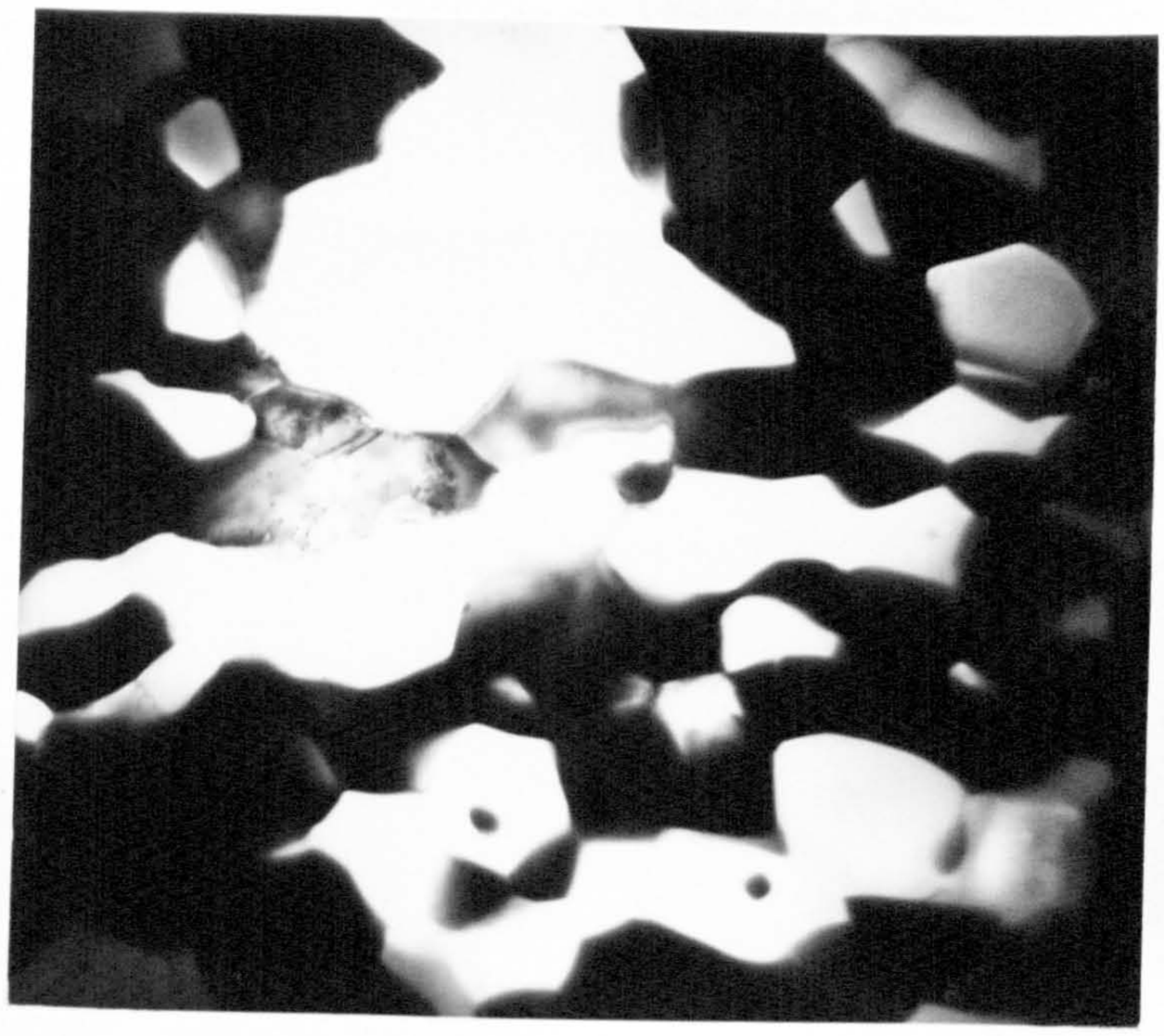

x12000

x30000

Figure 95a-Grip end of the specimen strained at 250°C and at the crosshead velocity of 0.2in/min.(TEM).

x12000

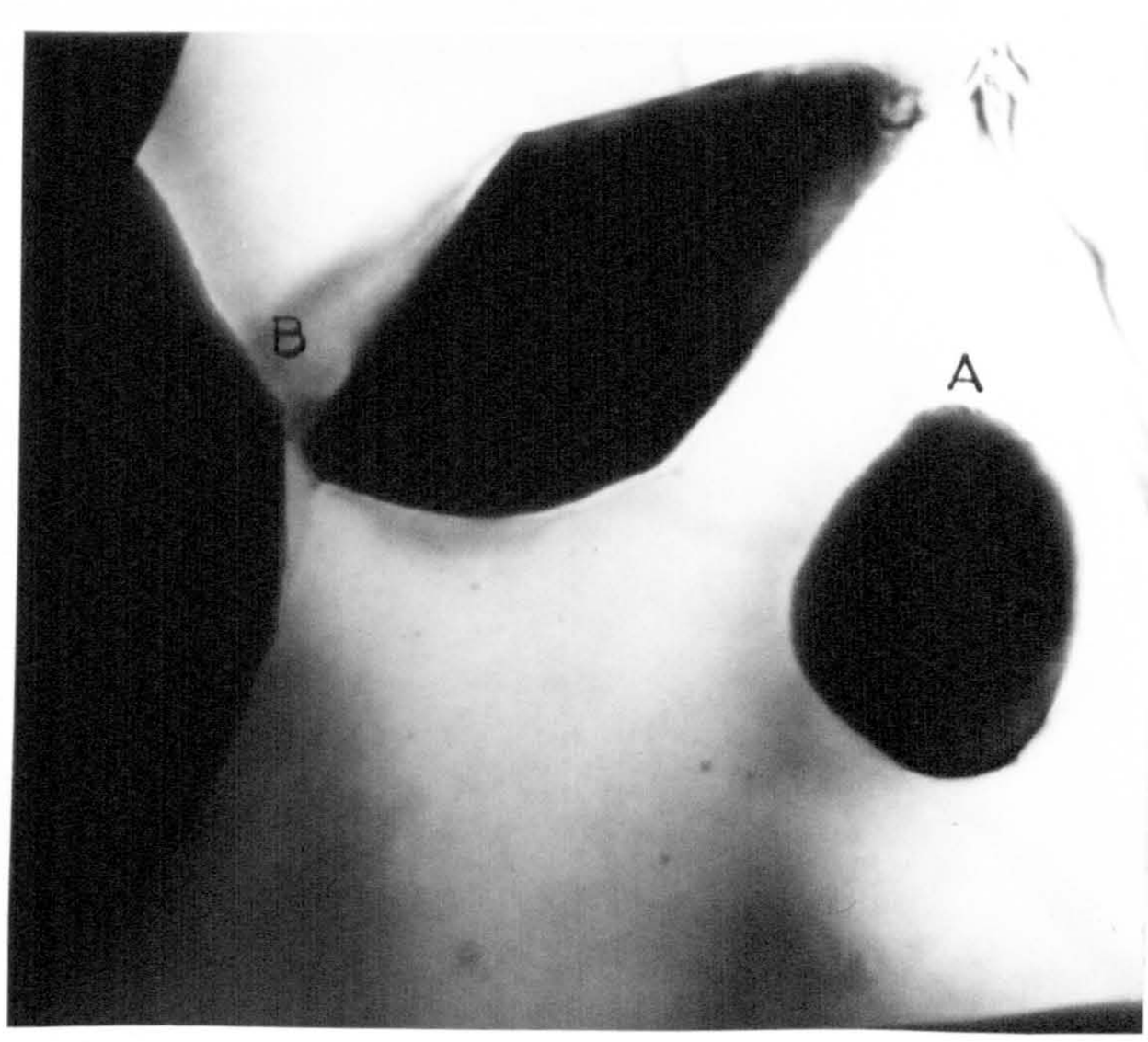

x51000

Figure 95b-Region strained 100% at 250°C and at the crosshead velocity of 0.2in/min.(TEM).

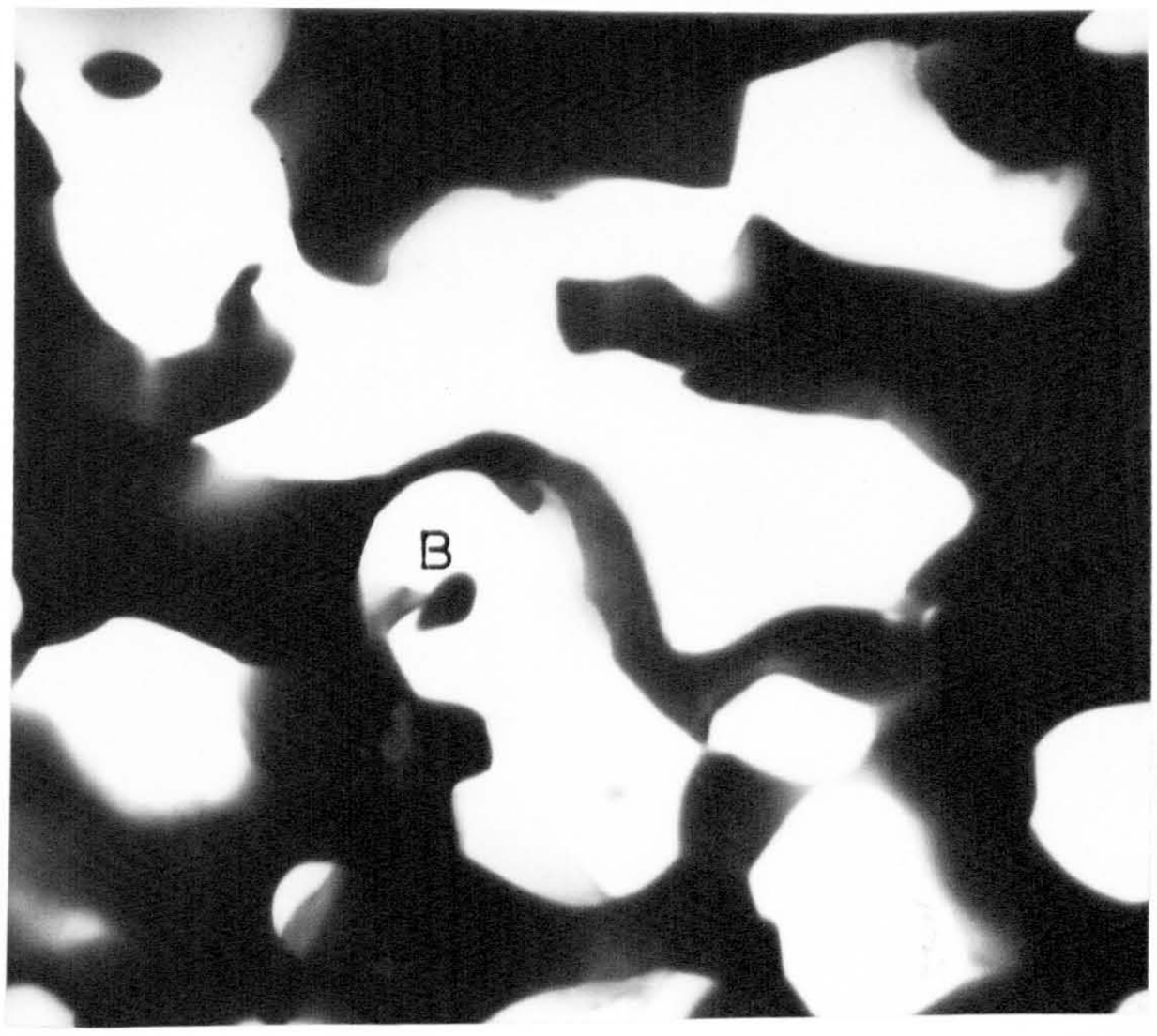

x12000

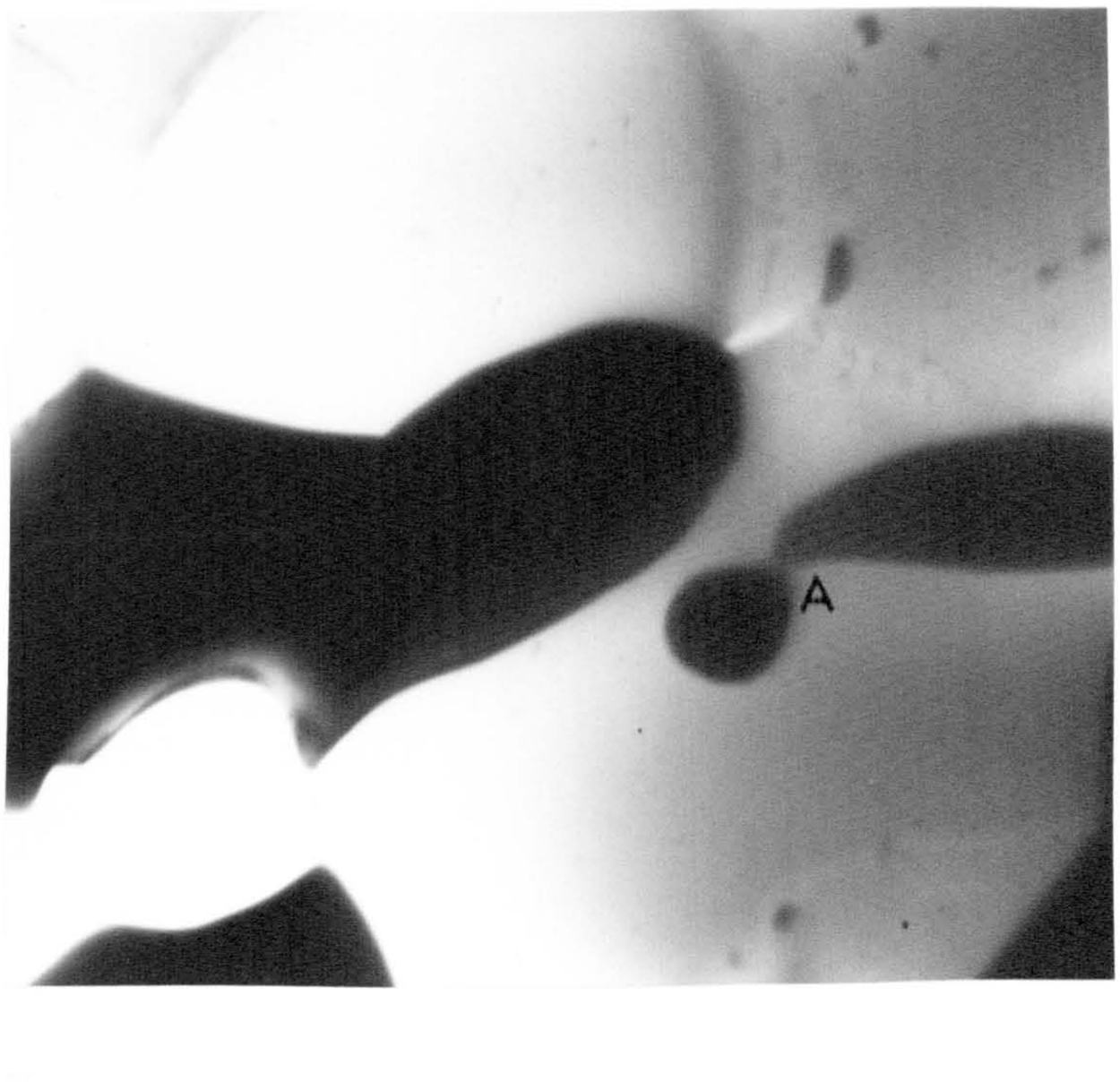

x30000

Figure95c-Region strained 300% at 250^{0}C and at the crosshead velocity of 0.2in/min.(TEM).

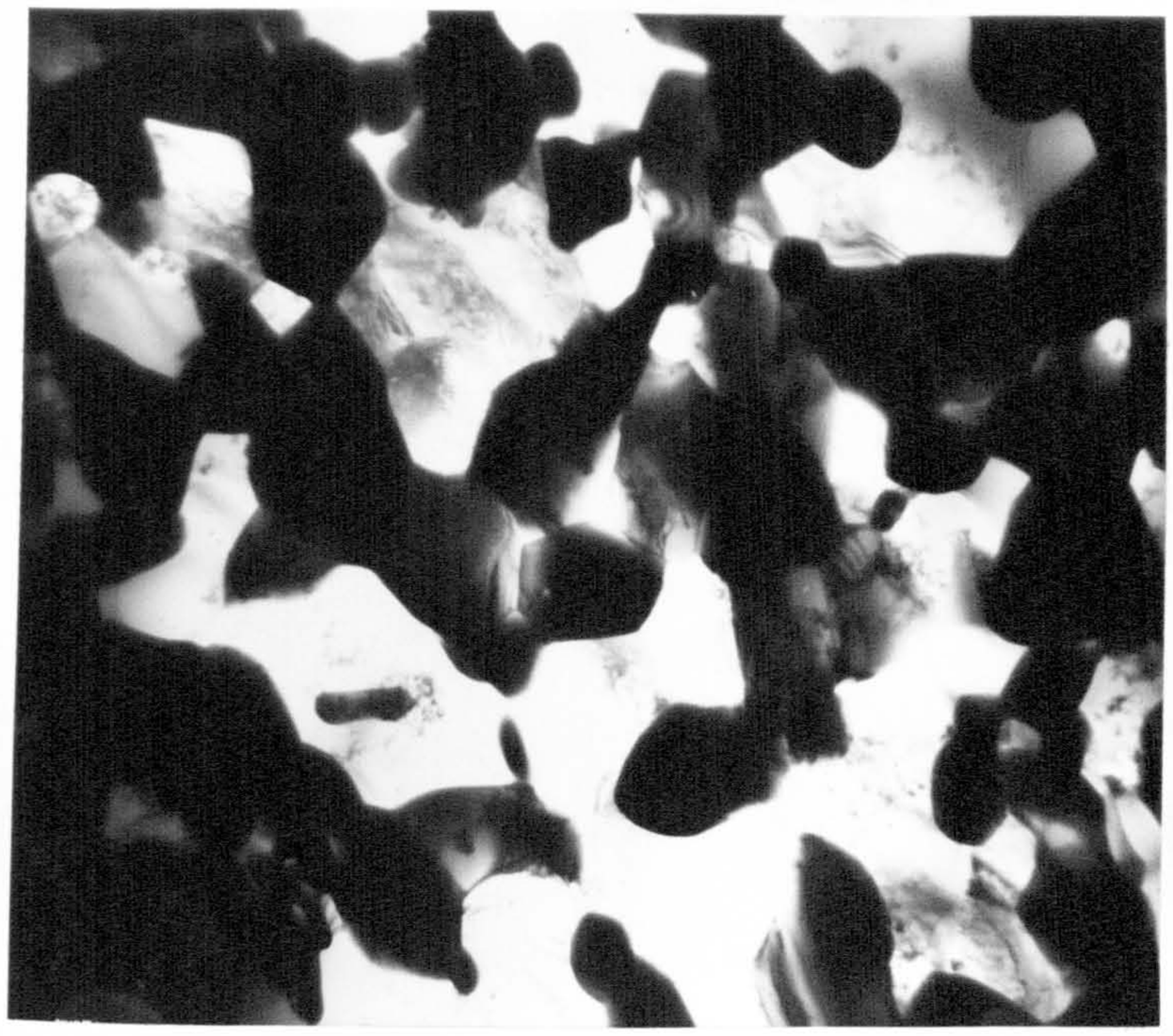

x12000

Figure 96a-Grip end of the specimen strained at 250°C and at the crosshead velocity of 2in/min.(TEM).

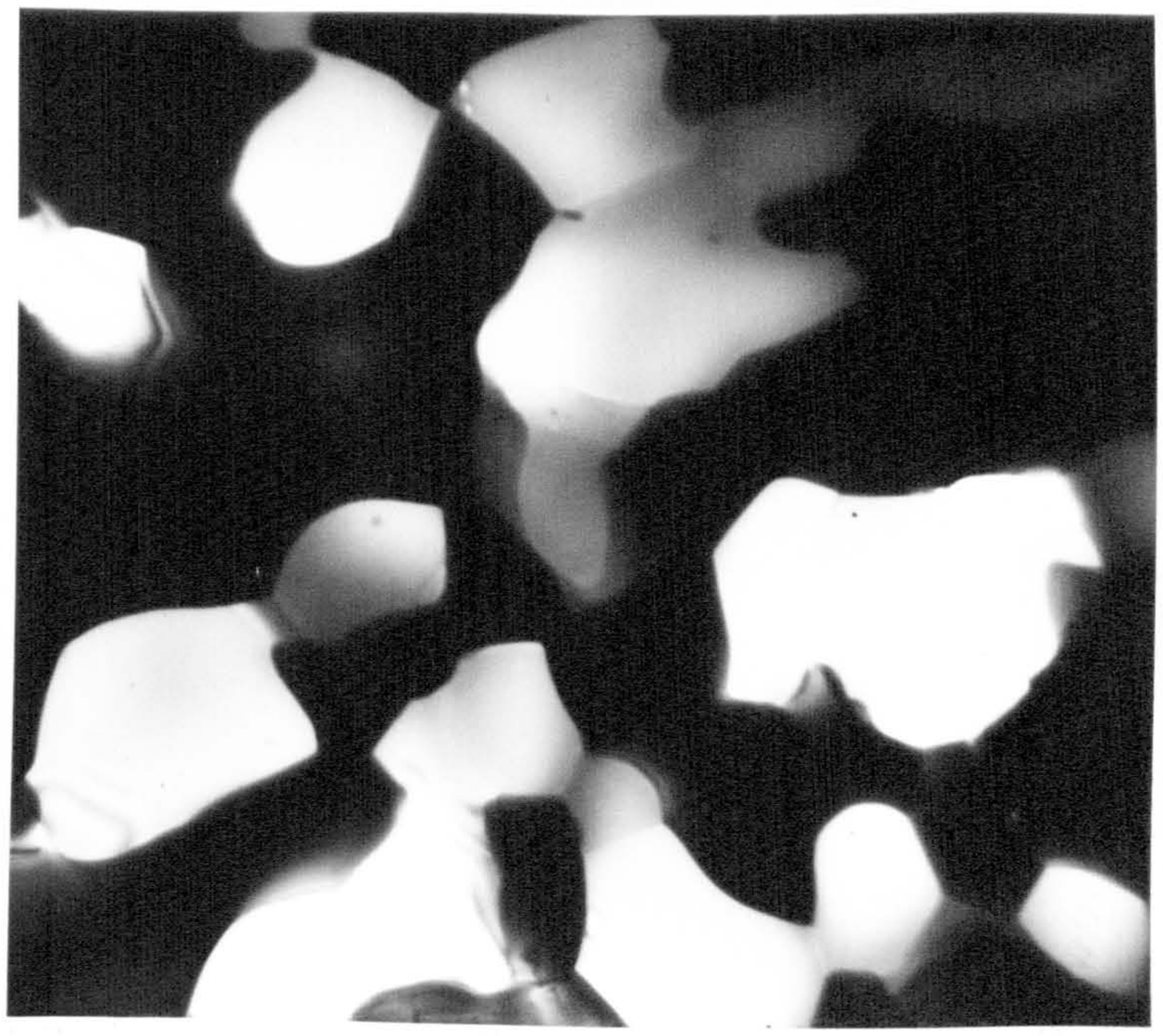

x12000

Figure 96b-Region strained 100% and at the crosshead velocity of 2in/min.(TEM).

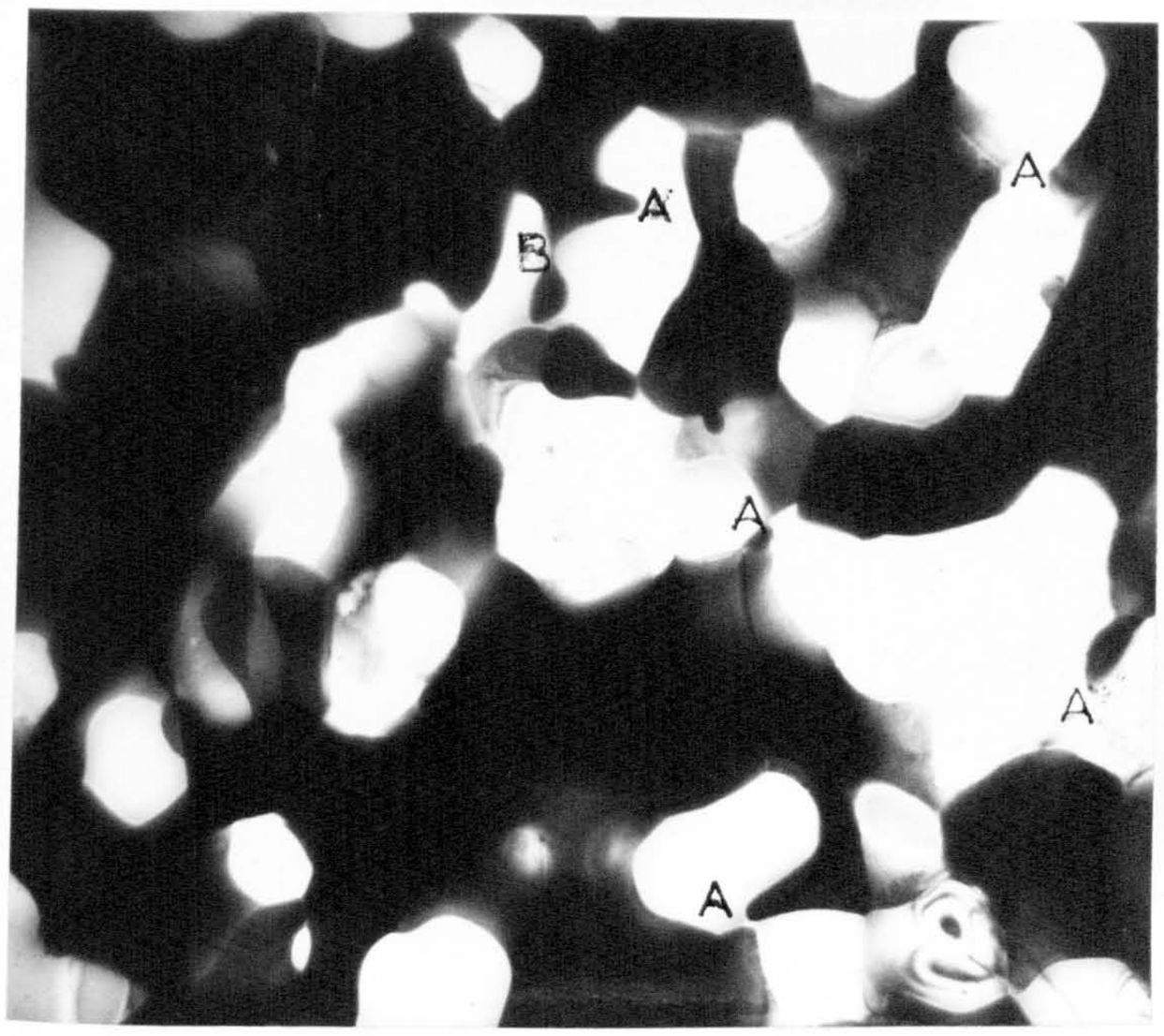

x12000

Figure 96c-Region strained 300% at 250°C and at the crosshead velocity of 2in/min.(TEM).

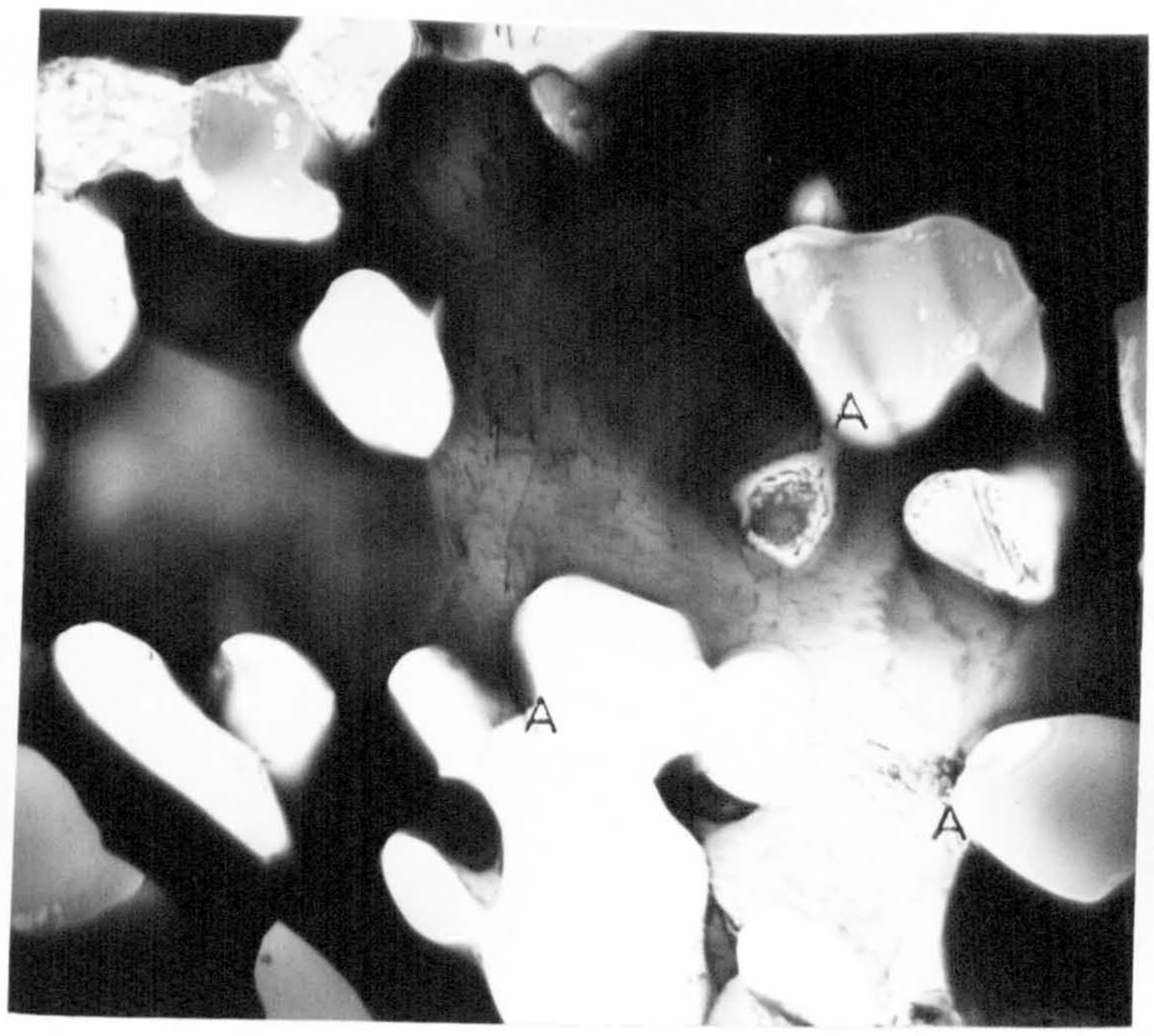

x12000

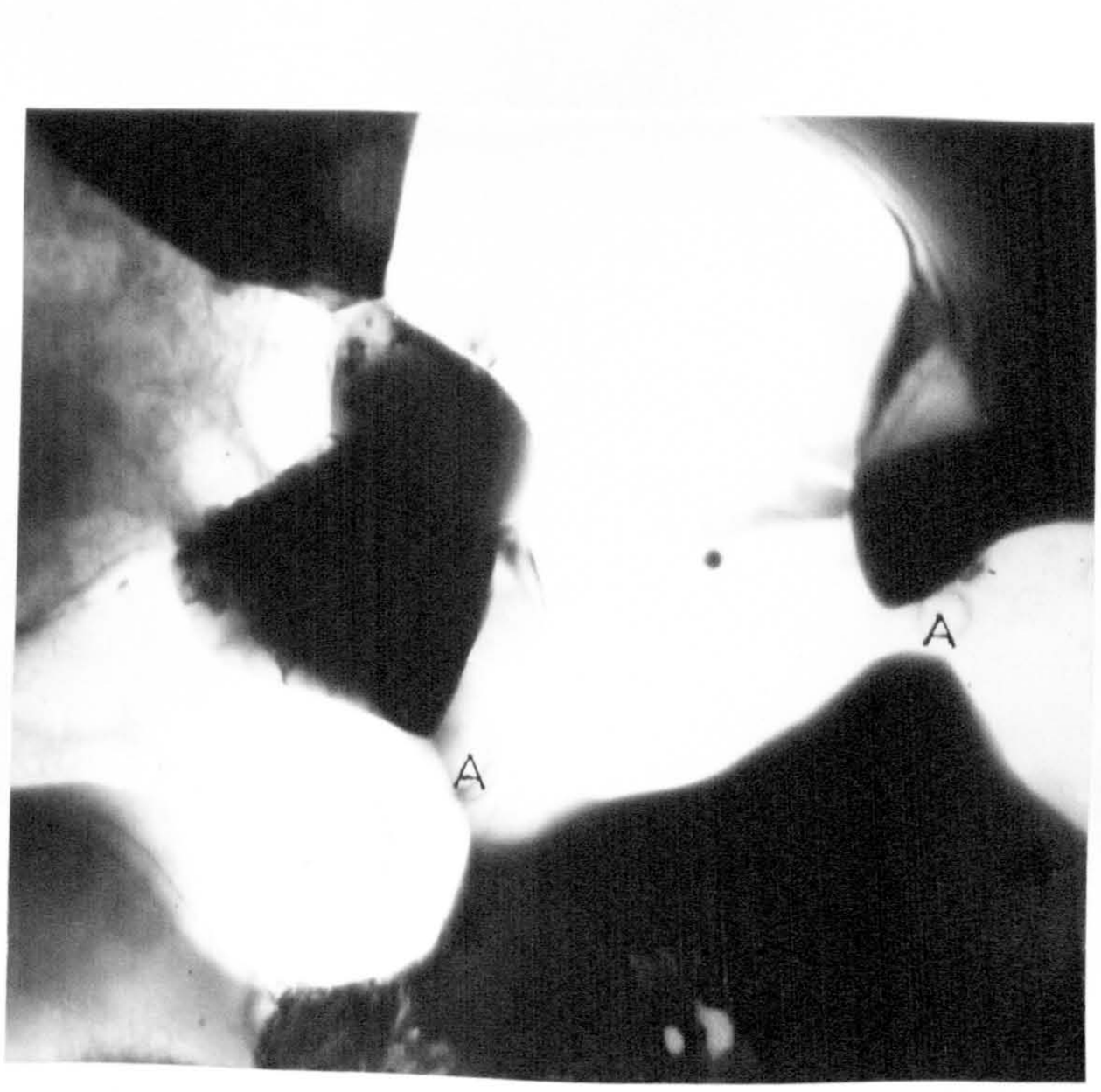

x30000

Figure 96d-Region strained 550% at 250°C and at the crosshead velocity of 2in/min.(TEM).

x12000

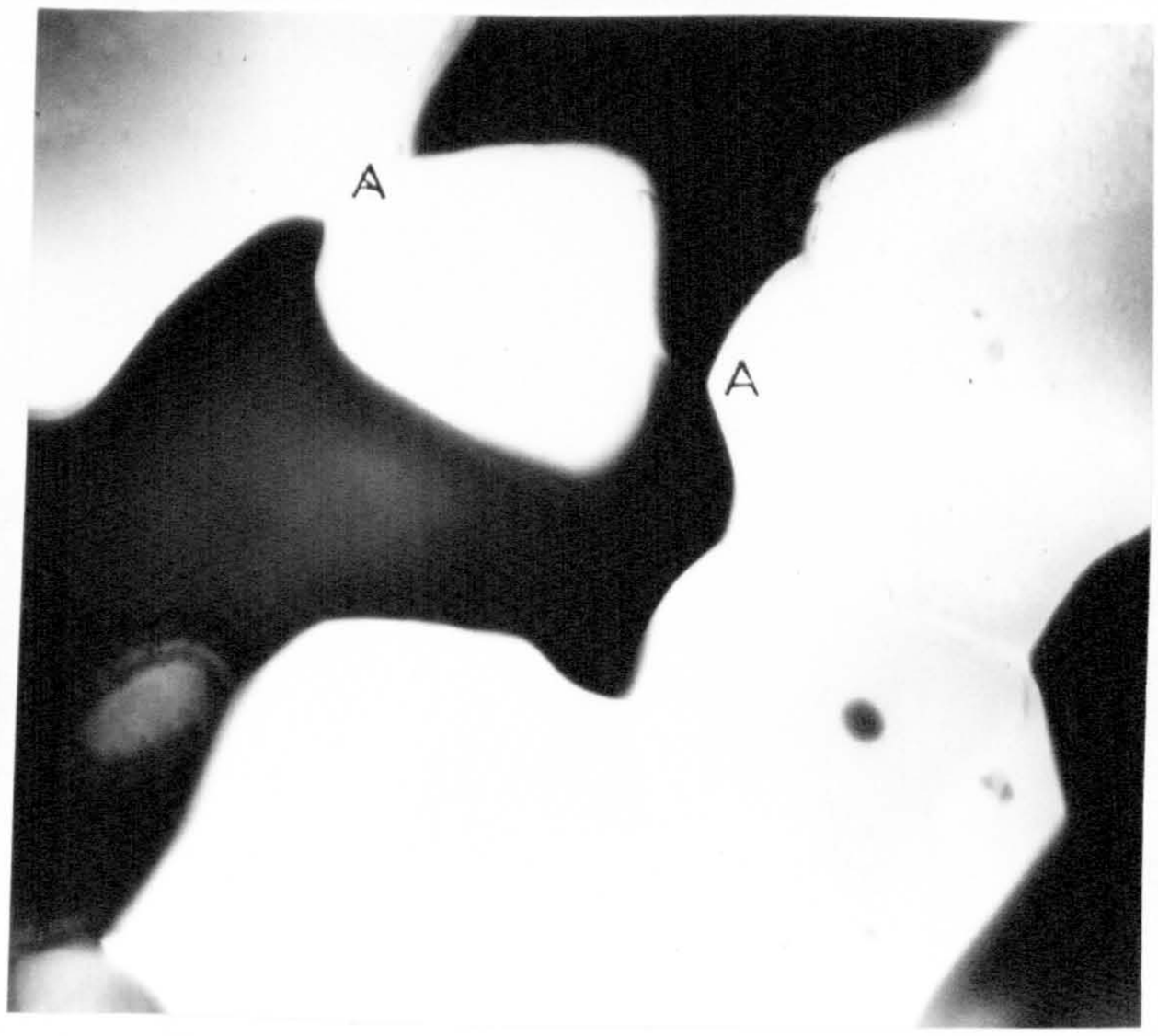

x30000

Figure 96e-Region strained 900% at 250°C and at the crosshead velocity of 2in/min.(TEM).

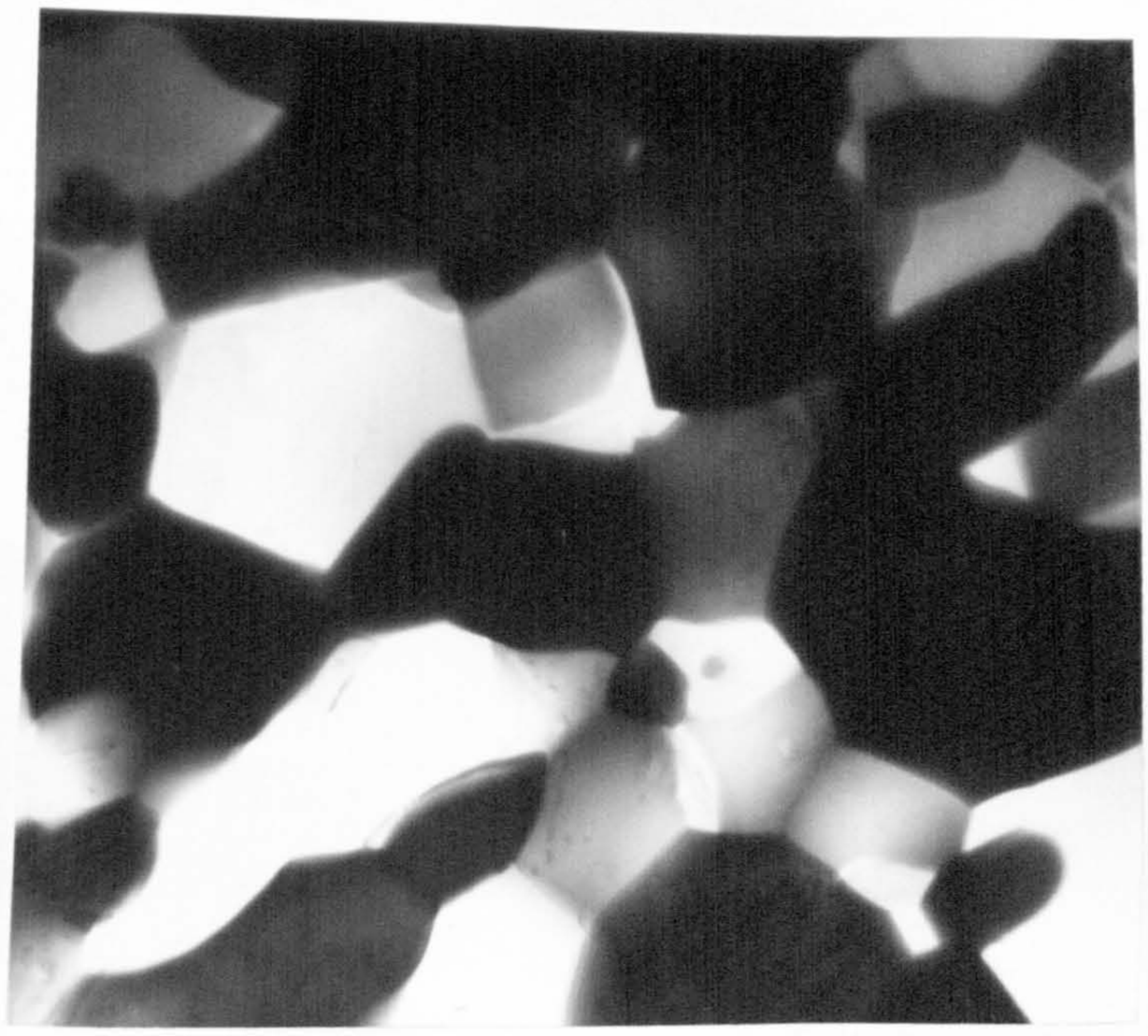

x12000

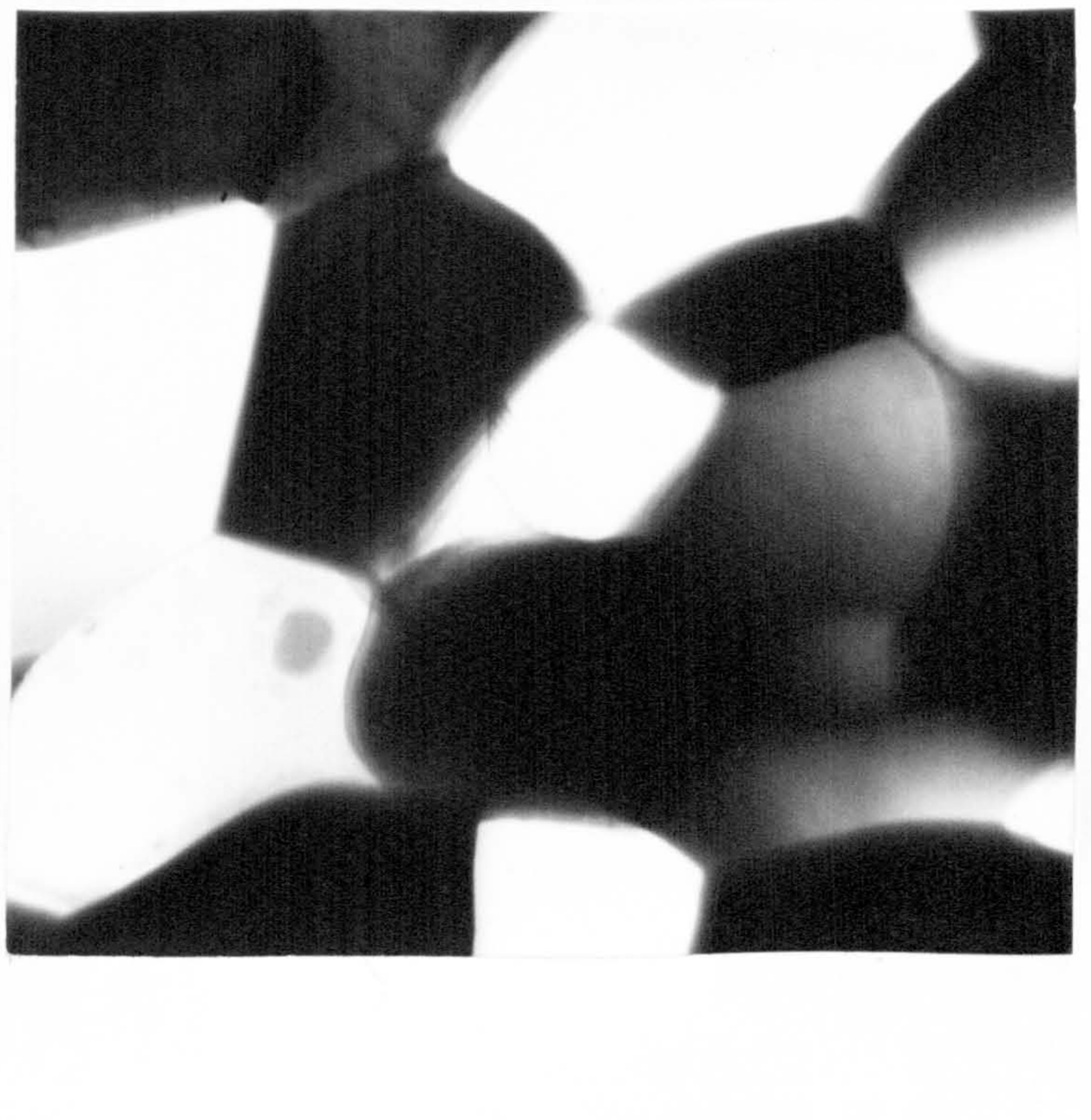

x30000

Figure 97a- Grip end of the specimen strained at 250°C and at the crosshead velocity of 20in/min.(TEM).

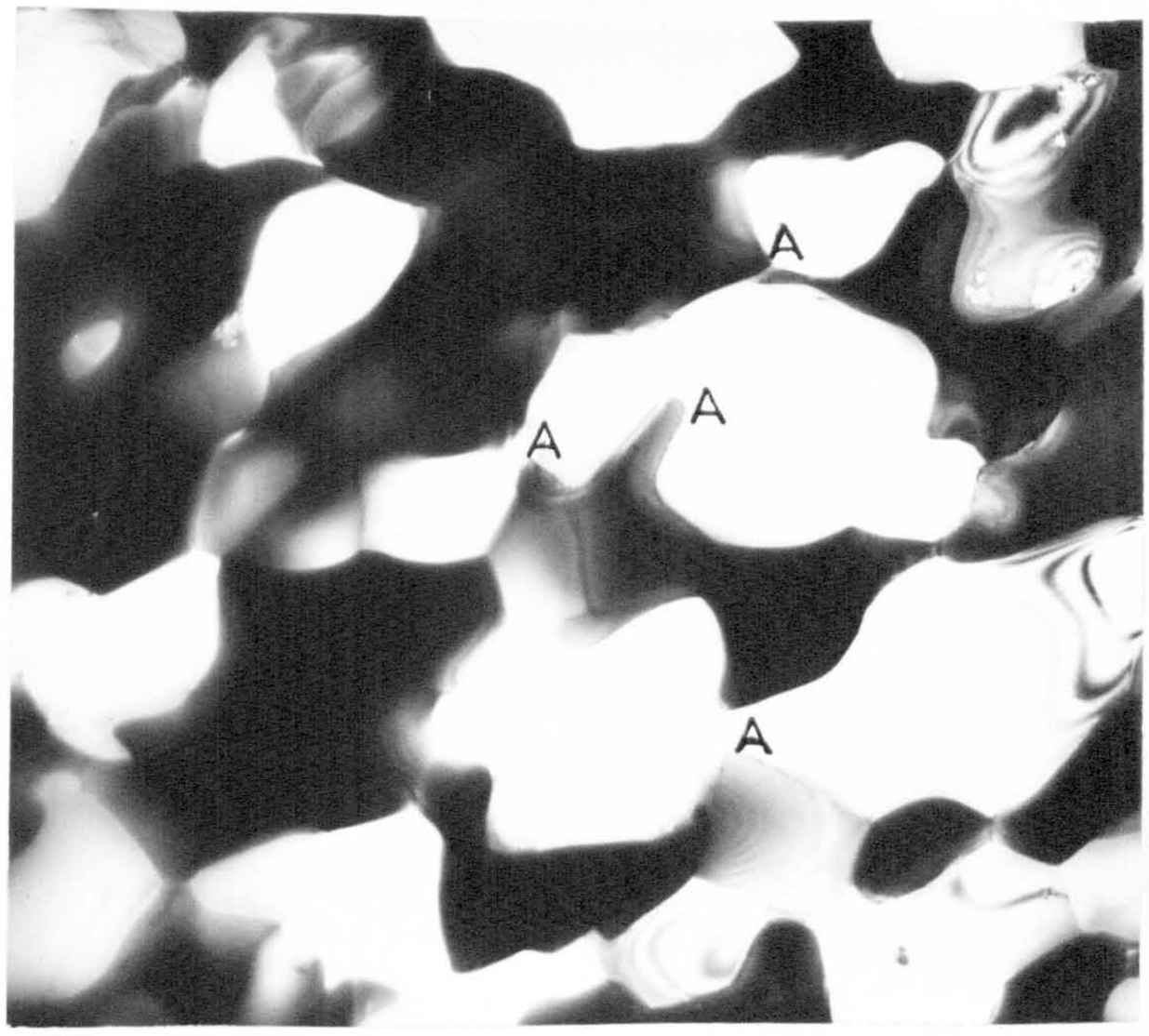

x12000

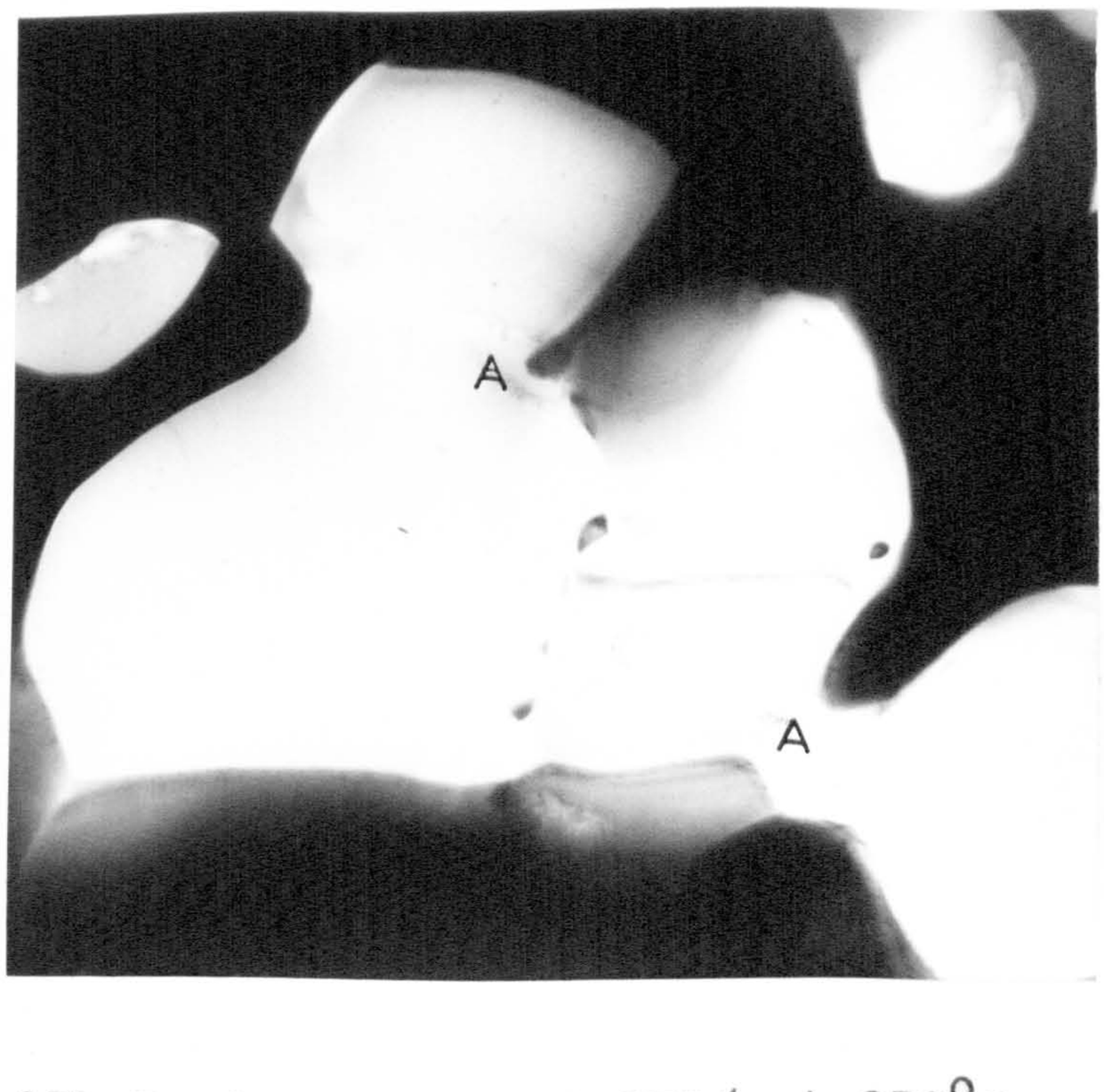

x30000

Figure 97b-Region strained 550% at 250°C and at the crosshead velocity of 20in/min.(TEM).

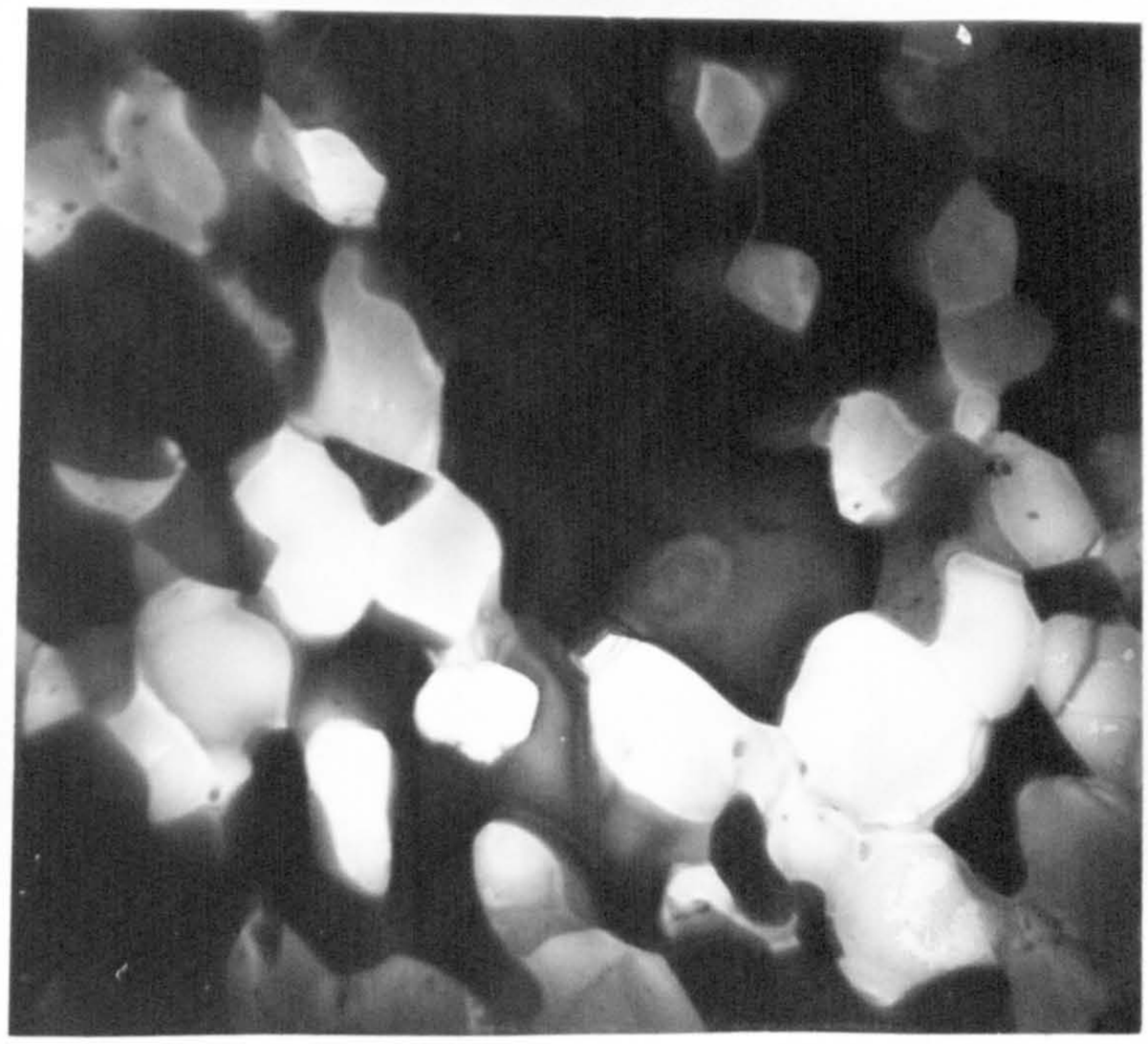

x12000

x30000

Figure 97c-Region strained 900% at 250°C and at the crosshead velocity of 20 in/min.(TEM).

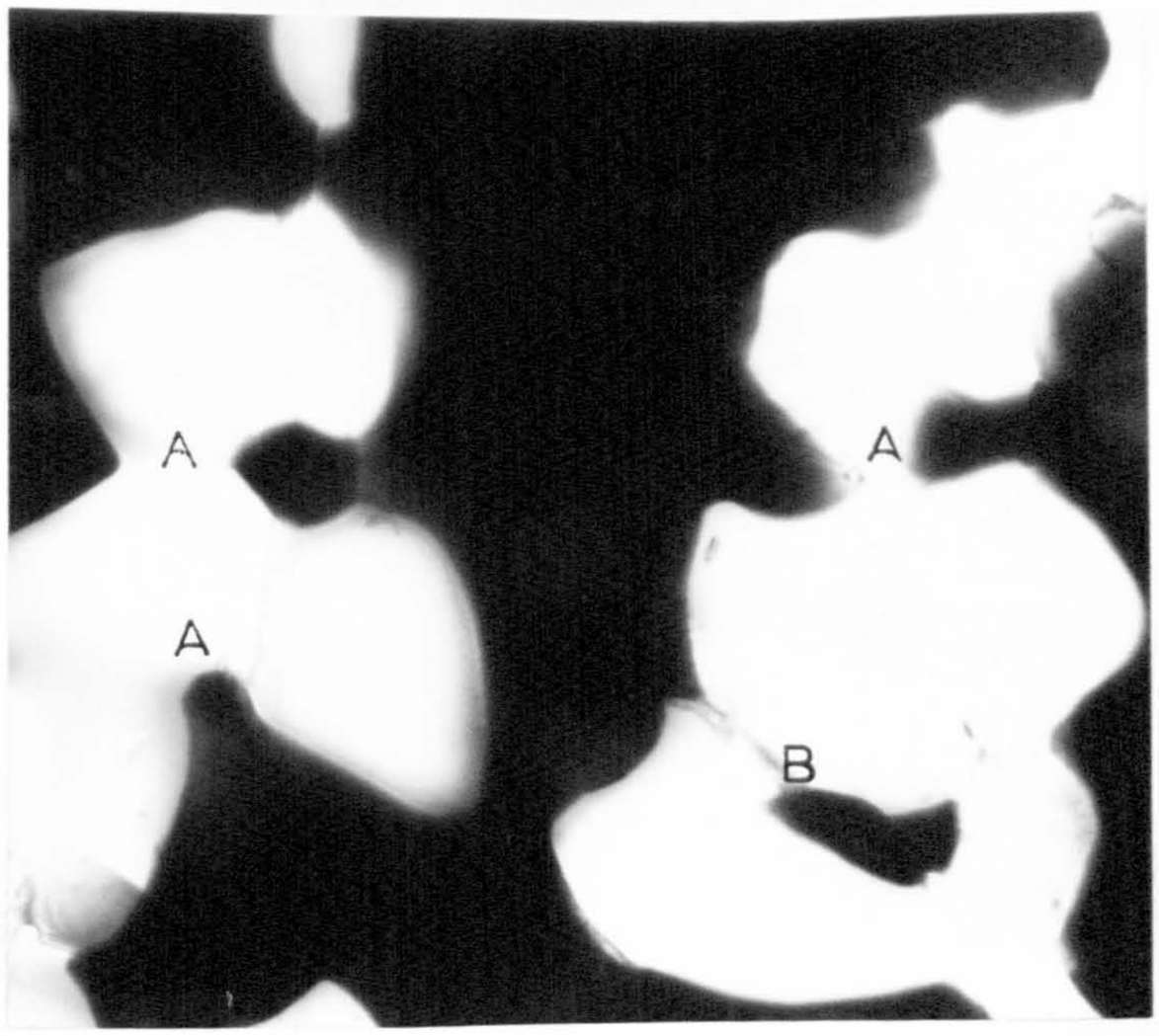

x19500

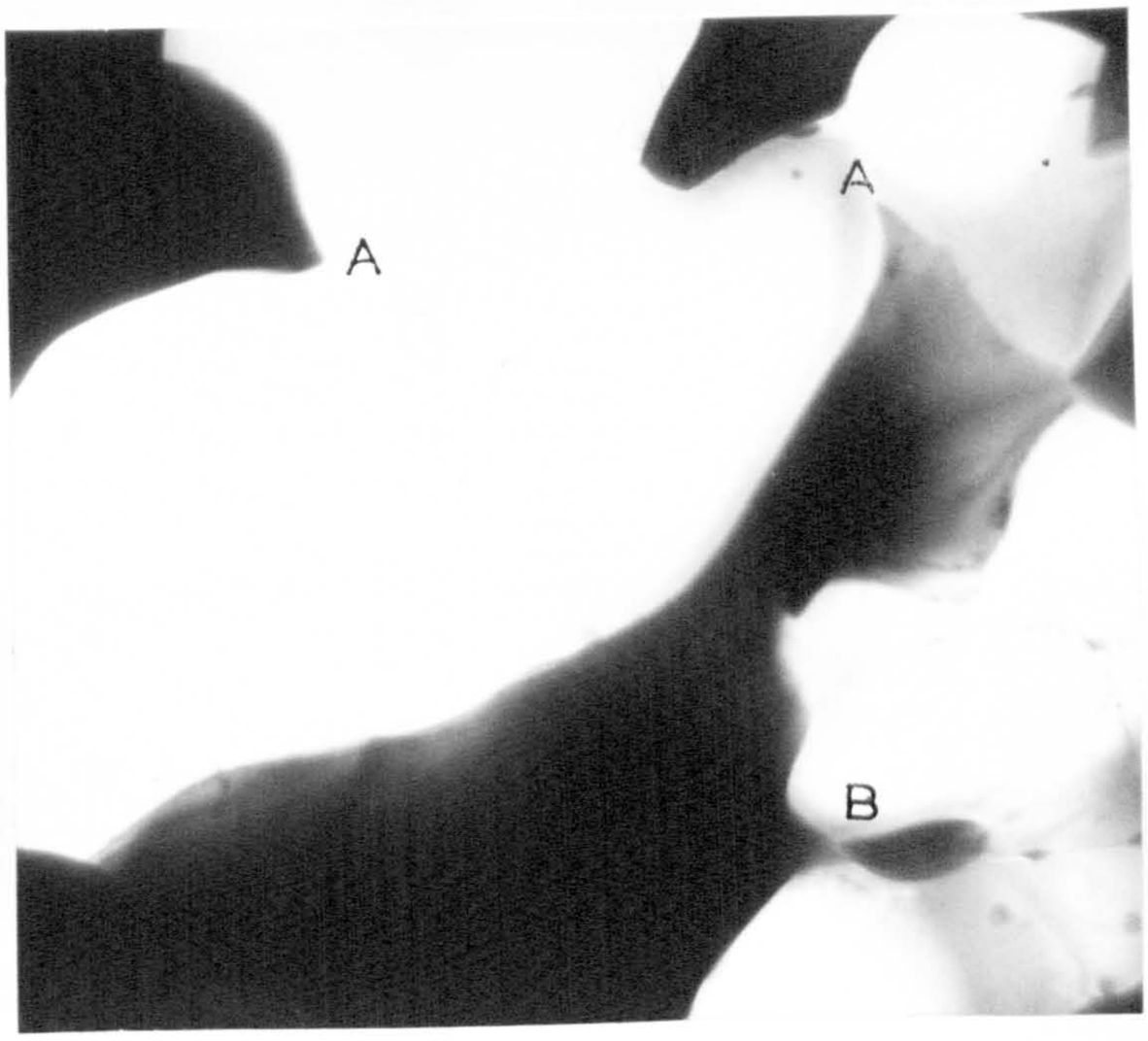

x30000

Figure 97d-Region strained ~2500% and at the crosshead velocity of 20 in/min.(TEM).

Grip end

Centre

Edge

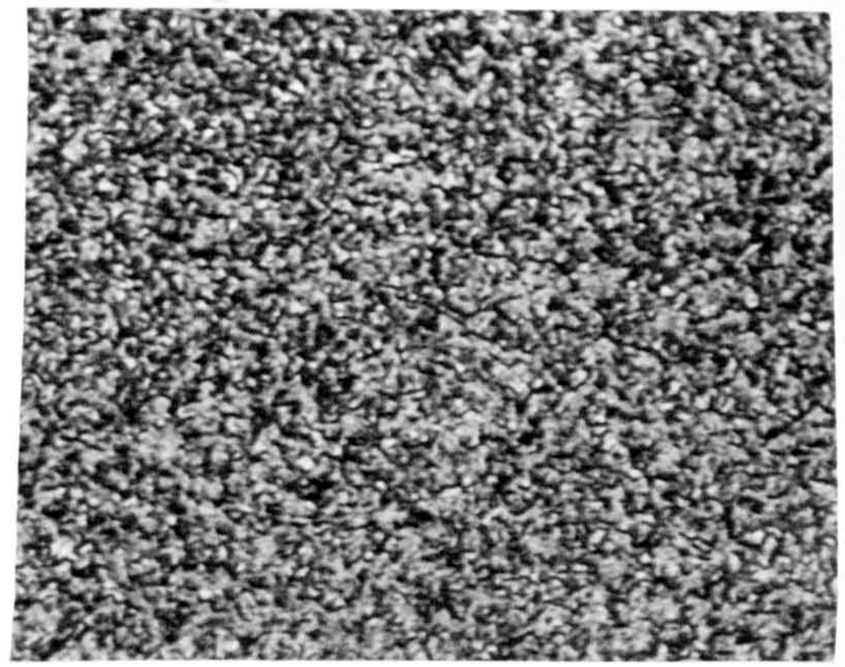

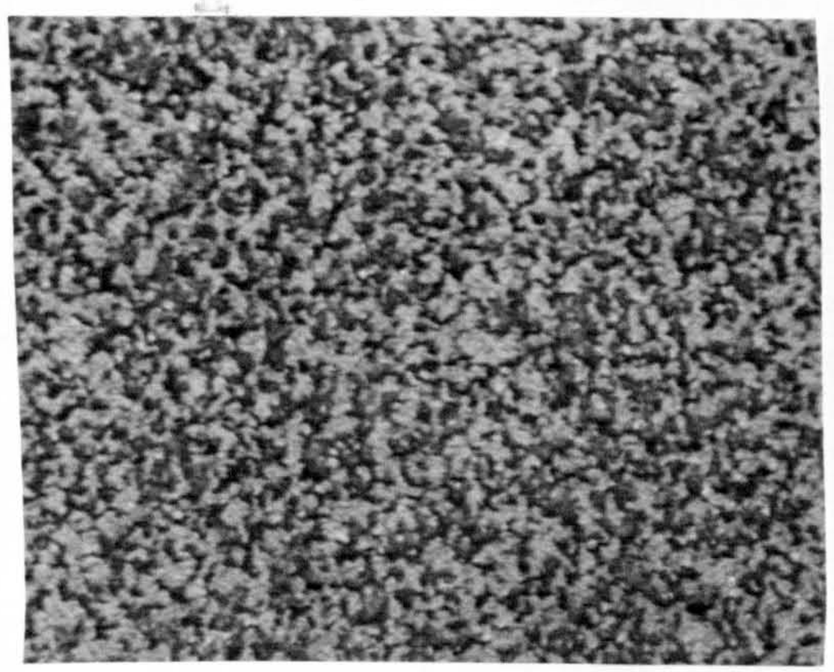

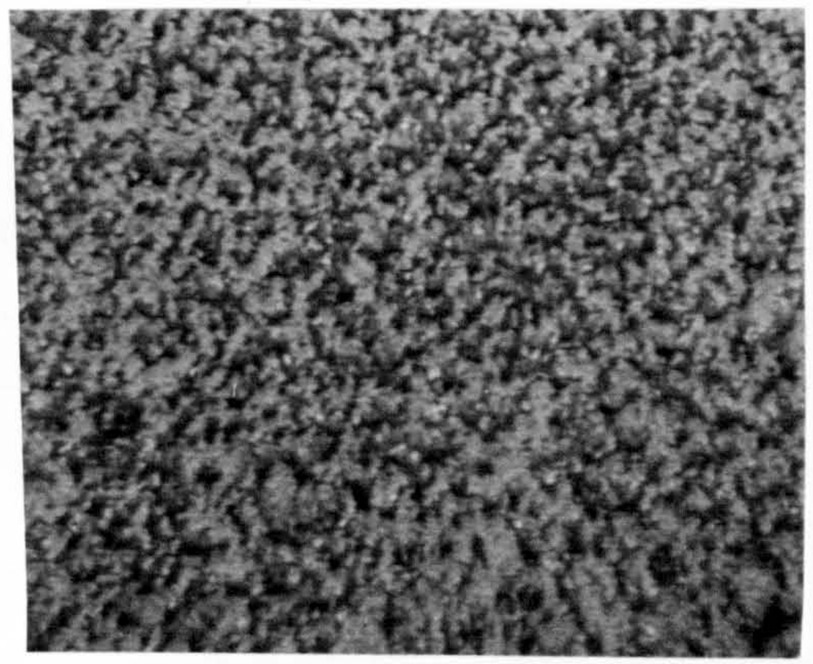

Strained at 250°C

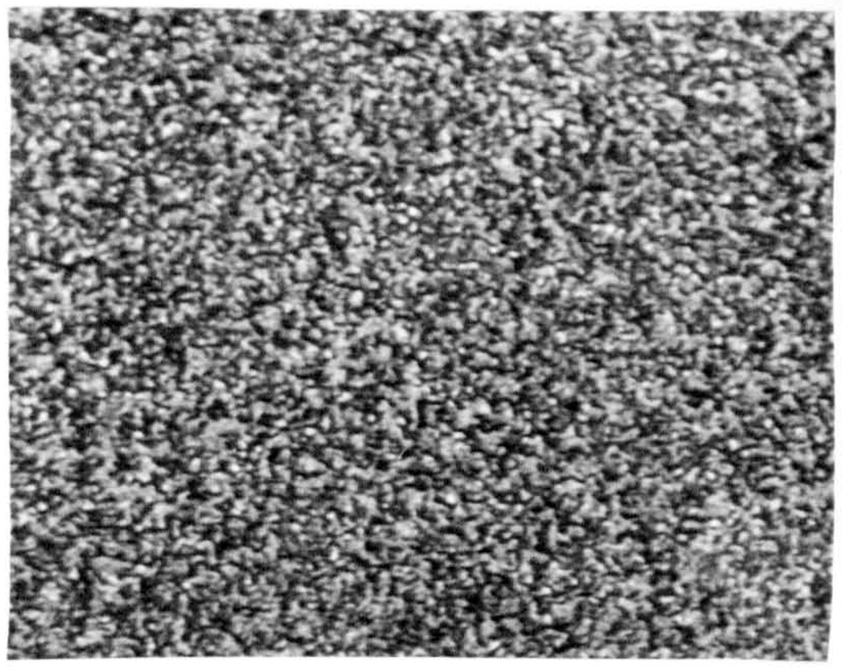

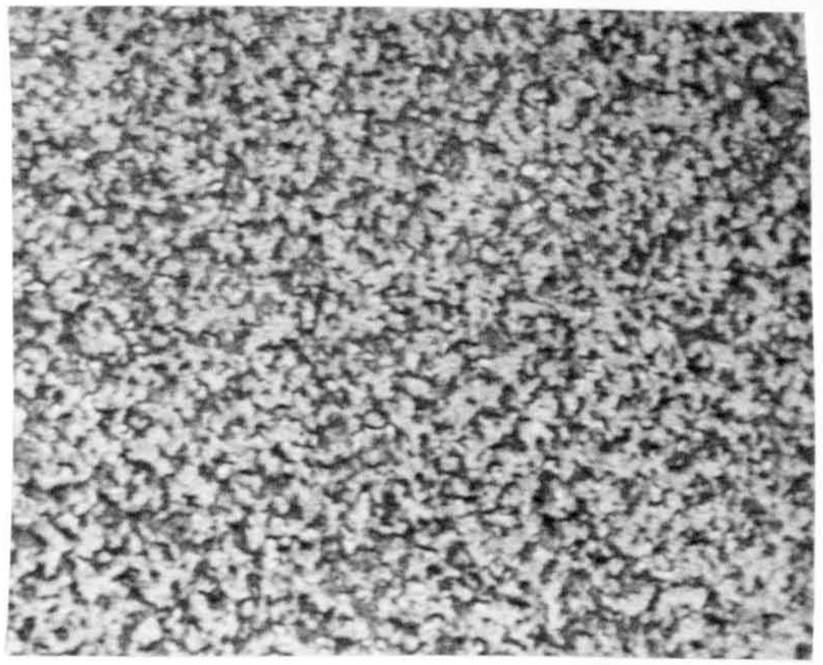

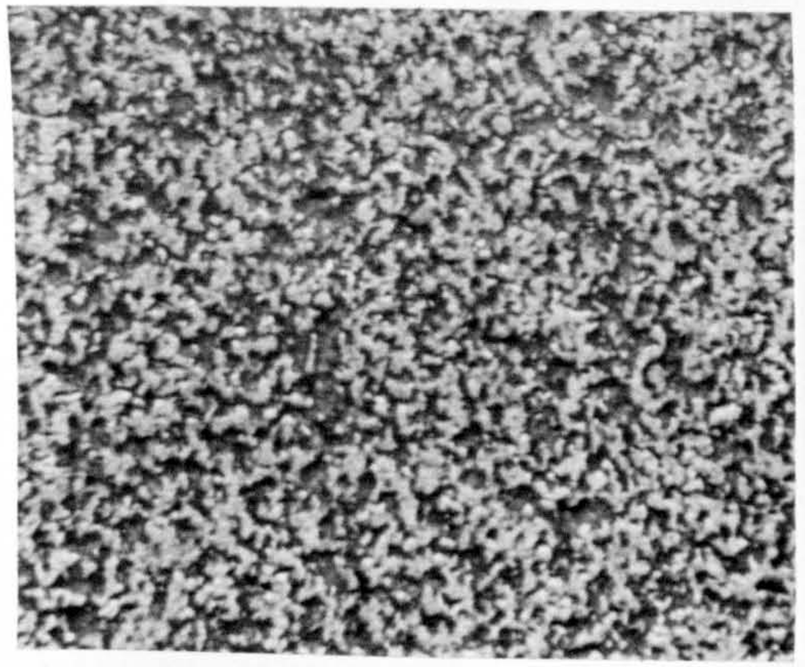

Strained at 150°C

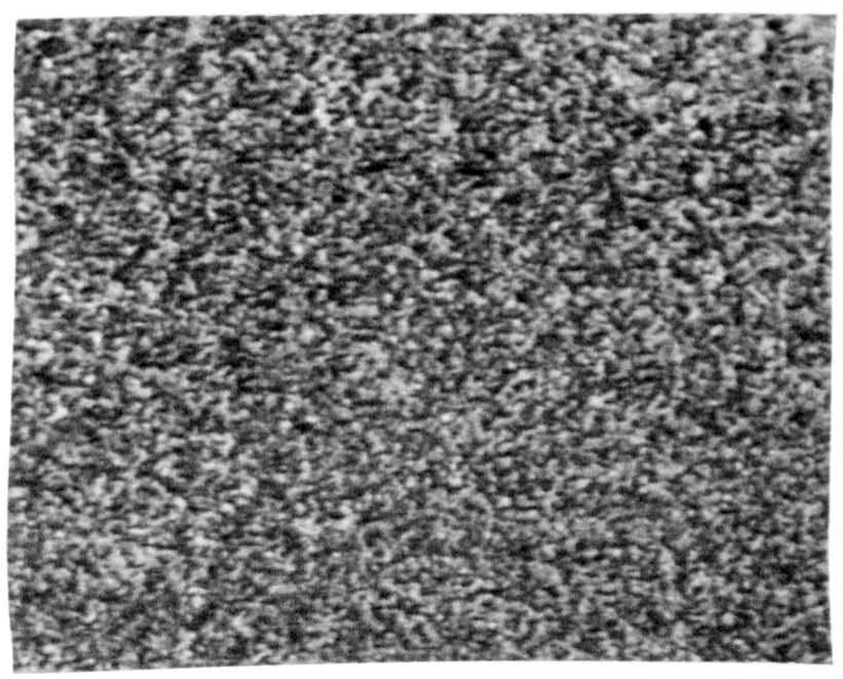

Starting Material

Figure 102-Microstructure of specimens strained in torsion at 390 rpm.(x1000).

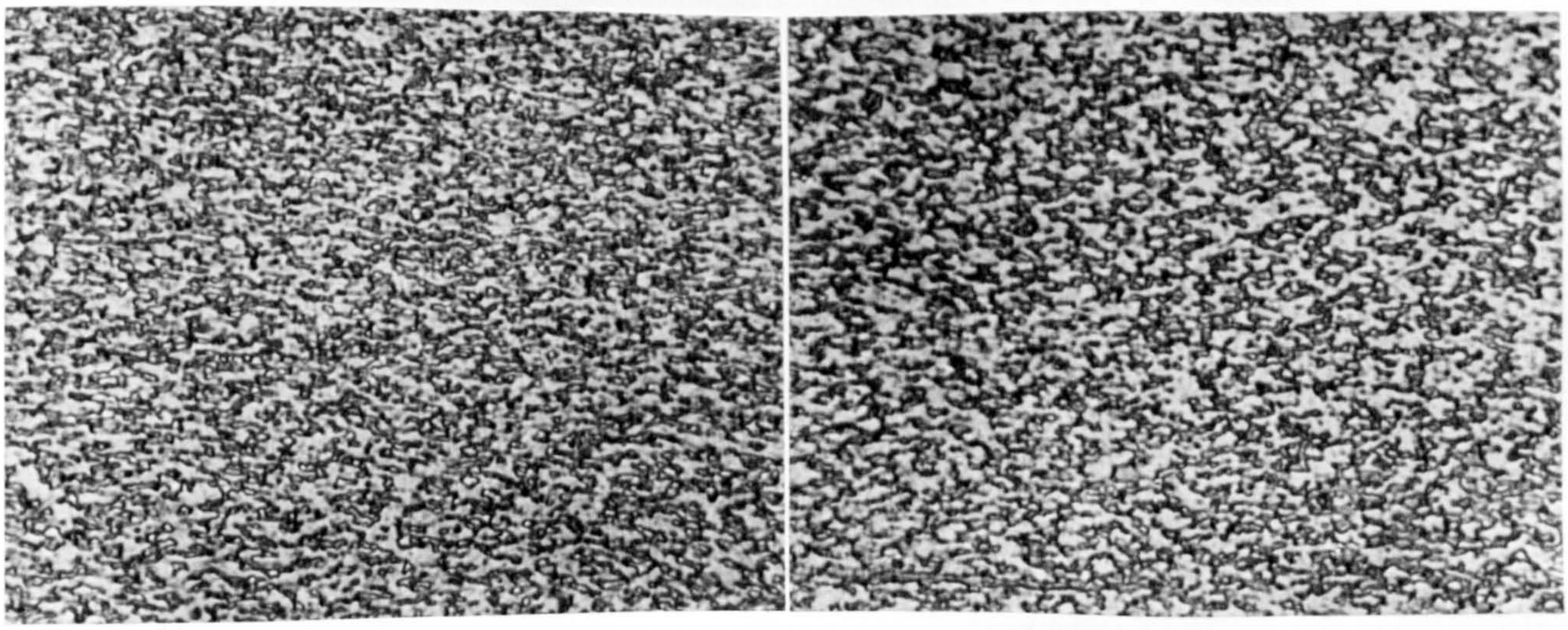

As recieved sheet

Grip end

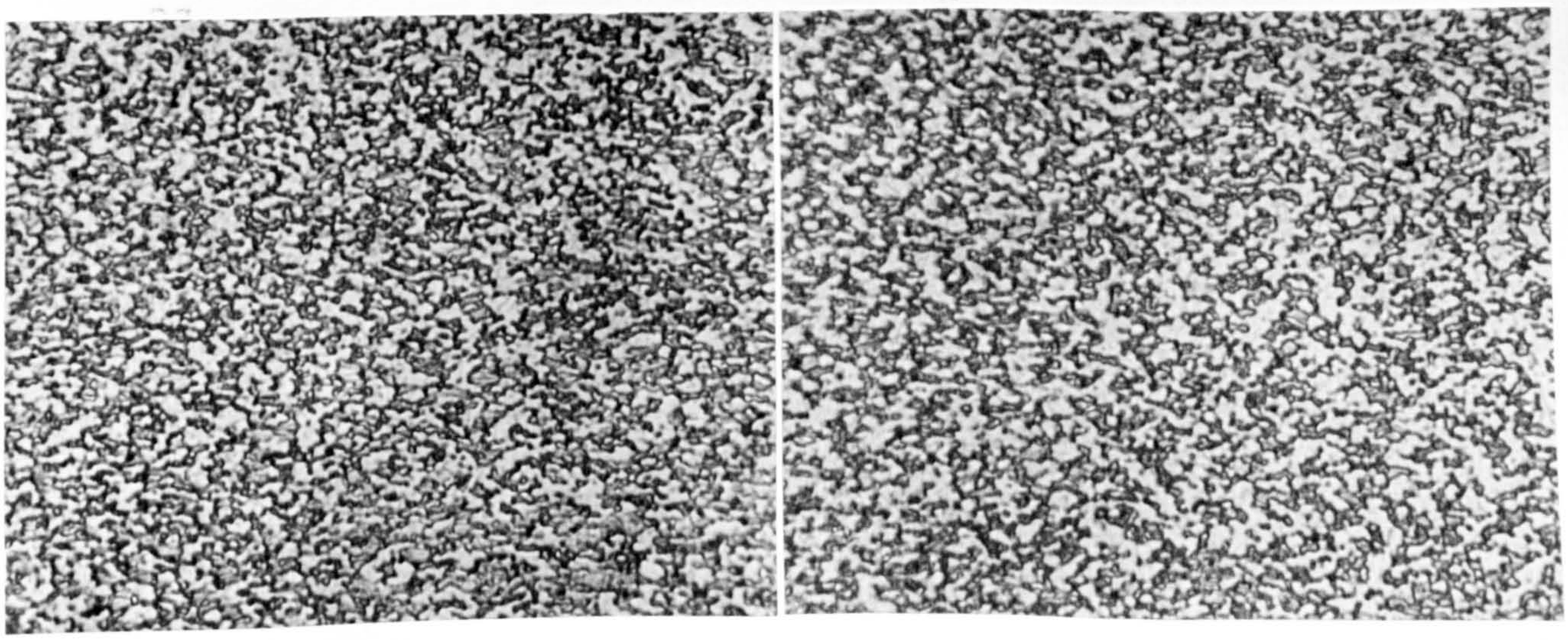

300%

500%

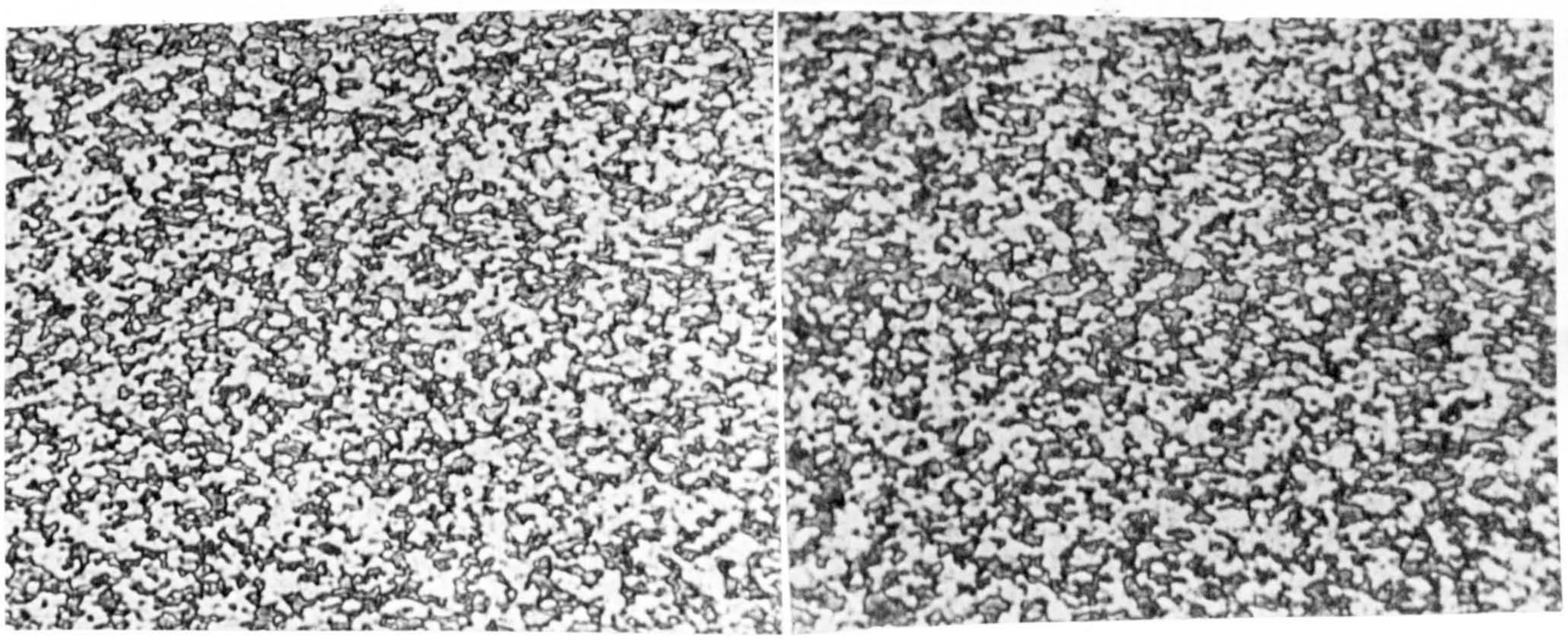

900%

~2000%

Figure 98-Regions strained different amount in a specimen strained at 250°C and at the crosshead velocity of 20in/min.(x1000).Longitudinal Section.

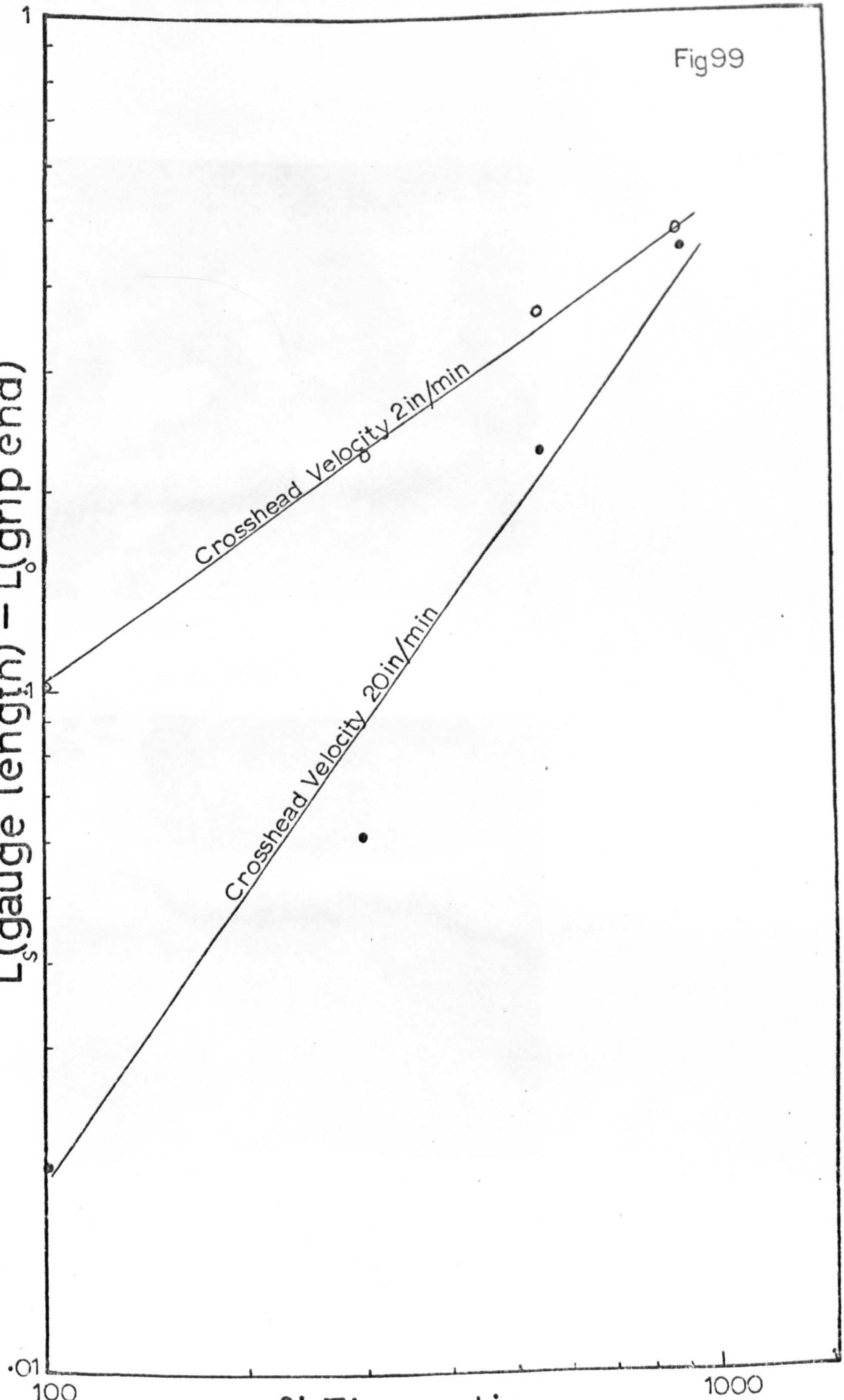

Figure 99- The actual grain size increase due to deformation (%elongation).

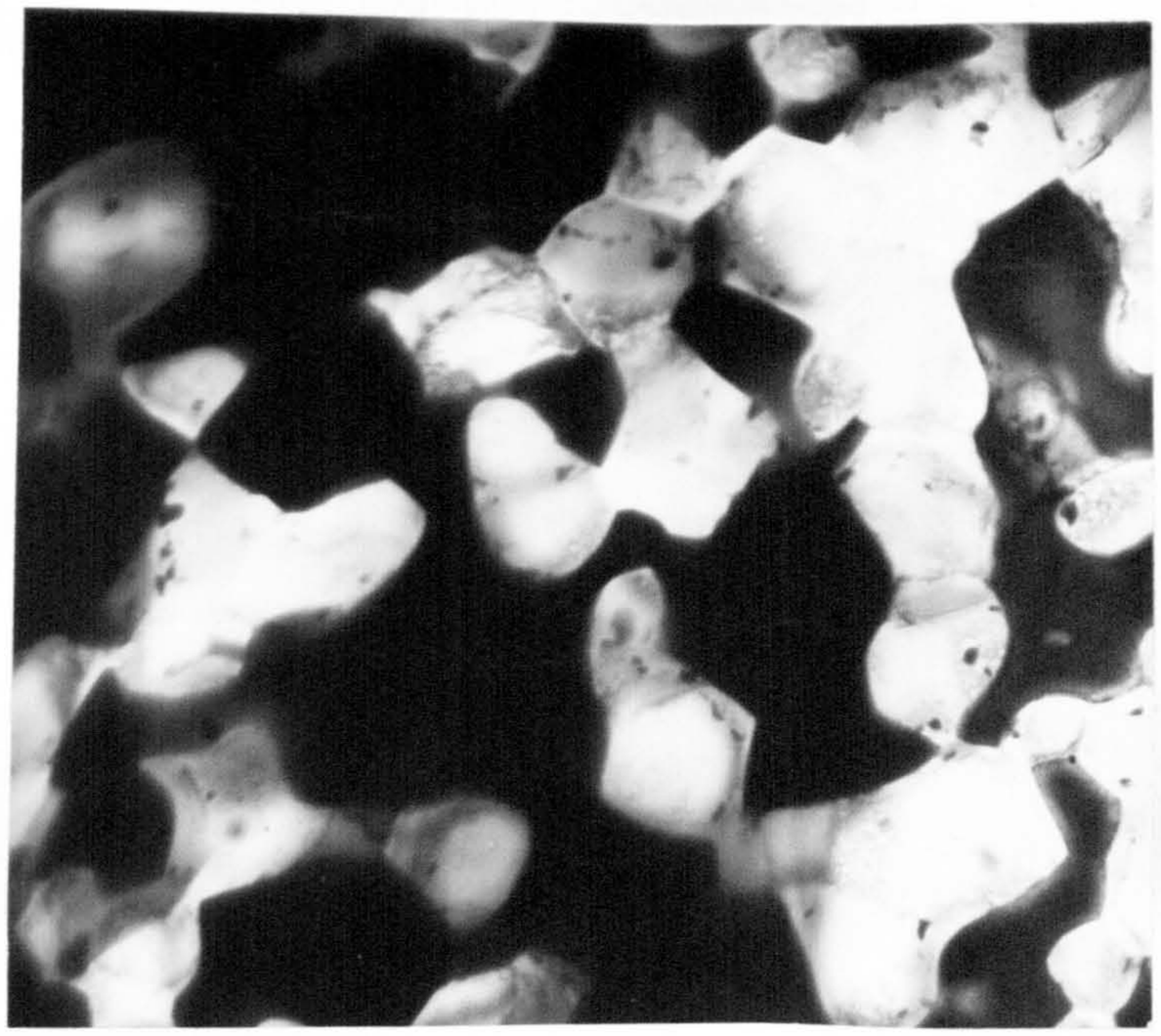

x16000

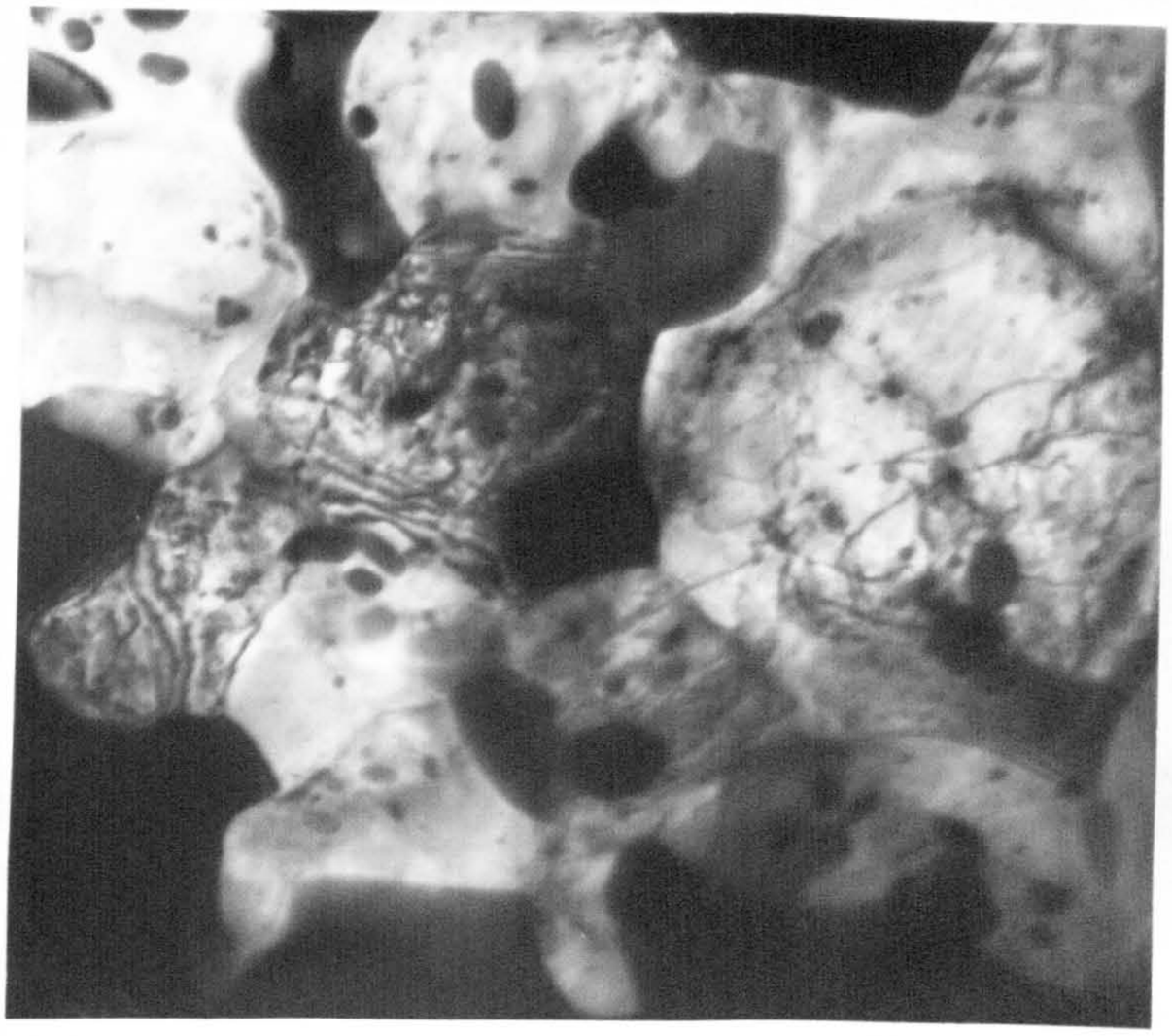

x29000

Figure 100- The microstructure of the torsion specimen(Figure 82b) strained to about 37 revolutions at 150°C and 390 rpm.(TEM).

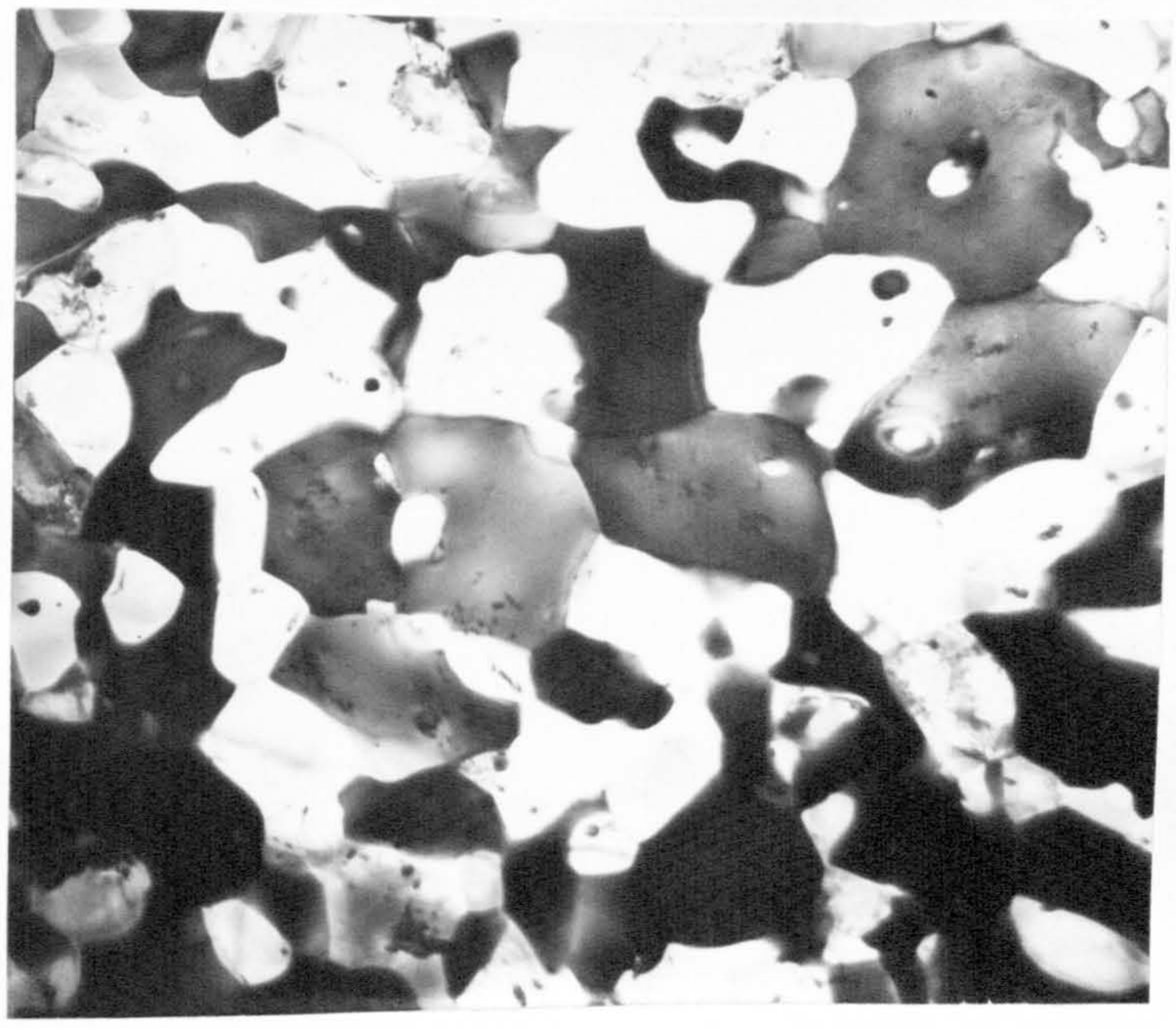

x10000

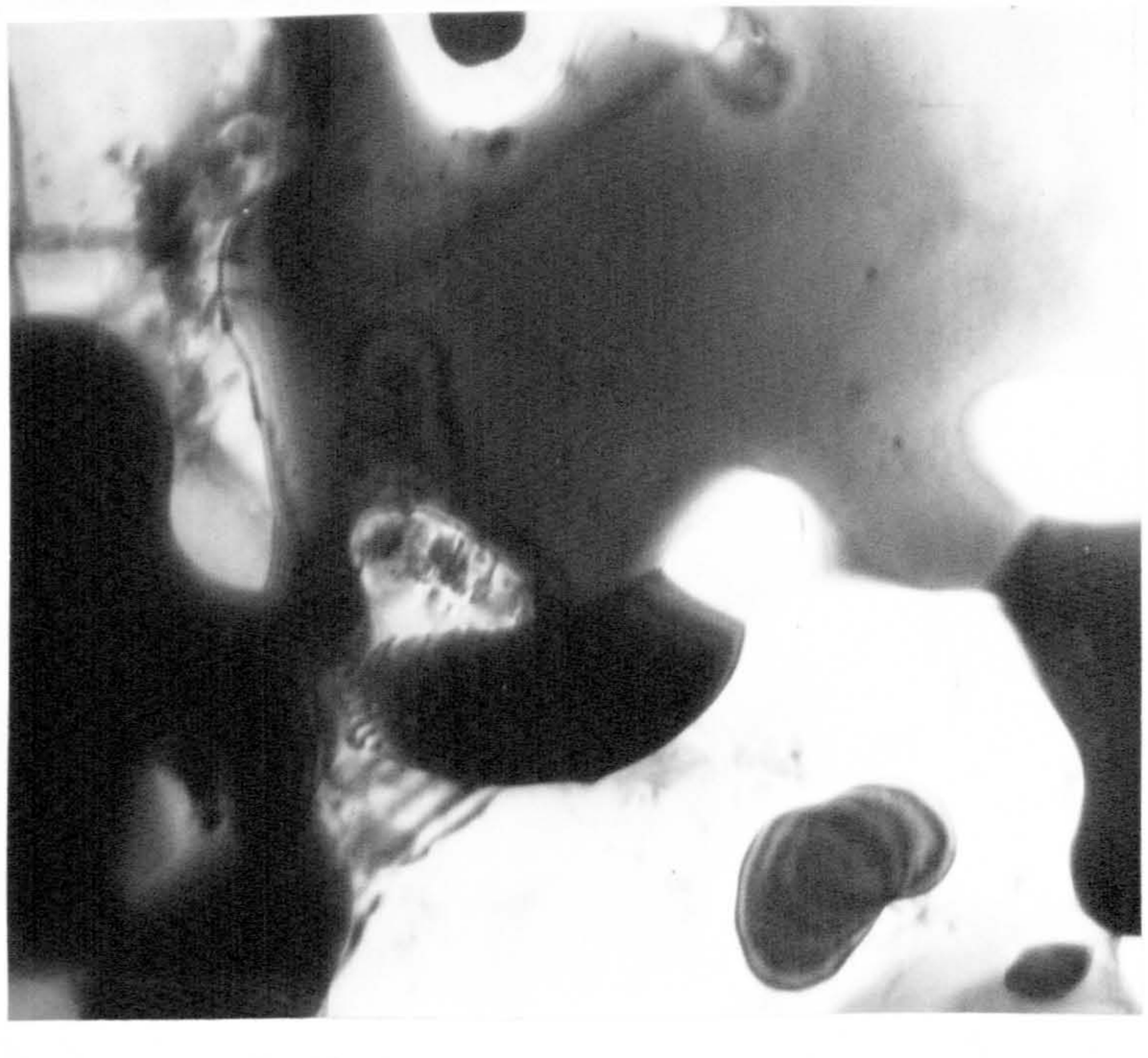

x40000

Figure 101-The microstructure of the torsion specimen (Figure 82b) strained to about 52 revolutions at 250°C and 390 rpm.(TEM).

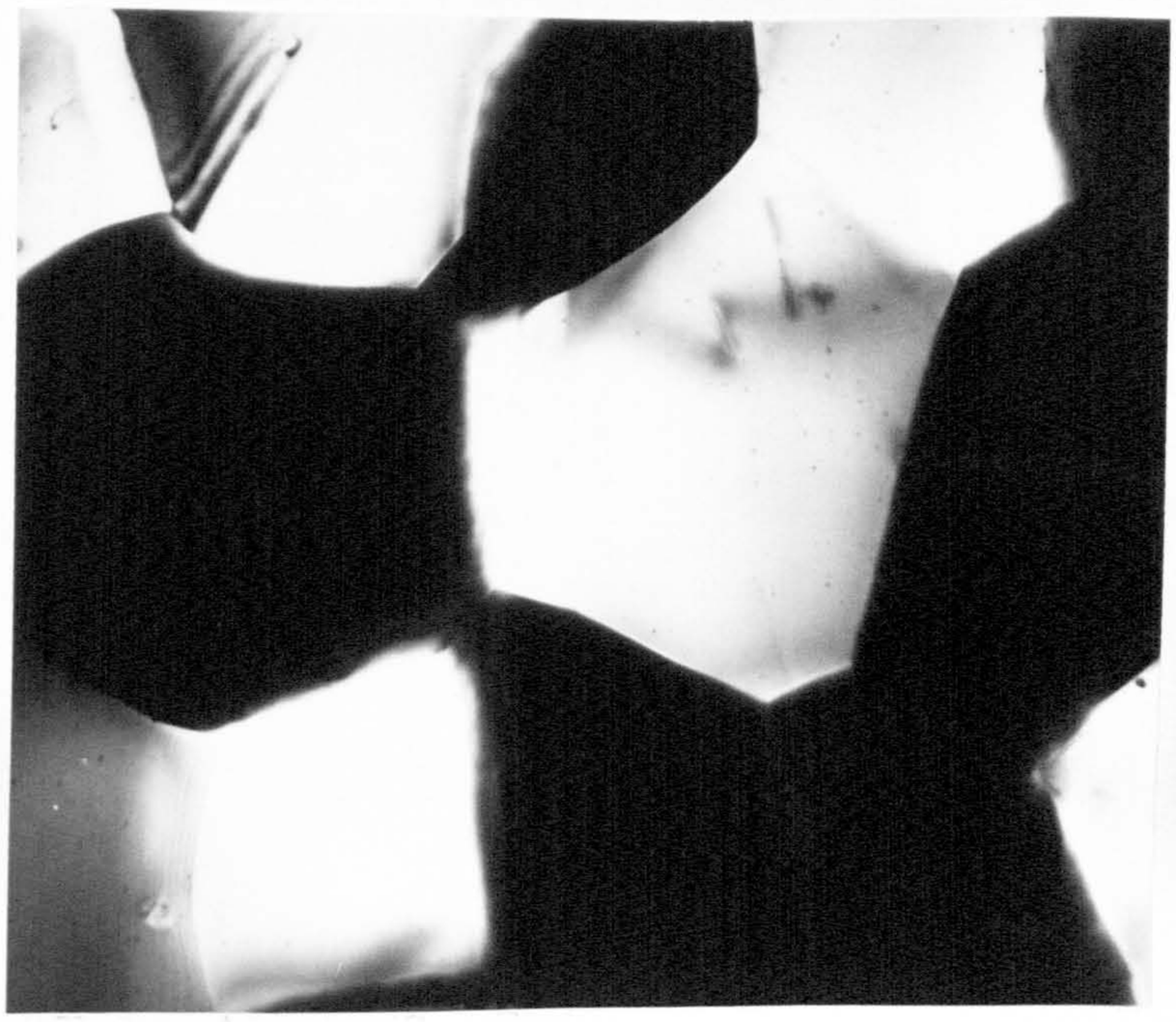

x30000

Figure 103a-Shows straight boundaries of an undeformed 1.05um grain size material.(TEM).

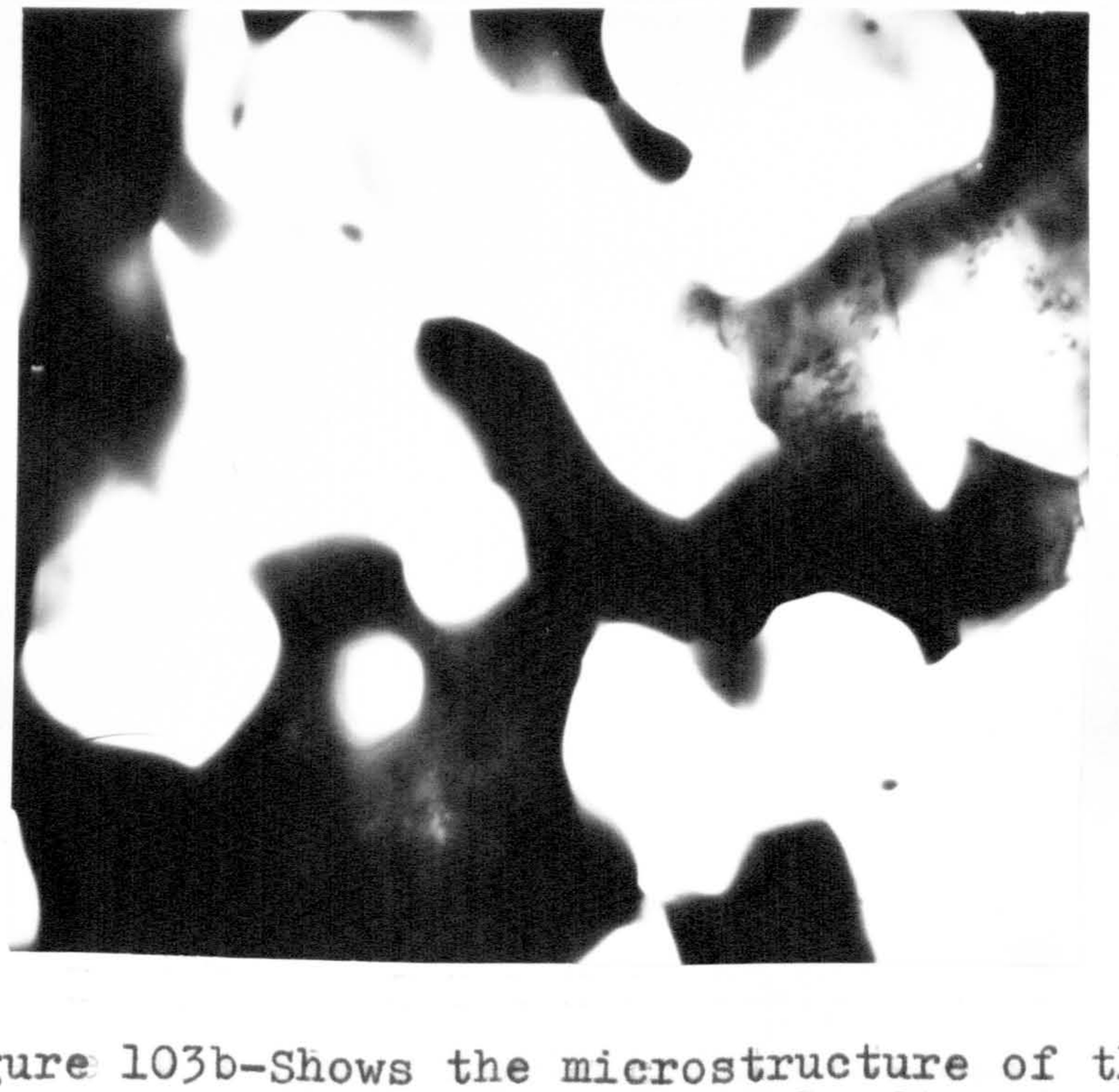

x12000

Figure 103b-Shows the microstructure of the 1.05um grain size material after it has been deformed(800%) at 250°C and at the crosshead velocity of 20 in/min.(TEM).

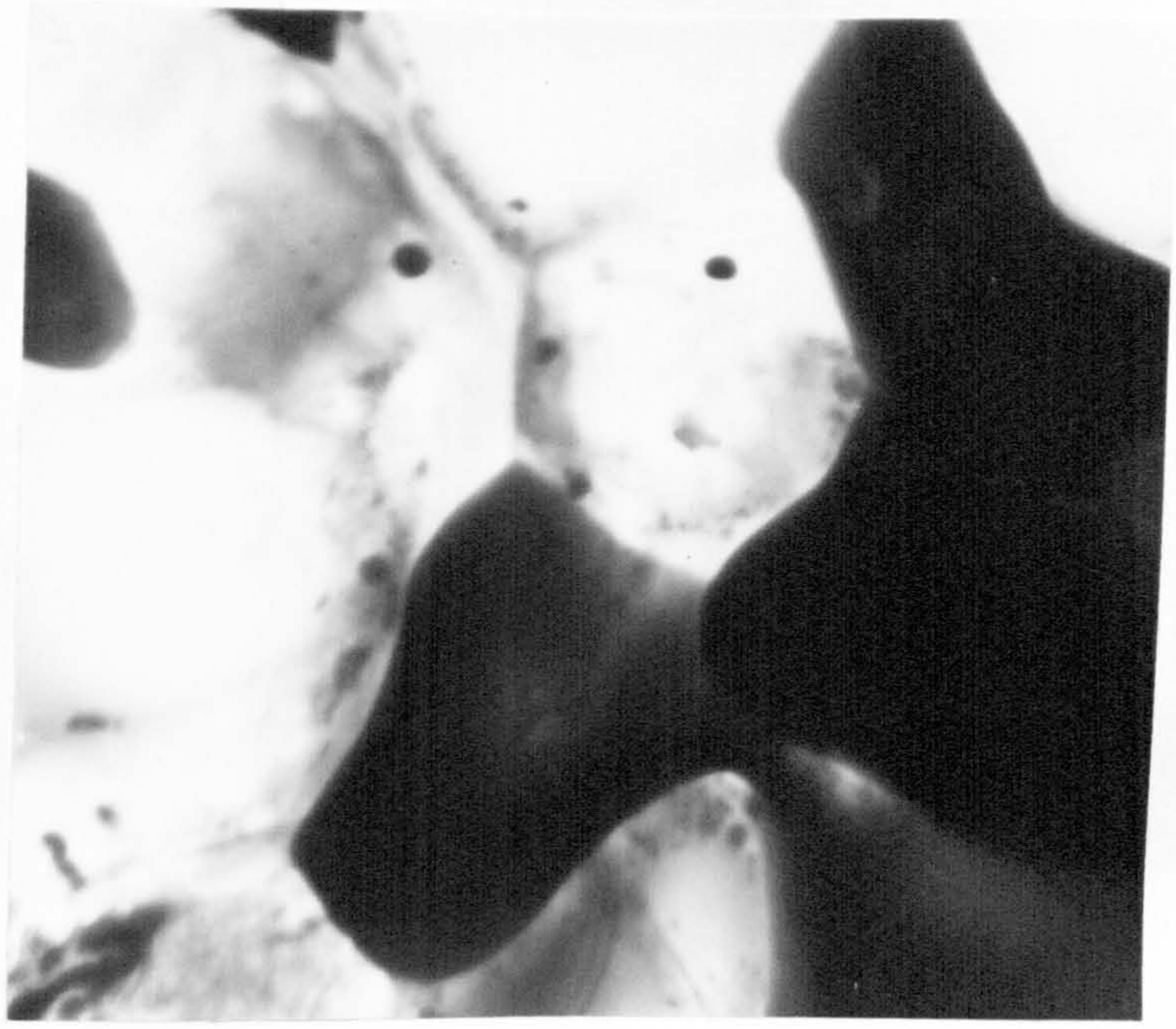

x30000

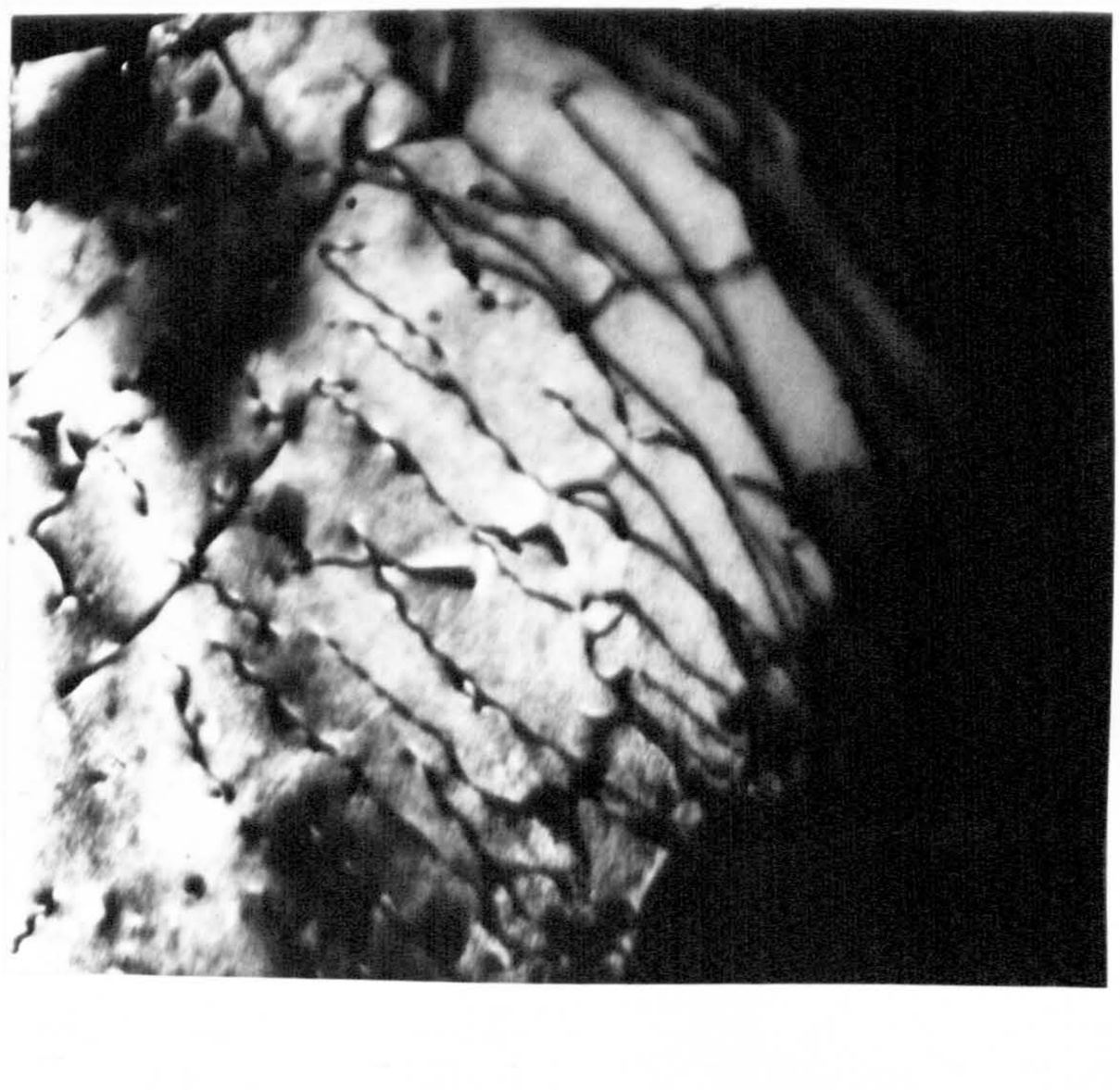

x60000

Figure 103c-Shows the microstructure of the 1.75um grain size material after it has been deformed(400%) at 250°C and at the crosshead velocity of 20 in/min.(TEM).

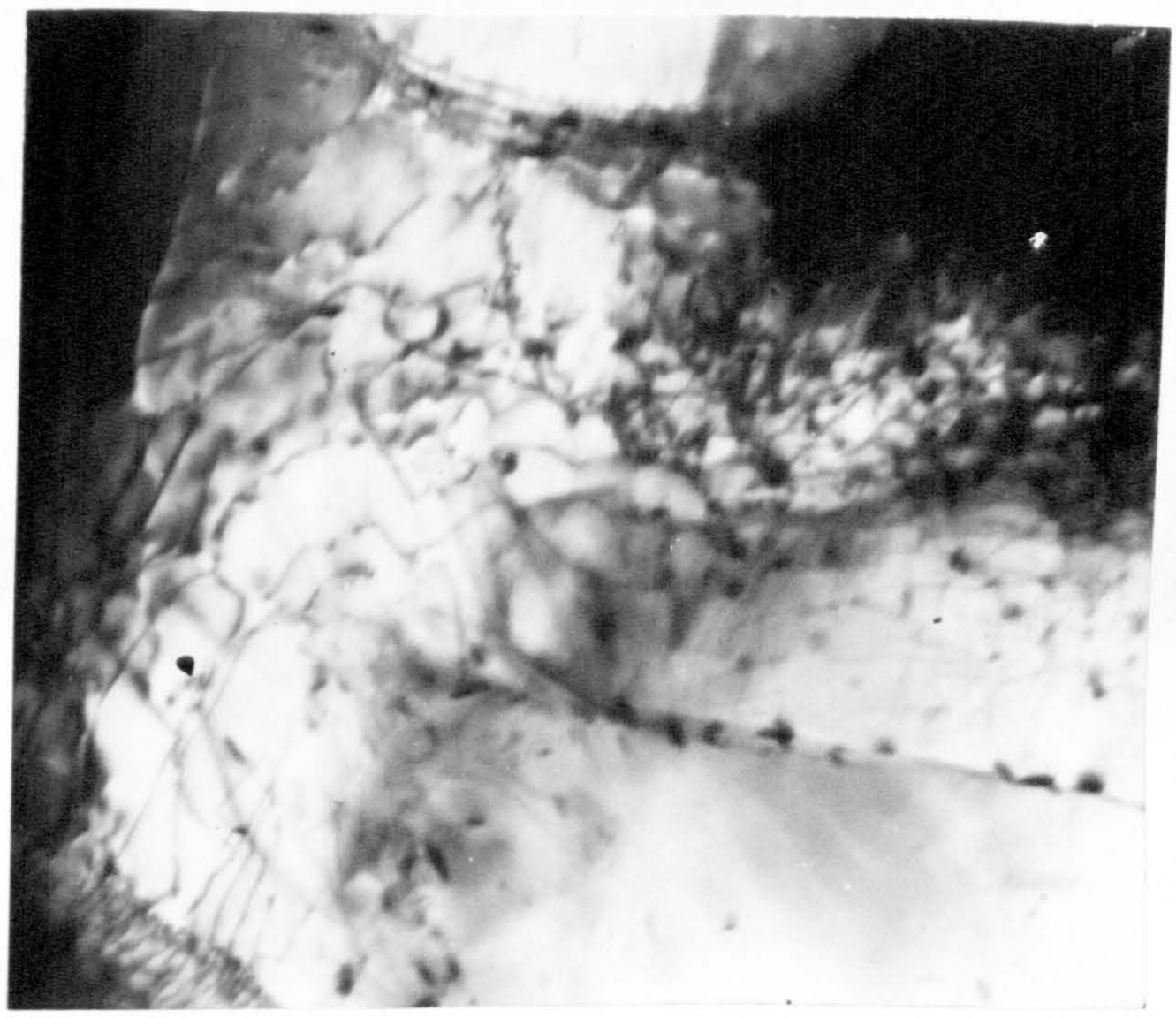

x60000

Figure 103d-Shows the microstructure of the 3.25um grain size material deformed (100%) at 250°C and at the crosshead velocity of 20 in/min.(TEM).

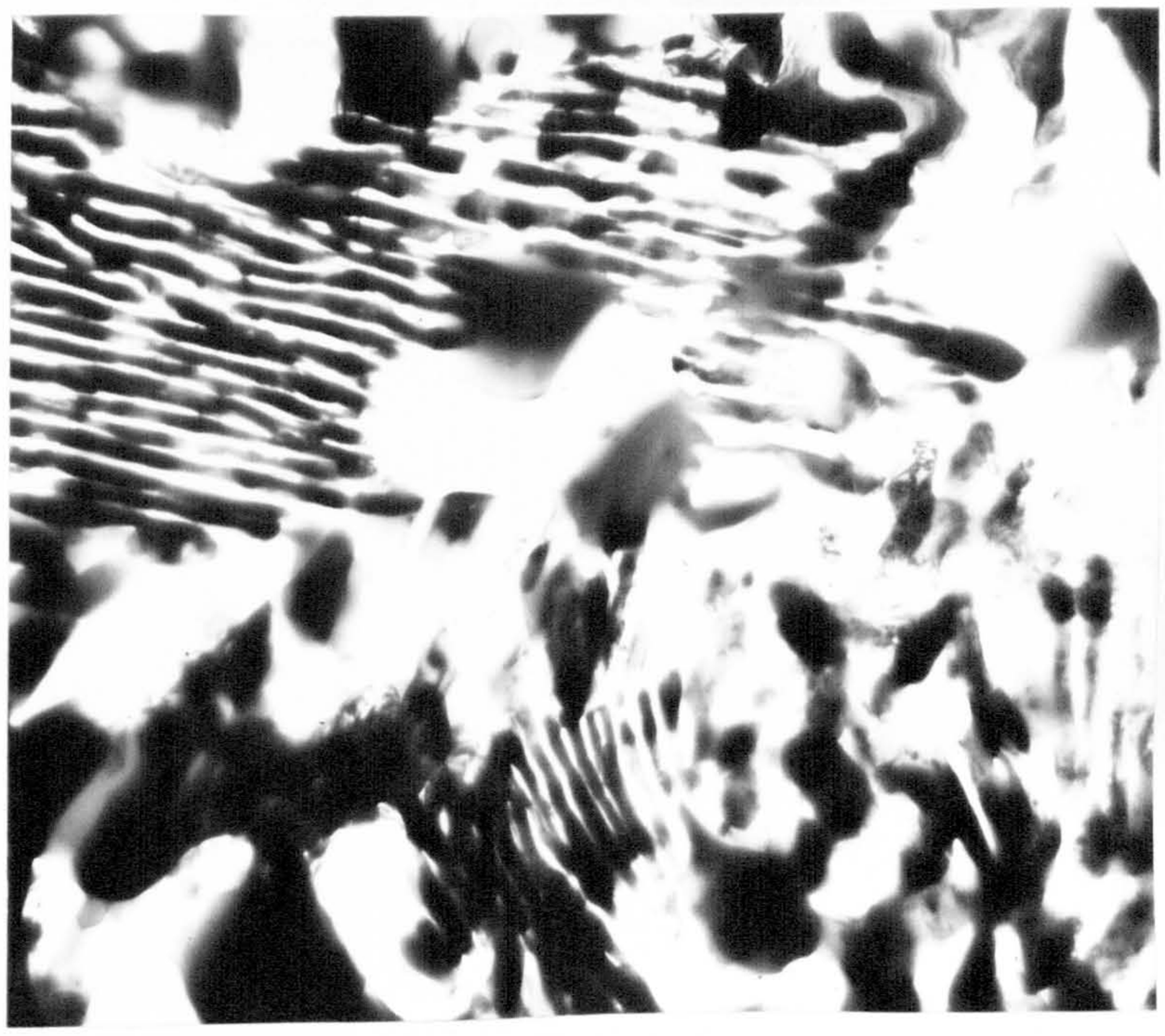

x19500

x60000

Figure 104- Specimen heated to 300°C and strained to fracture (150%) at the crosshead velocity of 20 in/min.(TEM).

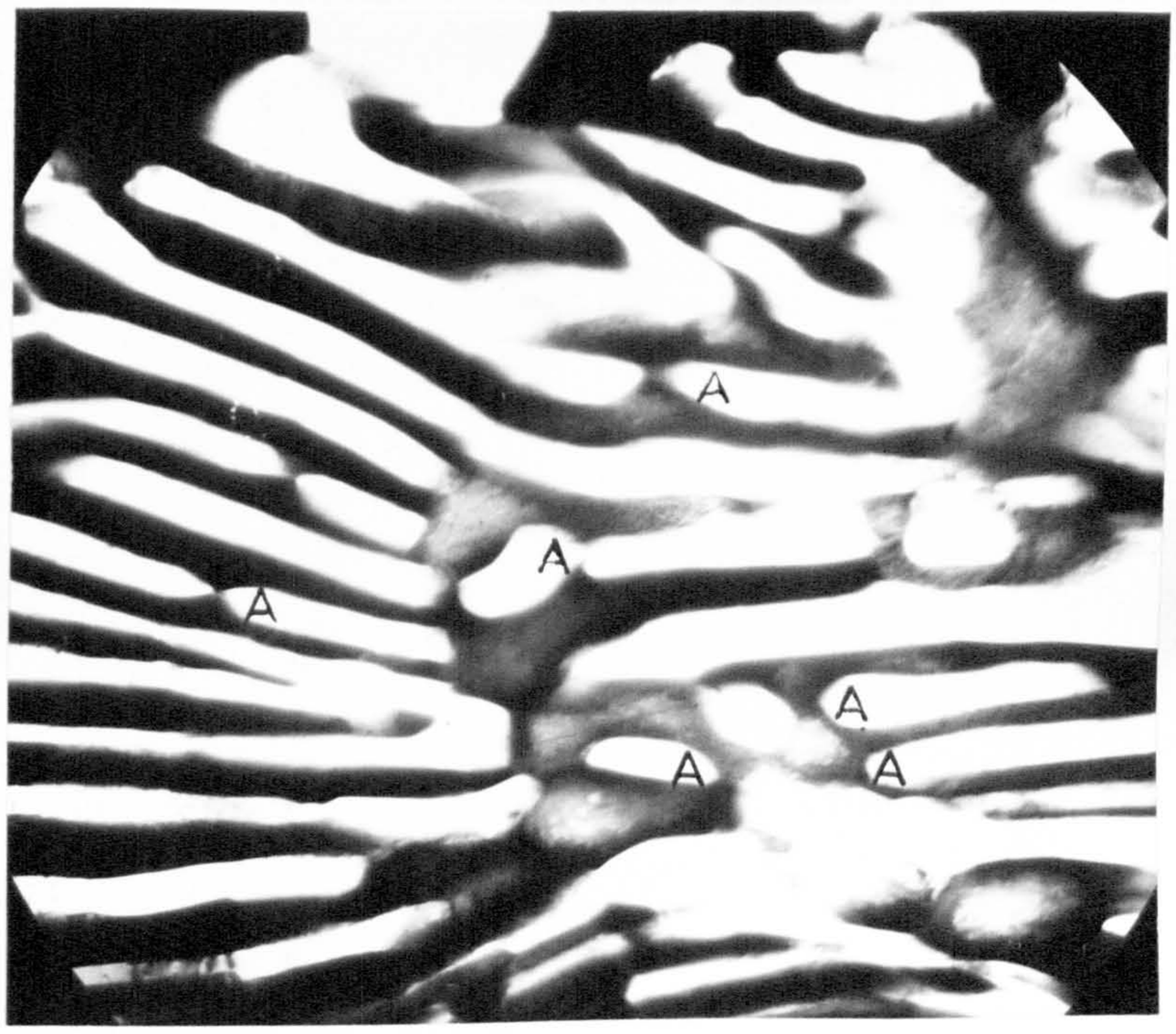

x20000

Figure 105- A lamellar structure specimen strained at 250°C and at the crosshead velocity of 20 in/min.(TEM).

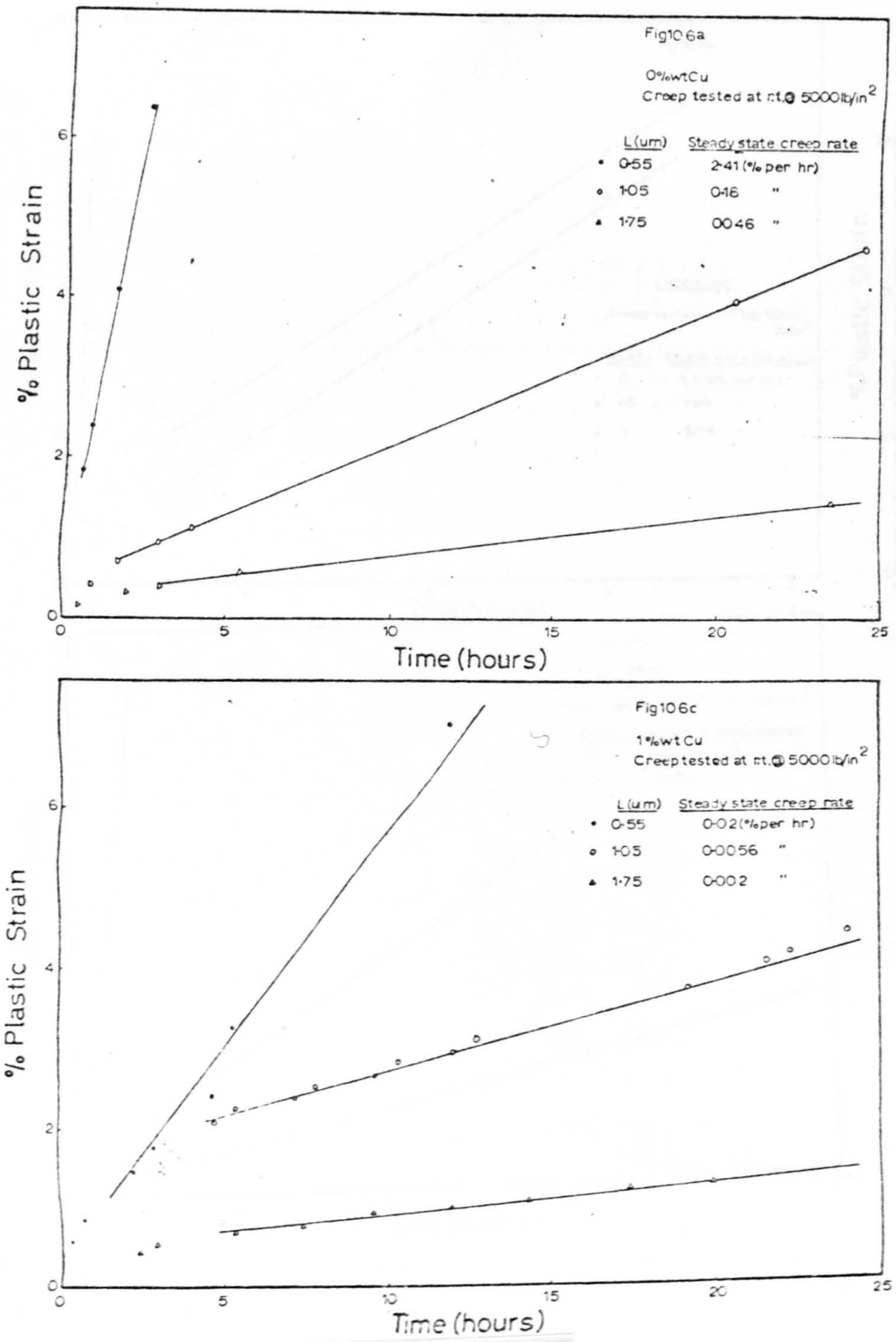

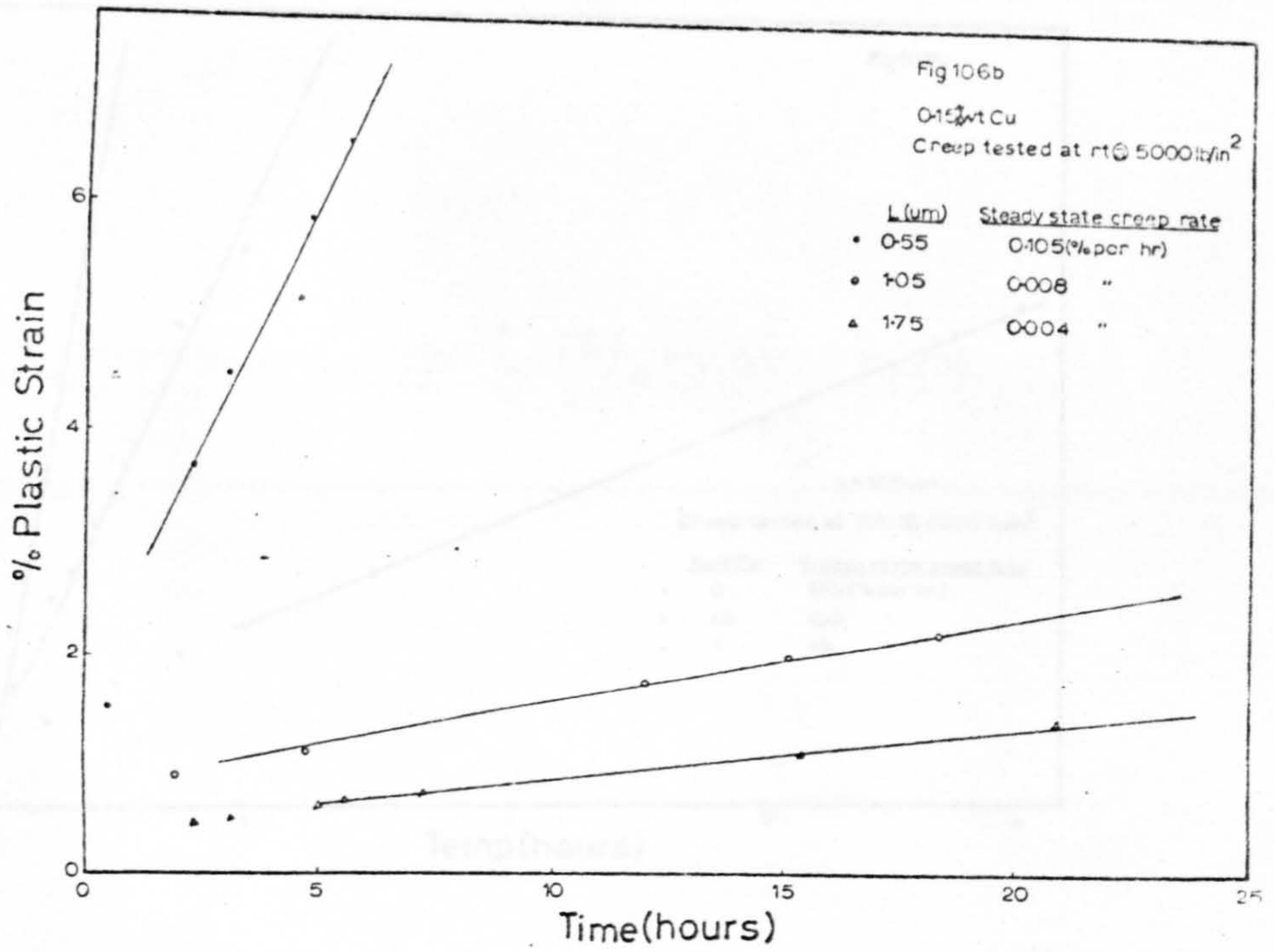

Figure 106a-c - The effect of copper additions and grain size on the steady state creep-rate at room temperature.

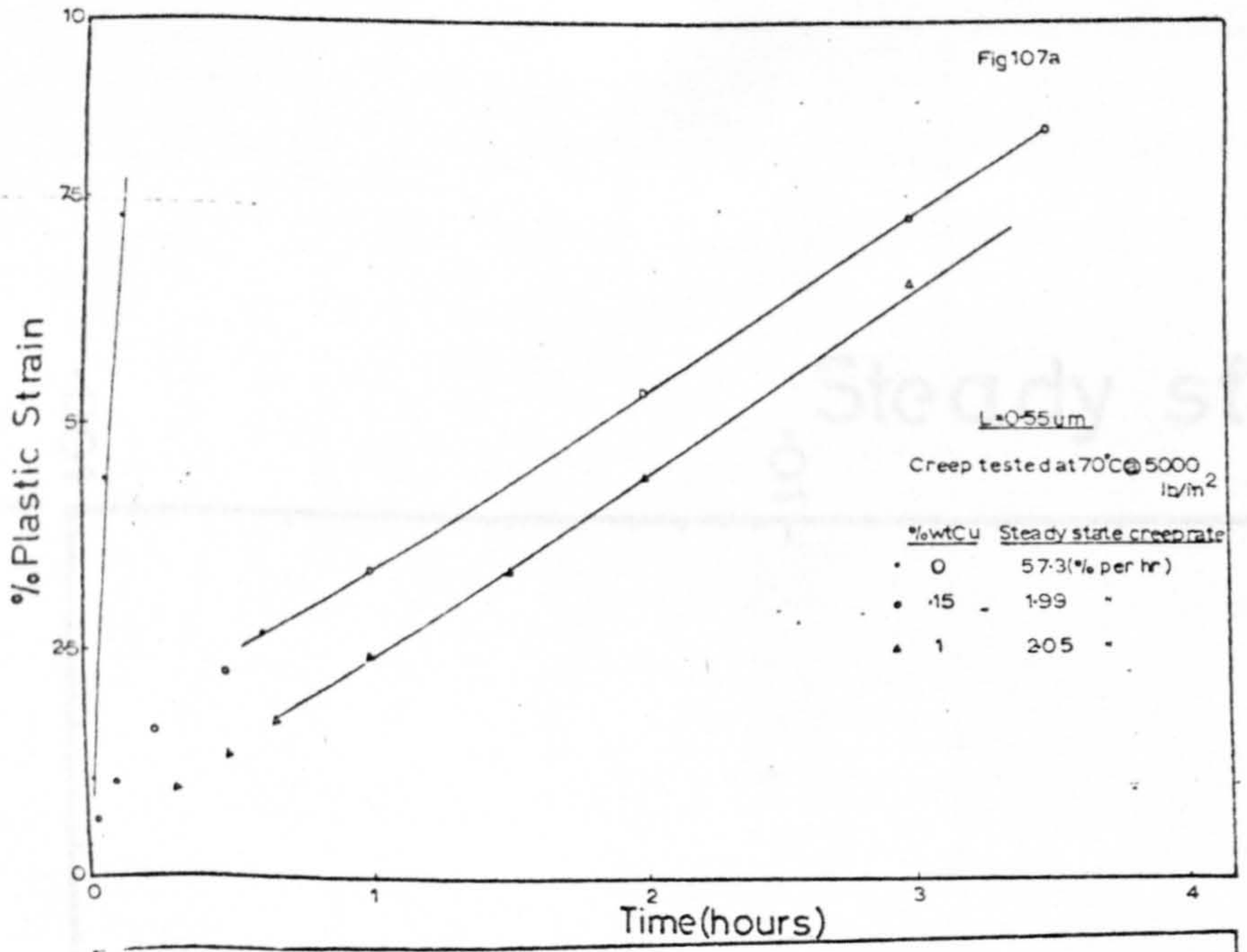

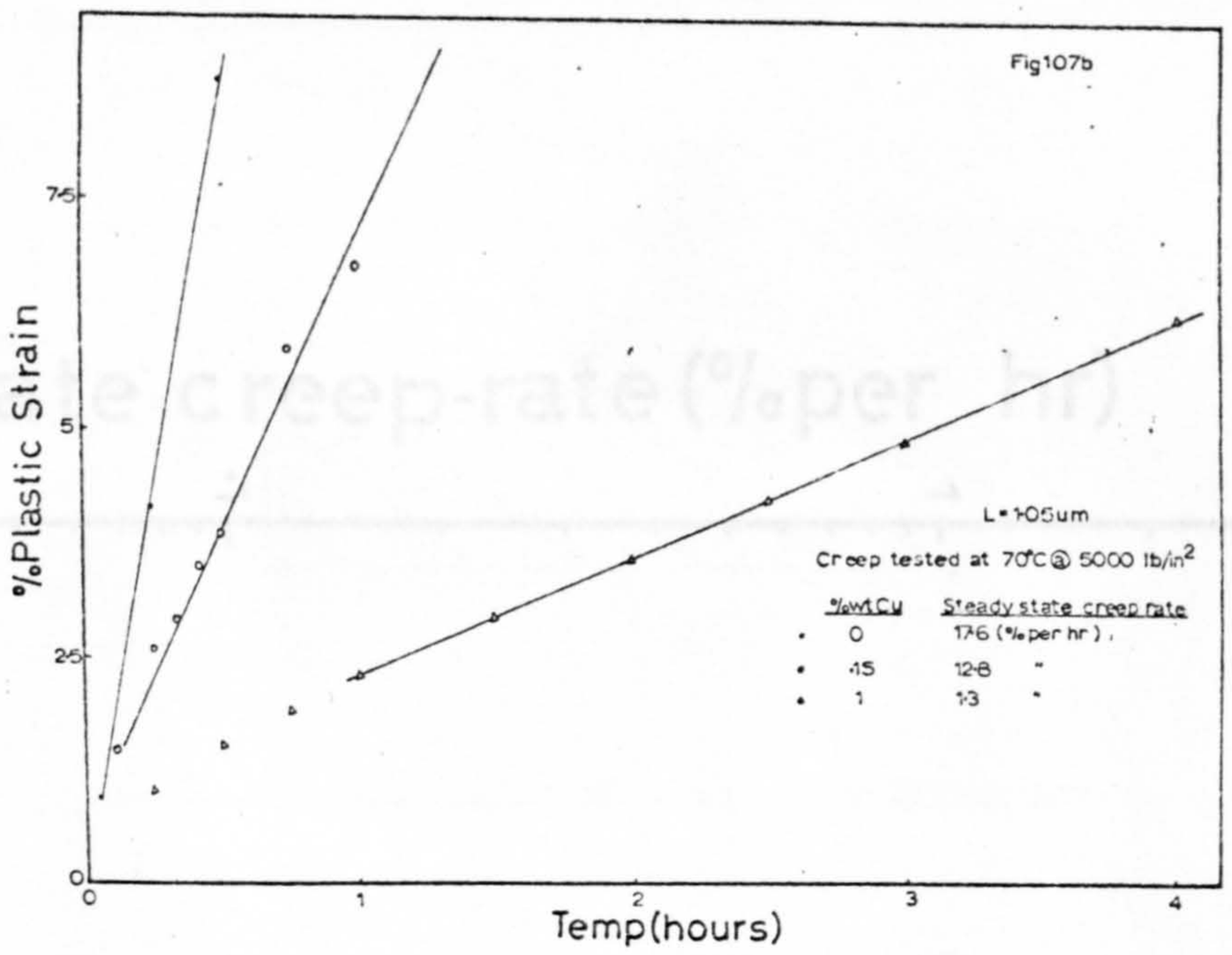

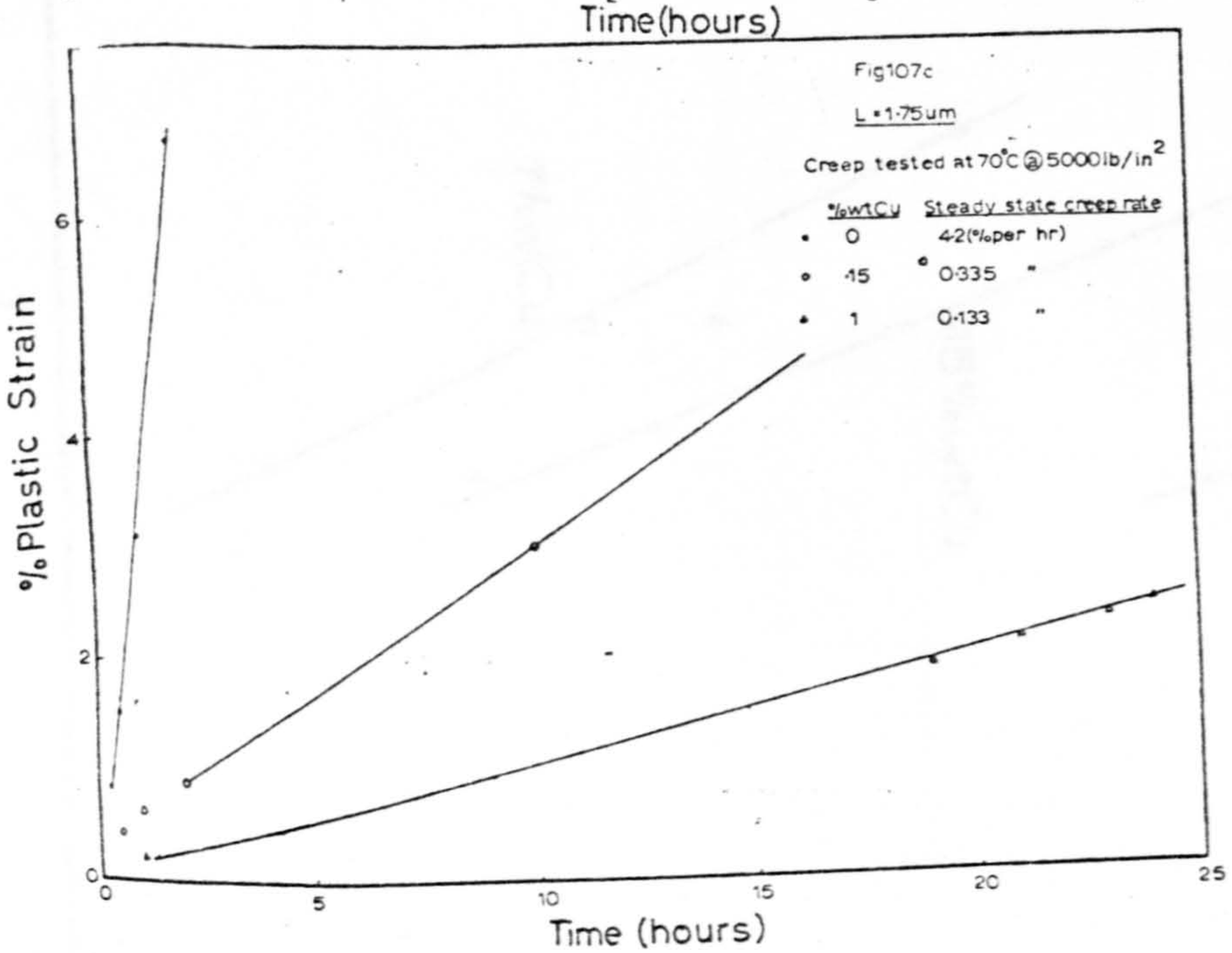

Figure 107a-c - The effect of copper additions and grain size on the steady state creep-rate at 70°C.

Fig 108

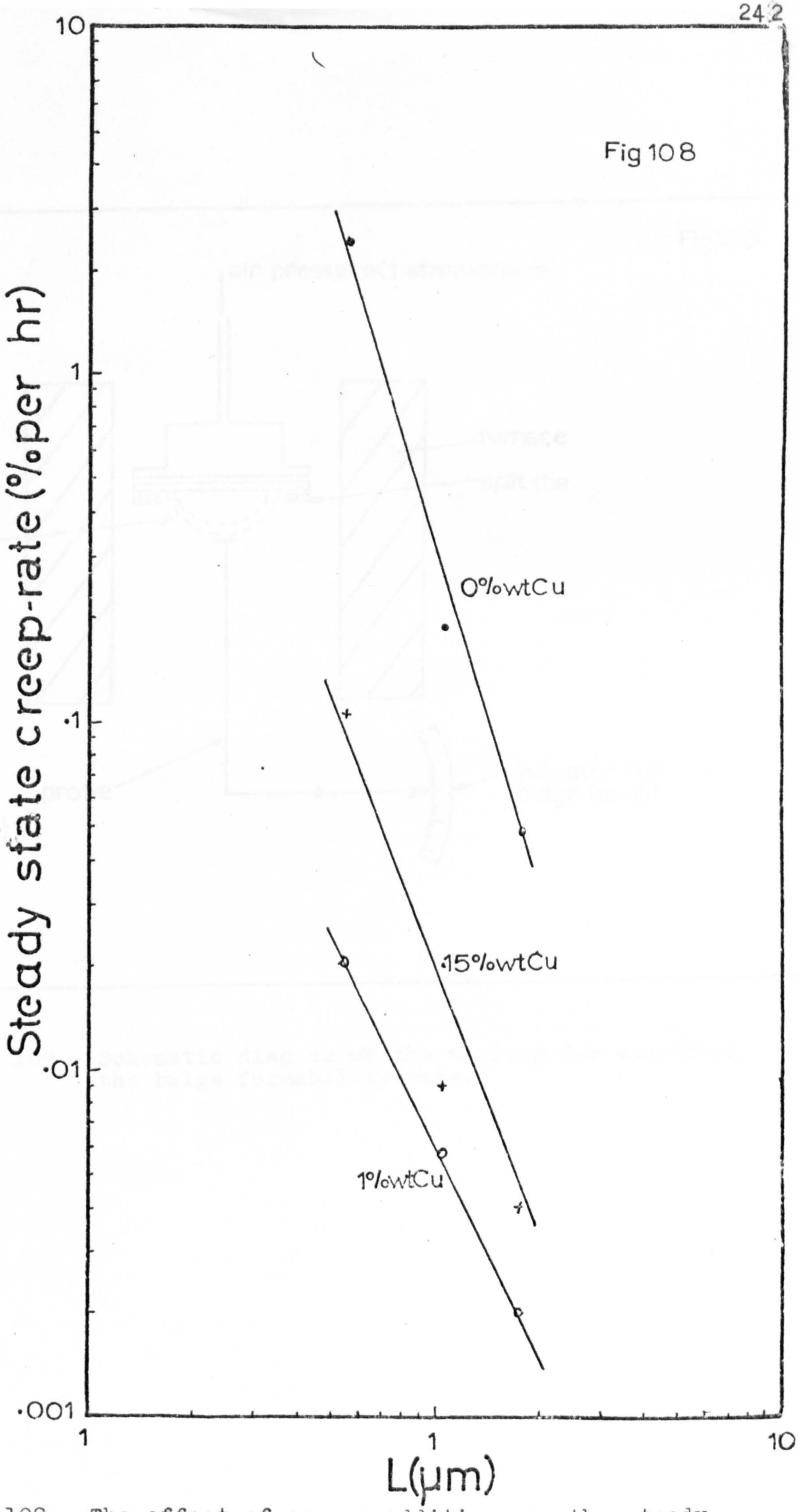

Figure 108 - The effect of copper additions on the steady state creep-rate with increasing grain size (room temperature).

Fig109

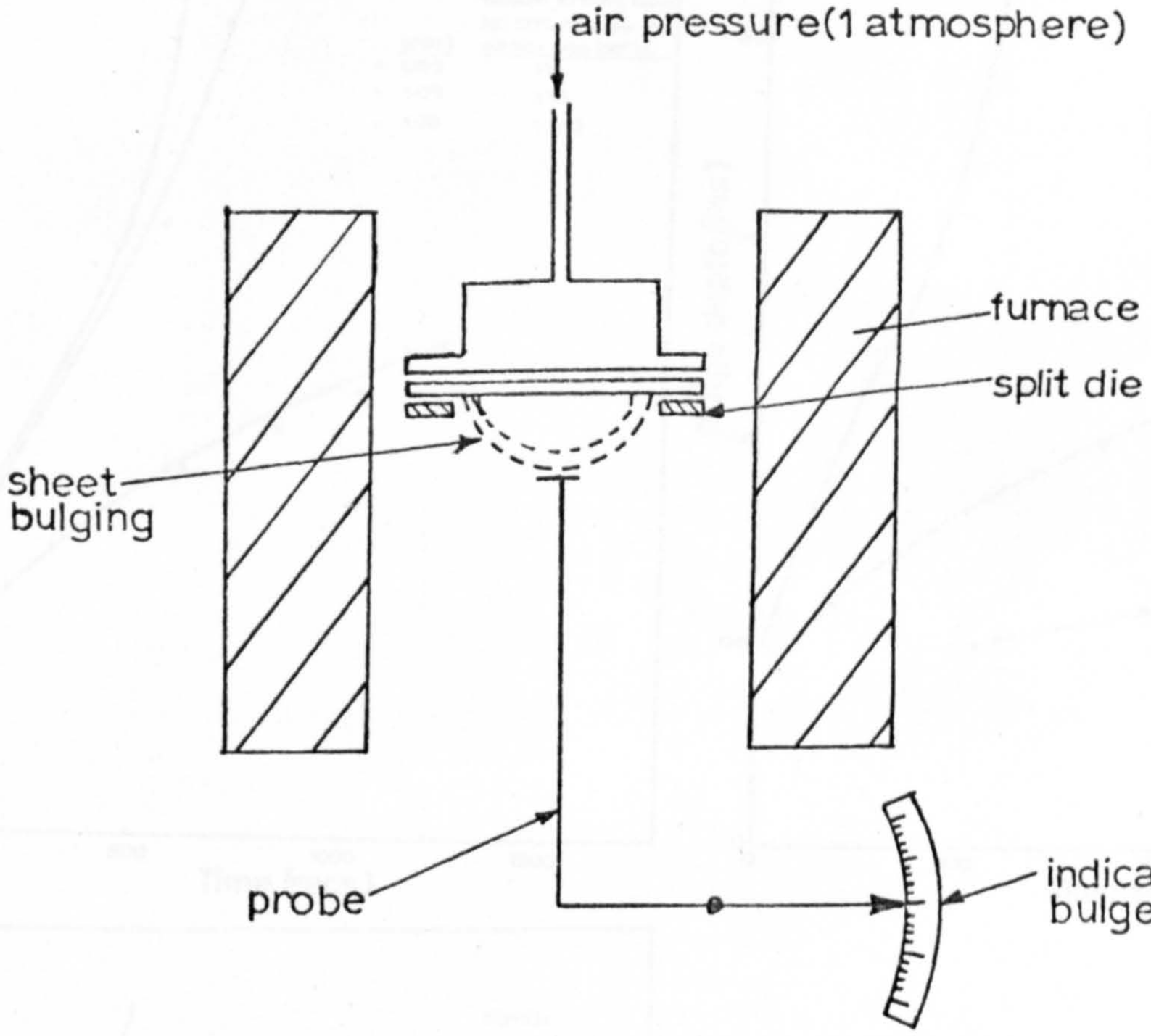

Figure 109 - Schematic diagram of the tooling for assessing the bulge formability-rate.

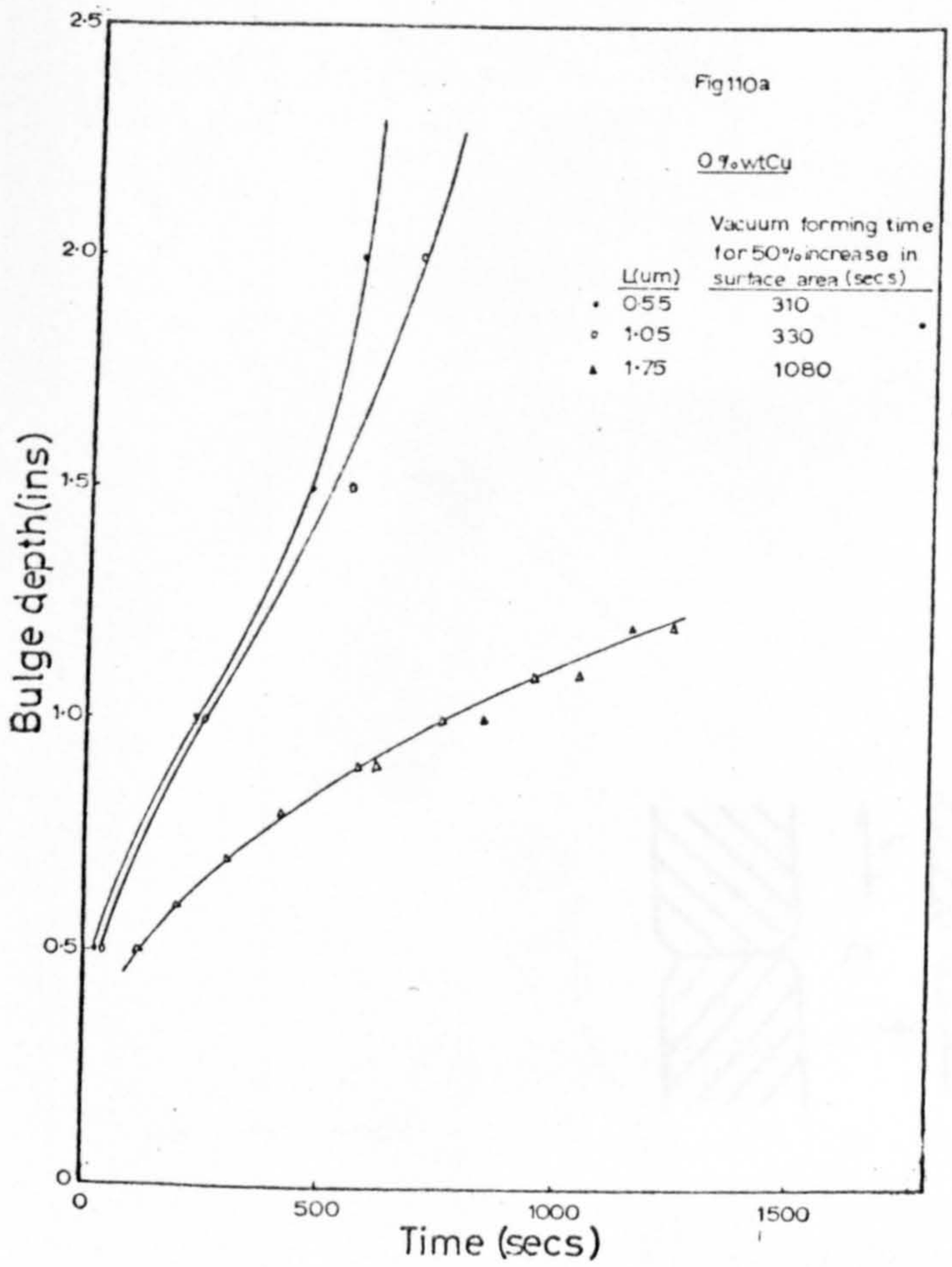

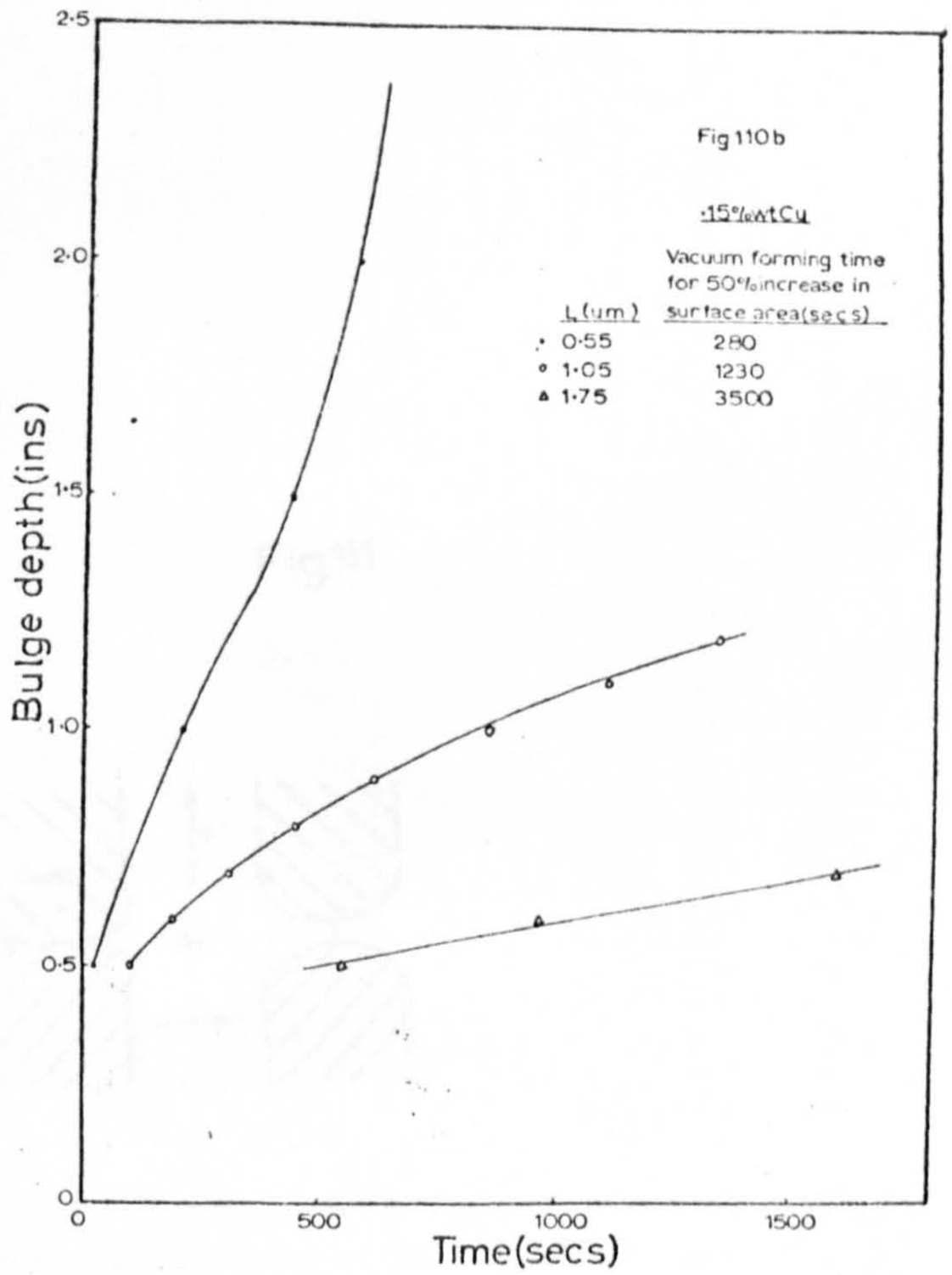

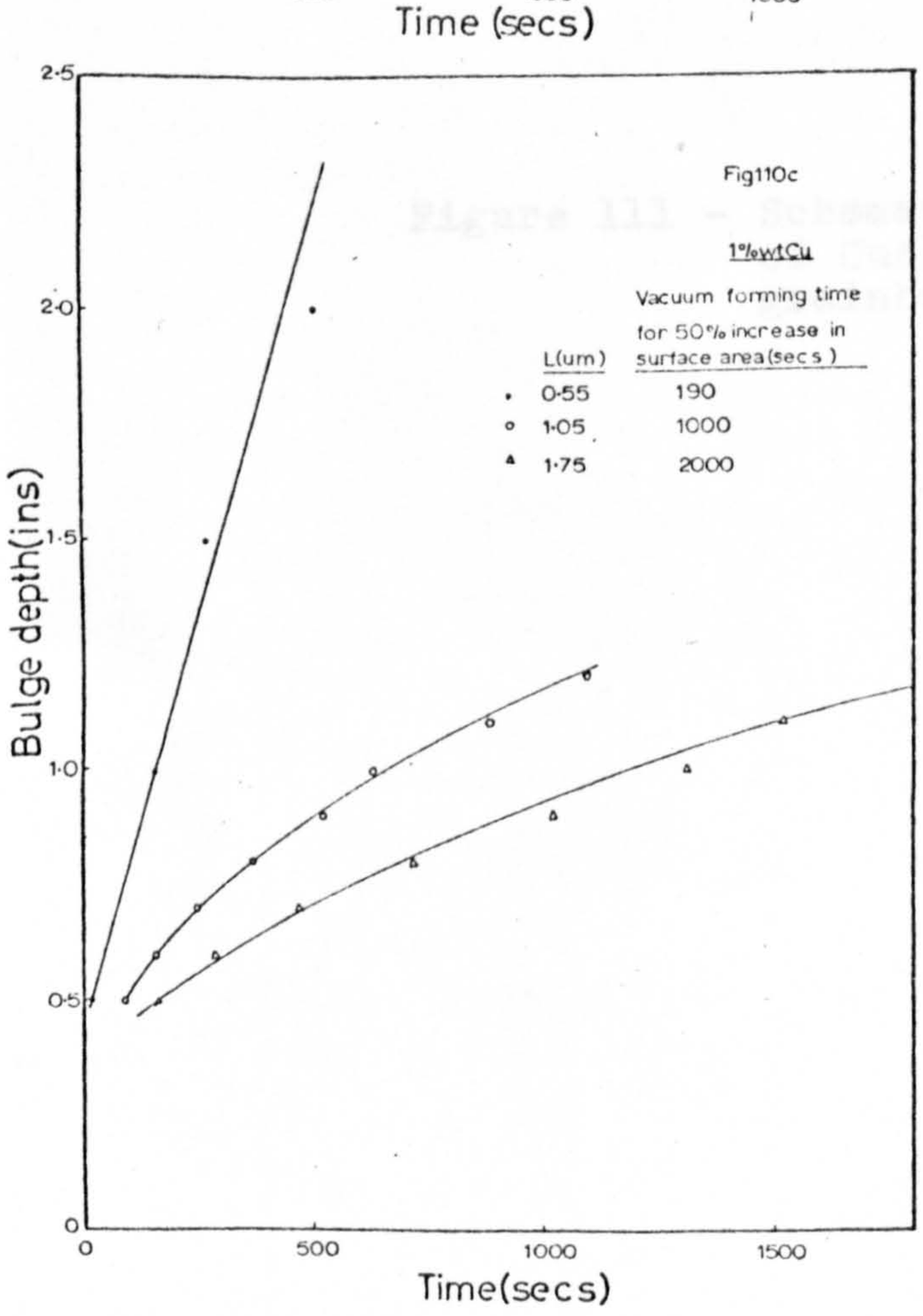

Figure 110a-c - The effect of copper additions and grain size on the bulge formability-rate.

Fig111

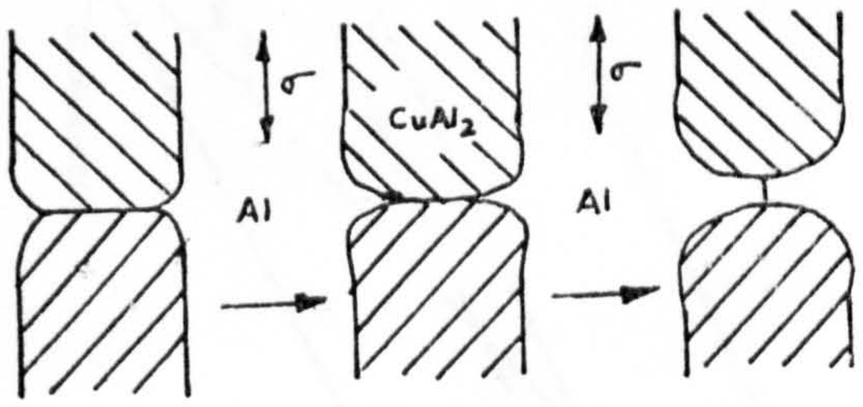

Figure 111 - Schematic diagram of the break-up of $CuAl_2$ particles by stress-assisted grainboundary grooving (Reference 57).

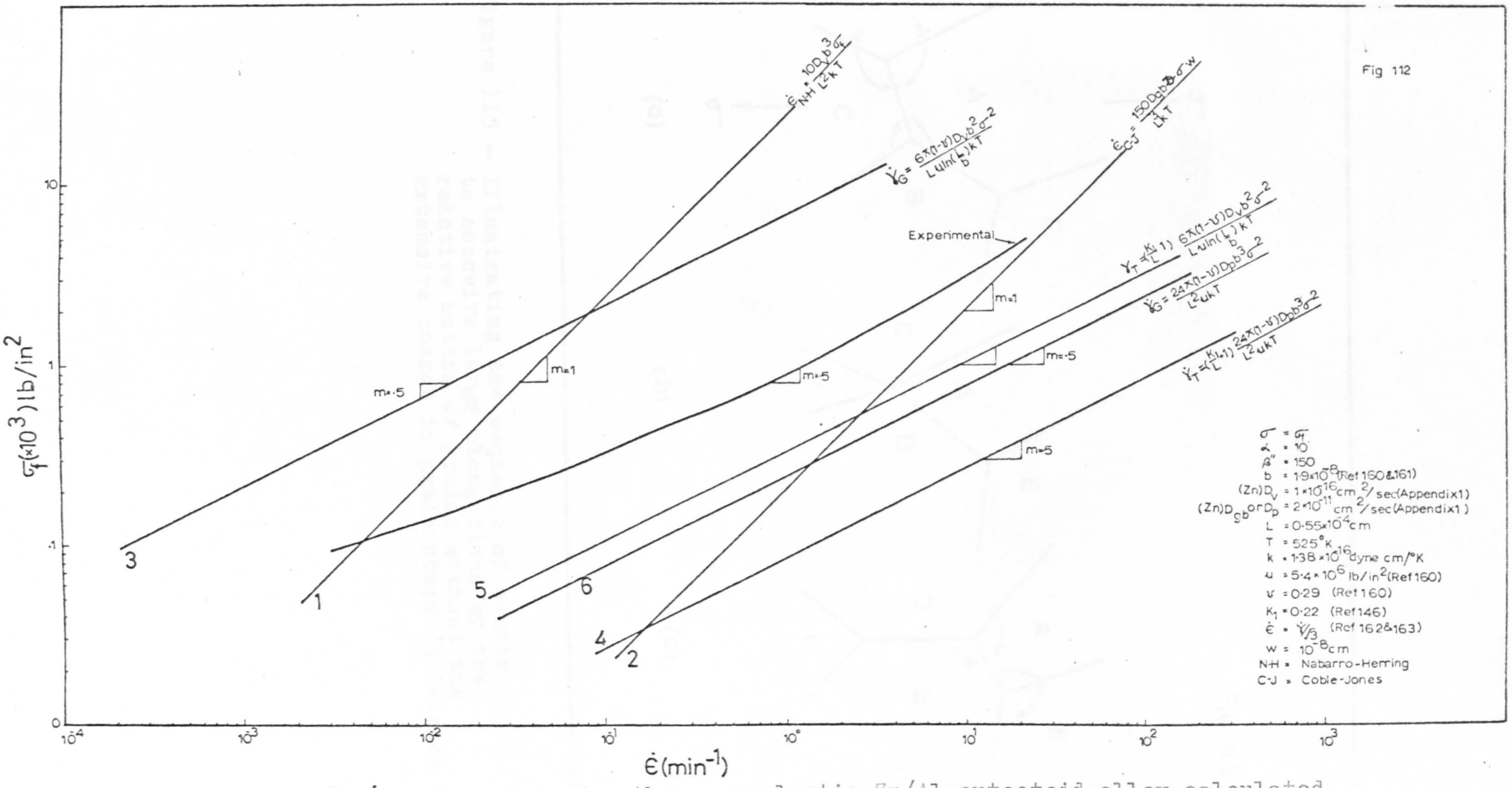

Figure 112-σ_f vs $\dot{\epsilon}$ relationship for the superplastic Zn/Al eutectoid alloy calculated from the various strain-rate contributing mechanisms.

Fig 113

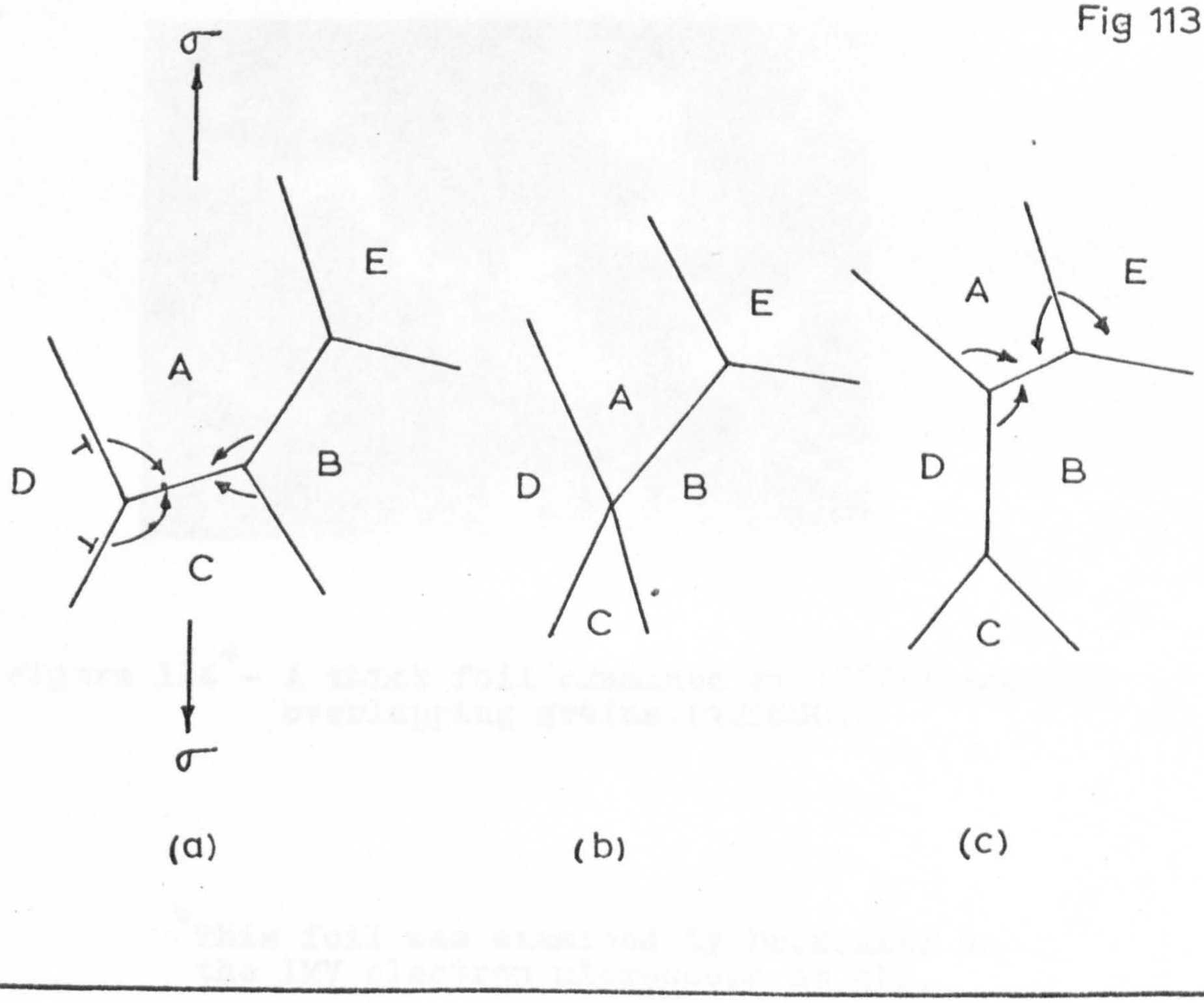

(a) (b) (c)

Figure 113 - Illustrating the sequence of events to conceive large elongations by the relative motion of grains without the extensive change in grain shape (Reference 143).

Figure 114*- A thick foil examined at 1000KV snowing overlapping grains.(x25000).

*This foil was examined by Dr.K.HALE on the 1MV electron microscope at NPL.